Identification, characterisation and optimisation of novel natural products and derivatives with antimicrobial activity against *Toxoplasma gondii*

Inaugural dissertation

for the attainment of the title of doctor
in the Faculty of Mathematics and Natural Sciences
at the Heinrich Heine University Düsseldorf

presented by

Flaminia Mazzone
from Catania

Düsseldorf, December 2023

from the Institute of Medical Microbiology and Hospital Hygiene
at the Heinrich Heine University Düsseldorf

Published by permission of the
Faculty of Mathematics and Natural Sciences at
Heinrich Heine University Düsseldorf

Supervisor: Prof. Dr. med. Klaus Pfeffer
Co-supervisor: Prof. Dr. rer. nat. Rainer Kalscheuer

Date of the oral examination:

L'amor che move il sole

e l'altre stelle.

(Dante Alighieri, Paradiso, XXXIII, v. 145)

Zusammenfassung

Toxoplasma gondii ist der Erreger der Toxoplasmose, einer weltweit beim Menschen verbreiteten Zoonose. Die verfügbaren Behandlungsmöglichkeiten sind in ihrer Anzahl begrenzt und mit Nebenwirkungen verbunden. Daher ist es dringend erforderlich, neue Behandlungsmethoden zu finden und zu entwickeln.

In der vorliegenden Arbeit wurden verschiedene Mini-Bibliotheken von Naturstoffen, Naturstoffanaloga und synthetischen kleinen Molekülen, die von Naturstoffgerüsten inspiriert sind, auf ihr Potenzial als neuartige Anti-Toxoplasma-Wirkstoffe *in vitro* untersucht. Der Forschungsartikel "*In vitro* biological activity of natural products from the endophytic fungus *Paraboeremia selaginellae* against *Toxoplasma gondii*" beschreibt die Isolierung, die Strukturaufklärung und die biologische Bewertung neuartiger Naturstoffe aus der Gattung *Paraboeremia*. Die Ergebnisse zeigen, dass Biphenylether, Bioxanthracene und 5S,6S-Phomalacton eine selektive Anti-Toxoplasma-Aktivität mit geringer oder keiner Zytotoxizität in menschlichen Zellen aufweisen. Die Veröffentlichung "Fluorescent Indolo[3,2-*a*]phenazines against *T. gondii*: Concise Synthesis by Gold-Catalyzed Cycloisomerization with 1,2-Silyl Migration and ipso-Iodination Suzuki Sequence" untersucht die Synthese, die biologische Bewertung und die Struktur-Eigenschaftsbeziehungen der Indolo[3,2-*a*]phenazine. Sie zeigten eine starke Aktivität gegen *T. gondii*, mit einem IC_{50}-Wert von bis zu 0,67 µM. Anschließend konzentrierten wir uns auf die Optimierung ihrer Strukturaktivität mit dem Ziel, ihre Struktur zu verändern, um das therapeutische Fenster zu erweitern. Die Leitverbindung LHP 091 zeigte eine starke Anti-Toxoplasma-Wirksamkeit ohne Zytotoxizität der Wirtszellen. Der Artikel "Modular Approach for the Synthesis and Bioactivity Profiling of 8,8'-Biflavones" stellt eine skalierbare Synthese für 55 monomere und dimere Flavone sowie die Bewertung ihres Antitoxoplasmaprofils, ihrer Zytotoxizität auf gesunde und Krebszellen und ihrer antioxidativen Kapazität vor. 8,8'-Biflavone zeigten eine hohe Wirksamkeit gegen die Proliferation von *T. gondii* und HeLa-Zellen. Das Manuskript "Synthesis and *In Vitro* Evaluation of Bichalcones as Novel Potential Anti-Toxoplasma Agents" beschreibt die Bioaktivität von A,A'-Bichalconen. Die *in vitro*-Untersuchungen auf ihre Anti-Toxoplasma-Kapazität haben A,A'-Bichalkone als Anti-Toxoplasma-Wirkstoffe herausgestellt. Die reinen Enantiomere (S_a) und (R_a) der aktivsten Verbindung wurden synthetisiert und biologisch bewertet. Die Ergebnisse zeigten, dass das Enantiomer (R_a) die höchste Aktivität aufwies. Das Manuskript "1-deoxy-d-xylulose 5-phosphate reductoisomerase (DXR) as target for

anti-*Toxoplasma gondii* agents: crystal structure, biochemical characterization and *in vitro* biological evaluation of fosmidomycin and reverse analogues as potent inhibitors" präsentiert die erste Röntgenstruktur der DXR von *T. gondii* im Komplex mit dem Inhibitor Fosmidomycin und dem Cofaktor NADPH, die entscheidende Bindungsinteraktionen aufdeckt. Es wurde eine biochemische Charakterisierung des Zielenzyms durchgeführt. Außerdem konnten reverse α-Phenyl-ß-thia-Analoga von Fosmidomycin als potente Inhibitoren identifiziert werden. Im Hinblick auf die Permeabilität wurde eine Analyse von Fosmidomycinderivaten und ihren entsprechenden POM-Estern durchgeführt. Letztere zeigten eine verbesserte Anti-Toxoplasma-Aktivität, was wahrscheinlich auf ihre erhöhte Lipophilie und potenzielle Prodrug-Aktivität zurückführen ist.
Diese Arbeit definiert Indolo[3,2-*a*]phenazine und Fosmidomycin-Derivate als neuartige Anti-Toxoplasma-Wirkstoffe und unterstreicht die Bedeutung von Naturstoffen und ihren Derivaten als Quelle für neue Leitstrukturen bei der Identifizierung von Anti-Toxoplasma-Wirkstoffen.

Summary

Toxoplasma gondii is the etiologic agent of toxoplasmosis, a zoonotic disease that is widespread in humans worldwide. The available treatment options are limited in number and associated with side effects. Thus, novel treatments are urgently needed to be identified and developed. In the present thesis, different small molecule mini-libraries of natural products, natural product analogues and synthetic small molecules inspired from natural product scaffolds were investigated for their potential as novel anti-toxoplasma agents *in vitro*. The research article "*In vitro* biological activity of natural products from the endophytic fungus *Paraboeremia selaginellae* against *Toxoplasma gondii*" details the isolation, the structure elucidation and the biological evaluation of novel natural products identified in the genus *Paraboeremia*. Results showed that biphenyl ethers, bioxanthracenes, and 5S,6S-phomalactone demonstrated a selective anti-toxoplasma activity with low or no cytotoxicity in human cells. The publication "Fluorescent Indolo[3,2-*a*]phenazines against *T. gondii*: Concise Synthesis by Gold-Catalyzed Cycloisomerization with 1,2-Silyl Migration and *ipso*-Iodination Suzuki Sequence" explores the synthesis, biological assessment, and the structure-property relationships of the indolo[3,2-*a*]phenazines. They showed potent activity against *T. gondii*, with an IC_{50} value of up to 0.67 µM. Afterwards, the focus was on their structure activity optimisation, with the aim to modify their structure to broaden the therapeutic window. The lead compound LHP 091 showed potent anti-toxoplasma efficacy without host cell cytotoxicity. The article "Modular Approach for the Synthesis and Bioactivity Profiling of 8,8'-Biflavones" evaluates the anti-toxoplasma profile, cytotoxicity on healthy and cancerous cells, and antioxidant capacity of 55 newly synthesised monomeric and dimeric flavones. 8,8'-Biflavones demonstrated high potency against the proliferation of *T. gondii* and HeLa cells. The manuscript "Synthesis and *In vitro* Evaluation of Bichalcones as Novel Potential Anti-Toxoplasma Agents" details the bioactivity of A,A'-bichalcones. The *in vitro* evaluation for their anti-toxoplasma capacity outlined A,A'-bichalcones as anti-toxoplasma agents. The pure enantiomers (S_a) and (R_a) of the most active compound were synthesised and biologically evaluated. Results showed that the enantiomer (R_a) exhibited the highest activity. The manuscript "1-deoxy-d-xylulose 5-phosphate reductoisomerase (DXR) as target for anti-*Toxoplasma gondii* agents: crystal structure, biochemical characterization and *in vitro* biological evaluation of fosmidomycin and reverse analogues as potent inhibitors" presents the first X-ray structure of the *T. gondii* DXR in complex with the inhibitor fosmidomycin and the cofactor NADPH, uncovering crucial binding interactions. Biochemical characterisation of the target-enzyme was performed. Moreover, reverse α-phenyl-ß-thia

analogues of fosmidomycin were identified as potent inhibitors. Addressing permeability issues, a screening of fosmidomycin derivatives and their corresponding POM esters was performed. The latter showed an improved anti-toxoplasma activity, probably be due to their increased lipophilicity and potential prodrug activity.

This thesis defines indolo[3,2-*a*]phenazines and fosmidomycin derivatives as novel anti-toxoplasma agents, highlighting the importance of natural products and their derivatives as a source of novel leads in the anti-toxoplasma drug discovery.

Table of Content

Zusammenfassung I

Summary III

Table of Content V

List of Tables VII

List of Figures VIII

List of Abbreviations IX

1 Introduction 1

1.1 Apicomplexa 1

1.2 *Toxoplasma gondii*: History of the Etiologic Agent 3

1.2.1 Life Cycle 3

1.3 Toxoplasmosis 6

1.3.1 Transmission to Humans 7

1.3.2 Clinical Manifestations of Toxoplasmosis 8

1.3.3 Treatment of Toxoplasmosis 10

1.3.4 Limits and Challenges of Anti-Toxoplasma Drugs 12

1.4 Natural Products and Derivatives in Drug Discovery 13

2 Aim of the Thesis 16

3 Publications 18

3.1 *In Vitro* Biological Activity of Natural Products from the Endophytic Fungus *Paraboeremia selaginellae* against *Toxoplasma gondii* 19

3.2 Fluorescent Indolo[3,2-*a*]phenazines against *Toxoplasma gondii*: Concise Sythesis by Gold-Catalyzed Cycloisomerization with 1,2-Silyl Migration and ipso Iodination Suzuki Sequence 35

3.2.1 Indolo[3,2-*a*]phenazines: Unpublished data 46

3.3 Modular Approach for the Synthesis and Bioactivity Profiling of 8,8´-Biflavones 53

3.4 Synthesis and *In Vitro* Evaluation of Bichalcones as Novel Anti-Toxoplasma Agents 74

3.5 1-deoxy-d-xylulose 5-phosphate reductoisomerase (DXR) as target for anti *Toxoplasma gondii* agents: crystal structure, biochemical characterization and *in vitro* biological evaluation of fosmidomycin and reverse analogues as potent inhibitors.....143

3.5.1 Inhibitors of 1-deoxy-D-xylulose 5-phosphate reductoisomerase: Unpublished data 201

4 Additional Unpublished Work 210

4.1 In vitro evaluation of a Histone Deacetilase Inhibitor (HDACi) library against *Toxoplasma gondii*.....210

5 Discussion 213

6 Concluding Remarks..... .229

Literature.....231

Acknowledgements XI

Statutory Declaration / Eidesstattliche Erklärung XV

List of Tables

Table 1: Indolo[3,2-*a*]phenazine derivates: *in vitro* activity against *T. gondii* ME49 tachyzoites and cytotoxicity on human fibroblasts Hs27 of the investigated compounds 52

Table 2: *In vitro* enzymatic inhibitory activity (IC_{50} and K_i values) of the investigated compounds against *Tg*DXR 203

Table 3: In vitro activity against *T. gondii* ME49 tachyzoites and their cytotoxicity on human fibroblasts Hs27 of DXR inhibitors. 207

Table 4: Anti-toxoplasma activity and cytotoxicity against human fibroblasts Hs27 of HDACi against *T. gondii*.....212

List of Figures

Figure 1: Classification of the phylum Apicomplexa 2
Figure 2: *T. gondii* life cycle 4
Figure 3: Lytic cycle and stage differentiation of *T. gondii* 5
Figure 4: Transmission of *T. gondii* in humans 7
Figure 5: Clinical manifestation of toxoplasmosis in humans 9
Figure 6: Mechanism of the action of antifolates 11
Figure 7: Discovery timeline of anti-toxoplasma medications currently in clinical use 12
Figure 8: Second cohort of indolo[3,2-*a*]phenazines.....47
Figure 9: Anti-toxoplasma activity of the novel investigated indolo[3,2-*a*]phenazines.....49
Figure 10: Effect of the novel investigated indolo[3,2-*a*]phenazines on the metabolic activity of human fibroblasts Hs27.....51
Figure 11: The novel free-phosphonate compound and their POM esters.....202
Figure 12: *In vitro* enzymatic inhibition of *Tg*DXR of the investigated compounds.....204
Figure 13: Anti-toxoplasma activity of the investigated free-phosphonate compounds ...205
Figure 14: Anti-toxoplasma activity of the investigated POM ester compounds 206
Figure 15: Effect of the investigated phosphonate and POM ester compounds on the viability of human fibroblasts Hs27.....208
Figure 16: Natural products isolated from the endophytic fungus *P. selaginella* with anti-toxoplasma activity.....214
Figure 17: The penta-heterocyclic structures of 8*H*-indolo[3,2-*a*]phenazine and berberine hemisulfate in comparison. 216
Figure 18: Most active indolo[3,2-*a*]phenazines of the first cohort against *T. gondii* 217
Figure 19: Chemical structure of the indolo[3,2-*a*]phenazine lead compound LHP 091 218
Figure 20. Chemical structure of the 8,8'-biflavone lead compound.....220
Figure 21. Chemical structures of bichalcones 12 and 13 222
Figure 22: Chemical structures of enantiomers R_a-12 and S_a-12 222
Figure 23: Chemical structures of bichalcone 12 and rhuschalcones IV and I 223
Figure 24: Chemical structure of the natural product fosmidomycin (FSM) 224
Figure 25: Chemical structures of fosmidomycin and the investigated reverse ß-thia and ß-oxa analogues of fosmidomycin.....225
Figure 26: Detailed view of the active site of *Tg*DXR 226
Figure 27: *T. gondii* under the scope: summary of the compound classes investigated 229

List of Abbreviations

AI	Artificial Intelligence
AIDS	Acquired Immunodeficiency Syndrome
C. gundi	*Ctenodactylus gundi*
CDC	Centre for Disease Control and Prevention
CNS	Central Nervous System
CUF	Cupressuflavone
DHFR	Dihydrofolate Reductase
DHPS	Dihydropteroate Synthase
DXR	1-deoxy-D-xylulose 5-phosphate reductoisomerase
E. coli	*Escherichia coli*
ECF	East Coast Fever
FPLC	Fast Protein Liquid Chromatography
FSM	Fosmidomycin
GRA	Dense Granule Proteins
HDAC	Histone Deacetylase
HPLC	High-Performance Liquid Chromatography
HTS	High-Throughput Screening
IC-MS	Ion Chromatography-Mass Spectrometry
M. tuberculosis	*Mycobacterium tuberculosis*
MEP	2-C-methyl-D-erythritol-4-phosphate
MS	Mass Spectrometry
MVA	Mevalonate Pathway
NCBI	National Center for Biotechnology Information
NPs	Natural Products
P. falciparum	*Plasmodium falciparum*

P. selaginellae	*Paraboeremia selaginellae*
POM	Pyvaloiloxymethyl
PV	Parasitophorous Vacuole
PVM	Parasitophorous Vacuole Membrane
PYR	Pyrimethamine
SAR	Structure-Activity Relationship
SAXS	Small-Angle X-ray Scattering
SDZ	Sulfadiazine
SIR2	Silent Information Regulator 2
SMLs	Synthetic Molecule Libraries
SMZ	Sulfamethoxazole
spp.	Species
T. gondii	*Toxoplasma gondii*
*Tg*DXR	*Toxoplasma gondii* 1-deoxy-D-xylulose 5-phosphate reductoisomerase
TMP	Trimethoprim
U.S.A.	United States of America
WHO	World Health Organisation

1 Introduction

1.1 Apicomplexa

The eukaryotic phylum Apicomplexa spans a large group of parasitic protists belonging to the superphylum Alveolata (Fast, Xue, Bingham, & Keeling, 2002), which encompasses over 6000 identified species and approximately one million of unnamed and undescribed species (Adl et al., 2007). Apicomplexans (from latin *apex* (top) and *complexus* (infolds)) are obligate intracellular parasitic protists sharing a common morphology (Votýpka, Modrý, Oborník, Šlapeta, & Lukeš, 2017). Their major feature consists in the presence of the apical complex, a structural and secretory formation containing unique organelles, the rhoptries, micronemes, and dense granules. These organelles are responsible for the invasion and interaction with the host cell, which are crucial processes for the establishment of the intracellular infection (Blackman & Bannister, 2001; Katris et al., 2014). Rhoptries are flask-shaped organelles bounded by membranes that are able to secrete membranous material. These organelles play a pivotal role in the establishment of parasitism, in particular to the invasion, expansion and maintenance of the parasitophorous vacuole membrane (PVM) (Sam-Yellowe, 1996). Much smaller than rhoptries are micronemes, fusiform or flask-shape organelles responsible of the host-invasion and motility of the parasites (Blackman & Bannister, 2001). The dense granules are secretory organelles bounded by a membrane with an electron dense crystalline protein core, involved in the maturation of the parasitophorous vacuole (PV) and the intracellular survival of the parasite. After the parasite invasion, dense granules secrete the dense granule proteins (GRA). The role of GRAs remains uncertain; however, recent data indicates a potential involvement in the construction of the PV network (Griffith, Pearce, & Heaslip, 2022; Mercier, Adjogble, Däubener, & Delauw, 2005). Alongside the apical complex, the apicoplast is another vital hallmark found in almost all Apicomplexans: discovered in the 1990s (McFadden, Reith, Munholland, & Lang-Unnasch, 1996), it is an unpigmented plastid with a small circular genome, originating from algae from secondary endosymbiosis, that have lost their photosynthetic metabolism (Lim & McFadden, 2010). Nevertheless, it houses several vital metabolic pathways for the parasite: the type II fatty acids biosynthetic pathway; the non-mevalonate pathway, for the production of crucial intermediates in the biosynthesis of isoprenoids; part of the haem biosynthesis; and other important functions (J. Kloehn, C. E. Lacour, & D. Soldati-Favre, 2021a).

Due their ability to infect a wide range of hosts, encompassing humans, Apicomplexans can be clinically significant pathogens, including: *Plasmodium spp.*, the causative agents of malaria

transmitted by Anopheles mosquitos (Hoffman, Subramanian, Collins, & Venter, 2002); *Babesia spp.*, pathogens of babesiosis, a zoonotic disease mostly being transmitted by its primary vector, the ixodid ticks (Yabsley & Shock, 2013); *Theileria spp.*, transmitted by ticks, where the most pathogenic representative *T.* parva is responsible for the East Coast Fever (ECF) (Fry et al., 2016); *Eimeria spp.* etiologic agents of coccidiosis, one of the major livestock disease in the world transmitted via the oral-fecal route (Blake & Tomley, 2014); *Cryptosporidium spp.*, leading cause of one of most common waterborne diarrheal disease outbreaks in humans and animals, the cryptosporidiosis (Khan & Witola, 2023) and *Toxoplasma gondii* (*T. gondii*), the pathogenic agent of the zoonotic disease toxoplasmosis (Jitender P Dubey, 2008) (**Figure 1**).

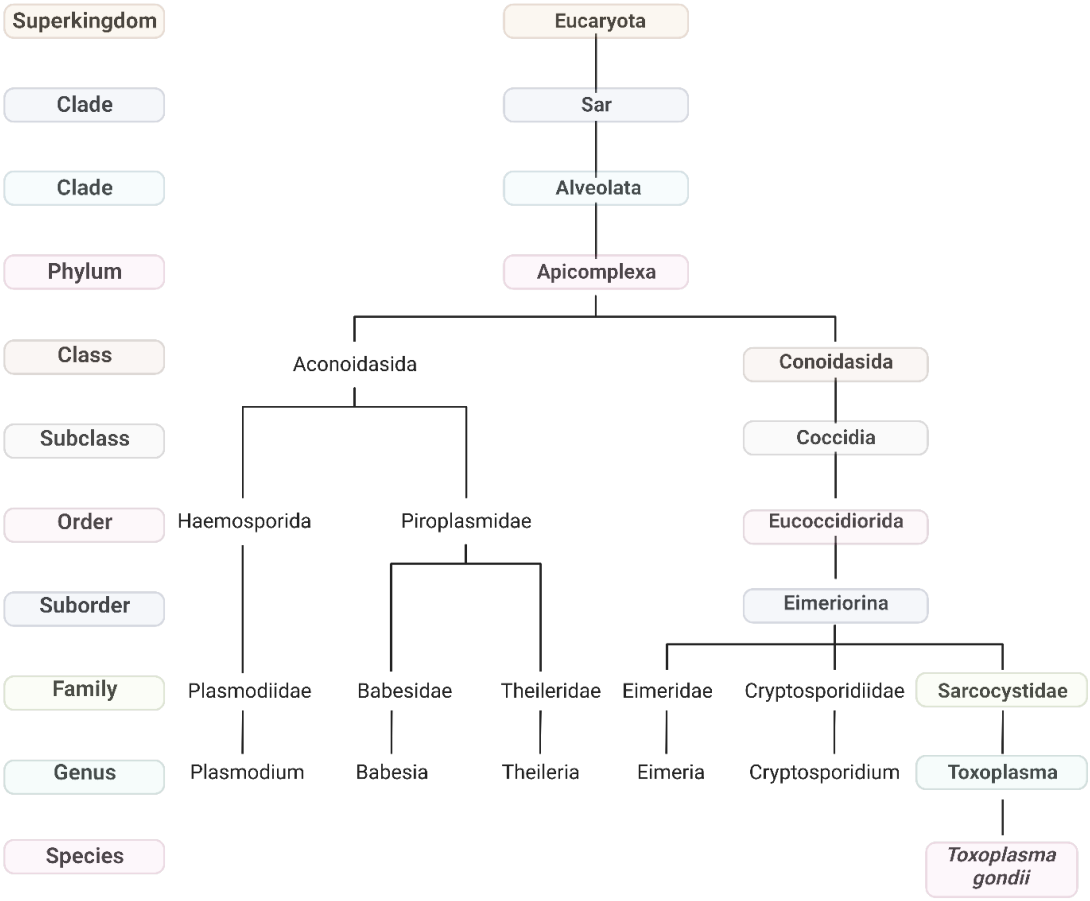

Figure 1: Classification of the phylum Apicomplexa

Phylogenetic tree of some of the clinical and veterinary relevant apicomplexan parasites according to NCBI taxonomy (Schoch et al., 2020). Taxonomy of *Toxoplasma gondii* is shown in bold and is coloured. Created with BioRender.com.

1.2 *Toxoplasma gondii*: History of the Etiologic Agent

T. gondii was identified and described for the first time in 1908 by Nicolle and Manceaux from the North-African rodent *Ctenodactylus gundi* (*C. gundi*) (Charles Nicolle, 1908), and concurrently, in Brazil in the same year, by Splendore from tissues of an infected rabbit (Splendore, 1908), both groups suspected that Toxoplasma is a protozoan belonging to the *Leishmania spp*. grouped into the *Euglenozoa* phylum. Realising that it was the discovery of a previously unknown organism, Nicolle and Manceaux proposed the name *Toxoplasma gondii,* referring to the morphology of the parasite (from Greek *toxon*: arc or bow, *plasma*: creature; and *gondii* resulting probably from a misspelling of the first identified host *C. gundi*) (C. Nicolle & Manceaux, 1909). After its discovery, several cases of *T. gondii* infections were reported in a variety of warm-blooded hosts, mainly bird species (J. Dubey, 2002).

In 1923, Janků probably documented the first human *T. gondii* infection in a eleven months old child in Prague affected by hydrocephalus (Janku, 1923) While Janků was unable to identify the causative agent of the infection, in 1939 Wolf *et al.* reported the first human isolate of *T. gondii,* establishing this parasite as a causative agent of the human disease toxoplasmosis (Wolf, Cowen, & Paige, 1939). Subsequently, numerous advancements were made for the comprehension and the elucidation of the disease in animals and humans (Frenkel & Jacobs, 1958; Hartley & Marshall, 1957). Remarkably, in 1948 Sabin *et al.* described the "Sabin-Feldman Dye-Test for Toxoplasmosis", a highly sensitive serological test for the detection and quantification of circulating Toxoplasma-specific antibodies in the serum of hosts upon infection (A. B. Sabin & Feldman, 1948). The realization of the first diagnostic test was an important epidemiological tool that enabled the revelation of the geographical dissemination and widespread occurrence of *T. gondii* infections in different warm-blooded hosts. There findings encouraged the investigation of the transmission routes of the parasite and the revelation of its life cycle (E. Innes, 2010). In 1995, Howe and Sibley described three clonal lineages of *T. gondii*, named types I, II, and III, which differ in virulence and their epidemiological prevalence pattern (D. K. Howe & L. D. Sibley, 1995; L. D. Sibley & Boothroyd, 1992). Type II has been identified as the most prevalent genotype for infections of humans (Chessa, Chisu, Porcu, & Masala, 2014; Howe, Honoré, Derouin, & Sibley, 1997; Mondragon, Howe, Dubey, & Sibley, 1998).

1.2.1 Life Cycle

In 1970, the life cycle of *T. gondii* was fully described when the two reproductive stages of the parasite were finally identified: the sexual stage that occurs exclusively in the members of

the family Felidae, that serve as definitive hosts; the asexual stage in intermediate hosts, occurring in a wide range of warm-blooded vertebrates, including humans (J. P. Dubey, Miller, & Frenkel, 1970) (**Figure 2**).

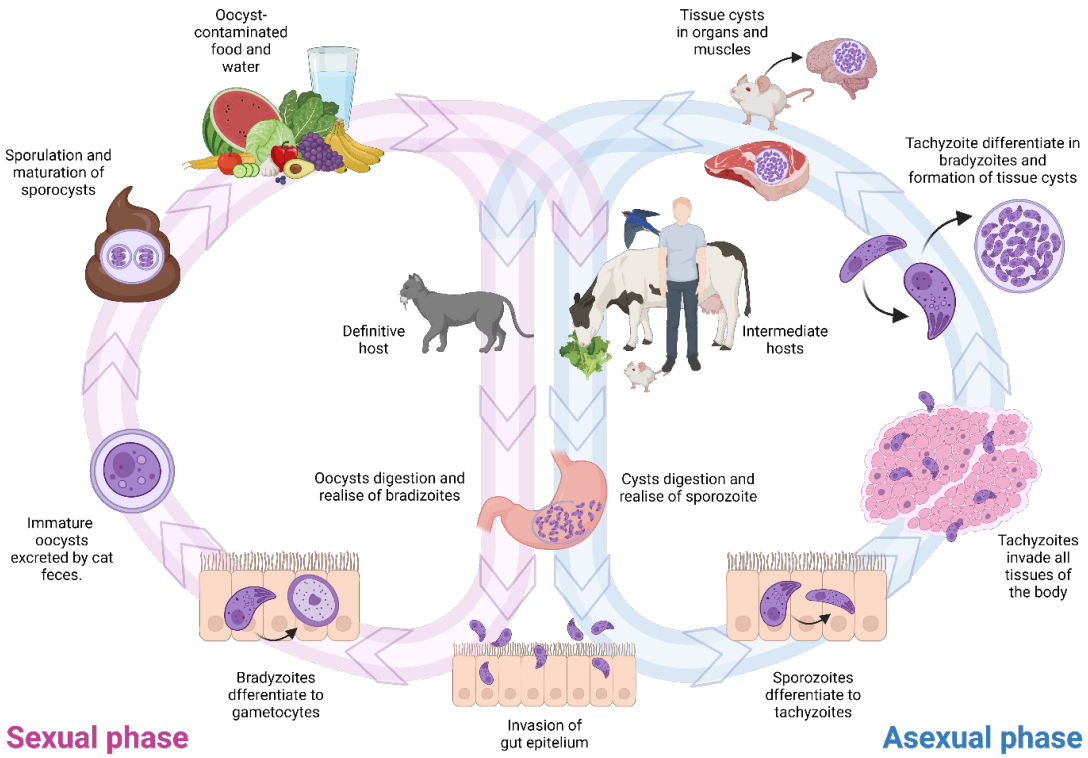

Figure 2: *T. gondii* life cycle

Biology, infection and replication of *T. gondii*. The sexual stage in the definite host is shown on the left, the asexual stage that occurs in the intermediate hosts in shown on the right. Modified from Farmhealthonline.com (Farmhealthonline.com). Created with BioRender.com.

The primary infection of felids can occur via the ingestion of tissue cysts within muscles or organs of infected animals, or the ingestion of the sporulated oocysts shed by another infected feline. Upon ingestion, the cysts or oocysts cell walls undergo digestion within the stomach, causing the release of sporozoite or bradyzoites that initiate to invade the felid gut epithelial cells (J. P. Dubey, Lindsay, & Speer, 1998). The latter are lacking the delta-6-desaturase activity leading to systemic excess of linoleic acid, responsible for the sexual reproduction of the parasite (Martorelli Di Genova, Wilson, Dubey, & Knoll, 2019). In the gut epithelium occur several schizogonic cycles, with the formation of 5 morphologically different schizonts, leading to the production of unsporulated and immature oocysts (zygotes) that are excreted by cat faeces. Outside of the cat, the oxygen-rich environment promotes sporulation, and following the maturation, sporocysts are then formed (J. P. Dubey

et al., 1970) (J. Dubey, 1998). The asexual stage commences with infection of intermediate hosts via ingestion of the highly infective oocyst, contained in food or water contaminated with cat faeces, or via the ingestion of tissue cysts contained in raw or undercooked meat. During the digestion, the breakdown of the oocysts or tissue cysts walls cause the release bradyzoites or sporozoites. The latter initiate the invasion of the epithelial cells, where happen then the conversion of sporozoites into tachyzoites, the fast-growing stage of the parasite that characterize the acute infection (J. P. Dubey et al., 1998; Harley G Sheffield & Melton, 1968). Tachyzoites undergo a lytic cycle, replicating by endodyogeny inside the parasitophorus vacuole (PV) established during host cells invasion. Afterwards, tachyzoites egress the host cell via a lytic process and continue the cycle through the invasion of novel host cells (Blader, Coleman, Chen, & Gubbels, 2015) (**Figure 3**). The spread of the parasite in all body tissues via the blood stream and lymphatic system is restricted by the activation of the immune system, triggering, after 10-14 days post-infection, the conversion of the actively-replicating tachyzoites into the slowly-replicating bradyzoites, encysted in tissue cysts throughout the body, responsible for the chronicity of the infection (Lyons, McLeod, & Roberts, 2002).

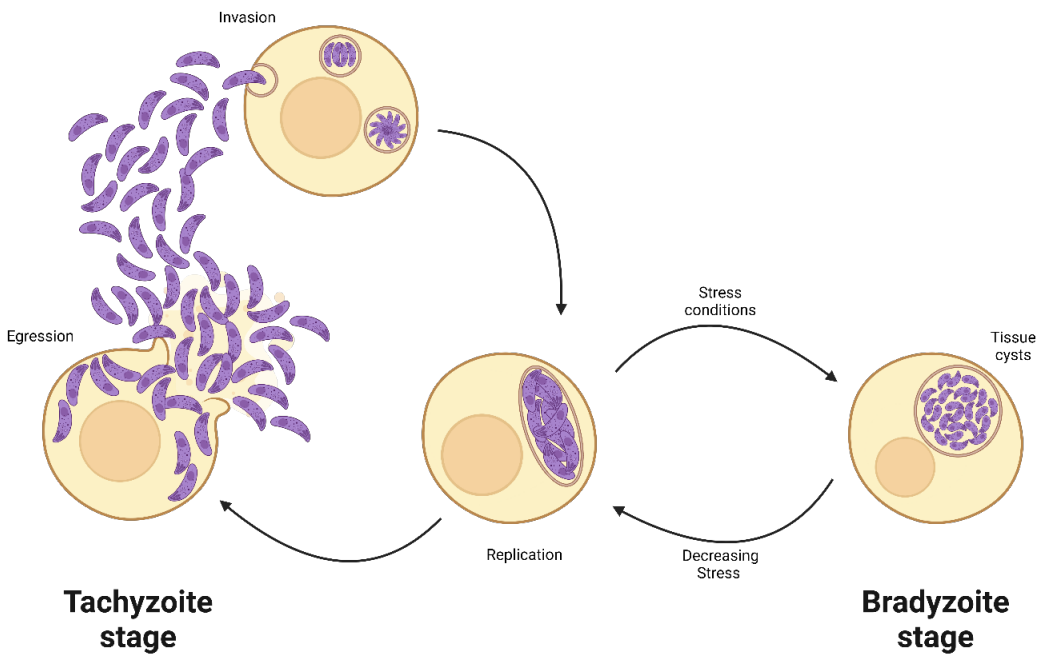

Figure 3: Lytic cycle and stage differentiation of *T. gondii*

Lytic cycle of *T. gondii* during the tachyzoite stage consists in the invasion, replication, and egression phases. Under stress conditions, tachyzoites convert into encysted bradyzoites. When the stress condition is decreasing,

bradyzoites convert into tachyzoites, starting the lytic cycle. Modified from Zhang *et al.* (M. Zhang, Joyce, Sullivan, & Nussenzweig, 2013). Created with BioRender.com.

1.3 Toxoplasmosis

T. gondii is the etiologic agent of toxoplasmosis, a zoonotic disease widely disseminated in humans and animals. Due to its worldwide distribution, *T. gondii* is referred as one of the most successful parasite, afflicting approximately a third of the global human population (Saadatnia & Golkar, 2012). According to the Centre for Disease Control and Prevention (CDC), approximately 11% of the U.S. population aged 6 years and older are seropositive to *T. gondii*, and in many countries characterized by hot and humid climate, it is estimated that the prevalence of the infection can reach more than 60% of the population (CDC, 2018).

1.3.1 Transmission to Humans

Infection of humans can occur via different routes: through the consumption of tissue cysts in contaminated raw meat; via ingestion of oocysts from the environment or contaminated food or water (as shown in **Figure 4**); congenitally, via mother-to-child transmission during pregnancy and rarely with blood transfusion and organ transplantation (Hill & Dubey, 2002)

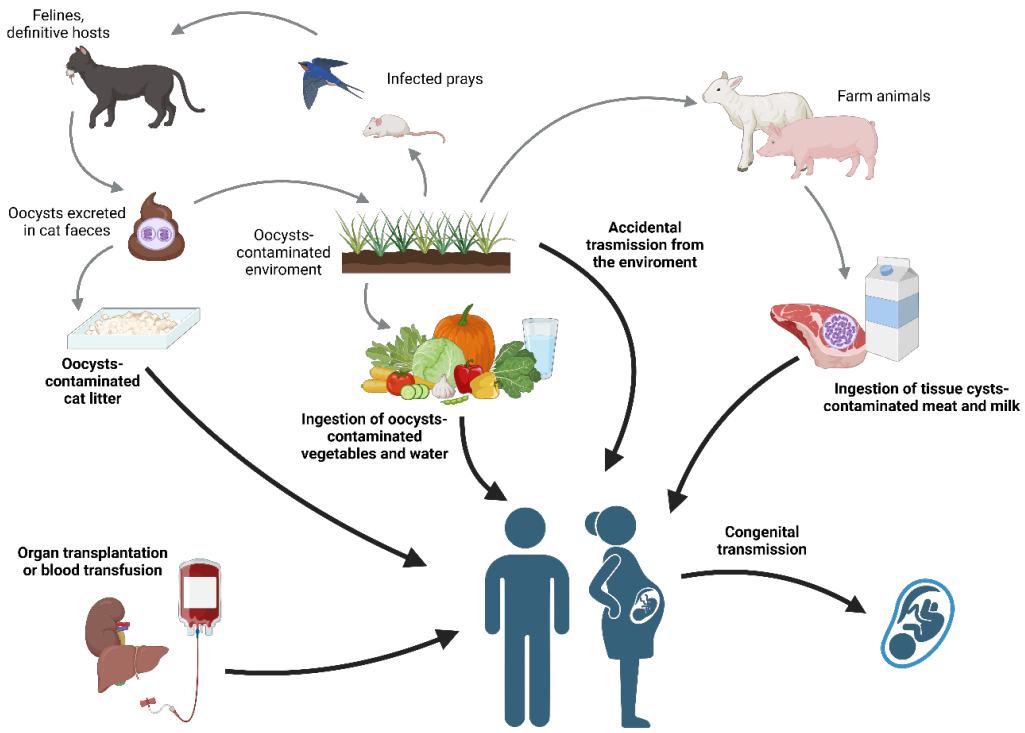

Figure 4: Transmission of *T. gondii* in humans

The various sources of foodborne and environmental contamination are shown. Modified from Deng *et al.* (Deng et al., 2021). Created with BioRender.com.

Tissue cysts, the cause of *T. gondii* foodborne transmission, are generally located in muscles and in the brain of infected livestock. After the consumption of undercooked contaminated meat, especially pork and lamb, walls of tissue cysts are subjected to digestion via the activity of proteolytic enzymes in the stomach, releasing bradyzoites (Al-Malki, 2021). The parasites have been demonstrated to be resistant to the proteolytic digestion in the gastric environment (Jacobs, Remington, & Melton, 1960), enabling the invasion of the host cells. The faecal *T. gondii* oocysts shed by felines in the environment represent a relevant health issue due their long viability and stability in the environment and their highly infectiousness to intermediate hosts (J. P. Dubey, 1996; Lélu et al., 2012). After sporulation, matured oocysts become a potential source of infection for humans, via the accidental ingestion of

contaminated vegetables and water or by inhalation from the environment (Torrey & Yolken, 2013). Additionally, the affliction of congenital transmission is very high (J. Dubey, Murata, Cerqueira-Cézar, Kwok, & Villena, 2021). Congenital infection can occur upon primary infection during pregnancy, with higher incidences during the third trimester of pregnancy, due to the higher permeability of the placenta during this phase, its protective role decrease, resulting an increased vulnerability to infection (Robert-Gangneux & Dardé, 2012).

Before pregnancy, the infection is generally low-risk for the foetus. The transmission of the infection occur only with some rare cases (Vogel et al., 1996). However, the precise mechanism how the congenital infection of *T. gondii* through the placenta can occur remains uncompletely understood (Bollani et al., 2022).

Other instances of *T. gondii* transmissions are solid organ transplantations, in which the transplant recipients can be affected by two different ways: transmission of the infection from a seropositive donor to a seronegative recipient, and the reactivation of a latent infection due to immune suppression after transplantation (Sumeeta Khurana & Nitya Batra, 2016). Additionally, infection can occur rarely via blood transfusion (Stopić et al., 2022).

1.3.2 Clinical Manifestations of Toxoplasmosis

From a clinical perspective, *T. gondii* infection can be unnoticed or can manifest by a various spectrum of symptoms, depending on the immune status of the host, characterized by: immunocompetent status: mainly asymptomatic and in seldom instances symptomatic; immunocompromised conditions and congenital toxoplasmosis: symptomatic (J. G. Montoya & Liesenfeld, 2004) (**Figure 5**).

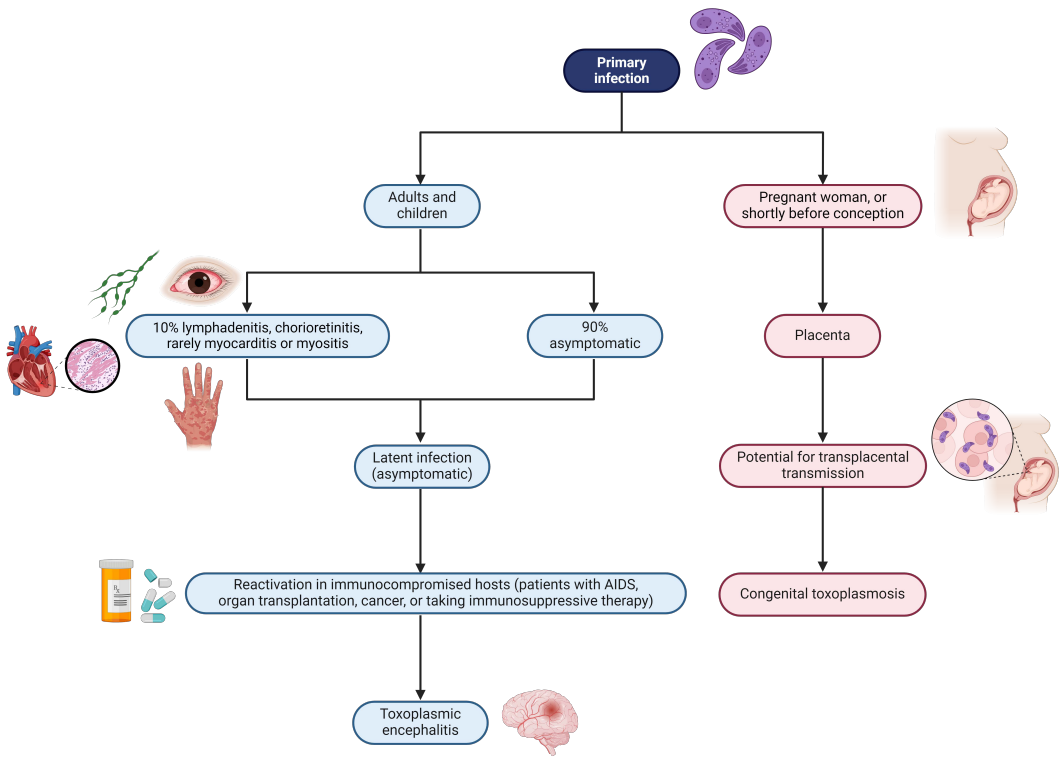

Figure 5: Clinical manifestation of toxoplasmosis in humans

Modified from Montoya *et al.* (J. G. Montoya & Liesenfeld, 2004). Created with BioRender.com.

In immunocompetent adults and children, the course of the primary infection with *T. gondii* is usually asymptomatic. In North America, symptomatic toxoplasmosis has been observed in approximately 10 to 20% of cases (J. S. Remington, 1974). This rate could be higher in certain geographic areas where the burden and the prevalence of the infection is superior, such as Brazil (Jones et al., 2006; Prestes-Carneiro et al., 2013; Strang et al., 2020). When the clinical course of acute infection is symptomatic, the major manifestations are flu-like symptoms that rarely require treatments, and asymptomatic isolated cervical lymphadenopathy. Rarely, more severe clinical manifestations can develop, including myocarditis, myositis and choriorenitis (José G. Montoya, Boothroyd, & Kovacs, 2015). The latter, has been reported as the consequence of the reoccurrence of the congenital infection or of acquired infection (Park & Nam, 2013), causing retinal lesions and vitreous inflammation (Holland, 2004). *T. gondii* parasite can be grouped into three major genotypes known as I, II and III, as well as distinct lineages commonly recognized as "exotic or atypical genotypes", which diverge significantly from the major three (Daniel K. Howe & L. David Sibley, 1995; L. David Sibley, Khan, Ajioka, & Rosenthal, 2009). However, the *T. gondii* type II strains are the most commonly associated with human toxoplasmosis (Howe et al., 1997).

In contrast with the favourable course of the disease in immunocompetent individuals, in immune-deficient patients lacking a proper cellular immunity, due to hematologic malignancies, cytotoxic anticancer regimen, immunosuppressive therapy for organ transplants or Acquired Immunodeficiency Syndrome (AIDS), toxoplasmosis can pose a life-threatening risk, usually due the reactivation of a latent infection (Ali, Abd El Wahab, Hamdy, & Hassan, 2019; S. Khurana & N. Batra, 2016; B. J. Luft & Chua, 2000; Pagano et al., 2004). For these patients, toxoplasmic encephalitis is the most common clinical manifestation, exhibiting a wide spectrum of signs and symptoms contingent upon the status of the infection, ranging from subacute signs to an acute confusion state, with severe neurological deficits which may rapidly devolve to severe outcomes, including hemiplegia, visual defects, psychosis, lethargy and coma up to lethality (Benjamin J. Luft & Remington, 1992).
As in immunocompetent individuals, primary infection in pregnant women is usually asymptomatic, but infection can be a potential risk for vertical transmission from mother to foetus, especially upon primary infection during pregnancy or, rarely, due to the reactivation of a chronic *T. gondii* infection in an immunodeficient pregnant mother (Goldstein, Montoya, & Remington, 2008). The frequency of the congenital transmission and the severity of the illness are dependent on which trimester of gestation the infection is acquired by the mother: the risk of vertical transmission in highest during the third trimester and the severity of illness is worst for the foetus if the infection is acquired during the first trimester (Jack S Remington & Klein, 2001). The clinical manifestations for the new born include jaundice, blindness, chorioretinitis, ventriculomegaly, hydrocephalus, intracranial calcifications, macrocephaly, microcephaly, seizure epilepsy, anaemia, encephalitis, and mental retardation (Jack S Remington, Wilson, Nizet, Klein, & Maldonado, 2010). Also, miscarriages / foetal death have been reported (Maldonado & Read, 2017).

1.3.3 Treatment of Toxoplasmosis

In 1942, the report of Sabin and Warren on the effectiveness of sulfonamides against experimental murine toxoplasmosis, acting as competitive inhibitors of the enzyme dihydropteroate synthase (DHPS) in the folate biosynthetic pathway, marked the beginning of anti-toxoplasma drug discovery (Henry, 1943; Albert B. Sabin & Warren, 1942). From that time onward, the effectiveness of other molecules on *in vitro* and *in vivo* models have been reported. Pyrimethamine, a synthetic diaminopyridine that inhibits the enzyme dihydrofolate reductase (DHFR) in the folate metabolic pathway (Hitchings, Falco, Vanderwerff, Russell, & Elion, 1952) and overall the parasite nuclear DNA replication

(McCabe & Oster, 1989), was reported to be effective against toxoplasmosis in mice in 1952 (Eyles & Coleman, 1952). Subsequently, Eyles and Coleman reported the synergistic effect of the combination treatment of pyrimethamine and sulfadiazine (PYR – SDZ). 70 years after, the regimen PYR – SDZ, targeting synergistically different steps in the folate synthetic pathway of the tachyzoite stage (H. G. Sheffield & Melton, 1975), still remains the gold-standard in treating human toxoplasmosis, which is administered in combination with folinic acid to prevent bone marrow suppression (Akira, 2000; Dunay, Gajurel, Dhakal, Liesenfeld, & Montoya, 2018; Y. Zhang, Li, Lu, & Zheng, 2022). Lately, other antifolate regimens were investigated, such us Trimethoprim (TMP) and sulfamethoxazole (SMZ) (Grossman & Remington, 1979) that are currently used in combination as an alternative treatment when the main regimen PYR – SDZ is not available (Hernandez et al., 2017) (**Figure 6**).

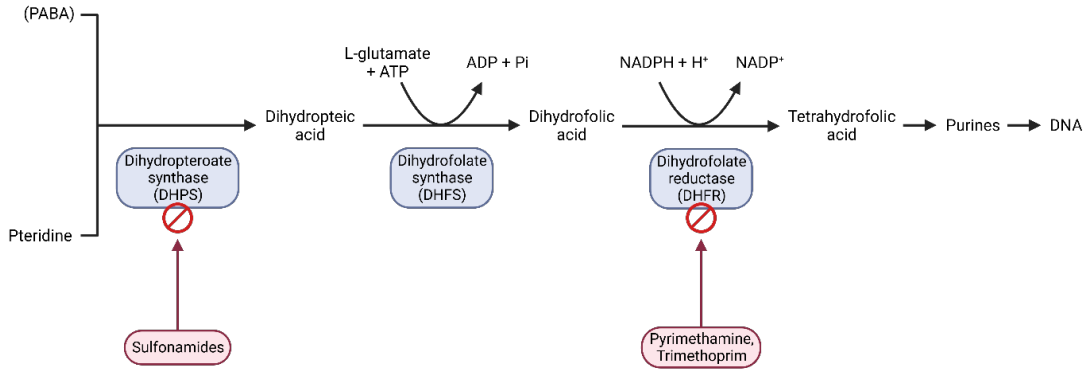

Figure 6: Mechanism of the action of antifolates

Modified from Cowell *et al.* (Cowell & Winzeler, 2019). Created with BioRender.com.

The anti-toxoplasma effectiveness of the macrolide spiramycin was first reported by Garin and Eyles in 1958 (Garin & Eyles, 1958). Following that discovery, several other macrolides have been found to exert an anti-toxoplasma activity, such as roxithromycin, azithromycin (F. Araujo, Shepard, & Remington, 1991; Chang & Pechère, 1988). For their mode-of-action an inhibitory activity of protein synthesis targeting the *T. gondii* apicoplast has been proposed (Beckers et al., 1995). Spiramycin is currently widely employed for prophylaxis and treatment of toxoplasmosis in pregnant women, due to its minimal side-effects and its inability to cross the placenta barrier. This makes it an ideal choice for the prevention of congenital infection, but ineffective when dealing with an already established foetal infection (Goldstein et al., 2008; Robert-Gangneux et al., 2011). In the early 1990s another noteworthy breakthrough emerged with the discovery of the anti-toxoplasma efficacy of atovaquone (F. G. Araujo, Huskinson, & Remington, 1991; Kovacs & AIDS, 1992), a naphthoquinone able to impact

the energy metabolism of the parasite acting as an inhibitor of the mitochondrial transport by targeting the cytochrome bc1 complex (Papich, 2016). Nowadays, together with clindamycin and azithromycin, it is widely used as alternative therapy for patients who are intolerant and allergic to sulfonamides regimens (Holmes, Kaplan, & Masur, 2002; Shiojiri, Kinai, Teruya, Kikuchi, & Oka, 2019) (**Figure 7**).

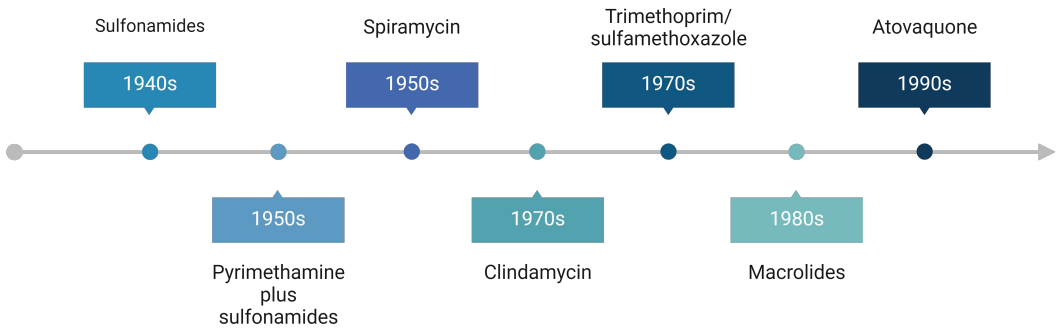

Figure 7: Discovery timeline of anti-toxoplasma medications currently in clinical use

Modified from Dunay *et al.* (Dunay et al., 2018). Created with BioRender.com

1.3.4 Limits and Challenges of Anti-Toxoplasma Drugs

According to the CDC, toxoplasmosis is referred to as a neglected parasitic infection in the USA (Jones, Parise, & Fiore, 2014; Scallan et al., 2011). The absence of market-driven interest by pharmaceutical industry in investing in novel and innovative anti-toxoplasma therapeutic entities has resulted in a deficiency of drug research and development (Trouiller et al., 2002). Thus, the approved anti-toxoplasma regimens still remain limited (Dunay et al., 2018), and are mostly acting as inhibitors against dihydrofolate reductase, NADH dehydrogenases, cysteine proteases and dihydropteroate synthase (Kortagere, 2012). Anti-toxoplasma drug discovery has been mostly based on repurposing of existing anti-Apicomplexan drugs, especially antimalarial ones (Secrieru, Costa, O'Neill, & Cristiano, 2020). Therefore, besides to be not exclusively used for *T. gondii* infection, over time current regimens are facing a reduced efficacy due the arising of parasite resistances against anti-infective drugs (Montazeri et al., 2018; Mzabi, Aubert, & Villena, 2017). Moreover, current treatment options are exclusively targeting the tachyzoite stage of the parasite, responsible for the acute infection. However, these treatments are unable to eradicate the tissue cysts harbouring bradyzoites, responsible for the development of the chronic infections (R McLeod, Van Tubbergen, Montoya, & Petersen, 2014). The main target of anti-toxoplasma drugs is the folate

biosynthetic pathway involved in DNA synthesis, particularly acting as inhibitors of the parasite DHFR and DHPS enzymes. Pyrimethamine, inhibitor of the DHFR enzyme, demonstrates lack of specificity on discerning between the parasite and host enzymes (Konstantinovic, Guegan, Stäjner, Belaz, & Robert-Gangneux, 2019), inducing severe side effects mainly related with the inhibition of the folate pathway in highly metabolic active tissue, such as bone marrow (Khan Assir, Ahmad, Akram, Yusuf, & Kamran, 2014), including bone marrow suppression, thrombocytopenia, diarrhoea, nausea, vomiting, cutaneous rush, and Steven–Johnson syndrome among others which may be even fatal (Ben-Harari, Goodwin, & Casoy, 2017; Rima McLeod et al., 2006). Significant adverse effect have been shown also in the other approved anti-toxoplasma medicaments (Shammaa, Powell, & Benmerzouga, 2021). As a consequence, the high level of toxicity leads to the lack of patient compliance, discontinuation of therapy and, as a drawback, extension of the drug administration (Konstantinovic et al., 2019). Thus, there is an urgent need to develop novel well-tolerated therapies that, in addition, are effective in acute, chronic and latent stages of the parasitic disease. Regrettably, a multitude of challenges hinder the discovery of novel anti-toxoplasma entities with such an idealistic profile, especially the effectiveness in bradyzoites, with their biology nowadays being mostly unclear. Enhancing the knowledge of the essential metabolic pathways of the bradyzoite stage and the identification of druggable targets could significantly improve the research in this field (Alday & Doggett, 2017). Moreover, *T. gondii* is able to cross the blood – brain barrier, leading to the invasion of brain tissue and to the conversion into encysted bradyzoites in the Central Nervous System (CNS) (Feustel, Meissner, & Liesenfeld, 2012) into which the available treatments are not able to penetrate (J. G. Montoya & Liesenfeld, 2004). Thus, the pharmacokinetic aspects of novel drugs must also be highly considered.

1.4 Natural Products and Derivatives in Drug Discovery

Natural products (NPs) have played a pivotal role in the history of drug discovery and have contributed to the development of modern drugs, especially in the field of cancer and infectious diseases, and nowadays they still maintain their crucial importance (Cragg, Newman, & Snader, 1997; Fernandes, da Silva Figueiredo, Monteiro, & Monteiro-Neto, 2023).

In 1928, Alexander Fleming's discovery of penicillin from *Penicillium notatum* initiated the 'golden era' of antibiotics, which peaked in the mid-1950s (Conly & Johnston, 2005). During this relatively short period, several classes of NPs antibiotics were discovered that are still in clinical use, such as ß-lactams, aminoglycosides and tetracyclines (Davies, 2006). Penicillins

are bactericidal agents that inhibit the synthesis of the cell wall consisting of a 6-aminopenicillanic acid core with a side chain attached via an amide bond, which identifies each penicillin (Miller, 2002). After Fleming's discovery, other natural products consisting of a four-member β-lactam ring were discovered, such as cephalosporin from *Cephalosporium spp.*, cephamycin and clavam from *Streptomyces spp.* and carbapenems and monocyclic β-lactams from actinomycetes (Demain & Elander, 1999).

Streptomycin, isolated in 1943 from *Streptomyces griseus*, was the first discovered aminoglycoside and the first clinical treatment for tuberculosis introduced in 1940 (Schatz, Bugle, & Waksman, 1944). This class of antibiotics is characterised by amino-modified sugars bound to an aminocyclitol nucleus, which exert their broad-spectrum bactericidal action through their irreversible binding to the 30s ribosomal subunit, inhibiting protein synthesis in the microorganism (Becker & Cooper, 2013).

Tetracyclines were discovered with the isolation of aureomycin from actinomycetes soil bacteria (Duggar, 1948) They are a class of inhibitors of bacterial protein synthesis, which act by inhibiting protein translation through their binding to the ribosomal subunit 30s and preventing the aminoacyl-tRNA from associating with the A-side of the bacterial ribosome (Chopra & Roberts, 2001).

Unfortunately, the high discovery of new antibiotic NPs in a short period of time has led to the overuse of these drugs, causing the rise of antimicrobial resistance (AMR) (Davies, 2006; Hutchings, Truman, & Wilkinson, 2019).

NPs are typically characterized by high molecular mass, high molecular rigidity and favourable physicochemical proprieties (Atanasov et al., 2021). Together with their vast array of scaffold diversity and their wide range of bioactivities, they are high value for the drug design and development (Atanas G Atanasov et al., 2015; Lachance, Wetzel, Kumar, & Waldmann, 2012) However, alongside the opportunities offered by their unique characteristics, several challenges have limited their use in drug discovery, such as the accessibility of the source of NPs, the complexity of their extraction and isolation processes and the incompatibility with high-throughput screening (HTS). These limitations have gradually reduced interest in natural product-based drug discovery, shifting the focus to synthetic molecule libraries (SMLs) and HTS (Atanas G. Atanasov et al., 2015). However, due to the lack of diversity, SMLs have only made limited contributions to the identification of novel bioactive scaffolds(Chan, Holmes, & Payne, 2004). Thus, with the AMR that are increasing worldwide (Smith & Coast, 2002), the urgent need for novel classes of antibiotics have renewed the interest in NPs as a source of new drug leads. The registration of

fidaxomicin, retapamulin, and daptomycin highlighted the re-emergence of NPs (Thaker, Waglechner, & Wright, 2014). Moreover, NPs could serve as starting materials for the design and the synthesis of semisynthetic NPs and total synthetic NPs derivatives, characterized by higher biological efficacy and improved pharmacokinetic and pharmacodynamic proprieties (da Rosa, Schenkel, & Campos Bernardes, 2020; Majhi & Das, 2021; Molinari, 2009). Several studies have demonstrated the invaluable potential and pivotal role of NPs in the research for potential anti-parasitic, including *T. gondii*, due to lower side-effects and higher availability (Adeyemi, Sugi, Han, & Kato, 2018; Harvey, Edrada-Ebel, & Quinn, 2015; Sharif et al., 2016). Actinobacteria and fungi have previously been the main producers of commercially important bioactive NPs (Conrado, Gomes, Roque, & De Souza, 2022; Genilloud, 2017). The main classes of antibiotics produced from actinomycetes include ß-lactams, aminoglycosides, lipopeptides, glycopeptides, asamycins, anthracyclines, nucleosides, peptides, polyenes, polyethers, tetracyclines and macrolides (Selim, Abdelhamid, & Mohamed, 2021). Current research suggests that these microorganisms, especially from the genus *Streptomyces*, and endophytic fungi continue to provide novel bioactive metabolites with unique chemical skeletons, such as alkaloids, coumarins, sesquiterpenoids, cytochalasins, tetracenediones, lactones, quinones, quinolones, xanthones that could be useful in preventing the growing AMR (Deshmukh et al., 2022; Donald et al., 2022; Igarashi, 2019; Jakubiec-Krzesniak, Rajnisz-Mateusiak, Guspiel, Ziemska, & Solecka, 2018).

In recent years, a variety of natural extracts of plants have shown inhibitory effects of *T. gondii* (Benoit-Vical, Santillana-Hayat, Kone-Bamba, Mallie, & Derouin, 2000), such as the sesquiterpene lactone artemisinin from the antimalarial plant *Artemisia annua* (Holfels, McAuley, Mack, Milhous, & McLeod, 1994), and its derivatives (D'Angelo, Bordon, Posner, Yolken, & Jones-Brando, 2009), indicating the high potential of NPs in anti-toxoplasma drug discovery.

2 Aim of the Thesis

Toxoplasmosis is a zoonotic disease widely distributed worldwide caused by the apicomplexan parasite *T. gondii* (Amouei et al., 2020). In Europe, *T. gondii* has been ranked as the second most important food-borne parasite in terms of public health, geographical distribution and economic impact (Bouwknegt, Devleesschauwer, Graham, Robertson, & van der Giessen, 2018). Toxoplasmosis is a serious burden for immunocompromised individuals and congenitally infected foetuses, causing severe and even fatal illness (J. Dubey et al., 2021; Machala et al., 2015). Even with enormous progress achieved toward understanding the biology of *T. gondii*, toxoplasmosis is still been considered a neglected parasitic disease, resulting in limited research in the realm of drug research and development, only leading to the approval of a limited number of anti-toxoplasma drugs (Boothroyd, 2009; Dunay et al., 2018; E. A. Innes, Hamilton, Garcia, Chryssafidis, & Smith, 2019; Trouiller et al., 2002). The most common treatment against acute toxoplasmosis is the combination of PYR – SLZ plus folinic acid. This and the other available regimens are associated with severe side effects, and additionally, no one is active against the chronic stage of the parasite. Thus, novel drug candidates are urgently needed for the development of novel, potent and safer anti-toxoplasma drugs (Antczak, Dzitko, & Długońska, 2016). In the history of drug discovery, nature has played a pivotal role as an inexhaustible source of novel and diverse bioactive NPs, serving as leads for the development of anti-infective drugs (Cragg et al., 1997; Shivaprasad, Sirisha Mulukuri, Chandrasekar, Baheti, & Pawar, 2023)

The aim of this thesis is the investigation of selected classes of NPs from natural sources, semisynthetic or total synthetic derivatives of NPs and synthetic molecules inspired from NP scaffolds for their potential as anti-toxoplasma agents. This process involves a comprehensive screening approach of various small molecule mini-libraries through *in vitro* evaluation to assess their effectiveness against *T. gondii*. Furthermore, it involves the assessment of the selectivity and the potential cytotoxic effects of these molecules on host cells. Following the initial screening step, the focus should shift to optimization of substances and towards conducting detailed structure-activity relationship (SAR) studies, aimed to identify the essential chemical features and structural characteristic of the investigated molecules that are crucial for their anti-toxoplasma bioactivity, and for the selection of lead compounds. This step is essential for the drug optimisation process, and should be conducted in collaboration with partner chemical research groups. The subsequent selected lead compounds are supposed to be investigated with the aim of the identification of the

toxoplasma targets and the characterisation of their mode-of-action, followed by the validation of the target *in vitro*. This purpose involves a multidisciplinary approach through biological end biochemical techniques and methodologies. Thus, this thesis aims to identify novel anti-Toxoplasma leads and to be the basis for further *in vivo* studies and *in vivo* investigation in the field of drug development against infectious diseases.

3 Publications

Mazzone, F., Simons, V. E., van Geelen, L., Frank, M., Mándi, A., Kurtán, T., Pfeffer, K., & Kalscheuer, R. (2022). In Vitro Biological Activity of Natural Products from the Endophytic Fungus *Paraboeremia selaginellae* against *Toxoplasma gondii*. *Antibiotics (Basel, Switzerland)*, *11*(9), 1176.

Merkt, F.K., **Mazzone, F.**, Sazzadeh, S.S., Bonda, L., Hinz, L.K., Gruber, I., Buchholz, K., Janiak, C., Pfeffer, K., & Müller, T.J. (2021). Fluorescent Indolo[3,2-*a*]phenazines against *Toxoplasma gondii*: Concise Synthesis by Gold-Catalyzed Cycloisomerization with 1,2-Silyl Migration and ipso-Iodination Suzuki Sequence. *Chemistry* (Weinheim an Der Bergstrasse, Germany), 27, 9774 - 9781.

Klischan, M.K.T., **Mazzone, F.**, Berning, L., Greb, J., Schlamkow, M., Haase, M., Frey, W., Stork, B., Pfeffer, K., Pietruszka, J. (2023). Modular Approach for the Synthesis and Bioactivity Profiling of 8,8'-Biflavones. *ACS Omega*, 8(44), 41816-41834.

Mazzone, F., Klischan, M.K.T., Greb, J., Smits, S.H.J., Pietruszka, J. & Pfeffer, K. Synthesis and *In Vitro* Evaluation of Bichalcones as Novel Anti-Toxoplasma Agents. (Manuscript to be submitted).

Mazzone, F., Hoeppner, A., Reiners, J., Abdullaziz, M.A., Gottstein, J., Wesemann, M., Kurz, T., Smits, S.H.J. & Pfeffer, K. 1-deoxy-d-xylulose 5-phosphate reductoisomerase (DXR) as target for anti *Toxoplasma gondii* agents: crystal structure, biochemical characterization and *in vitro* biological evaluation of fosmidomycin and reverse analogues as potent inhibitors. (Manuscript to be submitted).

In addition, the following manuscript has arisen from the present thesis.

Abdullaziz M.A., Takada S., Illarionov B., Pessanha de Carvalho L., Sakamoto Y., Höfmann S., Knak T., Kiffe-Delf A.L., **Mazzone F**., Pfeffer K, Kalscheuer R, Bacher A., Held J., Fischer M., Tanaka N., and Kurz T. Reverse *N*-substituted hydroxamic acid derivatives of fosmidomycin target a previously unknown sub-pocket of 1-deoxy-D-xylulose 5-phosphate reductoisomerase (DXR). (Manuscript submitted)

3.1 *In Vitro* Biological Activity of Natural Products from the Endophytic Fungus *Paraboeremia selaginellae* against *Toxoplasma gondii*

Authors

Flaminia Mazzone*, Viktor E. Simons*, Lasse van Geelen, Marian Frank, Attila Mándi, Tibor Kurtán, Klaus Pfeffer, Rainer Kalscheuer.

*These authors contributed equally to this work

Published in

MDPI Antibiotics

Impact factor

4.8 (2022)

DOI

10.3390/antibiotics11091176

Own contributions to this work

Overall: 50%

Conducted all of the following experiments:

- *Toxoplasma gondii* proliferation assays
- Cytotoxicity assays (MTT assays) in human fibroblasts Hs27

Other major contributions

Design of experiments, methodology, conduction of experiments, data analysis, manuscript preparation.

antibiotics

MDPI

Article

In Vitro Biological Activity of Natural Products from the Endophytic Fungus *Paraboeremia selaginellae* against *Toxoplasma gondii*

Flaminia Mazzone [1,†], Viktor E. Simons [2,†], Lasse van Geelen [2], Marian Frank [2], Attila Mándi [3], Tibor Kurtán [3], Klaus Pfeffer [1,*] and Rainer Kalscheuer [2,*]

1 Institute of Medical Microbiology and Hospital Hygiene, Heinrich Heine University, 40225 Duesseldorf, Germany
2 Institute of Pharmaceutical Biology and Biotechnology, Heinrich Heine University, 40225 Duesseldorf, Germany
3 Department of Organic Chemistry, University of Debrecen, 4002 Debrecen, Hungary
* Correspondence: klaus.pfeffer@hhu.de (K.P.); rainer.kalscheuer@hhu.de (R.K.); Tel.: +49-211-8112459 (K.P.); +49-211-8114180 (R.K.)
† These authors contributed equally to this work.

Abstract: *Toxoplasma gondii* is an apicomplexan pathogen able to infect a wide range of warm-blooded animals, including humans, leading to toxoplasmosis. Current treatments for toxoplasmosis are associated with severe side-effects and a lack efficacy to eradicate chronic infection. Thus, there is an urgent need for developing novel, highly efficient agents against toxoplasmosis with low toxicity. For decades, natural products have been a useful source of novel bioactive compounds for the treatment of infectious pathogens. In the present study, we isolated eight natural products from the crude extract of the endophytic fungus *Paraboeremia selaginellae* obtained from the leaves of the plant *Philodendron monstera*. The natural products were tested for inhibiting *Toxoplasma gondii* proliferation, and their cytotoxicity was evaluated in different human cell lines. Six natural products showed antitoxoplasma activity with low or no cytotoxicity in human cell lines. Together, these findings indicate that biphenyl ethers, bioxanthracenes, and 5*S*,6*S*-phomalactone from *P. selaginellae* are potential candidates for novel anti-toxoplasma drugs.

Keywords: *Toxoplasma gondii*; *Paraboeremia selaginellae*; endophytic fungi; natural products; bioactivity; biphenyl ether; bioxanthracene; phomalactone

check for updates

Citation: Mazzone, F.; Simons, V.E.; van Geelen, L.; Frank, M.; Mándi, A.; Kurtán, T.; Pfeffer, K.; Kalscheuer, R. In Vitro Biological Activity of Natural Products from the Endophytic Fungus *Paraboeremia selaginellae* against *Toxoplasma gondii*. *Antibiotics* **2022**, *11*, 1176. https://doi.org/10.3390/antibiotics11091176

Academic Editors: Valério Monteiro-Neto and Elizabeth S. Fernandes

Received: 12 August 2022
Accepted: 29 August 2022
Published: 31 August 2022

Publisher's Note: MDPI stays neutral with regard to jurisdictional claims in published maps and institutional affiliations.

Copyright: © 2022 by the authors. Licensee MDPI, Basel, Switzerland. This article is an open access article distributed under the terms and conditions of the Creative Commons Attribution (CC BY) license (https://creativecommons.org/licenses/by/4.0/).

1. Introduction

Toxoplasma gondii is an obligate intracellular protozoan parasite member of the phylum Apicomplexa, which includes known human pathogens such as *Plasmodium* sp., *Eimeria* sp., *Neospora*, *Babesia*, *Theileria*, and *Cryptosporidium* spp., with which it shares significant biological similarities [1]. Beyond these organisms, the study of *T. gondii* has experimental advantages since its basic biology and the methodology for the genetic manipulation and quantification of its different stages are well established. Thus, *T. gondii* is considered a major model for the study of apicomplexan biology and for anti-apicomplexan drug target validation [2]. *T. gondii* infections are among the most common human zoonoses, leading to toxoplasmosis disease [3]. *T. gondii* is considered one of the world's most successful parasites due its ability to infect a wide range of warm-blooded vertebrate intermediate hosts [4]. *T. gondii* is estimated to chronically infect one-third of the world's human population and is acquired mainly through two ways: by ingesting oocysts shed from feline hosts (the definitive hosts) in contaminated food or water and by the consumption of raw or undercooked meat containing viable tissue cysts [5]. Waterborne and food-borne outbreaks of toxoplasmosis have been reported from countries with diverse cultural, social,

and ethnic backgrounds [6]. In immunocompetent individuals, infection with *T. gondii* is usually asymptomatic or has a subclinical course with mild symptoms. In contrast, immunocompromised (i.e., acquired immune deficiency syndrome (AIDS), organ transplant or cancer) patients can develop the disease, leading to life-threatening cerebral and ocular toxoplasmosis due to a reactivation of the latent infection. Additionally, primary infection in pregnant women may result in fetal death, spontaneous abortion, and birth defects [7–9]. Although many gaps have been filled in the epidemiological, diagnostic, and biological fields to understand of the interaction of the parasite with the host, little progress has been made in drug discovery for the treatment of toxoplasmosis.

Current treatments of acute toxoplasmosis are largely limited to anti-folate therapy. Pyrimethamine and sulfadiazine, the current gold-standards for the treatment of toxoplasmosis, can suppress the parasite growth in the active stage of the infection by targeting the tachyzoite stage, but they have no effect in the bradyzoites stage. Additionally, they have been found to have high rates of toxic side effects, leading to discontinuation of therapy. Thus, there is an urgent need to identify novel potent candidates that would be well-tolerated to eradicate latency as well as to treat the acute infection [10,11]. Natural products profoundly impact the history of drug discovery, especially in the research of novel anti-cancer, anti-bacterial, and anti-parasitic treatments. Nature continues to provide diverse and unique chemical sources of bioactive lead compounds that inspire novel drug discoveries [12]. The antiparasitic bioactivity of natural products from various sources, especially plant-derived secondary metabolites, has been deeply investigated in in vitro and in vivo studies [13]. Many fungal metabolites have also been reported to exhibit antimicrobial properties against parasitic pathogens. However, most of these studies focused on bioactivity against *Plasmodium falciparum*, whereas there is a scarcity of investigations to explore the potential of fungi as a source of novel anti-toxoplasma agents [14].

In this study, we extracted and purified eight natural products from the crude extract of *Paraboeremia selaginellae*, an endophytic fungus isolated from the ornamental plant *Philodendron monstera*. Isolated compounds were structurally characterized and evaluated for their anti-toxoplasma activities. Biphenyl ethers, bioxanthracenes, and phomalactone showed substantial activity against *T. gondii* proliferation. Therefore, we suggest these compounds as promising candidates for novel anti-parasitic therapies.

2. Results

2.1. Isolation of Compounds from Paraboeremia selaginella

We isolated an endophytic fungus from fresh surface-sterilized leaves of the ornamental plant *Philodendron monstera*. The isolated strain was identified as *Paraboeremia selaginella* by the internal transcribed spacer (ITS) sequence with 99.56% identity in comparison with the ITS database of the National Center for Biotechnology Information. From the crude extract of a culture of *Paraboeremia selaginella* grown on solid rice medium, eight compounds were isolated by chromatographic methods and structurally elucidated by complementary spectroscopic analyses (Figure 1). All eight compounds have previously been reported from other sources but are reported here for the first time as natural products occurring in the genus *Paraboeremia*.

Different stereoisomers of phomalactone (**F**) were isolated and reported previously from various sources [15–18], and some papers did not specify the absolute configuration [19,20], while others assigned the (5*R*,6*R*) absolute configuration to the large positive specific rotation [21], which was opposite to previous studies [15–18,22]. In order to determine the absolute configuration of phomalactone independently and unambiguously, we performed TDDFT-ECD, TDDFT-OR, and DFT-VCD studies, which consistently confirmed the (+)-*cis*-(5*S*,6*S*) absolute configuration (see Supplementary Materials) [23,24]. Comparisons of the experimental and computed VCD spectra of *cis*-(5*S*,6*S*) are shown in Figure 2, which produced good agreement. Other computational results are shown in the Supplementary Materials.

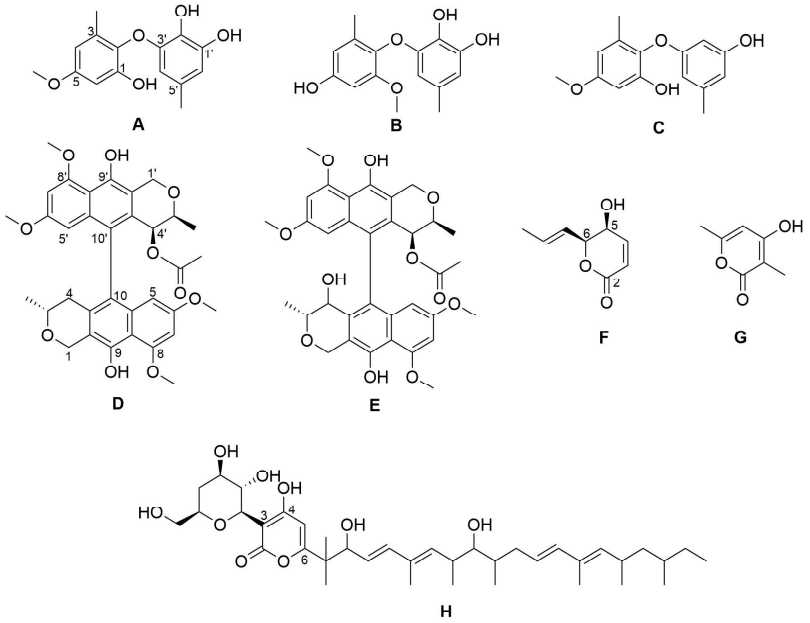

Figure 1. Chemical structures of the isolated compounds. NK-A 17e233 (**A**); 1,2-benzenediol, 3-(4-hydroxy-2-methoxy-6-methylphenoxy)-5-methyl-(ACI) (**B**); cyperin (**C**); ES-242-1 (**D**); ES-242-3 (**E**); 5*S*,6*S*-phomalactone (**F**); methyltriaceticlactone (**G**); S 39163/F-1 (**H**).

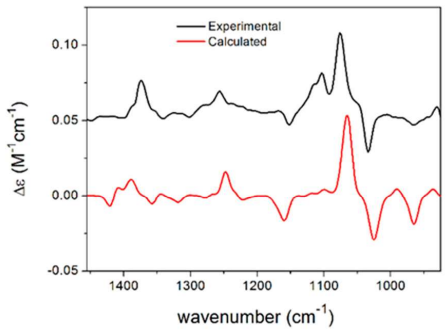

Figure 2. Comparison of the experimental VCD spectrum of **F** measured in $CDCl_3$ and the calculated VCD spectrum of *cis*-(5*S*,6*S*)-**F** computed at the B3LYP/TZVP PCM/$CHCl_3$ level for the eight lowest-energy conformers gained from the DFT optimization performed at the same level.

2.2. Anti-*T. gondii* Activity

The eight natural products isolated from *P. selaginellae* were tested for anti-*T. gondii* activity. Interestingly, **A–F** showed activity against *T. gondii* growth, with IC_{50} values of 5.75, 22.16, 27.22, 7.38, 17.99, and 5.13 μM, respectively (Table 1 and Figure 3). Therefore, we further explored the in vitro cytotoxicity of the natural compounds in different human cell lines.

Table 1. In vitro activity (IC_{50} values) of the natural compounds (**A–H**) from *P. selaginellae* against the *T. gondii* strain ME49. All experiments were conducted in triplicate.

Compound	IC_{50} (μM)
NK-A 17e233 (**A**)	5.75
1,2-benzenediol, 3-(4-hydroxy-2-methoxy-6-methylphenoxy)-5-methyl-(ACI) (**B**)	22.16
cyperin (**C**)	27.22
ES-242-1 (**D**)	7.38
ES-242-3 (**E**)	17.99
5*S*,6*S*-phomalactone (**F**)	5.13
methyltriaceticlactone (**G**)	Not active
S 39163/F-1 (**H**)	Not active
pyrimethamine	0.06

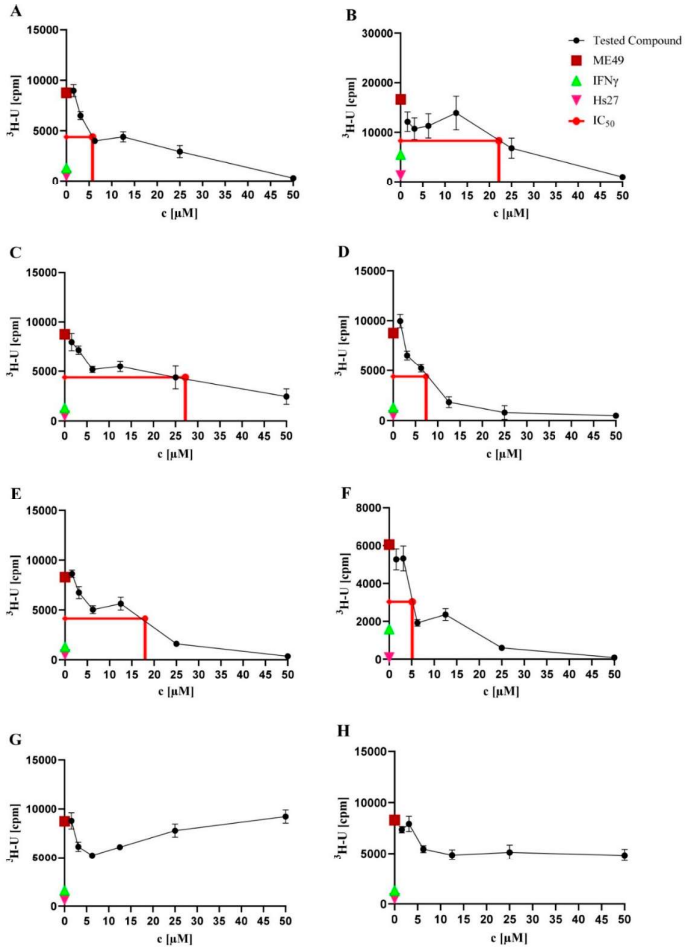

Figure 3. Toxoplasma proliferation assays. Toxoplasma proliferation assays were performed to investigate the activity of the natural products against *T. gondii* strain ME49. Hs27 cells were cultured in a monolayer in 96-well plates and infected with *T. gondii* (3×10^4). Cultures were treated with the

natural products at the concentration range of 0.56–50.00 µM for 48 h at 37 °C. Afterwards, the cultures were labelled with ^{3}H-U (5 mCi, diluted 1:30) for 28–30 h at 37 °C. Based on the incorporation of ^{3}H-U into the parasite nucleic acid, the parasite growth was quantified. As controls, uninfected Hs27 cells without treatment (pink triangles) and IFNγ pre-stimulated infected Hs27 cells (green triangles) were used, while untreated *T. gondii*-infected Hs27 cells (red squares) served as a negative control. Values shown in (**A–H**) represent the means of three independent experiments each done in duplicate (n = 6) ± SEM. The mean of the IC_{50} values (red line) of each compound is shown. Activity of NK-A 17e233 (**A**); 1,2-benzenediol, 3-(4-hydroxy-2-methoxy-6-methylphenoxy)-5-methyl-(ACI) (**B**); cyperin (**C**); ES-242-1 (**D**); ES-242-3 (**E**); 5*S*,6*S*-phomalactone (**F**); methyltriaceticlactone (**G**); S 39163/F-1 (**H**).

2.3. Cytotoxicity Assays

First, we evaluated the cytotoxicity of compounds **A** to **F** in an MTT assay against Hs27 human fibroblasts (same cell type used for the *T. gondii* proliferation assay). The results of the MTT assay are shown in Figure 4 and Table 2. **A–E** showed no cytotoxicity at 100 µM against Hs27 cells. Only **F** showed moderate cytotoxicity with a cytotoxic concentration CC_{50} = 81 ± 2.16 µM.

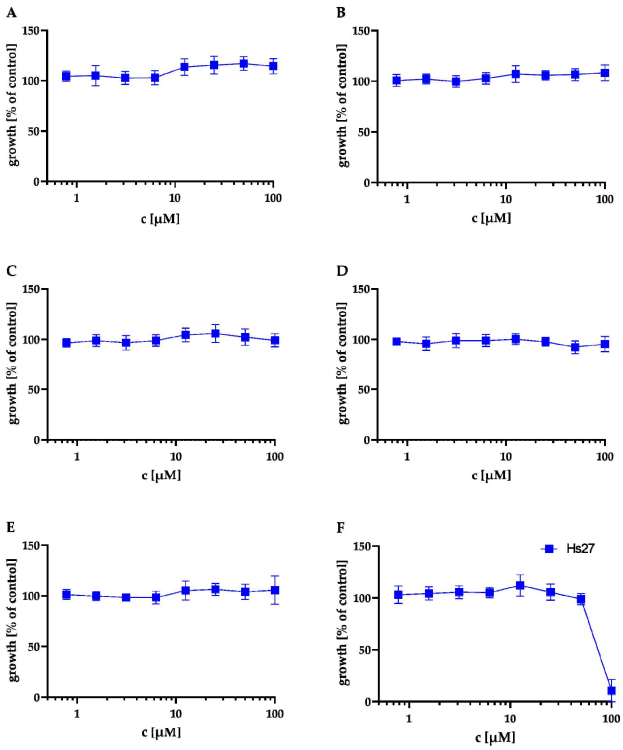

Figure 4. Effect of the natural products on the metabolic activity of Hs27 cells via MTT assay. Hs27 cells were plated in 96-well plates and grown to confluence prior to incubation at 37 °C for 24 h with the natural products in the concentration range of 0.56–100.00 µM. The cultures were incubated with 10 µL of the 12 mM MTT stock solution for approximately 4 h. Afterwards, 100 µL of SDS dissolved in HCl was added to each well and incubated again for 4 h at 37 °C. Finally, the absorbance was measured at 570 nm by spectrophotometry. Values shown in (**A–F**) represent the means of three independent experiments each done in duplicate (n = 6) ± SEM. Cytotoxicity in Hs27 cells of NK-A 17e233 (**A**); 1,2-benzenediol, 3-(4-hydroxy-2-methoxy-6-methylphenoxy)-5-methyl-(ACI) (**B**); cyperin (**C**); ES-242-1 (**D**); ES-242-3 (**E**); 5*S*,6*S*-phomalactone (**F**).

Table 2. In vitro cytotoxicity (CC_{50} values) of the natural compounds (**A–F**) from *P. selaginellae* against human fibroblasts Hs27. Concentration >100 μM indicates no activity in the experimental setup. All experiments were conducted in triplicate.

Compound	CC_{50} (μM)
A	>100
B	>100
C	>100
D	>100
E	>100
F	81
Pyrimethamine	44

These compounds also were tested against the THP-1, Huh-7, and Hek 293 cell lines in a Resazurin assay. The mean IC_{50} values of the Resazurin assay are shown in Table 3. While compounds **A–C** showed no cytotoxic effect in concentrations < 100 μM against any of the tested cell lines, **D** had only a weak cytotoxic activity against the Hek 293 cell line with an IC_{50} of 93.8 μM. **E** showed moderate cytotoxic activity against all of the three tested cell lines and thus was the most cytotoxic of the tested compounds. **F** showed no or weak cytotoxic effects against the Huh-7 and Hek-293 cell lines. The cytotoxic effect against the THP-1 cell line was higher, with an IC_{50} of 24.3 μM. The graphs for the Resazurin assay are shown in Figure 5.

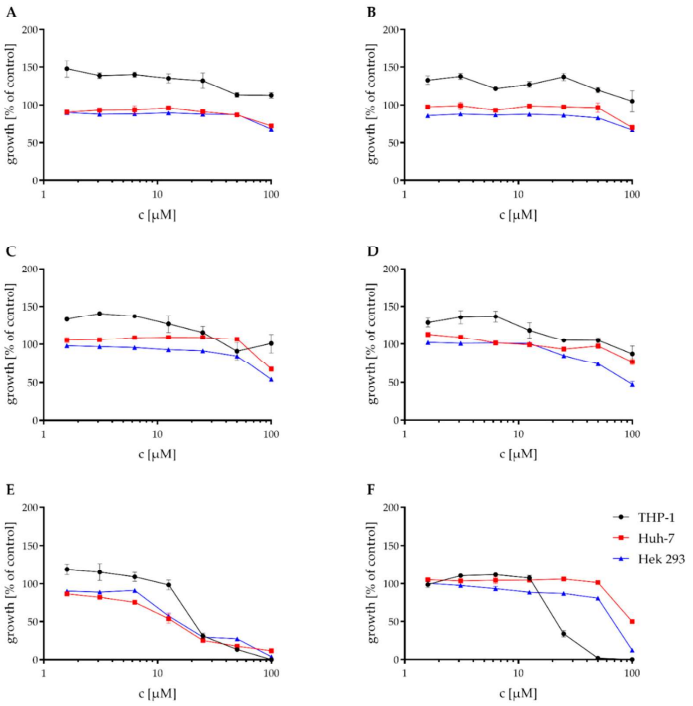

Figure 5. Effect of the natural products on the viability of THP-1, Huh-7, and HEK-293 cells. Cytotoxic effect of NK-A17e233 (**A**); 1,2-benzenediol,3-(4-hydroxy-2-methoxy-6-methylphenoxy)-5-methyl-(ACI) (**B**); cyperin (**C**); ES-242-1 (**D**); ES-242-3 (**E**); 5*S*,6*S*-phomalactone (**F**) against the human cell lines THP-1, Huh-7, and HEK-293 as determined by resazurin assay. 100% growth control DMSO, 0% growth control cycloheximide. Values represent the means of triplicates ± SEM.

Table 3. Mean IC_{50} values of compounds **A–F** against human cell lines THP-1, Huh-7, and Hek293. All concentrations are shown in μM. Concentration >100 μM indicates no activity in the experimental setup. All experiments were conducted in triplicate. The IC_{50} values were calculated using GraphPad Prism 7.

Compound	Mean IC_{50} [μM]		
	THP1	Huh-7	HEK-293
A	>100	>100	>100
B	>100	>100	>100
C	>100	>100	>100
D	>100	>100	93.8
E	21.9	13	16.95
F	24.3	100	66.9

2.4. Determination of Anti-Bacterial Activity

In our ongoing research for antibacterial and particularly antitubercular compounds, **A** to **H** were also tested in a minimal inhibitory concentration assay against *S. aureus* ATCC 700699, *P. aeruginosa* ATCC 87110, and *M. tuberculosis* H37Rv. Compounds **A** to **H** had no inhibitory effect on *S. aureus* ATCC 700699 and *P. aeruginosa* ATCC 87110, except for compound **F**, which showed a weak inhibitory effect on *P. aeruginosa* ATCC 87110 with an MIC_{90} of 100 μM. Compounds **A**, **B**, **C**, **F**, **G**, and **H** had no inhibitory effect on the growth of *M. tuberculosis*, and compounds **D** and **E** showed a weak inhibitory effect with an MIC_{90} of 50 and 100 μM, respectively. The results are shown in Table 4, highlighting that compounds **A** to **F** had a specific anti-toxoplasma effect and were devoid of broad, unspecific antimicrobial activity.

Table 4. MIC_{90} against *S. aureus* ATCC 700699, *P. aeruginosa* ATCC 87110, and *M. tuberculosis* H37Rv. All concentrations are shown in μM. Concentration >100 μM indicates no activity in the experimental setup. All experiments were conducted in triplicate.

Compound	MIC_{90} [μM]		
	S. aureus ATCC 700699	*P. aeruginosa* ATCC 87110	*M. tuberculosis* H37Rv
A	>100	>100	>100
B	>100	>100	>100
C	>100	>100	>100
D	>100	>100	50
E	>100	>100	100
F	>100	100	>100
G	>100	>100	>100
H	>100	>100	>100

3. Discussion

Natural products have played an important role in the history of drug discovery for infectious disease. In the quest for new anti-*T. gondii* drugs, natural products have been proven to exhibit high potential for the discovery and development of new lead compounds with strong anti-*T. gondii* activity [25,26]. In this study, we isolated eight natural products from the crude extract of the endophytic fungus *P. selaginellae*. A previous report on the inhibitory activity of one of these compounds (phomalactone, **F**) against the apicomplexan parasite *Plasmodium falciparum* with an IC_{50} of 84.32 μM [27] prompted us to test the natural products for anti-*T. gondii* activity. Interestingly, six compounds showed activity against *T. gondii* proliferation with no or low cytotoxicity in different human cell lines and no or low antibacterial activity against a gram-positive, a gram-negative, and a mycobacterial representative, revealing reasonable anti-*T. gondii* specificity and promising therapeutic windows. These results establish diphenyl ethers, bioxanthracenes, and lactones from *P. selaginellae* as potential candidates for further preclinical development of novel anti-toxoplasma therapeutics.

Some of the isolated compounds share similar structural elements, which give insights into a structure–activity relationship of the natural products against the tested *T. gondii* strain ME49. Compounds **A**, **B**, and **C** are biphenyl ether derivatives that differ either in the position of the methoxy group or in the number of substituted hydroxyl groups. The most potent of these compounds is **A** (IC_{50} = 5.75 μM), followed by **B** (IC_{50} = 19.35 μM) and **C** (IC_{50} = 27.22 μM). While **A** only differs from **B** by a switch in the position of the methoxylated hydroxyl group from position 2 to 4, it differs from **C** only by an additional hydroxyl group in position 2′, which it shares with **B**. Because of the higher potency of **A** in the toxoplasma proliferation assay compared to **B** and **C**, the position of the methoxy group in 4 and the amount and position of hydroxyl groups in 2′ and 3′ both are likely to have an influence on the antitoxoplasma activity of these derivatives. This suggestion, nevertheless, needs further experimental evidence. Furthermore, diphenyl ethers **A**, **B**, and **C** are structurally related to triclosan, a well-known broad spectrum antifungal and antibacterial agent targeting lipid synthesis [28]. It has been shown that triclosan also inhibits the growth of apicomplexans by inhibition of the enoyl reductase ENR (FabI) enzyme, the second reductive step in the type II fatty acid biosynthesis pathway. Nevertheless, due the poor solubility of triclosan, there is considerable interest in finding novel potent triclosan analogs with improved properties such as solubility, activity, and toxicity [29,30]. The mechanism of action of **A**, **B**, and **C** may be similar to that of triclosan, but further studies are necessary to explore and confirm their mode of action and cellular target. Furthermore, in vitro and in vivo pharmacokinetic characterization is needed to reveal whether any of the compounds reported here has superior properties compared to triclosan.

Compounds **D** and **E** represent bioxanthracenes belonging to the ES-242 class and share the same structure, differing only in position 4′ by the hydroxyl group that is present only in **E**. The IC_{50} values in the toxoplasma proliferation assay were 7.38 μM and 17.99 μM for **D** and **E**, respectively, suggesting a reduction in the antitoxoplasma activity if position 4′ is substituted by a hydroxyl group. The bioxanthracenes **D** and **E** were previously isolated from *Verticillium* spp. and are well-known to act as *N*-methyl-*D*-aspartate receptor antagonists [31]. Both compounds were also found to be active against the apicomplexan parasite *P. falciparum* with IC_{50} values of 8.44 and 13.22 μM, respectively [32]. Interestingly, the activities of **D** and **E** against *T. gondii* in this study were comparable to their reported activity in *P. falciparum* with IC_{50} values of 7.38 μM and 17.99 μM (see Table 1). Nevertheless, the mechanism of action of **D** and **E** on apicomplexans is still unknown and is probably independent from their activity as NMDA receptor antagonists [32].

Compounds **F** and **G** are small δ-lactonic molecules; 5*S*,6*S*-phomalactone (**F**) differs from methyltriaceticlactone (**G**) in the length of the sidechain in position 6, the hydroxyl group in position 5, and in the absence of the methyl group that is present in methyltriaceticlactone in position 2. Interestingly, antitoxoplasmal activity was observed for **F**, but not for **G**, suggesting that one or more of these structural differences and not only the presence of the δ-lactonic base structure plays a crucial role in the bioactivity against *T. gondii*. Phomalactone (**F**) is a frequent fungal metabolite and was first isolated from the plant-pathogenic fungus *Nigrospora* sp. [16]. It has a wide range of activities such as antifungal, immunomodulating, insecticide, nematocidal, and phytotoxic activity [15,19,33–35]. In addition, it has been found to be active against the apicomplexan parasite *P. falciparum*, with an IC_{50} of 84.32 μM [27]. In the present study, we tested **F** for inhibition of *T. gondii* proliferation and, interestingly, it showed a more potent activity with an IC_{50} of 5.13 μM (see Table 1). No target or mode of action has been suggested for phomalactone in *P. falciparum*, and the target of this compound in *T. gondii* also remains elusive and has to be determined in the future. Importantly, the newly identified natural products with inhibitory activity against *T. gondii* showed very little in vitro toxicity and should be evaluated in in vivo infection model systems in the future. In general, this study highlights the potential of endophytic fungi as a promising source for novel antitoxoplasma compounds.

4. Materials and Methods

4.1. General Experimental Procedures

Optical rotations were measured on a Jasco P-2000 polarimeter (Jasco, Pfungstadt, Germany). UV-spectra were obtained by the use of a Dionex P580 system in combination with a diode array detector (UVD340S) and an Eurosphere 10 C18 column (125 mm × 4 mm). ECD spectra were measured on a JASCO J-810 spectropolarimeter. VCD spectra were recorded on a BioTools Chiral-IR-2X at a resolution of 4 cm^{-1} under ambient temperature for 18 × 3000 scans. Samples were dissolved in $CDCl_3$, and the solution was placed in a 100 µm BaF_2 cell. 1D and 2D NMR spectra were recorded on a Bruker Avance III (^1H, 600 MHz; ^{13}C 150 MHz) spectrometer. Mass spectra were measured on a Finnigan LCQ Deca (Thermo Quest, Egelsbach, Germany) mass spectrometer and for HRESIMS, on a UHR-QTOF maXis 4G (Bruker Daltonics, Bremen, Germany) mass spectrometer. Semipreperative HPLC was performed on a Lachrom-Merck Hitachi system (pump L7100, UV-detector L7400, Eurospher 100 C18 column 300 mm × 8 mm, Knauer, Everswinkel, Germany). VLC and non-vacuum-column chromatography were accomplished using Macherey Nagel silica gel 60M (0.04–0.063 mm). Precoated TLC silica gel 60 F254 plates (Merck, Darmstadt, Germany) were used for tracking separation using detection under UV light at 254 and 365 nm wavelengths or spraying anisaldehyde–sulfuric acid reagent. Sephadex LH20 (GE Healthcare Bio.Sciences AB, Uppsala, Sweden) was used as a stationary phase for column chromatography. The measurement of optical rotations was accomplished by using spectral grade solvents.

4.2. Fungal Material

The fungus was obtained from the leaves of the plant *Philodendron monstera* as an endophyte. A single leaf was surface sterilized by soaking it with 70% ethanol for 30 s and letting it dry under sterile conditions. With a heat-sterilized scalpel, the leaf was cut into pieces and put onto a YPD agar plate, which was enriched with 100 mg/L chloramphenicol to suppress bacterial growth. After seven days of incubation at room temperature, distinct fungal growth was observed on the plate. A 1 cm^2 piece of the fungus was cut out of the agar medium using a heat-sterilized scalpel under sterile conditions and was transferred onto a new sterile YPD agar plate to isolate a pure organism. The isolated strain was identified as *Paraboeremia selaginella* by the internal transcribed spacer (ITS) sequence with 99.56% identity in comparison with the ITS database of the National Center for Biotechnology Information (GenBank Accession ON231784).

4.3. Fermentation and Extraction

The fungus was fermented on solid rice medium. Ten Erlenmeyer flasks were used; 100 g of rice and 100 mL of demineralized water were added to each flask and autoclaved at 121 °C for 15 min. Under sterile conditions, 1 cm^2 of fungal material was cut out of an agar plate using a sterile scalpel and transferred onto the autoclaved rice medium. The fungus was grown for 4 weeks under static conditions at room temperature. Each flask was soaked with 250 mL of ethylacetate for at least 12 h. The rice medium was then cut into small pieces and shaken for 8 h at 150 rpm. The liquid crude extract was filtrated into round flasks and evaporated using a rotary evaporator to yield 14.66 g of dry crude extract.

4.4. Isolation

The crude extract (14.66 g) obtained from the fermentation was separated using vacuum liquid chromatography with silica gel as a stationary phase. A step gradient from 100% hexane to 100% ethylacetate followed by a step gradient from 100% dichloromethane to 100% methanol gave 18 fractions (V1–V18). Two fractions (V4 and V6) were chosen based on initial bioactivity observed against *Candida albicans*. However, this bioactivity was lost during the purification process. Fraction V4 (200.7 mg) was further separated using a Sephadex LH20 column with MeOH as eluent to give five subfractions (V4-S1–S5). Fraction V4S3 (47.3 mg) was subjected to semipreparative HPLC using a MeOH-H_2O step gradient

from 50% to 80% MeOH followed by a washing step with 100% MeOH to yield **A** (20.7 mg), **B** (2.8 mg), and **C** (7.7 mg). Fraction V6 (1010 mg) was purified using a Sephadex LH20 column with CH_2Cl_2 and MeOH (50/50) as eluent to yield six subfractions (V6-S1–S6). Subfraction S2 (72.0 mg) was purified using a silica column with 40% hexane and 60% ethylacetate to elute **D** (25.0 mg) and **E** (8.6 mg) as pure compounds. Subfraction V6-S4 (516 mg) was further purified by using a Sephadex LH20 column with MeOH as eluent to yield five subfractions (V6S4-S1–S5). Subfraction V6S4S2 (496 mg) was subjected to a silica column with a mixture of CH_2Cl_2 and MeOH (95/5) as eluent to give four subfractions (V6S4S2-K1–K4). Silica subfraction V6S4S2K2 (47 mg) was then purified by semipreparative HPLC using a MeOH-H_2O step gradient from 10% to 30% MeOH followed by a washing step with 100% MeOH to yield **F** (22.2 mg) and **G** (4.5 mg). Fraction V12 (744.1 mg) was separated using a Sephadex LH20 column with 50% MeOH and 50% CH_2Cl_2 to yield six subfractions (V12-S1–S6). Subfraction S2 (180.3 mg) was then further separated using a silica column with 10% MeOH and 90% CH_2Cl_2 as eluent to give seven subfractions (V12S2-K1–K7). Silica subfraction K7 (56.1 mg) was subjected to semipreparative HPLC using a step gradient from 70% to 100% MeOH to yield **H** (5.0 mg).

NK-A 17e233 (A): Brown oil; UV (MeOH) λ_{max} 220.0, 234.3, 279.7 nm; ^{1}H NMR (DMSO-d6) see Supplementary Materials Figure S1; HRESIMS *m/z* 277.1075 [M + H]$^+$ (calcd. for $C_{15}H_{17}O_5$ 277.1071 *m/z*).

3-(4-Hydroxy-2-methoxy-6-methylphenoxy)-5-methylbenzene-1,2-diol (B): Brown oil; UV (MeOH) λ_{max} 211.7, 286.3 nm; ^{1}H NMR ($CDCl_3$), see Supplementary Materials Figure S6; HRESIMS *m/z* 277.1065 [M + H]$^+$ (calcd. for $C_{15}H_{17}O_5$ 277.1071 *m/z*).

Cyperin (C): Brown oil; UV (MeOH) λ_{max} 212.1, 279.8 nm; ^{1}H NMR ($CDCl_3$), see Supplementary Materials Figure S10; HRESIMS *m/z* 261.1126 [M + H]$^+$ (calcd. for $C_{15}H_{17}O_4$ 261.1121 *m/z*).

ES-242-1 (D): Brown amorphous powder; $[\alpha]^{24}{}_D$ *+18* (c 1.0, MeOH); UV (MeOH) λ_{max} 239.0, 309.8, 345.8 nm; ^{1}H NMR ($CDCl_3$) and ^{13}C NMR ($CDCl_3$), see Supplementary Materials Figures S14 and S15; HRESIMS *m/z* 622.2644 [M + $NH_4]^+$ (calcd. for $C_{34}H_{40}NO_{10}$ 622.2647 *m/z*).

ES-242-3 (E): Brown amorphous powder; $[\alpha]^{24}{}_D$ *+66* (c 1.0, $CHCl_3$); UV (MeOH) λ_{max} 239.2, 298.6, 309.4 nm; ^{1}H NMR ($CDCl_3$) and ^{13}C NMR ($CDCl_3$), see Supplementary Materials Figures S19 and S20; HRESIMS *m/z* 638.2588 [M + $NH_4]^+$ (calcd. for $C_{34}H_{40}NO_{11}$ 638.2596 *m/z*).

Phomalactone (F): light yellowish oil; $[\alpha]^{24}{}_D$ *+172* (c 1.0, EtOH); UV (MeOH) λ_{max} 216.0 nm; For the details of VCD, ECD, and OR calculations, see Supplementary Materials; ^{1}H NMR ($CDCl_3$) and ^{13}C NMR ($CDCl_3$), see Supplementary Materials Figures S24 and S25; HRESIMS *m/z* 155.0702 [M + H]$^+$ (calcd. for $C_8H_{11}O_3$ 155.0703 *m/z*) and *m/z* 137.0597 [M − OH^-]$^+$ (calcd. for $C_8H_9O_2$ 137.0597 *m/z*).

Methyltriaceticlactone (G): White amorphous powder; UV (MeOH) λ_{max} 290.5 nm; ^{1}H NMR (DMSO-d6) and ^{13}C NMR (DMSO-d6), see Supplementary Materials Figures S29 and S30; HRESIMS *m/z* 141.0549 [M + H]$^+$ (calcd. for $C_7H_9O_3$ 141.0546 *m/z*).

S 39163/F-1 (H): Brown amorphous gum; $[\alpha]^{24}{}_D$ *−11* (c 1.0, MeOH); UV (MeOH) λ_{max} 218.2, 238.8, 291.9 nm; ^{1}H NMR ($CDCl_3$), see Supplementary Materials Figure S34; HRESIMS *m/z* 661.4312 [M + H]$^+$ (calcd. for $C_{38}H_{61}O_9$ 661.4310 *m/z*).

4.5. Preparation of Compounds for T. gondii Proliferation Assay

The purified natural products **A–F** and pyrimethamine [36] were dissolved in DMSO as 10 mM stocks and stored at −20 °C. The compounds were diluted in Iscove's Modified Dulbecco's medium (Gibco–Thermo Fisher Scientific, Braunschweig, Germany) immediately prior to use.

4.6. Parasites and Cell Culture for T. gondii Proliferation Assay

T. gondii ME49 tachyzoites (ATCC/LGC Standards GmbH, Wesel, Germany) were cultured in human foreskin fibroblast Hs27 cells (ATCC/LGC Standards GmbH, Wesel, Germany)

as host cells as described previously [37]. The cells were maintained in Iscove's modified Dulbecco's medium (Gibco–Thermo Fisher Scientific, Braunschweig, Germany) supplemented with 10% heat-inactivated fetal bovine serum (Invitrogen, Karlsruhe, Germany) and 50 mM 2-mercaptoethanol (Gibco–Thermo Fisher Scientific, Braunschweig, Germany) and were grown in a humidified incubator at 37 °C with 5% CO_2 in air atmosphere. For toxoplasma propagation, 25 cm^2 cell culture flasks, containing a confluent monolayer of Hs27 cells, were infected with 5×10^6 *T. gondii* tachyzoites after medium change. After three days, the supernatant of the cell culture containing parasites was harvested and transferred to a 15 mL centrifuge tube and centrifuged at 700 rpm for five minutes and resuspended in cell culture medium. The number of parasites was counted using a hemocytometer.

4.7. T. gondii Proliferation Assay

Microtiter plates (96-well) with a final volume of 200 μL per well were used for the assay. Hs27 fibroblast monolayers were infected with 3×10^4 freshly harvested tachyzoites per well (MOI = 1) and incubated for 48 h at 37 °C, after which various concentrations of the tested compounds (0.04, 0.09, 0.19, 0.39, 0.78, 1.5, 3.12, 6.25, 12.5, 25, 50 μM) in culture medium were added to the cells. Pyrimethamine (0.007, 0.01, 0.03, 0.06, 0.125, 0.25, 0.5, 1 μM) was added under identical conditions as a positive drug control [37]. Hs27 cells were pre-stimulated for 24 h with IFNγ (300 U/mL) and infected with *T. gondii* cells without further treatment as the growth inhibition control. After 48 h, proliferating toxoplasma parasites were radioactively labelled with tritiated uracil (5 mCi, Hartmann Analytic, Braunschweig, Germany) and diluted 1:30 (10 μL per 200 μL total culture volume per well) in order to determine parasite proliferation [38]. After 28–30 h, the microtiter plates were frozen at −20 °C. To evaluate the assay, the microtiter plates were thawed at room temperature. Cells were transferred to glass-fiber filters (Printed Filtermat A 102 mm × 258 mm, PerkinElmer, Waltham, MA, USA) using a cell harvester (Basic96 Harvester, Zinsser Analytic, Skatron Instruments, Northridge, CA, USA). The filters were dried for 20 min at 130 °C in a drying cabinet and were then soaked in 10 mL of scintillation fluid (Betaplate Scint, PerkinElmer, Waltham, MA, USA) and shrink-wrapped in plastic covers (Sample Bag for Betaplate, PerkinElmer, Waltham, MA, USA). The filters were then clamped in cassettes and evaluated using a beta-counter device (Betaplate Liquid Scintillation Counter 1205, LKB-WALLAK, Melbourne, Australia) to measure the Cherenkov radiation, which refers to the amount of incorporation of tritiated uracil into the RNA of *T. gondii*. IC_{50} values, the concentration of inhibitors necessary to inhibit the growth of tachyzoites by 50%, were determined for each experiment with the use of Prism GraphPad version 9.2.0 software.

4.8. Cell Viability Assay against Hs27 Cells

The 3-[4,5-dimethylthiazole-2-yl]-2,5-diphenyltetrazolium bromide (MTT) test was used to assess cell viability of the isolated active compounds against Hs27 cells. The MTT assay is a colorimetric reaction based on the enzymatic reduction of MTT to MTT-formazan, which is catalyzed by mitochondrial succinate dehydrogenase [39].

In brief, Hs27 cells were seeded 96-well plates in a monolayer in Iscove's modified Dulbecco's medium (Gibco–Thermo Fisher Scientific, Braunschweig, Germany) and incubated at 37 °C with different concentrations of the tested natural products (1.56, 3,12, 6.25, 12,5, 25, 50, 100 μM) in the culture media. Staurosporine (0.007, 0.01, 0.03, 0.06, 1.25, 0.25, 0.5, 1 μM), a well-known cytotoxicity-inducing kinase inhibitor [40], untreated Hs27 cells, and DMSO were used as controls. After 24 h, the medium of the culture was removed and replaced with 100 μL of DMEM without red phenol (Gibco–Thermo Fisher Scientific, Braunschweig, Germany) plus 10% heat-inactivated fetal bovine serum (Invitrogen, Karlsruhe, Germany), and 50 mM 2-mercaptoethanol (Gibco–Thermo Fisher Scientific, Braunschweig, Germany). Afterwards, the 12 mM MTT solution was added to each well according to the manufacturer's instruction (Vybrant MTT Cell Proliferation Assay Kit, Thermo Fisher Scientific, Braunschweig, Germany). The OD value of each well was assayed at the wavelength of 570 nm on a microplate reader (TECAN Sunrise, Männedorf, Switzerland). The 50%

cytotoxic concentration (CC_{50} values) of the tested natural products on Hs27 cells was calculated and all data were analyzed using Prism GraphPad version 9.2.0 software.

4.9. Determination of the Minimal Inhibitory Concentration against Different Pathogenic Bacteria

Testing for antibacterial activity was done as described previously [37]. Briefly, a single colony of Methicillin-resistant *Staphylococcus aureus* (MRSA strain Mu50, ATCC 700699) or *Pseudomonas aeruginosa* (strain PAO1, ATCC 87110) were grown in Mueller-Hinton broth (MHB) at 37 °C shaking at 120 rpm to reach an optical density of approx. 0.4. The cell suspension was adjusted to 10^6 CFU/mL, of which 50 µL was seeded into a prepared 96-well polystyrene round-bottom plate containing test compounds diluted in MHB in a 1:1 serial dilution ranging from 100 µM to 0.78 µM. The plates were incubated at 37 °C statically for 24 h, and readout was performed using the BacTiter Glo assay (Promega) following the manufacturer's instructions. Briefly, BacTiter Glo reagent was added to a white flat-bottom 96-well plate, and an equal volume of bacteria suspension was added to each well and mixed carefully. After 5 min, the luminescence was measured using a TECAN plate reader. The growth was calculated in regard to the vehicle (DMSO) and sterile control. Moxifloxacin and cefuroxime were used as a positive and negative control, respectively. All compounds were tested in triplicate.

For the testing against *M. tuberculosis* H37Rv, the Minimal Inhibitory Concentration (MIC) was determined in 96-well microtiter plates containing a total volume of 100 µL employing a resazurin reduction assay [41]. Briefly, a 96-well plate was prepared containing 7H9 medium supplemented with 10% ADS (0.81% NaCl, 5% BSA, 2% dextrose), 0.5% glycerol, and 0.05% tyloxapol. Compounds were two-fold serially diluted with the highest tested concentration of 100 µM. A *M. tuberculosis* culture was pre-grown to an $OD_{600\ nm}$ of approx. 0.4–0.6 by shaking at 37 °C in PETG square bottles (ThermoFisher Scientific, Braunschweig, Germany) containing 10 mL supplemented 7H9 medium. The cell density was adjusted to an $OD_{600\ nm}$ of 0.08 (10^6 CFU/mL, and 5×10^4 CFU were added to each well). Rifampicin and DMSO were used as a positive and solvent control, respectively. The 96-well plates were incubated for 5 days at 37 °C and 5% CO_2 in humidified atmosphere. Afterwards, 10 µL of a 100 mg/mL resazurin solution was added to each well and resuspended carefully. After another 24 h at room temperature, the cells were fixed by adding 100 µL of a 10% formalin solution to each well. The readout was performed using a TECAN plate reader at 535 nm excitation and 590 nm emission. The growth was calculated in relation to the solvent control being 100% growth. The experiment was performed in triplicate.

4.10. Cytotoxicity Assay against Different Human Cell Lines

The cytotoxicity study was carried out using the THP-1 (human monocytic leukemia cell line), Huh-7 (Human liver carcinoma cell line), and HEK293 (human embryonic kidney cell line) cell lines as described before [37]. The THP-1 cells were cultured using RPMI 1640 medium containing 2 mM L-glutamine and supplemented with 10% fetal calf serum (FCS) and 1% sodium pyruvate. Huh-7 cells were cultured using a 1:1 mixture of RPMI 1640 medium containing 2 mM L-glutamine and 10% FCS medium and DMEM containing 10% FCS and 1% sodium pyruvate. The HEK-293 cells were cultured with DMEM including 2 mM L-glutamine and supplemented with 1% NE amino acids, 1% 1.0 mM sodium pyruvate and 10% FCS. All three cell lines were then incubated at 37 °C in an atmosphere of 5% CO_2 under humid conditions for 2 weeks while renewing the medium twice weekly. Subsequently, the cells were suspended and adjusted to a density of 2×10^5 cells/mL. In a 96-well flat-bottom microtiter plate, the cells were adjusted to a total volume of 100 µL containing 2-fold serial dilutions of the tested compounds **A–F** ranging from 100 to 1.56 µM. Cycloheximide (4, 2, 1, 0.5, 0.25, 0.13, 0.06, 0.03 µg/mL) was used as a positive control. After an incubation time of 48 h at 37 °C in an atmosphere of 5% CO_2 under humid conditions, 10 µL resazurin solution (100 µg/mL) was added to each well and incubated for another 4 h. The fluorescence was then quantified using a Tecan Infinite 200pro microplate reader

(excitation 540 nm, emission 590 nm). The residual growth was calculated relative to non-inoculated conditions (0% growth) and controls treated with DMSO (100% growth).

Supplementary Materials: The following supporting information can be downloaded at: https://www.mdpi.com/article/10.3390/antibiotics11091176/s1, Figures S1–S58: Spectroscopic data used for the structure elucidation of compounds A–H; Figure S59: Comparison of the experimental ECD spectrum of F measured in MeCN and the calculated ECD spectra of (5S,6S)-F computed at various levels of theory for the 10 lowest-energy ωB97X/TZVP PCM/MeCN conformers; Figure S60: Geometries of the low-energy ωB97X/TZVP PCM/MeCN conformers of (5S,6S)-F; Figure S61: Geometries of the low-energy B3LYP/TZVP PCM/CHCl3 conformers of (5S,6S)-F; Table S1: Boltzmann populations and specific optical rotations of the low-energy conformers of (5S,6S)-F computed at various levels for the low-energy ωB97X conformers. References [42–45] are cited in Supplementary Materials.

Author Contributions: Conceptualization, R.K. and K.P.; methodology, F.M., V.E.S., T.K., R.K. and K.P.; investigation, F.M., V.E.S., L.v.G. and A.M.; data curation, F.M., V.E.S., M.F., T.K., R.K. and K.P.; writing—original draft preparation, F.M. and V.E.S.; writing—review and editing, funding acquisition, T.K., R.K. and K.P. All authors have read and agreed to the published version of the manuscript.

Funding: This work was supported by the Deutsche Forschungsgemeinschaft (DFG, German Research Foundation)–project number 270650915/GRK 2158 (to RK and KP). T.K. and A.M. were supported by the National Research, Development and Innovation Office (K138672 and FK134653).

Institutional Review Board Statement: Not applicable.

Informed Consent Statement: Not applicable.

Data Availability Statement: All data presented in this study are contained within the article and the supplementary materials. The internal transcribed spacer (ITS) sequence for *Paraboeremia selaginellae* has been deposited in the National Center for Biotechnology Information (NCBI) GenBank under accession number ON231784.

Acknowledgments: We thank the CeMSA@HHU (Center for Molecular and Structural Analytics@Heinrich Heine University) for recording the mass-spectrometric and the NMR-spectroscopic data. We thank Heike Goldbach-Gecke for testing and measuring the cytotoxic effect of the isolated compounds against the tested human cell lines. The Governmental Information-Technology Development Agency (KIFÜ) is acknowledged for CPU time. We thank Karin Buchholz for expert technical assistance and Daniel Degrandi as well as Ursula Sorg for scientific advice and discussions.

Conflicts of Interest: The authors declare no conflict of interest. The funders had no role in the design of the study; in the collection, analyses, or interpretation of data; in the writing of the manuscript, or in the decision to publish the results.

References

1. Frolich, S.; Entzeroth, R.; Wallach, M. Comparison of protective immune responses to apicomplexan parasites. *J. Parasitol. Res.* **2012**, *2012*, 852591. [CrossRef] [PubMed]
2. Kim, K.; Weiss, L.M. Toxoplasma gondii: The model apicomplexan. *Int. J. Parasitol.* **2004**, *34*, 423–432. [CrossRef] [PubMed]
3. Toxoplasmosis of Animals and Man. By J.P. Dubey and C. P. Beattie. 220 pages. ISBN 0 8493 4618 5. CRC Press, Boca Raton, 1988. £108.00. *Parasitology* **2009**, *100*, 500–501. [CrossRef]
4. Dubey, J.P. *Toxoplasmosis of Animals and Humans*; CRC Press: Boca Raton, FL, USA, 2016.
5. Saadatnia, G.; Golkar, M. A review on human toxoplasmosis. *Scand. J. Infect. Dis.* **2012**, *44*, 805–814. [CrossRef] [PubMed]
6. Dubey, J.P. Outbreaks of clinical toxoplasmosis in humans: Five decades of personal experience, perspectives and lessons learned. *Parasites Vectors* **2021**, *14*, 263. [CrossRef] [PubMed]
7. Furtado, J.M.; Smith, J.R.; Belfort, R., Jr.; Gattey, D.; Winthrop, K.L. Toxoplasmosis: A global threat. *J. Glob. Infect. Dis.* **2011**, *3*, 281–284. [CrossRef]
8. de Jong, P.T. Ocular toxoplasmosis; common and rare symptoms and signs. *Int. Ophthalmol.* **1989**, *13*, 391–397. [CrossRef]
9. Elbez-Rubinstein, A.; Ajzenberg, D.; Dardé, M.L.; Cohen, R.; Dumètre, A.; Yera, H.; Gondon, E.; Janaud, J.C.; Thulliez, P. Congenital toxoplasmosis and reinfection during pregnancy: Case report, strain characterization, experimental model of reinfection, and review. *J. Infect. Dis.* **2009**, *199*, 280–285. [CrossRef]
10. Dunay, I.R.; Gajurel, K.; Dhakal, R.; Liesenfeld, O.; Montoya, J.G. Treatment of Toxoplasmosis: Historical Perspective, Animal Models, and Current Clinical Practice. *Clin. Microbiol. Rev.* **2018**, *31*, e00057-17. [CrossRef]

11. Gopalakrishnan, A.M.; López-Estraño, C. Comparative analysis of stage specific gene regulation of apicomplexan parasites: Plasmodium falciparum and Toxoplasma gondii. *Infect. Disord. Drug Targets* **2010**, *10*, 303–311. [CrossRef]
12. Newman, D.J.; Cragg, G.M. Natural Products as Sources of New Drugs over the Nearly Four Decades from 01/1981 to 09/2019. *J. Nat. Prod.* **2020**, *83*, 770–803. [CrossRef] [PubMed]
13. Cheraghipour, K.; Masoori, L.; Ezzatpour, B.; Roozbehani, M.; Sheikhian, A.; Malekara, V.; Niazi, M.; Mardanshah, O.; Moradpour, K.; Mahmoudvand, H. The Experimental Role of Medicinal Plants in Treatment of Toxoplasma gondii Infection: A Systematic Review. *Acta Parasitol.* **2021**, *66*, 303–328. [CrossRef] [PubMed]
14. Lenzi, J.; Costa, T.M.; Alberton, M.D.; Goulart, J.A.G.; Tavares, L.B.B. Medicinal fungi: A source of antiparasitic secondary metabolites. *Appl. Microbiol. Biotechnol.* **2018**, *102*, 5791–5810. [CrossRef] [PubMed]
15. Fukushima, T.; Tanaka, M.; Gohbara, M.; Fujimori, T. Phytotoxicity of three lactones from Nigrospora sacchari. *Phytochemistry* **1998**, *48*, 625–630. [CrossRef]
16. Evans, R.H.; Ellestad, G.A.; Kunstmann, M.P. Two new metabolites from an unidentified nigrospora species. *Tetrahedron Lett.* **1969**, *10*, 1791–1794. [CrossRef]
17. Gusmao, A.S.; Abreu, L.S.; Tavares, J.F.; de Freitas, H.F.; Silva da Rocha Pita, S.; Dos Santos, E.G.; Caldas, I.S.; Vieira, A.A.; Silva, E.O. Computer-Guided Trypanocidal Activity of Natural Lactones Produced by Endophytic Fungus of Euphorbia umbellata. *Chem. Biodivers* **2021**, *18*, e2100493. [CrossRef]
18. Hussain, H.; Kock, I.; Al-Harrasi, A.; Al-Rawahi, A.; Abbas, G.; Green, I.R.; Shah, A.; Badshah, A.; Saleem, M.; Draeger, S.; et al. Antimicrobial chemical constituents from endophytic fungus Phoma sp. *Asian Pac. J. Trop. Med.* **2014**, *7*, 699–702. [CrossRef]
19. Khambay, B.P.S.; Bourne, J.M.; Cameron, S.; Kerry, B.R.; Zaki, M.J. A nematicidal metabolite from Verticillium chlamydosporium. *Pest Manag. Sci. Former. Pestic. Sci.* **2000**, *56*, 1098–1099. [CrossRef]
20. Meepagala, K.M.; Johnson, R.D.; Techen, N.; Wedge, D.E.; Duke, S.O. Phomalactone from a Phytopathogenic Fungus Infecting ZINNIA elegans (ASTERACEAE) Leaves. *J. Chem. Ecol.* **2015**, *41*, 602–612. [CrossRef]
21. Trisuwan, K.; Rukachaisirikul, V.; Sukpondma, Y.; Preedanon, S.; Phongpaichit, S.; Sakayaroj, J. Pyrone derivatives from the marine-derived fungus *Nigrospora* sp. PSU-F18. *Phytochemistry* **2009**, *70*, 554–557. [CrossRef]
22. Wu, S.H.; Chen, Y.W.; Shao, S.C.; Wang, L.D.; Yu, Y.; Li, Z.Y.; Yang, L.Y.; Li, S.L.; Huang, R. Two new solanapyrone analogues from the endophytic fungus *Nigrospora* sp. YB-141 of Azadirachta indica. *Chem. Biodivers* **2009**, *6*, 79–85. [CrossRef] [PubMed]
23. Mandi, A.; Kurtan, T. Applications of OR/ECD/VCD to the structure elucidation of natural products. *Nat. Prod. Rep.* **2019**, *36*, 889–918. [CrossRef] [PubMed]
24. Szabo, Z.; Paczal, A.; Kovacs, T.; Mandi, A.; Kotschy, A.; Kurtan, T. Synthesis and Vibrational Circular Dichroism Analysis of N-Heterocyclic Carbene Precursors Containing Remote Chirality Centers. *Int. J. Mol. Sci* **2022**, *23*, 3471. [CrossRef]
25. Atanasov, A.G.; Zotchev, S.B.; Dirsch, V.M.; Orhan, I.E.; Banach, M.; Rollinger, J.M.; Barreca, D.; Weckwerth, W.; Bauer, R.; Bayer, E.A.; et al. Natural products in drug discovery: Advances and opportunities. *Nat. Rev. Drug Discov.* **2021**, *20*, 200–216. [CrossRef] [PubMed]
26. Guo, H.-Y.; Jin, C.; Zhang, H.-M.; Jin, C.-M.; Shen, Q.-K.; Quan, Z.-S. Synthesis and Biological Evaluation of (+)-Usnic Acid Derivatives as Potential Anti-Toxoplasma gondii Agents. *J. Agric. Food Chem.* **2019**, *67*, 9630–9642. [CrossRef] [PubMed]
27. Jiménez-Romero, C.; Ortega-Barría, E.; Arnold, A.E.; Cubilla-Rios, L. Activity against *Plasmodium falciparum* of Lactones Isolated from the Endophytic Fungus *Xylaria* sp. *Pharm. Biol.* **2008**, *46*, 700–703. [CrossRef]
28. McMurry, L.M.; Oethinger, M.; Levy, S.B. Triclosan targets lipid synthesis. *Nature* **1998**, *394*, 531–532. [CrossRef]
29. McLeod, R.; Muench, S.P.; Rafferty, J.B.; Kyle, D.E.; Mui, E.J.; Kirisits, M.J.; Mack, D.G.; Roberts, C.W.; Samuel, B.U.; Lyons, R.E.; et al. Triclosan inhibits the growth of Plasmodium falciparum and Toxoplasma gondii by inhibition of apicomplexan Fab I. *Int. J. Parasitol.* **2001**, *31*, 109–113. [CrossRef]
30. Tipparaju, S.K.; Muench, S.P.; Mui, E.J.; Ruzheinikov, S.N.; Lu, J.Z.; Hutson, S.L.; Kirisits, M.J.; Prigge, S.T.; Roberts, C.W.; Henriquez, F.L.; et al. Identification and development of novel inhibitors of Toxoplasma gondii enoyl reductase. *J. Med. Chem.* **2010**, *53*, 6287–6300. [CrossRef]
31. Toki, S.; Ando, K.; Kawamoto, I.; Sano, H.; Yoshida, M.; Matsuda, Y. ES-242-2, -3, -4, -5, -6, -7, and -8, novel bioxanthracenes produced by *Verticillium* sp., which act on the N-methyl-D-aspartate receptor. *J. Antibiot.* **1992**, *45*, 1047–1054. [CrossRef]
32. Jaturapat, A.; Isaka, M.; Hywel-Jones, N.L.; Lertwerawat, Y.; Kamchonwongpaisan, S.; Kirtikara, K.; Tanticharoen, M.; Thebtaranonth, Y. Bioxanthracenes from the insect pathogenic fungus. Cordyceps pseudomilitaris BCC 1620. I. Taxonomy, fermentation, isolation and antimalarial activity. *J. Antibiot.* **2001**, *54*, 29–35. [CrossRef] [PubMed]
33. Komai, S.-I.; Hosoe, T.; Nozawa, K.; Okada, K.; de Campos Takaki, G.M.; Fukushima, K.; Miyaji, M.; Horie, Y.; Kawai, K.-I. Antifungal activity of pyranone and furanone derivatives, isolated from *Aspergillus* sp. IFM51759, against *Aspergillus fumigatus*. *MYCOTOXINS-TOKYO-* **2003**, *53*, 11–18. [CrossRef]
34. Krasnoff, S.B.; Gupta, S. Identification of the antibiotic phomalactone from the entomopathogenic fungusHirsutella thompsonii var. synnematosa. *J. Chem. Ecol.* **1994**, *20*, 293–302. [CrossRef] [PubMed]
35. Krivobok, S.; Thomasson, F.; Seigle-Murandi, F.; Steiman, R.; Bottex-Gauthier, C. 6-Allyl-5, 6-dihydro-5-hydroxypyran-2-one, a lactone produced by a new Drechslera species: Specified 1H and 13C NMR assignments, mutagenic and immunomodulating testings. *Die Pharm.* **1994**, *49*, 605–607.

36. Kumarihamy, M.; Ferreira, D.; Croom, E.M., Jr.; Sahu, R.; Tekwani, B.L.; Duke, S.O.; Khan, S.; Techen, N.; Nanayakkara, N.P.D. Antiplasmodial and Cytotoxic Cytochalasins from an Endophytic Fungus, *Nemania* sp. UM10M, Isolated from a Diseased *Torreya taxifolia* Leaf. *Molecules* **2019**, *24*, 777. [CrossRef]
37. Meier, D.; Hernandez, M.V.; van Geelen, L.; Muharini, R.; Proksch, P.; Bandow, J.E.; Kalscheuer, R. The plant-derived chalcone Xanthoangelol targets the membrane of Gram-positive bacteria. *Bioorg Med. Chem.* **2019**, *27*, 115151. [CrossRef]
38. Pfefferkorn, E.R.; Pfefferkorn, L.C. Specific Labeling of Intracellular Toxoplasma gondii with Uracil. *J. Protozool.* **1977**, *24*, 449–453. [CrossRef]
39. Mosmann, T. Rapid colorimetric assay for cellular growth and survival: Application to proliferation and cytotoxicity assays. *J. Immunol. Methods* **1983**, *65*, 55–63. [CrossRef]
40. Tamaoki, T.; Nomoto, H.; Takahashi, I.; Kato, Y.; Morimoto, M.; Tomita, F. Staurosporine, a potent inhibitor of phospholipid/Ca++dependent protein kinase. *Biochem. Biophys. Res. Commun.* **1986**, *135*, 397–402. [CrossRef]
41. Rehberg, N.; Akone, H.S.; Ioerger, T.R.; Erlenkamp, G.; Daletos, G.; Gohlke, H.; Proksch, P.; Kalscheuer, R. Chlorflavonin Targets Acetohydroxyacid Synthase Catalytic Subunit IlvB1 for Synergistic Killing of *Mycobacterium tuberculosis*. *ACS Infect. Dis.* **2018**, *4*, 123–134. [CrossRef]
42. MacroModel; Schrödinger LLC. 2015. Available online: http://www.schrodinger.com/MacroModel (accessed on 31 July 2022).
43. Frisch, M.J.; Trucks, G.W.; Schlegel, H.B.; Scuseria, G.E.; Robb, M.A.; Cheeseman, J.R.; Scalmani, V.; Barone, G.; Mennucci, B.; Petersson, G.A.; et al. *Gaussian 09 (Revision E.01)*; Gaussian, Inc.: Wallingford, CT, USA, 2013.
44. Stephens, P.J.; Harada, N. ECD cotton effect approximated by the Gaussian curve and other methods. *Chirality* **2009**, *22*, 229–233. [CrossRef] [PubMed]
45. Varetto, U. *Molekel 5.4*; Swiss National Supercomputing Centre: Manno, Switzerland, 2009.

Supporting Information

In Vitro Biological Activity of Natural Products from the Endophytic Fungus *Paraboeremia selaginellae* against *Toxoplasma gondii*

Authors

Flaminia Mazzone*, Viktor E. Simons*, Lasse van Geelen, Marian Frank, Attila Mándi, Tibor Kurtán, Klaus Pfeffer, Rainer Kalscheuer

*These authors contributed equally to this work

Supporting Information link

The following supporting information can be downloaded at:
https://www.mdpi.com/article/10.3390/antibiotics11091176/s1

GUID: 9C19E02F-F859-488B-A093-EDEAAC33DE8E

3.2 Fluorescent Indolo[3,2-*a*]phenazines against *Toxoplasma gondii*: Concise Sythesis by Gold-Catalyzed Cycloisomerization with 1,2-Silyl Migration and ipso Iodination Suzuki Sequence

Authors

Franziska K. Merkt, **Flaminia Mazzone**, Shabnam Shaneh Sazzadeh, Lorand Bonda, Larissa K. E. Hinz, Irina Gruber, Karin Buchholz, Christoph Janiak, Klaus Pfeffer, Thomas J.J. Müller.

Published in

Chemistry – Wiley

Impact factor

5.020 (2021)

DOI

10.1002/chem.202101391

Own contributions to this work

Overall: 30%

Conducted all of the following experiments:

- *Toxoplasma gondii* proliferation assays
- Cytotoxicity assays (MTT assays) in human fibroblasts Hs27

Other major contributions

Design of experiments, methodology, conduction of experiments, data analysis, manuscript preparation.

Chemistry–A European Journal

Full Paper
doi.org/10.1002/chem.202101391

Chemistry Europe
European Chemical Societies Publishing

Fluorescent Indolo[3,2-*a*]phenazines against *Toxoplasma gondii*: Concise Synthesis by Gold-Catalyzed Cycloisomerization with 1,2-Silyl Migration and *ipso*-Iodination Suzuki Sequence

Franziska K. Merkt,[a] Flaminia Mazzone,[b] Shabnam Shaneh Sazzadeh,[b] Lorand Bonda,[a] Larissa K. E. Hinz,[a] Irina Gruber,[c] Karin Buchholz,[b] Christoph Janiak,[c] Klaus Pfeffer,[b] and Thomas J. J. Müller*[a]

Dedicated to Prof. Dr. Ari M. P. Koskinen on the occasion of his 65th birthday

Abstract: A gold-catalyzed cycloisomerization of 2-indolyl-3-[(trimethylsilyl)ethynyl)]quinoxalines with concomitant 1,2-silyl shift forms 6-(trimethylsilyl)indolo[3,2-*a*]phenazines in moderate to excellent yield. These silylated heterocycles are readily transformed into 6-aryl-indolo[3,2-*a*]phenazines in moderate to good yield by one-pot *ipso*-iodination Suzuki coupling. The title compounds represent a novel type of tunable luminophore. Structure-property relationships for 6-aryl-indolo[3,2-*a*]phenazines obtained from Hammett correlations with σ_{p^+} substituent parameters indicate that emission maxima, Stokes shifts, and fluorescence quantum yields can be fine-tuned by the remote *para*-aryl substituent. Furthermore, indolo[3,2-*a*]phenazines were found to exhibit interesting activities against medically relevant pathogens such as the Apicomplexa parasite *Toxoplasma gondii* with an IC_{50} of up to 0.67 ± 0.13 μM. Thus, these compounds are promising candidates for novel anti-parasitic therapies.

Introduction

Indolo[3,2-*a*]phenazine (**1**; Figure 1) represents a highly interesting fused pentaheterocyclic structure consisting of the angular anellation of electron-rich indole to the electron-poor phenazine, which has not been deeply explored in its properties to date. By in silico docking studies indolo[3,2-*a*]phenazine **2** was identified as a novel inhibitor of NAD(P)H quinone oxidoreductase,[1] due to strong interaction with gene NQO1,

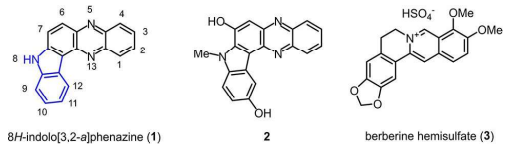

Figure 1. 8*H*-indolo[3,2-*a*]phenazine (**1**), a potentially potent anticancer agent **2** (from in silico docking studies), and berberine hemisulfate (**3**).

which can be responsible for the overexpression of tumor cells and inhibitors of this enzyme have been proposed as potent anticancer agents.[2] The pentacyclic structure with donor-acceptor separation additionally resembles to that of berberine hemisulfate (**3**), belonging to the protoberberine group of benzylisoquinoline alkaloids with considerable pharmacological applications in many different indications.[3] In particular, berberine and derivatives are considered as alternative treatment options against the parasite *Toxoplasma gondii*.[4]

T. gondii is an obligate intracellular parasite belonging to the phylum Apicomplexa, which includes known human pathogens such as the agent of tropical malaria *Plasmodium falciparum*, with which it shares significant biological similarities.[5] *T. gondii* is the causative agent of toxoplasmosis and is considered one of the world's most successful parasites due its ability to infect a wide range of warm-blooded vertebrate intermediate hosts, including humans.[6] It is estimated that one-third of the human population is chronically

[a] Dr. F. K. Merkt, L. Bonda, L. K. E. Hinz, Prof. Dr. T. J. J. Müller
Institut für Organische Chemie und Makromolekulare Chemie
Heinrich-Heine-Universität Düsseldorf
Universitätsstraße 1, 40225 Düsseldorf (Germany)
E-mail: ThomasJJ.Mueller@hhu.de

[b] F. Mazzone, Dr. S. S. Sazzadeh, K. Buchholz, Prof. Dr. K. Pfeffer
Institut für Medizinische Mikrobiologie und Krankenhaushygiene
Heinrich-Heine-Universität Düsseldorf
Universitätsstraße 1, 40225 Düsseldorf (Germany)

[c] Dr. I. Gruber, Prof. Dr. C. Janiak
Institut für Anorganische Chemie und Strukturchemie
Heinrich-Heine-Universität Düsseldorf
Universitätsstraße 1, 40225 Düsseldorf (Germany)

Supporting information for this article is available on the WWW under https://doi.org/10.1002/chem.202101391

© 2021 The Authors. Published by Wiley-VCH GmbH. This is an open access article under the terms of the Creative Commons Attribution Non-Commercial NoDerivs License, which permits use and distribution in any medium, provided the original work is properly cited, the use is non-commercial and no modifications or adaptations are made.

Chemistry–A European Journal
Full Paper
doi.org/10.1002/chem.202101391
Chemistry Europe
European Chemical Societies Publishing

infected with *T. gondii*[7] which is acquired mainly through two ways: by ingesting tissue cysts from raw or undercooked meat or by ingesting oocysts shed from feline hosts (the definitive hosts) with contaminated food or water.[8] In immunocompetent individuals, the infection with *T. gondii* is usually inapparent with minor or no symptoms, but it can be fatal in immunocompromised individuals due to reactivation of latent infections.[9] In addition, early maternal infection during pregnancy may result in fetal death, spontaneous abortion, and birth defects.[10] Treatments of acute toxoplasmosis are largely limited to antifolate therapy, based on the combination of pyrimethamine and sulfadiazine supplemented with folic acid. As the second-line treatments, the antibiotics co-trimoxazole and clindamycin are used.[11] These regimens have high rates of toxic side effects leading to discontinuation of therapy. Thus, there is need to develop well-tolerated and less or nontoxic treatments options to improve the care of patients with toxoplasmosis.[12]

While phenazines have found entry in various dyes, such as *induline*,[13] *neutral red*,[14] or *safranin T*,[13] their indolo-fused analogues have remained unknown as chromophores. In synthetic chemistry only very few syntheses have been reported so far (Scheme 1).

While the parent system **1** was already assessed in 1954 by Teuber and Staiger by cyclocondensation of 3*H*-carbazol-3,4(9*H*)-dione and *ortho*-phenylene diamine (Scheme 1A),[15] similarly to the Hinsberg synthesis of quinoxaline, the title compounds remained unexplored. Only a few years ago, the groups of Kurth and Haddadin presented an acid-catalyzed Friedländer synthesis with 2,3-dihydro-1*H*-cyclopenta[*b*]quinoxalinen-1-one and 2-aminobenzaldehyde furnishing a mixture of 8*H*-indolo[3,2-*a*]phenazine and quinolin[2,3-*c*]cyclopentadienone[2,3-*b*]quinoxaline, however, with 8*H*-indolo[3,2-*a*]phenazine as the minor product.[16] Recently, Kumar and Pal reported a general synthesis of indolo[3,2-*a*]phenazines in good yield by trifluoroacetic acid catalyzed cycloisomerization of indole-substituted 3-ethynylquinoxalines (Scheme 1B).[17] Interestingly, gold-catalyzed cycloisomerization of 3-ethynylquinoxalines was not reported in this study. Based upon our long standing experience in consecutive multicomponent syntheses of quinoxalines[18] and their photophysical properties,[18b–f,19] we envisioned that our multicomponent access to 3-ethynylquinoxalines provides an excellent basis for developing syntheses of specifically substituted 8*H*-indolo[3,2-*a*]phenazines in the sense of diversity-oriented level-2 transformations (Scheme 1C). Here, we report on a novel synthesis of 6-trimethylsilyl 8*H*-indolo[3,2-*a*]phenazines, their one-pot *ipso*-iodination-Suzuki coupling to 6-arylsubstituted 8*H*-indolo[3,2-*a*]phenazines, the photophysical characteristics of these novel systems as well as the biological testing of their activity against the parasite *T. gondii*.

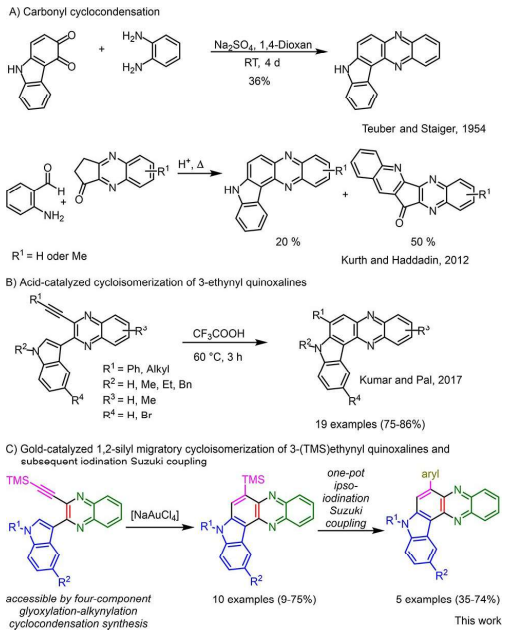

Scheme 1. Synthetic approaches to 8*H*-indolo[3,2-*a*]phenazines.

Results and Discussion

Synthesis and structure

In past years, we have disclosed several consecutive multicomponent syntheses of various 2-indolyl-3-[(trimethylsilyl)ethynyl)]quinoxalines based upon glyoxylation-alkynylation-cyclocondensation (GACC) or activation-alkynylation-cyclocondensation (AACC) strategies furnishing 3-ethynyl quinoxalines as key intermediates.[18b–f] To quickly provide suitable substrates for testing the cycloisomerization of 3-ethynyl quinoxalines to 8*H*-indolo[3,2-*a*]phenazines, we chose the GACC synthesis starting from various indoles (**4**), oxalylchloride (**5**), (trimethylsilyl)acetylene (**6**), and *ortho*-phenylenediamine (**7**) to give 2-indolyl-3-[(trimethylsilyl)ethynyl)]-quinoxalines **8** in good to excellent yield (Scheme 2).

With 3-[(trimethylsilyl)ethynyl)]quinoxaline **8a** and its desilyated congener 3-(ethynyl)quinoxaline **8l** in hand (compound **8l** was prepared from compound **8a** by desilylation with KF in MeOH[18e]), we set out with two model reactions to screen conditions for the cycloisomerization to indolo[3,2-*a*]phenazines **9a** and **9l** (Scheme 3, for details, see the Supporting Information, Chapter 3, and Table S2). Among several carbophilic Lewis acids[20] only auric chloride ($AuCl_3$) cycloisomerizes alkyne **8l** to indolo[3,2-*a*]phenazine **9l** in moderate yield and $NaAuCl_4$ proves to be an inefficient catalyst for this substrate. However, while for alkyne **8a** Kumar's and Pal's conditions (excess of trifluoroacetic acid)[17] failed $NaAuCl_4$ turns out to be the catalyst of choice in toluene at 80 °C for cycloisomerizing compound **8a** to indolo[3,2-*a*]phenazine **9a**. Most interestingly the cycloisomerization proceeds with concomitant 1,2-silyl migration.

© 2021 The Authors. Published by Wiley-VCH GmbH

Chemistry–A European Journal
Full Paper
doi.org/10.1002/chem.202101391
Chemistry Europe
European Chemical Societies Publishing

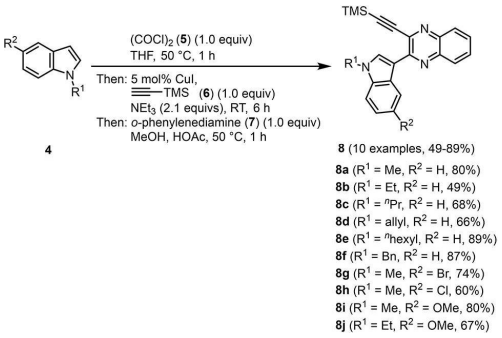

Scheme 2. Consecutive four-component GACC synthesis of 2-indolyl-3-[(trimethylsilyl)ethynyl)]quinoxalines **8**.

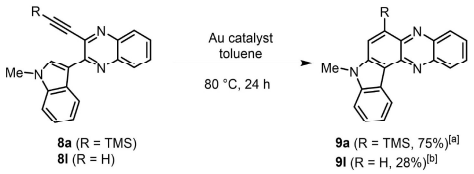

Scheme 3. Test reaction for the cycloisomerization of compounds **8** to indolo[3,2-*a*]phenazines **9**. [a] 2 mol% $NaAuCl_4$; [b] 40 mol% $AuCl_3$.

The structures of the cycloisomerization products **9a** and **9k** are unambiguously supported by extensive NMR spectroscopy, and in addition the structure of indolo[3,2-*a*]phenazine **9a** was corroborated by an X-ray structure analysis (Figure 2).[21] The crystal structure additionally reveals π-π interactions.

The gold-catalyzed cycloisomerization of 3-[(trimethylsilyl)-ethynyl)]quinoxaline **8a** to furnish 8-methyl-6-(trimethylsilyl)-indolo[3,2-*a*]phenazine (**9a**) represents a 6-*endo*-*dig* cyclization of the indole moiety and the alkyne unit with concomitant 1,2-silyl migration. Group IV elements (carbon, silicon, germanium, and tin) might undergo 1,2-migrations in alkyne-vinylidene isomerization via a gold carbenoid[22] and with related 1,2-silyl-shifts of the vinyl-gold species[23] as intermediates. To gain some mechanistic insight, we treated a selectively deuterated substrate **8k** with 100% deuterium at position 2 of the indole part to give 53% of indolo[3,2-*a*]phenazine **9k** containing 70% deuterium at position 7 (Scheme 4). Obviously not only the silyl group undergoes a 1,2-shift but also 1,2-hydride shift occurs in the sequence. This observation can be rationalized by two alternative scenarios. Assuming an Au carbenoid pathway (Scheme 4, pathway A) after coordination of the catalyst to the triple bond the 1,2-silyl shift generates gold vinylidene complex **10a**, which cyclizes to give carbenoid **11a** according to Gevorgyan's rationale.[22b] The subsequent 1,2-H(D) shift furnishes the zwitterion **12a** that produces the product upon deauration. Alternatively, pathway B (Scheme 4) commences with the intramolecular nucleophilic attack of the indole moiety at the Au-activated triple bond to give the cyclized zwitterionic vinyl-gold intermediate **13a** according to Fürstner's rationale.[23] The subsequent 1,2-H(D) shift first generates the β-silyl stabilized indoliminium intermediate **14a**, which then undergoes a 1,2-silyl shift maintaining the β-silyl cation stabilization in intermediate **15a**. Finally, deauration closes the catalytic

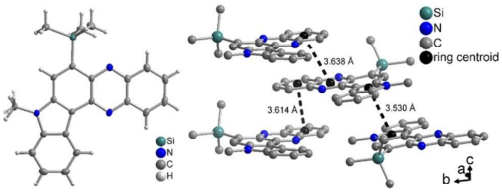

Figure 2. Left: Molecular structure of compound **9a** (thermal ellipsoids shown at the 50% probability level). Right: Section of the packing diagram of **9a** showing significant π-π interactions (labeled with their centroid–centroid distances; H atoms omitted for clarity). For further details, see Section 13 in the Supporting Information.

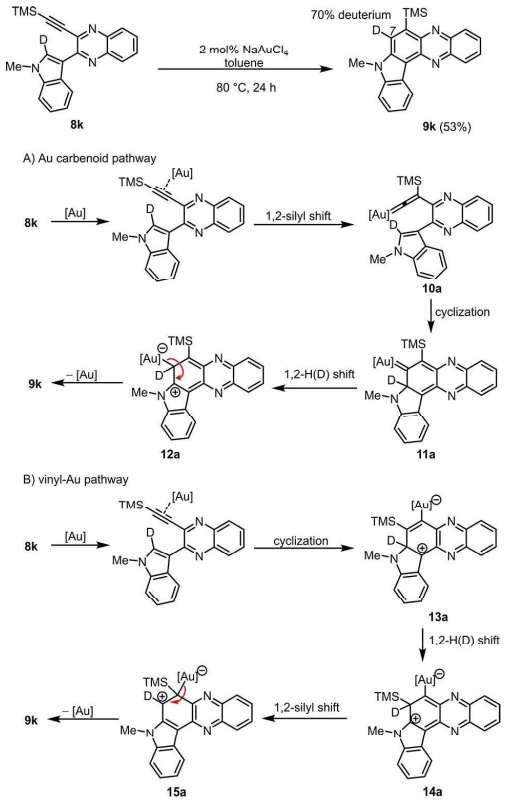

Scheme 4. Cycloisomerization with concomitant 1,2-silyl migration of selectively deuterated compound **8k** to give deuterated indolo[3,2-*a*] phenazine **9k** and two mechanistic scenarios.

© 2021 The Authors. Published by Wiley-VCH GmbH

Chemistry–A European Journal
Full Paper
doi.org/10.1002/chem.202101391
Chemistry Europe
European Chemical Societies Publishing

cycle and liberates the cycloisomerization product **9k**. At this stage, both scenarios are in agreement of the result of the control experiment with the deuterated substrate **8k**.

With optimal conditions for the cycloisomerization of 3-[(trimethylsilyl)ethynyl)]quinoxalines **8** with concomitant 1,2-silylmigration in hand (see the Supporting Information, Chapter 3, and Table S2, entry 15) the stage was set for screening scope and limitation with respect to the substitution pattern on the indole moiety. Upon heating 3-[(trimethylsilyl)ethynyl)] quinoxalines **8** in toluene to 80 °C for 24 h in the presence of catalytic amounts of sodium tetrachloroaurate various indolo [3,2-*a*]phenazines **9** were obtained in moderate to good yield (Scheme 5). The proposed structures were unambiguously supported by ^{1}H and ^{13}C NMR spectroscopy, mass spectrometry, IR spectroscopy, and combustion analysis. From the N-substitution pattern, it can be seen that increasing steric bulk (from Me over Et, Pr, allyl, and hexyl to benzyl) causes a significant decrease in yield. Substitution in position 11 of the indolo[3,2-*a*] phenazine allows access to the electronically diverse derivatives, that is, 11-halogen- or 11-methoxy-substituted molecules.

Silyl (hetero)arenes are perfectly suited for functionalization by *ipso*-substitution,[24] a particular case of electrophilic aromatic substitution operating by efficient stabilization of β-silyl cation σ-complex intermediates. This transformation was probed by converting compound **9a** into 6-iodo-indolo[3,2-*a*]phenazine **16** (Scheme 6), which could be favorably employed as a substrate in subsequent coupling reactions. The optimal conditions are the use of 1.7 equiv. of ICl in dichloromethane and after stirring at −78 °C for 5 min and at room temp for 30 min the 6-iodo-indolo[3,2-*a*]phenazine **16** was obtained after isolation in 76% yield (for details, see the Supporting Information, Chapters 5 and 6, Table S4).

For arylation of iodo indolo[3,2-*a*]phenazine **16** we selected the Suzuki coupling.[25] In a quick optimization study with *p*-methoxyphenylboronic acid (**17a**) as a coupling partner, optimal conditions were identified with potassium carbonate as a base in a 2:1 DMF/water mixture at 100 °C for 18.5 h giving 6-(*p*-anisyl)-8-methyl-indolo[3,2-*a*]phenazine (**18a**) after isolation by flash chromatography in 75% yield (Scheme 7, for details, see the Supporting Information, Chapter 7, Table S5, entry 3).

To establish a novel one-pot *ipso*-iodination-Suzuki synthesis of 6-(*p*-anisyl)-8-methyl-indolo[3,2-*a*]phenazine (**18a**) starting from indolo[3,2-*a*]phenazine **9a**, a ^{1}H NMR-based optimization study was launched (for details, see the Supporting Information Chapter 8, Table S6). It is noteworthy to mention that for the optimal conditions (see the Supporting Information, Table S6, entry 10) the yield of compound **18a** after chromatography with this novel one-pot sequence (72%) is considerably higher than the combined yield (57%) of stepwise *ipso*-iodination (76%, Scheme 6) and Suzuki coupling (75%, Scheme 7). Besides practicality, this also underlines the superiority, efficiency and efficacy of one-pot processes over stepwise transformations.

With these optimized conditions in hand the one-pot *ipso*-iodination-Suzuki coupling synthesis of 6-aryl-indolo[3,2-*a*] phenazines **18** was illustrated with indolo[3,2-*a*]phenazine **9a** and boronic acids/boroate **17** in seven examples to give the targeted products after chromatography in 35–74% yield (Scheme 8).

The proposed structures were unambiguously supported by ^{1}H and ^{13}C NMR spectroscopy, mass spectrometry, IR spectroscopy, and combustion analysis, and in addition the structure of 6-aryl-indolo[3,2-*a*]phenazine **18e** was corroborated by an X-ray structure analysis (Figure 3).[21] The structure elucidation of compound **18e** shows full planarity of the pentacyclic indolo [3,2-*a*]phenazine scaffold with a torsional angle of 54.3° of the *p*-cyanophenyl substituent with respect to the indolo[3,2-*a*] phenazine mean plane. The crystal structure additionally reveals distinct dipolar π-π interactions (as low as 3.38 Å).

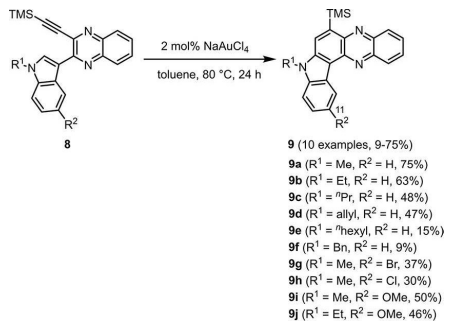

Scheme 5. Synthesis of indolo[3,2-*a*]phenazines **9** by gold-catalyzed cycloisomerization-1,2-silyl shift of 3-[(trimethylsilyl)ethynyl)]quinoxalines **8**.

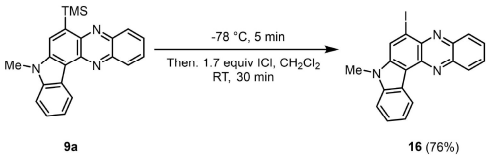

Scheme 6. Synthesis of 6-iodo-8-methyl-8*H*-indolo[3,2-*a*]phenazine (**16**) by electrophilic *ipso*-iodination with iodine monochloride.

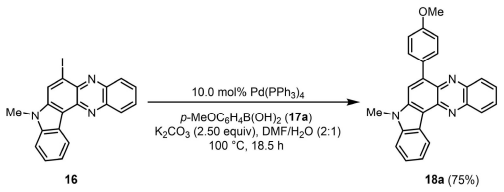

Scheme 7. Synthesis of compound **18a** by Suzuki coupling of 6-iodo-indolo [3,2-*a*]phenazine **16** with *p*-methoxyphenylboronic acid (**17a**).

© 2021 The Authors. Published by Wiley-VCH GmbH

Chemistry–A European Journal
Full Paper
doi.org/10.1002/chem.202101391
Chemistry Europe
European Chemical Societies Publishing

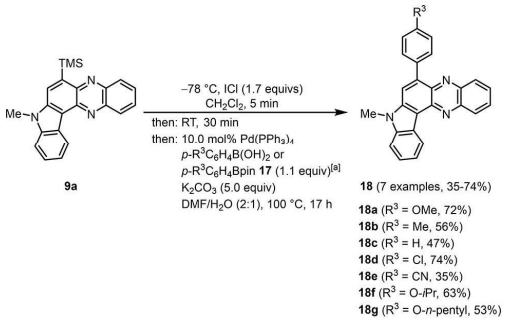

Scheme 8. One-pot *ipso*-iodination Suzuki coupling synthesis of 6-aryl-indolo[3,2-*a*]phenazines **18** from 6-(trimethylsilyl)indolo[3,2-*a*]phenazine **9a**.
[a] Boronate **17** was formed by bromine-lithium exchange and borylation, then the solution formed in situ was transferred to the iodo compound **16** formed in situ by syringe.

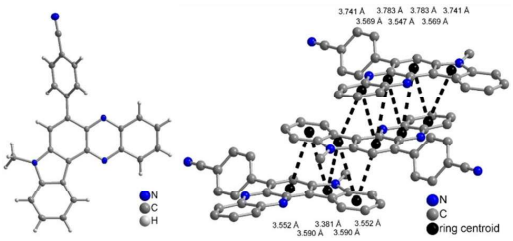

Figure 3. Left: Molecular structure of compound **18e** (thermal ellipsoids shown at the 50% probability level). Right: Section of the packing diagram of **18e** showing significant π-π interactions (with their centroid–centroid distances given; H atoms omitted for clarity). For further details, see Chapter 13 in the Supporting Information.

Photophysical properties and electronic structure of 6-substituted Indolo[3,2-*a*]phenazines

The luminescence of solutions of 6-substituted indolo[3,2-*a*]phenazines **9** and **18** in dichloromethane after excitation under a handheld UV lamp can be seen even by the naked eye (for a detailed analysis, see the Supporting Information, Chapter 11). The emission intensity of 6-(trimethylsilyl)indolo[3,2-*a*]phenazines **9** grows with the increasing electron-donor character of substituent R^3 to a maximum for the fluorescence quantum yield Φ_f of 28% (Table S8). The presence of two basic nitrogen atoms in 6-(trimethylsilyl)indolo[3,2-*a*]phenazine **9** suggests halochromicity of the underlying chromophore. Indeed, protonation of indolo[3,2-*a*]phenazine **9a** with trifluoroacetic acid (TFA) gives a pK_a of 5.60 for the protonated chromophore **9a-H$^+$**, that is, about four orders of magnitude less acidic than simple phenazine-H$^+$ ($pK_a = 1.2$).[26] Upon protonation the fluorescence signal is quenched (see the Supporting Information, Figure S57B).

As found for compounds **9**, 6-arylindolo[3,2-*a*]phenazines **18** display an increase of the fluorescence quantum yield Φ_f with increasing donor strength of substituent R^3 from 16% (R^3=CN) to 52% (R^3=OMe; see the Supporting Information, Table S9). Structure-property correlations based upon free energy linear relationships (LFER) with Hammett parameters σ^+ were unanimously found for absorption maxima $\lambda_{max,abs}$, emission maxima $\lambda_{max,em}$, Stokes shifts $\Delta\tilde{\nu}$ (see the Supporting Information, Figure S60A), and relative fluorescence quantum yields Φ_f (see the Supporting Information, Figure S60B). While only a minor polarity effect on the electronic ground state $\lambda_{max,abs}$ can be assigned from slope of the Hammett correlation, all effects reflecting the excited state ($\lambda_{max,em}$, $\Delta\tilde{\nu}$, Φ_f) strongly depend on stabilization of positive partial charges as supported by the σ_{p+} substituent parameter.

In addition, all compounds **18** are also luminescent in the solid state, however, with variable emission color (Figure 4). While compound **18a** (R^3=OMe) is yellow under the handheld UV-lamp, electron-deficient substituted **18e** (R^3=CN) is orange.

A deeper understanding of the electronic transitions in the absorption spectra of selected 6-aryl-8*H*-indolo[3,2-*a*]phenazines **18a**, **18c**, and **18e** was sought by calculating UV/Vis absorption spectra on the DFT level of theory using Gaussian09[27] with CAM–B3LYP[28] as a functional and the Pople 6-311+G(d,p) basis set.[29] Since the absorption spectra were recorded in dichloromethane solutions, the polarizable continuum model (PCM) with dichloromethane as a solvent was applied.[30]

The experimentally determined longest wavelength absorption bands are reasonably well reproduced by the TD-DFT calculations (see the Supporting Information, Table S10). As expected, the longest wavelength absorption bands of all three calculated 6-aryl-8*H*-indolo[3,2-*a*]phenazines originate from dominant contributions of HOMO–LUMO based transitions. In the HOMO of structures **18** the coefficient density is predominantly localized on the carbazole moiety of the indolo[3,2-*a*]phenazine, while the coefficient density in the LUMO almost exclusively is localized on the phenazine part (see the Supporting Information, Figure S61). This is in agreement with an angular charge transfer transition from donor (carbazole moiety) to acceptor (phenazine moiety).

Biological properties and activity against *T. gondii*

Indolo[3,2-*a*]phenazines are structurally related to the natural product berberine hemisulfate, which demonstrated anti-

Figure 4. Solid state fluorescence of 6-aryl-8*H*-indolo[3,2-*a*]phenazines **18a** (left) and **18e** (right; λ_{ex} = 365 nm).

© 2021 The Authors. Published by Wiley-VCH GmbH

Chemistry–A European Journal
Full Paper
doi.org/10.1002/chem.202101391
Chemistry Europe
European Chemical Societies Publishing

toxoplasma activity.[4] Also in this study, an IC_{50} was determined for berberine hemisulfate (**3**) of 0.94 μM against *T. gondii* ME49 (Table 1, for experimental details, see the Supporting Information). The aim of this part of the study was to investigate the anti-toxoplasma activities of seven selected synthetic indolo[3,2-*a*]phenazines (**9a**, **18a–d**, **18f–g**) and to compare them with the anti-*T. gondii* activity of berberine hemisulfate. To achieve this aim, *T. gondii* proliferation assays were performed.

Table 1. *In vitro* activity of the selected synthetic indolo[3,2-*a*]phenazines **9** and **18** and berberine hemisulfate (**3**) against the *T. gondii* strain ME49.[a]

Compound[a]	IC50 ± SD [μM]	Compound[a]	IC50 ± SD [μM]
3	0.94 ± 0.48	**18c**	0.73 ± 0.27
9a	1.68 ± 0.88	**18d**	2.38 ± 0.86
18a	2.58 ± 1.68	**18f**	3.3 ± 2.29
18b	0.67 ± 0.13	**18g**	3.07 ± 1.75

[a] Toxoplasma proliferation assays were performed to investigate the activity of the selected synthetic indolo[3,2-*a*]phenazines against the *T. gondii* ME49 strain. Hs27 cells in a monolayer were cultured in 96-well plates and infected with *T. gondii* (2×10^4). Infected cells were treated with indolo[3,2-*a*]phenazines **9**, **18a–d**, **18f–g**, and berberine hemisulfate (**3**) at the concentration range of 0.15–20.00 μM at 37 °C for 48 h. Afterwards, the assays were labelled with ^{3}H–U (5mCi, diluted 1:30) at 37 °C for 28–30 h. Based on the incorporation of ^{3}H–U into the parasite nucleic acid, the parasite growth was quantified. As controls, uninfected Hs27 cells without treatment, IFNγ pre-stimulated infected cells and only *T. gondii* infected cells were used (Figure S63). Three independent assays, in duplicates, were performed. IC_{50} values and mean ± SD of each compound of the three independent experiments are shown.

All the tested compounds showed an anti-toxoplasma activity with an IC_{50} lower than 3.5 μM (Table 1 and Figure S63). The comparison with the IC_{50} value of berberine hemisulfate (**3**; 0.94 μM), demonstrated that **18b** and **18c** were slightly more effective inhibitors than berberine hemisulfate (**3**) with IC_{50} values 0.67 and 0.73 μM, respectively.

In order to evaluate whether the selected synthetic indolo[3,2-*a*]phenazines inhibit cell mitochondria of the host cell, MTT assays were performed. The synthetic indolo[3,2-*a*]phenazines **9** and **18** were, at the concentration range between 0.15-5.00 μM, not cytotoxic to Hs27 cells comparable to berberine hemisulfate (**3**). The synthetic indolo[3,2-*a*]phenazines **9**, **18a–d**, and **18f–g** showed moderate toxicity against Hs27 fibroblasts at concentrations starting at 10.00 μM (Figure 5). These results indicate that indolo[3,2-*a*]phenazines are effective inhibitors of *T. gondii* proliferation, and compounds **18b** and **18c** were found to be most effective.

With regard to the anti-toxoplasma activity of indolo[3,2-*a*] phenazines, compounds containing TMS-, phenyl, *p*-chlorophenyl, *p*-tolyl, *p*-methoxyphenyl, *p*-pentoxyphenyl and *p*-isopropyloxyphenyl moieties bound to the phenazine core-structure inhibited *T. gondii* (type II, strain ME49) very efficiently with $IC_{50} < 3.5$ μM (Table 1). Interestingly, the activity of berberine hemisulfate (**3**) in this study was very comparable to the previous report by Kryvogorsky et al.[4] using the RH *T. gondii* strain. Thus, promising leads of this study (**18b** and **18c**) are well suited for developing modified and even more active analogues in the future.

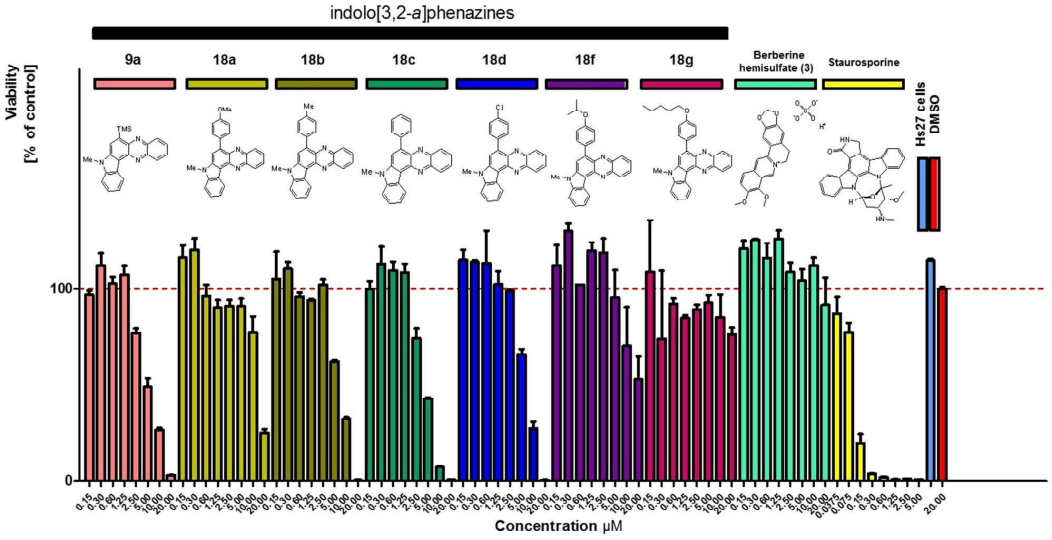

Figure 5. Effect of indolo[3,2-*a*]phenazines and **9** and **18** and berberine hemisulfate (**3**) on the metabolic activity of Hs27 cells. Hs27 cells were plated in 96-well plates and grown to confluence prior to incubation at 37 °C for 24 h with the selected synthetic indolo[3,2-*a*]phenazines and berberine hemisulfate at concentrations of 0.15–20.00 μM. The cultures were incubated with 10 μL of the 12 mM MTT stock solution for approximately 4 h. Afterwards, 100 μL of SDS dissolved in HCl was added to each well, and the plate was incubated again for 4 h at 37 °C. Finally, the absorbance was measured at 570 nm by spectrophotometry. Staurosporine (yellow) at concentrations of 0.0375–5.00 μL, Hs27 cells without treatment (blue) and DMSO (red) at the concentration of 20.00 μM were used as controls. Three independent assays were performed in duplicate; mean values ± SD are shown.

© 2021 The Authors. Published by Wiley-VCH GmbH

Chemistry–A European Journal
Full Paper
doi.org/10.1002/chem.202101391
Chemistry Europe
European Chemical Societies Publishing

Conclusion

In summary, by gold-catalyzed cycloisomerization with a concomitant 1,2-silyl shift, 6-(trimethylsilyl)indolo[3,2-*a*]phenazines have been synthesized in moderate to excellent yield from 2-indolyl-3-[(trimethylsilyl)ethynyl)]quinoxalines, which were obtained by consecutive four-component synthesis. This novel type of indolo[3,2-*a*]phenazine is readily transformed in a one-pot *ipso*-iodination Suzuki coupling synthesis into 6-aryl-indolo[3,2-*a*]phenazines in moderate to good yield. Indolo[3,2-*a*]phenazines, as rigid pentaheterocyclic scaffolds consisting of a fused carbazole (donor) and phenazine (acceptor) moieties, represent an interesting novel type of luminophore that can be tuned in their emission characteristics, such as emission color and fluorescence quantum yield, by substituent decoration. Structure-property relationships were obtained for 6-aryl-indolo[3,2-*a*]phenazines from Hammett correlations with σ_{p+} substituent parameters, indicating that excited state properties, such as emission maxima, Stokes shifts and fluorescence quantum yields, in particular are affected and tunable by the remote *para*-aryl substituent. Furthermore, none of the synthetic indolo[3,2-*a*]phenazines showed relevant cytotoxicity against Hs27 cells over the concentration range 0.15–5.00 μM. Phenyl- and *p*-tolyl-substituted derivatives possess an intriguing Toxoplasma inhibitory effect with IC_{50} values lower than berberine hemisulfate and therefore do not have a relevant effect on the metabolic activity of Hs27 cells. This establishes the phenyl and toluene moieties connected to the phenazine core-structure as suitable substituents, with more attractive structure-activity properties against *T. gondii* than the other synthetic indolo[3,2-*a*]phenazines tested in this study. Therefore, the next step to be considered is the in vivo testing of the lead indolo[3,2-*a*]phenazines for toxicity and activity against *T. gondii* infections.

Acknowledgements

This work was supported by the Deutsche Forschungsgemeinschaft (GRK 2158, Mu 1088/9-1) and the Fonds der Chemischen Industrie. Open access funding enabled and organized by Projekt DEAL.

Conflict of Interest

The authors declare no conflict of interest.

Keywords: bioactivity · cycloisomerization · heterocycles · iodination · multicomponent reactions · *Toxoplasma gondii*

[1] K. A. Nolan, D. J. Timson, I. J. Stratforda, R. A. Bryce, *Bioorg. Med. Chem. Lett.* **2006**, *16*, 6246–6254.
[2] a) J. Bian, X. Qian, B. Deng, X. Xu, X. Guo, Y. Wang, X. Li, H. Sun, Q. You, X. Zhang, *RSC Adv.* **2015**, *5*, 49471–49479; b) K. A. Scott, J. Barnes, R. C. Whitehead, I. J. Stratford, K. A. Nolan, *Biochem. Pharmacol.* **2011**, *81*, 355–363.
[3] For lead reviews on the pharmacological profile and applications of berberine, see, e.g., a) K. Zou, Z. Li, Y. Zhang, H.-y. Zhang, B. Li, W.-l. Zhu, J.-y. Shi, Q. Jia, Y.-m. Li, *Acta Pharmacol. Sin.* **2017**, *38*, 157–167; b) M. Tillhon, L. M. G. Ortiz, P. Lombardi, A. I. Scovassi, *Biochem. Pharmacol.* **2012**, *84*, 1260–1267; c) J. Tang, Y. Feng, S. Tsao, N. Wang, R. Curtain, Y. Wang, *J. Ethnopharmacol.* **2009**, *126*, 5–17; d) M. Imanshahidi, H. Hosseinzadeh, *Phytother. Res.* **2008**, *22*, 999–1012.
[4] B. Krivogorsky, J. A. Pernat, K. A. Douglas, N. J. Czerniecki, P. Grundt, *Bioorg. Med. Chem. Lett.* **2012**, *22*, 2980–2982.
[5] I. Tardieux, R. Ménard, *Traffic* **2008**, *9*, 627–635.
[6] J. P. Webster, *Parasites Vectors* **2010**, *3*, 112.
[7] G. Pappas, N. Roussos, M. E. Falagas, *Int. J. Parasitol.* **2009**, *39*, 1385–1394.
[8] J. C. Sepúlveda-Arias, J. E. Gómez-Marin, B. Bobić, C. A. Naranjo-Galvis, O. Djurković-Djaković, *Travel. Med. Infect. Dis.* **2014**, *12*, 592–601.
[9] L. Machala, P. Kodym, M. Malý, M. Geleneky, O. Beran, D. Jilich, *Epidemiol. Mikrobiol. Imunol.* **2015**, *64*, 59–65.
[10] A. Elbez-Rubinstein, D. Ajzenberg, M.-L. Dardé, R. Cohen, A. Dumètre, H. Yera, E. Gondon, J.-C. Janaud, P. Thulliez, *J. Infect. Dis.* **2009**, *199*, 280–285.
[11] H. B. Fung, H. L. Kirschenbaum, *Clin. Ther.* **1996**, *18*, 1037–1056.
[12] P. Alday, J. Doggett, *Drug Des. Dev. Ther.* **2017**, *11*, 273–293.
[13] H. Berneth, *Azine Dyes, Ullmann's Encyclopedia of Industrial Chemistry, Vol. 4*, Wiley-VCH, Weinheim, **2012**, pp 475–514.
[14] G. Repetto, A. del Peso, J. L. Zurita, *Nat. Protoc.* **2008**, *3*, 1125–1131.
[15] H.-J. Teuber, G. Staiger, *Chem. Ber.* **1954**, *87*, 1251–1253.
[16] T. A. Shoker, K. I. Ghattass, J. C. Fettinger, M. J. Kurth, M. J. Haddadin, *Org. Lett.* **2012**, *14*, 3704–3707.
[17] K. S. Kumar, B. Bhaskar, M. S. Ramulu, N. P. Kumar, M. A. Ashfaq, M. Pal, *Org. Biomol. Chem.* **2017**, *15*, 82–87.
[18] a) P. Niesobski, I. Santana Martínez, S. Kustosz, T. J. J. Müller, *Eur. J. Org. Chem.* **2019**, 5214–5218; b) F. K. Merkt, K. Pieper, M. Klopotowski, C. Janiak, T. J. J. Müller, *Chem. Eur. J.* **2019**, *25*, 9447–9455; c) F. K. Merkt, S. P. Höwedes, C. F. Gers-Panther, I. Gruber, C. Janiak, T. J. J. Müller, *Chem. Eur. J.* **2018**, *24*, 8114–8125; d) F. K. Merkt, T. J. J. Müller, *Sci. China Chem.* **2018**, *61*, 909–924; e) C. F. Gers-Panther, H. Fischer, J. Nordmann, T. Seiler, T. Behnke, C. Würth, W. Frank, U. Resch-Genger, T. J. J. Müller, *J. Org. Chem.* **2017**, *82*, 567–578; f) C. F. Gers, J. Nordmann, C. Kumru, W. Frank, T. J. J. Müller, *J. Org. Chem.* **2014**, *79*, 3296–3310.
[19] a) M. M. Lindic, M. Zajonz, C. Gers-Panther, T. J. J. Müller, M. Schmitt, *Spectrochim. Acta Part A* **2020**, *228*, 117574; b) N. Nirmalananthan, T. Behnke, K. Hoffmann, D. Kage, C. F. Gers-Panther, W. Frank, T. J. J. Müller, U. Resch-Genger, *J. Phys. Chem. C* **2018**, *122*, 11119–11127.
[20] For reviews on π-Lewis acids, see e.g. a) A. Fürstner, P. W. Davies, *Angew. Chem. Int. Ed.* **2007**, *46*, 3410–3449; *Angew. Chem.* **2007**, *119*, 3478–3519; *Angew. Chem.* **2007**, *119*, 3478–3519; *Angew. Chem. Int. Ed.* **2007**, *46*, 3410–3449; b) A. S. K. Hashmi, *Chem. Rev.* **2007**, *107*, 3180–3211; c) D. J. Gorin, D. Toste, *Nature* **2007**, *446*, 395–403.
[21] Deposition numbers 2061296 (for **9a**) and CCDC-2061297 (for **18e**) contain the supplementary crystallographic data for this paper. These data are provided free of charge by the joint Cambridge Crystallographic Data Centre and Fachinformationszentrum Karlsruhe Access Structures service.
[22] a) I. V. Seregin, V. Gevorgyan, *J. Am. Chem. Soc.* **2006**, *128*, 12050–12051; b) I. Nakamura, T. Sato, M. Terada, Y. Yamamoto, *Org. Lett.* **2007**, *9*, 4081–4083; c) Y. Xia, A. S. Dudnik, Y. Li, V. Gevorgyan, *Org. Lett.* **2010**, *12*, 5538–5541.
[23] V. Mamane, P. Hannen, A. Fürstner, *Chem. Eur. J.* **2004**, *10*, 4556–4575.
[24] For selected reviews, see e.g. a) S. M. Bonesi, M. Fagnoni, *Chem. Eur. J.* **2010**, *16*, 13572–13589; b) B. A. Keay, *Chem. Soc. Rev.* **1999**, *28*, 209–215; c) T. H. Chan, I. Fleming, *Synthesis* **1969**, 761–786; d) B. Bennetau, J. Dunogues, *Synlett* **1993**, 171–176.
[25] For selected reviews on Suzuki coupling, see, e.g., a) A. Suzuki, *Angew. Chem. Int. Ed.* **2011**, *50*, 6722–6737; *Angew. Chem.* **2011**, *123*, 6854–6869; *Angew. Chem.* **2011**, *123*, 6854–6869; *Angew. Chem. Int. Ed.* **2011**, *50*, 6722–6737; b) H. Doucet, *Eur. J. Org. Chem.* **2008**, 2013–2030; c) N. Miyaura, A. Suzuki, *Chem. Rev.* **1995**, *95*, 2457–2483.
[26] U. Urleb, S. Gobec, *Product Class 16: Phenazines, Science of Synthesis, Vol. 16*, Thieme, Stuttgart, **2004**, pp 913–943.
[27] M. J. Frisch, G. W. Trucks, H. B. Schlegel, G. E. Scuseria, M. A. Robb, J. R. Cheeseman, G. Scalmani, V. Barone, B. Mennucci, G. A. Petersson, H. Nakatsuji, M. Caricato, X. Li, H. P. Hratchian, A. F. Izmaylov, J. Bloino, G. Zheng, J. L. Sonnenberg, M. Hada, M. Ehara, K. Toyota, R. Fukuda, J. Hasegawa, M. Ishida, T. Nakajima, Y. Honda, O. Kitao, H. Nakai, T. Vreven, J. A. Montgomery, Jr., J. E. Peralta, F. Ogliaro, M. Bearpark, J. J. Heyd, E.

© 2021 The Authors. Published by Wiley-VCH GmbH

Chemistry–A European Journal
Full Paper
doi.org/10.1002/chem.202101391
Chemistry Europe
European Chemical Societies Publishing

Brothers, K. N. Kudin, V. N. Staroverov, R. Kobayashi, J. Normand, K. Raghavachari, A. Rendell, J. C. Burant, S. S. Iyengar, J. Tomasi, M. Cossi, N. Rega, J. M. Millam, M. Klene, J. E. Knox, J. B. Cross, V. Bakken, C. Adamo, J. Jaramillo, R. Gomperts, R. E. Stratmann, O. Yazyev, A. J. Austin, R. Cammi, C. Pomelli, J. W. Ochterski, R. L. Martin, K. Morokuma, V. G. Zakrzewski, G. A. Voth, P. Salvador, J. J. Dannenberg, S. Dapprich, A. D. Daniels, O. Farkas, J. B. Foresman, J. V. Ortiz, J. Cioslowski, D. J. Fox, *Gaussian 09 (Revision A.02)* Gaussian, Inc., Wallingford CT, **2009**.

[28] a) C. Lee, W. Yang, R. G. Parr, *Phys. Rev. B* **1988**, *37*, 785–789; b) A. D. Becke, *J. Chem. Phys.* **1993**, *98*, 1372–1377; c) A. D. Becke, *J. Chem. Phys.* **1993**, *98*, 5648–5652; d) K. Kim, K. D. Jordan, *J. Phys. Chem.* **1994**, *98*, 10089–10094; e) P. J. Stephens, F. J. Devlin, C. F. Chabalowski, M. J. Frisch, *J. Phys. Chem.* **1994**, *98*, 11623–11627.

[29] R. Krishnan, J. S. Binkley, R. Seeger, J. A. Pople, *J. Chem. Phys.* **1980**, *72*, 650–654.

[30] G. Scalmani, M. J. Frisch, *J. Chem. Phys.* **2010**, *132*, 114110.

Manuscript received: April 18, 2021
Accepted manuscript online: April 21, 2021
Version of record online: May 27, 2021

© 2021 The Authors. Published by Wiley-VCH GmbH

Supporting Information

Fluorescent Indolo[3,2-*a*]phenazines against *Toxoplasma gondii*: Concise Sythesis by Gold-Catalyzed Cycloisomerization with 1,2-Silyl Migration and ipso Iodination Suzuki Sequence

Authors

Franziska K. Merkt, **Flaminia Mazzone**, Shabnam Shaneh Sazzadeh, Lorand Bonda, Larissa K. E. Hinz, Irina Gruber, Karin Buchholz, Christoph Janiak, Klaus Pfeffer, Thomas J.J. Müller.

Supporting Information link

https://chemistry-europe.onlinelibrary.wiley.com/action/downloadSupplement?doi=10.1002%2Fchem.202101391&file=chem202101391-sup-0001-misc_information.pdf

GUID: 8DE52C48-4F34-40B1-ADB1-0D4FF40038FA

3.2.1 Indolo[3,2-*a*]phenazines: Unpublished data

Manuscript in preparation. Submission expected: 2024

The second cohort of indolo[3,2-*a*]phenazines

Indolo[3,2-*a*]phenazines investigated in chapter 3.2 exhibited relevant cytotoxic effect on human fibroblasts (Hs27) at the concentration of 5 μM, suggesting a small therapeutic window and lack of selectivity. Moreover, certain compounds presented limited solubility in water, underscoring the necessity of novel derivatives with enhanced chemical and biological profiles. Thus, it was commenced a systematic approach on the derivatization on the indolo[3,2-*a*]phenazine scaffold in positions 6 and 11 with a variety of substituents, possessing either electron-withdrawing or electron-donating capabilities. In total, fifteen novel derivatives (**Figure 8**) were synthesised. All the compounds were employed for the evaluation of their activity against *T. gondii* and their cytotoxic effect on *T. gondii* host cells (Hs27 fibroblasts).

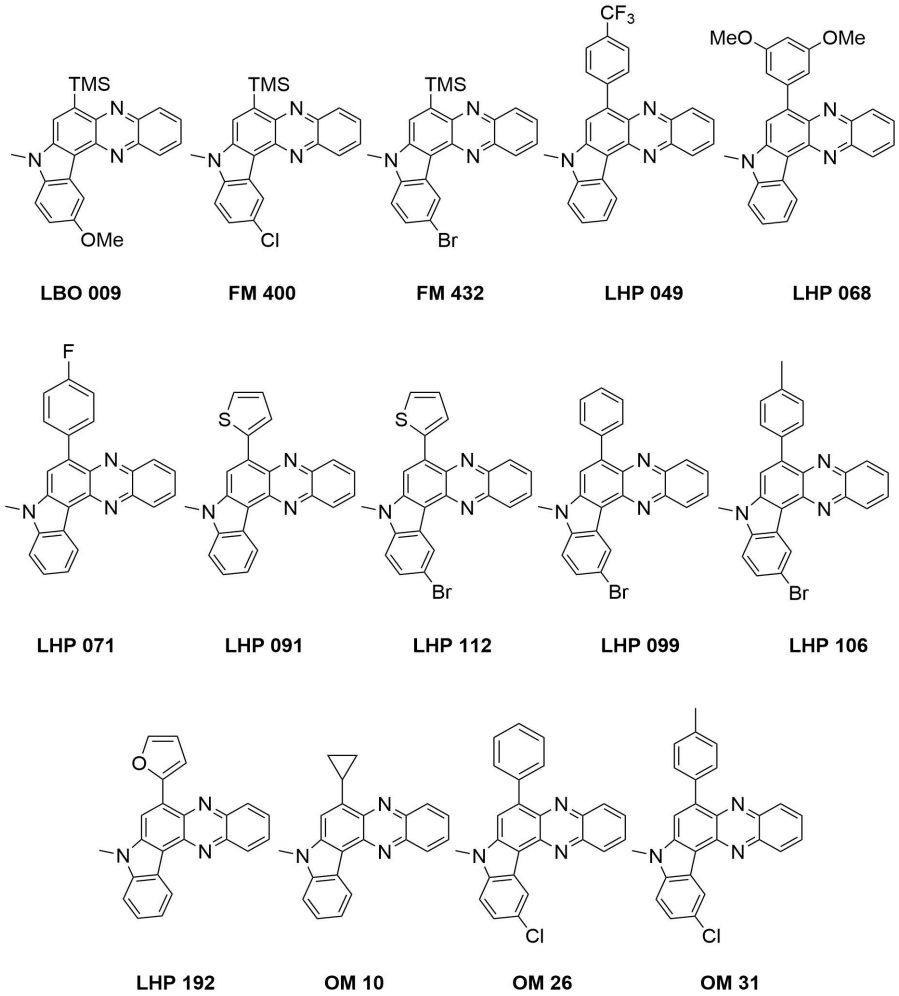

Figure 8: Second cohort of indolo[3,2-*a*]phenazines.

Chemical structures are shown. Molecules were synthesised by Larissa K.E Hinz.

Anti-*T. gondii* proliferation assay

The novel indolo[3,2-*a*]phenazines were tested against *T. gondii* ME49 proliferation using the [^{3}H]-uracil incorporation assay detailed in the Materials and Method section of chapter 3.2. All compounds showed potent activity against *T. gondii*, except of the compounds **FM 400**, **FM 432**, and **OM 31**, they showed an IC_{50} value higher than 2 μM (**Figure 9** and **Table 1**).

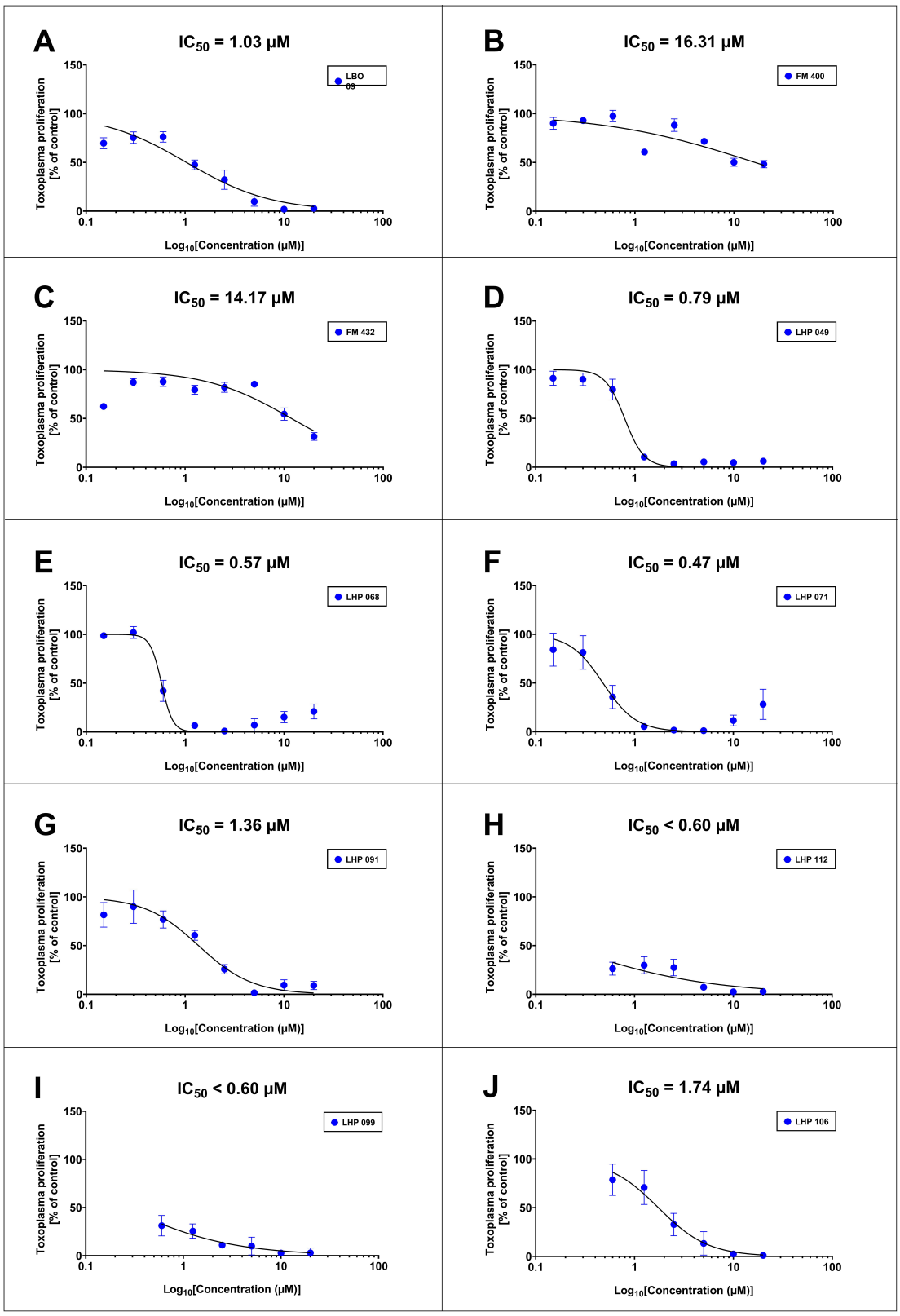
A
IC50 = 1.03 µM
LBO 09
B
IC50 = 16.31 µM
FM 400
C
IC50 = 14.17 µM
FM 432
D
IC50 = 0.79 µM
LHP 049
E
IC50 = 0.57 µM
LHP 068
F
IC50 = 0.47 µM
LHP 071
G
IC50 = 1.36 µM
LHP 091
H
IC50 < 0.60 µM
LHP 112
I
IC50 < 0.60 µM
LHP 099
J
IC50 = 1.74 µM
LHP 106
Toxoplasma proliferation [% of control]
Log10[Concentration (µM)]
150
100
50
0
0.1
1
10
100

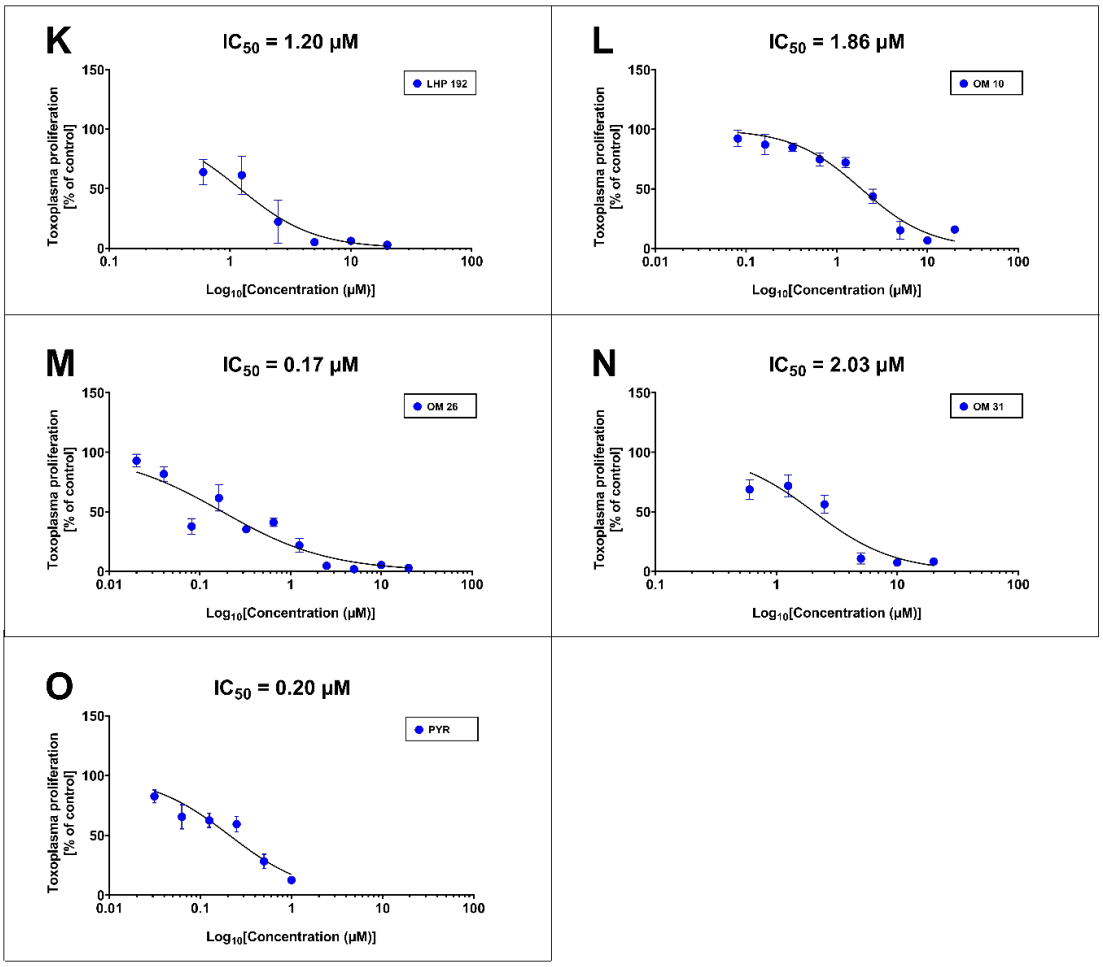

Figure 9: Anti-toxoplasma activity of the novel investigated indolo[3,2-*a*]phenazines

The inhibitory activities of **LBO 09** (**A**), **FM 400** (**B**), **FM 432** (**C**), **LHP 049** (**D**), **LHP 068** (**E**), **LHP 071** (**F**), **LHP 091** (**G**), **LHP 112** (**H**), **LHP 099** (**I**), **LHP 106** (**J**), **LHP 192** (**K**), **OM 10** (**L**), **OM 26** (**M**), **OM 31** (**N**), **Pyrimethamine** (**O**), were determined by the *T. gondii in vitro* inhibition assay via [^{3}H]-uracil incorporation into the RNA of the parasite. Data shown are from the means of three independent experiments each performed in duplicate (n = 6) ± SEM. IC_{50} values of each compound are shown.

Cytotoxicity assay

Following the evaluation of their anti-toxoplasma capacity, I conducted the investigation of their cytotoxic effect on human fibroblasts (Hs27) which served as host cells in the proliferation assay, aiming to evaluate the selectivity of their activity. The experiments were conducted as reported in the Material and Method section in chapter 3.2. The investigated compounds showed a diverse array of outcomes: Compounds **LBO 009**, **LHP 068**, **LHP 071**, **LHP 112**, **LHP 099**, **LHP 106** and **OM 26** showed high cytotoxic rates with CC_{50} values lower that 10 µM; compounds LH 049 and OM 31 presented a medium cytotoxicity lower than 20 µM; and compounds FM 400, FM 432, LHP 091, LHP 192, OM 10 showed low or no cytotoxic effects (**Figure 10** and **Table 1**).

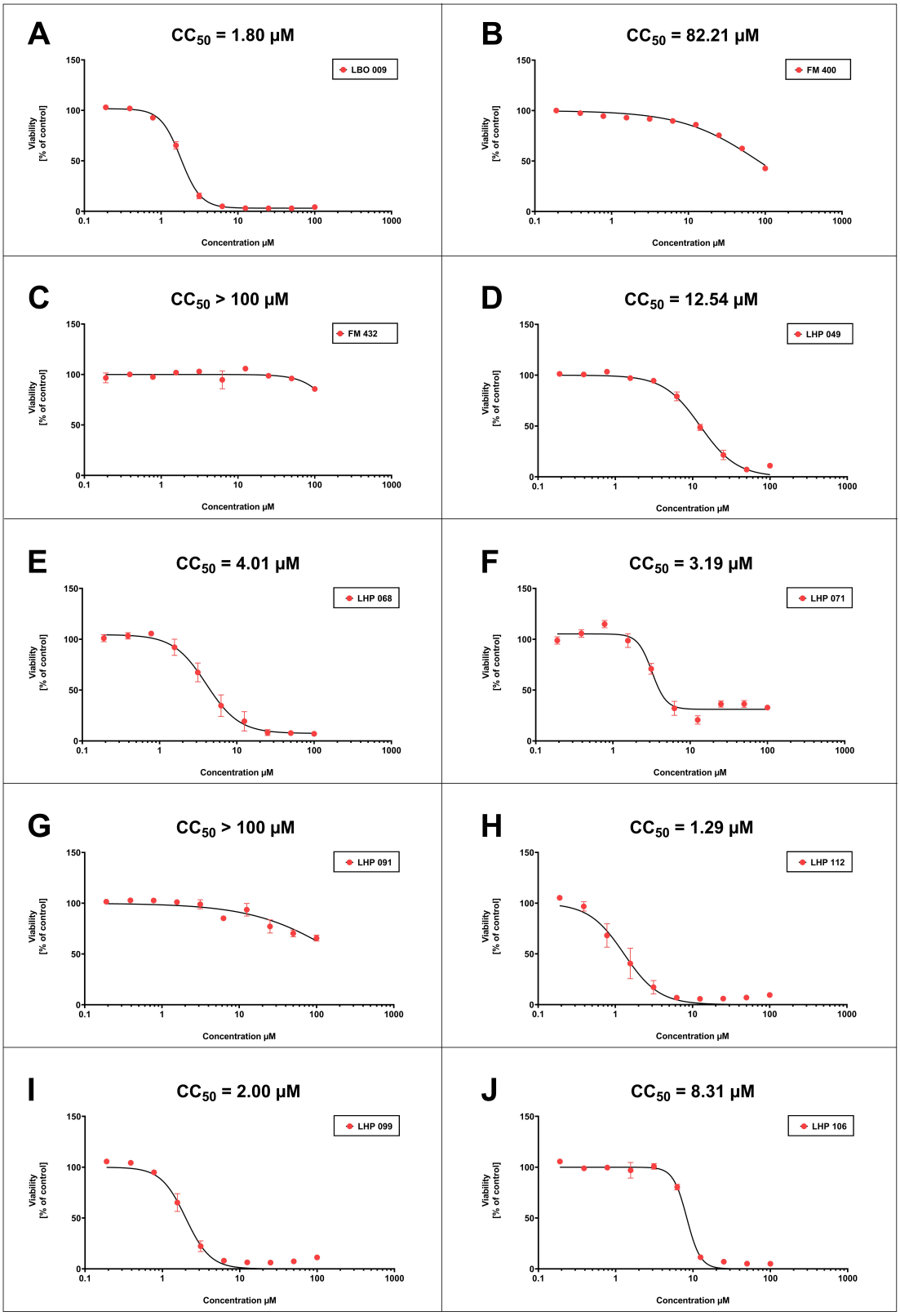
A
CC50 = 1.80 µM
LBO 009
B
CC50 = 82.21 µM
FM 400
C
CC50 > 100 µM
FM 432
D
CC50 = 12.54 µM
LHP 049
E
CC50 = 4.01 µM
LHP 068
F
CC50 = 3.19 µM
LHP 071
G
CC50 > 100 µM
LHP 091
H
CC50 = 1.29 µM
LHP 112
I
CC50 = 2.00 µM
LHP 099
J
CC50 = 8.31 µM
LHP 106
Viability [% of control]
Concentration µM
150
100
50
0
0.1
1
10
100
1000

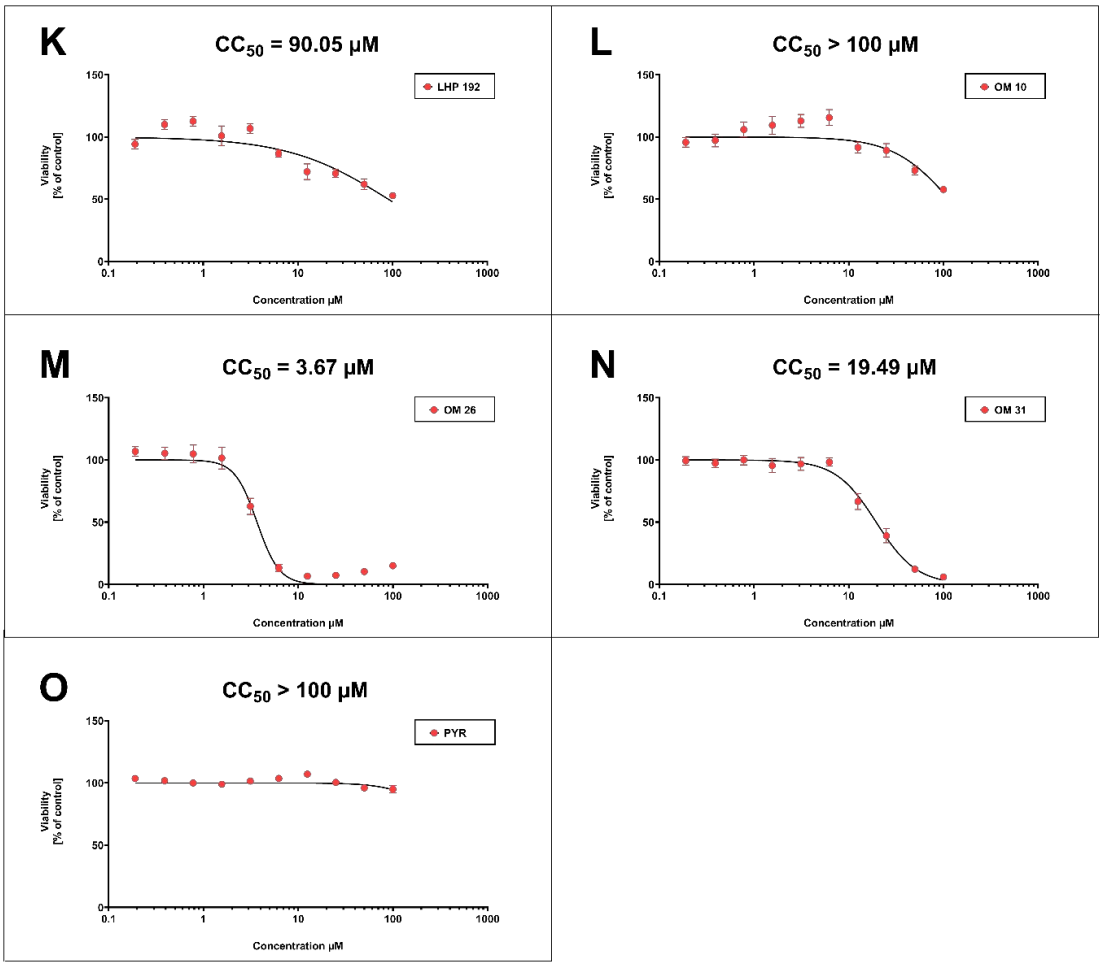

Figure 10: Effect of the novel investigated indolo[3,2-*a*]phenazines on the metabolic activity of human fibroblasts Hs27

Cytotoxic effect of **LBO 09** (**A**); **FM 400** (**B**); **FM 432** (**C**); **LHP 049** (**D**); **LHP 068** (**E**); **LHP 071** (**F**); **LHP 091** (**G**); **LHP 112** (**H**); **LHP 099** (**I**); **LHP 106** (**J**); **LHP 192** (**K**); **OM 10** (**L**); **OM 26** (**M**); **OM 31** (**N**); **Pyrimethamine** (**O**) against human cell lines Hs27 as determined by MTT assay. 100% growth control DMSO, 0% growth control staurosporine. Values shown in the figures represent the means of three independent experiments each done in duplicate (n = 6) ± SEM.

Compound	IC_{50} ± S.D. (µM)	CC_{50} ± S.D. (µM)
LBO 09	1.03 ± 0.18	1.80 ± 0.12
FM 400	16.31 ± 0.86	82.21 ± 3.63
FM 432	14.17 ± 3.46	> 100
LHP 049	0.79 ± 0.20	12.54 ± 2.77
LHP 068	0.57 ± 0.19	4.01 ± 3.43
LHP 071	0.47 ± 0.31	3.19 ± 0.66
LHP 091	1.36 ± 0.68	> 100
LHP 112	< 0.60	1.29 ± 1.08
LHP 099	< 0.60	2.00 ± 0.62
LHP 106	1.74 ± 0.51	8.31 ± 0.46
LHP 192	1.20 ± 0.47	90.05 ± 20.20
OM 10	1.86 ± 0.65	> 100
OM 26	0.17 ± 0.13	3.67 ± 0.65
OM 31	2.03 ± 1.39	19.49 ± 6.07
Pyrimethamine	0.20 ± 0.06	> 100

Table 1: Indolo[3,2-*a*]phenazine derivates: *in vitro* activity against *T. gondii* ME49 tachyzoites and cytotoxicity on human fibroblasts Hs27 of the investigated compounds

Values shown in the table represent the means of three independent experiments each done in duplicate (n = 6) ± S.D.

3.3 Modular Approach for the Synthesis and Bioactivity Profiling of 8,8´-Biflavones

Authors

Moritz K.T. Klischan, **Flaminia Mazzone***, Lena Berning*, Julian Greb*, Max Schlamkow, Mona Haase, Wolfgang Frey, Björn Stork, Klaus Pfeffer, Jörg Pietruszka.

*These authors share the second authorship

Published in

ACS Omega – American Chemical Society

Impact factor

4.1 (2022)

DOI

https://doi.org/10.1021/acsomega.3c06503

Own contributions to this work

Overall: 25%

Conducted all of the following experiments:

- *Toxoplasma gondii* proliferation assays
- Cytotoxicity assays (MTT assays) in human fibroblasts Hs27

Other major contributions

Design of experiments, methodology, conduction of experiments, data analysis, manuscript preparation.

ACS OMEGA

Open Access
This article is licensed under CC-BY-NC-ND 4.0

http://pubs.acs.org/journal/acsodf
Article

Modular Approach for the Synthesis and Bioactivity Profiling of 8,8′-Biflavones

Moritz K. T. Klischan, Flaminia Mazzone,[#] Lena Berning,[#] Julian Greb,[#] Max Schlamkow, Mona Haase, Wolfgang Frey, Björn Stork, Klaus Pfeffer, and Jörg Pietruszka*

Cite This: *ACS Omega* 2023, 8, 41816−41834

Read Online

ACCESS | Metrics & More | Article Recommendations | Supporting Information

ABSTRACT: In this work, we report the scalable and modular synthesis of a library of 55 monomeric and dimeric flavonoids including 14 8,8′-biflavones. The sterically demanding tetra-*ortho*-substituted axis of an acetophenone dimer key intermediate was constructed in a regioselective manner using Fe-mediated oxidative coupling. This step was systematically optimized and performed on up to multigram scale. The biological activities of this compound library were evaluated, including cytotoxicity against healthy and malignant human cell lines, antimicrobial activity against the apicomplexan parasite *Toxoplasma gondii*, and antioxidant capacity. A marked increase in activity for the 8,8′-dimeric structures compared to that of their monomeric counterparts was observed. Several biflavones were identified with high selectivity indices (low cytotoxicity and high antiprotozoal activity), showing that this class of natural products may serve as lead structures for further investigations.

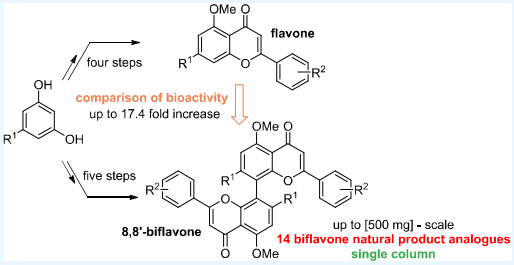

Downloaded via 109.42.179.195 on December 7, 2023 at 12:14:27 (UTC).
See https://pubs.acs.org/sharingguidelines for options on how to legitimately share published articles.

■ INTRODUCTION

Biflavones are naturally occurring biaryl-based compounds present among a range of gymnosperms.[1−4] First isolated in 1966 from *Cupressus torulosa* where its name is derived from,[1] the naturally occurring 8,8′-biflavone cupressuflavone (CUF) was subsequently also isolated from plants of the genus *Araucaria cunninghamii*.[5] So far, very few structural modifications with the exception of glycosylations have been observed in nature.[6] While biological activities of non-C_2-symmetrical biflavones are reported comprehensively in the literature (Figure 1A),[7−13] 8,8′-biflavones are a more elusive subclass of flavonoid natural products. CUF has thus far only been investigated in some limited capacity regarding pharmacological effects.[14−19]

In many cases, dimeric natural products show higher activities than their monomeric counterparts.[20−22] Apigenin—the monomeric unit of CUF—exerts similar activities in some cases;[19] in others, they are exclusively found for CUF,[23] highlighting the importance of comparing the activity of dimers to monomers. Additionally, 8,8′-biflavones can also, in some cases, be thought of as structurally simplified analogues of polyketides such as gonytolid A as was proposed and successfully shown by Kikuchi et al. in their synthesis of Me,Me′-CUF (Figure 1B).[24] This exemplifies a key strategy in the natural product-inspired drug design by simplifying complex natural structures to leverage the ease of synthesis but retain bioactivity.[25] Further, the merging of spherical shapes of *ortho*-substituted-biaryl-based natural products[26] with a biologically relevant flavone scaffold[27] qualifies this compound class as potent drug candidates.

Total syntheses of CUF are established since the late 1960s via different methods.[28−34] However, only singular examples of 8,8′-biflavones were synthesized to this date, showing the lack of a systematic and diversity-oriented approach (Figure 1B). The construction of these sterically demanding tetra-*ortho*-substituted biaryls poses a synthetic challenge.[35,36] Syntheses of these biaryl-based natural products often suffer from a narrow substrate scope involving the coupling of highly functionalized monomers[37,38] or involve multistep functionalization or coupling under harsh reaction conditions.[39−42] We herein report the first modular synthesis of a dedicated library of 8,8′-biflavones (Figure 1C) and the systematic investigation of their biological activity.

■ RESULTS AND DISCUSSION

To ensure scalability, which is highly desirable in natural product synthesis,[43] a synthesis route was chosen that allowed for the diversification of target structures and isolation by recrystallization. We chose the protocol developed by Li et al.

Received: August 30, 2023
Revised: September 20, 2023
Accepted: September 25, 2023
Published: October 27, 2023

ACS Publications
© 2023 The Authors. Published by American Chemical Society

https://doi.org/10.1021/acsomega.3c06503
ACS Omega 2023, 8, 41816−41834

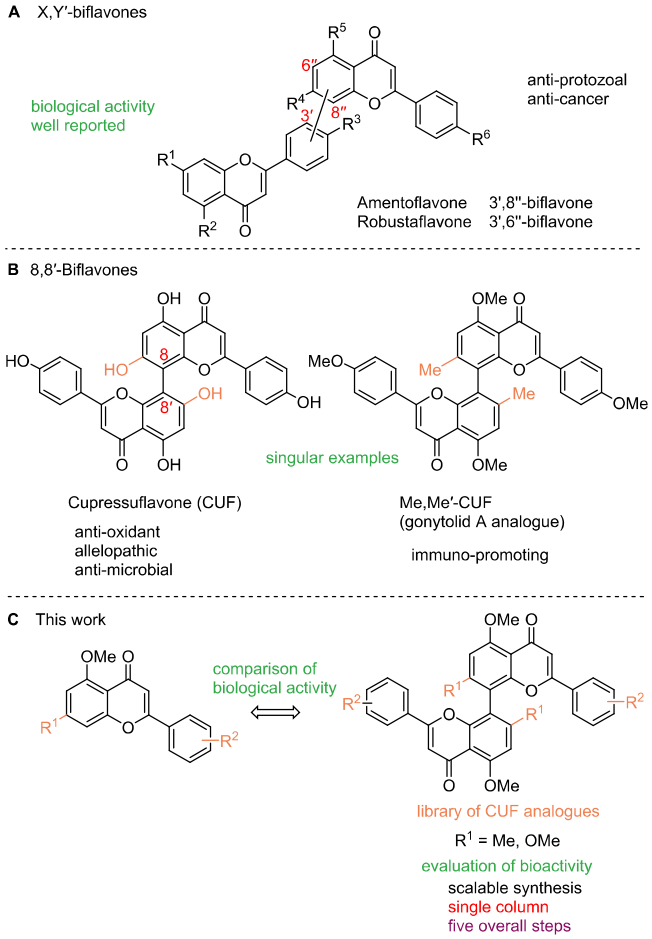

Figure 1. Biflavones as bioactive natural products with 8,8′-biflavones as a subclass.

as the basis for our investigations.[30] Starting from commercially available phenols **1a** and **1b**, all monomeric and dimeric target compounds should be accessible. After acylation to acetophenones **2**, the key intermediates **3** and **4** should be accessible: while acetophenones **3a** and **3b** will be available based on the modified literature-known procedures (Scheme 1),[30,44,45] the acetophenone dimers **4a** and **4b** were to be synthesized by the oxidative coupling without the involvement of toxicologically relevant transition metals. Finally, the Claisen−Schmidt condensation using aldehydes **5** provides chalcones **6** and bichalcones **7**. Subsequent I_2-catalyzed oxidation to synthesize flavones **8** and biflavones **9** was to be conducted. A variety of aldehydes were chosen to obtain the natural substitution pattern of CUF in addition to various more electron-rich and electron-deficient 8,8′-biflavones. Overall, a multigram scale synthesis route for the key intermediates **4** is outlined that avoids the use of column purification.

We initiated our studies with the synthesis of the acetophenone starting materials **3a** and **3b**, employed for both the oxidative coupling and the synthesis of the monomers. Acetylation and subsequent selective monomethylation of commercially available phenols **1a** and **1b** proceeded smoothly on decagram-scale, with yields of 74% (**3a**) and 70% (**3b**) over two steps, respectively (Scheme 2).

Starting from acetophenones **3a** and **3b**, the corresponding chalcone monomers **6** were synthesized via the typical Claisen−Schmidt condensations under alkaline conditions in ethanol with seven different benzaldehyde derivatives **5a−g** (Scheme 2). In some cases, conversions were incomplete. This was mitigated by the addition of an additional 0.6 equiv of the corresponding aldehyde after 6 h, which led to full conversion overnight. With the synthesis of the chalcones **6** in place, we continued with the synthesis of the target flavone monomers **8**. Following literature-known conditions, the oxidative cyclization using catalytic amounts of I_2 in DMSO proceeded smoothly.[46] All flavones were obtained in yields ranging from 36 to 93%. Thus, starting from phenols **1a** and **1b**, the procedure yielded 14 monomeric flavones **8aa−g** and **8ba−g**

https://doi.org/10.1021/acsomega.3c06503
ACS Omega 2023, 8, 41816−41834

Scheme 1. Retrosynthesis of Flavones and Biflavones Starting from Commercially Available Phenols 1 via the Key Intermediates 4

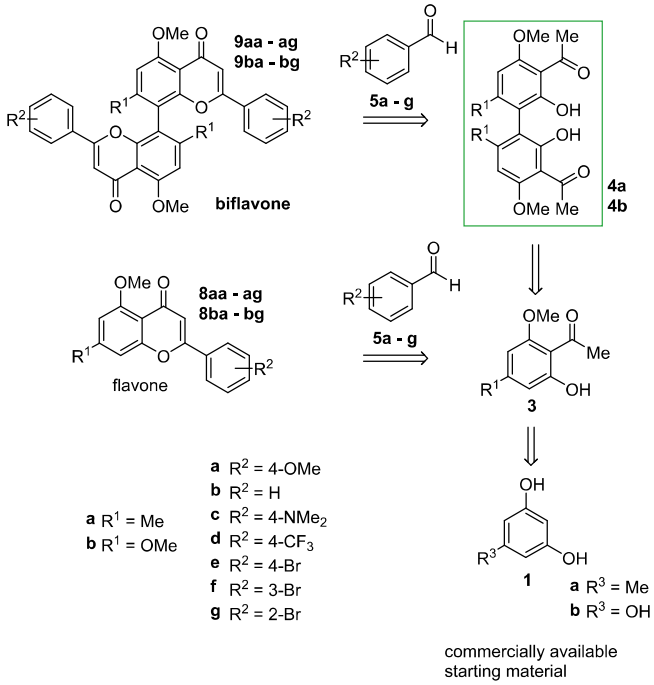

Scheme 2. Synthesis of Acetophenones 3a and 3b via Acetylation and Subsequent Methylation

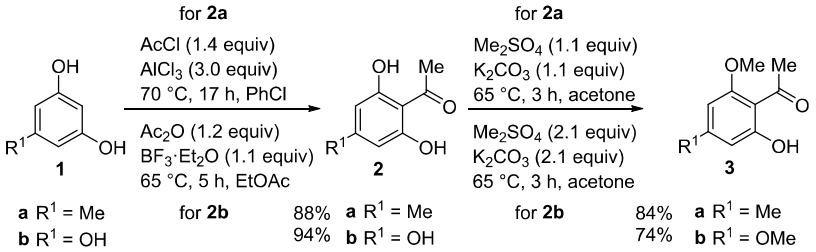

in four steps, requiring only a single column chromatographic purification step each (Scheme 3).

With a satisfactory synthesis of the monomeric flavones **8** in place, we directed our efforts toward the synthesis of acetophenone dimers **4a** and **4b** to ultimately provide the target biflavones **9**. The oxidative coupling of naphthol using $FeCl_3$ to form BINOL is known since the 1870s[47] and was later improved upon by solid-phase synthesis.[48] The first application of $FeCl_3$ on silica ($FeCl_3/SiO_2$) was the elimination of water from alcohols.[49] Jempty et al. conducted the first oxidative coupling of arenes using $FeCl_3/SiO_2$.[50] In their total synthesis, Li et al. used silica-bound $FeCl_3$ to synthesize hexamethyl-CUF,[30] in addition to the application of this method in the subsequent total syntheses of a variety of natural products.[24,40,51,52] While naphthol is well-known to form radicals in the *ortho* position to the hydroxy-group in the presence of oxidative transition metals,[48] phenols tend to form less localized radicals. The regioselectivity of Fe-based oxidative homocouplings has to the best of our knowledge hardly been investigated.[53−58]

We next directed our efforts toward the oxidative coupling of acetophenone **3a**. A variety of recent catalytic methods were evaluated for the synthesis of **4a** and **4b** (Table S7). After extensive efforts, we concluded that the use of stoichiometric amounts of oxidant is crucial for the conversion of 2′-hydroxy acetophenones **3a** and **3b**. As such, the use of classic oxidative systems such as $FeCl_3/SiO_2$ as was shown by Li et al. seemed more promising.[30] $FeCl_3/SiO_2$ was prepared using Et_2O as a solvent at 40 °C. When conducting solid-phase oxidative couplings using $FeCl_3{\cdot}6H_2O$ on SiO_2 (50% w/w), we observed the formation of small amounts of product **4a**. However, we also noted a major side product that was subsequently identified as chlorinated acetophenone **10a** among other minor chlorinated side products **10**. This regioselective

https://doi.org/10.1021/acsomega.3c06503
ACS Omega 2023, 8, 41816−41834

Scheme 3. Synthesis of Flavones 8[a]

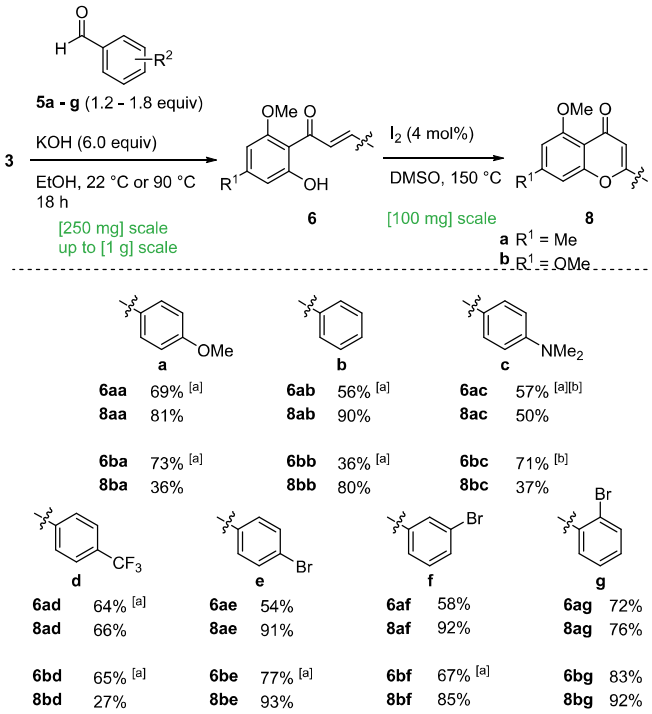

[a]Yields of isolated products; [a] with 1.8 equiv of aldehyde **5** and [b] at 90 °C.

Table 1. Oxidative Coupling of Acetophenones 3a and 3b by Solid-Phase Synthesis, with the Main Side Product 10a Formation under Varying Conditions for the Preparation of $FeCl_3/SiO_2$

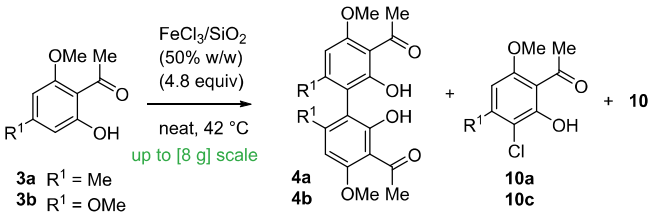

entry	4	$FeCl_3/SiO_2$	conversion[a] [%]	10a/c [%]	yield[b] [%]
1	**4a**	I	21	45	
2	**4a**	II	6	94	
3	**4a**	III	76	18	39
4	**4a**	IV	50	7	23
5	**4a**	V	51	43	
6[c]	**4a**	III	88	9	58
7[c]	**4b**	I	81	4	52

[a]Conversion to main product **4a**/**4b** relative to **10** and **3** according to ^{1}H NMR. [b]Isolated yield. [c]8 g scale, improved workup; **I**: $FeCl_3/SiO_2$ prepared at 40 °C in Et_2O using $FeCl_3{\cdot}6H_2O$; **II**: $FeCl_3/SiO_2$ prepared at 40 °C in Et_2O/MeOH (9:1) using $FeCl_3{\cdot}6H_2O$; **III**: $FeCl_3/SiO_2$ prepared at 40 °C, then 60 °C in anhydr. Et_2O/MeOH (9:1) using $FeCl_3$; **IV**: $FeCl_3/SiO_2$ prepared at 40 °C, then 60 °C in (nonanhydr.) Et_2O/MeOH (9:1) using $FeCl_3$, **V**: $FeCl_3/SiO_2$ prepared at 40 °C, then 60 °C in anhydr. Et_2O/MeOH (9:1) using newly purchased $FeCl_3{\cdot}6H_2O$ (refer to Supporting Information Table S4).

formation of the chlorinated side product has already been reported in the literature.[30]

To address this lack of chemoselectivity, we first conducted a full factorial screening[59] regarding the %weight/weight (%w/w) composition of $FeCl_3/SiO_2$, equivalents, and reaction time

https://doi.org/10.1021/acsomega.3c06503
ACS Omega 2023, 8, 41816−41834

Scheme 4. Synthesis of a Library of Bichalcones 8 and Biflavones 9[a]

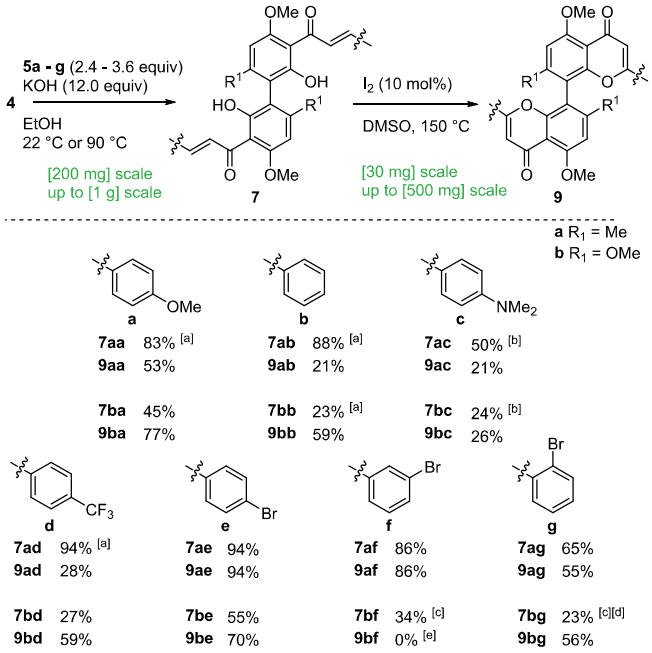

[a]Yields of isolated products: [a] with 3.6 equiv of aldehyde **5**; [b] at 90 °C; [c] presumed mixture of chalcone and flavanones and monoaddition product; [d] 1 h reaction time; and [e] complex mixture according to ^{1}H NMR.

(Table S5). More equivalents of $FeCl_3{\cdot}6H_2O$ gave a higher conversion of acetophenone **3a**. A higher %w/w $FeCl_3{\cdot}6H_2O/SiO_2$ resulted not only in an increase in the conversion of **3a** but also in a significant increase in the side product formation **10a**. A longer reaction time resulted in a higher conversion of acetophenone **3a** but an increase in the chlorinated side product formation **10a** (Table S6).

With these assessments in place, we resumed our preparative screening efforts. The use of methanol as a cosolvent during the $FeCl_3/SiO_2$ preparation did not increase selectivity (procedure II, Table 1 entry 2). To our delight, the use of anhydrous $FeCl_3$ instead of $FeCl_3{\cdot}6H_2O$ in combination with anhydrous solvents resulted in the formation of less chlorinated side product (preparation III, Table 1 entry 3). The use of anhydrous solvents and by effect the method of $FeCl_3/SiO_2$ preparation proved crucial in increasing the selectivity as the use of nonanhydrous solvents gave lower selectivity (preparation IV, Table 1 entry 4). Again, we observed an increase in the formation of side product **10a** over time. $FeCl_3$ may deteriorate over time, and thus a fast reaction may be beneficial for the selective conversion of the starting material. We also considered that the exposure to moisture might have deteriorated the $FeCl_3{\cdot}6H_2O$. $FeCl_3/SiO_2$ prepared under otherwise anhydrous conditions using the newly purchased $FeCl_3{\cdot}6H_2O$ gave better conversion and selectivity (procedure V, Table 1 entry 4) albeit still with significant side product formation. Ultimately, 4.8 equiv of anhydrous $FeCl_3$ with 50% w/w of SiO_2 in combination with anhydrous solvents resulted in the most selective conversion to acetophenone dimer **4a** in 2.5 h with a conversion of >95% (according to ^{1}H NMR) and an isolated yield of 58%. We obtained the complementary acetophenone dimer **4b** in a yield of 52% on a scale of 8 g, further underlining the utility of this reaction. We attribute the remaining mass balance to polymerization side products. This is in accordance with the previous observation of a fast reaction being more selective, whereas a long reaction time resulted in complex reaction mixtures and low yields. With the optimized protocol established, the sterically demanding products could be obtained without protecting groups and without selective functionalization of the monomeric acetophenones **3**. We were able to adapt the protocol by Li et al.[30] to synthesize acetophenone **4a** via this route and synthesize **4b** accordingly, lowering the literature-reported reaction time significantly. The X-ray structure of the acetophenone dimer **4a** supports the regioselectivity of the coupling in addition to the NMR 2D data (Figure 1 and Figures S71–S73).

With a scalable and robust synthesis of the acetophenone dimers in hand, we commenced the synthesis of the biflavone library (Scheme 4). It is noteworthy that again for some reactions, under the appropriately modified conditions of the chalcone **6** synthesis, the addition of a further 1.2 equiv of aldehyde after 6 h gave full conversion of acetophenone **4** (2.4–3.6 equiv aldehyde **5** in total). The use of an ionic liquid as a solvent to address low solubility gave chalcone dimer **7ac** in comparable yield but appeared less generally applicable (Table S7). During the reaction, a complex mixture of side products and intermediates could form and as such the isolation of these highly insoluble compounds proved difficult. However, scaleup and purification by recrystallization gave

https://doi.org/10.1021/acsomega.3c06503
ACS Omega 2023, 8, 41816–41834

chalcone dimers **7** in acceptable yield and purity. Only for **7bf** and **7bg**, the isolation of bichalcone in acceptable purity proved to not be possible. These compounds were obtained as a mixture of bichalcone and flavanone side products and significant amounts of an additional side product, presumably the monoaddition product.

With a scalable synthesis of bichalcones **7** with yields of up to 94% on a 0.2−1 g scale established, we proceeded with the synthesis of biflavones **9**. Modified conditions of the monomer synthesis were successfully transferred to the chalcone dimers. Only biflavone **9bf** was not obtained under the given conditions attributed to the difficulty in isolation of chalcone **7bf** in sufficient purity. Overall, we were able to obtain a library of 13 8,8′-biflavones with up to 38% yield (**9ae**) over five steps in a scalable fashion on up to 500 mg scale in the final step, with only a single column chromatographic purification over the full synthesis route.

■ BIOLOGICAL DATA

With a dedicated library at hand, we initiated the biological evaluation of flavones and biflavones (Figure 2). Bioactivity assays against *Toxoplasma gondii* (*T. gondii*) proliferation and the viability of healthy and malignant human cell lines were performed. Overall, this allowed for a systematic comparison of the natural product 8,8-biflavone analogues **9** with the corresponding monomers **8**.

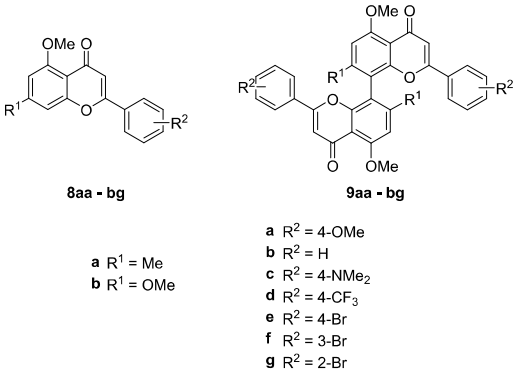

Figure 2. Structure of flavones **8** and biflavones **9** and the associated library evaluated regarding their bioactivity against *T. gondii* proliferation and against human cell lines.

T. gondii, the causative agent of toxoplasmosis, is an obligate intracellular protozoan parasite member of the phylum Apicomplexa.[60] It is referred to as one of the most successful parasites due to its ability to infect and persist in virtually all warm-blooded animals as intermediate hosts, including humans.[61] According to the World Health Organization (WHO), it is estimated that up to a third of the world's human population is infected with this parasite.[62] This unmet medical need has yet to be resolved. As biflavones such as the structurally related 3′,8″-biflavone amentoflavone are known to exert activity against kinetoplastid parasites, we wished to investigate the activity of our compound library (Table 2 and Figure 3).[13]

First, the cytotoxicity of this compound library was assessed by in vitro screening against Hs27 fibroblasts used as hosts in the *T. gondii* proliferation assay. Comparison of the activities against *T. gondii* proliferation revealed that in many cases biflavones **9** exerted higher bioactivity (lower IC_{50}) than their respective flavone counterpart **8** (Table 2). Overall, biflavone **9ac** was the most active compound regarding the inhibition of *T. gondii* proliferation with an IC_{50} of 1.6 μM. By dividing the cytotoxicity ($IC_{50\ (Hs27)}$ value against fibroblasts; Table S1) by the $IC_{50\ (T.\ gondii)}$ value (*T. gondii* proliferation inhibition), we obtained the selectivity index (SI) for each tested compound, giving us a measure of the therapeutic potential (Table 2). Of the seven compounds with the highest SI, six are biflavones, one of which is hexa-*O*-methyl-CUF (**9ba**). Five of these most active non-natural analogues have higher SIs than hexa-*O*-methyl-CUF (**9ba**).

Table 2. $IC_{(50\ HeLa)}$, $IC_{(50\ T.gondii)}$, and $IC_{(50\ Hs27)}$ and Selectivity Index (SI) of Flavones (8) and Biflavones (9) against *T. gondii* Proliferation[a]

	$IC_{50\ (HeLa)}$ [μM]	$IC_{50\ (T.\ gondii)}$ [μM]	$IC_{50\ (Hs27)}$ [μM]	SI[a]
8aa	28.4	13.7	>200	>14.6
8ab	82.5	6.68	>200	>29.9
8ac	24.2	7.98	140.6	19.1
8ad	>100	> 50	>200	-
8ae	>100	2.33	>200	>85.6
8af	32.9	4.09	104.0	25.4
8ag	76.3	7.46	130.0	17.4
8ba	33	4.86	>200	>41.1
8bb	73.7	4.61	>200	>43.3
8bc	55.7	22.9	>200	>8.7
8bd	>100	4.03	>200	>49.5
8be	85.8	3.44	>200	>58.0
8bf	72	8.10	128.1	15.6
8bg	>100	6.02	>200	>33.2
9aa	41.4	3.20	>200	>62.5
9ab	11.8	5.12	>200	> 39.0
9ac	1.4	1.58	179.9	113.4
9ad	>100	10.4	>200	>19.2
9ae	35.8	2.21	>200	>90.4
9af	>100	12.3	>200	> 16.2
9ag	18.5	39.6	>200	> 5.0
9ba	39.5	3.33	>200	>59.9
9bb	22.1	2.28	>200	>87.5
9bc	43.8	12.3	>200	>16.3
9bd	>100	4.16	>200	>48.0
9be	96.1	2.29	>200	>87.1
9bf	N/A	-	-	-
9bg	10.4	11.4	>200	>17.6

[a]SI ≥ 50 (Highlighted in Gray). [a] SI = ($IC_{(50\ Hs27)}$)/($IC_{(50\ T.\ gondii)}$). For Confidence Intervals of IC_{50}, refer to Tables S1 and S2

Next, the cytotoxicity toward malignant human cells [HeLa cells ($IC_{50\ (HeLa)}$)] was assessed (Table 2). Broadly speaking, biflavones **9** again display higher activities compared to flavones **8**, the most active compound again being biflavone **9ac**. Compounds with 4-CF_3 substituents **8ad**, **8bd**, **9ad**, and **9bd** appeared to be noncytotoxic against either human cell line while exhibiting moderate to good activity against *T. gondii* proliferation. 4-NMe_2-substituted biflavone **9ac** exerted the highest bioactivity ($IC_{50\ (HeLa)}$ = 1.4 μM and $IC_{50\ (T.\ gondii)}$ =

https://doi.org/10.1021/acsomega.3c06503
ACS Omega 2023, 8, 41816−41834

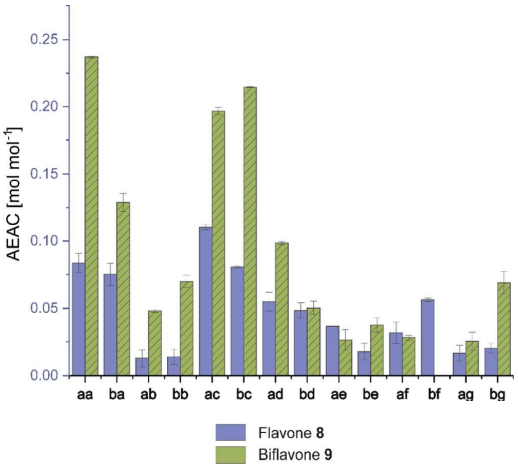

Figure 3. Ascorbic acid equivalent antioxidant capacity (AEAC) of flavones **8** and biflavones **9** relative to ascorbic acid (mol mol^{-1}) determined by the ABTS decolorization assay with standard deviation.[63] For absolute values, refer to Table S3.

1.58 μM) as well as the highest SI (113.4) of all tested compounds (Figure 4). Additionally, biflavone **9be** exerts high

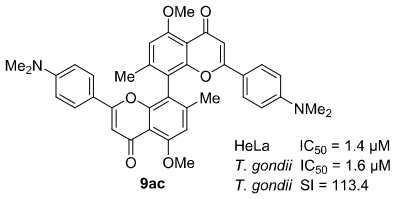

Figure 4. Most overall active compound biflavone **9ac**.

activity against *T. gondii* while exhibiting little activity against HeLa cells ($IC_{50\ (Hs27)}$ > 200 μM, $IC_{50\ (HeLa)}$ 96.1 μM, $IC_{50\ (T.\ gondii)}$ 2.3 μM). Biflavone **9ag** exerts moderate activity against HeLa cells, while no cytotoxicity and little activity against *T. gondii* is observed ($IC_{50\ (Hs27)}$ > 200 μM, $IC_{50\ (HeLa)}$ 18.5 μM, $IC_{50\ (T.\ gondii)}$ 39.6 μM). Overall, all tested compounds and particularly biflavones **9** that show moderate to high cytotoxicity against malignant HeLa cells exert little to no cytotoxicity against healthy fibroblasts Hs27.

Additionally, electron-rich arenes such as flavones are known to exhibit antioxidant properties.[64] Therefore, we assessed the ascorbic acid equivalent antioxidant capacity (AEAC) of our dedicated library using an ABTS decolorization assay.[63] We found that electron-rich biflavone **9aa** (0.25 equiv ascorbic acid [mol mol^{-1}]) exerts the highest antioxidant activity with similarly electron-rich **9bc**, **9ac**, and **9ba** following suit (Figure 3).

To show the usefulness of our synthesis route, we scaled-up the reaction to gram-scale. Biflavone **9ac** was chosen as it exerted the lowest IC_{50} regarding HeLa cells while also having one of the highest selectivity indices (SI) toward *T. gondii* proliferation inhibition. We found that slightly lower yields were obtained, which we attribute to the necessity for an intermediate workup as no further conversion was observed after adding additional 1.2 equiv of aldehyde **5c**. Following the procedure of the chalcone synthesis, we performed the flavone synthesis on a 575 mg scale. The pure biflavone was isolated in a yield of 21%. This scaleup allowed for additional modification of the biflavone by cleavage of the methoxy groups using BCl_3 (Scheme 5). This was to showcase the potential for further functionalization. The obtained biflavone **11** was isolated in a 44% yield and showed no biological activity ($IC_{50\ (HeLa)}$ > 100 μM, $IC_{50\ (T.\ gondii)}$ > 50 μM, $IC_{50\ (Hs27)}$ > 200 μM) and less antioxidant capacity (0.037 equiv (**11**) vs 0.197 equiv (**9ac**) ascorbic acid (mol mol^{-1})) compared to the protected biflavones **9ac**.

■ CONCLUSIONS

In summary, we were able to establish a scalable synthesis of a library of non-natural 8,8′-biflavones. The lack of a diversity-oriented approach for the synthesis of 8,8′-biflavones was addressed, and synthesis protocols were set in place that allow for further investigations. To provide the necessary acetophenone dimer key intermediates, we investigated a one-step oxidative coupling procedure. By doing so, we were able to overcome chemoselectivity issues by investigating the chlorinated side product formation. The reaction was then performed on a scale of up to 8 g without the need for column chromatographic isolation. Using our established protocols, we managed to synthesize a library of 14 flavones and 13 biflavones. Further, we were able to show the antiproliferative biological activity of the said library against *T. gondii* as well as selective cytotoxicity against malignant human cell lines (HeLa) and antioxidant capacity. Most biflavones **9** were more active than their respective monomeric flavone counterparts **8**. The most potent biflavone **9ac** showed the strongest activity against both *T. gondii* proliferation and

Scheme 5. Selective Deprotection of the Methoxy Groups of Biflavone 9ac for the Synthesis of Biflavone 11. Yield of Isolated Product

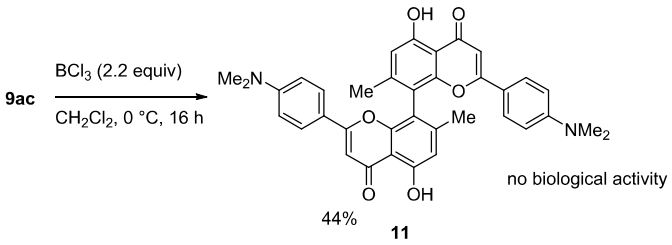

https://doi.org/10.1021/acsomega.3c06503
ACS Omega 2023, 8, 41816−41834

HeLa viability while exerting low cytotoxicity against healthy fibroblasts (SI = 113.4, $IC_{50\ (T.\ gondii)}$ = 1.6 μM, $IC_{50\ (HeLa)}$ = 1.4 μM), making it a lead structure in further studies. The synthesis of this compound was scaled up to 500 mg scale to show the viability of our approach. While this study highlights the potential use of flavones and biflavones as novel anti-*Toxoplasma* agents, further research is needed to assess their efficacy and safety in humans. The modes of action are undergoing further investigations.

■ EXPERIMENTAL SECTION

Experimental Synthesis Procedures. *General Information.* All chemicals not synthesized or present in the group were purchased from Sigma-Aldrich Co., Alfa Aesar GmbH & Co. KG, Merck KGaA, or Fluorochem Ltd. All reactants were used without any further purification unless stated otherwise. Methanol was dried using the activated molecular sieve (3 Å). DMSO was degassed via freeze−pump−thaw. Anhyd. diethyl ether and dichloromethane were taken from the solvent purifier MB SPS-800 by MBraun. Silica gel 60 (0.040−0.063 mm, 230−400 mesh) by Merck used for synthesis was dried in an oven at 110 °C overnight. Anhyd. solid reagents were stored in a desiccator under an atmosphere of N_2. All glassware and stirring bars used for reactions under anhyd. or inert conditions were put in an oven at 110 °C for at least 12 h. When removing glassware from the oven, it was sealed airtight using septa and stopcocks. It was then attached to a Schlenk line and left to cool under nitrogen gas, which was itself dried over SICAPENT, for several minutes. Glassware was then dried using the Schlenk technique by heating the glassware under vacuum for several minutes and then letting it cool to room temperature under a N_2 flow. This process was repeated three times. Septa were only opened briefly during the addition of reactants under a N_2 countercurrent. Liquid reactants, solvents, and solutions of reactants were transferred using syringes flushed three times with N_2. Solvents were removed using rotary evaporators at a bath temperature of 40 °C under reduced pressure. Analytical balance AE 163 by Mettler Toledo was used to determine and weigh yields and reactants. Sonication of reactions was conducted using an ultrasonic cleaning bath T310 by Elma Schmidbauer GmbH. Distillations of liquid aldehydes were conducted using Kugelrohrofen Glass Oven B-580 and Glass Oven B-585 by Büchi under reduced pressure. For thin-layer chromatography (TLC), silica gel plates (Polygram SIL G/UV 254) by Machery-Nagel with a fluorescent indicator were used. Spots were made visible under UV light, using aqueous potassium permanganate solution, CAM, Molydip, anisaldehyde. Column chromatographic purification was conducted using the appropriate solvent mixture and silica gel 60 (0.040−0.063 mm, 230−400 mesh) by Merck in cylindric glass columns by applying pressure with compressed air. IR spectra were recorded using a SpectrumTwo FT-IR by PerkinElmer with attenuated total reflection (ATR). The absorption bands were given in units of wave numbers (cm^{-1}). ^{1}H-, ^{13}C-, 135DEPT-, COSY-, HSQC-, and HMBC-NMR spectra were measured on the spectrometer Bruker Avance/DRX 600 at a frequency of 600 MHz (^{1}H) and 151 MHz (^{13}C). ^{19}F- and select ^{1}H- and ^{13}C NMR spectra were measured on the spectrometer Bruker Avance/DRX 300 at a frequency of 282 MHz (^{19}F), 300 MHz (^{1}H), and 75 MHz (^{13}C). Deuterated chloroform with 0.03 vol % of TMS ($CDCl_3$) or deuterated d^6-DMSO was used as a solvent. The ^{1}H- and ^{13}C-spectra were referenced to the solvent peak ($CDCl_3$ δ = 7.26 ppm (^{1}H), δ = 77.16 ppm (^{13}C); DMSO-d^6 δ = 2.50 ppm (^{1}H), δ = 39.52 ppm (^{13}C)). Data was evaluated using the software MNova (MestReNova) version 14.1 by Mestrelab Research. Coupling constants J were given in Hz, and chemical shifts δ were given in ppm (parts per million). Multiplicities are abbreviated as the following: singlet (s), broad singlet (brs), doublet (d), triplet (t), quartet (q), and multiplet (m).

General Procedures. *General Procedure A Chalcone Monomer (**6**).* A vial with a stir bar was charged with acetophenone (**3**) (250 mg, 1.0 equiv), ethanol (2.50 mL), and aq. KOH solution (3 m, 6.0 equiv, 2.78 mL). The mixture was stirred for 5 min until all solids were dissolved. Aldehyde (**5**) (1.2 equiv) was added at once. The reaction was stirred at room temperature unless stated otherwise. If stated, after 6 h, another portion of aldehyde was added (0.6 equiv). The reaction mixture was left to stir overnight. After the completion of the reaction, aq. HCl (1 M, 10 mL) was added and solids precipitated. The suspension was filtered, and the filtrate was washed with some methanol. The filtrate was then dissolved in CH_2Cl_2 (10 mL), MeOH (10% v/v) was added, and the solvent was removed in vacuo. The crude product was washed with MeOH (4 mL) at 70 °C and left to cool to room temperature, and the solids were filtered off to isolate the title compound.

*General Procedure B Chalcone Dimer (**7**).* A vial with a stir bar was charged with acetophenone (**4**) (200 mg, 1.0 equiv), ethanol (2.50 mL), and aq. KOH solution (3 M, 12.0 equiv). The mixture was stirred for 5 min until all solids were dissolved. Aldehyde (**5**) (2.4 equiv) was added at once. The reaction was stirred at room temperature unless stated otherwise. If stated, after 6 h, another portion of aldehyde was added (1.2 equiv). The reaction mixture was left to stir overnight unless stated otherwise. After the completion of the reaction, aq. HCl (1 M, 10 mL) was added unless stated otherwise, and solids precipitated. The suspension was filtered, and the filtrate was washed with some methanol. The filtrate was then dissolved in CH_2Cl_2, MeOH (10% v/v) was added, and the solvent was removed in vacuo. The crude product was washed with MeOH (10 mL) at 22 °C and filtered off to isolate the title compound.

*General Procedure C Flavone Monomer (**8**).* A 10 mL microwave vial with a stir bar was charged with chalcone (**6**) (100 mg, 1.00 equiv) and capped with a septum. The degassed DMSO (1.70 mL) and a solution of I_2 in degassed DMSO (78.8 mM, 4 mol %) were added. The reaction solution was then heated to 150 °C and stirred for 3 h. After complete conversion, sat. aq. Na_2SO_3 solution (4 mL) was added. The aq. phase was extracted with ethyl acetate (3 × 20 mL). The combined org. layers were washed with cold water (3 × 20 mL) and sat. NaCl solution (2 × 20 mL), and the solvent was removed in vacuo. The product was isolated by filtration over a plug of silica (CH_2Cl_2/MeOH, 9:1 v/v).

*General Procedure D Flavone Dimer (**9**).* A 10 mL microwave vial with a stir bar was charged with bichalcone (**7**) (30 mg, 1.00 equiv) and capped with a septum. Degassed DMSO (0.24 mL) and a solution of I_2 in degassed DMSO (78.8 mM, 10 mol %) were added. The reaction solution was then heated to 150 °C and stirred for 3 h unless stated otherwise. After complete conversion, sat. aq. Na_2SO_3 solution (4 mL) was added. The aq. phase was extracted with ethyl acetate (3 × 20 mL). The combined org. layers were washed with cold water (3 × 20 mL) and sat. NaCl solution (2 × 20

https://doi.org/10.1021/acsomega.3c06503
ACS Omega 2023, 8, 41816−41834

mL), and the solvent was removed in vacuo. The product was isolated by column chromatography unless otherwise stated.

*(E)-1-(2-Hydroxy-6-methoxy-4-methylphenyl)-3-(4-methoxyphenyl)prop-2-en-1-one (**6aa**).* Synthesized in accordance with **General Procedure A**. Starting from acetophenone **3a** (250 mg, 1.39 mmol, 1.0 equiv) and 4-methoxybenzaldehyde (**5a**) (0.30 mL, 2.50 mmol, 1.2 + 0.6 equiv). The product was isolated as orange solids (286 mg, 0.96 mmol, 69%). **^{1}H NMR** (600 MHz, $CDCl_3$): δ 2.33 (s, 3H), 3.86 (s, 3H), 3.94 (s, 3H), 6.24 (d, J = 1.5 Hz, 1H), 6.44 (dd, J = 1.5, 0.8 Hz, 1H), 6.94 (d, J = 8.8 Hz, 2H), 7.58 (d, J = 8.8 Hz, 2H), 7.80 (s, 2H), 13.49 (s, 1H). **^{13}C NMR** (151 MHz, $CDCl_3$): δ 22.53, 55.56, 56.01, 103.00, 110.01, 111.52, 114.56, 125.51, 128.43, 130.34, 142.87, 147.51, 161.02, 161.64, 165.33, 193.94. **IR** (ATR film): 3003, 2838, 1627, 1605, 1561, 1511, 1483, 1457, 1422, 1410, 1305, 1289, 1255, 1223, 1207, 1172, 1113, 1035, 982, 828, 814, 768, 742, 722, 662, 557, 539 **HR-MS (ESI):** m/z calcd for $[C_{18}H_{19}O_4]^+$ ([M + H$^+$]): 299.1278, found: 299.1284. **Melting point:** 113−114 °C.

*(E)-1-(2-Hydroxy-6-methoxy-4-methylphenyl)-3-phenylprop-2-en-1-one (**6ab**).* Synthesized in accordance with **General Procedure A**. Starting from acetophenone **3a** (250 mg, 1.39 mmol, 1.0 equiv) and benzaldehyde (**5b**) (0.26 mL, 2.50 mmol, 1.2 + 0.6 equiv). The product was isolated as orange solids (209 mg, 0.78 mmol, 56%). **^{1}H NMR** (600 MHz, $CDCl_3$): δ 2.33 (s, 3H), 3.94 (s, 3H), 6.24 (s, 1H), 6.45 (s, 1H), 7.40−7.61 (m, 5H), 7.80 (d, J = 15.6 Hz, 1H), 7.89 (d, J = 15.6 Hz, 1H), 13.37 (s, 1H). **^{13}C NMR** (151 MHz, $CDCl_3$): δ 22.59, 56.01, 102.97, 109.89, 111.46, 127.83, 128.56, 129.04, 130.31, 135.61, 142.72, 147.89, 161.04, 165.31, 194.02. **IR** (ATR film): 3091, 3036, 2980, 2951, 1641, 1576, 1495, 1459, 1418, 1378, 1344, 1284, 1232, 1216, 1168, 1124, 1082, 985, 954, 878, 853, 824. **HR-MS (ESI):** m/z calcd for $[C_{17}H_{17}O_3]^+$ ([M + H$^+$]): 269.1172, found: 269.1173. **Melting point:** 169.6−170.2 °C.

*(E)-3-(4-(Dimethylamino)phenyl)-1-(2-hydroxy-6-methoxy-4-methylphenyl)prop-2-en-1-one (**6ac**).* Synthesized in accordance with **General Procedure A**. Starting from acetophenone **3a** (250 mg, 1.39 mmol, 1.0 equiv) and 4-(dimethylamino)benzaldehyde (**5c**) (373 mg, 2.50 mmol, 1.2 + 0.6 equiv) at 90 °C. The product was isolated as red solids (264 mg, 0.85 mmol, 61%). **^{1}H NMR** (600 MHz, $CDCl_3$): δ 2.31 (s, 3H), 3.04 (s, 6H), 3.93 (s, 3H), 6.22 (d, J = 1.6 Hz, 1H), 6.43 (d, J = 1.6 Hz, 1H), 6.70 (d, J = 8.6 Hz, 2H), 7.50−7.55 (m, 2H), 7.74 (d, J = 15.4 Hz, 1H), 7.84 (d, J = 15.4 Hz, 1H), 13.72 (s, 1H). **^{13}C NMR** (151 MHz, $CDCl_3$): δ 22.47, 40.28, 55.93, 102.90, 110.06, 111.40, 112.00, 122.40, 123.41, 130.59, 144.39, 146.89, 152.02, 160.88, 165.24, 193.67. **IR** (ATR film): 3121, 3009, 2968, 2808, 2645, 2169, 2052, 1628, 1593, 1525, 1476, 1462, 1435, 1413, 1375, 1336, 1296, 1257, 1223, 1198, 1168, 1113, 1069, 1031, 984, 948, 883, 838, 819, 807, 768, 732, 711, 680, 665, 638, 600, 546, 529, 514, 501, 470. **HR-MS (ESI):** m/z calcd for $[C_{19}H_{22}O_3N]^+$ ([M + H$^+$]): 312.1594, found: 312.1596. **Melting point:** 182−183 °C.

*(E)-1-(2-Hydroxy-6-methoxy-4-methylphenyl)-3-(4-(trifluoromethyl)phenyl)prop-2-en-1-one (**6ad**).* Synthesized in accordance with **General Procedure A**. Starting from acetophenone **3a** (250 mg, 1.39 mmol, 1.0 equiv) and 4-(trifluoromethyl)benzaldehyde (**5d**) (0.34 mL, 2.50 mmol, 1.2 + 0.6 equiv). The product was isolated as orange solids (299 mg, 0.89 mmol, 64%). **^{1}H NMR** (600 MHz, $CDCl_3$): δ 2.36 (s, 3H), 3.97 (s, 3H), 6.27 (s, 1H), 6.48 (s, 1H), 7.69 (d, J = 8.1 Hz, 2H), 7.72 (d, J = 8.1 Hz, 2H), 7.78 (d, J = 15.7 Hz, 1H), 7.94 (d, J = 15.7 Hz, 1H), 13.26 (d, J = 2.3 Hz, 1H). **^{13}C NMR** (151 MHz, $CDCl_3$): δ 22.63, 56.05, 103.00, 109.77, 111.53, 124.05 (q, J = 272.1 Hz), 125.98 (q, J = 3.8 Hz), 128.53, 130.21, 131.62 (q, J = 32.6 Hz), 139.06, 140.37, 148.42, 161.03, 165.40, 193.63. **^{19}F NMR** (282 MHz, $CDCl_3$): δ −62.77. **IR** (ATR film): 3746, 3123, 3051, 2974, 1635, 1614, 1565, 1487, 1456, 1410, 1368, 1317, 1287, 1266, 1223, 1169, 1066, 1031, 1015, 983, 909, 843, 813, 768, 747, 732, 683, 666, 626, 593, 558, 530, 506, 492 **HR-MS (ESI):** m/z calcd for $[C_{18}H_{16}O_3F_3]^+$ ([M + H$^+$]): 337.1046, found: 337.1050. **Melting point:** 124−126 °C.

*(E)-3-(4-Bromophenyl)-1-(2-hydroxy-6-methoxy-4-methylphenyl)prop-2-en-1-one (**6ae**).* Synthesized in accordance with **General Procedure A**. Starting from acetophenone **3a** (250 mg, 1.39 mmol, 1.0 equiv) and 4-bromobenzaldehyde (**5e**) (309 mg 1.66 mmol, 1.2 equiv). The product was isolated as yellow solids (261 mg, 0.75 mmol, 54%). **^{1}H NMR** (600 MHz, $CDCl_3$): δ 2.33 (s, 3H), 3.93 (s, 3H), 6.23 (d, J = 1.6 Hz, 1H), 6.45 (s, 1H), 7.46 (d, J = 8.4 Hz, 2H), 7.54 (d, J = 8.4 Hz, 2H), 7.70 (d, J = 15.6 Hz, 1H), 7.85 (d, J = 15.6 Hz, 1H), 13.30 (s, 1H). **^{13}C NMR** (151 MHz, $CDCl_3$): δ 22.60, 56.04, 102.98, 109.82, 111.51, 124.48, 128.43, 129.88, 132.28, 134.56, 141.20, 148.13, 161.00, 165.36, 193.74. **IR** (ATR film): 2970, 2850, 1632, 1571, 1486, 1454, 1402, 1369, 1331, 1270, 1222, 1206, 1159, 1114, 1072, 1031, 1009, 979, 945, 874, 820, 790, 764, 712, 595, 572, 557, 529. **HR-MS (ESI):** m/z calcd for $[C_{17}H_{16}O_3Br]^+$ ([M + H$^+$]): 347.0277, found: 347.0279. **Melting point:** 122−124 °C.

*(E)-3-(3-Bromophenyl)-1-(2-hydroxy-6-methoxy-4-methylphenyl)prop-2-en-1-one (**6af**).* Synthesized in accordance with **General Procedure A**. Starting from acetophenone **3a** (250 mg, 1.39 mmol, 1.0 equiv) and 3-bromobenzaldehyde (**5f**) (0.20 mL, 1.66 mmol, 1.2 equiv). The product was isolated as yellow solids (279 mg, 0.81 mmol, 58%). **^{1}H NMR** (600 MHz, $CDCl_3$): δ 2.33 (s, 3H), 3.94 (s, 3H), 6.24 (d, J = 1.5 Hz, 1H), 6.43−6.46 (m, 1H), 7.28 (t, J = 7.8 Hz, 1H), 7.51 (dd, J = 7.9, 1.8 Hz, 2H), 7.67 (d, J = 15.6 Hz, 1H), 7.74 (t, J = 1.8 Hz, 1H), 7.84 (d, J = 15.6 Hz, 1H), 13.27 (s, 1H). **^{13}C NMR** (151 MHz, $CDCl_3$): δ 22.61, 56.09, 102.99, 109.79, 111.49, 123.15, 127.21, 129.18, 130.53, 131.03, 132.97, 137.80, 140.70, 148.23, 161.03, 165.35, 193.65. **IR** (ATR film): 2918, 2850, 1633, 1571, 1454, 1410, 1368, 1329, 1307, 1276, 1222, 1204, 1159, 1114, 1072, 1031, 978, 945, 898, 863, 815, 787, 760, 699, 667, 626, 606, 583, 557, 529, 485. **HR-MS (ESI):** m/z calcd for $[C_{17}H_{16}O_3Br]^+$ ([M + H$^+$]): 347.0277, found: 347.0278. **Melting point:** 123−124 °C.

*(E)-3-(2-Bromophenyl)-1-(2-hydroxy-6-methoxy-4-methylphenyl)prop-2-en-1-one (**6ag**).* Synthesized in accordance with **General Procedure A**. Starting from acetophenone **3a** (250 mg, 1.39 mmol, 1.0 equiv) and 2-bromobenzaldehyde (**5g**) (0.19 mL, 1.66 mmol, 1.2 equiv). The product was isolated as yellow solids (347 mg, 1.00 mmol, 72%). **^{1}H NMR** (600 MHz, $CDCl_3$): δ 2.33 (s, 3H), 3.92 (s, 3H), 6.23 (s, 1H), 6.45 (s, 1H), 7.23 (td, J = 7.6, 1.6 Hz, 1H), 7.35 (t, J = 7.5 Hz, 1H), 7.63 (dd, J = 8.0, 1.2 Hz, 1H), 7.69 (dd, J = 7.9, 1.6 Hz, 1H), 7.80 (d, J = 15.4 Hz, 1H), 8.11 (d, J = 15.5 Hz, 1H), 13.29 (s, 1H). **^{13}C NMR** (151 MHz, $CDCl_3$): δ 22.61, 56.03, 102.95, 109.80, 111.50, 126.07, 127.77, 128.03, 130.45, 131.10, 133.69, 135.66, 140.78, 148.17, 161.02, 165.38, 193.65. **IR** (ATR film): 3065, 1629, 1577, 1487, 1466, 1451, 1438, 1367, 1334, 1278, 1225, 1208, 1191, 1159, 1113, 1049, 1025, 996, 966, 944, 893, 858, 839, 813, 768, 745, 713, 656, 625, 606, 561, 530, 511, 489. **HR-MS (ESI):** m/z calcd for

https://doi.org/10.1021/acsomega.3c06503
ACS Omega 2023, 8, 41816−41834

$[C_{17}H_{16}O_3Br]^+$ ([M + H$^+$]): 347.0277, found: 347.0281. **Melting point:** 162−164 °C.

*(E)-1-(2-Hydroxy-4,6-dimethoxyphenyl)-3-(4-methoxyphenyl)prop-2-en-1-one or Flavokavain A (**6ba**).* Synthesized in accordance with **General Procedure A**. Starting from acetophenone **3b** (250 mg, 1.27 mmol, 1.0 equiv) and 4-methoxybenzaldehyde (**5a**) (0.28 mL, 2.29 mmol, 1.2 + 0.6 equiv). The product was isolated as yellow solids (292 mg, 0.93 mmol, 73%). The analytical data was in accordance with the literature.[65] **^{1}H NMR** (600 MHz, $CDCl_3$): δ 3.84 (s, 3H), 3.86 (s, 3H), 3.92 (s, 3H), 5.97 (dd, J = 5.1, 2.4 Hz, 1H), 6.11 (d, J = 2.3 Hz, 1H), 6.93 (d, J = 8.8 Hz, 2H), 7.57 (d, J = 8.7 Hz, 2H), 7.80 (m, 2H), 14.43 (s, 1H). **^{13}C NMR** (151 MHz, $CDCl_3$): δ 55.39, 55.56, 55.84, 91.26, 93.86, 106.41, 114.38, 125.19, 128.37, 130.10, 142.45, 161.38, 162.48, 166.03, 168.38, 192.61. **IR** (ATR film): 3005, 2838, 1622, 1580, 1559, 1511, 1488, 1455, 1440, 1421, 1391, 1344, 1304, 1289, 1255, 1216, 1172, 1158, 1112, 984, 939, 870, 828, 766, 721, 697, 674, 615, 559, 539, 520. **HR-MS (ESI):** m/z calcd for $[C_{18}H_{19}O_5]^+$ ([M + H$^+$]): 315.1227, found: 315.1230. **Melting point:** 113−114 °C (110 °C).[66]

*(E)-1-(2-Hydroxy-4,6-dimethoxyphenyl)-3-phenylprop-2-en-1-one (**6bb**).* Synthesized in accordance with **General Procedure A**. Starting from acetophenone **3b** (250 mg, 1.27 mmol, 1.0 equiv) and benzaldehyde (**5b**) (0.23 mL, 2.29 mmol, 1.2 + 0.6 equiv) at 50 °C. The product was isolated as yellow solids (130 mg, 0.46 mmol, 36%). The analytical data was in accordance with the literature.[65] **^{1}H NMR** (600 MHz, $CDCl_3$): δ 3.84 (s, 3H), 3.92 (s, 3H), 5.97 (d, J = 2.4 Hz, 1H), 6.11 (d, J = 2.4 Hz, 1H), 7.36−7.44 (m, 3H), 7.58−7.63 (m, 2H), 7.79 (d, J = 15.6 Hz, 1H), 7.91 (d, J = 15.6 Hz, 1H), 14.31 (s, 1H). **^{13}C NMR** (151 MHz, $CDCl_3$): δ 55.59, 55.87, 91.31, 93.86, 106.41, 127.60, 128.36, 128.88, 130.04, 135.64, 142.32, 162.55, 166.27, 168.43, 192.67. **IR** (ATR film): 3082, 3059, 3025, 3004, 2969, 2940, 2849, 1615, 1558, 1494, 1415, 1340, 1284, 1211, 1155, 1112, 1072, 1055, 1033, 984, 939, 888, 869, 818, 788, 742, 691, 673, 647, 623, 577, 562, 534, 495, 459 **HR-MS (ESI):** m/z calcd for $[C_{17}H_{17}O_4]^+$ ([M + H$^+$]): 285.1121, found: 285.1122. **Melting point:** 83−84 °C (85−86 °C).[65]

*(E)-3-(4-(Dimethylamino)phenyl)-1-(2-hydroxy-4,6-dimethoxyphenyl)prop-2-en-1-one (**6bc**).* Synthesized in accordance with **General Procedure A**. Starting from acetophenone **3b** (250 mg, 1.27 mmol, 1.0 equiv) and 4-(dimethylamino)benzaldehyde (**5c**) (228 mg, 1.53 mmol, 1.2 equiv) at 90 °C. The product was isolated as red solids (296 mg, 0.91 mmol, 71%). The analytical data was in accordance with the literature.[67] **^{1}H NMR** (600 MHz, $CDCl_3$): δ 3.03 (s, 6H), 3.82 (s, 3H), 3.91 (s, 3H), 5.95 (d, J = 2.4 Hz, 1H), 6.10 (d, J = 2.4 Hz, 1H), 6.69 (d, J = 8.5 Hz, 2H), 7.52 (d, J = 8.7 Hz, 2H), 7.75 (d, J = 15.3 Hz, 1H), 7.83 (d, J = 15.4 Hz, 1H), 14.66 (s, 1H). **^{13}C NMR** (151 MHz, $CDCl_3$): δ 40.16, 55.52, 55.78, 91.12, 93.83, 106.45, 111.90, 122.09, 123.40, 130.37, 143.99, 151.84, 162.39, 165.63, 168.31, 192.47. **IR** (ATR film): 3004, 2962, 2850, 1621, 1587, 1528, 1481, 1436, 1415, 1379, 1346, 1296, 1209, 1172, 1154, 1111, 1031, 1001, 986, 941, 920, 864, 810, 765, 711, 677, 638, 616, 547, 516, 503, 461. **HR-MS (ESI):** m/z calcd for $[C_{19}H_{22}O_4]^+$ ([M + H$^+$]): 328.1543, found: 328.1546. **Melting point:** 203−204 °C (153 °C).[66]

*(E)-1-(2-Hydroxy-4,6-dimethoxyphenyl)-3-(4-(trifluoromethyl)phenyl)prop-2-en-1-one (**6bd**).* Synthesized in accordance with **General Procedure A**. Starting from acetophenone **3b** (250 mg, 1.27 mmol, 1.0 equiv) and 4-(trifluoromethyl)benzaldehyde (**5d**) (0.31 mL, 2.29 mmol, 1.2 + 0.6 equiv). The product was isolated as yellow solids (293 mg, 0.83 mmol, 65%). **^{1}H NMR** (600 MHz, $CDCl_3$): δ 3.84 (s, 3H), 3.92 (s, 3H), 5.97 (d, J = 2.4 Hz, 1H), 6.11 (d, J = 2.4 Hz, 1H), 7.65 (d, J = 8.3 Hz, 2H), 7.68 (d, J = 8.3 Hz, 2H), 7.74 (d, J = 15.6 Hz, 1H), 7.93 (d, J = 15.6 Hz, 1H), 14.14 (s, 1H). **^{13}C NMR** (151 MHz, $CDCl_3$): δ 55.78, 56.05, 91.53, 94.00, 106.43, 124.07 (q, J = 272.1 Hz), 125.96 (q, J = 3.8 Hz), 128.47, 130.12, 131.51 (q, J = 32.6 Hz), 139.19, 140.13, 162.65, 166.72, 168.66, 192.32. **^{19}F NMR** (282 MHz, $CDCl_3$): δ −62.76. **IR** (ATR film): 3022, 2980, 2948, 1633, 1613, 1579, 1488, 1456, 1438, 1414, 1342, 1324, 1287, 1216, 1101, 1067, 1030, 1016, 955, 936, 906, 872, 838, 827, 815, 768, 750, 732, 693, 676, 605, 590, 535, 504, 461. **HR-MS (ESI):** m/z calcd for $[C_{18}H_{16}O_4F_3]^+$ ([M + H$^+$]): 353.0995, found: 353.0997. **Melting point:** 148−149 °C.

*(E)-3-(4-Bromophenyl)-1-(2-hydroxy-4,6-dimethoxyphenyl)prop-2-en-1-one (**6be**).* Synthesized in accordance with **General Procedure A**. Starting from acetophenone **3b** (250 mg, 1.27 mmol, 1.0 equiv) and 4-bromobenzaldehyde (**5e**) (423 mg, 2.29 mmol, 1.2 + 0.6 equiv). The product was isolated as a yellow solid (356 mg, 0.98 mmol, 77%). The analytical data was in accordance with the literature.[65] **^{1}H NMR** (600 MHz, $CDCl_3$): δ 3.82 (s, 3H), 3.90 (s, 3H), 5.94 (d, J = 2.4 Hz, 1H), 6.09 (d, J = 2.4 Hz, 1H), 7.44 (d, J = 8.2 Hz, 2H), 7.52 (d, J = 8.2 Hz, 2H), 7.67 (d, J = 15.6 Hz, 1H), 7.85 (d, J = 15.6 Hz, 1H), 14.23 (s, 1H). **^{13}C NMR** (151 MHz, $CDCl_3$): δ 55.72, 55.99, 91.42, 93.95, 106.39, 124.30, 128.26, 129.78, 132.20, 134.63, 140.88, 162.58, 166.49, 168.57, 192.40. **IR** (ATR film): 3016, 2996, 2978, 1627, 1586, 1564, 1484, 1440, 1420, 1336, 1303, 1289, 1272, 1215, 1158, 1114, 1069, 1029, 1007, 986, 973, 936, 891, 818, 792, 758, 709, 666, 604, 564, 534, 505, 483, 460. **HR-MS (ESI):** m/z calcd for $[C_{17}H_{16}O_4Br]^+$ ([M + H$^+$]): 363.0226, found: 363.0231. **Melting point:** 169−170 °C (166 °C)[68] (150−151 °C).[65]

*(E)-3-(3-Bromophenyl)-1-(2-hydroxy-4,6-dimethoxyphenyl)prop-2-en-1-one (**6bf**).* Starting from acetophenone **3b** (250 mg, 1.27 mmol, 1.0 equiv) and 3-bromobenzaldehyde (**5f**) (0.27 mL, 2.29 mmol, 1.2 + 0.6 equiv). The product was isolated as a yellow solid (310 mg, 0.85 mmol, 67%). The analytical data was in accordance with the literature.[69] **^{1}H NMR** (600 MHz, $CDCl_3$): δ 3.83 (s, 3H), 3.92 (s, 3H), 5.96 (d, J = 2.4 Hz, 1H), 6.10 (d, J = 2.4 Hz, 1H), 7.27 (t, J = 7.9 Hz, 1H), 7.49 (dd, J = 7.9, 1.8 Hz, 2H), 7.66 (d, J = 15.6 Hz, 1H), 7.72 (t, J = 1.8 Hz, 1H), 7.85 (d, J = 15.6 Hz, 1H), 14.18 (s, 1H). **^{13}C NMR** (151 MHz, $CDCl_3$): δ 55.75, 56.07, 91.47, 93.96, 106.42, 123.12, 127.12, 129.05, 130.49, 130.99, 132.84, 137.90, 140.43, 162.63, 166.59, 168.59, 192.35. **IR** (ATR film): 2942, 2852, 1619, 1578, 1469, 1454, 1440, 1416, 1392, 1340, 1319, 1303, 1262, 1216, 1158, 1114, 1072, 1055, 1030, 983, 939, 911, 863, 819, 787, 758, 688, 670, 647, 624, 582, 564, 533, 492. **HR-MS (ESI):** m/z calcd for $[C_{17}H_{16}O_4Br]^+$ ([M + H$^+$]): 363.0226, found: 363.0230. **Melting point:** 115−116 °C.

*(E)-3-(2-Bromophenyl)-1-(2-hydroxy-4,6-dimethoxyphenyl)prop-2-en-1-one (**6bg**).* Synthesized in accordance with **General Procedure A**. Starting from acetophenone **3b** (250 mg, 1.27 mmol, 1.0 equiv) and 2-bromobenzaldehyde (**5g**) (0.18 mL, 1.53 mmol, 1.2 equiv). The product was isolated as yellow solids (385 mg, 1.06 mmol, 83%). The analytical data was in accordance with the

https://doi.org/10.1021/acsomega.3c06503
ACS Omega 2023, 8, 41816−41834

literature.[70] **^{1}H NMR** (600 MHz, $CDCl_3$): δ 3.83 (s, 3H), 3.89 (s, 3H), 5.95 (d, J = 2.4 Hz, 1H), 6.10 (d, J = 2.4 Hz, 1H), 7.21 (td, J = 7.6, 1.6 Hz, 1H), 7.34 (td, J = 7.6, 1.3 Hz, 1H), 7.62 (dd, J = 8.1, 1.2 Hz, 1H), 7.67 (dd, J = 7.8, 1.7 Hz, 1H), 7.81 (d, J = 15.5 Hz, 1H), 8.09 (d, J = 15.5 Hz, 1H), 14.21 (s, 1H). **^{13}C NMR** (151 MHz, $CDCl_3$): δ 55.73, 56.01, 91.41, 93.96, 106.41, 125.96, 127.75, 127.99, 130.32, 130.98, 133.62, 135.73, 140.51, 162.62, 166.55, 168.60, 192.34. **IR** (ATR film): 3005, 2976, 1627, 1579, 1565, 1490, 1464, 1437, 1416, 1343, 1321, 1307, 1269, 1216, 1160, 1113, 1048, 1027, 971, 939, 874, 814, 797, 770, 744, 695, 663, 646, 622, 586, 535, 507. **HR-MS (ESI):** m/z calcd for $[C_{17}H_{16}O_4Br]^+$ ([M + H$^+$]): 363.0226, found: 363.0233. **Melting point:** 147−148 °C (146−147 °C).[70]

*5-Methoxy-2-(4-methoxyphenyl)-7-methyl-4H-chromen-4-one (**8aa**).* Synthesized in accordance with **General Procedure C**. Starting from chalcone **6aa** (100 mg, 0.34 mmol, 1.0 equiv) and I_2 (78.8 mM, 173 μL, 0.01 mmol, 4 mol %). The product was isolated as white solids (81.0 mg, 0.28 mmol, 81%). **^{1}H NMR** (600 MHz, $CDCl_3$): δ 2.46 (s, 3H), 3.88 (s, 3H), 3.98 (s, 3H), 6.62 (d, J = 1.4 Hz, 1H), 6.63 (s, 1H), 6.94 (dd, J = 1.6, 0.8 Hz, 1H), 7.00 (d, J = 8.9 Hz, 2H), 7.83 (d, J = 8.9 Hz, 2H). **^{13}C NMR** (151 MHz, $CDCl_3$): δ 22.42, 55.63, 56.59, 107.88, 110.39, 112.60, 114.54, 124.13, 127.86, 145.01, 158.44, 159.67, 161.04, 162.28, 178.34. **IR** (ATR film): 2840, 1639, 1606, 1575, 1512, 1483, 1423, 1377, 1340, 1300, 1220, 1180, 1115, 1050, 955, 903, 833, 611, 586. **HR-MS (ESI):** m/z calcd for $[C_{18}H_{17}O_4]^+$ ([M + H$^+$]): 297.1121, found: 297.1126. **Melting point:** 173−174 °C.

*5-Methoxy-7-methyl-2-phenyl-4H-chromen-4-one (**8ab**).* Synthesized in accordance with **General Procedure C**. Starting from chalcone **6ab** (100 mg, 0.38 mmol, 1.0 equiv) and I_2 (78.8 mM, 192 μL, 0.02 mmol, 4 mol %). The product was isolated as white solids (90.3 mg, 0.34 mmol, 90%). **^{1}H NMR** (600 MHz, $CDCl_3$): δ 2.45 (s, 3H), 3.98 (s, 3H), 6.62 (s, 1H), 6.70 (s, 1H), 6.95 (s, 1H), 7.49 (m, 3H), 7.87 (dd, J = 7.5, 2.3 Hz, 2H). **^{13}C NMR** (151 MHz, $CDCl_3$): δ 22.40, 56.55, 107.93, 109.17, 110.39, 112.62, 126.14, 129.05, 131.34, 131.77, 145.26, 158.45, 159.65, 160.97, 178.28. **IR** (ATR film): 3068, 2914, 2851, 2236, 1637, 1610, 1577, 1566, 1482, 1463, 1449, 1410, 1375, 1337, 1298, 1263, 1219, 1188, 1163, 1118, 1079, 1049, 1014, 1001, 973, 956, 919, 901, 848, 825, 769, 729, 691, 676, 610, 566, 545, 528, 488. **HR-MS (ESI):** m/z calcd for $[C_{17}H_{15}O_3]^+$ ([M + H$^+$]): 267.1016, found: 267.1020. **Melting point:** 162−163 °C.

*2-(4-(Dimethylamino)phenyl)-5-methoxy-7-methyl-4H-chromen-4-one (**8ac**).* Synthesized in accordance with **General Procedure C**. Starting from chalcone **6ac** (100 mg, 0.32 mmol, 1.0 equiv) and I_2 (78.8 mM, 162 μL, 0.01 mmol, 4 mol %). The product was isolated as orange solids (50.0 mg, 0.16 mmol, 50%). **^{1}H NMR** (600 MHz, $CDCl_3$): δ 2.44 (s, 3H), 3.05 (s, 6H), 3.97 (s, 3H), 6.57 (s, 1H), 6.60 (s, 1H), 6.73 (d, J = 8.9 Hz, 2H), 6.92 (s, 1H), 7.76 (d, J = 8.9 Hz, 2H). **^{13}C NMR** (151 MHz, $CDCl_3$): δ 22.38, 40.24, 56.54, 106.13, 107.60, 110.36, 111.76, 112.55, 118.36, 127.49, 144.54, 152.37, 158.38, 159.53, 161.89, 178.42. **IR** (ATR film): 2924, 2853, 2235, 1629, 1597, 1523, 1481, 1463, 1445, 1412, 1366, 1339, 1300, 1253, 1223, 1197, 1170, 1118, 1092, 1049, 1015, 972, 947, 914, 776, 758, 728, 677, 643, 611, 577, 541, 528, 510, 480 **HR-MS (ESI):** m/z calcd for $[C_{19}H_{20}NO_3]^+$ ([M + H$^+$]): 310.1438, found: 310.1441. **Melting point:** 198 °C (decomposition).

*5-Methoxy-7-methyl-2-(4-(trifluoromethyl)phenyl)-4H-chromen-4-one (**8ad**).* Synthesized in accordance with **General Procedure C**. Starting from chalcone **6ad** (100 mg, 0.30 mmol, 1.0 equiv) and I_2 (78.8 mM, 152 μL, 0.01 mmol, 4 mol %). The product was isolated as white solids (65.7 mg, 0.20 mmol, 66%). **^{1}H NMR** (600 MHz, $CDCl_3$): δ 2.46 (s, 3H), 3.98 (s, 3H), 6.64 (s, 1H), 6.74 (s, 1H), 6.96 (s, 1H), 7.75 (d, J = 8.2 Hz, 2H), 7.98 (d, J = 8.1 Hz, 2H). **^{13}C NMR** (151 MHz, $CDCl_3$): δ 22.44, 56.59, 108.19, 110.34, 112.63, 122.91 (q, J = 271.2 Hz), 126.07 (q, J = 3.8 Hz), 126.48, 132.97 (q, J = 32.8 Hz), 135.23, 145.73, 158.35, 159.23, 159.73, 177.89. **^{19}F NMR** (282 MHz, $CDCl_3$): δ −62.95. **IR** (ATR film): 3074, 2920, 1645, 1612, 1567, 1518, 1486, 1466, 1417, 1379, 1319, 1295, 1257, 1219, 1202, 1159, 1114, 1071, 1049, 1016, 958, 902, 889, 849, 823, 776, 731, 702, 677, 649, 635, 612, 585, 566, 551, 530, 497. **HR-MS (ESI):** m/z calcd for $[C_{18}H_{14}O_3F_3]^+$ ([M + H$^+$]): 335.0890, found: 335.0895. **Melting point:** 226−228 °C.

*2-(4-Bromophenyl)-5-methoxy-7-methyl-4H-chromen-4-one (**8ae**).* Synthesized in accordance with **General Procedure C**. Starting from chalcone **6ae** (100 mg, 0.29 mmol, 1.0 equiv) and I_2 (78.8 mM, 147 μL, 0.01 mmol, 4 mol %). The product was isolated as white solids (90.5 mg, 0.26 mmol, 91%). **^{1}H NMR** (600 MHz, $CDCl_3$): δ 2.46 (s, 3H), 3.98 (s, 3H), 6.64 (s, 1H), 6.69 (s, 1H), 6.94 (s, 1H), 7.63 (d, J = 8.6 Hz, 2H), 7.74 (d, J = 8.6 Hz, 2H). **^{13}C NMR** (151 MHz, $CDCl_3$): δ 22.48, 56.60, 108.05, 109.29, 110.35, 112.54, 126.02, 127.61, 130.71, 132.39, 145.53, 158.34, 159.67, 159.95, 178.13. **IR** (ATR film): 3072, 2236, 1612, 1588, 1567, 1483, 1463, 1404, 1375, 1334, 1300, 1265, 1218, 1188, 1164, 1120, 1074, 1048, 1008, 956, 828, 776, 731, 677, 644, 566, 550, 529, 495, 475. **HR-MS (ESI):** m/z calcd for $[C_{17}H_{14}O_3Br]^+$ ([M + H$^+$]): 345.0121, found: 345.0121. **Melting point:** 203−206 °C.

*2-(3-Bromophenyl)-5-methoxy-7-methyl-4H-chromen-4-one (**8af**).* Synthesized in accordance with **General Procedure C**. Starting from chalcone **6af** (100 mg, 0.29 mmol, 1.0 equiv) and I_2 (78.8 mM, 147 μL, 0.01 mmol, 4 mol %). The product was isolated as white solids (92.1 mg, 0.27 mmol, 92%). **^{1}H NMR** (600 MHz, $CDCl_3$): δ 2.39 (s, 3H), 3.91 (s, 3H), 6.57 (d, J = 8.3 Hz, 2H), 6.86 (t, J = 1.1 Hz, 1H), 7.29 (t, J = 7.9 Hz, 1H), 7.54 (ddd, J = 8.0, 2.0, 1.0 Hz, 1H), 7.68 (dt, J = 7.9, 1.4 Hz, 1H), 7.92 (t, J = 1.9 Hz, 1H). **^{13}C NMR** (151 MHz, $CDCl_3$): δ 22.28, 56.37, 107.88, 109.44, 110.17, 112.29, 123.08, 124.44, 128.84, 130.40, 133.49, 133.99, 145.44, 158.03, 158.97, 159.40, 177.71. **IR** (ATR film): 2921, 1644, 1613, 1560, 1483, 1465, 1417, 1375, 1301, 1266, 1217, 1165, 1121, 1098, 1077, 1050, 998, 977, 956, 846, 825, 791, 744, 721, 693, 612, 566, 529, 487. **HR-MS (ESI):** m/z calcd for $[C_{17}H_{14}O_3Br]^+$ ([M + H$^+$]): 345.0121, found: 345.0125. **Melting point:** 165−166 °C.

*2-(2-Bromophenyl)-5-methoxy-7-methyl-4H-chromen-4-one (**8ag**).* Synthesized in accordance with **General Procedure C**. Starting from chalcone **6ag** (100 mg, 0.29 mmol, 1.0 equiv) and I_2 (78.8 mM, 147 μL, 0.01 mmol, 4 mol %). The product was isolated as white solids (76.4 mg, 0.22 mmol, 76%). **^{1}H NMR** (600 MHz, $CDCl_3$): δ 2.45 (s, 3H), 3.99 (s, 3H), 6.45 (s, 1H), 6.64 (s, 1H), 6.88 (s, 1H), 7.35 (td, J = 7.7, 1.7 Hz, 1H), 7.43 (td, J = 7.5, 1.2 Hz, 1H), 7.55 (dd, J = 7.7, 1.7 Hz, 1H), 7.70 (dd, J = 8.0, 1.1 Hz, 1H). **^{13}C NMR** (151 MHz, $CDCl_3$): δ 22.43, 56.58, 108.06, 110.45, 112.62, 114.33, 122.05, 127.70, 130.98, 131.81, 134.02, 134.05, 145.50, 158.71, 159.75, 161.65, 177.90. **IR** (ATR film): 2931, 1650, 1616, 1483, 1466, 1436, 1411, 1332, 1298, 1267, 1217, 1164, 1117,

https://doi.org/10.1021/acsomega.3c06503
ACS Omega 2023, 8, 41816−41834

1061, 1040, 1026, 854, 764, 727, 683, 567, 545, 500. **HR-MS (ESI):** m/z calcd for $[C_{17}H_{14}O_3Br]^+$ ($[M + H^+]$): 345.0121, found 345.0125. **Melting point:** 146−148 °C.

*5,7-Dimethoxy-2-(4-methoxyphenyl)-4H-chromen-4-one or Apigenin Trimethyl Ether (**8ba**).* Synthesized in accordance with **General Procedure C**. Starting from chalcone **6ba** (100 mg, 0.32 mmol, 1.0 equiv) and I_2 (78.8 mM, 162 μL, 0.01 mmol, 4 mol %). The product was isolated as white solids (35.7 mg, 0.12 mmol, 36%). The analytical data was in accordance with the literature.[71] **^{1}H NMR** (600 MHz, $CDCl_3$): δ 3.88 (s, 3H), 3.91 (s, 3H), 3.96 (s, 3H), 6.37 (d, J = 2.3 Hz, 1H), 6.56 (d, J = 2.3 Hz, 1H), 6.60 (s, 1H), 7.00 (d, J = 8.9 Hz, 2H), 7.82 (d, J = 8.9 Hz, 2H). **^{13}C NMR** (151 MHz, $CDCl_3$): δ 55.62, 55.87, 56.59, 93.02, 96.25, 107.92, 109.46, 114.53, 124.09, 127.76, 160.03, 160.83, 161.12, 162.22, 164.07, 177.75. **IR** (ATR film): 2941, 1640, 1605, 1513, 1491, 1460, 1422, 1347, 1301, 1259, 1218, 1202, 1180, 1161, 1114, 1057, 1032, 908, 833, 773, 620, 599, 559. **HR-MS (ESI):** m/z calcd for $[C_{18}H_{17}O_5]^+$ ($[M + H^+]$): 313.1071, found: 313.1075. **Melting point:** 155−157 °C (155−157 °C).[71]

*5,7-Dimethoxy-2-phenyl-4H-chromen-4-one or Dimethylchrysin (**8bb**).* Synthesized in accordance with **General Procedure C**. Starting from chalcone **6bb** (100 mg, 0.35 mmol, 1.0 equiv) and I_2 (78.8 mM, 178 μL, 0.01 mmol, 4 mol %). The product was isolated as white solids (80.1 mg, 0.28 mmol, 80%). The analytical data was in accordance with the literature.[72] **^{1}H NMR** (600 MHz, $CDCl_3$): δ 3.91 (s, 3H), 3.95 (s, 3H), 6.37 (d, J = 2.3 Hz, 1H), 6.57 (d, J = 2.3 Hz, 1H), 6.68 (s, 1H), 7.47−7.52 (m, 3H), 7.84−7.90 (m, 2H). **^{13}C NMR** (151 MHz, $CDCl_3$): δ 55.89, 56.57, 93.02, 96.35, 109.26, 109.52, 126.09, 129.06, 131.29, 131.75, 160.08, 160.78, 161.12, 164.22, 177.69. **IR** (ATR film): 3017, 2948, 2922, 2844, 2326, 2226, 2015, 1646, 1605, 1491, 1465, 1451, 1422, 1392, 1348, 1302, 1268, 1215, 1204, 1189, 1161, 1120, 1104, 1079, 1058, 1035, 1022, 1000, 962, 949, 915, 851, 819, 803, 766, 723, 689, 642, 614, 556, 530, 483. **HR-MS (ESI):** m/z calcd for $[C_{17}H_{15}O_4]^+$ ($[M + H^+]$): 283.0965, found: 283.0969. **Melting point:** 80.0 °C (brown discoloration), 141−142 °C (145−146 °C).[72]

*2-(4-(Dimethylamino)phenyl)-5,7-dimethoxy-4H-chromen-4-one (**8bc**).* Synthesized in accordance with **General Procedure C**. Starting from chalcone **6bc** (100 mg, 0.31 mmol, 1.0 equiv) and I_2 (78.8 mM, 157 μL, 0.01 mmol, 4 mol %). The product was isolated as orange solids (37.1 mg, 0.11 mmol, 37%). **^{1}H NMR** (600 MHz, $CDCl_3$): δ 3.06 (s, 6H), 3.91 (s, 3H), 3.95 (s, 3H), 6.36 (d, J = 2.3 Hz, 1H), 6.55 (s, 2H), 6.74 (d, J = 9.0 Hz, 2H), 7.75 (d, J = 9.0 Hz, 2H). **^{13}C NMR** (151 MHz, $CDCl_3$): δ 40.25, 55.83, 56.57, 93.03, 96.03, 106.23, 111.83, 112.16, 118.48, 127.44, 152.39, 160.00, 161.04, 161.72, 163.79, 177.87. **IR** (ATR film): 2943, 1635, 1601, 1525, 1489, 1458, 1369, 1347, 1303, 1253, 1217, 1200, 1161, 1117, 1057, 1029, 1002, 908, 819, 729, 674, 642, 618, 592, 511, 467. **HR-MS (ESI):** m/z calcd for $[C_{19}H_{20}NO_4]^+$ ($[M + H^+]$): 326.1387, found: 326.1388. **Melting point:** 211−214 °C.

*5,7-Dimethoxy-2-(4-(trifluoromethyl)phenyl)-4H-chromen-4-one (**8bd**).* Synthesized in accordance with **General Procedure C**. Starting from chalcone **6bd** (100 mg, 0.29 mmol, 1.0 equiv) and I_2 (78.8 mM, 147 μL, 0.01 mmol, 4 mol %). The product was isolated as white solids (26.8 mg, 0.08 mmol 27%). The analytical data was in accordance with the literature.[73] **^{1}H NMR** (600 MHz, $CDCl_3$): δ 3.91 (s, 3H), 3.95 (s, 3H), 6.38 (d, J = 2.3 Hz, 1H), 6.57 (d, J = 2.3 Hz, 1H), 6.70 (s, 1H), 7.74 (d, J = 8.1 Hz, 2H), 7.97 (d, J = 8.1 Hz, 2H). **^{13}C NMR** (151 MHz, $CDCl_3$): δ 55.80, 56.45, 92.88, 96.41, 109.36, 110.30, 123.68 (q, J = 272.2 Hz), 125.91 (q, J = 3.8 Hz), 126.26, 132.77 (q, J = 32.8 Hz), 135.02, 158.87, 159.84, 161.04, 164.34, 177.11. **^{19}F NMR** (282 MHz, $CDCl_3$): δ −62.93. **IR** (ATR film): 2945, 2240, 1645, 1574, 1491, 1459, 1416, 1386, 1322, 1295, 1264, 1218, 1203, 1161, 1070, 1057, 1027, 1016, 908, 841, 807, 731, 675, 635, 616, 586, 564, 528, 514, 493, 468. **HR-MS (ESI):** m/z calcd for $[C_{18}H_{14}F_3O_4]^+$ ($[M + H^+]$): 351.0839, found: 351.0843. **Melting point:** 185−186 °C.

*2-(4-Bromophenyl)-5,7-dimethoxy-4H-chromen-4-one (**8be**).* Synthesized in accordance with **General Procedure C**. Starting from chalcone **6be** (100 mg, 0.28 mmol, 1.0 equiv) and I_2 (78.8 mM, 142 μL, 0.01 mmol, 4 mol %). The product was isolated as white solids (92.6 mg, 0.26 mmol, 93%). The analytical data was in accordance with the literature.[74] **^{1}H NMR** (600 MHz, $CDCl_3$): δ 3.90 (s, 3H), 3.94 (s, 3H), 6.36 (d, J = 2.3 Hz, 1H), 6.54 (d, J = 2.3 Hz, 1H), 6.63 (s, 1H), 7.61 (d, J = 8.6 Hz, 2H), 7.71 (d, J = 8.6 Hz, 2H). **^{13}C NMR** (151 MHz, $CDCl_3$): δ 55.91, 56.57, 92.93, 96.40, 109.33, 109.38, 125.88, 127.47, 130.60, 132.33, 159.64, 159.91, 161.06, 164.28, 177.44. **IR** (ATR film): 2842, 1644, 1607, 1572, 1488, 1459, 1422, 1404, 1380, 1341, 1277, 1217, 1202, 1161, 1118, 1105, 1073, 1057, 1008, 905, 827, 773, 738, 718, 674, 635, 616, 529, 491, 475. **HR-MS (ESI):** m/z calcd for $[C_{17}H_{14}O_4Br]^+$ ($[M + H^+]$): 361.0070, found: 361.0073. **Melting point:** 194−195 °C (197−198 °C).[74]

*2-(3-Bromophenyl)-5,7-dimethoxy-4H-chromen-4-one (**8bf**).* Synthesized in accordance with **General Procedure C**. Starting from chalcone **6bf** (100 mg, 0.28 mmol, 1.0 equiv) and I_2 (78.8 mM, 142 μL, 0.01 mmol, 4 mol %). The product was isolated as white solids (84.9 mg, 0.24 mmol, 85%). The analytical data was in accordance with the literature.[75] **^{1}H NMR** (600 MHz, $CDCl_3$): δ 3.92 (s, 3H), 3.96 (s, 3H), 6.39 (d, J = 2.3 Hz, 1H), 6.58 (d, J = 2.3 Hz, 1H), 6.65 (s, 1H), 7.37 (t, J = 7.9 Hz, 1H), 7.63 (dd, J = 8.0, 1.5 Hz, 1H), 7.77 (dt, J = 7.9, 1.4 Hz, 1H), 8.03 (d, J = 1.9 Hz, 1H). **^{13}C NMR** (151 MHz, $CDCl_3$): δ 55.82, 56.46, 92.85, 96.41, 109.35, 109.75, 123.16, 124.50, 128.93, 130.45, 133.66, 134.00, 158.95, 159.84, 161.00, 164.26, 177.21. **IR** (ATR film): 2949, 1649, 1609, 1571, 1489, 1421, 1384, 1268, 1201, 1160, 1115, 1099, 1063, 1024, 910, 854, 825, 764, 728, 636, 611, 566, 554, 531, 504, 480. **HR-MS (ESI):** m/z calcd for $[C_{17}H_{14}O_4Br]^+$ ($[M + H^+]$): 361.0070, found: 361.0077. **Melting point:** 134−136 °C (278−280 °C)[75] The melting point deviated strongly from the literature-reported value.

*2-(2-Bromophenyl)-5,7-dimethoxy-4H-chromen-4-one (**8bg**).* Synthesized in accordance with **General Procedure C**. Starting from chalcone **6bg** (100 mg, 0.28 mmol, 1.0 equiv) and I_2 (78.8 mM, 142 μL, 0.01 mmol, 4 mol %). The product was isolated as white solids (92.3 mg, 0.26 mmol, 92%). **^{1}H NMR** (600 MHz, $CDCl_3$): δ 3.88 (s, 3H), 3.96 (s, 3H), 6.39 (d, J = 2.3 Hz, 1H), 6.43 (s, 1H), 6.50 (d, J = 2.3 Hz, 1H), 7.35 (td, J = 7.7, 1.7 Hz, 1H), 7.43 (td, J = 7.5, 1.2 Hz, 1H), 7.54 (dd, J = 7.6, 1.7 Hz, 1H), 7.70 (dd, J = 8.1, 1.2 Hz, 1H). **^{13}C NMR** (151 MHz, $CDCl_3$): δ 55.89, 56.59, 92.99, 96.51, 109.48, 114.41, 122.05, 127.71, 130.98, 131.80, 133.97, 134.02, 160.35, 161.20, 161.34, 164.35, 177.28. **IR** (ATR film): 2843, 1644, 1607, 1489, 1459, 1421, 1383, 1334, 1306, 1269, 1217, 1202, 1161, 1119, 1101, 1079, 1057, 1028, 997, 965, 953, 916, 876, 846, 824, 790, 772, 754, 726, 692, 674, 643, 616, 566, 529, 483 **HR-MS (ESI):** m/z calcd for $[C_{17}H_{14}O_4Br]^+$ ($[M +$

https://doi.org/10.1021/acsomega.3c06503
ACS Omega 2023, 8, 41816−41834

H^+]): 361.0070, found: 361.0074. **Melting point:** 162−163 °C.

*rac-(2E,2′E)-1,1′-(2,2′-Dihydroxy-4,4′-dimethoxy-6,6′-dimethyl-[1,1′-biphenyl]-3,3′-diyl)bis(3-(4-methoxyphenyl)-prop-2-en-1-one) (**7aa**).* Synthesized in accordance with **General Procedure B**. Starting from acetophenone **4a** (200 mg, 0.56 mmol, 1.0 equiv) and 4-methoxybenzaldehyde (**5a**) (0.24 mL, 2.01 mmol, 2.4 equiv +1.2 equiv). The product was isolated as orange solids (278 mg, 0.46 mmol, 83%). **^{1}H NMR** (600 MHz, $CDCl_3$): δ 2.11 (s, 6H), 3.86 (s, 6H), 3.99 (s, 6H), 6.43 (s, 2H), 6.94 (d, J = 8.7 Hz, 4H), 7.58 (d, J = 8.7 Hz, 4H), 7.79 (d, J = 15.6 Hz, 2H), 7.84 (d, J = 15.6 Hz, 2H), 13.80 (s, 2H). **^{13}C NMR** (151 MHz, $CDCl_3$): δ 20.87, 55.40, 55.77, 103.30, 109.96, 114.38, 117.73, 125.66, 128.37, 130.16, 142.50, 147.05, 160.12, 161.41, 162.70, 194.03. **IR** (ATR film): 2970, 2839, 1623, 1603, 1558, 1510, 1464, 1422, 1363, 1327, 1304, 1291, 1256, 1216, 1170, 1114, 1037, 908, 871, 828, 770, 647, 619, 559, 536, 521, 487. **HR-MS (ESI):** m/z calcd for $[C_{36}H_{35}O_8]^+$ ([M + H^+]): 595.2327, found: 595.2335. **Melting point:** 212−214 °C.

*rac-(2E,2′E)-1,1′-(2,2′-Dihydroxy-4,4′-dimethoxy-6,6′-dimethyl-[1,1′-biphenyl]-3,3′-diyl)bis(3-phenylprop-2-en-1-one) (**7ab**).* Synthesized in accordance with **General Procedure B**. Starting from acetophenone **4a** (200 mg, 0.56 mmol, 1.0 equiv) and benzaldehyde (**5b**) (0.20 mL, 2.01 mmol, 2.4 + 1.2 equiv). The product was isolated as orange solids (263 mg, 0.49 mmol, 88%). **^{1}H NMR** (600 MHz, $CDCl_3$): δ 2.12 (s, 6H), 4.00 (s, 6H), 6.44 (s, 2H), 7.37−7.45 (m, 6H), 7.59−7.65 (m, 4H), 7.80 (d, J = 15.6 Hz, 2H), 7.94 (d, J = 15.6 Hz, 2H), 13.71 (s, 2H). **^{13}C NMR** (151 MHz, $CDCl_3$): δ 21.06, 55.96, 103.50, 110.07, 117.82, 128.16, 128.56, 129.04, 130.24, 135.76, 142.55, 147.57, 160.38, 162.89, 194.30. **IR** (ATR film): 3104, 3026, 2970, 2942, 2250, 1628, 1609, 1564, 1448, 1388, 1361, 1329, 1272, 1214, 1179, 1115, 1073, 1038, 976, 948, 907, 869, 817, 789, 758, 725, 688, 647, 565, 534, 494. **HR-MS (ESI):** m/z calcd for $[C_{34}H_{31}O_6]^+$ ([M + H^+]): 535.2115, found: 535.2122. **Melting point:** 213−215 °C.

*rac-(2E,2′E)-1,1′-(2,2′-Dihydroxy-4,4′-dimethoxy-6,6′-dimethyl-[1,1′-biphenyl]-3,3′-diyl)bis(3-(4-(dimethylamino)-phenyl)prop-2-en-1-one) (**7ac**).* Synthesized in accordance with **General Procedure B**. Starting from acetophenone **4a** (200 mg, 0.56 mmol, 1.0 equiv) and 4-(dimethylamino)-benzaldehyde (**5c**) (200 mg, 1.34 mmol, 2.4 equiv) at 90 °C. The product was isolated as red solids (175 mg, 0.28 mmol, 50%).

Scaleup: in a 50 mL round-bottom flask, acetophenone **4a** (1.00 g, 2.80 mmol, 1.0 equiv) and 4-(dimethylamino)-benzaldehyde (**5c**) (1.00 g, 6.70 mmol, 2.4 equiv) were given in EtOH (10 mL). Aq. KOH solution was added (3 M, 11 mL, 33.5 mmol, 12.0 equiv). The reaction mixture was stirred at 90 °C. After 24 h, 4-(dimethylamino)benzaldehyde (**5c**) (500 mg, 3.40 mmol, 1.2 equiv) was added. After an additional 24 h heating was stopped, KPi-buffer (1 M, pH 7, 20 mL) was added. The organic phases were extracted using CH_2Cl_2 (3x 100 mL). The combined organic phases were washed with sat. aq. NaCl solution (50 mL) and dried over $MgSO_4$. The solvent was removed in vacuo. The mixture was then resuspended in MeOH (10 mL). Aq. KOH solution was added (3 M, 11.0 mL, 33.5 mmol, 12.0 equiv). Then, 4-(dimethylamino)-benzaldehyde (**5c**) (500 mg, 3.40 mmol, 1.2 equiv) was added and the mixture was stirred at 90 °C for 16 h. The reaction was stopped, and KPi-buffer (1 M, pH 7, 20 mL) was added. The organic phases were extracted using CH_2Cl_2 (3 × 100 mL). The combined organic phases were washed with sat. aq. NaCl solution (50 mL) and dried over $MgSO_4$. MeOH (15 mL) was added to the solution, and the solvent was carefully removed in vacuo. The resulting mixture was macerated with MeOH (15 mL). The solids were filtered off and washed with copious amounts of MeOH. The product was obtained as red solids (607 mg, 0.98 mmol, 35%). **^{1}H NMR** (600 MHz, $CDCl_3$): δ 2.10 (s, 6H), 3.04 (s, 12H), 3.98 (s, 6H), 6.41 (s, 2H), 6.70 (d, J = 8.6 Hz, 4H), 7.53 (d, J = 8.5 Hz, 4H), 7.78 (d, J = 15.4 Hz, 2H), 7.84 (d, J = 15.5 Hz, 2H), 13.96 (s, 2H). **^{13}C NMR** (151 MHz, $CDCl_3$): δ 20.98, 40.30, 55.87, 103.40, 110.29, 112.07, 118.01, 122.95, 123.69, 129.01, 130.54, 144.05, 146.58, 152.03, 160.15, 162.83, 193.97. **IR** (ATR film): 1602, 1543, 1525, 1472, 1445, 1414, 1364, 1316, 1298, 1228, 1211, 1167, 1113, 1067, 979, 947, 866, 815, 732, 703, 651, 613, 569, 541, 469. **HR-MS (ESI):** m/z calcd for $[C_{38}H_{41}N_2O_6]^+$ ([M + H^+]): 621.2959, found: 621.2962. **Melting point:** 265 °C (decomposition).

*rac-(2E,2′E)-1,1′-(2,2′-Dihydroxy-4,4′-dimethoxy-6,6′-dimethyl-[1,1′-biphenyl]-3,3′-diyl)bis(3-(4-(trifluoromethyl)-phenyl)prop-2-en-1-one) (**7ad**).* Synthesized in accordance with **General Procedure B**. Starting from acetophenone **4a** (200 mg, 0.56 mmol, 1.0 equiv) and 4-(trifluoromethyl)-benzaldehyde (**5d**) (0.25 mL, 2.01 mmol, 2.4 + 1.2 equiv). The product was isolated as orange solids (232 mg, 0.35 mmol, 62%). **^{1}H NMR** (600 MHz, $CDCl_3$): δ 2.12 (s, 6H), 4.00 (s, 6H), 6.45 (s, 2H), 7.67 (d, J = 8.2 Hz, 4H), 7.71 (d, J = 8.1 Hz, 4H), 7.76 (d, J = 15.6 Hz, 2H), 7.97 (d, J = 15.7 Hz, 2H), 13.59 (s, 2H). **^{13}C NMR** (151 MHz, $CDCl_3$): δ 21.10, 56.03, 103.55, 109.97, 117.77, 124.09 (q, J = 271.5), 126.00 (q, J = 3.8 Hz), 128.54, 130.49, 131.65 (q, J = 33.4 Hz), 139.17, 140.30, 148.08, 160.41, 162.94, 193.93. **^{19}F NMR** (282 MHz, $CDCl_3$): δ −62.76. **IR** (ATR film): 2946, 2852, 1609, 1570, 1481, 1452, 1414, 1389, 1362, 1321, 1288, 1273, 1216, 1180, 1116, 1068, 1034, 1017, 979, 954, 834, 734, 716, 673, 652, 593, 571, 535. **HR-MS (ESI):** m/z calcd for $[C_{36}H_{29}F_6O_6]^+$ ([M + H^+]): 671.1863, found: 671.1866. **Melting point:** 208−209 °C.

*rac-(2E,2′E)-1,1′-(2,2′-Dihydroxy-4,4′-dimethoxy-6,6′-dimethyl-[1,1′-biphenyl]-3,3′-diyl)bis(3-(4-bromophenyl)prop-2-en-1-one) (**7ae**).* Synthesized in accordance with **General Procedure B**. Starting from acetophenone **4a** (200 mg, 0.56 mmol, 1.0 equiv) and 4-bromobenzaldehyde (**5e**) (248 mg 1.34 mmol, 2.4 equiv). The product was isolated as orange solids (364 mg, 0.53 mmol, 94%). **^{1}H NMR** (600 MHz, $CDCl_3$): δ 2.11 (s, 6H), 3.99 (s, 6H), 6.43 (s, 2H), 7.47 (d, J = 8.5 Hz, 4H), 7.54 (d, J = 8.4 Hz, 3H), 7.71 (d, J = 15.6 Hz, 2H), 7.90 (d, J = 15.6 Hz, 2H), 13.65 (s, 2H). **^{13}C NMR** (151 MHz, $CDCl_3$): δ 21.06, 56.00, 103.51, 110.00, 117.80, 124.43, 128.73, 129.88, 132.29, 134.68, 141.07, 147.79, 160.35, 162.90, 194.02. **IR** (ATR film): 2970, 2941, 2848, 2251, 1627, 1605, 1559, 1485, 1389, 1359, 1323, 1213, 1178, 1141, 1114, 1072, 1035, 1009, 979, 946, 908, 875, 819, 801, 786, 731, 648, 632, 604, 571, 535, 507, 491. **HR-MS (ESI):** m/z calcd for $[C_{34}H_{29}O_6Br_2]^+$ ([M + H^+]): 691.0325, found: 691.0324. **Melting point:** 230−236 °C.

*rac-(2E,2′E)-1,1′-(2,2′-Dihydroxy-4,4′-dimethoxy-6,6′-dimethyl-[1,1′-biphenyl]-3,3′-diyl)bis(3-(3-bromophenyl)prop-2-en-1-one) (**7af**).* Synthesized in accordance with **General Procedure B**. Starting from acetophenone **4a** (200 mg, 0.56 mmol, 1.0 equiv) and 3-bromobenzaldehyde (**5f**) (0.16 mL, 1.34 mmol, 2.4 equiv). The product was isolated as orange

https://doi.org/10.1021/acsomega.3c06503
ACS Omega 2023, 8, 41816−41834

solids (335 mg, 0.48 mmol, 86%). **^{1}H NMR** (600 MHz, $CDCl_3$): δ 2.11 (s, 6H), 4.00 (s, 6H), 6.44 (s, 2H), 7.29 (t, J = 7.8 Hz, 2H), 7.51 (dt, J = 8.1, 1.5 Hz, 4H), 7.68 (d, J = 15.6 Hz, 2H), 7.74 (t, J = 1.8 Hz, 2H), 7.89 (d, J = 15.6 Hz, 2H), 13.63 (s, 2H). **^{13}C NMR** (151 MHz, $CDCl_3$): δ 21.09, 56.04, 103.51, 109.92, 117.71, 123.15, 127.20, 129.43, 130.53, 131.06, 132.94, 137.88, 140.62, 147.92, 160.37, 162.90, 193.93. **IR** (ATR film): 2922, 1630, 1469, 1389, 1323, 1274, 1180, 1116, 1035, 907, 864, 795, 778, 730, 648. **HR-MS (ESI):** m/z calcd for $[C_{34}H_{29}O_6Br_2]^+$ ([M + H$^+$]): 691.0325, found: 691.0324. **Melting point:** 110 °C (decomposition).

*rac-(2E,2′E)-1,1′-(2,2′-Dihydroxy-4,4′-dimethoxy-6,6′-dimethyl-[1,1′-biphenyl]-3,3′-diyl)bis(3-(2-bromophenyl)prop-2-en-1-one) (**7ag**).* Synthesized in accordance with **General Procedure B**. Starting from acetophenone **4a** (200 mg, 0.56 mmol, 1.0 equiv) and 2-bromobenzaldehyde (**5g**) (0.16 mL, 1.34 mmol, 2.4 equiv). The product was isolated as orange solids (253 mg, 0.36 mmol, 65%). **^{1}H NMR** (600 MHz, $CDCl_3$): δ 2.11 (s, 6H), 3.98 (s, 6H), 6.43 (s, 2H), 7.24 (td, J = 7.7, 1.6 Hz, 2H), 7.36 (td, J = 7.4, 1.0 Hz, 2H), 7.64 (dd, J = 8.0, 1.3 Hz, 2H), 7.70 (dd, J = 7.8, 1.6 Hz, 2H), 7.85 (d, J = 15.5 Hz, 2H), 8.11 (d, J = 15.6 Hz, 2H), 13.61 (s, 2H). **^{13}C NMR** (151 MHz, $CDCl_3$): δ 20.93, 55.83, 103.33, 109.85, 117.63, 125.88, 127.62, 127.96, 130.69, 130.86, 133.54, 135.70, 140.43, 147.70, 160.21, 162.79, 193.76. **IR** (ATR film): 2851, 1610, 1573, 1465, 1361, 1214, 1180, 1117, 1027, 907, 730, 535. **HR-MS (ESI):** m/z calcd for $[C_{34}H_{29}O_6Br_2]^+$ ([M + H$^+$]): 691.0325, found: 691.0323. **TLC** (petroleum ether/EtOAc, 6:4 v/v): R_f = 0.44 **Melting point:** 220−221 °C.

*rac-(2E,2′E)-1,1′-(2,2′-Dihydroxy-4,4′,6,6′-tetramethoxy-[1,1′-biphenyl]-3,3′-diyl)bis(3-(4-methoxyphenyl)prop-2-en-1-one) (**7ba**).* Synthesized in accordance with **General Procedure B**. Starting from acetophenone **4b** (200 mg, 0.56 mmol, 1.0 equiv) and 4-methoxybenzaldehyde (**5a**) (0.15 mL, 1.23 mmol, 2.4 equiv). The product was isolated as yellow solids (145 mg, 0.25 mmol, 45%). The analytical data is in accordance with the literature.[29] **^{1}H NMR** (600 MHz, $CDCl_3$): δ 3.86 (s, 12H), 4.01 (s, 6H), 6.14 (s, 2H), 6.93 (d, J = 8.6 Hz, 4H), 7.56 (d, J = 8.5 Hz, 4H), 7.76 (d, J = 15.5 Hz, 2H), 7.82 (d, J = 15.6 Hz, 2H), 14.20 (s, 2H). **^{13}C NMR** (151 MHz, $CDCl_3$): δ 55.55, 55.98, 56.08, 87.20, 103.27, 106.93, 114.50, 125.90, 128.69, 130.18, 142.07, 161.40, 162.93, 164.02, 164.78, 193.18. **IR** (ATR film): 1739, 1622, 1604, 1510, 1466, 1407, 1371, 1290, 1255, 1215, 1171, 1122, 829, 801, 776, 603, 559, 539, 520. **HR-MS (ESI):** m/z calcd for $[C_{36}H_{35}O_{10}]^+$ ([M + H$^+$]): 627.2225, found: 627.2227. **Melting point:** 284−285 °C (282−285 °C).[29]

*rac-(2E,2′E)-1,1′-(2,2′-Dihydroxy-4,4′,6,6′-tetramethoxy-[1,1′-biphenyl]-3,3′-diyl)bis(3-phenylprop-2-en-1-one) (**7bb**).* Synthesized in accordance with **General Procedure B**. Starting from acetophenone **4b** (200 mg, 0.51 mmol, 1.0 equiv) and benzaldehyde (**5b**) (0.19 mL, 1.85 mmol, 2.4 + 1.2 equiv). The product was isolated as yellow solids (65.8 mg, 0.13 mmol, 23%). **^{1}H NMR** (600 MHz, $CDCl_3$): δ 3.86 (s, 6H), 4.02 (s, 6H), 6.15 (s, 2H), 7.37−7.44 (m, 6H), 7.61 (d, J = 7.1 Hz, 4H), 7.77 (d, J = 15.6 Hz, 2H), 7.91 (d, J = 15.6 Hz, 2H), 14.11 (s, 2H). **^{13}C NMR** (151 MHz, $CDCl_3$): δ 56.00, 56.10, 87.20, 103.20, 106.90, 128.25, 128.47, 129.00, 130.04, 135.94, 141.97, 163.06, 164.25, 164.80, 193.25. **IR** (ATR film): 2918, 2850, 1737, 1617, 1560, 1470, 1450, 1435, 1373, 1331, 1287, 1217, 1179, 1155, 1122, 1037, 870, 804, 762, 726, 703, 685, 662, 633, 576, 532, 477 **HR-MS (ESI):** m/z calcd for $[C_{34}H_{31}O_8]^+$ ([M + H$^+$]): 567.2013, found: 567.2020. **Melting point:** 272 °C (decomposition).

*rac-(2E,2′E)-1,1′-(2,2′-Dihydroxy-4,4′,6,6′-tetramethoxy-[1,1′-biphenyl]-3,3′-diyl)bis(3-(4-(dimethylamino)phenyl)-prop-2-en-1-one) (**7bc**).* Synthesized in accordance with **General Procedure B**. Starting from acetophenone **4b** (200 mg, 0.51 mmol, 1.0 equiv) and 4-(dimethylamino)-benzaldehyde (**5c**) (183.4 mg, 1.23 mmol, 2.4 equiv) at 90 °C. The product was isolated as red solids (80.2 mg, 0.13 mmol, 24%). (Due to poor solubility in $CDCl_3$, and d_6-DMSO, only a ^{1}H NMR spectrum could be obtained.) **^{1}H NMR** (600 MHz, $CDCl_3$): δ 3.04 (s, 12H), 3.84 (s, 6H), 4.00 (s, 6H), 6.13 (s, 2H), 6.70 (d, J = 8.6 Hz, 4H), 7.52 (d, J = 8.5 Hz, 4H), 7.76 (d, J = 15.4 Hz, 2H), 7.81 (d, J = 15.4 Hz, 2H), 14.37 (s, 2H). **IR** (ATR film): 2850, 1598, 1542, 1527, 1467, 1434, 1411, 1370, 1334, 1295, 1214, 1168, 1114, 1038, 996, 982, 970, 863, 818, 776, 722, 702, 662, 605, 543. **HR-MS (ESI):** m/z calcd for $[C_{38}H_{41}N_2O_8]^+$ ([M + H$^+$]): 653.2857, found: 653.2851. **Melting point:** 302 °C (decomposition).

*rac-(2E,2′E)-1,1′-(2,2′-Dihydroxy-4,4′,6,6′-tetramethoxy-[1,1′-biphenyl]-3,3′-diyl)bis(3-(4-(trifluoromethyl)phenyl)-prop-2-en-1-one) (**7bd**).* Synthesized in accordance with **General Procedure B**. Starting from acetophenone **4b** (200 mg, 0.51 mmol, 1.0 equiv) and 4-(trifluoromethyl)-benzaldehyde (**5d**) (0.17 mL, 1.23 mmol, 2.4 equiv). The product was isolated as yellow solids (95.0 mg, 0.15 mmol, 27%). **^{1}H NMR** (600 MHz, $CDCl_3$): δ 3.87 (s, 6H), 4.02 (s, 6H), 6.15 (s, 2H), 7.66 (d, J = 8.2 Hz, 4H), 7.69 (d, J = 8.2 Hz, 4H), 7.73 (d, J = 15.7 Hz, 2H), 7.94 (d, J = 15.7 Hz, 2H), 13.99 (s, 2H). **^{13}C NMR** (151 MHz, $CDCl_3$): δ 56.05, 56.12, 87.21, 103.14, 106.80, 124.12 (q, J = 271.3 Hz), 125.96 (q, J = 3.8 Hz), 128.45, 130.61, 131.46 (q, J = 32.7 Hz), 139.36, 139.75, 163.13, 164.57, 164.83, 192.79. **^{19}F NMR** (282 MHz, $CDCl_3$): δ −62.74. **IR** (ATR film): 2921, 2852, 1731, 1611, 1566, 1467, 1405, 1321, 1286, 1215, 1122, 1067, 1032, 1016, 954, 907, 834, 775, 732, 649, 597, 531. **HR-MS (ESI):** m/z calcd for $[C_{36}H_{29}F_6O_8]^+$ ([M + H$^+$]): 703.1761, found: 703.1767. **Melting point:** 251 °C (decomposition).

*rac-(2E,2′E)-1,1′-(2,2′-Dihydroxy-4,4′,6,6′-tetramethoxy-[1,1′-biphenyl]-3,3′-diyl)bis(3-(4-bromophenyl)prop-2-en-1-one) (**7be**).* Synthesized in accordance with **General Procedure B**. Starting from acetophenone **4b** (200 mg, 0.56 mmol, 1.0 equiv) and 4-bromobenzaldehyde (**5e**) (227 mg, 1.23 mmol, 2.4 equiv). The product was isolated as yellow solids (202 mg, 0.31 mmol, 55%). **^{1}H NMR** (600 MHz, $CDCl_3$): δ 3.86 (s, 6H), 4.01 (s, 6H), 6.14 (s, 2H), 7.45 (d, J = 8.4 Hz, 4H), 7.53 (d, J = 8.3 Hz, 4H), 7.67 (d, J = 15.6 Hz, 2H), 7.88 (d, J = 15.6 Hz, 2H), 14.05 (s, 2H). **^{13}C NMR** (151 MHz, $CDCl_3$): δ 56.03, 56.10, 87.20, 103.17, 106.83, 124.19, 128.83, 129.79, 132.24, 134.86, 140.51, 163.05, 164.38, 164.80, 192.92. **IR** (ATR film): 2918, 2850, 1738, 1628, 1556, 1486, 1471, 1436, 1399, 1372, 1328, 1291, 1214, 1180, 1154, 1090, 1073, 1033, 1009, 974, 820, 648, 631. **HR-MS (ESI):** m/z calcd for $[C_{34}H_{29}Br_2O_8]^+$ ([M + H$^+$]): 723.0220, found: 723.0224. **Melting point:** 274 °C (decomposition).

*rac-(2E,2′E)-1,1′-(2,2′-Dihydroxy-4,4′,6,6′-tetramethoxy-[1,1′-biphenyl]-3,3′-diyl)bis(3-(3-bromophenyl)prop-2-en-1-one) (**7bf**).* Synthesized in accordance with **General Procedure B**. Starting from acetophenone **4b** (200 mg, 0.56 mmol, 1.0 equiv) and 3-bromobenzaldehyde (**5f**) (0.14 mL, 1.23 mmol, 2.4 equiv). The product was obtained as yellow solids (124 mg). A 3:1 mix of chalcone:flavanone with monoaddition product present (according to ^{1}H NMR). ^{1}H

https://doi.org/10.1021/acsomega.3c06503
ACS Omega 2023, 8, 41816−41834

NMR reported for the major chalcone product. **^{1}H NMR** (600 MHz, $CDCl_3$): δ 3.86 (d, 6H), 4.03 (s, 6H), 6.15 (s, 2H), 7.29 (t, J = 7.9 Hz, 2H), 7.50 (d, J = 7.8 Hz, 4H), 7.65 (d, J = 15.5 Hz, 2H), 7.73 (s, 2H), 7.87 (d, J = 15.6 Hz, 2H), 14.03 (s, 2H). **HR-MS (ESI):** m/z calcd for $[C_{34}H_{29}Br_2O_8]^+$ ($[M + H^+]$): 723.0221, found: 723.0224.

*rac-(2E,2′E)-1,1′-(2,2′-Dihydroxy-4,4′,6,6′-tetramethoxy-[1,1′-biphenyl]-3,3′-diyl)bis(3-(2-bromophenyl)prop-2-en-1-one) (**7bg**).* Synthesized in accordance with **General Procedure B**. Starting from acetophenone **4b** (200 mg, 0.56 mmol, 1.0 equiv) and 2-bromobenzaldehyde (**5g**) (0.14 mL, 1.23 mmol, 2.4 equiv), 1.5 h reaction time. The product was obtained as yellow solids (84.7 mg). A 5:1 mix of chalcone:flavanone with monoaddition product present (according to ^{1}H NMR). ^{1}H NMR reported for the major chalcone product. **^{1}H NMR** (600 MHz, $CDCl_3$): δ 3.86 (s, 6H), 4.00 (s, 6H), 6.13 (s, 2H), 7.22 (t, J = 7.7 Hz, 2H), 7.35 (t, J = 7.8 Hz, 2H), 7.63 (d, J = 8.0 Hz, 2H), 7.69 (d, J = 7.6 Hz, 3H), 7.82 (d, J = 15.6 Hz, 2H), 8.07 (d, J = 15.6 Hz, 2H), 13.96 (s, 1H). **HR-MS (ESI):** m/z calcd for $[C_{34}H_{29}Br_2O_8]^+$ ($[M + H^+]$): 723.0216, found: 723.0224.

*rac-5,5′-Dimethoxy-2,2′-bis(4-methoxyphenyl)-7,7′-dimethyl-4H,4′H-[8,8′-bichromene]-4,4′-dione (**9aa**).* Synthesized in accordance with **General Procedure D**. Starting from bichalcone **7ab** (30.0 mg, 50.7 μmol, 1.00 equiv) and I_2 (78.8 mM, 63 μL, 5.1 μmol, 10 mol %) in 1 h. The product was isolated by column chromatography (EtOAc/MeOH, 95:5 v/v) and was obtained as white solids (15.8 mg, 30.2 μmol, 53%). The analytical data was in accordance with the literature.[24] **^{1}H NMR** (600 MHz, $CDCl_3$): δ 2.18 (s, 6H), 3.79 (s, 6H), 4.11 (s, 6H), 6.64 (s, 2H), 6.78 (d, J = 8.9 Hz, 4H), 6.88 (s, 2H), 7.23 (d, J = 8.9 Hz, 4H). **^{13}C NMR** (151 MHz, $CDCl_3$): δ 20.76, 55.63, 56.72, 107.23, 108.34, 112.96, 114.66, 116.56, 123.48, 127.32, 144.67, 155.77, 159.28, 160.94, 162.32, 178.62. **IR** (ATR film): 2844, 2238, 1605, 1576, 1512, 1496, 1478, 1464, 1442, 1423, 1371, 1335, 1301, 1207, 1116, 1062, 1031, 976, 956, 909, 730, 644, 590. **TLC** (EtOAc/MeOH, 95:5 v/v): R_f = 0.26 **HR-MS (ESI):** m/z calcd for $[C_{36}H_{31}O_8]^+$ ($[M + H^+]$): 591.2013, found: 591.2020. **Melting point:** 295−296 °C.

*rac-5,5′-Dimethoxy-7,7′-dimethyl-2,2′-diphenyl-4H,4′H-[8,8′-bichromene]-4,4′-dione (**9ab**).* Synthesized in accordance with **General Procedure D**. Starting from bichalcone **7ab** (30.0 mg, 56.5 μmol, 1.00 equiv) and I_2 (78.8 mM, 72 μL, 5.7 μmol, 10 mol %). The product was isolated by column chromatography (EtOAc/MeOH, 98:2 v/v) and was obtained as white solids (6.2 mg, 12 μmol, 21%). **^{1}H NMR** (600 MHz, $CDCl_3$): δ 2.19 (s, 6H), 4.11 (s, 6H), 6.73 (s, 2H), 6.89 (s, 2H), 7.26−7.33 (m, 8H), 7.34−7.40 (m, 2H). **^{13}C NMR** (151 MHz, $CDCl_3$): δ 20.65, 56.57, 108.28, 108.50, 112.92, 116.35, 125.44, 129.01, 131.09, 131.29, 144.81, 155.66, 159.20, 160.64, 178.44. **IR** (ATR film): 3005, 2848, 1640, 1597, 1578, 1495, 1479, 1464, 1450, 1370, 1333, 1307, 1281, 1258, 1207, 1189, 1122, 1062, 976, 955, 908, 850, 771, 730, 689, 665, 645, 612, 551, 531. **TLC** (EtOAc/MeOH, 98:2 v/v): R_f = 0.28 **HR-MS (ESI):** m/z calcd for $[C_{34}H_{27}O_6]^+$ ($[M + H^+]$): 531.1802, found: 531.1805. **Melting point:** 296 °C.

*rac-2,2′-Bis(4-(dimethylamino)phenyl)-5,5′-dimethoxy-7,7′-dimethyl-4H,4′H-[8,8′-bichromene]-4,4′-dione (**9ac**).* Synthesized in accordance with **General Procedure D**. Starting from bichalcone **7ac** (30.0 mg, 48.6 μmol, 1.00 equiv) and I_2 (78.8 mM, 62 μL, 4.9 μmol, 10 mol %). The product was isolated by column chromatography and was obtained as orange solids (6.3 mg, 10 μmol, 21%). The reaction was repeatedly scaled up with bichalcone **7ac** (575 mg, 0.93 mmol, 1.00 equiv). The product was isolated as orange solids (123 mg, 0.20 μmol, 21%). The purity of biflavone **9ac** was assessed by reverse-phase HPLC (97.3%) and was in accordance with purity determined by ^{1}H NMR (96.9%). Stability experiments revealed that biflavone **9ac** was stable in DMSO at up to 40 °C over 24 h. **^{1}H NMR** (600 MHz, $CDCl_3$): δ 2.17 (s, 3H), 2.97 (s, 6H), 4.10 (s, 3H), 6.51 (d, J = 9.1 Hz, 4H), 6.58 (s, 1H), 6.86 (s, 1H), 7.16 (d, J = 9.0 Hz, 4H). **^{13}C NMR** (151 MHz, $CDCl_3$): δ 20.71, 40.17, 56.64, 105.38, 108.02, 111.79, 112.83, 116.66, 117.70, 127.05, 144.20, 152.28, 155.70, 159.00, 161.92, 178.80. **IR** (ATR film): 2923, 2237, 1731, 1604, 1591, 1524, 1495, 1364, 1335, 1302, 1284, 1251, 1197, 1171, 1120, 1063, 908, 819, 761, 728, 662, 642, 582, 570, 544, 531, 512. **TLC** ($EtOAc/CH_2Cl_2$/MeOH, 7:2.5:0.5 v/v): R_f = 0.16 **HR-MS (ESI):** m/z calcd for $[C_{38}H_{37}N_2O_6]^+$ ($[M + H^+]$): 617.2646, found: 617.2653. **Melting point:** 196−197 °C.

*rac-5,5′-Dimethoxy-7,7′-dimethyl-2,2′-bis(4-(trifluoromethyl)phenyl)-4H,4′H-[8,8′-bichromene]-4,4′-dione (**9ad**).* Synthesized in accordance with **General Procedure D**. Starting from bichalcone **7ad** (30.0 mg, 45.0 μmol, 1.00 equiv) and I_2 (78.8 mM, 57 μL, 4.5 μmol, 10 mol %) for 2 h. The product was isolated by column chromatography (petroleum ether/EtOAc/isopropanol, 6:3:1 v/v) and was obtained as a white viscous semisolid (8.5 mg, 13 μmol, 28%). **^{1}H NMR** (600 MHz, $CDCl_3$): δ 2.21 (s, 6H), 4.12 (s, 6H), 6.78 (s, 2H), 6.93 (s, 2H), 7.40 (d, J = 8.2 Hz, 4H), 7.56 (d, J = 8.3 Hz, 4H). **^{13}C NMR** (151 MHz, $CDCl_3$): δ 20.83, 56.78, 108.68, 109.89, 113.06, 116.21, 123.61 (q, J = 272.1 Hz), 125.84, 126.22 (q, J = 3.7 Hz), 133.12 (q, J = 33.1 Hz), 134.59, 145.37, 155.68, 159.03, 159.52, 178.08. **^{19}F NMR** (282 MHz, $CDCl_3$): δ −63.13. **IR** (ATR film): 2854, 1817, 1646, 1600, 1579, 1497, 1480, 1466, 1445, 1417, 1323, 1295, 1207, 1125, 1063, 1015, 977, 957, 909, 844, 777, 731, 625, 557, 532, 518. **TLC** (petroleum ether/EtOAc/isopropanol, 6:3:1 v/v): R_f = 0.21 **HR-MS (ESI):** m/z calcd for $[C_{36}H_{25}F_6O_6]^+$ ($[M + H^+]$): 667.1555, found: 667.1550. **Melting point:** 263−265 °C.

*rac-2,2′-Bis(4-bromophenyl)-5,5′-dimethoxy-7,7′-dimethyl-4H,4′H-[8,8′-bichromene]-4,4′-dione (**9ae**).* Synthesized in accordance with **General Procedure D**. Starting from bichalcone **7ae** (30.0 mg, 43.6 μmol, 1.00 equiv) and I_2 (78.8 mM, 55 μL, 4.4 μmol, 10 mol %). The product was obtained as white solids (27.7 mg, 40.1 μmol, 94%). **^{1}H NMR** (600 MHz, $CDCl_3$): δ 2.18 (s, 6H), 4.10 (s, 6H), 6.69 (s, 2H), 6.89 (s, 2H), 7.14 (d, J = 8.7 Hz, 4H), 7.42 (d, J = 8.7 Hz, 4H). **^{13}C NMR** (151 MHz, $CDCl_3$): δ 20.82, 56.74, 108.49, 108.77, 112.94, 116.23, 126.19, 126.93, 130.08, 132.49, 145.14, 155.62, 159.37, 159.72, 178.26. **IR** (ATR film): 3005, 2931, 2851, 2240, 1773, 1638, 1597, 1562, 1479, 1464, 1403, 1368, 1329, 1303, 1275, 1260, 1207, 1187, 1167, 1122, 1061, 1030, 1008, 977, 955, 907, 830, 794, 681, 645, 626, 573, 557, 532, 499, 478. **HR-MS (ESI):** m/z calcd for $[C_{34}H_{25}O_4Br_2]^+$ ($[M + H^+]$): 687.0012, found: 687.0017. **Melting point:** 245 °C (decomposition).

*rac-2,2′-Bis(3-bromophenyl)-5,5′-dimethoxy-7,7′-dimethyl-4H,4′H-[8,8′-bichromene]-4,4′-dione (**9af**).* Synthesized in accordance with **General Procedure D**. Starting from bichalcone **7af** (30.0 mg, 43.6 μmol, 1.00 equiv) and I_2 (78.8 mM, 55 μL, 4.4 μmol, 10 mol %) for 1 h. The product was isolated by column chromatography (EtOAc 100%) and

https://doi.org/10.1021/acsomega.3c06503
ACS Omega 2023, 8, 41816−41834

was obtained as white solids (25.4 mg, 37.5 μmol, 86%). **^{1}H NMR** (600 MHz, $CDCl_3$): δ 2.24 (s, 6H), 4.11 (s, 6H), 6.70 (s, 2H), 6.94 (s, 2H), 7.18 (t, *J* = 7.9 Hz, 2H), 7.31 (dt, *J* = 8.0, 1.4 Hz, 2H), 7.34 (t, *J* = 1.9 Hz, 2H), 7.49 (ddd, *J* = 8.0, 2.0, 1.0 Hz, 2H). **^{13}C NMR** (151 MHz, $CDCl_3$): δ 20.84, 56.73, 108.62, 109.16, 113.03, 116.16, 123.38, 123.91, 128.77, 130.58, 133.21, 134.18, 145.20, 155.49, 158.77, 159.50, 178.11. **IR** (ATR film): 2851, 2241, 1642, 1598, 1561, 1496, 1478, 1442, 1417, 1367, 1299, 1266, 1206, 1124, 1062, 998, 956, 917, 847, 790, 730, 692, 646, 619, 571, 551, 532. **TLC** (EtOAc 100%): R_f = 0.26 **HR-MS (ESI):** *m/z* calcd for $[C_{34}H_{25}O_4Br_2]^+$ ([M + H$^+$]): 687.0012, found: 687.0005. **Melting point:** 276−278 °C.

*rac-2,2′-Bis(2-bromophenyl)-5,5′-dimethoxy-7,7′-dimethyl-4H,4′H-[8,8′-bichromene]-4,4′-dione (**9ag**).* Synthesized in accordance with **General Procedure D**. Starting from bichalcone **7ag** (30.0 mg, 43.6 μmol, 1.00 equiv) and I_2 (78.8 mM, 55 μL, 4.4 μmol, 10 mol %) for 2 h. The product was obtained as white solids (16.5 mg, 24.0 μmol, 55%). **^{1}H NMR** (600 MHz, $CDCl_3$): δ 2.12 (s, 6H), 4.02 (s, 6H), 6.46 (s, 2H), 6.78 (s, 2H), 7.20 (td, *J* = 7.4, 6.9, 2.0 Hz, 2H), 7.21−7.29 (m, 4H), 7.51 (dd, *J* = 7.8, 1.5 Hz, 2H). **^{13}C NMR** (151 MHz, $CDCl_3$): δ 20.93, 56.54, 108.54, 113.00, 114.33, 116.56, 121.57, 127.67, 130.73, 131.78, 133.49, 134.22, 144.91, 156.39, 159.23, 161.62, 178.19. **IR** (ATR film): 3300, 2924, 2869, 2852, 1733, 1653, 1600, 1562, 1496, 1464, 1437, 1370, 1327, 1279, 1263, 1206, 1115, 1065, 976, 954, 912, 855, 763, 733, 703, 680, 645, 612. **HR-MS (ESI):** *m/z* calcd for $[C_{34}H_{25}O_4Br_2]^+$ ([M + H$^+$]): 687.0012, found: 687.0011. **Melting point:** 250 °C (decomposition).

*rac-5,5′,7,7′-Tetramethoxy-2,2′-bis(4-methoxyphenyl)-4H,4′H-[8,8′-bichromene]-4,4′-dione or Hexa-O-methylcupressuflavone (**9ba**).* Synthesized in accordance with **General Procedure D**. Starting from bichalcone **7ba** (30.0 mg, 48.2 μmol, 1.00 equiv) and I_2 (78.8 mM, 61 μL, 4.8 μmol, 10 mol %). The product was isolated by column chromatography (EtOAc/MeOH, 9:1 v/v) and was obtained as white solids (23.1 mg, 37.1 μmol, 77%). The analytical data was in accordance with the literature.[29] **^{1}H NMR** (600 MHz, $CDCl_3$): δ 3.77 (s, 6H), 3.86 (s, 6H), 4.12 (s, 6H), 6.58 (s, 2H), 6.59 (s, 2H), 6.77 (d, *J* = 8.9 Hz, 4H), 7.29 (d, *J* = 8.9 Hz, 4H). **^{13}C NMR** (151 MHz, $CDCl_3$): δ 55.47, 56.13, 56.60, 91.78, 102.13, 106.80, 109.05, 114.39, 123.54, 127.15, 156.57, 160.66, 161.29, 161.74, 162.03, 178.14. **IR** (ATR film): 1637, 1593, 1465, 1424, 1388, 1338, 1304, 1180, 1111, 1033, 919, 834, 588, 567. **TLC** (EtOAc/MeOH, 9:1 v/v): R_f = 0.22 **HR-MS (ESI):** *m/z* calcd for $[C_{36}H_{31}O_{10}]^+$ ([M + H$^+$]): 623.1912, found: 623.1912. **Melting point:** 240.0 °C (brown discoloration) 285−286 °C (294−295 °C).[29]

*rac-5,5′,7,7′-Tetramethoxy-2,2′-diphenyl-4H,4′H-[8,8′-bichromene]-4,4′-dione (**9bb**).* Synthesized in accordance with **General Procedure D**. Starting from **7bb** (30.0 mg, 53.3 μmol, 1.00 equiv) and I_2 (78.8 mM, 68 μL, 5.3 μmol, 10 mol %) for 2 h. The product was isolated by column chromatography (EtOAc/MeOH, 98:2 v/v) and was obtained as white solids (17.6 mg, 31.4 μmol, 59%). The analytical data was in accordance with the literature.[34] **^{1}H NMR** (600 MHz, $CDCl_3$): δ 3.85 (s, 6H), 4.12 (s, 6H), 6.59 (s, 2H), 6.68 (s, 2H), 7.28 (d, *J* = 7.4 Hz, 4H), 7.33−7.40 (m, 6H). **^{13}C NMR** (151 MHz, $CDCl_3$): δ 56.25, 56.72, 91.92, 102.19, 108.36, 109.29, 125.56, 129.01, 131.23, 131.42, 156.77, 160.62, 161.51, 161.99, 178.19. **IR** (ATR film): 3067, 2844, 2238, 1635, 1590, 1508, 1491, 1465, 1450, 1435, 1388, 1333, 1299, 1265, 1214, 1190, 1172, 1125, 1109, 1087, 1036, 1022, 957, 917, 849, 812, 771, 728, 689, 672, 644, 618, 570, 546, 514. **TLC** (EtOAc/MeOH, 98:2 v/v): R_f = 0.12 **HR-MS (ESI):** *m/z* calcd for $[C_{34}H_{27}O_8]^+$ ([M + H$^+$]): 563.1700, found: 563.1707. **Melting point:** 312−313 °C (318−319 °C).[34]

*rac-2,2′-Bis(4-(dimethylamino)phenyl)-5,5′,7,7′-tetramethoxy-4H,4′H-[8,8′-bichromene]-4,4′-dione (**9bc**).* Synthesized in accordance with **General Procedure D**. Starting from **7bc** (30.0. mg, 46.3 μmol, 1.00 equiv) and I_2 (78.8 mM, 59 μL, 4.6 μmol, 10 mol %). The product was isolated by column chromatography (CH_2Cl_2/EtOAc/MeOH, 5:4.5:0.5 v/v) and obtained as orange solids (7.7 mg, 12 μmol, 26%). **^{1}H NMR** (600 MHz, $CDCl_3$): δ 2.95 (s, 12H), 3.86 (s, 6H), 4.11 (s, 6H), 6.50 (d, *J* = 8.9 Hz, 4H), 6.53 (s, 2H), 6.56 (s, 2H), 7.21 (d, *J* = 9.0 Hz, 4H). **^{13}C NMR** (151 MHz, $CDCl_3$): δ 40.19, 56.24, 56.71, 91.82, 102.44, 105.21, 109.21, 111.78, 118.11, 127.09, 152.25, 156.70, 161.21, 161.61, 161.82, 178.44. **IR** (ATR film): 2942, 2234, 1630, 1601, 1586, 1524, 1487, 1465, 1434, 1387, 1366, 1336, 1305, 1253, 1214, 1198, 1171, 1124, 1064, 1030, 1001, 947, 917, 840, 819, 783, 766, 729, 664, 643, 582, 563, 513, 486. **TLC** (CH_2Cl_2/EtOAc/MeOH, 5:4.5:0.5 v/v): R_f = 0.14 **HR-MS (ESI):** *m/z* calcd for $[C_{38}H_{37}N_2O_8]^+$ ([M + H$^+$]): 649.2544, found: 649.2546.

*rac-5,5′,7,7′-Tetramethoxy-2,2′-bis(4-(trifluoromethyl)-phenyl)-4H,4′H-[8,8′-bichromene]-4,4′-dione (**9bd**).* Synthesized in accordance with **General Procedure D**. Starting from **7bd** (30.0 mg, 42.9 μmol, 1.00 equiv) and I_2 (78.8 mM, 54 μL, 4.3 μmol, 10 mol %) for 2 h. The product was isolated by column chromatography (petroleum ether/EtOAc/*i*PrOH, 2:7:1 v/v) and obtained as white solids (17.7 mg, 25.3 μmol, 59%). **^{1}H NMR** (600 MHz, $CDCl_3$): δ 3.89 (s, 6H), 4.15 (s, 6H), 6.62 (s, 2H), 6.73 (s, 2H), 7.46 (d, *J* = 8.2 Hz, 4H), 7.56 (d, *J* = 8.3 Hz, 4H). **^{13}C NMR** (151 MHz, $CDCl_3$): δ 56.32, 56.77, 92.04, 101.94, 109.24, 109.63, 123.64 (q, *J* = 271.8 Hz), 125.80, 126.09 (q, *J* = 3.6 Hz), 132.92 (q, *J* = 32.9 Hz), 134.79, 156.67, 158.84, 161.72, 162.24, 177.67. **^{19}F NMR** (282 MHz, $CDCl_3$): δ −63.08. **IR** (ATR film): 1622, 1594, 1416, 1388, 1324, 1216, 1170, 1128, 1070, 1027, 958, 919, 843, 812. **TLC** (petroleum ether/EtOAc/*i*PrOH, 2:7:1 v/v): R_f = 0.35 **HR-MS (ESI):** *m/z* calcd for $[C_{36}H_{25}N_2O_8]^+$ ([M + H$^+$]): 699.1448, found: 699.1450. **Melting point:** 261−262 °C.

*rac-2,2′-Bis(4-bromophenyl)-5,5′,7,7′-tetramethoxy-4H,4′H-[8,8′-bichromene]-4,4′-dione (**9be**).* Synthesized in accordance with **General Procedure D**. Starting from **7be** (30.0 mg, 41.6 μmol, 1.00 equiv) and I_2 (78.8 mM, 53 μL, 4.2 μmol, 10 mol %) for 2 h. The product was isolated by column chromatography (petroleum ether/EtOAc/*i*PrOH, 2:7:1 v/v) and obtained as white solids (20.9 mg, 29.1 μmol, 70%). **^{1}H NMR** (600 MHz, $CDCl_3$): δ 3.86 (s, 6H), 4.12 (s, 6H), 6.58 (s, 2H), 6.64 (s, 2H), 7.20 (d, *J* = 8.4 Hz, 4H), 7.42 (d, *J* = 8.5 Hz, 4H). **^{13}C NMR** (151 MHz, $CDCl_3$): δ 56.28, 56.74, 91.93, 101.96, 108.51, 109.17, 125.95, 126.92, 130.30, 132.35, 156.60, 159.53, 161.60, 162.07, 177.85. **IR** (ATR film): 2885, 2239, 1638, 1590, 1508, 1487, 1465, 1435, 1403, 1388, 1331, 1302, 1274, 1215, 1190, 1171, 1127, 1107, 1073, 1027, 1009, 958, 828, 782, 730, 687, 644, 626, 572, 545, 517, 477. **TLC** (petroleum ether/EtOAc/*i*PrOH, 2:7:1 v/v): R_f = 0.21 **HR-MS (ESI):** *m/z* calcd for $[C_{34}H_{25}O_8Br_2]^+$ ([M + H$^+$]): 718.9911, found: 718.9915. **Melting point:** 251−255 °C.

*rac-2,2′-Bis(2-bromophenyl)-5,5′,7,7′-tetramethoxy-4H,4′H-[8,8′-bichromene]-4,4′-dione (**9bg**).* Synthesized in accordance with **General Procedure D**. Starting from **7bg** (30.0 mg, 41.6 μmol, 1.00 equiv) and I_2 (78.8 mM, 53 μL, 4.2

https://doi.org/10.1021/acsomega.3c06503
ACS Omega 2023, 8, 41816−41834

μmol, 10 mol %) for 1 h. The product was isolated by column chromatography (EtOAc/MeOH, 9:1 v/v) and obtained as white solids (16.7 mg, 23.3 μmol, 56%). **^{1}H NMR** (600 MHz, $CDCl_3$): δ 3.84 (s, 6H), 4.06 (s, 6H), 6.47 (s, 2H), 6.50 (s, 2H), 7.23 (ddd, *J* = 7.8, 4.0, 2.4 Hz, 4H), 7.27−7.29 (m, 2H), 7.53−7.57 (m, 2H). **^{13}C NMR** (151 MHz, $CDCl_3$): δ 56.20, 56.58, 91.98, 102.18, 109.12, 114.04, 121.57, 127.62, 130.63, 131.65, 133.50, 134.24, 157.33, 161.14, 161.41, 162.13, 177.82. **IR** (ATR film): 3493, 2940, 2842, 2244, 1646, 1593, 1472, 1434, 1389, 1336, 1214, 1109, 1025, 730. **TLC** (EtOAc/MeOH, 9:1 v/v): R_f = 0.32 **HR-MS (ESI):** *m/z* calcd for $[C_{34}H_{25}O_8Br_2]^+$ ([M + H$^+$]): 718.9911, found: 718.9916 **Melting point:** 260 °C (decomposition).

*rac-2,2′-Bis(4-(dimethylamino)phenyl)-5,5′-dihydroxy-7,7′-dimethyl-4H,4′H-[8,8′-bichromene]-4,4′-dione (**11**).* A dry 25 mL Schlenk round-bottom flask was charged with biflavone **9ac** (40.0 mg, 0.06 mmol, 1.0 equiv) and anhydr. CH_2Cl_2 (2.5 mL). The solution was cooled to −78 °C, and BCl_3 (1 M in CH_2Cl_2, 0.14 mL, 0.14 mmol, 2.2 equiv) was added dropwise. The cooling bath was left to warm up overnight. After 16 h of reaction time, KPi-buffer (K_2HPO_4/KH_2PO_4, 1 M, pH 7, 10 mL) was added. The aqueous phase was extracted with CH_2Cl_2 (3 × 10 mL), and the combined organic phases were washed with sat. aq. NaCl solution (20 mL). The crude product was isolated by column chromatography (EtOAc/MeOH, 9:1 v/v) and obtained as orange crystals (16.9 mg, 0.03 μmol, 44%). **^{1}H NMR** (600 MHz, $CDCl_3$): δ 2.15 (s, 6H), 3.01 (s, 12H), 6.56 (s, 2H), 6.58 (d, *J* = 9.0 Hz, 4H), 6.87 (s, 2H), 7.28 (d, *J* = 9.0 Hz, 4H), 12.99 (s, 2H). **^{13}C NMR** (151 MHz, $CDCl_3$): δ 20.78, 40.17, 102.04, 109.12, 111.85, 112.58, 113.33, 117.29, 127.63, 146.42, 152.81, 153.79, 160.16, 165.32, 183.41. **IR** (ATR film): 2923, 1649, 1588, 1520, 1482, 1360, 1246, 1201, 1163, 1110, 1034, 814. **TLC** (petroleum ether/EtOAc, 55:45 v/v): R_f = 0.3 **HR-MS (ESI):** *m/z* calcd for $[C_{36}H_{33}N_2O_6]^+$ ([M + H$^+$]): 589.2333, found: 589.2340 **Melting point:** 280−283 °C.

■ ASSOCIATED CONTENT

Supporting Information

The Supporting Information is available free of charge at https://pubs.acs.org/doi/10.1021/acsomega.3c06503

Coordinates of the X-ray structure of compound **4a**; bioactivity data; additional synthesis procedures; computational details including all coordinates; copies of all ^{1}H and ^{13}C spectral data; HPLC chromatograms; and material and methods for biological assays as well as biological activity graphs (PDF)

Compound **4a** piet13 (CIF)

■ AUTHOR INFORMATION

Corresponding Author

Jörg Pietruszka − *Institute of Bioorganic Chemistry, Heinrich Heine University Düsseldorf, Forschungszentrum Jülich, 52426 Jülich, Germany; Institut für Bio- und Geowissenschaften (IBG-1: Bioorganische Chemie) Forschungszentrum, 52428 Jülich, Germany;* orcid.org/0000-0002-9819-889X; Email: j.pietruszka@fz-juelich.de

Authors

Moritz K. T. Klischan − *Institute of Bioorganic Chemistry, Heinrich Heine University Düsseldorf, Forschungszentrum Jülich, 52426 Jülich, Germany*

Flaminia Mazzone − *Institute of Medical Microbiology and Hospital Hygiene, Medical Faculty and University Hospital Düsseldorf, Heinrich Heine University Düsseldorf, 40225 Düsseldorf, Germany;* orcid.org/0000-0003-1429-230X

Lena Berning − *Institute of Molecular Medicine I, Medical Faculty and University Hospital Düsseldorf, Heinrich Heine University Düsseldorf, 40225 Düsseldorf, Germany*

Julian Greb − *Institute of Bioorganic Chemistry, Heinrich Heine University Düsseldorf, Forschungszentrum Jülich, 52426 Jülich, Germany*

Max Schlamkow − *Institute of Bioorganic Chemistry, Heinrich Heine University Düsseldorf, Forschungszentrum Jülich, 52426 Jülich, Germany; Institut für Bio- und Geowissenschaften (IBG-1: Bioorganische Chemie) Forschungszentrum, 52428 Jülich, Germany*

Mona Haase − *Institute of Bioorganic Chemistry, Heinrich Heine University Düsseldorf, Forschungszentrum Jülich, 52426 Jülich, Germany*

Wolfgang Frey − *Institute of Organic Chemistry, University of Stuttgart, 70569 Stuttgart, Germany*

Björn Stork − *Institute of Molecular Medicine I, Medical Faculty and University Hospital Düsseldorf, Heinrich Heine University Düsseldorf, 40225 Düsseldorf, Germany;* orcid.org/0000-0002-4167-7806

Klaus Pfeffer − *Institute of Medical Microbiology and Hospital Hygiene, Medical Faculty and University Hospital Düsseldorf, Heinrich Heine University Düsseldorf, 40225 Düsseldorf, Germany*

Complete contact information is available at: https://pubs.acs.org/10.1021/acsomega.3c06503

Author Contributions

#F.M., L.B. and J.G. contributed equally to this work.

Notes

The authors declare no competing financial interest.

■ ACKNOWLEDGMENTS

The authors gratefully acknowledge the DFG (GRK2158), the Forschungszentrum Jülich GmbH, and the Heinrich Heine University (HHU) for their generous support. The authors thank Ruth Ganardi, Sebastian Myllek, Karin Buchholz, Daniel Degrandi, and Ursula Sorg for their scientific consultation, Birgit Henßen for HPLC support, and Vera Ophoven for synthesis support.

■ REFERENCES

(1) Murti, V.; Raman, P.; Seshadri, T. Cupressuflavone, a new biflavonyl pigment. *Tetrahedron* **1967**, *23*, 397−404.

(2) Molyneux, R.; Waiss, A., Jr; Haddon, W. Oxidative coupling of apigenin. *Tetrahedron* **1970**, *26*, 1409−1416.

(3) Rahman, W.; Bhatnagar, S. A new biflavonyl AC3 from Araucaria cunninghamii. *Tetrahedron Lett.* **1968**, *9*, 675−678.

(4) Murti, V.; Raman, P.; Seshadri, T. Cupressuflavone, a new member of the biflavonyl group. *Tetrahedron Lett.* **1964**, *5*, 2995−2997.

(5) Natarajan, S.; Murti, V.; Seshadri, T. Biflavones of some Cupressaceae plants. *Phytochemistry* **1970**, *9*, 575−579.

(6) Inatomi, Y.; Iida, N.; Murata, H.; Inada, A.; Murata, J.; Lang, F. A.; Iinuma, M.; Tanaka, T.; Nakanishi, T. A pair of new atropisomeric cupressuflavone glucosides isolated from Juniperus communis var. depressa. *Tetrahedron Lett.* **2005**, *46*, 6533−6535.

(7) Yu, S.; Yan, H.; Zhang, L.; Shan, M.; Chen, P.; Ding, A.; Li, S. F. Y. A review on the phytochemistry, pharmacology, and pharmacoki-

netics of amentoflavone, a naturally-occurring biflavonoid. *Molecules* **2017**, *22*, No. 299.
(8) Kim, H. P.; Park, H.; Son, K. H.; Chang, H. W.; Kang, S. S. Biochemical pharmacology of biflavonoids: implications for anti-inflammatory action. *Arch. Pharmacal. Res.* **2008**, *31*, 265−273.
(9) Lin, Y.-M.; Flavin, M. T.; Schure, R.; Chen, F.-C.; Sidwell, R.; Barnard, D. I.; Huffmann, J. H.; Kern, E. R. Antiviral activities of biflavonoids. *Planta Med.* **1999**, *65*, 120−125.
(10) Adnan, M.; Rasul, A.; Hussain, G.; Shah, M. A.; Zahoor, M. K.; Anwar, H.; Sarfraz, I.; Riaz, A.; Manzoor, M.; Adem, Ş.; Selamoglu, Z. Ginkgetin: A natural biflavone with versatile pharmacological activities. *Food Chem. Toxicol.* **2020**, *145*, No. 111642.
(11) Yamaguchi, L. F.; Kato, M. J.; Di Mascio, P. Biflavonoids from Araucaria angustifolia protect against DNA UV-induced damage. *Phytochemistry* **2009**, *70*, 615−620.
(12) Gontijo, V. S.; dos Santos, M. H.; Viegas, C., Jr Biological and chemical aspects of natural biflavonoids from plants: a brief review. *Mini Rev. Med. Chem.* **2017**, *17*, 834−862.
(13) Tasdemir, D.; Kaiser, M.; Brun, R.; Yardley, V.; Schmidt, T. J.; Tosun, F.; Rüedi, P. Antitrypanosomal and antileishmanial activities of flavonoids and their analogues: in vitro, in vivo, structure-activity relationship, and quantitative structure-activity relationship studies. *Antimicrob. Agents Chemother.* **2006**, *50*, 1352−1364.
(14) Al-Sayed, E.; Gad, H. A.; El-Shazly, M.; Abdel-Daim, M. M.; Singab, A. N. Anti-inflammatory and analgesic activities of cupressuflavone from Cupressus macrocarpa: Impact on pro-inflammatory mediators. *Drug Dev. Res.* **2018**, *79*, 22−28.
(15) Freitas, A.; Almeida, M.; Andrighetti-Fröhner, C.; Cardozo, F.; Barardi, C.; Farias, M.; Simões, C. Antiviral activity-guided fractionation from Araucaria angustifolia leaves extract. *J. Ethnopharmacol.* **2009**, *126*, 512−517.
(16) Siddiqui, J. A.; Swarnkar, G.; Sharan, K.; Chakravarti, B.; Sharma, G.; Rawat, P.; Kumar, M.; Khan, F. M.; Pierroz, D.; Maurya, R. 8, 8 ″-Biapigeninyl stimulates osteoblast functions and inhibits osteoclast and adipocyte functions: Osteoprotective action of 8, 8 ″-biapigeninyl in ovariectomized mice. *Mol. Cell. Endocrinol.* **2010**, *323*, 256−267.
(17) Al-Sayed, E.; Abdel-Daim, M. M. Protective role of Cupressuflavone from Cupressus macrocarpa against carbon tetrachloride-induced hepato-and nephrotoxicity in mice. *Planta Med.* **2014**, *80*, 1665−1671.
(18) Sasaki, H.; Kitoh, Y.; Tsukada, M.; Miki, K.; Koyama, K.; Juliawaty, L. D.; Hakim, E. H.; Takahashi, K.; Kinoshita, K. Inhibitory activities of biflavonoids against amyloid-β peptide 42 cytotoxicity in PC-12 cells. *Bioorg. Med. Chem. Lett.* **2015**, *25*, 2831−2833.
(19) DeForest, J. C.; Du, L.; Joyner, P. M. 4′, 4‴, 7, 7 ″-Tetra-O-methylcupressuflavone Inhibits Seed Germination of Lactuca sativa. *J. Nat. Prod.* **2014**, *77*, 1093−1096.
(20) Frank, M.; Niemann, H.; Böhler, P.; Stork, B.; Wesselborg, S.; Lin, W.; Proksch, P. Phomoxanthone A-from mangrove forests to anticancer therapy. *Curr. Med. Chem.* **2015**, *22*, 3523−3532.
(21) Zhang, W.; Krohn, K.; Flörke, U.; Pescitelli, G.; Di Bari, L.; Antus, S.; Kurtán, T.; Rheinheimer, J.; Draeger, S.; Schulz, B. New Mono-and Dimeric Members of the Secalonic Acid Family: Blennolides A−G Isolated from the Fungus Blennoria sp. *Chem. - Eur. J.* **2008**, *14*, 4913−4923.
(22) Kikuchi, H.; Isobe, M.; Sekiya, M.; Abe, Y.; Hoshikawa, T.; Ueda, K.; Kurata, S.; Katou, Y.; Oshima, Y. Structures of the dimeric and monomeric chromanones, gonytolides A−C, isolated from the fungus Gonytrichum sp. and their promoting activities of innate immune responses. *Org. Lett.* **2011**, *13*, 4624−4627.
(23) Sirimangkalakitti, N.; Juliawaty, L. D.; Hakim, E. H.; Waliana, I.; Saito, N.; Koyama, K.; Kinoshita, K. Naturally occurring biflavonoids with amyloid β aggregation inhibitory activity for development of anti-Alzheimer agents. *Bioorg. Med. Chem. Lett.* **2019**, *29*, 1994−1997.
(24) Kikuchi, H.; Hoshikawa, T.; Kurata, S.; Katou, Y.; Oshima, Y. Design and synthesis of Structure-Simplified derivatives of Gonytolide for the promotion of innate immune responses. *J. Nat. Prod.* **2016**, *79*, 1259−1266.
(25) Wender, P. A.; Verma, V. A.; Paxton, T. J.; Pillow, T. H. Function-oriented synthesis, step economy, and drug design. *Acc. Chem. Res.* **2008**, *41*, 40−49.
(26) Brown, D. G.; Bostrom, J. Analysis of past and present synthetic methodologies on medicinal chemistry: where have all the new reactions gone? Miniperspective. *J. Med. Chem.* **2016**, *59*, 4443−4458.
(27) Singh, M.; Kaur, M.; Silakari, O. Flavones: An important scaffold for medicinal chemistry. *Eur. J. Med. Chem.* **2014**, *84*, 206−239.
(28) Ahmad, S.; Razaq, S. A new approach to the synthesis of symmetrical biflavones. *Tetrahedron Lett.* **1971**, *12*, 4633−4636.
(29) Ahmad, S.; Razaq, S. New synthesis of biflavones of cupressuflavone series. *Tetrahedron* **1976**, *32*, 503−506.
(30) Li, H.-Y.; Nehira, T.; Hagiwara, M.; Harada, N. Total Synthesis and Absolute Stereochemistry of the Natural Atropisomer of the Biflavone 4′, 4″′, 7, 7″-Tetra-O-methylcupressuflavone. *J. Org. Chem.* **1997**, *62*, 7222−7227.
(31) Lin, G.-Q.; Zhong, M. The first enantioselective synthesis of optically pure (R)-and (S)-5, 5″-dihydroxy-4′, 4″′, 7, 7″-tetramethoxy-8, 8″-biflavone and the reconfirmation of their absolute configuration. *Tetrahedron Lett.* **1997**, *38*, 1087−1090.
(32) Parthasarathy, M.; Gupta, S. Oxidative coupling of phloroacetophenone dimethyl ether, resacetophenone and resacetophenone monomethyl ether using silica-bound FeCl3. *Indian J. Chem., Sect. B: Org. Chem. Incl. Med. Chem.* **1984**, *23*, 227−230.
(33) Lee, C. Y.; Cheon, C. H. Diastereomeric Resolution of a Racemic Biarylboronic Acid and Its Application to Divergent Asymmetric Total Syntheses of Some Axially Chiral Natural Products. *Adv. Synth. Catal.* **2016**, *358*, 549−554.
(34) Zhang, F. J.; Lin, G. Q. Synthesis of the optically pure 5, 5″-dihydroxy-7, 7″-dimethoxy-8, 8″-biflavone and its derivatives. *Chin. J. Chem.* **1997**, *15*, 464−471.
(35) Bringmann, G.; Mortimer, A. J. P.; Keller, P. A.; Gresser, M. J.; Garner, J.; Breuning, M. Atropselektive Synthese axial-chiraler Biaryle. *Angew. Chem.* **2005**, *117*, 5518−5563.
(36) Bringmann, G.; Günther, C.; Ochse, M.; Schupp, O.; Tasler, S.Biaryls in nature: a multi-facetted class of stereochemically, biosynthetically, and pharmacologically intriguing secondary metabolites. In *Progress in the Chemistry of Organic Natural Products*; Springer, 2001; Vol. *82*, pp 1−249.
(37) Wu, X.; Iwata, T.; Scharf, A.; Qin, T.; Reichl, K. D.; Porco, J. A., Jr Asymmetric synthesis of gonytolide A: strategic use of an aryl halide blocking group for oxidative coupling. *J. Am. Chem. Soc.* **2018**, *140*, 5969−5975.
(38) Qin, T.; Skraba-Joiner, S. L.; Khalil, Z. G.; Johnson, R. P.; Capon, R. J.; Porco, J. A., Jr Atropselective syntheses of (−) and (+) rugulotrosin A utilizing point-to-axial chirality transfer. *Nat. Chem.* **2015**, *7*, 234−240.
(39) Giles, R. G.; Sargent, M. Naturally-Occurring Dibenzofurans. X. A New Synthesis of Di-O-Methylstrepsilin. *Aust. J. Chem.* **1986**, *39*, 2177−2181.
(40) Drochner, D.; Hüttel, W.; Bode, S. E.; Müller, M.; Karl, U.; Nieger, M.; Steglich, W. Dimeric orsellinic acid derivatives: Valuable intermediates for natural product synthesis. *Eur. J. Org. Chem.* **2007**, *2007*, 1749−1758.
(41) Hauser, F. M.; Gauuan, P. J. F. Total synthesis of (±)-Biphyscion. *Org. Lett.* **1999**, *1*, 671−672.
(42) Rahman, M.; Riaz, M.; Desai, U. R. Synthesis of biologically relevant biflavanoids—a review. *Chem. Biodiversity* **2007**, *4*, 2495−2527.
(43) Kuttruff, C. A.; Eastgate, M. D.; Baran, P. S. Natural product synthesis in the age of scalability. *Nat. Prod. Rep.* **2014**, *31*, 419−432.
(44) Wang, J.; Zhou, R.-G.; Wu, T.; Yang, T.; Qin, Q.-X.; Li, L.; Yang, B.; Yang, J. Total synthesis of apigenin. *J. Chem. Res.* **2012**, *36*, 121−122.

https://doi.org/10.1021/acsomega.3c06503
ACS Omega 2023, 8, 41816−41834

(45) Königs, P.; Rinker, B.; Maus, L.; Nieger, M.; Rheinheimer, J.; Waldvogel, S. Structural revision and synthesis of altechromone A. *J. Nat. Prod.* **2010**, *73*, 2064−2066.
(46) Freitas, M.; Ribeiro, D.; Tome, S. M.; Silva, A. M.; Fernandes, E. Synthesis of chlorinated flavonoids with anti-inflammatory and pro-apoptotic activities in human neutrophils. *Eur. J. Med. Chem.* **2014**, *86*, 153−164.
(47) Dianin, A. About Products from the Oxidation of Naphthols with Ferric Chloride. *Zh. Russ. Fiz.-Khim. O-va.* **1874**, *6*, 183−193.
(48) Tanaka, K.; Toda, F. Oxidative coupling reactions of phenols with FeCl3 in the solid state. *Mol. Cryst. Liq. Cryst. Incorporating Nonlinear Opt.* **1990**, *187*, 49−52.
(49) Keinan, E.; Mazur, Y. Reactions in dry media. Ferric chloride adsorbed on silica gel. A multipurpose, easily controllable reagent. *J. Org. Chem.* **1978**, *43*, 1020−1022.
(50) Jempty, T. C.; Miller, L. L.; Mazur, Y. Oxidative coupling reactions using silica-bound ferric chloride. *J. Org. Chem.* **1980**, *45*, 749−751.
(51) Drochner, D.; Hüttel, W.; Nieger, M.; Müller, M. Unselective Phenolic Coupling of Methyl 2-Hydroxy-4-methoxy-6-methylbenzoate—A Valuable Tool for the Total Synthesis of Natural Product Families. *Angew. Chem.* **2003**, *115*, 961−963.
(52) Hüttel, W.; Nieger, M.; Müller, M. A Short and Efficient TotalSynthesis of the Naturally Occurring Coumarins Siderin, Kotanin, Isokotanin A and Desertorin C. *Synthesis* **2003**, 1803−1808.
(53) Nieves-Quinones, Y.; Paniak, T. J.; Lee, Y. E.; Kim, S. M.; Tcyrulnikov, S.; Kozlowski, M. C. Chromium-salen catalyzed cross-coupling of phenols: mechanism and origin of the selectivity. *J. Am. Chem. Soc.* **2019**, *141*, 10016−10032.
(54) Libman, A.; Shalit, H.; Vainer, Y.; Narute, S.; Kozuch, S.; Pappo, D. Synthetic and predictive approach to unsymmetrical biphenols by iron-catalyzed chelated radical−anion oxidative coupling. *J. Am. Chem. Soc.* **2015**, *137*, 11453−11460.
(55) Kang, H.; Herling, M. R.; Niederer, K. A.; Lee, Y. E.; Vasu Govardhana Reddy, P.; Dey, S.; Allen, S. E.; Sung, P.; Hewitt, K.; Torruellas, C.; et al. Enantioselective vanadium-catalyzed oxidative coupling: development and mechanistic insights. *J. Org. Chem.* **2018**, *83*, 14362−14384.
(56) Lee, Y. E.; Cao, T.; Torruellas, C.; Kozlowski, M. C. Selective oxidative homo-and cross-coupling of phenols with aerobic catalysts. *J. Am. Chem. Soc.* **2014**, *136*, 6782−6785.
(57) Shalit, H.; Libman, A.; Pappo, D. meso-Tetraphenylporphyrin iron chloride catalyzed selective oxidative cross-coupling of phenols. *J. Am. Chem. Soc.* **2017**, *139*, 13404−13413.
(58) Shalit, H.; Dyadyuk, A.; Pappo, D. Selective oxidative phenol coupling by iron catalysis. *J. Org. Chem.* **2019**, *84*, 1677−1686.
(59) Montgomery, D. C. *Design and Analysis of Experiments*; John Wiley & Sons, 2017.
(60) Dardé, M.; Ajzenberg, D.; Smith, J.Population structure and epidemiology of Toxoplasma gondii. In *Toxoplasma Gondii*; Elsevier, 2007; pp 49−80.
(61) Flegr, J.; Prandota, J.; Sovičková, M.; Israili, Z. H. Toxoplasmosis−a global threat. Correlation of latent toxoplasmosis with specific disease burden in a set of 88 countries. *PLoS One* **2014**, *9*, No. e90203.
(62) EFSA, E. 2019; p e05926.
(63) Re, R.; Pellegrini, N.; Proteggente, A.; Pannala, A.; Yang, M.; Rice-Evans, C. Antioxidant activity applying an improved ABTS radical cation decolorization assay. *Free Radical Biol. Med.* **1999**, *26*, 1231−1237.
(64) Catarino, M. D.; Alves-Silva, J. M.; Pereira, O. R.; Cardoso, S. M. Antioxidant capacities of flavones and benefits in oxidative-stress related diseases. *Curr. Top. Med. Chem.* **2015**, *15*, 105−119.
(65) Boeck, P.; Falcão, C. A. B.; Leal, P. C.; Yunes, R. A.; Cechinel Filho, V.; Torres-Santos, E. C.; Rossi-Bergmann, B. Synthesis of chalcone analogues with increased antileishmanial activity. *Bioorg. Med. Chem.* **2006**, *14*, 1538−1545.
(66) Thieury, C.; Lebouvier, N.; Le Guével, R.; Barguil, Y.; Herbette, G.; Antheaume, C.; Hnawia, E.; Asakawa, Y.; Nour, M.; Guillaudeux, T. Mechanisms of action and structure-activity relationships of cytotoxic flavokawain derivatives. *Bioorg. Med. Chem.* **2017**, *25*, 1817−1829.
(67) Mai, C. W.; Yaeghoobi, M.; Abd-Rahman, N.; Kang, Y. B.; Pichika, M. R. Chalcones with electron-withdrawing and electron-donating substituents: anticancer activity against TRAIL resistant cancer cells, structure−activity relationship analysis and regulation of apoptotic proteins. *Eur. J. Med. Chem.* **2014**, *77*, 378−387.
(68) Sinyeue, C.; Matsui, M.; Oelgemöller, M.; Bregier, F.; Chaleix, V.; Sol, V.; Lebouvier, N. Synthesis and Investigation of Flavanone Derivatives as Potential New Anti-Inflammatory Agents. *Molecules* **2022**, *27*, No. 1781.
(69) Akçok, İ.; Çağır, A. Synthesis of stilbene-fused 2′-hydroxychalcones and flavanones. *Bioorg. Chem.* **2010**, *38*, 139−143.
(70) Cabrera, M.; Simoens, M.; Falchi, G.; Lavaggi, M. L.; Piro, O. E.; Castellano, E. E.; Vidal, A.; Azqueta, A.; Monge, A.; de Cerain, A. L. Synthetic chalcones, flavanones, and flavones as antitumoral agents: Biological evaluation and structure−activity relationships. *Bioorg. Med. Chem.* **2007**, *15*, 3356−3367.
(71) Schwarz, M.; Eno, R. F.; Freitag-Pohl, S.; Coxon, C. R.; Straker, H. E.; Wortley, D. J.; Hughes, D. J.; Mitchell, G.; Moore, J.; Cummins, I.; et al. Flavonoid-based inhibitors of the Phi-class glutathione transferase from black-grass to combat multiple herbicide resistance. *Org. Biomol. Chem.* **2021**, *19*, 9211−9222.
(72) Basílio, N.; Lima, J. C.; Cruz, L.; de Freitas, V.; Pina, F.; Ando, H.; Kimura, Y.; Oyama, K. I.; Yoshida, K. Unveiling the 6, 8-rearrangement in 8-phenyl-5, 7-dihydroxyflavylium and 8-methyl-5, 7-dihydroxyflavylium through host−guest complexation. *Eur. J. Org. Chem.* **2017**, *2017*, 5617−5626.
(73) Zheng, X.; Cao, J.-G.; Meng, W.-D.; Qing, F.-L. Synthesis and anticancer effect of B-ring trifluoromethylated flavonoids. *Bioorg. Med. Chem. Lett.* **2003**, *13*, 3423−3427.
(74) Shih, T.-L.; Chou, C.-E.; Liao, W.-Y.; Hsiao, C.-A. Copper-mediated trimethylsilyl azide in amination of bromoflavonoids to synthesize unique aminoflavonoids. *Tetrahedron* **2014**, *70*, 3657−3664.
(75) Wu, C.; Dunaway-Mariano, D.; Mariano, P. S. Design, synthesis, and evaluation of inhibitors of pyruvate phosphate dikinase. *J. Org. Chem.* **2013**, *78*, 1910−1922.

https://doi.org/10.1021/acsomega.3c06503
ACS Omega 2023, 8, 41816−41834

Supporting Information

Modular Approach for the Synthesis and Bioactivity Profiling of 8,8´-Biflavones

Authors

Moritz K.T. Klischan, **Flaminia Mazzone***, Lena Berning*, Julian Greb*, Max Schlamkow, Mona Haase, Wolfgang Frey, Björn Stork, Klaus Pfeffer, Jörg Pietruszka.

*These authors share the second authorship

Supporting Information link

The following supporting information can be downloaded at:

https://pubs.acs.org/doi/10.1021/acsomega.3c06503

GUID: 4C574A8E-7F9D-48B6-BFB4-7FCB3040FFC7

3.4 Synthesis and *In Vitro* Evaluation of Bichalcones as Novel Anti-Toxoplasma Agents

Authors

Flaminia Mazzone*, Moritz K.T. Klischan*, Julian Greb*, Sander H.J. Smits, Jörg Pietruszka, Klaus Pfeffer.

*These authors share the first authorship

Published in

Manuscript to be submitted

Impact factor

-

DOI

-

Own contributions to this work

Overall: 55%

Conducted all of the following experiments:

- *Toxoplasma gondii* proliferation assays
- Cytotoxicity assays (MTT assays) in human fibroblasts Hs27

Other major contributions

Design of experiments, methodology, conduction of experiments, data analysis, manuscript preparation.

Synthesis and In Vitro Evaluation of Bichalcones as Novel Anti-Toxoplasma Agents

Flaminia Mazzone[1] †, Moritz K. T. Klischan[2] †, Julian Greb[2] †, Sander H. J. Smits[3], Jörg Pietruszka[2,4*] and Klaus Pfeffer[1*]

[1]Institute of Medical Microbiology and Hospital Hygiene, Heinrich Heine University Düsseldorf, Düsseldorf, Germany

[2]Institute of Biorganic Chemistry, Heinrich Heine University Düsseldorf, Forschungszentrum Jülich GmbH, Jülich, Germany

[3]Institute of Biochemistry, Heinrich Heine University Düsseldorf, Düsseldorf, Germany

[4]Institute of Bio- and Geosciences (IBG-1): Biotechnology, Forschungszentrum Jülich GmbH, Jülich, Germany

†These authors share first authorship

*** Correspondence:**

Klaus Pfeffer

klaus.pfeffer@hhu.de

Jörg Pietrusza

j.pietruszka@fz-juelich.de

Keywords: *Toxoplasma gondii*, bichalcones, antiinfective, antitoxoplasma, stereoisomers, bioactivity.

Abstract

Toxoplasmosis is a zoonotic disease caused by *Toxoplasma gondii*, an apicomplexan that infects a third of the world's human population. This disease can cause serious complications during pregnancy and can be fatal in immunocompromised hosts. The current treatments for toxoplasmosis are few in number and face several limitations. Thus, to address the urgent medical need on the discovery of novel anti-toxoplasma potential drug candidates, our research focused on exploring a series of monomeric and dimeric chalcones, polyphenolic molecules belonging to the class of flavonoids. Chalcones and bichalcones were evaluated *in vitro* against the proliferation of the parasite in a cell-based assay. Comparison of the efficacy demonstrated that, in several cases, bichalcones exhibited increased bioactivity compared to their corresponding monomeric counterpart. Among these compounds, A-A'-connected bichalcone with a benzene as the B-ring and a methyl moiety **2ab** showed the most potent and selective inhibitory activity in the nanomolar range. Both enantiomers of **2ab** were synthesized using as common building block biphenol (**3**). The biaryl bond was forged using Suzuki-cross-coupling in water with amphiphilic surfactants/detergents. Separation of the enantiomers of **3** was conducted by chiral HPLC on preparative scale. The biological evaluation of the enantiomers, revealed that (R_a)-**2ab** is the eutomer. These studies suggest that bichalcones may be important drug candidates for further *in vivo* evaluations for the discovery of anti-toxoplasma drugs.

1 Introduction

Toxoplasma gondii (*T. gondii*), the causative agent of toxoplasmosis, is a coccidian parasite that belongs to the phylum Apicomplexa (Hill & Dubey, 2018; Montoya & Liesenfeld, 2004). This large phylum includes also other unicellular eukaryotes (LEVINE, 1988) that survive by infecting a wide range of hosts and causing severe diseases such as malaria (*Plasmodium falciparum* (Phillips et al., 2017)), babesiosis (*Babesia* spp. (Homer, Aguilar-Delfin, Telford, Krause, & Persing, 2000)), or cryptosporidiosis (*Cryptosporidium parvum* (Helmy & Hafez, 2022)). Like all other apicomplexans, *T. gondii* displays a heteroxenous and complex life cycle. It alternates between sexual replication that occurs exclusively in the *Felidae* family members (the definitive hosts), and asexual replication in a variety of warm-blooded intermediate hosts, including humans, via three infectious stages: tachyzoites, bradyzoites and sporozoites (J. Dubey, Lindsay, & Speer, 1998; Tenter, Heckeroth, & Weiss, 2000). Due to its

widespread distribution, *T. gondii* is often referred to as one of the most successful parasites (Delgado et al., 2022). There are multiple modes of transmission that result in human infections: foodborne, via ingestion of contaminated water and raw or undercooked meat; faecal-oral, via unintentional ingestion of oocysts from cat faeces; and also via several minor modes such as congenital transmission and blood or organ transplantation (J. P. Dubey, 2021). According to the Centers for Disease Control and Prevention (CDC), it has been estimated that more than 40 million people have been infected with *T. gondii* in the USA alone Centers for Disease Control and Prevention. "Parasites - Toxoplasmosis (Toxoplasma infection). Toxoplasmosis Epidemiology & Risk Factors." 2018. https://www.cdc.gov/parasites/toxoplasmosis/epi.html. Accessed June 19, 2023..

In immunocompetent individuals, the infection is often subclinical or asymptomatic in the acute phase, but can trigger behavioural disorder during the latent phase (Fekadu, Shibre, & Cleare, 2010). Without proper treatment, severe disease, or even death, can occur in immunocompromised individuals or in foetuses infected congenitally (Strang et al., 2020; Wang et al., 2017). An increased frequency of toxoplasmic encephalitis has been reported in patients with AIDS (Acquired Immunodeficiency Syndrome) with significant immunosuppression (Lejeune et al., 2011).

The current gold-standard treatment for toxoplasmosis relies on the administration of pyrimethamine (PYR) and sulfadiazine (SDZ) (Konstantinovic, Guegan, Stäjner, Belaz, & Robert-Gangneux, 2019). Since its discovery in 1953 by Eyles and Coleman (Eyles & Coleman, 1953), the synergistic nature of this combination therapy has been well-established. This synergy is achieved because both drugs interfere with different steps in the folate pathway of the tachyzoite stage of the parasite, and therefore the acute phase of the infection (Sheffield & Melton, 1975). To mitigate harmful side-effects associated with this PYR-SDZ regimen, among which is bone marrow myelosuppression, folinic acid (leucovorin) has been included in the combination (Alday & Doggett, 2017; Van Delden & Hirschel, 1996). Unfortunately, the resulting and other current regimens are still burdened with strong side effects, frequently resulting in a lack of patient compliance and discontinuation of the therapy. Moreover, the absence of drugs able to specifically target the cyst form of the parasite, responsible of the chronic and latent infection, remain a critical limitation. Thus, there is an urgent need for the discovery and development of novel, potent and well-tolerated treatments to overcome these challenges and improve the wellbeing of patients inflicted with toxoplasmosis (Konstantinovic et al., 2019).

Natural products play a crucial role in the field of drug discovery for infectious disease (Newman & Cragg, 2020). These compounds usually offer a wide and diverse range of biological activities, although during their preliminary evaluations often they show only moderate or weak potency. Thus, synthetic work on natural products is important for the identification of natural product analogues as novel hits and lead compounds (Deng, Wu, Zhai, & Li, 2019).

A very prominent class of natural products are flavonoids. Among these phenylpropanoid-based organic compounds are chalcones, polyphenolic secondary metabolites of plants (Elkanzi et al., 2022). These molecules have gathered high interest in medicinal chemistry and nowadays are considered privileged structures for their simple scaffold and their wide variety of pharmacological activities and characteristics (Zhuang et al., 2017), including antibacterial (Dan & Dai, 2020), anti-inflammatory (Vale, Lucas, Ribeiro, & Fernandes, 2023), antiviral (Fu et al., 2020), anticancer (Ouyang et al., 2021), antioxidant (Bale et al., 2021), antidiabetic (Rocha, Ribeiro, Fernandes, & Freitas, 2020), and antimalarial (Qin, Zhang, Lekkala, Alsulami, & Rakesh, 2020) properties among others. In addition, several studies have demonstrated the potential of chalcones as novel anti-toxoplasma agents (AL-Hilli, Ghazzay, Hasan, Al-Kelaby, & Zarka, 2021; Ghazzay, Hasan, DeliKhudhair, & Abbas, 2023; Jiang et al., 2022; Si et al., 2018; Touquet et al., 2018), but their mode of action on *T. gondii* remains unclear. Bichalcones (also commonly referred to as 'bis-chalcones'), a sub-class of chalcones and thus of the broader class of flavonoids, have shown to possess intriguing biological activities and among others also antiplasmodial activity (Domínguez et al., 2013; Ram, Saxena, Srivastava, & Chandra, 2000; Sharma et al., 2018). Nevertheless, these molecules have hardly been investigated in comparison to chalcones (Pereira, Silva, Ribeiro, Silva, & Fernandes, 2023). These observations indicate that more research into bichalcones may display valuable insights and novel potential therapeutic applications of these molecules.

Bichalcones exist in a variety of different connectivities regarding the monomeric unit (**Figure 1**). Depending on their scaffolds, different bioactivities was observed. Common scaffolds include linker-connected, such as with urea or alkyl linker exerting anti-malarial activity (Domínguez et al., 2013; Ram et al., 2000), A-B-type, showing anti-protozoal activity (Mihigo, Mammo, Bezabih, Andrae-Marobela, & Abegaz, 2010) and B-B-type bichalcones exhibiting antiplasmodial efficacy (Sharma et al., 2018) among others (Arslan et al., 2016; Karaman et al., 2018; Masesane, Yeboah, Liebscher, Mügge, & Abegaz, 2000; Mdee, Yeboah, & Abegaz, 2003; Menezes & Diederich, 2019; Pereira et

al., 2023; Zhang, Wang, Guo, & Liu, 2013; Zhuang et al., 2017). To this date, only few A-A′-bichalcones have been synthesized and their bioactivities have hardly been investigated. Lin *et al.* (Lin & Zhong, 1997) and Li *et al.* (Li, Nehira, Hagiwara, & Harada, 1997) independently investigated synthetic routes towards enantiopure 8,8′-biflavones, obtaining enantiopure A-A′-bichalcones as key intermediates. Both strategies employed the use of chiral auxiliaries to access the enantiopure products limiting the scalability of their approaches.

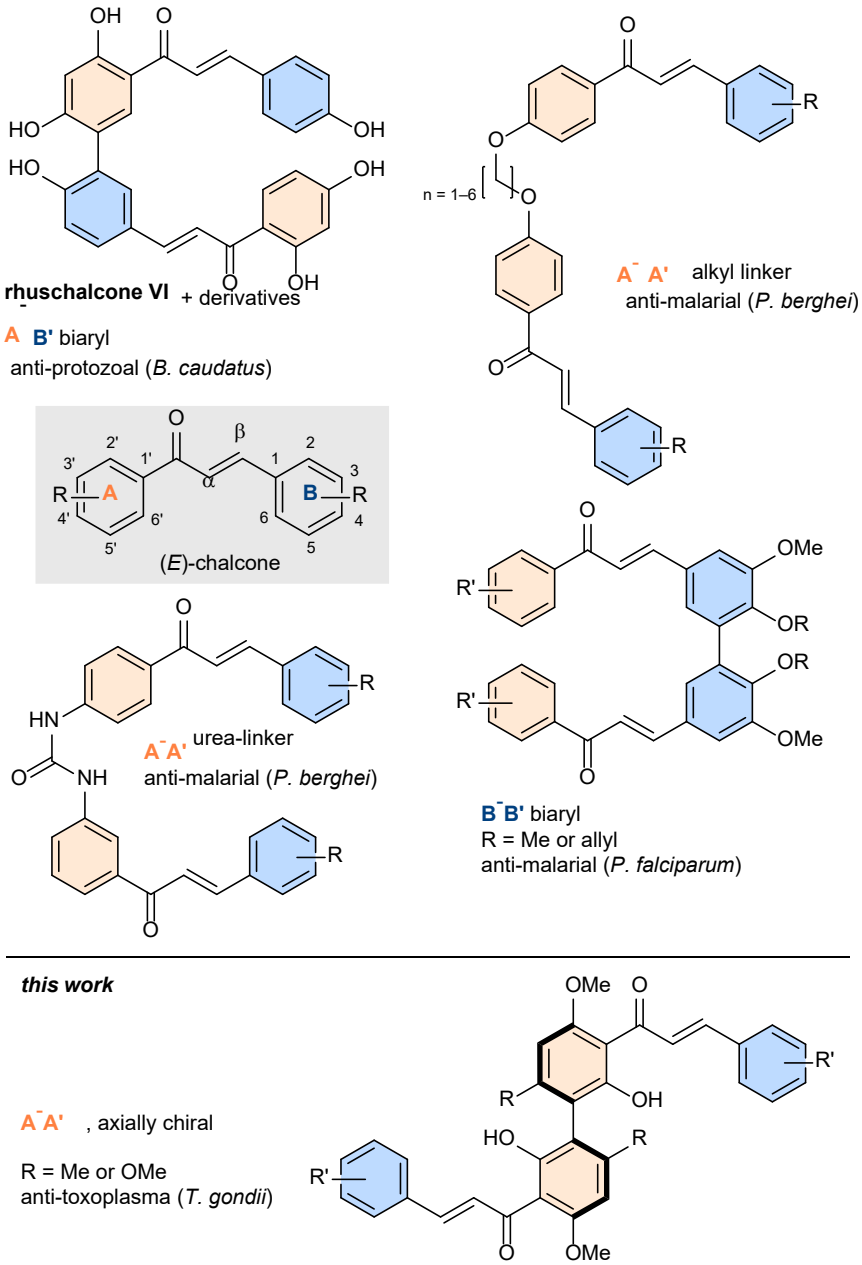

Figure 1: General structure of chalcones and various bichalcones with different linkages and their respective bioactivities.

In the present study, we report a novel synthetic pathway towards enantiopure A-A′-bichalchones and the first biological evaluation of this elusive class of flavonoids. Their *in vitro* anti-toxoplasma activities were evaluated against *T. gondii* type II ME49 strain and compared with their monomer chalcone counterparts.

2 Materials and Methods

2.1 Synthesis of chalcones and bichalcones

Chalcones and racemic bichalcones investigated in the present study were synthesized following established procedures from our previous investigations on the bioactivity of biflavones (Klischan et al., 2023). Synthetic schemes, methodologies and analytical data are available in the Supporting Information in the sections Experimental Procedures and Synthetic Procedures.

2.2 Parasite and cell culture

The tachyzoite stage of the ME49 strain type II of *T. gondii* (ATCC/LGC Standards GmbH, Wesel, Germany, #50611) was maintained and propagated by regular passages infecting monolayers of human foreskin fibroblasts Hs27 (ATCC/LGC Standards GmbH, Wesel, Germany, #CRL-1634), in 25 cm^2 cell culture flasks, with $5x10^6$ tachyzoites. The cultures were grown in Iscove's Modified Dulbecco's medium (IMDM; Gibco-Thermo Fisher Scientific, Braunschweig, Germany, #12440053) supplemented with 10% heat-inactivated foetal bovine serum (FBS Standard; South America origin, foetal bovine serum, 2µm sterile filtered, PAN-Biotech, Aidenbach, Germany, #P30-3306) and 50 mM 2-mercaptoethanol (Gibco-Thermo Fisher Scientific, Braunschweig, Germany, #21985023) at 37°C and 5% CO_2 for 72 hours. After incubation, the cell culture supernatant was centrifuged at a speed of 700 rpm for 5 minutes. The density of the parasite was then measured using a hemocytometer and adjusted accordingly of *in vitro* experimental infection analysis.

2.3 Compounds for *in vitro* analysis

Pyrimethamine, staurosporine and all the synthesized chalcones and bichalcones were dissolved in DMSO (Dimethylsulfoxide, ≥ 99%, Thermo Scientific Chemicals, Braunschweig, Germany, #A12380.36) as 10 mM stock solutions and stored at -20 °C. Before use, these solutions were thawed and diluted in culture medium to produce the appropriate concentrations (ranging from 200 µM to 0.02 µM).

2.4 *Toxoplasma gondii in vitro* inhibition assay

To evaluate the efficacy of the investigated chalcones and bichalcones against *T. gondii* proliferation, we conducted *in vitro* inhibition assays using a similar protocol to the previously reported articles (Klischan et al., 2023; Mazzone et al., 2022; Merkt et al., 2021). In brief, we seeded $3x10^4$ Hs27 cells in 96-well microtiter plates with a total culture volume of 200 µL each well. To avoid edge effects, only the inner 60 wells of each plate were used. After the aforementioned process of harvesting *T. gondii*, the host cells were then infected with $3x10^4$ tachyzoites per well, with a multiplicity of infection (MOI, parasite/host cell) ratio of 1:1. At the same time, the compounds were added to the cultures at various concentrations as previous described (ranging from 50 µM to 0.02 µM). As controls were used pyrimethamine (Alday & Doggett, 2017; Konstantinovic et al., 2019) (Merck, Darmstadt, Germany, #219864), *T. gondii* infected cells only and human interferon γ (IFN γ) (E. Pfefferkorn, 1986) (300 U/ml) (Merck, Darmstadt, Germany, #I17001) pre-stimulated and infected Hs27 cells for 24 hours. To quantify the proliferation of *T. gondii*, after 48 hours incubation the parasite was labelled with tritiated uracil (^{3}H-U; 5 mCi, Hartmann Analytic, Braunschweig, Germany, #ART1782, diluted 1:30) (E. R. Pfefferkorn & Pfefferkorn, 1977) and incubated for another 28-30 hours. Before the evaluation of the assay, the experimental 96-well microtiter plates were frozen at -20°C. Then, the plates were thawed at room temperature, the cells were extracted through a harvester device (Basic96 Harvester; Zinsser Analytic, Skatron Instruments, Northridge, CA, USA) and transferred into glass-fibre filters (Printed Filtermat A 102 mm × 258 mm; PerkinElmer, Waltham, MA, USA). The filters were then dried in a cabinet at 130°C for 20 minutes, wetted in 10 mL of scintillation solution (Betaplate Scint; PerkinElmer, Waltham, MA, USA, #1205-440), and sealed with plastic covers (Sample Bag for Betaplate; PerkinElmer, Waltham, MA, USA, #1205-441). The filters

were clamped in cassettes and evaluated using a beta-counter device (Betaplate Liquid Scintillation Counter 1205; LKB-WALLAK, Melbourne, Australia) to quantify the amount of radioactive uracil in the RNA of *T. gondii*. The IC_{50} values (minimal concentration of compounds required for 50% inhibition *in vitro*) were determined by non-linear regression analysis through the statistics software GraphPad PRISM™ (Version 9.5.1; San Diego, CA).

2.5 Cytotoxicity assay

To assess the cytotoxic effects of the examined chalcones and bichalcones on the host cells, the MTT [3- (4,5-dimethylthiazole-2-yl)-2,5-diphenyltetrazolium bromide] reduction assay (Mosmann, 1983) was used for quantification. To avoid edge effects, only the inner 60 wells of each plate were used. In summary, $5x10^4$ per well of Hs27 cells were cultured in 96-well microtiter plates in Iscove's modified Dulbecco's medium (IMDM, Gibco–Thermo Fisher Scientific, Braunschweig, Germany, #12440053) with a volume of 100 µL per well and incubated at 37°C overnight till confluence. Then, different concentrations of the investigated compounds (ranging from 200 µM to 0.09 µM) were added to the Hs27 cells. As controls were used untreated Hs27 cells, DMSO and staurosporine (0.031, 0.062, 0.125, 0.25, 0.5, 1 µM) (Merck, Darmstadt, Germany, #S4400), a natural product well known for its potent activity as apoptosis inducer (Belmokhtar, Hillion, & Ségal-Bendirdjian, 2001). After an incubation of 24 hours, the culture media was replaced with 100 µL of Dulbecco's Modified Eagle Medium (DMEM) medium without red phenol (Gibco-Thermo Fisher Scientific, Braunschweig, Germany, #21041025) plus 10 % heat-inactivated foetal bovine serum (FBS Standard, South America origin, foetal bovine serum, 2µm sterile filtered, PAN-Biotech, Aidenbach, Germany, #P30-3306), and 50 mM 2-mercaptoethanol (Gibco-Thermo Fisher Scientific, Braunschweig, Germany, #21985023). The experiment was performed following the manufacture instructions (CyQuant MTT Cell Viability Assay Kit, Thermo Fisher Scientific, Braunschweig, Germany, #V-13154). The optical density (O.D.) was measured at 570 nm on a microplate reader (TECAN Sunrise, Männedorf, Switzerland). The half maximal cytotoxic concentration (CC_{50} values) of each compound against Hs27 cells relative to DMSO treated samples were determinated using GraphPad PRISM™ statistics software package (Version 9.5.1; San Diego, CA).

3 Results

3.1 Bichalcones and chalcones are effective inhibitors of *T. gondii* tachyzoite growth

In our previous study we investigated the anti-toxoplasma activities of various flavones and biflavones (Klischan et al., 2023). There, chalcones **1** and A-A′-bichalcones **2** were obtained as intermediate products. In this work we report the anti-toxoplasma activities for this dedicated library of simplified natural product analogues (**Figure 2**). Additionally, both enantiomers of the most active bichalcone were synthesized and their activities compared with the racemic mixture.

In view of previous studies demonstrating the effectiveness of chalcones against apicomplexans (AL-Hilli et al., 2021; Domínguez et al., 2013; Ghazzay et al., 2023; Jiang et al., 2022; Qin et al., 2020; Ram et al., 2000; Sharma et al., 2018; Si et al., 2018; Touquet et al., 2018), we evaluated and compared the activity of 14 chalcones and 14 of their dimeric bichalcone counterparts (**Figure 2**). In order to determine their potential against *T. gondii* ME49 tachyzoites, we performed an *in vitro* proliferation assay based on the uptake of radioactively labelled ^{3}H-uracil. We then assessed their IC_{50} values. As shown in **Table 1** and **Figure S26**, chalcones and bichalcones exhibited bioactivity against *T. gondii* proliferation.

Chalcone	IC_{50} ± S.D. (µM)	Bichalcone	IC_{50} ± S.D. (µM)
1aa	21.81 ± 3.07	**2aa**	6.63 ± 0.77
1ab	14.05 ± 2.62	**2ab**	0.11 ± 0.02
1ac	> 50	**2ac**	> 50
1ad	> 50	**2ad**	24.74 ± 3.52
1ae	10.60 ± 1.05	**2ae**	7.91 ± 1.14
1af	6.18 ± 0.55	**2af**	30.48 ± 7.21
1ag	> 50	**2ag**	18.44 ± 0.10
1ba	8.08 ± 2.06	**2ba**	> 50
1bb	6.01 ± 2.54	**2bb**	9.75 ± 1.95
1bc	> 50	**2bc**	> 50
1bd	> 50	**2bd**	3.09 ± 0.15
1be	> 50	**2be**	8.55 ± 1.28
1bf	11.32 ± 0.61	**2bf**	12.4 ± 2.09
1bg	4.46 ± 0.46	**2bg**	> 50

Table 1. *In vitro* activity of chalcones (1aa – bg) and bichalcones (2aa – bg) against *T. gondii* ME49 tachyzoites

Values shown in the table represent the means of three independent experiments each done in duplicate (n = 6) ± S.D.

Especially, bichalcone **2ab** showed an IC_{50} of 0.11 µM, more potent than its monomeric counterpart (**1ab**, 14.05 µM) by two orders of magnitude and overall, more active than all other compounds in our dedicated library (3.09 to 30.48 µM). **2ab** contains a benzene moiety as the B-ring and a methyl (Me) at R (**Figure 2**). Interestingly the latter appears to be important for the anti-toxoplasma activity, since **2bb** with a methoxy group (OMe) at R showed a comparably low IC_{50} of 9.75 µM (**Table 1** and **Figure S26**).

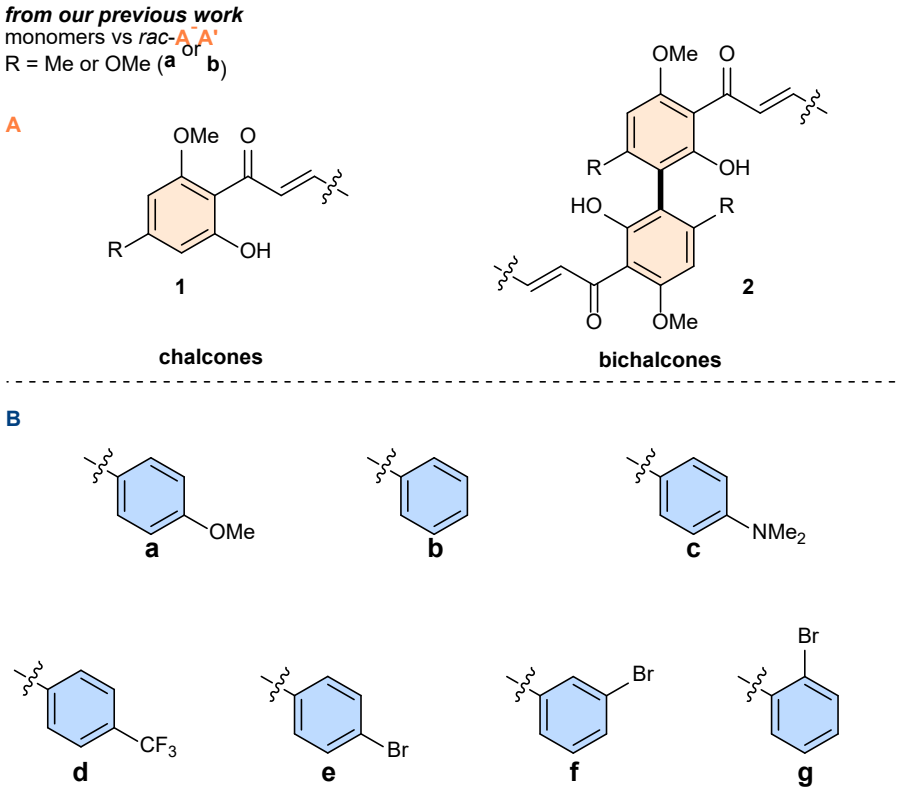

Figure 2: Library of chalcones and bichalcones.

3.2 Bichalcone 2ab is a strong and selective inhibitor of *T. gondii*

To investigate the selectivity of our (bi)chalcone library regarding parasite inhibition versus human host cell cytotoxicity, we assessed their cytotoxic potential in human fibroblasts Hs27 with the MTT reduction assay. The screening revealed weak to no cytotoxicity for chalcones, and no cytotoxicity for all bichalcones (**Table 2** and **Figure S27**). **2ab** possessed the highest selectivity on toxoplasma, with a selectivity index (SI) of > 6994. Thus, it was selected as our lead compound for further investigations.

Chalcone	CC_{50} (µM)	SI	Bichalcone	CC_{50} (µM)	SI
1aa	179.7 ± 32.18	8.23	**2aa**	> 200	> 30.13
1ab	132.8 ± 27.85	13.17	**2ab**	> 200	> 6994
1ac	> 200	-	**2ac**	> 200	-
1ad	> 200	-	**2ad**	> 200	> 8.08
1ae	190.3 ± 99.30	17.95	**2ae**	> 200	> 25.28
1af	133.8 ± 78.14	21.65	**2af**	> 200	> 6.56
1ag	> 200	-	**2ag**	> 200	> 10.84
1ba	> 200	> 24.73	**2ba**	> 200	-
1bb	87.81 ± 16.78	14.61	**2bb**	> 200	> 20.51
1bc	> 200	-	**2bc**	> 200	-
1bd	> 200	-	**2bd**	> 200	> 64.72
1be	> 200	-	**2be**	> 200	> 23.39
1bf	> 200	> 17.66	**2bf**	> 200	> 16.12
1bg	132.8 ± 72.40	29.77	**2bg**	> 200	-

Table 2. *In vitro* cytotoxicity of chalcones (1aa – bg) and bichalcones (2aa – bg) on human fibroblasts Hs27 and their selectivity indexes (SI)

Values shown in the table represent the means of three independent experiments each done in duplicate (n = 6).

3.3 Enantiopure synthesis of (S_a)- and (R_a)-2ab enantiomers

Since **2ab** exhibits axial chirality and only its racemic mixture was investigated so far, we turned our focus on the investigation of the pure enantiomers of **2ab**. This investigation aims to discern potential variations in activity and selectivity between the individual enantiomers. To gain access to both enantiomers of enantiopure bichalcones, our synthetic strategy involved the use of biphenol **3**, a building block used in previous studies in the synthesis of various natural product analogues (Ganardi, Greb, Henssen, & Pietruszka; Greb et al., 2023) (**Scheme 1**). Readily available brominated starting material **4** was transformed into the corresponding boronic acid ester **5** in a scalable fashion. Next, we investigated the aryl-aryl bond formation. The sterically demanding tetra-*ortho*-substituted biaryl bond of **6** was constructed by Suzuki cross-coupling. After screening for various conditions (SI), we were able to leverage the use of Lipshutz amphiphiles in

water drastically reducing the amount of palladium required (compared to our previous protocol (Ganardi et al.)). We next needed to gain access to enantiopure biphenol **3**. To our delight we found that separation of both enantiomers was possible by preparative normal phase HPLC using Lux i-Amylose-1 as the column. This process could be scaled up to 500 mg per run exceeding the scale of previously established protocols towards enantiopure bichalcones (Li et al., 1997; Lin & Zhong, 1997).

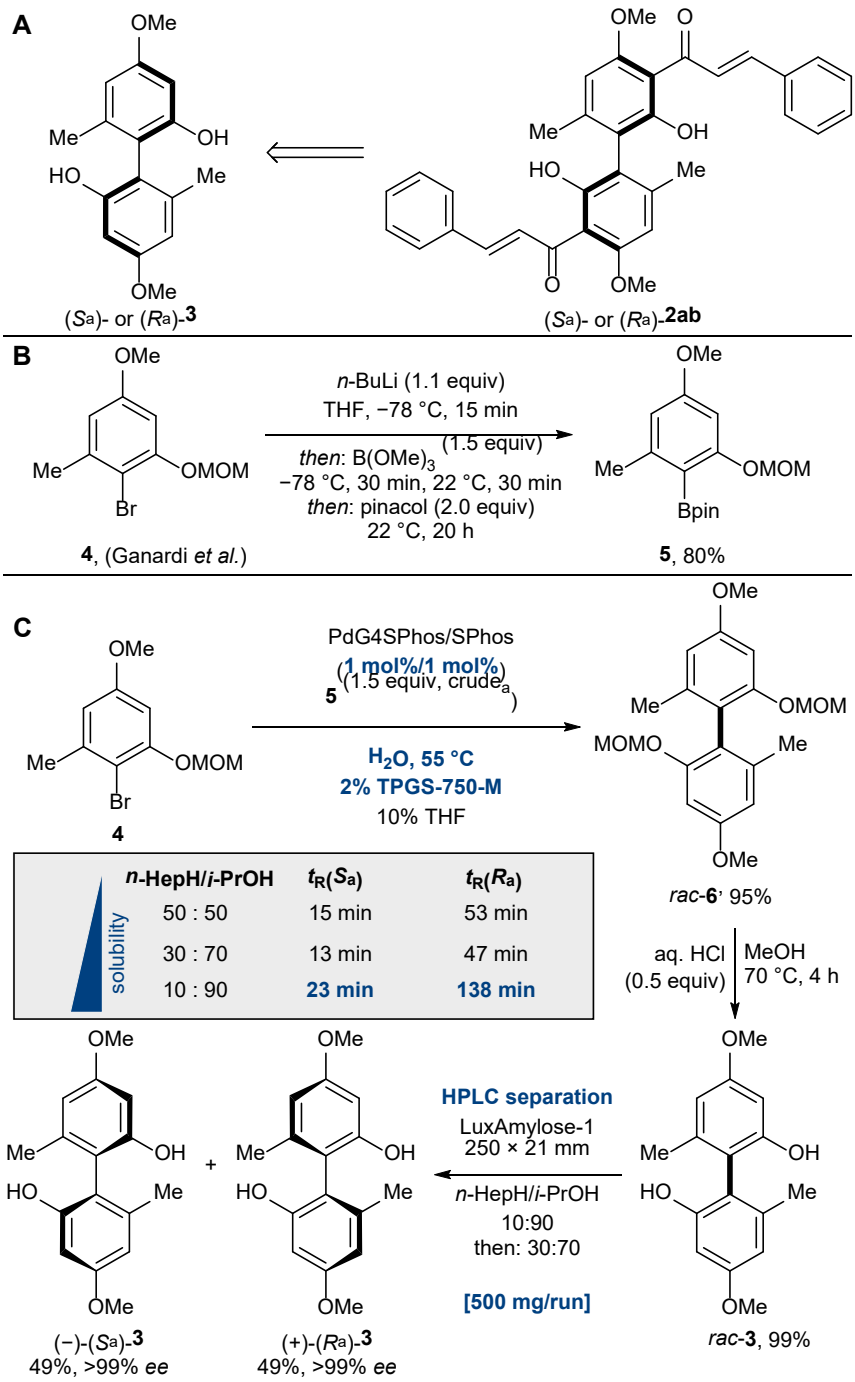

Scheme 2: (A) Synthesis strategy of both enantiomers of bichalcone 2ab. (B) Scalable borylation of readily available brominated starting material 4. (C) Pd-catalyzed (1 mol% Pd) Suzuki cross

coupling using amphiphile TPGS-750-M. Separation of the enantiomers was achieved by HPLC because of drastically different elution times (Δt_R = 115 min for *n*-heptane:*i*-propanol 10:90 v/v) for both enantiomers using Lux i-Amylose-1.

With both enantiomers of biphenol **3** in hand, we directed our efforts at the synthesis of both enantiomers of bichalcone **2ab**. The synthesis of acetophenone **7** following our previously established protocol (Greb et al., 2023) proceeded smoothly for both enantiomers in yields of 83% (S_a) and 76% (R_a) respectively (**Scheme 3**).

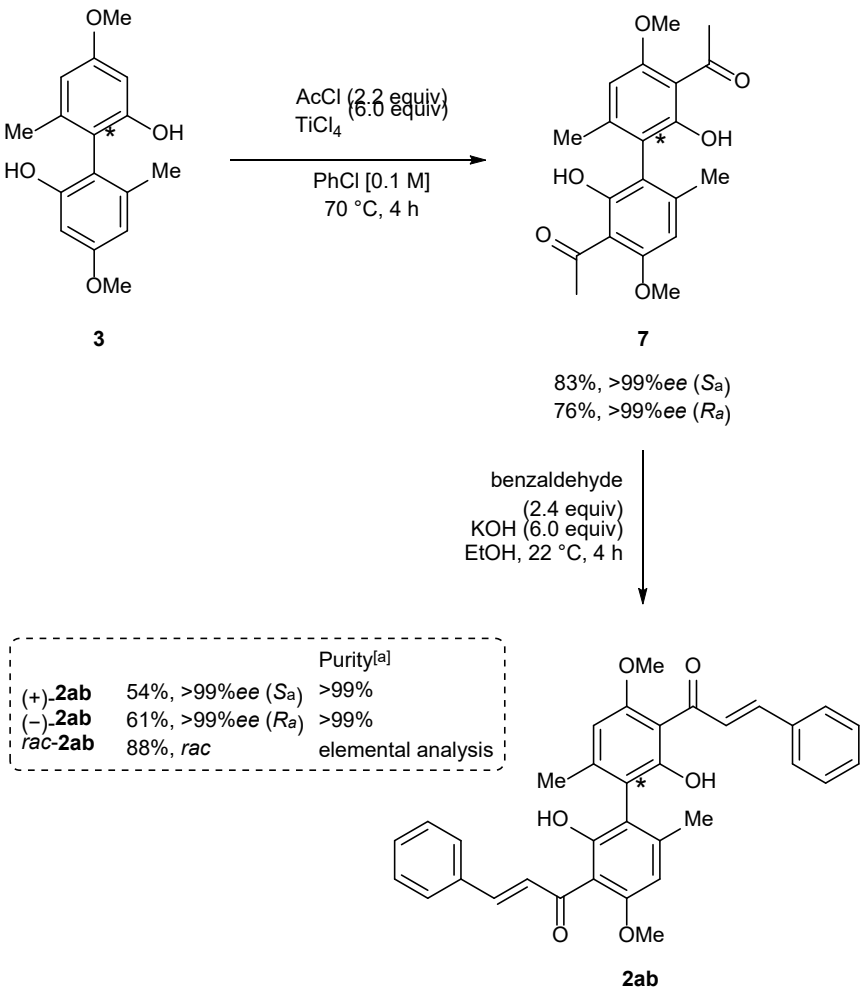

Scheme 4: Synthesis of both enantiomers of bichalcone 2ab.

[a] Purity by normal phase and reversed phase HPLC.

We continued with the synthesis of both enantiomers of bichalcone **2ab**. Racemic bichalcone **2ab** was conveniently obtained from our previous investigations on the bioactivity of biflavones (Klischan et al., 2023). In contrast to the racemic mixture of **2ab** isolation by column chromatography was feasible. Both enantiomers were obtained in

yields of 54% (S_a) and 61% (R_a) respectively with >99%*ee* each according to HPLC. We attribute the lower yield compared to the racemic mixture to increased formation of flavanone side products.

3.4 Biological evaluation of the enantiomers of bichalcone 2ab

After the successful synthesis of enantiopure (S_a)-**2ab** and (R_a)-**2ab**, we commenced our evaluation on their activity against *T. gondii* tachyzoites and their potential cytotoxicity on Hs27 with the aim of comparing their selectivity and determine if their absolute configuration influences their activity. As shown in **Table 3** and **Figure S28**, both enantiomers are strongly active against *T. gondii* proliferation with IC_{50} values in the nanomolar range and no cytotoxicity on Hs27, similarly to the racemic mixture. Interestingly, (R_a)-**2ab** resulted to be the eutomer (more potent enantiomer) with an IC_{50} of 0.10 µM, more than two fold higher than the enantiomer (S_a)-**2ab**. And slightly more active that the racemic mixture. A comparison with PYR-the gold-standard treatment for toxoplasmosis (Konstantinovic et al., 2019)-(IC_{50} of 0.222 µM, literature 0.4 µM) highlights the significance of our findings (**Table 3**).

Compound	IC_{50} (µM)	CC_{50} (µM)
(S_a)-2ab	0.31 ± 0.03	> 100
(R_a)-2ab	0.10 ± 0.01	> 100
2ab	0.11 ± 0.02	> 100
PYR	0.22 ± 0.05	> 100

Table 3. *In vitro* activity (IC_{50}) against *T. gondii*, cytotoxicity (CC_{50}) on human Hs27 cells of bichalcone 2ab and pyrimethamine (PYR)

Values shown in the table represent the means of three independent experiments each done in duplicate (n = 6) ± S.D.

4 Discussion

Toxoplasmosis, the disease caused by the apicomplexan parasite *T. gondii*, is the most common infection worldwide, affecting virtually all warm-blooded animals, including humans. The current available treatments options are only able to control the acute infection caused by the actively replicating tachyzoite stage, while having low or no effect on the chronic infection caused by the slowly replicating bradyzoite stage. Moreover, after more than 60 years from its discovery, the combination therapy pyrimethamine – sulfadiazine (PYR – SDZ) still remain the frontline treatment and only few novel medicinal entities have been approved for the human treatment of toxoplasmosis (Dunay, Gajurel, Dhakal, Liesenfeld, & Montoya, 2018).

Prior research has shown the potential of flavonoids as novel anti-toxoplasma entities *in vitro* and *in vivo*, and among them, flavones (Abugri, Witola, Russell, & Troy, 2018; Klischan et al., 2023) and chalcones (AL-Hilli et al., 2021; Ghazzay et al., 2023; Jiang et al., 2022; Qin et al., 2020; Si et al., 2018; Touquet et al., 2018)

We recently showed that biflavones are more potent than their monomeric counterpart, for both their antioxidant capacity and anti-toxoplasma *in vitro* activity (Klischan et al., 2023). Therefore, the objective of the present study was to explore the anti-toxoplasma *in vitro* activity of chalcones, crucial synthetic intermediates of flavones obtained in our previous study. With a specific focus at the biological comparison between monomers and dimers, this study aims to demonstrate the potential of the less investigated bichalcone counterparts.

Comparison of the anti-toxoplasma *in vitro* potential of monomers and their dimeric counterparts revealed that in some cases bichalcones are more potent than chalcones. In addition, all bichalcones exerted no cytotoxic effect on human fibroblasts Hs27, thus possessing a better cytotoxic profile than their monomeric counterparts. The bichalcone **2ab** exhibits the highest potency and selectivity, the only one with an IC_{50} in the nanomolar range. Thus, it possesses the potential to be a novel anti-toxoplasma lead compound.

With a target identified, we commenced with the synthesis of both enantiomers of **2ab**. The core biaryl motif of the A,A'-bichalcones contains a stereogenic axis, resulting in the presence of two atropenantiomers within the racemic mixture **2ab**. Synthesis of both enantiomers was successfully performed with the use of low amounts of Pd-catalyst. Comparison on the activity of the two enantiomers (S_a)- **2ab** and (R_a)-**2ab**, showed that

stereochemistry plays a key role on the potency, resulting (R_a)-**2ab** the eutomer. In addition, comparison on the activity of the gold-standard treatment PYR demonstrated that the enantiomer (R_a)-**2ab** and the racemic mixture are more potent.

Interestingly, Karaman *et al.* (2018) performed a structure-based virtual screening for the identification of novel sirtuin inhibitors and modulators. Docking analysis resulted in two bichalcones, a rhuschalcone IV and a rhuschalcone I analogue, identified as active inhibitors of human SIRT-1 and SIRT-2 (Karaman et al., 2018). Sirtuins are highly conserved enzymes dependent on nicotinamide adenine dinucleotide (NAD^+). In humans, seven sirtuins are classified as class III histone deacetylases (HDACs), regulating a wide range of important intracellular activities, such as metabolism, transcription and genome stability (Abbotto et al., 2022; Finkel, Deng, & Mostoslavsky, 2009). The *T. gondii* genome encodes for one SIR2 subtype homologue (class III) (Yu, Chen, et al., 2021; Yu, Lu, et al., 2021). The function of SIR2-like proteins in apicomplexans has not been fully explored, although they have been shown to be involved in the epigenetic regulation of virulence genes that are vital for the pathogenesis and persistence of *P. falciparum* (Religa & Waters, 2012).Thus, we performed a docking analysis of (S_a)- **2ab** and (R_a)-**2ab** with the *Tg*SIR2 homolog, to explore if it could be a potential target for compound **2ab**. Unfortunately, the performed docking studies did not result into a stable protein-ligand complex which might explain the inhibitory properties. Since these are *in silico* experiments, there might be several reasons to explain this, but first, initial *in vitro* binding studies need to be performed to conclusively suggest that this *Tg*SIR2 protein is actually the target. Thus, more research is needed to explore the mechanism of action and the target in *T. gondii* of **2ab**, and in particular, investigations of the binding interaction with the two enantiomers of **2ab**. Furthermore, *in vivo* investigations are needed to explore their activity and safety in the mouse model system in the future.

5 Conflict of Interest

The authors declare that the research was conducted in the absence of any commercial or financial relationships that could be construed as a potential conflict of interest.

6 Author Contributions

JP and KP contributed to conception and design of the study. MK and JG performed the synthesis. FM performed the biological investigation. SS performed docking analysis. FM wrote the first draft of the manuscript. FM, MK, JG and SS wrote sections of the manuscript. SS, JP and KP performed writing-review and editing of the manuscript. All authors contributed to manuscript revision, read, and approved the submitted version.

7 Funding

This work was supported by the Deutsche Forschungsgemeinschaft (DFG, German Research Foundation)–project number 270650915/GRK 2158 (to SS, JP and KP)

8 Acknowledgments

We gratefully acknowledge the DFG (GRK2158), the Heinrich Heine University (HHU) and Forschungszentrum Jülich GmbH for their generous support. We thank Karin Buchholz, Daniel Degrandi, Ursula Sorg and Max Schlamkow for scientific consultation and synthesis support.

9 Supplementary Material

The Supplementary Material for this article can be found online at:

10 Data Availability Statement

The original contributions presented in the study are included in the in the article/Supplementary Material. Further inquiries can be directed to the corresponding authors.

11 References

Abbotto, E., Scarano, N., Piacente, F., Millo, E., Cichero, E., & Bruzzone, S. (2022). Virtual Screening in the Identification of Sirtuins' Activity Modulators. *Molecules, 27*(17), 5641.

Abugri, D. A., Witola, W. H., Russell, A. E., & Troy, R. M. (2018). In vitro activity of the interaction between taxifolin (dihydroquercetin) and pyrimethamine against Toxoplasma gondii. *Chemical Biology & Drug Design, 91*(1), 194-201.

AL-Hilli, E. S. A., Ghazzay, M. H., Hasan, S. A., Al-Kelaby, K. K. A., & Zarka, M. A. (2021). THERAPEUTIC EFFECT OF CHALCONE ON TOXOPLASMA GONDII ISOLATED FROM RECURRENT PREGNANCY LOSS CASES IN AL-NAJAF CITY" INVITRO STUDY". *Journal of Natural Remedies, 22*(1 (2)), 32-40.

Alday, P. H., & Doggett, J. S. (2017). Drugs in development for toxoplasmosis: advances, challenges, and current status. *Drug design, development and therapy*, 273-293.

Arslan, T., Celik, G., Celik, H., Şentürk, M., Yaylı, N., & Ekinci, D. (2016). Synthesis and biological evaluation of novel bischalcone derivatives as carbonic anhydrase inhibitors. *Archiv der Pharmazie, 349*(9), 741-748.

Bale, A. T., Salar, U., Khan, K. M., Chigurupati, S., Fasina, T., Ali, F., . . . Perveen, S. (2021). Chalcones and Bis-Chalcones Analogs as DPPH and ABTS Radical Scavengers. *Letters in Drug Design & Discovery, 18*(3), 249-257.

Belmokhtar, C. A., Hillion, J., & Ségal-Bendirdjian, E. (2001). Staurosporine induces apoptosis through both caspase-dependent and caspase-independent mechanisms. *Oncogene, 20*(26), 3354-3362.

Dan, W., & Dai, J. (2020). Recent developments of chalcones as potential antibacterial agents in medicinal chemistry. *European Journal of Medicinal Chemistry, 187*, 111980.

Delgado, I. L. S., Zúquete, S., Santos, D., Basto, A. P., Leitão, A., & Nolasco, S. (2022). The Apicomplexan Parasite Toxoplasma gondii. *Encyclopedia, 2*(1), 189-211. Retrieved from https://www.mdpi.com/2673-8392/2/1/12

Deng, Y., Wu, T., Zhai, S.-Q., & Li, C.-H. (2019). Recent progress on anti-Toxoplasma drugs discovery: Design, synthesis and screening. *European Journal of Medicinal Chemistry, 183*, 111711.

Domínguez, J. N., Gamboa de Dominguez, N., Rodrigues, J., Acosta, M. E., Caraballo, N., & León, C. (2013). Synthesis and antimalarial activity of urenyl Bis-chalcone in vitro and in vivo. *Journal of Enzyme Inhibition and Medicinal Chemistry, 28*(6), 1267-1273.

Dubey, J., Lindsay, D., & Speer, C. (1998). Structures of Toxoplasma gondii tachyzoites, bradyzoites, and sporozoites and biology and development of tissue cysts. *Clinical Microbiology Reviews, 11*(2), 267-299.

Dubey, J. P. (2021). *Toxoplasmosis of animals and humans*: CRC press.

Dunay, I. R., Gajurel, K., Dhakal, R., Liesenfeld, O., & Montoya, J. G. (2018). Treatment of toxoplasmosis: historical perspective, animal models, and current clinical practice. *Clinical Microbiology Reviews, 31*(4), e00057-00017.

Elkanzi, N. A., Hrichi, H., Alolayan, R. A., Derafa, W., Zahou, F. M., & Bakr, R. B. (2022). Synthesis of chalcones derivatives and their biological activities: a review. *ACS omega, 7*(32), 27769-27786.

Eyles, D., & Coleman, N. (1953). Synergistic Effect of Sulfadiazlne and Daraprim against Experimental Toxoplasmosis in the Mouse. *Antibiotics & chemotherapy, 3*(5), 483-490.

Fekadu, A., Shibre, T., & Cleare, A. J. (2010). Toxoplasmosis as a cause for behaviour disorders-overview of evidence and mechanisms. *Folia parasitologica, 57*(2), 105.

Finkel, T., Deng, C.-X., & Mostoslavsky, R. (2009). Recent progress in the biology and physiology of sirtuins. *Nature, 460*(7255), 587-591.

Fu, Y., Liu, D., Zeng, H., Ren, X., Song, B., Hu, D., & Gan, X. (2020). New chalcone derivatives: synthesis, antiviral activity and mechanism of action. *RSC advances, 10*(41), 24483-24490.

Ganardi, R., Greb, J., Henssen, B., & Pietruszka, J. Atroposelective Total Synthesis of (+)-Isokotanin A via Combined Metal and Enzyme Catalysis. *Advanced Synthesis & Catalysis*.

Ghazzay, M. H., Hasan, S. A., DeliKhudhair, O., & Abbas, K. K. (2023). Synthesis, Characterization, and Anti-parasitic Activity Evaluation of the Synthesized Chalcone against Toxoplasma Gondii Isolated from Cases of Abortion in Al-Najaf City.

Greb, J., Drennhaus, T., Klischan, M. K., Schroeder, Z. W., Frey, W., & Pietruszka, J. (2023). A Common C2-Symmetric 2, 2′-Biphenol Building Block and its Application in the Synthesis of (+)-di-epi-Gonytolide A. *Chemistry–A European Journal, 29*(34), e202300941.

Helmy, Y. A., & Hafez, H. M. (2022). Cryptosporidiosis: From Prevention to Treatment, a Narrative Review. *Microorganisms, 10*(12), 2456. Retrieved from https://www.mdpi.com/2076-2607/10/12/2456

Hill, D. E., & Dubey, J. P. (2018). Toxoplasma gondii. In Y. R. Ortega & C. R. Sterling (Eds.), *Foodborne Parasites* (pp. 119-138). Cham: Springer International Publishing.

Homer, M. J., Aguilar-Delfin, I., Telford, S. R., Krause, P. J., & Persing, D. H. (2000). Babesiosis. *Clinical Microbiology Reviews, 13*(3), 451-469. doi:doi:10.1128/cmr.13.3.451

Jiang, L., Liu, B., Hou, S., Su, T., Fan, Q., Alyafeai, E., . . . Li, J. (2022). Discovery and evaluation of chalcone derivatives as novel potential anti-Toxoplasma gondii agents. *European Journal of Medicinal Chemistry, 234*, 114244.

Karaman, B., Alhalabi, Z., Swyter, S., Mihigo, S. O., Andrae-Marobela, K., Jung, M., . . . Ntie-Kang, F. (2018). Identification of bichalcones as sirtuin inhibitors by virtual screening and in vitro testing. *Molecules, 23*(2), 416.

Klischan, M. K. T., Mazzone, F., Berning, L., Greb, J., Schlamkow, M., Haase, M., . . . Pietruszka, J. (2023). Modular Approach for the Synthesis and Bioactivity Profiling of 8,8′-Biflavones. *ACS omega, 8*(44), 41816-41834. doi:10.1021/acsomega.3c06503

Konstantinovic, N., Guegan, H., Stäjner, T., Belaz, S., & Robert-Gangneux, F. (2019). Treatment of toxoplasmosis: Current options and future perspectives. *Food and waterborne parasitology, 15*, e00036.

Lejeune, M., Miró, J. M., De Lazzari, E., García, F., Claramonte, X., Martínez, E., . . . Group, t. S. T. g. S. (2011). Restoration of T Cell Responses to Toxoplasma gondii after Successful Combined Antiretroviral Therapy in Patients with AIDS with Previous Toxoplasmic Encephalitis. *Clinical Infectious Diseases, 52*(5), 662-670. doi:10.1093/cid/ciq197

LEVINE, N. D. (1988). Progress in taxonomy of the Apicomplexan protozoa. *J Protozool, 35*(4), 518-520.

Li, H.-Y., Nehira, T., Hagiwara, M., & Harada, N. (1997). Total Synthesis and Absolute Stereochemistry of the Natural Atropisomer of the Biflavone 4 ‘, 4 ‘‘‘, 7, 7 ‘‘-Tetra-O-methylcupressuflavone. *The Journal of organic chemistry, 62*(21), 7222-7227.

Lin, G.-Q., & Zhong, M. (1997). The first enantioselective synthesis of optically pure (R)-and (S)-5, 5 ″-dihydroxy-4′, 4‴, 7, 7 ″-tetramethoxy-8, 8 ″-biflavone and the reconfirmation of their absolute configuration. *Tetrahedron Letters, 38*(6), 1087-1090.

Masesane, I. B., Yeboah, S. O., Liebscher, J., Mügge, C., & Abegaz, B. M. (2000). A bichalcone from the twigs of Rhus pyroides. *Phytochemistry, 53*(8), 1005-1008.

Mazzone, F., Simons, V. E., van Geelen, L., Frank, M., Mándi, A., Kurtán, T., . . . Kalscheuer, R. (2022). In Vitro Biological Activity of Natural Products from the Endophytic Fungus Paraboeremia selaginellae against Toxoplasma gondii. *Antibiotics, 11*(9), 1176.

Mdee, L. K., Yeboah, S. O., & Abegaz, B. M. (2003). Rhuschalcones II− VI, Five New Bichalcones from the Root Bark of Rhus p yroides. *J Nat Prod, 66*(5), 599-604.

Menezes, J. C., & Diederich, M. F. (2019). Natural dimers of coumarin, chalcones, and resveratrol and the link between structure and pharmacology. *European Journal of Medicinal Chemistry, 182*, 111637.

Merkt, F. K., Mazzone, F., Sazzadeh, S. S., Bonda, L., Hinz, L. K., Gruber, I., . . . Müller, T. J. (2021). Fluorescent Indolo [3, 2-a] phenazines against Toxoplasma gondii: Concise Synthesis by Gold-Catalyzed Cycloisomerization with 1, 2-Silyl Migration and ipso-Iodination Suzuki Sequence. *Chemistry–A European Journal, 27*(38), 9774-9781.

Mihigo, S. O., Mammo, W., Bezabih, M., Andrae-Marobela, K., & Abegaz, B. M. (2010). Total synthesis, antiprotozoal and cytotoxicity activities of rhuschalcone VI and analogs. *Bioorganic & Medicinal Chemistry, 18*(7), 2464-2473.

Montoya, J. G., & Liesenfeld, O. (2004). Toxoplasmosis. *The Lancet, 363*(9425), 1965-1976. doi:https://doi.org/10.1016/S0140-6736(04)16412-X

Mosmann, T. (1983). Rapid colorimetric assay for cellular growth and survival: application to proliferation and cytotoxicity assays. *J Immunol Methods, 65*(1-2), 55-63. doi:10.1016/0022-1759(83)90303-4

Newman, D. J., & Cragg, G. M. (2020). Natural Products as Sources of New Drugs over the Nearly Four Decades from 01/1981 to 09/2019. *J Nat Prod, 83*(3), 770-803. doi:10.1021/acs.jnatprod.9b01285

Ouyang, Y., Li, J., Chen, X., Fu, X., Sun, S., & Wu, Q. (2021). Chalcone derivatives: Role in anticancer therapy. *Biomolecules, 11*(6), 894.

Pereira, R., Silva, A. M., Ribeiro, D., Silva, V. L., & Fernandes, E. (2023). Bis-chalcones: A review of synthetic methodologies and anti-inflammatory effects. *European journal of medicinal chemistry, 252*, 115280.

Pfefferkorn, E. (1986). *Interferon gamma and the growth of Toxoplasma gondii in fibroblasts.* Paper presented at the Annales de l'Institut Pasteur/Microbiologie.

Pfefferkorn, E. R., & Pfefferkorn, L. C. (1977). Specific labeling of intracellular Toxoplasma gondii with uracil. *J Protozool, 24*(3), 449-453. doi:10.1111/j.1550-7408.1977.tb04774.x

Phillips, M. A., Burrows, J. N., Manyando, C., van Huijsduijnen, R. H., Van Voorhis, W. C., & Wells, T. N. C. (2017). Malaria. *Nature Reviews Disease Primers, 3*(1), 17050. doi:10.1038/nrdp.2017.50

Qin, H.-L., Zhang, Z.-W., Lekkala, R., Alsulami, H., & Rakesh, K. (2020). Chalcone hybrids as privileged scaffolds in antimalarial drug discovery: A key review. *European Journal of Medicinal Chemistry, 193*, 112215.

Ram, V. J., Saxena, A. S., Srivastava, S., & Chandra, S. (2000). Oxygenated chalcones and bischalcones as potential antimalarial agents. *Bioorganic & Medicinal Chemistry Letters, 10*(19), 2159-2161.

Religa, A. A., & Waters, A. P. (2012). Sirtuins of parasitic protozoa: In search of function(s). *Molecular and biochemical parasitology, 185*(2), 71-88. doi:https://doi.org/10.1016/j.molbiopara.2012.08.003

Rocha, S., Ribeiro, D., Fernandes, E., & Freitas, M. (2020). A systematic review on anti-diabetic properties of chalcones. *Current medicinal chemistry, 27*(14), 2257-2321.

Sharma, U. K., Mohanakrishnan, D., Sharma, N., Equbal, D., Sahal, D., & Sinha, A. K. (2018). Facile synthesis of vanillin-based novel bischalcones identifies one that induces apoptosis and displays synergy with Artemisinin in killing chloroquine resistant Plasmodium falciparum. *European journal of medicinal chemistry, 155*, 623-638.

Sheffield, H. G., & Melton, M. L. (1975). Effect of Pyrimethamine and Sulfadiazine on the Fine Structure and Multiplication of Toxoplasma gondii in Cell Cultures. *J Parasitol, 61*(4), 704-712. doi:10.2307/3279470

Si, H., Xu, C., Zhang, J., Zhang, X., Li, B., Zhou, X., & Zhang, J. (2018). Licochalcone A: an effective and low-toxicity compound against Toxoplasma gondii in vitro and in vivo. *International Journal for Parasitology: Drugs and Drug Resistance, 8*(2), 238-245.

Strang, A. G., Ferrari, R. G., do Rosário, D. K., Nishi, L., Evangelista, F. F., Santana, P. L., . . . Guilherme, A. L. F. (2020). The congenital toxoplasmosis burden in Brazil: Systematic review and meta-analysis. *Acta Tropica, 211*, 105608.

Tenter, A. M., Heckeroth, A. R., & Weiss, L. M. (2000). Toxoplasma gondii: from animals to humans. *International journal for parasitology, 30*(12), 1217-1258. doi:https://doi.org/10.1016/S0020-7519(00)00124-7

Touquet, B., Pelissier, L., Cavailles, P., Yi, W., Bellini, V., Mercier, C., . . . Aldebert, D. (2018). High-content imaging assay to evaluate Toxoplasma gondii infection and proliferation: a multiparametric assay to screen new compounds. *PloS one, 13*(8), e0201678.

Vale, A., Lucas, M., Ribeiro, D., & Fernandes, E. (2023). *Research into New Molecules with Anti-Inflammatory Activity.* Paper presented at the Medical Sciences Forum.

Van Delden, C., & Hirschel, B. (1996). Folinic acid supplements to pyrimethamine-sulfadiazine for Toxoplasma encephalitis are associated with better outcome. *Journal of Infectious Diseases, 173*(5), 1294-1295.

Wang, Z.-D., Liu, H.-H., Ma, Z.-X., Ma, H.-Y., Li, Z.-Y., Yang, Z.-B., . . . Liu, Q. (2017). Toxoplasma gondii Infection in Immunocompromised Patients: A Systematic Review and Meta-Analysis. *Frontiers in Microbiology, 8*. doi:10.3389/fmicb.2017.00389

Yu, Z., Chen, S., Aleem, M., He, S., Yang, Y., Zhou, T., . . . Xu, L. (2021). Histone deacetylase SIR2 in Toxoplasma gondii modulates functions of murine macrophages in vitro and protects mice against acute toxoplasmosis in vivo. *Microbial Pathogenesis, 154*, 104835.

Yu, Z., Lu, Y., Cao, W., Aleem, M. T., Liu, J., Luo, J., . . . Li, X. (2021). Nano DNA vaccine encoding Toxoplasma gondii histone deacetylase SIR2 enhanced protective immunity in Mice. *Pharmaceutics, 13*(10), 1582.

Zhang, E.-H., Wang, R.-F., Guo, S.-Z., & Liu, B. (2013). An update on antitumor activity of naturally occurring chalcones. *Evidence-Based Complementary and Alternative Medicine, 2013*.

Zhuang, C., Zhang, W., Sheng, C., Zhang, W., Xing, C., & Miao, Z. (2017). Chalcone: a privileged structure in medicinal chemistry. *Chemical Reviews, 117*(12), 7762-7810.

Supplementary Material

Synthesis and *In Vitro* Evaluation of Bichalcones as Novel Anti-Toxoplasma Agents

Flaminia Mazzone[1] †, Moritz K. T. Klischan[2] †, Julian Greb[2] †, Sander H. J. Smits[3], Jörg Pietruszka[2,4*] and Klaus Pfeffer[1*]

[1]Institute of Medical Microbiology and Hospital Hygiene, Heinrich Heine University Düsseldorf, Düsseldorf, Germany

[2]Institute of Biorganic Chemistry, Heinrich Heine University Düsseldorf, Forschungszentrum Jülich GmbH, Jülich, Germany

[3]Institute of Biochemistry, Heinrich Heine University Düsseldorf, Düsseldorf, Germany

[4]Institute of Bio- and Geosciences (IBG-1): Biotechnology, Forschungszentrum Jülich GmbH, Jülich, Germany

†These authors share first authorship

*** Correspondence:**

Klaus Pfeffer

klaus.pfeffer@hhu.de

Jörg Pietrusza

j.pietruszka@fz-juelich.de

1 Experimental Procedures

1.1 General Information

Prior to use in synthesis benzaldehyde was washed with saturated aqueous Na_2CO_3 solution, dried over $MgSO_4$ and then isolated by vacuum distillation ($1 \cdot 10^{-1}$ mbar) at 94 °C (58 °C head temperature).

1.1.1 Optimization of Suzuki Coupling in Micellar Aqueous Media

The required biphenol building block **3** can be formed via double methoxymethyl (MOM)-protected intermediate 6. While the synthesis of such tetra-*ortho*-substituted biaryls can be challenging, efficient syntheses have been developed recently (**Figure S1**). Besides formation via oxidation of the corresponding biaryl Lipshutz cuprates, a one-pot Miyaura borylation Suzuki coupling (MBSC) sequence has been developed. While being scalable and efficient, these approaches either involved the use of superstoechiometric amount of pyrophoric *tert*-butyllithium and toxic copper cyanide or rather high effective palladium loadings relative to the amount of isolated product.

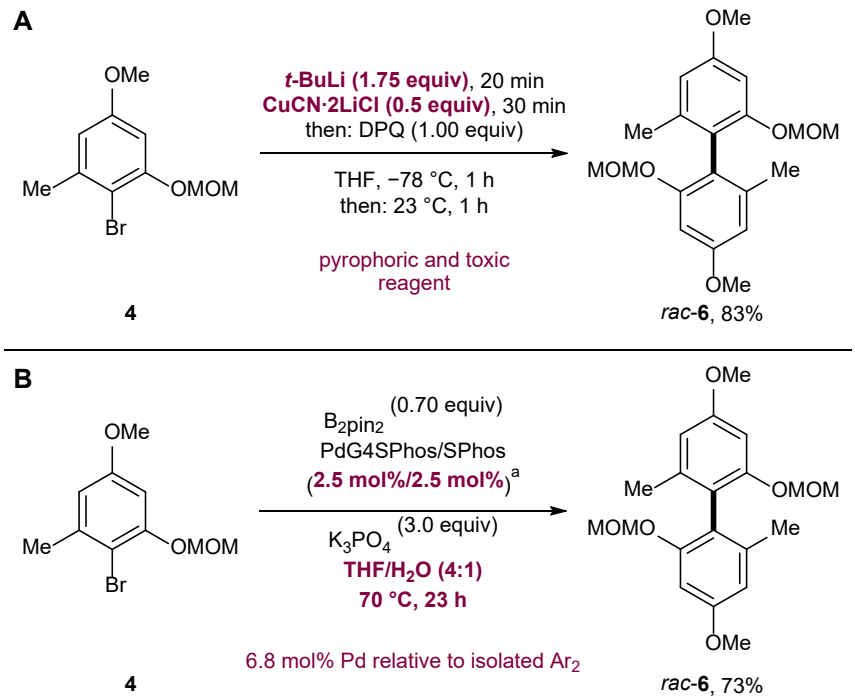

Figure S1: Previous coupling approach.
Via the oxidation of a biaryl Lipshutz cuprate (A) or using a Miyaura borylation-Suzuki coupling (MBSC) one-pot approach (B).

We wondered whether the challenging Suzuki coupling step could be further improved with respect to temperature, solvent and especially palladium loadings. The needed aryl boronic acid pinacol ester **5** was made available via a classic borylation approach. With the boronate in hand, we systematically optimized our previous Suzuki coupling conditions. The corresponding optimization results are shown in **Table S1**.

A solvent mixture of 4:1 THF/water was confirmed to be superior compared to pure organic solvent systems like tetrahydrofuran and toluene (entries 1 – 3) (Christine Ganardi, Greb, Henßen, & Pietruszka; Tietze, Ma, & Jackenkroll, 2014). Most notably, we found that the use an aqueous micellar reaction medium based on Lipshutz's TPGS-750-M surfactant significantly facilitated the coupling reaction, enabling conversions at room temperature (entry 4) (Lipshutz et al., 2011). Addition of 10% cosolvent was employed to ensure a stable emulsion (Gabriel et al., 2017). The use of Buchwald's SPhosG4 precatalyst in combination with slight heating further improved conversions at significantly reduced palladium loadings from 3.5 to 1.0 mol% (entry 5). Scaling was performed using slightly increased amounts of aryl boronate, which could be employed as crude product. Full conversions were observed, and the desired product could be isolated in 95% yield (entry 7). Further reduction of catalyst loadings let to an incomplete conversion (entry 6).

Table S1. **Optimization of Suzuki Coupling in Water**

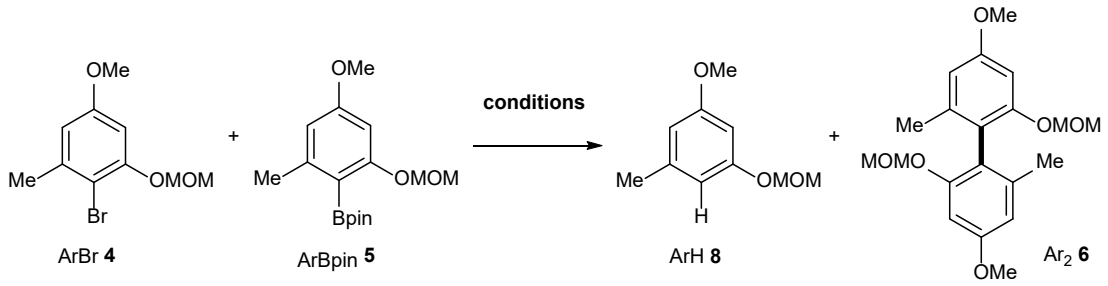

Entry	Conditions	Conversions [%][a]				Comment
		ArBr	ArH	ArBpin	Ar_2	

1	$Pd(OAc)_2$/ SPhos (3.5/ 7.0 mol%) ArBr (1.0 equiv) ArBpin (1.25 equiv) K_3PO_4 (3.0 equiv) **THF** 70 °C, 15 h	43 <97>	32 <72>	0 <0>	25 <56>	[0.05 mmol] <Integral(Ar) = 225>
2	$Pd(OAc)_2$/ SPhos (3.5/ 7.0 mol%) ArBr (1.0 equiv) ArBpin (1.25 equiv) K_3PO_4 (3.0 equiv) **PhMe** 70 °C, 15 h	45 <101>	31 <70>	13 <29>	11 <25>	[0.05 mmol] <Integral(Ar) = 225>
3	$Pd(OAc)_2$/ SPhos (3.5/ 7.0 mol%) ArBr (1.0 equiv) ArBpin (1.25 equiv) K_3PO_4 (3.0 equiv) **THF/H_2O (4:1)** 70 °C, 17 h	23 <52>	28 <63>	0 <0>	49 <110>	[0.05 mmol] <Integral(Ar) = 225>
4	$Pd(OAc)_2$/ SPhos (3.5/ 7.0 mol%) ArBr (1.00 equiv) ArBpin (1.25 equiv) K_3PO_4 (3.0 equiv) **2% TPGS-750-M in H_2O** 10% THF **22 °C, 2 h**	25 <57>	34 <76>	0 <0>	41 <93>	**reaction at room temperature** [0.1 mmol] <Integral(Ar) = 225>
5	**PdG4SPhos/ SPhos (1.0/ 1.0 mol%)** ArBr (1.00 equiv) ArBpin (1.25 equiv)	22 <50>	11 <24>	13 <29> 0	54 <122>	**precatalyst superior** [0.1 mmol] <Integral(Ar) = 225>

	K_3PO_4 (3.0 equiv) 2% TPGS-750-M in H_2O 10% THF 55 °C, 0.5 h 55 °C, 3.5 h	16 <37>	18 <41>	<0>	65 <147>	
6	PdG4SPhos/ SPhos **(0.5/ 0.5 mol%)** ArBr (1.00 equiv) **crude ArBpin** **(1.50 equiv)** K_3PO_4 (3.0 equiv) 2% TPGS-750-M in H_2O 10% THF 50 °C, 22 h	13 <32>	37 <93>	0 <1>	50 <126> (**61**)	**ArBpin crude** **(15% ArH)** [5.66 mmol] <Integral(Ar) = 250>
7	PdG4SPhos/ SPhos **(1.0/ 1.0 mol%)** ArBr (1.00 equiv) **crude ArBpin** **(1.50 equiv)** K_3PO_4 (3.0 equiv) 2% TPGS-750-M in H_2O 10% THF 55 °C, 16 h	0 <0>	23 <67>	0 <0>	73 <183> (**95**)	**ArBpin crude** **(15% ArH)** [5.66 mmol] **Isolated: 1.9 g** <Integral(Ar) = 250>

[a] Observed rations by ^{1}H-NMR analysis of worked-up reaction samples or crude products (integral sum of all common parent aryl group signals 'Integral(Ar)' set to 100). In chevrons ('<>') the same ratio is give with the integral sum of aryl group signals set to the total amount of ArBr **and** ArBpin **starting material 'aryl equivalents' (e.g. Integral(Ar) = 225 for 1.00 equiv** ArBr **+ 1.25 equiv** ArBpin**). While maybe a bit unusual, this procedure allows for a more direct determination of the individual conversions of** ArBr **and** ArBpin**, which carry the same parent aryl motif. Isolated yields are given in parentheses.**

The fully optimized Suzuki coupling conditions are summarized in **Figure S2**. The overall yield of biaryl **6** relative to the employed aryl bromide **4** is 68% over two steps. While the yield is comparable to the previous one-pot borylation-Suzuki coupling approach (**Figure S1**), a significant decrease in palladium loading could be achieved (1.1 mol% instead of 6.8 mol% relative to the amount of isolated product).

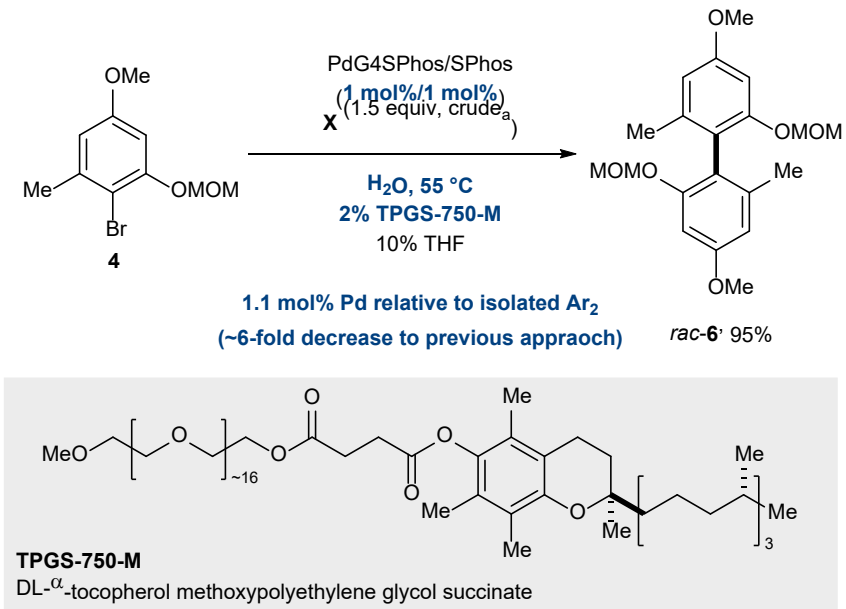

Figure S2: Optimized Suzuki coupling with reduced Pd-loading, temperature and solvent using micellar catalysis.
[a] determined by ^{1}H-NMR, protodehalogenated aryl side product as impurity.

Figure S3: Reaction mixture of Suzuki coupling under aqueous micellar conditions.
From left to right: (a) starting materials and reagents as homogeneous water/TPGS-750-M emulsion (2% surfactant, 10% tetrahydrofuran cosolvent) before base addition; (b) reaction emulsion after base addition, the yellow color is indicative for precatalyst activation; (c) reaction mixture after 16 h mild heating and stirring; (d) reaction mixture after standing for a while, an organic crude product layer formed.

1.1.2 Systematic Evaluation of Preparative HPLC-Conditions

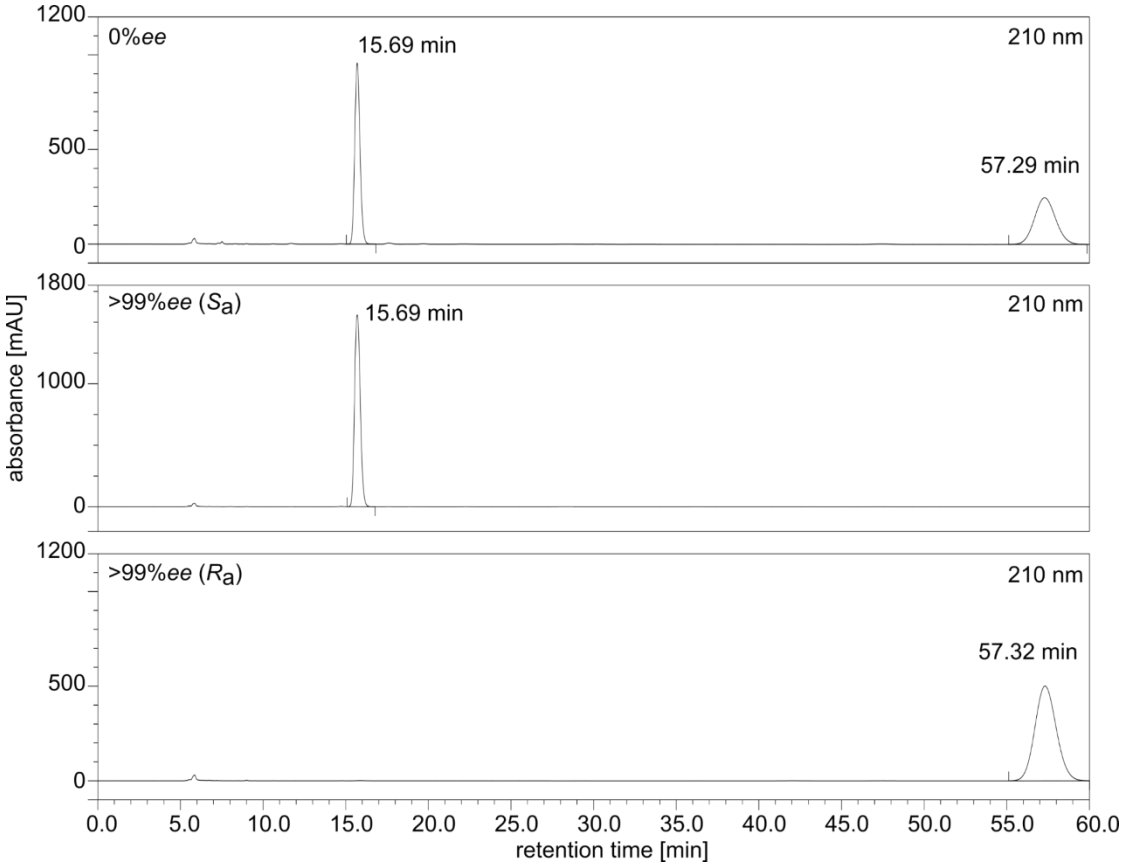

Figure S4: Comparative HPLC analysis of racemic and enantio-pure biphenol 3.
Racemic mixture (top), (S_a)-configured- (middle) and (R_a)-configured biphenol (bottom). Analytical HPLC conditions: LuxAmylose-1 (*Phenomenex*), 250.0 × 4.6 mm, 5 µm, 25 °C, 0.5 mL min^{-1}, 210 m, 50:50 (v/v) *n*-heptane/*i*-propanol.

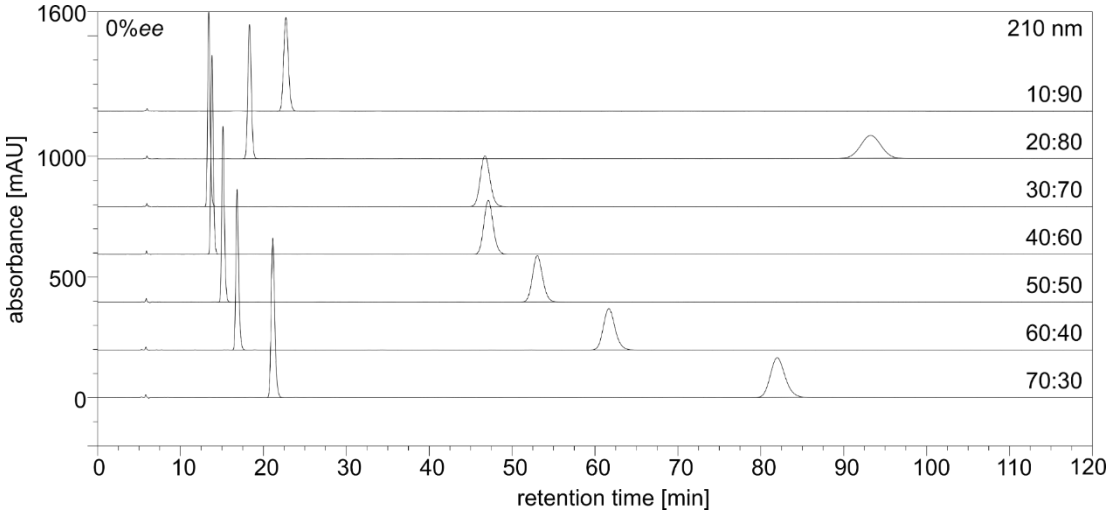

Figure S5: HPLC-separation behavior of racemic biphenol 3 on an analytical column.
LuxAmylose-1 (*Phenomenex*), 250.0 × 4.6 mm, 5 µm, 25 °C, 0.5 mL min^{-1}, 210 m, *n*-heptane/*i*-propanol; retention times for (S_a)-3/(R_a)-3 at a different *n*-heptane : *i*-propanol (v/v) mixtures were 21.1 min/82.2 min (70:30), 16.8 min/61.7 min (60:40), 15.1 min/53.0 min (50:50), 13.8 min/47.1 min (40:60), 13.4 min/46.7 min (30:70), 18.2 min/93.5 min (20:80), 22.7 min/>120.0 min (10:90).

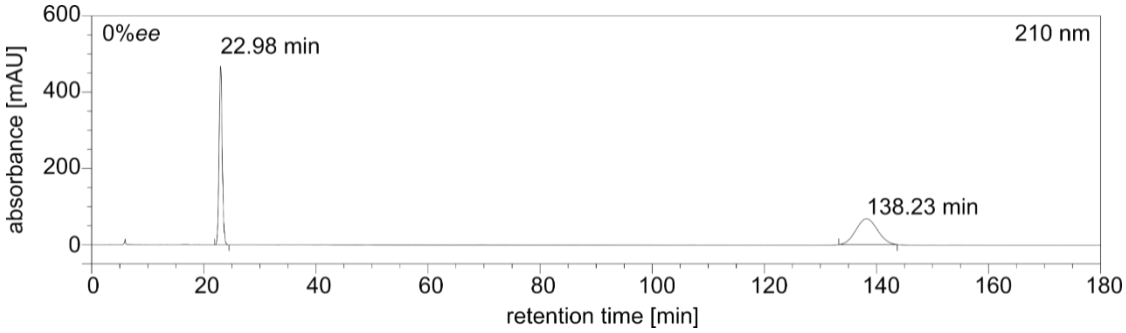

Figure S6: HPLC-separation of racemic biphenol 3 on an analytical column with 10:90 (v/v) *n*-heptane/*i*-propanol and increased runtime. LuxAmylose-1 (*Phenomenex*), 250.0 × 4.6 mm, 5 µm, 25 °C, 0.5 mL min^{-1}, 210 m, *n*-heptane/*i*-propanol.

Based on the observed retention times t_{R1}(S_a-**3**), t_{R2}(R_a-**3**) and the void time t_{R0}, retention factors $k_1 = (t_{R1} - t_{R0})/t_{R0}$ and $k_2 = (t_{R2} - t_{R0})/t_{R0}$ as well as a separation factors (chiral selectivities) $\alpha = k_2/k_1$ could be calculated for eluents of different polarities. These are listed in **Table 2**.

Table 2: Retention Factors k_1/k_2 and Separation Factors α for Eluents with Increasing Polarity.

HepH/*i*-PrOH	$t_{R1}(S_a)$ [min]	$k_1(S_a)$	$t_{R0}(R_a)$ [min]	$k_2(R_a)$	α
70 : 30	21.1	2.6	82.2	13.2	5.0
60 : 40	16.8	1.9	61.7	9.6	5.1
50 : 50	15.1	1.6	53.0	8.1	5.1
40 : 60	13.8	1.4	47.1	7.1	5.2
30 : 70	13.4	1.3	46.7	**7.1**	5.4
20 : 80	18.2	2.1	93.5	15.1	7.1
10 : 90	23.0	3.0	138.2	22.8	**7.7**

Based on analytical separation runs on LuxAmylose-1 (*Phenomenex*), 250.0 × 4.6 mm, 5 µm, 25 °C, 0.5 mL min^{-1}, 210 m (Figures S4, S5 and S6); the void time t_{R0} was determined to be 5.8 min based on the injection peak; for an eluent mixture of 10: 90 the highest separation factor was observed, at an eluent mixture of 30: 70 the lowest retention factor for the later-eluting enantiomer was observed.

The chiral stationary phase (CSP) of LuxAmylose-1 (*Phenomenx*) is based on the well-known chiral selector amylose tris(3,5-dimethylphenyl)carbamate (ADMPC) in combination with a silica gel matrix. The same chiral selector is used in other commercial HPLC columns like Chiralpak AD (*Daicel*) or Chiralpak IA (*Daicel*). Good separation factors of 2 – 5 for the separation of atrop-enantiomeric analytes has been reported recently (Rizzo, Benincori, Fontana, Pasini, & Cirilli, 2022; Sechi et al., 2023). The structure of polymeric ADMPC (shown in **Figure S7**) is known do adopt a helical conformation (Yamamoto, Yashima, & Okamoto, 2002). Also, unusual separation behaviours as a function of the eluent composition including for example inversion of the elution order of enantiomers have been observed by others (Wang & Chen, 1999; Wang, Chen, & Vailaya, 2000). These have been attributed to an alteration of the CSP's chiral cavities (stereo environment) by solvent incorporation or changes in the higher order structure of ADMPC, such as the degree of twisting of the amylose helix or differences in crystallinity, especially for higher concentration of branched alcohols, such as *i*-propanol or *t*-butanol (Wang & Wenslow, 2003).

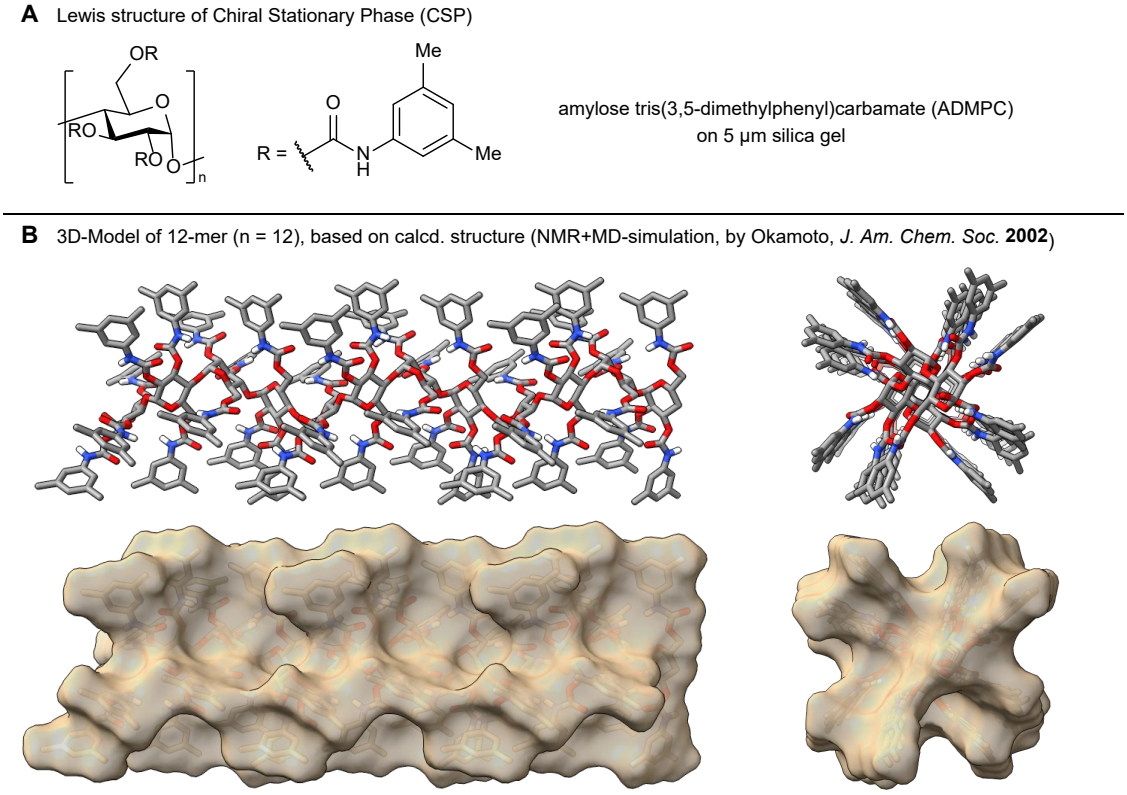

Figure S7: Structural Representations of the LuxAmylose-1 Chiral Selector ADMPC. Polymer 2D-Lewis structure (A) and helical 3D-model (B); the 3D-model was generated based on the structural data published by Ye (Ye, Bai, Vyas, & Wirth, 2007), which in turn has been calculated by Okamato and coworkers via experimental NMR-constraints in combination with MD-simulations (Yamamoto et al., 2002). The visualization was generated based on the published pdb-file using ChimeraX (Pettersen et al., 2021) and is depicted from the side (B, left) or top (B, right) as stick model without (B, top) and with surface (solvent-excluded surfaces, 2.0 Å probe radius) (B, bottom).

1.2 Synthetic Procedures

In the following, the synthetic procedures used in this work are outlined. The syntheses of monomeric chalcones as well as the racemic synthesis of bichalcones has previously been published.(Klischan et al., 2023) Our enantioselective bichalcone synthesis commenced with methoxymethyl (MOM)-protected 2-bromophenol **4**, which was synthesized following a scalable and column-free procedure starting from commercially available orcinol (Greb et al., 2023).

1.2.1 Synthesis of 2-(4-methoxy-2-(methoxymethoxy)-6-methylphenyl)-4,4,5,5-tetramethyl-1,3,2-dioxaborolane (5)

A dry 50-mL Schlenk-tube was equipped with a magnetic stirring bar and septum and charged with 2-bromo-5-methoxy-1-(methoxymethoxy)-3-methylbenzene (**4**, 522 mg, 2.0 mmol, 1.0 equiv) (Greb et al., 2023) under a nitrogen atmosphere. The starting

material was stirred at room temperature and degassed by three cycles of evacuation and nitrogen backflushing. Subsequently, 20 mL dry and degassed tetrahydrofuran were added, and the resulting solution was cooled to −78 °C. A solution of *n*-butyllithium (2.18 M in hexane, 1.0 mL, 2.2 mmol, 1.1 equiv) was added dropwise and stirring was continued for 30 min. Dry trimethyl borate (340 µL, 3.0 mmol, 1.5 equiv) was added dropwise and stirring was continued for 30 min, after which the solution was allowed to warm to room temperature for 30 min. Subsequently, pinacol (473 mg, 4.0 mmol, 2.0 equiv) was added in a single portion. The resulting solution was stirred for 20 h at room temperature. After cooling to 0 °C, the solution was poured into 40 mL of an ice-cold and stirred, saturated aqueous solution of ammonium chloride. If needed, the mixture was carefully adjusted to pH 5 – 7 using 1 M aqueous hydrogen chloride. The mixture was transferred into a separation funnel, rinsing the used glass ware with water and ethyl acetate. After adding 50 mL ethyl acetate, the resulting two-phase system was mixed, the phases were separated, and the aqueous phase was extracted twice using 50 mL ethyl acetate. The combined organic phases were washed with brine, dried over magnesium sulphate, and concentrated in vacuo. The resulting crude product, a clear yellow oil, was analysed by ^{1}H-NMR and purified by column chromatography (petroleum ether:ethyl acetate, 90:10 → 80:20 v/v) yielding the title compound as colourless oil in a yield of 491 mg (1.6 mmol, 80%).

In a separate experiment the reaction was scaled including slight adjustments of the reagent equivalents, but otherwise identical conditions as described above. In a 100-mL Schlenk-tube 2-bromo-5-methoxy-1-(methoxymethoxy)-3-methylbenzene (2.6 mg, 10.0 mmol, 1.00 equiv) in 50 mL dry tetrahydrofuran was reacted with *n*-butyllithium (2.30 M in hexane, 4.4 mL, 10.2 mmol, 1.02 equiv), dry trimethyl borate (1.18 mL, 10.5 mmol, 1.05 equiv) and pinacol (1.3 g, 11.0 mmol, 1.10 equiv). After 16 h reaction time, quenching, and work up, the crude product was determined to be 85% pure (by ^{1}H-NMR, 15% protodehalogenated side product) and could be used in the subsequent coupling step without further purification.

The analytical data was in accordance with previously published results.(Ganardi, Greb, Henssen, & Pietruszka, 2023)

TLC (petroleum ether:ethyl acetate, 90:10 v/v): $R_f = 0.20$.

: δ [ppm] = 1.36 (s, 12H; 6′-H, 7′-H, 8′-H, 9′-H), 2.34 (s, 3H; 10-H), 3.46 (s, 3H; 8-H), 3.76 (s, 3H; 9-H), 5.11 (s, 2H; 7-H); 6.36 (d, J = 2.1 Hz; 5-H), 6.41 (d, J = 2.1 Hz; 3-H).

^{13}C NMR (151 MHz, $CDCl_3$): δ [ppm] = 22.3 (C-10), 24.9 (C-6′, C-7′, C-8′, C-9′), 55.3 (C-9), 56.1 (C-8), 83.6 (C-4′, C-5′), 94.7 (C-7), 98.3 (C-3), 108.6 (C-5), 112.5 (C-1, very weak), 144.5 (C-6), 161.8 (C-4), 162.0 (C-2).

^{11}B NMR (96 MHz, $CDCl_3$): δ [ppm] = 31.3 (B-2′).

IR (ATR film): ṽ [cm^{-1}] = 2977, 1603, 1371, 1337, 1299, 1141, 1052, 1035, 926, 857, 834, 670.

HR-MS (ESI): m/z calcd. for $[C_{16}H_{26}BO_5]^+$ ([M + H^+]) = 309.1868, found: 309.1876.

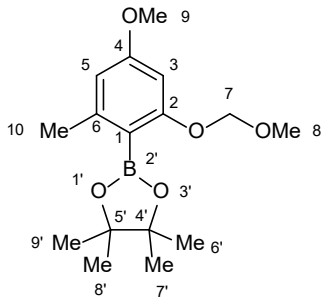

5

1.2.2 Synthesis of 4,4'-dimethoxy-2,2'-bis(methoxymethoxy)-6,6'-dimethyl-1,1'-biphenyl (6)

A 100 mL-Schlenk tube or flask was charged with 2-bromo-5-methoxy-1-(methoxymethoxy)-3-methylbenzene (**4**, 1.48 g, 5.66 mmol, 1.00 equiv) (Greb et al., 2023), crude 2-(4-methoxy-2-(methoxymethoxy)-6-methylphenyl)-4,4,5,5-tetramethyl-1,3,2-dioxaborolane (**5**, 85% purity (see above), 3.08 g, 8.49 mmol, 1.50 equiv), PdSPhosG4 precatalyst (45 mg, 0.57 mmol, 1.0 mol%) and SPhos (23 mg, 0.57 mmol, 1.0 mol%) under a nitrogen atmosphere. The starting materials were stirred at room temperature and degassed by three cycles of evacuation and nitrogen backflushing. As it simplified the set-up operation, TPGS-750-M (1.00 g, 2%(w/w) relative to aqueous part of the final solvent mix) was degassed analogously in a separate 10 mL-Schlenk-tube and dissolved in 5.5 mL dry degassed tetrahydrofuran. Subsequently, the organic surfactant solution was added to the starting materials and reagents forming a yellowish clear solution. While stirring, 30 mL of degassed water were added to the organic solution resulting in the formation of a white homogeneous emulsion (see **Figure S3**). A separate 50-mL Schlenk-flask was charged with potassium phosphate (3.60 g, 16.98 mmol, 3.00 equiv) under a nitrogen atmosphere, which was dissolved in 20 mL degassed water. The aqueous base solution was added to the emulsion, which turned yellow indicting

precatalyst activation and start of the reaction (see **Figure S3**). Subsequently, the reaction mixture was subjected to mild heating at 55 °C under vigorously stirring for 16 h. Upon full conversion, as indicated by TLC, stirring was stopped and the reaction mixture was warmed to room temperature. While standing, the emulsion separated, and an orange organic crude product phase formed on the surface of the aqueous layer (see **Figure S3**). The reaction mixture was diluted with ethyl acetate and transferred into a separation funnel. The reaction vessel was rinsed properly with water and ethyl acetate. After mixing of the resulting two-phase system, the layers were separated, and the aqueous phase was extracted three times with 30 mL ethyl acetate. The combined organic layers were washed with brine, dried over magnesium sulphate and concentrated in vacuo. The resulting crude product was analysed by ^{1}H-NMR and purified by column chromatography (petroleum ether:ethyl acetate, 80:20 v/v) yielding the racemic title compound as slightly orange oil in a yield of 1.94 g (5.35 mmol, 95%).

The analytical data was in accordance with previously published results (Christine Ganardi et al.; Greb et al., 2023):

TLC (petroleum ether:ethyl acetate, 80:20 v/v): $R_f = 0.27$.

: δ [ppm] = 6.64 (d, J = 2.5 Hz, 2H; 3-H, 3′-H), 6.52 (d, J = 2.5 Hz, 2H; 5-H, 5′-H), 5.01 (d, J = 6.6 Hz, 2H; 7b-H, 7b′-H), 4.97 (d, J = 6.6 Hz, 2H; 7a-H, 7a′-H), 3.82 (s, 6H; 9-H, 9′-H), 3.30 (s, 6H; 8-H, 8′-H), 1.95 (s, 6H; 10-H, 10′-H).

^{13}C NMR (151 MHz, $CDCl_3$): δ [ppm] = 159.5 (C-4, C-4′). 156.0 (C-2, C-2′), 139.5 (C-6, C-6′), 119.8 (C-1, C-1′), 108.5 (C-5, C-5′), 99.6 (C-3, C-3′), 94.9 (C-7, C-7′), 55.8 (C-8, C-8′), 55.3 (C-9, C-9′), 20.3 (C-10, C-10′).

IR (ATR film): ṽ [cm^{-1}] = 2952, 1602, 1466, 1310, 1209, 1145, 1041, 994, 923, 833, 635, 516.

MS (ESI): m/z = 385.2 ([M + Na^{+}]).

HR-MS (ESI): m/z calcd. for $[C_{20}H_{26}O_6Na]^{+}$ ([M + Na^{+}]) = 385.1622, found: 385.1618.

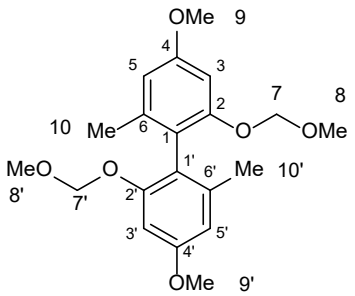

6

1.2.3 Synthesis of 4,4'-dimethoxy-6,6'-dimethyl-[1,1'-biphenyl]-2,2'-diol (3)

A 100-mL round-bottom flask equipped with a magnetic string bar as well as a reflux condenser and charged with 4,4'-dimethoxy-2,2'-bis(methoxymethoxy)-6,6'-dimethyl-1,1'-biphenyl (**6**, 1.2 g, 3.31 mmol, 1.0 equiv) in 33 mL degassed methanol under a nitrogen atmosphere. Aqueous hydrochloric acid (4 M, 0.83 mL, 3.31 mmol, 1.0 equiv) was added and the resulting mixture was heated at 70 °C for 1 – 2 h. Careful TLC monitoring was performed to avoid methyl ether-cleavage. Upon full conversion, as indicated by TLC, the reaction was cooled to room temperature neutralized using a saturated aqueous solution of sodium bicarbonate. The resulting mixture was transferred into a separation funnel and diluted with 30 mL water and 30 mL ethyl acetate, rinsing the used glass ware properly. After mixing, the phases were separated, and the aqueous layer was extracted three times with 30 mL ethyl acetate. The combined organic layers were washed twice with brine and dried over magnesium sulphate. Removal of the solvent at reduced pressure yielded the racemic title compound as slightly yellow crystalline solid in a yield of 899 mg (3.27 mmol, 99%), which could be used without further purification. The analytical data was in accordance with previously published results (Christine Ganardi et al.; Greb et al., 2023):

TLC (petroleum ether:ethyl acetate, 80:20 v/v): $R_f = 0.12$.

Melting point: 148 – 150 °C (*rac*).

: δ [ppm] = 6.48 (d, J = 2.5 Hz, 2H; 5-H, 5′-H), 6.46 (d, J = 2.5 Hz, 2H; 3-H, 3′-H), 4.86 (s, 2H; 2-OH, 2′-OH), 3.80 (s, 6H; 7-H, 7′-H), 1.97 (bs, 6H; 8-H, 8′ H).

^{13}C NMR (151 MHz, $CDCl_3$): δ [ppm] = 161.2 (C-4, C-4′), 155.5 (C-2, C-2′), 140.5 (C-6, C-6′), 111.4 (C-1, C-1′), 109.0 (C-5, C-5′), 98.5 (C-3, C-3′), 55.4 (C-7, C-7′), 19.9 (C-8, C-8′).

IR (ATR film): $\tilde{\nu}$ [cm^{-1}] = 3505, 3360, 2960, 1612, 1575, 1446, 1310, 1197, 1141, 1069, 1038, 934, 840, 824, 608, 497.

MS (ESI): m/z = 275.0 ([M + H^+]).

HR-MS (ESI): m/z calcd. for $[C_{16}H_{17}O_4]^-$ ([M – H^+]) = 273.1132, found: 273.1128.

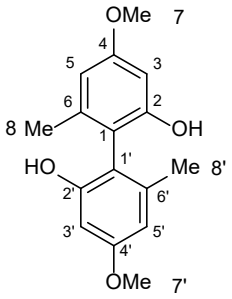

3

1.2.4 Resolution of 4,4'-dimethoxy-6,6'-dimethyl-[1,1'-biphenyl]-2,2'-diol (3)

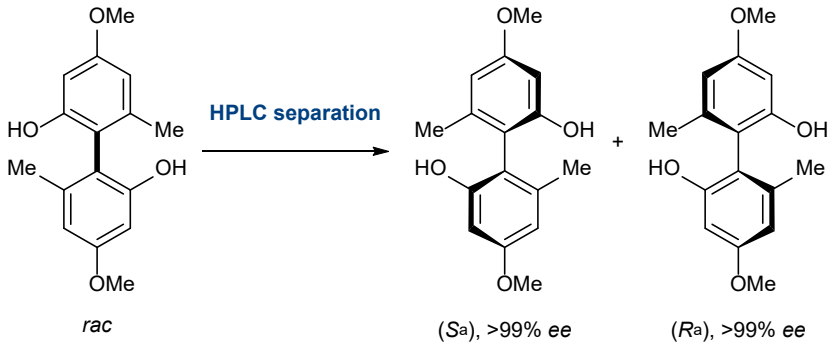

A saturated solution of racemic 4,4'-dimethoxy-6,6'-dimethyl-[1,1'-biphenyl]-2,2'-diol (**3**, 530 mg, 1.94 mmol) in 10:90 (v/v) *n*-heptane/*i*-propanol was prepared by stirring and sonication. After standing at room temperature for 1 – 2 h or overnight (to avoid later precipitate formation, potential temperature/solubility increase due to sonication), the solution was passed through a syringe filter. Enantiomer separation was performed using a Lux® Amylose-1, 5 µm, 250.0 × 21.2 mm, AXIA™ (*Phenomenex*) preparative HPLC column with a suitable HPLC pump system and a diode array (detection at 210 nm). Depending on the polarity of the eluent used, flow rates between 8 and 12 mL/min were used to, conservatively, not exceed maximal backpressures of 100 – 110 bar (250 bar suggested by manufacturer). After column equilibration with 10:90 (v/v) *n*-heptane/*i*-propanol, the prepared solution of racemic biphenol was injected using an appropriate sample loop. Within the loop, the sample solution has been 'sandwiched' (15% eluent, 70% sample, 15% eluent) to avoid compound loss during loading. Fractions were collected based on the live diode array signal. Due to the high selectivity factor α of 7.7, maximal loading/overloading the column did not at all impede a clean separation. Once

roughly half of the earlier enantiomer had been eluted (roughly 20 – 25 min at 8 – 10 mL/min), the eluent was changed to 30:70 (v/v) *n*-heptane/*i*-propanol (lowest k_2 observed) and flowrates were increased, staying within the pressure limits, to shorten overall runtimes. After complete elution, the column was equilibrated to storage conditions and the collected fractions were concentrated at reduced pressure yielding 262 mg (0.946 mmol, 49%, >99%*ee* S_a) and 257 mg (0.937 mmol, 49%, >99%*ee* R_a) respectively.

The stereochemistry-specific analytical data was in accordance with previously published results (Christine Ganardi et al.; Greb et al., 2023):

Melting point: 148 – 150 °C (*rac*).

172 – 174 °C (S_a, >99%*ee*).

Optical rotation: $[\alpha]^{25}_D = -31.9°$ (c = 1.04, $CHCl_3$, S_a, >99%*ee*).

$[\alpha]^{25}_D = +32.6°$ (c = 1.22, $CHCl_3$, R_a, >99%*ee*).

HPLC: Lux® Amylose-1 (*Phenomenex*), 250 × 4.6 mm, 25 °C, 0.5 mL min^{-1}, 210 nm, *n*-heptane:*i*-propanol 50:50 (v/v): $t_R(S_a)$ = 15.1 min, $t_R(R_a)$ = 53.0 min.

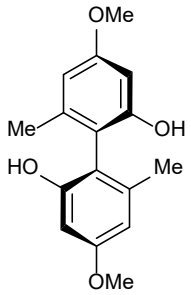

(−)-(S_a)-**3**

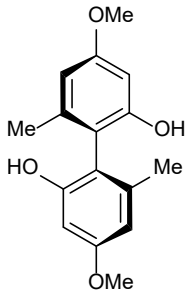

(+)-(R_a)-**3**

1.2.5 Synthesis of 1,1'-(2,2'-dihydroxy-4,4'-dimethoxy-6,6'-dimethyl-[1,1'-biphenyl]-3,3'-diyl)bis(ethan-1-one) (7)

Following our literature known procedure (Greb et al., 2023) a 50 mL Schlenk-vial equipped with stir bar was charged with biphenol **3** (274 mg, 1.0 equiv, 1.00 mmol, >99%*ee* S_a) and anhydr. chlorobenzene (10 mL, 0.1 M). The solution was stirred at 0 °C, acetyl chloride (157 µL, 2.2 equiv, 2.20 mmol) added dropwise and then the mixture stirred at room temperature for 30 minutes. $TiCl_4$ (658 µL, 6.0 equiv, 6.00 mmol) was added dropwise and the reaction mixture stirred at 70 °C for 4 h. The reaction mixture was transferred into a 250 mL Erlenmeyer beaker equipped with stir bar with K_2HPO_4/KH_2PO_4-buffer (KPi-buffer, 1 M, 100 mL, pH 7) at 0 °C. The pH was then

adjusted to pH 4 by the addition of 1 M HCl-solution. The resulting white suspension was then stirred for 15 mins, sonicated for 15 mins, and then stirred for 30 mins. The mixture was filtered over a pad of celite using a wide Buchner-type funnel. The filter cake was washed with CH_2Cl_2 (100 mL) water, then with CH_2Cl_2 (800 mL). The filter cake was then transferred into an Erlenmeyer flask and stirred with CH_2Cl_2 overnight. The suspension was then again filtered over celite. The filtrates were combined, and the aqueous phase extracted with CH_2Cl_2 (4 × 250 mL). The combined aqueous phases were washed with sat. aq. NaCl solution, dried over $MgSO_4$ and the solvent removed in vacuo. The product was isolated by column chromatography (CH_2Cl_2:PhMe 1:9 v/v) and obtained as pale yellow solids in a yield of 297 mg (0.829 mmol, 83%, >99%*ee*, S_a).

In a repeat experiment using biaryl **X** (343 mg, 1.0 equiv, 1.25 mmol, >99%*ee*, R_a) the product was isolated as pale yellow solids in a yield of 271 mg (0.756 mmol, 76%, >99%*ee* R_a).

TLC (petroleum ether:ethyl acetate, 7:3 v/v): R_f = 0.32.

Melting point: 233 – 235 °C (*rac*) (233 – 236 °C) (Greb et al., 2023).
230 – 232 °C (S_a, >99%ee) (209 – 210 °C) (Greb et al., 2023).
231 – 234 °C (R_a, >99%ee).

: δ [ppm] = 2.06 (s, 3H, Me), 2.67 (s, 3H, CO*Me*), 3.93 (s, 3H, OMe), 6.38 (s, 1H, H-5), 13.68 (s, 1H, OH).

^{13}C NMR (151 MHz, $CDCl_3$): δ [ppm] = 20.97 (Me), 33.66 (CO*Me*), 55.58 (OMe), 102.97 (C-5), 109.41 (C-3), 117.38 (C-1), 147.54 (C-6), 160.79 (C-4), 162.40 (C-2), 204.77 (*CO*Me).

IR (ATR film): $\tilde{\nu}$ [cm^{-1}] = 1599, 1360, 1283, 1202, 1119, 9693, 865, 834, 655, 573, 534.

HR-MS (ESI): m/z calcd. for $[C_{20}H_{23}O_6]^+$ ([M + H$^+$]) = 359.1489, found: 359.1492.

Optical rotation: $[\alpha]^{25}_D$ = +51.2° (±0.2°, duplicate) (*c* = 1.02, $CHCl_3$, S_a, >99%*ee*) (+43.1) (Greb et al., 2023).

HPLC: Lux® Amylose-1 (*Phenomenex*) 250 × 4.6 mm, 25 °C, 0.5 mL min^{-1}, 274 nm, *n*-heptane:*i*-propanol 50:50 (v/v): $t_R(S_a)$ = 7.4 min, $t_R(R_a)$ = 11.0 min.

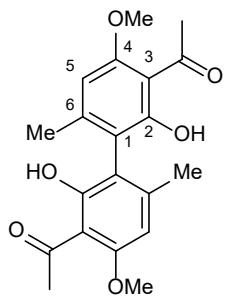

7

1.2.6 (2*E*,2′*E*)-1,1'-(2,2'-dihydroxy-4,4'-dimethoxy-6,6'-dimethyl-[1,1'-biphenyl]-3,3'-diyl)bis(3-phenylprop-2-en-1-one) (2ab)

A vial equipped with a stir bar was charged with acetophenone **7** (100 mg, 0.279 mmol, 1.0 equiv, >99%*ee* S_a) and ethanol (1.0 mL, 0.28 M) and an aqueous solution of KOH (1.12 mL, 3.35 mmol, 12.0 equiv). Once fully dissolved, benzaldehyde (67.7 µL, 0.670 mmol, 2.4 equiv) were added at once. The mixture was stirred for 4 h at 22 °C after which aq. HCl-solution (1 M, 4 mL) was added. The forming solids were filtered off and washed with MeOH:H_2O (8:2, 10 mL). The solids were then dissolved into a round bottom flask using CH_2Cl_2 and solvents removed in vacuo. The product was isolated by column chromatography (100% CH_2Cl_2). The isolated product was suspended in *n*-pentane (2 × 5 mL) and sonicated to remove traces of CH_2Cl_2. The solvent was then removed in vacuo. The product was isolated as orange amorphous solids in a yield of 81.0 mg (0.152 mmol, 54%, >99%*ee* S_a).

In a repeat experiment starting from (100 mg, 0.279 mmol, 1.0 equiv, >99%*ee* R_a) the product was isolated as orange amorphous solids in a yield of 91.1 mg (0.170 mmol, 61%, >99%*ee* R_a).

TLC (100% CH_2Cl_2): R_f = 0.36 (yellow spot)

Melting point: 213 – 215 °C (*rac*)
190 – 192 °C (S_a)
191 – 192 °C (R_a)

: δ [ppm] = 2.12 (s, 6H, Me), 4.00 (s, 6H, OMe), 6.44 (s, 2H, H-5), 7.37 – 7.45 (m, 6H, H-3’’+H-4’’), 7.59 – 7.65 (m, 4H, H-2’’), 7.80 (d, *J* = 15.6 Hz, 2H, H-3’), 7.94 (d, *J* = 15.6 Hz, 2H, H-2’), 13.71 (s, 2H, OH).

^{13}C NMR (151 MHz, $CDCl_3$): δ [ppm] = 21.06 (Me), 55.96 (OMe), 103.50 (C-5), 110.07 (C-3), 117.82 (C-1), 128.16 (C-2'), 128.56 (C-2''), 129.04 (C-3''), 130.24 (C-4''), 135.76 (C-1''), 142.55 (C-3'), 147.57 (C-6), 160.38 (C-4), 162.89 (C-2), 194.30 (C-1').

IR (ATR film): ṽ [cm^{-1}] = 3104, 3026, 2970, 2942, 2250, 1628, 1609, 1564, 1448, 1388, 1361, 1329, 1272, 1214, 1179, 1115, 1073, 1038, 976, 948, 907, 869, 817, 789, 758, 725, 688, 647, 565, 534, 494.

HR-MS (ESI): m/z calcd. for $[C_{34}H_{31}O_6]^+$ ([M + H^+]) = 535.2115, found: 535.2122.

elemental analysis (calcd., found for $C_{34}H_{30}O_6$): C (76.39, 76.31), H (5.66, 5.59). (*rac*)

elemental analysis (calcd., found for $C_{34}H_{30}O_6$): C (76.39, 76.13), H (5.66, 5.62). (S_a)

elemental analysis (calcd., found for $C_{34}H_{30}O_6$): C (76.39, 75.91), H (5.66, 5.72). (R_a)

Chiral HPLC: >99% ee (S_a)
>99% ee (R_a)

Purity: >99% (normal phase HPLC), >99% (reverse phase HPLC) (S_a)
>99% (normal phase HPLC), >99% (reverse phase HPLC) (R_a)
96% (reverse phase HPLC), (elemental Analysis) (*rac*)

Optical rotation: $[\alpha]^{20}_D$ = +128.7° (±0.1°, duplicate) (c = 0.964, $CHCl_3$, S_a, >99%*ee*)

HPLC: Lux® Amylose-1 (*Phenomenex*) 2504.6 mm, 25 °C, 0.5 mL min^{-1}, 331 nm, *n*-heptane:*i*-propanol 50:50 (v/v): $t_R(S_a)$ = 14.7 min, $t_R(R_a)$ = 24.2 min.

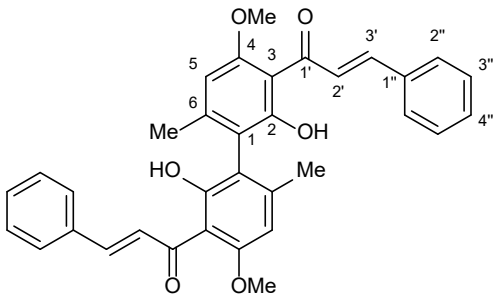

2ab

2 HPLC Chromatograms

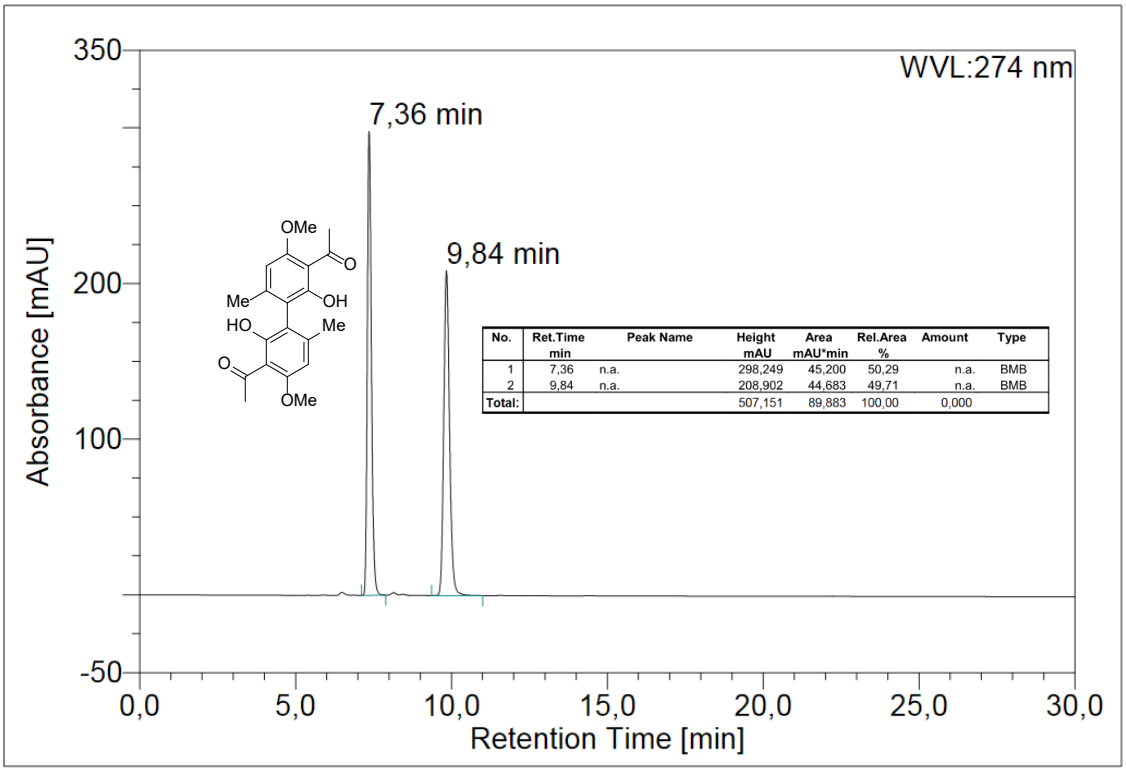

No.	Ret.Time min	Peak Name	Height mAU	Area mAU*min	Rel.Area %	Amount	Type
1	7,36	n.a.	298,249	45,200	50,29	n.a.	BMB
2	9,84	n.a.	208,902	44,683	49,71	n.a.	BMB
Total:			507,151	89,883	100,00	0,000	

Figure S8: HPLC Chromatogram of biacetophenone 7 (*rac*)

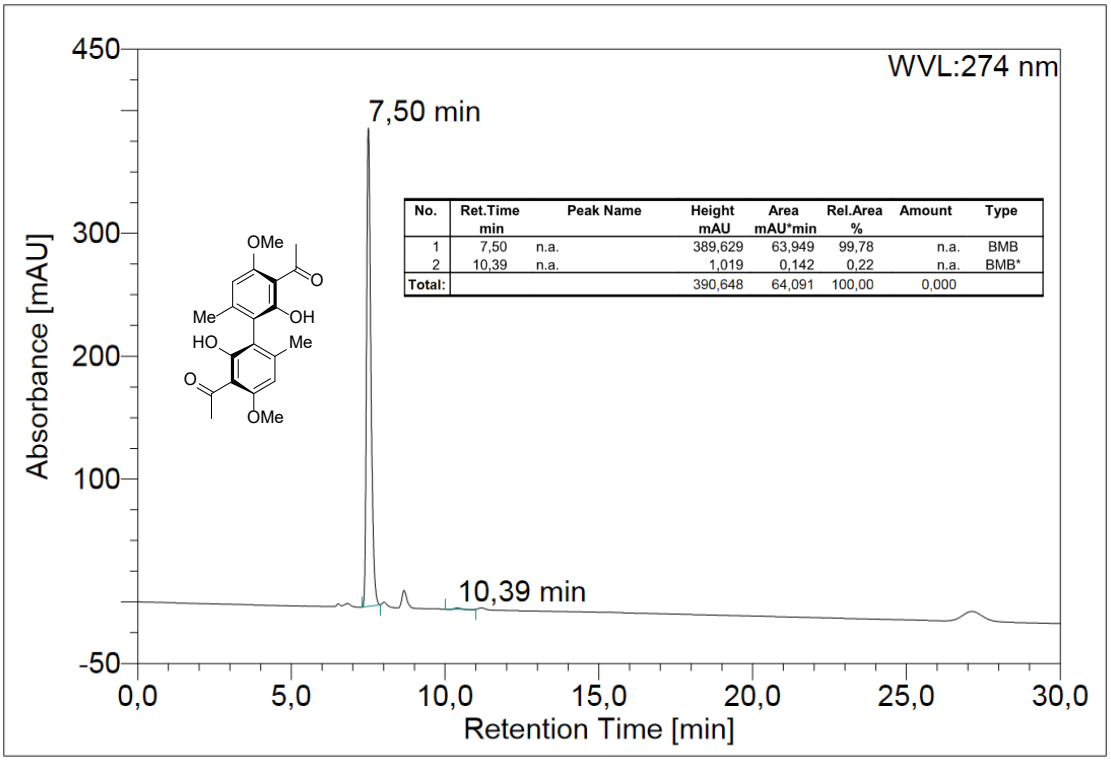

No.	Ret.Time min	Peak Name	Height mAU	Area mAU*min	Rel.Area %	Amount	Type
1	7,50	n.a.	389,629	63,949	99,78	n.a.	BMB
2	10,39	n.a.	1,019	0,142	0,22	n.a.	BMB*
Total:			390,648	64,091	100,00	0,000	

Figure S9: HPLC Chromatogram of biacetophenone 7 >99%*ee* (S_a).

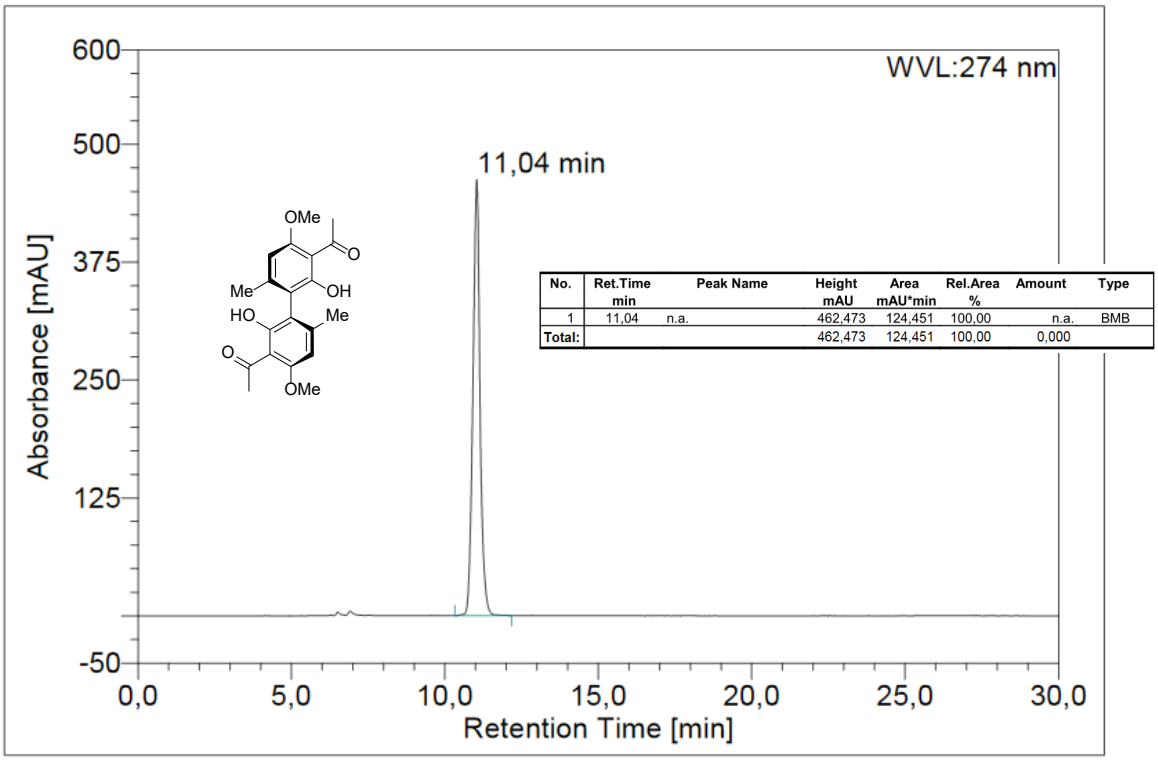

No.	Ret.Time min	Peak Name	Height mAU	Area mAU*min	Rel.Area %	Amount	Type
1	11,04	n.a.	462,473	124,451	100,00	n.a.	BMB
Total:			462,473	124,451	100,00	0,000	

Figure S10: HPLC Chromatogram of biacetophenone 7 >99%*ee* (R_a).

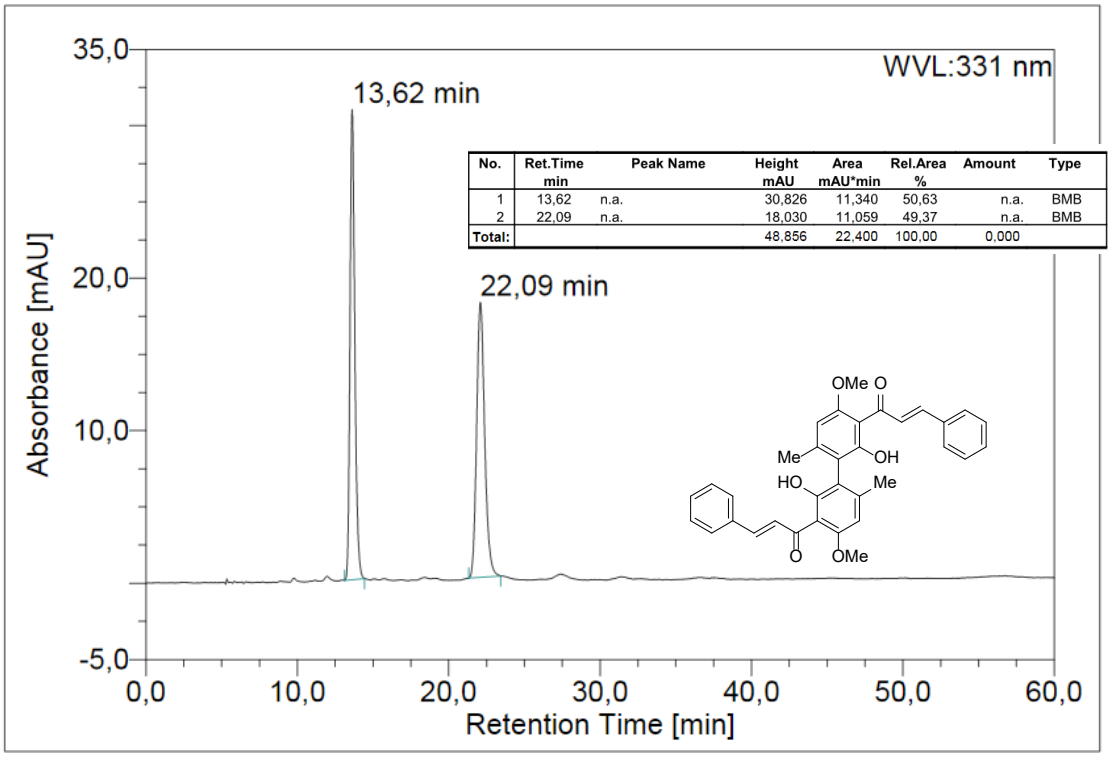

No.	Ret.Time min	Peak Name	Height mAU	Area mAU*min	Rel.Area %	Amount	Type
1	13,62	n.a.	30,826	11,340	50,63	n.a.	BMB
2	22,09	n.a.	18,030	11,059	49,37	n.a.	BMB
Total:			48,856	22,400	100,00	0,000	

Figure S11: HPLC Chromatogram of bichalcone 2ab (*rac*).

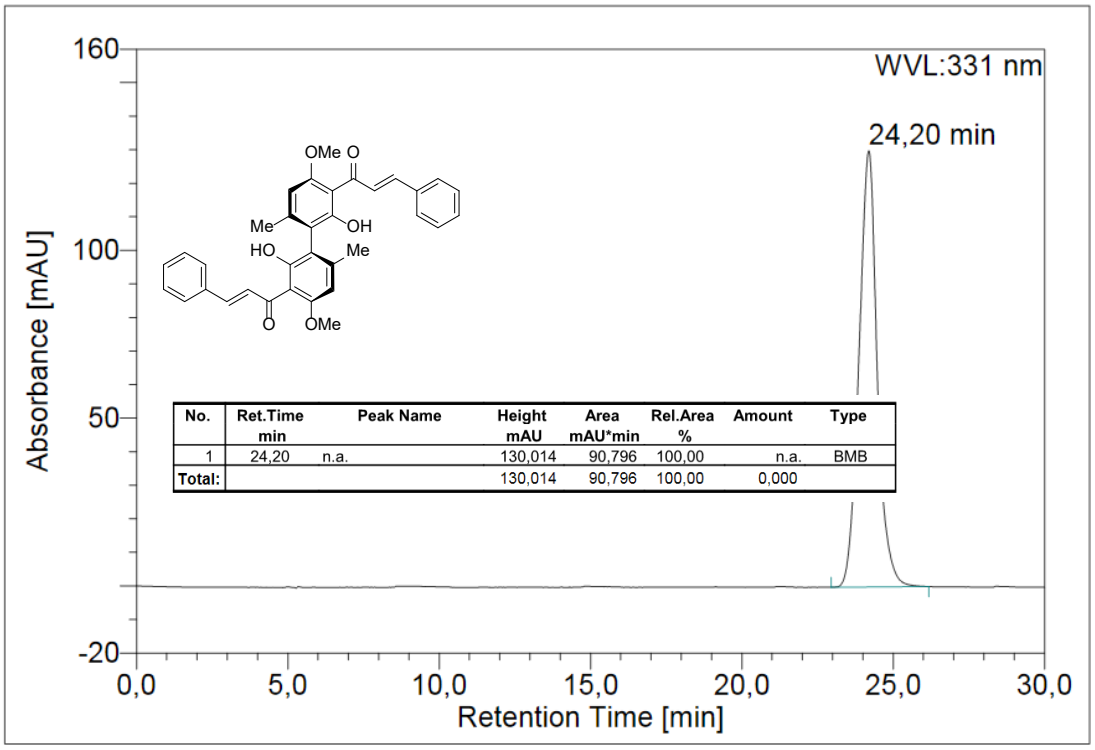

No.	Ret.Time min	Peak Name	Height mAU	Area mAU*min	Rel.Area %	Amount	Type
1	24,20	n.a.	130,014	90,796	100,00	n.a.	BMB
Total:			130,014	90,796	100,00	0,000	

Figure S12: HPLC Chromatogram of bichalcone 2ab >99%*ee* (R_a).

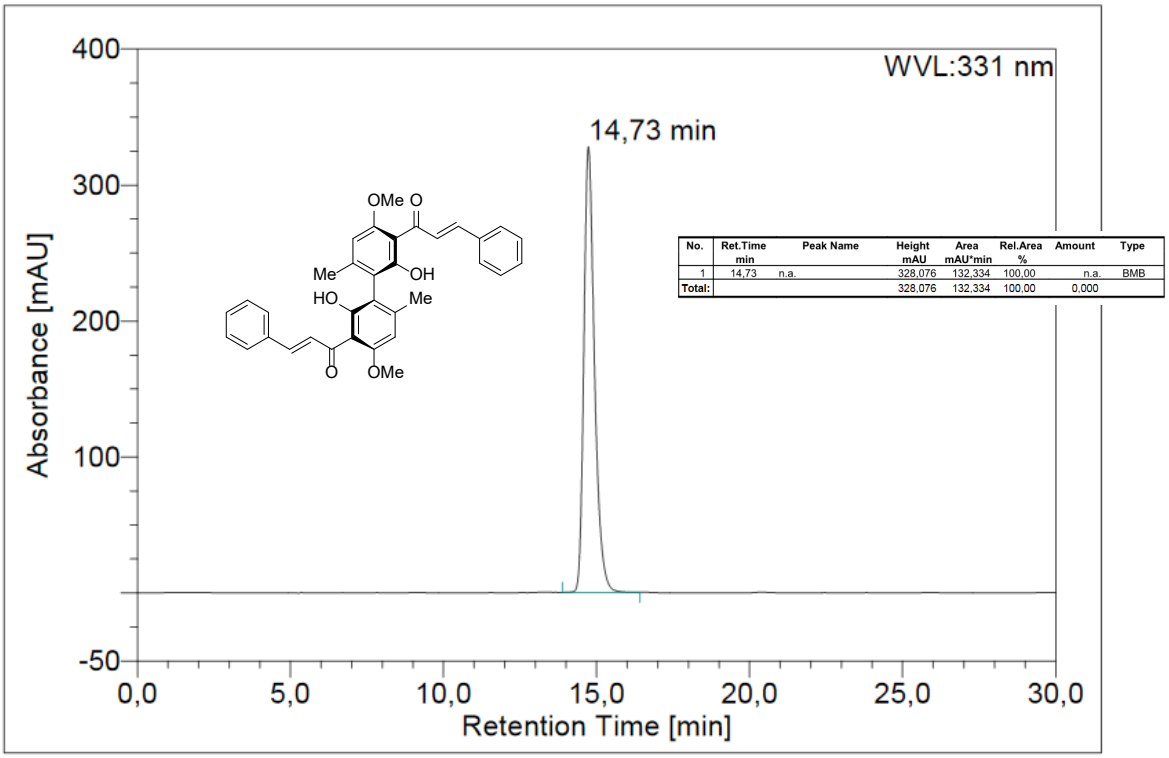

No.	Ret.Time min	Peak Name	Height mAU	Area mAU*min	Rel.Area %	Amount	Type
1	14,73	n.a.	328,076	132,334	100,00	n.a.	BMB
Total:			328,076	132,334	100,00	0,000	

Figure S13: HPLC Chromatogram of bichalcone 2ab >99%*ee* (S_a)

2.1 Stability Experiments

To investigate the stability of bichalcone **2ab**, we submitted the racemic mixture to various conditions.

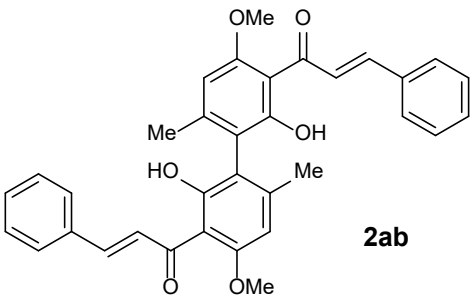

Method:

Hyperclone 5 µ ODS (C18), 125*4 mm, 120 Å, Fa. Phenomenex, 1 mL/min, A: H_2O; B: Methanol

Gradient:	0-2 min	10% B/90% A
	2-15 min	Gradient 10% B/90% A to 100% B/0% A
	15-20 min	100% B/0% A
	20-21 min	Gradient 100% B/0% A to 10% B/90% A
	21-30 min	10% B/90% A

Table S3: Purity results of the stability experiments over a varying time span at different temperatures.

Entry	Variations	Time	Purity [%]
1	22 °C, DMSO	24 h	75.9
2	40 °C, DMSO	24 h	76.6
3	-20 °C, DMSO	6 months	96.2
3	40 °C, MeOH, KOH	24 h	35.6
4	40 °C, MeOH	24 h	89.7

Table S4: Reverse Phase HPLC chromatogram of bichalcone 2ab (*rac*) in DMSO stock solution at 22 °C for 24 h.

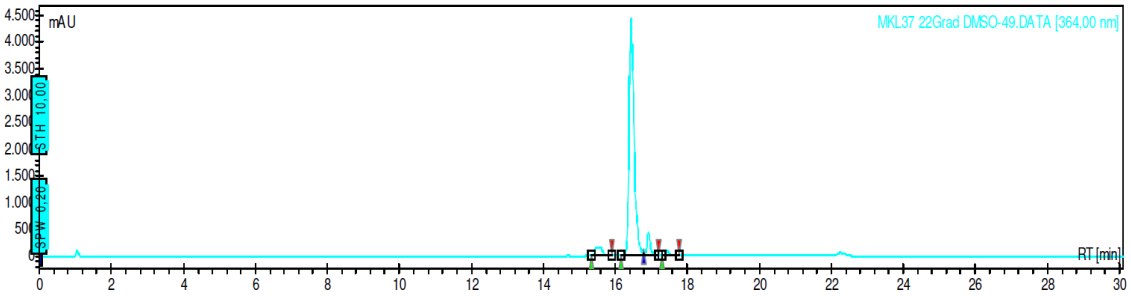

Index	Name	Time [Min]	Quantity [% Area]	Height [mAU]	Area [mAU.Min]	Area % [%]
1	UNKNOWN	15,479	5,01	164,3	39,7	5,008
2	UNKNOWN	16,439	87,93	4437,9	696,2	87,931
4	UNKNOWN	16,905	5,98	428,5	47,3	5,980
3	UNKNOWN	17,439	1,08	78,6	8,6	1,081
Total			100,00	5109,3	791,8	100,000

Table S5: Reverse Phase HPLC chromatogram of bichalcone 2ab (*rac*) in DMSO stock solution at 40 °C for 24 h.

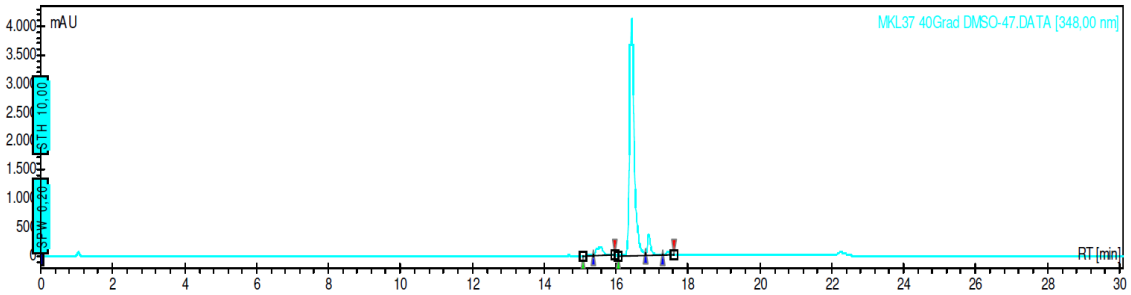

Index	Name	Time [Min]	Quantity [% Area]	Height [mAU]	Area [mAU.Min]	Area % [%]
1	UNKNOWN	15,239	0,23	19,0	1,6	0,234
3	UNKNOWN	15,559	4,99	147,8	34,9	4,986
2	UNKNOWN	16,425	88,23	4142,5	617,8	88,234
4	UNKNOWN	16,905	5,67	367,5	39,7	5,666
5	UNKNOWN	17,425	0,88	60,0	6,2	0,880
Total			100,00	4736,8	700,2	100,000

Table S6: Reverse Phase HPLC chromatogram of bichalcone 2ab (*rac*) in DMSO at -78 °C for 6 months.

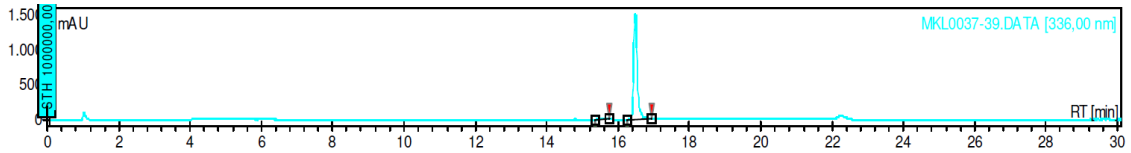

Index	Name	Time [Min]	Quantity [% Area]	Height [mAU]	Area [mAU.Min]	Area % [%]
2	UNKNOWN	15,546	1,91	14,8	3,0	1,910
1	UNKNOWN	16,545	98,09	1353,7	153,2	98,090
Total			100,00	1368,5	156,2	100,000

Table S7: Reverse Phase HPLC chromatogram of bichalcone 2ab (*rac*) in MeOH/aq. KOH solution at 40 °C for 24 h.

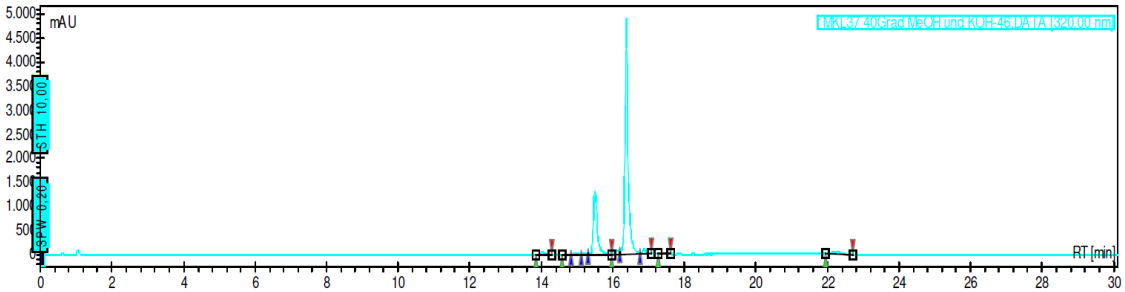

Index	Name	Time [Min]	Quantity [% Area]	Height [mAU]	Area [mAU.Min]	Area % [%]
1	UNKNOWN	14,026	1,04	56,6	7,1	1,043
2	UNKNOWN	14,732	0,11	6,4	0,8	0,113
3	UNKNOWN	14,932	0,41	21,2	2,8	0,413
4	UNKNOWN	15,212	0,24	13,1	1,6	0,238
5	UNKNOWN	15,506	24,66	1318,7	168,8	24,655
6	UNKNOWN	16,119	1,48	89,1	10,1	1,477
7	UNKNOWN	16,372	67,71	4914,3	463,6	67,707
8	UNKNOWN	16,879	1,53	98,2	10,5	1,529
9	UNKNOWN	17,399	0,32	18,4	2,2	0,315
10	UNKNOWN	22,225	2,51	60,7	17,2	2,508
Total			100,00	6596,6	684,7	100,000

Table S8: Reverse Phase HPLC chromatogram of bichalcone 2ab (*rac*) in MeOH at 40 °C for 24 h.

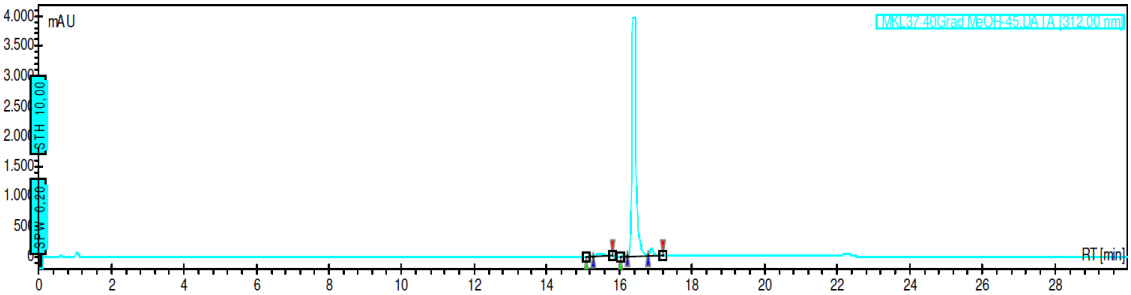

Index	Name	Time [Min]	Quantity [% Area]	Height [mAU]	Area [mAU.Min]	Area % [%]
1	UNKNOWN	15,212	0,13	10,0	0,7	0,129
2	UNKNOWN	15,439	2,19	48,8	11,6	2,187
3	UNKNOWN	16,132	0,18	8,1	0,9	0,177
4	UNKNOWN	16,372	94,89	3972,3	504,6	94,895
5	UNKNOWN	16,879	2,61	128,4	13,9	2,612
Total			100,00	4167,6	531,8	100,000

2.2 TIMS-HPLC-HRMS

The additional peaks observed when stirring (S_a)-bichalcone **2ab** at elevated Temperature in KOH/MeOH were investigated by Bruker® timsTOF Pro (PASEF®) at a flow rate of 3 µL min^{-1} and ionized using ESI-MS, with TIMS-on. In total, six isomeric peaks could be observed, which is in line with the expected number of isomers for bichalcone (1x), flavanone-chalcone (2x) and biflavanone (3x).

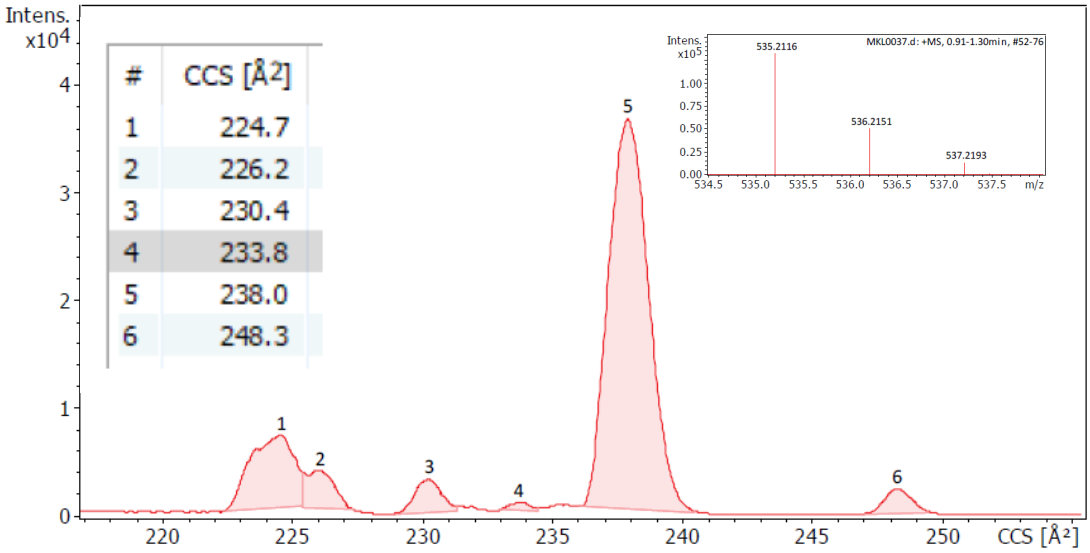

Figure S14: Extracted mobilogram for [M+H$^+$] of 535.2115 separated by trapped ion mobility using collisional cross section (CCS) analysis

2.3 Reverse Phase purity

We assessed the purity of both enantiomers of bichalcone **2ab** and the racemic mixture by reverse phase HPLC.

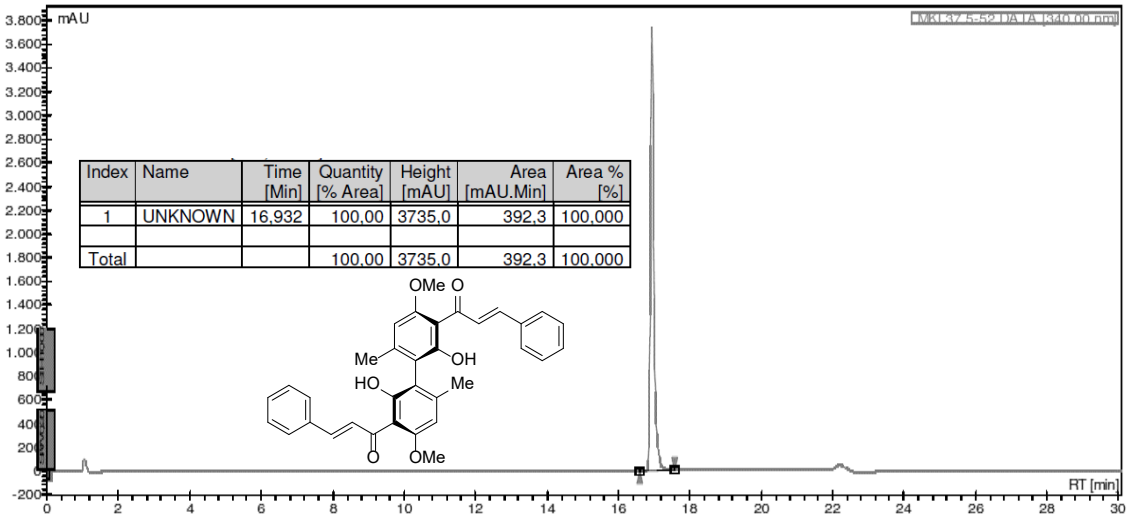

Figure S15: Reverse Phase HPLC chromatogram of bichalcone 2ab (S_a).

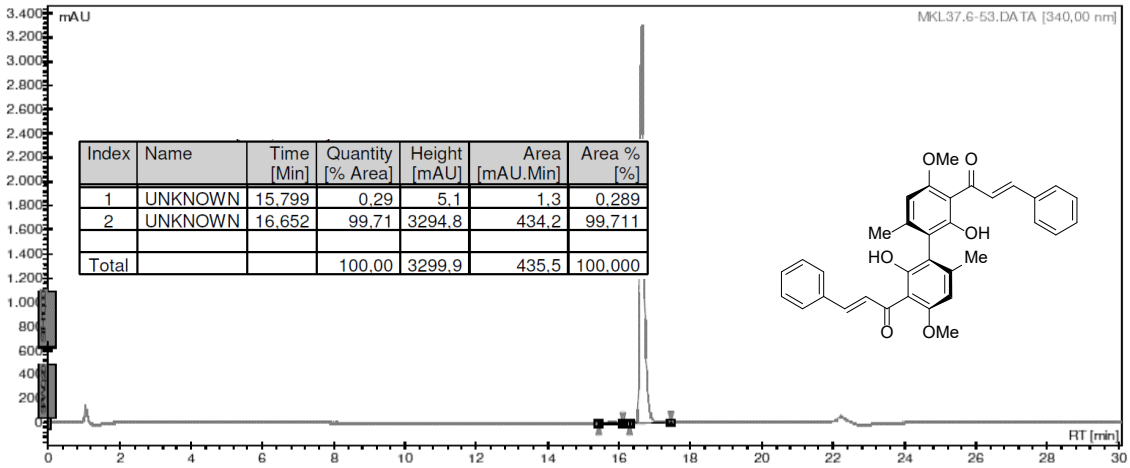

Figure S16: Reverse Phase HPLC chromatogram of bichalcone 2ab (R_a).

3 NMR spectra

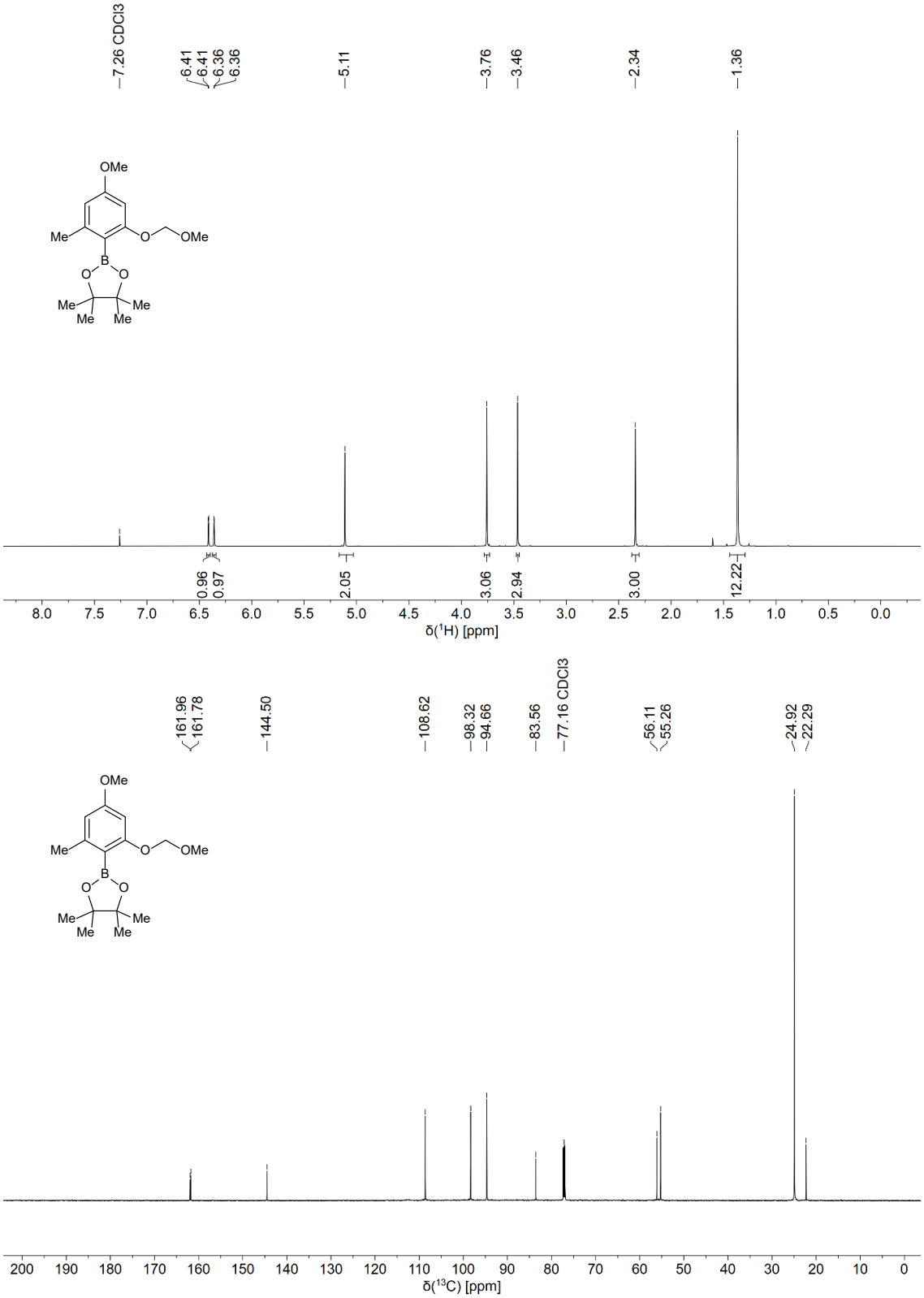

Figure S17: ^{1}H- and ^{13}C-NMR spectra (600 / 151 MHz, $CDCl_3$) of 2-(4-methoxy-2-(methoxymethoxy)-6-methylphenyl)-4,4,5,5-tetramethyl-1,3,2-dioxaborolane (5).

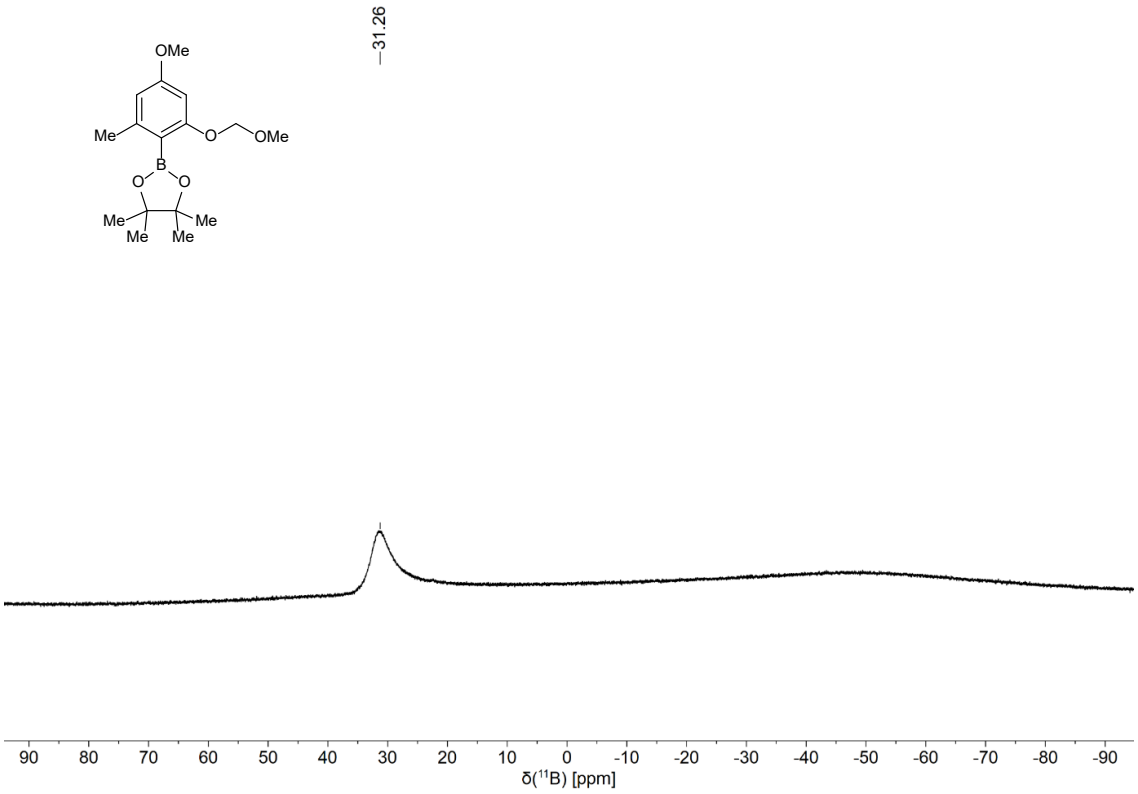

Figure S18: ^{11}B-NMR spectrum (x MHz, $CDCl_3$) of ArBpin (5).

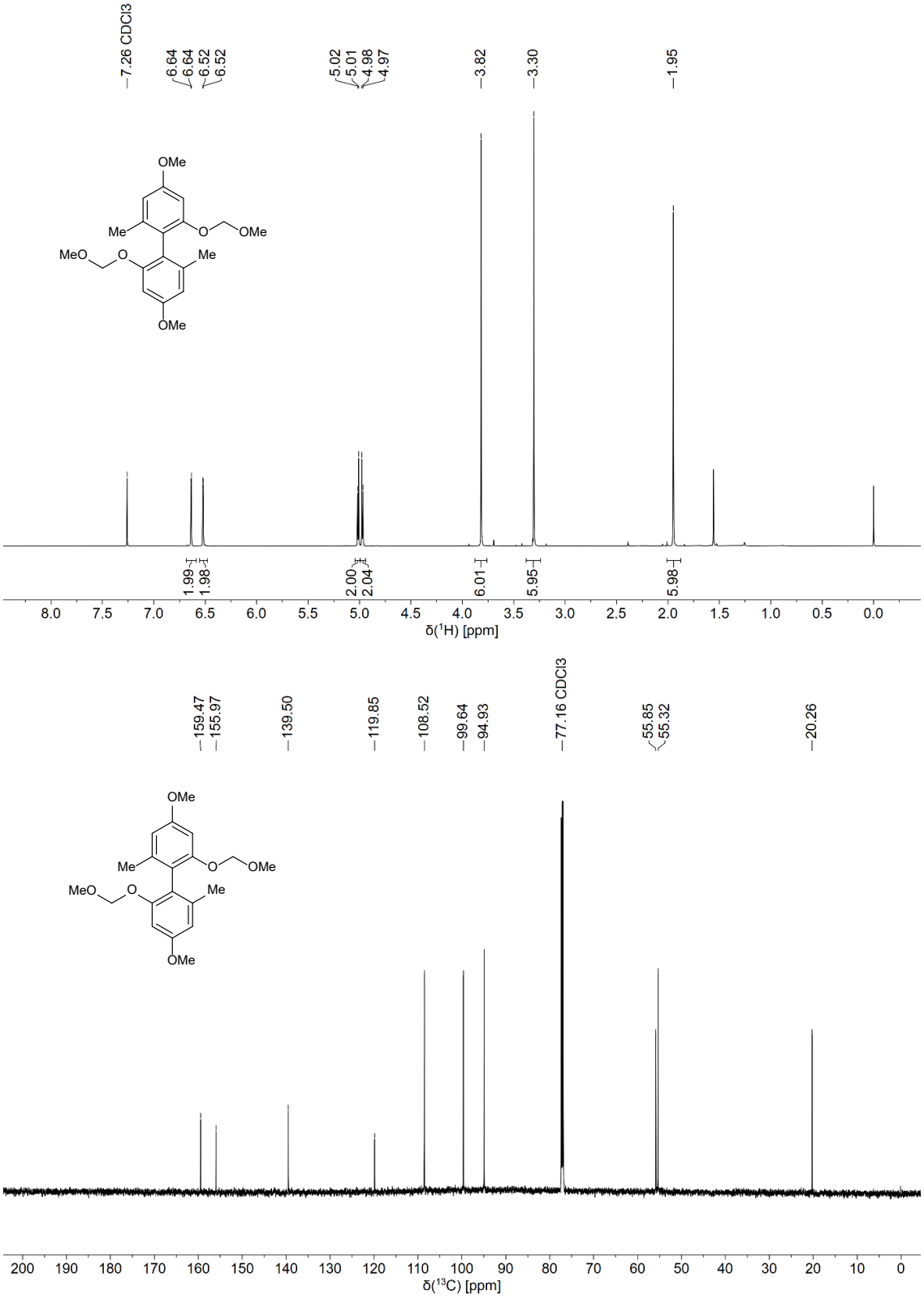

Figure S19: ^{1}H- and ^{13}C-NMR spectra (600 / 151 MHz, $CDCl_3$) of 4,4'-dimethoxy-2,2'-bis(methoxymethoxy)-6,6'-dimethyl-1,1'-biphenyl (6).

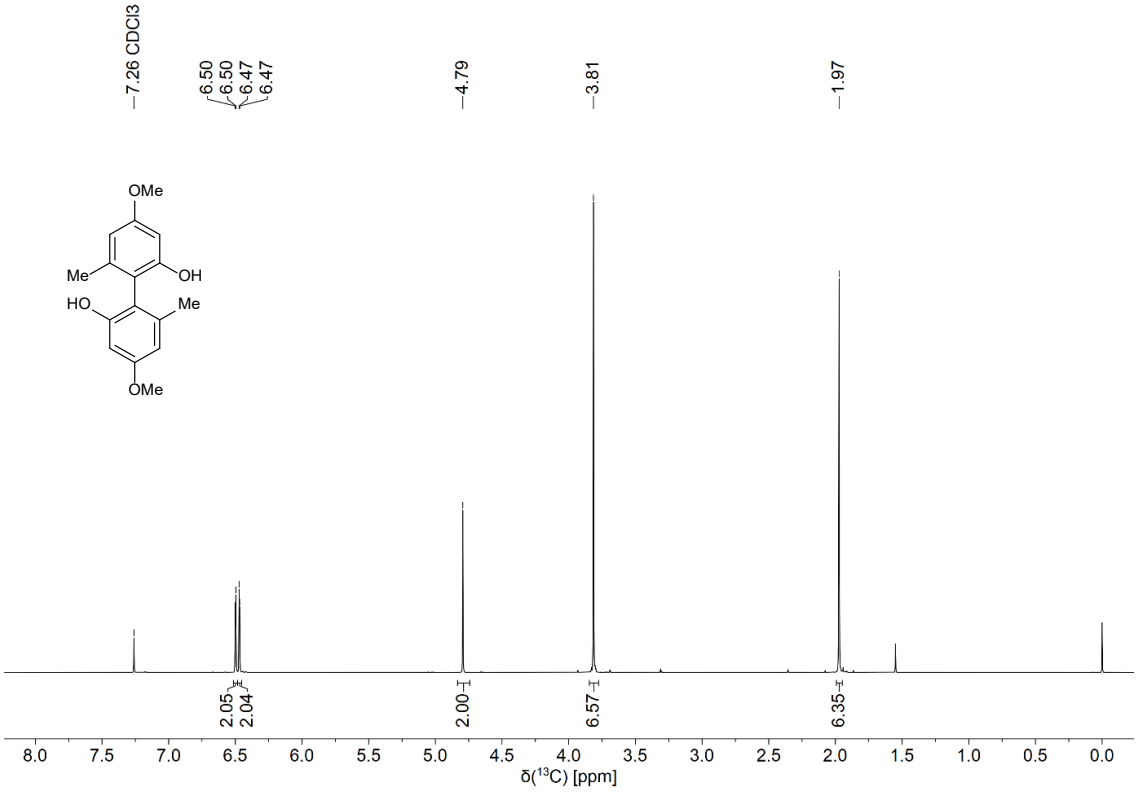

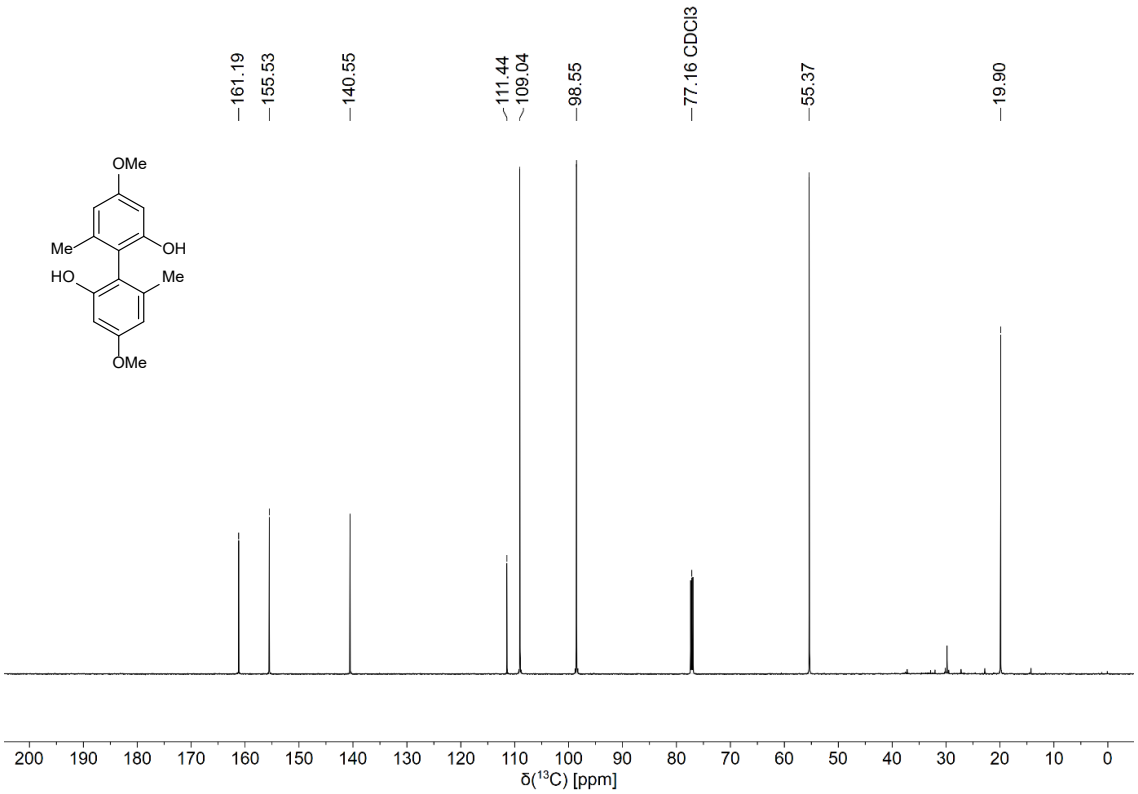

Figure S20: ^{1}H- and ^{13}C-NMR spectra (600 / 151 MHz, $CDCl_3$) of 4,4'-dimethoxy-6,6'-dimethyl-[1,1'-biphenyl]-2,2'-diol (3).

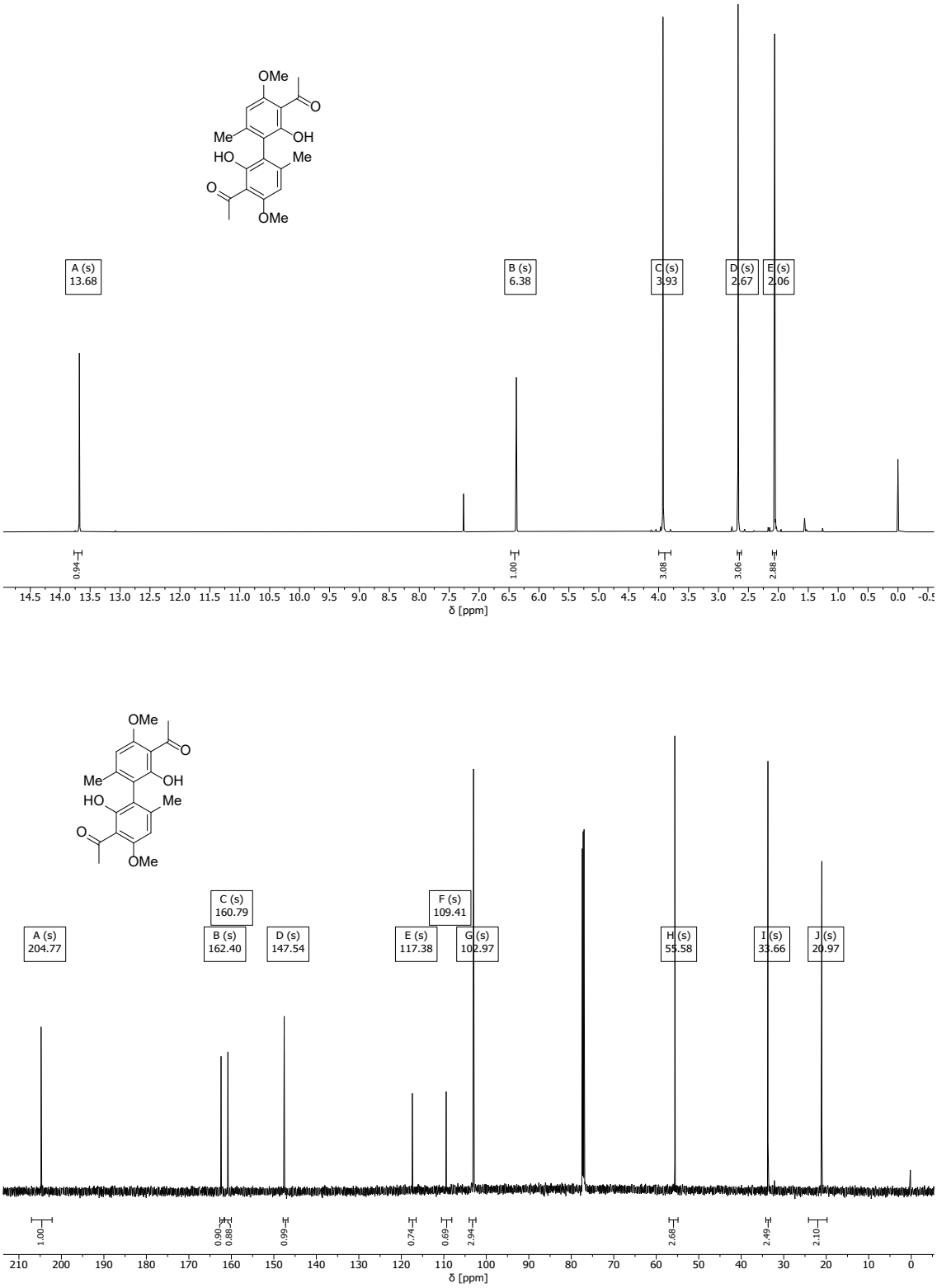

Figure S21: ^{1}H- and ^{13}C-NMR spectra (600 / 151 MHz, $CDCl_3$) of rac-1-(2-hydroxy-6-methoxy-4-methylphenyl)ethan-1-one (7).

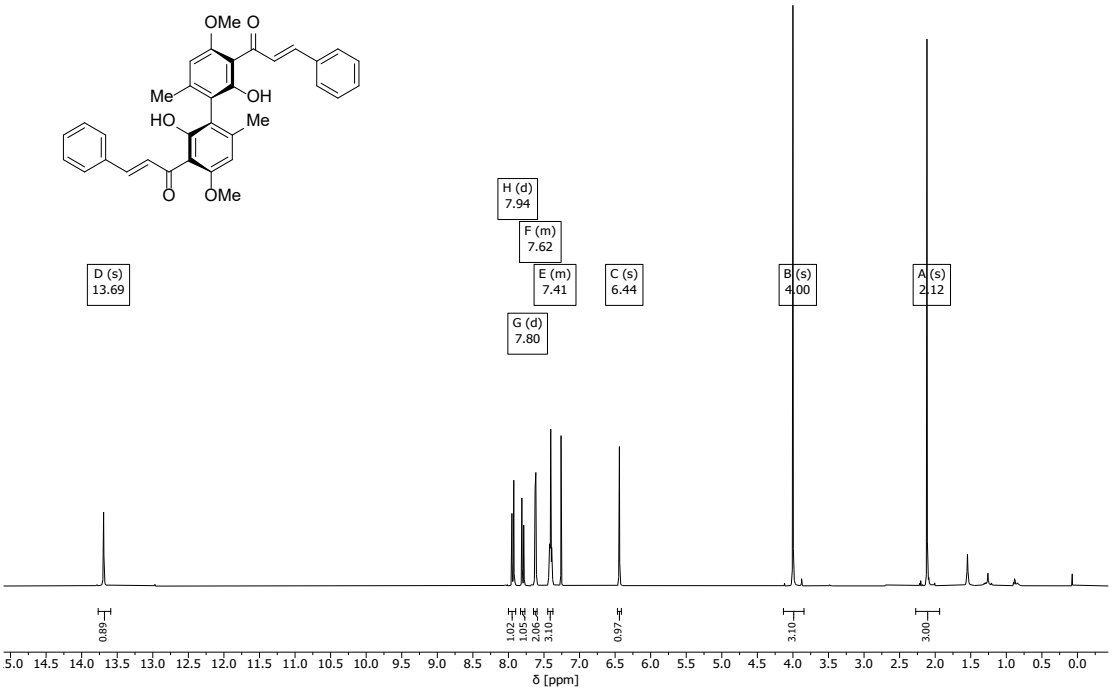

Figure S22: ^{1}H- spectrum (600 MHz, $CDCl_3$) of (+)-(2*E*,2′*E*)-1,1'-(2,2'-dihydroxy-4,4'-dimethoxy-6,6'-dimethyl-[1,1'-biphenyl]-3,3'-diyl)bis(3-phenylprop-2-en-1-one) (2ab, S_a).

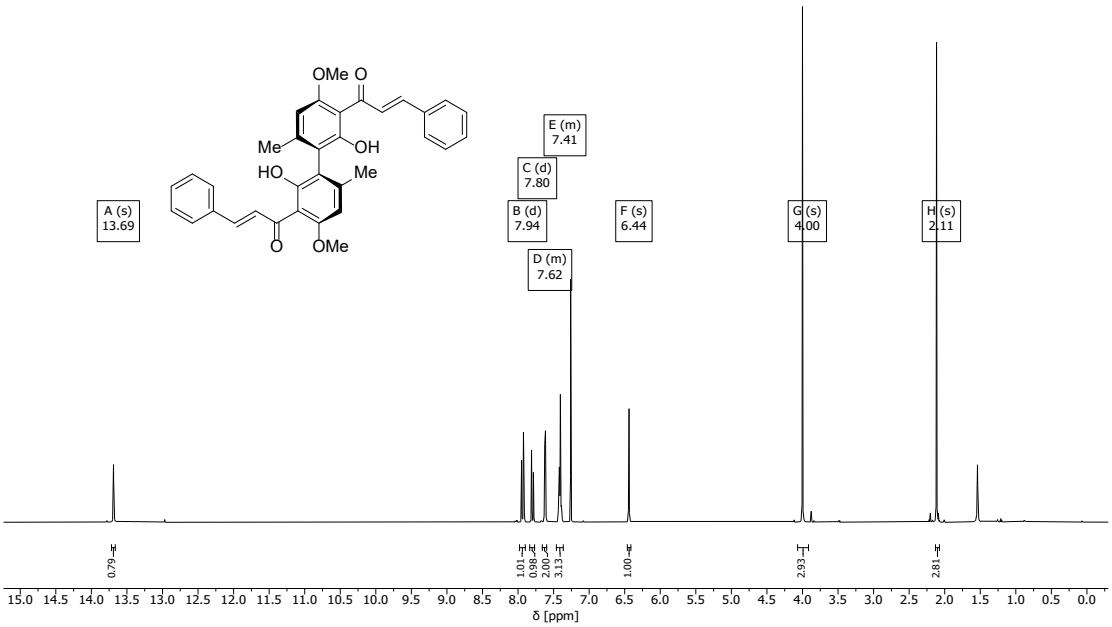

Figure S23: ^{1}H- spectrum (600 MHz, $CDCl_3$) of (−)-(2*E*,2′*E*)-1,1'-(2,2'-dihydroxy-4,4'-dimethoxy-6,6'-dimethyl-[1,1'-biphenyl]-3,3'-diyl)bis(3-phenylprop-2-en-1-one) (2ab, R_a).

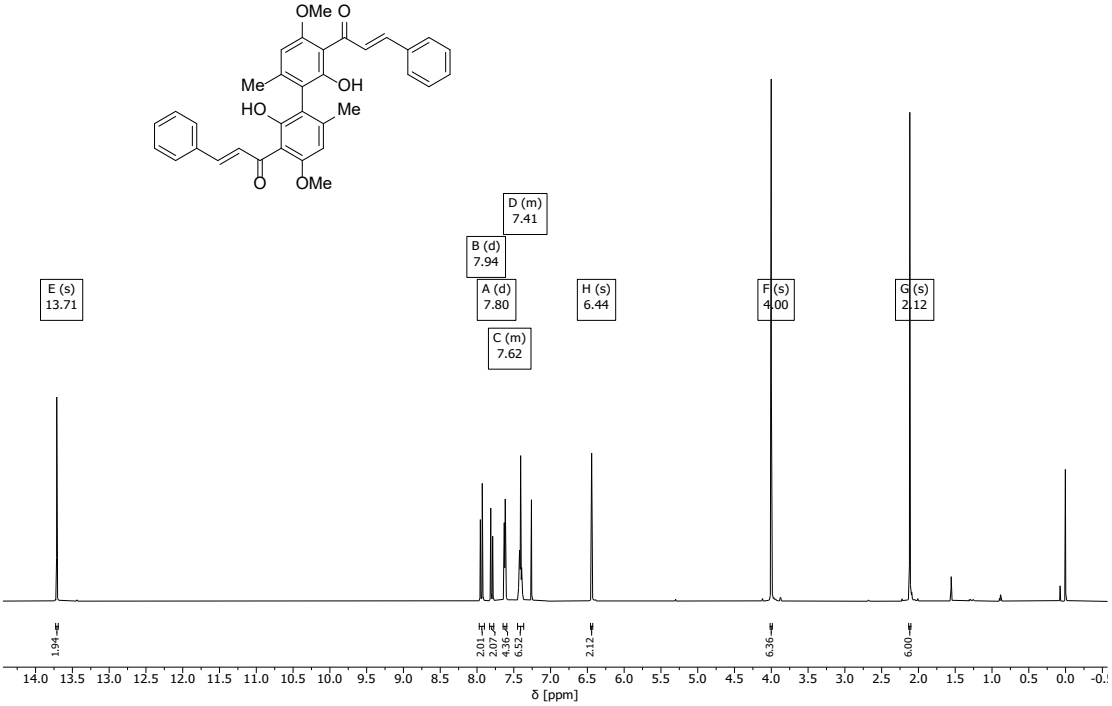

Figure S24: ^{1}H- spectrum (600 MHz, $CDCl_3$) of *rac*-(2*E*,2′*E*)-1,1'-(2,2'-dihydroxy-4,4'-dimethoxy-6,6'-dimethyl-[1,1'-biphenyl]-3,3'-diyl)bis(3-phenylprop-2-en-1-one) (2ab, *rac*).

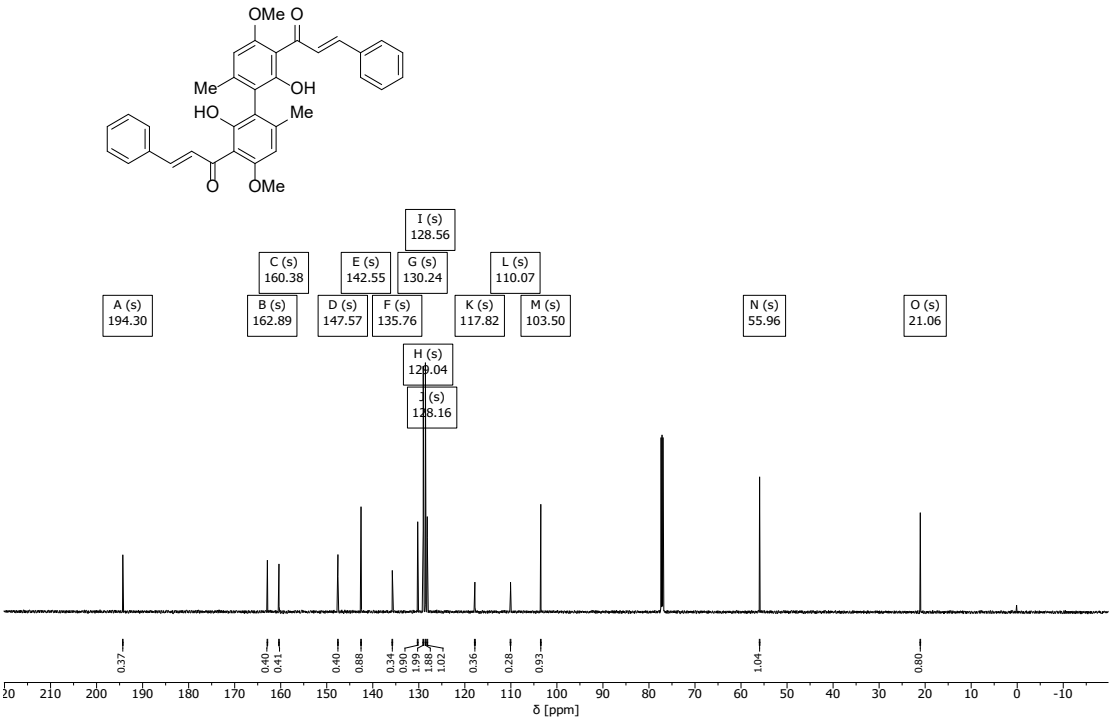

Figure S25: ^{13}C- spectrum (151 MHz, $CDCl_3$) of *rac*-(2*E*,2′*E*)-1,1'-(2,2'-dihydroxy-4,4'-dimethoxy-6,6'-dimethyl-[1,1'-biphenyl]-3,3'-diyl)bis(3-phenylprop-2-en-1-one) (2ab, *rac*).

Biological data

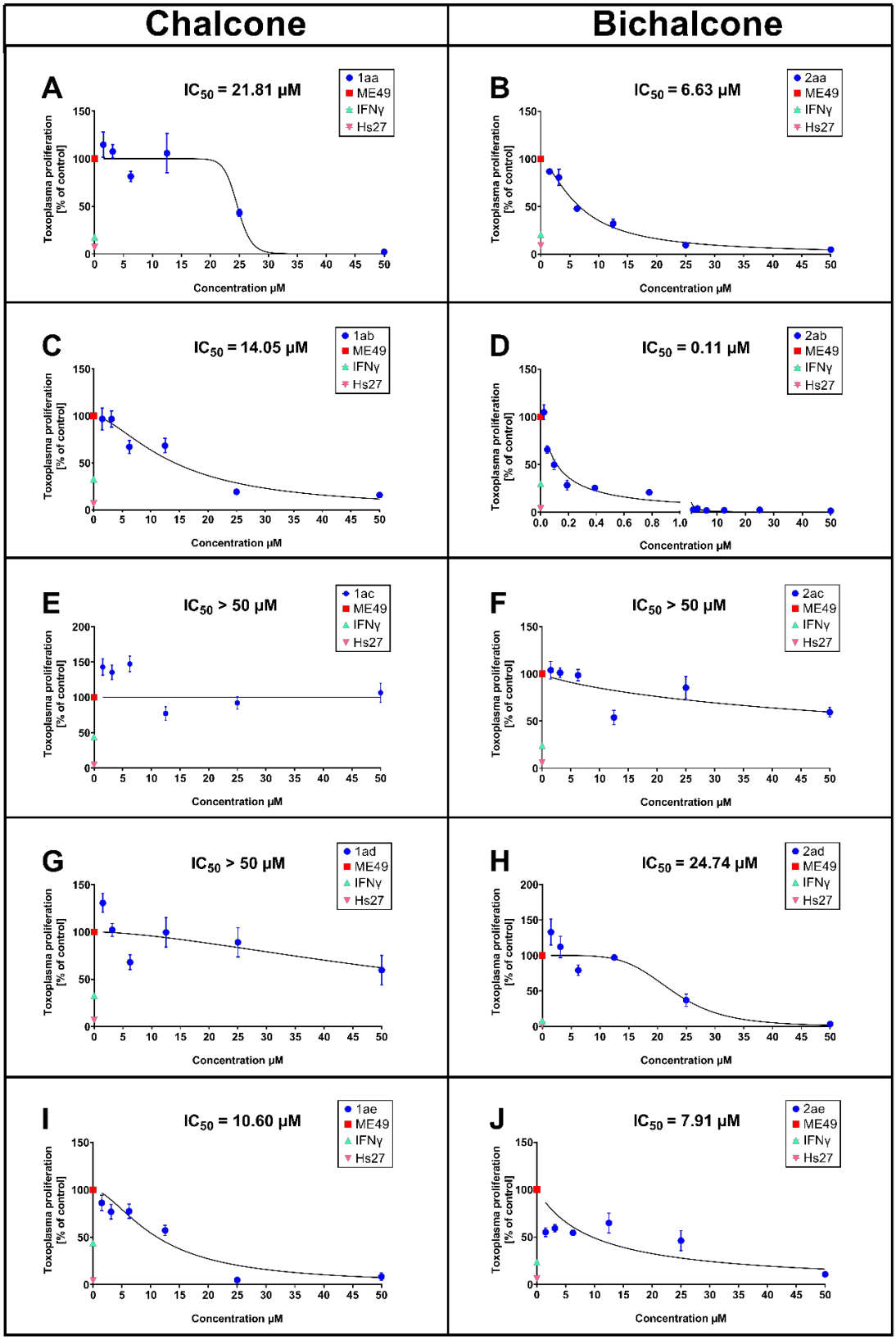
Chalcone
Bichalcone
A
IC50 = 21.81 µM
1aa
ME49
IFNγ
Hs27
B
IC50 = 6.63 µM
2aa
C
IC50 = 14.05 µM
1ab
D
IC50 = 0.11 µM
2ab
E
IC50 > 50 µM
1ac
F
IC50 > 50 µM
2ac
G
IC50 > 50 µM
1ad
H
IC50 = 24.74 µM
2ad
I
IC50 = 10.60 µM
1ae
J
IC50 = 7.91 µM
2ae
Toxoplasma proliferation [% of control]
Concentration µM

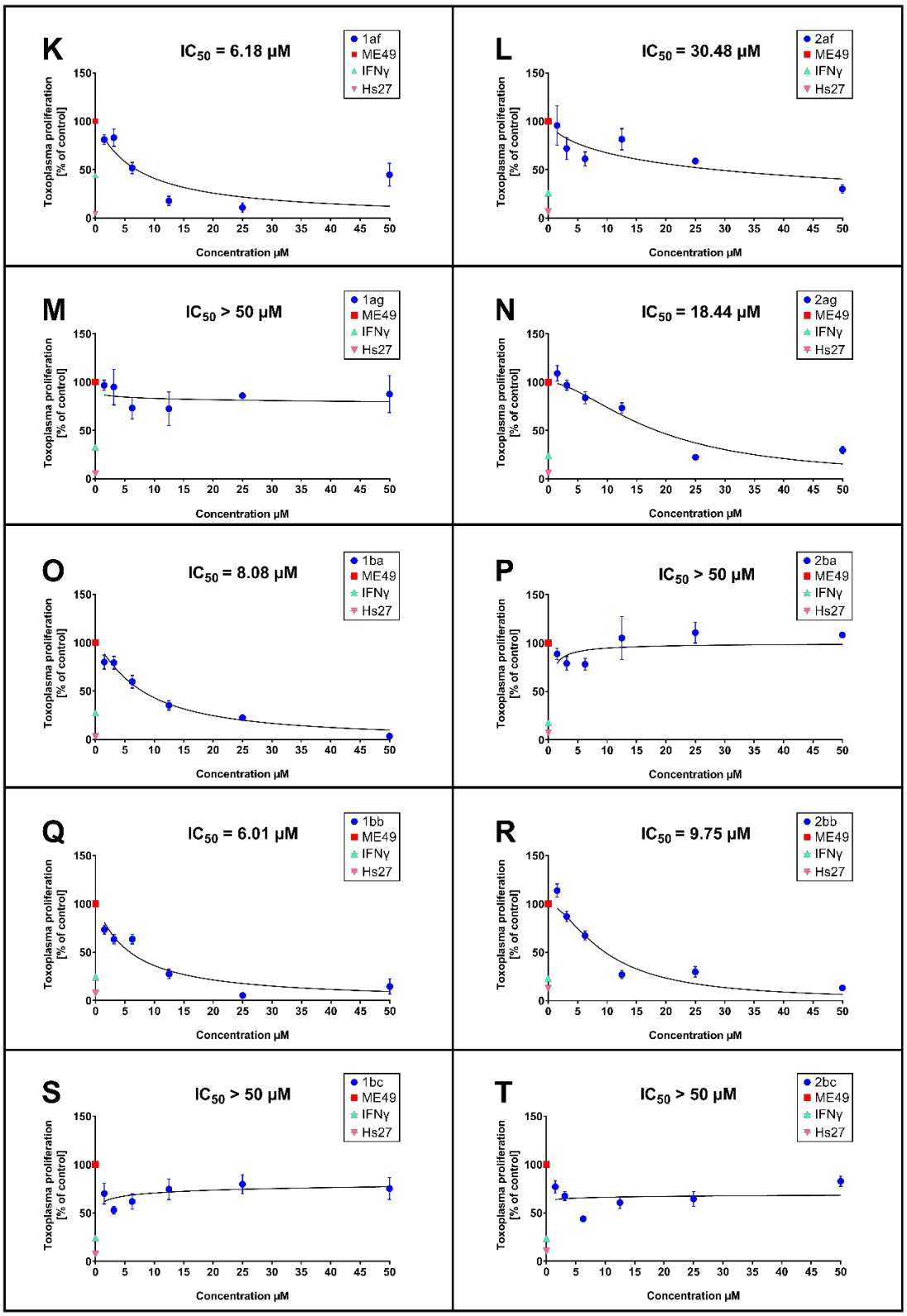
K
IC50 = 6.18 µM
1af
ME49
IFNγ
Hs27
L
IC50 = 30.48 µM
2af
M
IC50 > 50 µM
1ag
N
IC50 = 18.44 µM
2ag
O
IC50 = 8.08 µM
1ba
P
IC50 > 50 µM
2ba
Q
IC50 = 6.01 µM
1bb
R
IC50 = 9.75 µM
2bb
S
IC50 > 50 µM
1bc
T
IC50 > 50 µM
2bc
Toxoplasma proliferation [% of control]
Concentration µM

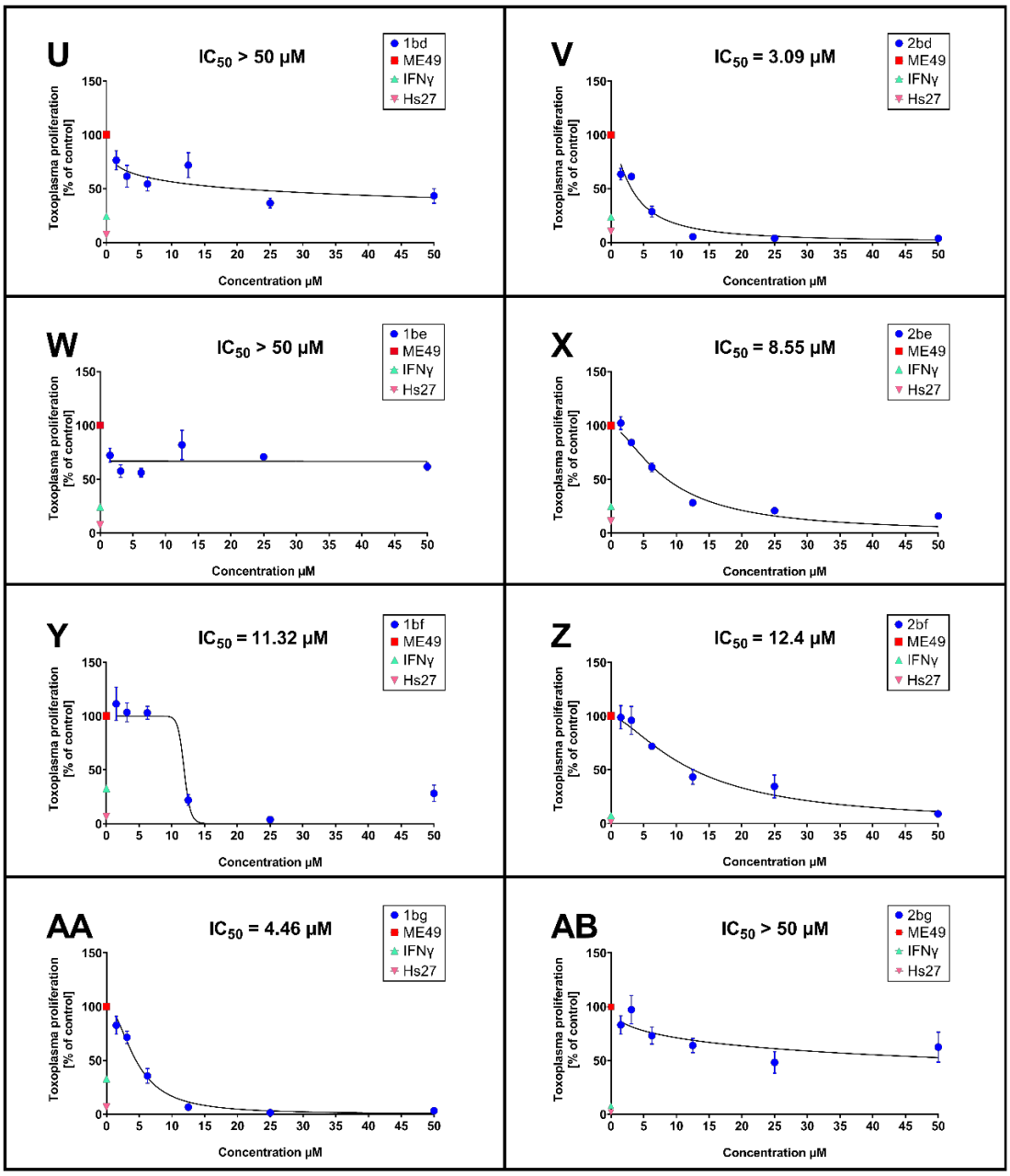

Figure S26: Effects and IC_{50} values of chalcones and bichalcones on *T. gondii* proliferation.
T. gondii ME49 tachyzoites were incubated with various concentrations of chalcones and bichalcones and the [^{3}H]-uracil incorporation assay was performed to assess their activity as described in the Materials and Methods. Plots represent nonlinear regression curves and IC_{50} values of **1aa** (**A**); **2aa** (**B**); **1ab** (**C**); **2ab** (**D**); **1ac** (**E**); **2ac** (**F**); **1ad** (**G**); **2ad** (**H**); **1ae** (**I**); **2ae** (**J**); **1af** (**K**); **2af** (**L**); **1ag** (**M**); **2ag** (**N**); **1ba** (**O**); **2ba** (**P**); **1bb** (**Q**); **2bb** (**R**); **1bc** (**S**); **2bc** (**T**); **1bd** (**U**); **2bd** (**V**); **1be** (**W**); **2be** (**X**); **1bf** (**Y**); **2bf** (**Z**); **1bg** (**AA**); **2bg** (**AB**) against *T. gondii* proliferation. The control samples included untreated and uninfected Hs27 cells (represented by pink triangles), infected Hs27 cells pre-stimulated with IFNγ for 18 h (represented by green triangles) and untreated *T. gondii*-infected Hs27 cells (represented by red squares). Values presented in the tables indicated the means of three independent experiments each performed in duplicate (n = 6) ± SEM. IC_{50} values are shown.

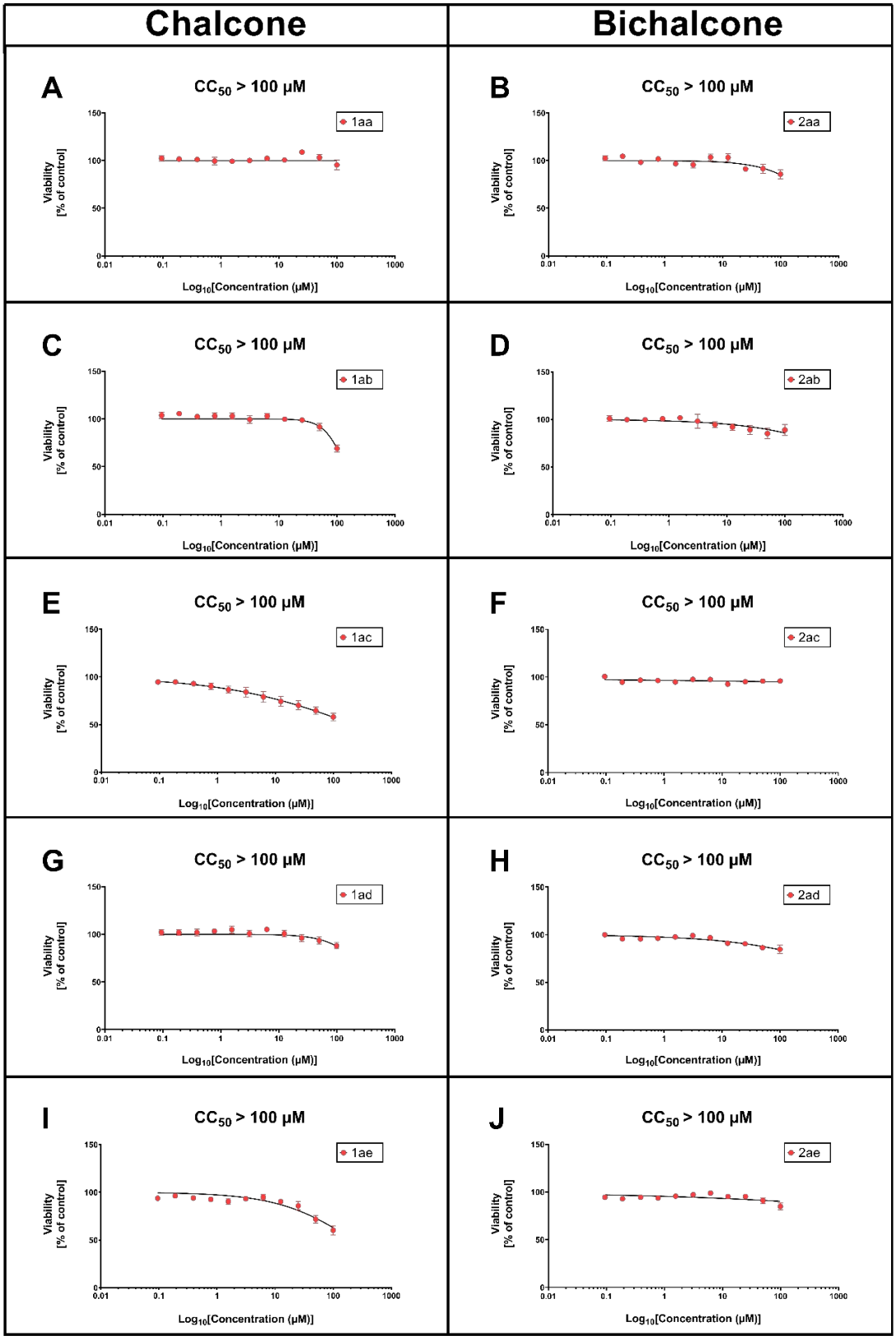
Chalcone
Bichalcone
A
CC50 > 100 µM
1aa
B
CC50 > 100 µM
2aa
C
CC50 > 100 µM
1ab
D
CC50 > 100 µM
2ab
E
CC50 > 100 µM
1ac
F
CC50 > 100 µM
2ac
G
CC50 > 100 µM
1ad
H
CC50 > 100 µM
2ad
I
CC50 > 100 µM
1ae
J
CC50 > 100 µM
2ae
Viability [% of control]
Log10[Concentration (µM)]

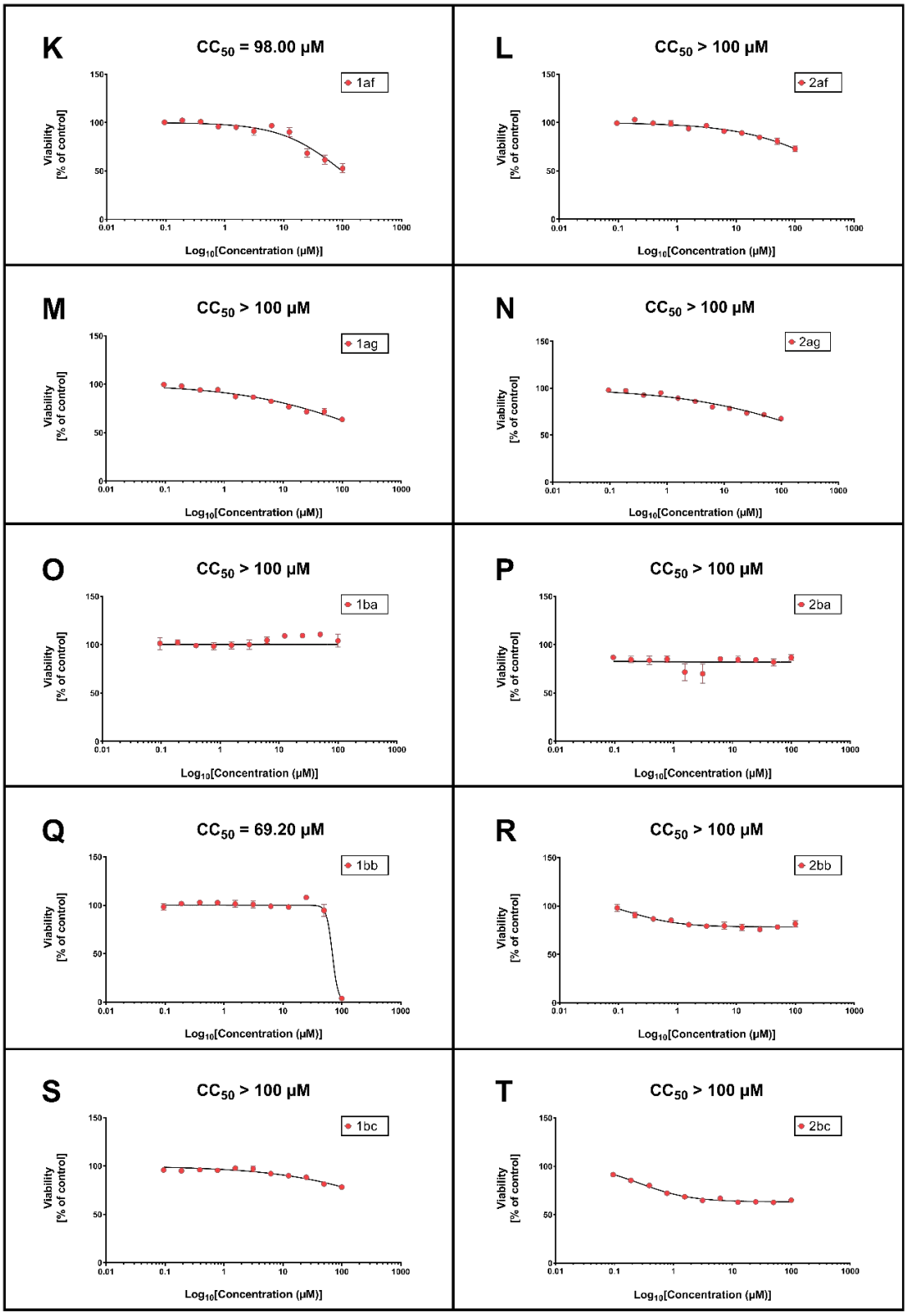
K
CC50 = 98.00 µM
1af
L
CC50 > 100 µM
2af
M
CC50 > 100 µM
1ag
N
CC50 > 100 µM
2ag
O
CC50 > 100 µM
1ba
P
CC50 > 100 µM
2ba
Q
CC50 = 69.20 µM
1bb
R
CC50 > 100 µM
2bb
S
CC50 > 100 µM
1bc
T
CC50 > 100 µM
2bc
Viability [% of control]
Log10[Concentration (µM)]

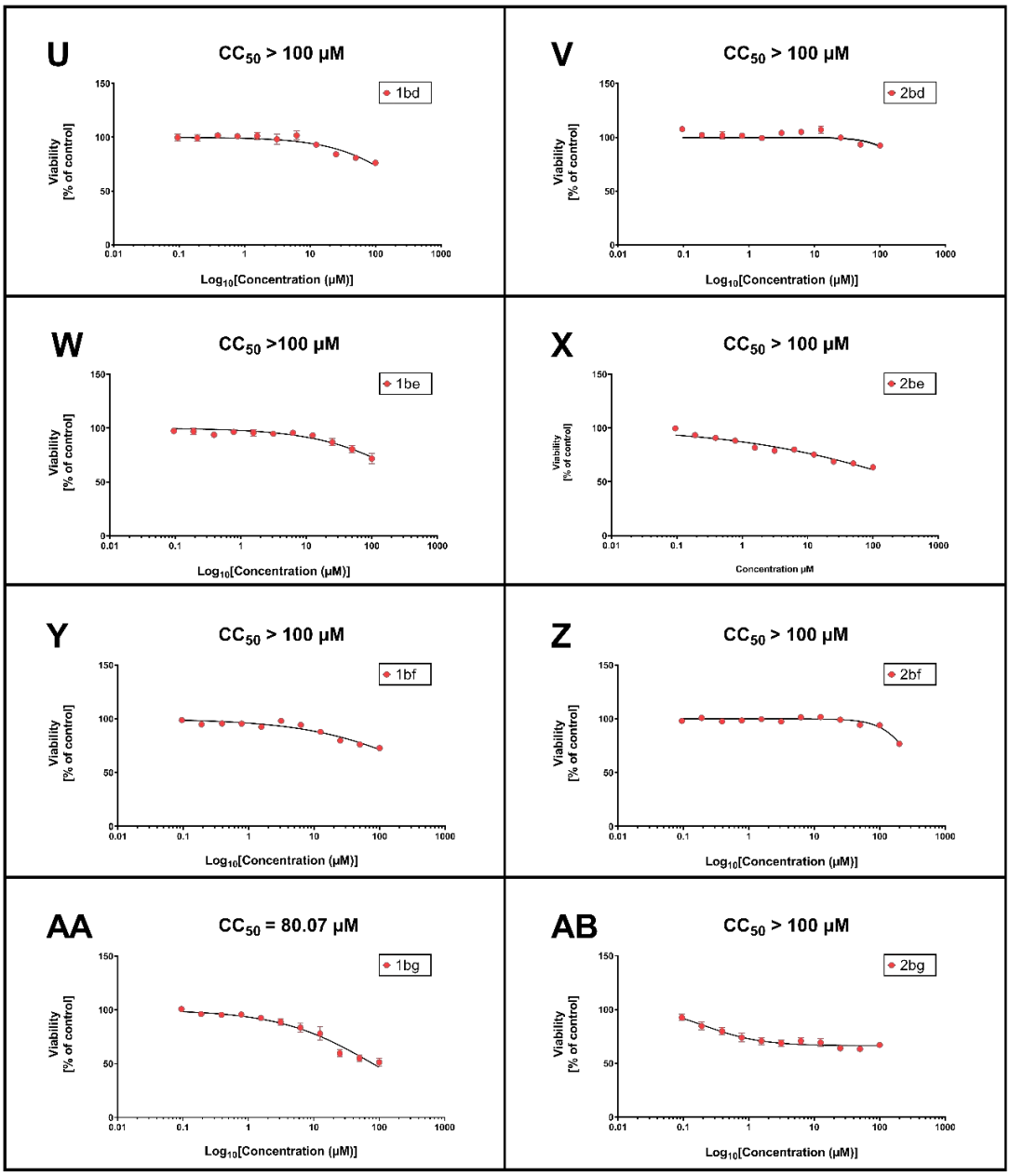

Figure S27: Effect of chalcones and bichalcones on the viability of human Hs27 fibroblasts. Cytotoxic effect of **1aa** (**A**); **2aa** (**B**); **1ab** (**C**); **2ab** (**D**); **1ac** (**E**); **2ac** (**F**); **1ad** (**G**); **2ad** (**H**); **1ae** (**I**); **2ae** (**J**); **1af** (**K**); **2af** (**L**); **1ag** (**M**); **2ag** (**N**); **1ba** (**O**); **2ba** (**P**); **1bb** (**Q**); **2bb** (**R**); **1bc** (**S**); **2bc** (**T**); **1bd** (**U**); **2bd** (**V**); **1be** (**W**); **2be** (**X**); **1bf** (**Y**); **2bf** (**Z**); **1bg** (**AA**); **2bg** (**AB**) against human cell lines Hs27 as determined by MTT assay. 100% growth control DMSO, 0% growth control staurosporine. Values shown in the figures represent the means of three independent experiments each done in duplicate (n = 6) ± SEM.

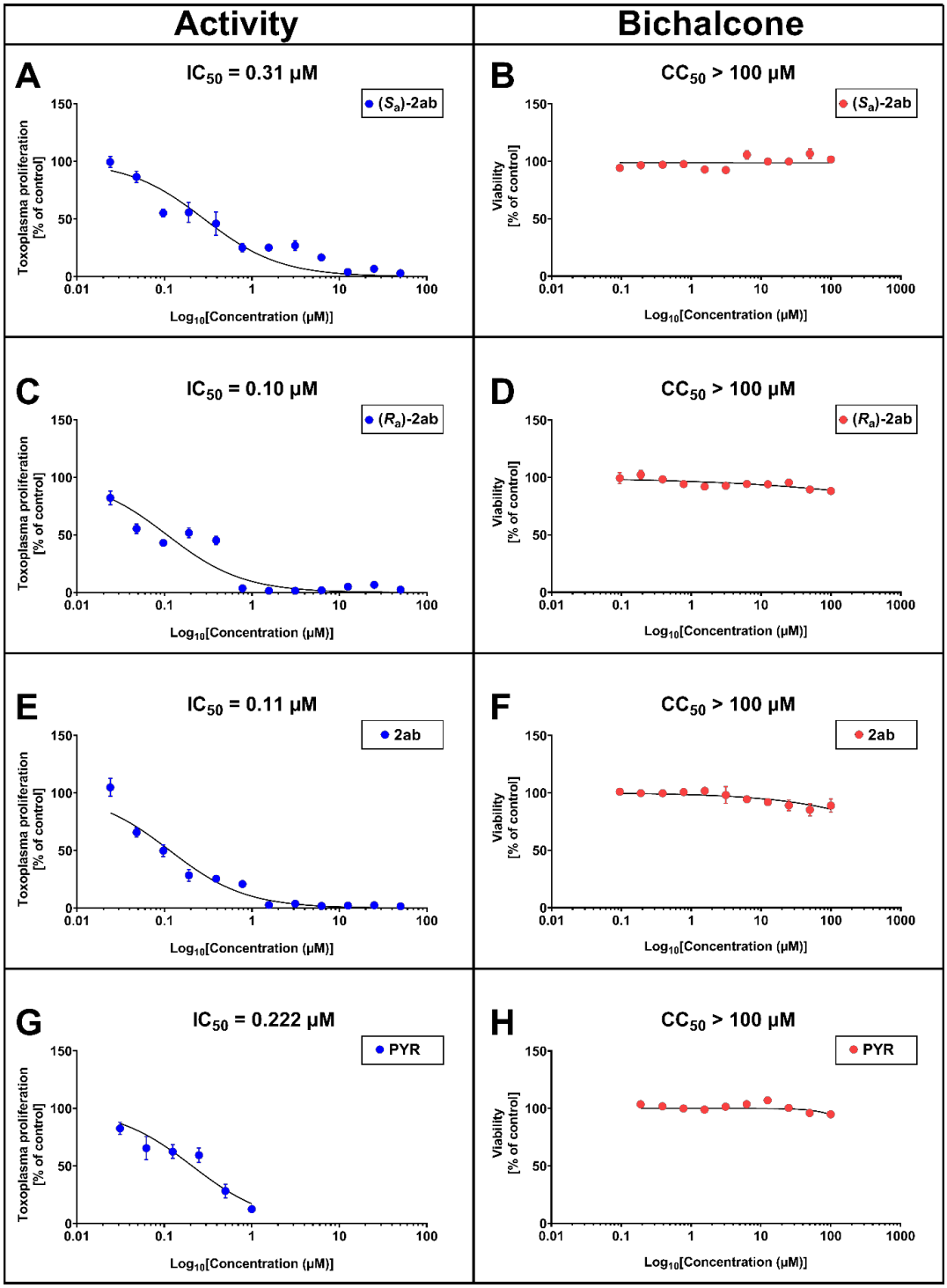

Figure S28: The anti-toxoplasma activity and cytotoxicity of the pure enantiomers (*S*a)-2ab and (*R*a)-2ab and the racemic solution 2ab compared with pyrimethamine.
The inhibitory activities of the enantiomers **(*S*a)-2ab** (**A**), **(*R*a)-2ab** (**C**), the racemic solution **2ab** (**E**) and **PYR** (**G**) were determined by the *T. gondii in vitro* inhibition assay via the [^{3}H]-uracil incorporation into the RNA of the parasite. The cytotoxicity of **(*S*a)-2ab** (**B**), **(*R*a)-2ab** (**D**), the racemic solution **2ab** (**F**) and **PYR** (**H**) was measured by MTT assays. Data shown are from the means of three independent experiments each performed in duplicate (n = 6) ± SEM. IC_{50} and CC_{50} values of each compound are shown.

4 Bibliography

Christine Ganardi, R., Greb, J., Henßen, B., & Pietruszka, J. Atroposelective Total Synthesis of (+)-Isokotanin A via Combined Metal and Enzyme Catalysis. *Advanced Synthesis & Catalysis, n/a*(n/a). doi:https://doi.org/10.1002/adsc.202300698

Gabriel, C. M., Lee, N. R., Bigorne, F., Klumphu, P., Parmentier, M., Gallou, F., & Lipshutz, B. H. (2017). Effects of Co-solvents on Reactions Run under Micellar Catalysis Conditions. *Organic Letters, 19*(1), 194-197. doi:10.1021/acs.orglett.6b03468

Ganardi, R., Greb, J., Henssen, B., & Pietruszka, J. (2023). Atroposelective Total Synthesis of (+)-Isokotanin A via Combined Metal and Enzyme Catalysis. *Advanced Synthesis & Catalysis, 365,*, 3512–3520. doi:doi.org/10.1002/adsc.202300698

Greb, J., Drennhaus, T., Klischan, M. K. T., Schroeder, Z. W., Frey, W., & Pietruszka, J. (2023). A Common C2-Symmetric 2,2'-Biphenol Building Block and its Application in the Synthesis of (+)-di-epi-Gonytolide A. *Chemistry – A European Journal, 29*(34), e202300941. doi:https://doi.org/10.1002/chem.202300941

Klischan, M. K. T., Mazzone, F., Berning, L., Greb, J., Schlamkow, M., Haase, M., . . . Pietruszka, J. (2023). Modular Approach for the Synthesis and Bioactivity Profiling of 8,8′-Biflavones. *ACS Omega, 8*(44), 41816–41834. doi:10.1021/acsomega.3c06503

Lipshutz, B. H., Ghorai, S., Abela, A. R., Moser, R., Nishikata, T., Duplais, C., . . . Gadwood, R. C. (2011). TPGS-750-M: A Second-Generation Amphiphile for Metal-Catalyzed Cross-Couplings in Water at Room Temperature. *The Journal of Organic Chemistry, 76*(11), 4379-4391. doi:10.1021/jo101974u

Pettersen, E. F., Goddard, T. D., Huang, C. C., Meng, E. C., Couch, G. S., Croll, T. I., . . . Ferrin, T. E. (2021). UCSF ChimeraX: Structure visualization for researchers, educators, and developers. *Protein Science, 30*(1), 70-82. doi:10.1002/pro.3943

Rizzo, S., Benincori, T., Fontana, F., Pasini, D., & Cirilli, R. (2022). HPLC Enantioseparation of Rigid Chiral Probes with Central, Axial, Helical, and Planar Stereogenicity on an Amylose (3,5-Dimethylphenylcarbamate) Chiral Stationary Phase. *Molecules, 27*(23), 8527. Retrieved from https://www.mdpi.com/1420-3049/27/23/8527

Sechi, B., Mamane, V., Dallocchio, R., Dessì, A., Cossu, S., Jibuti, G., & Peluso, P. (2023). Enantioseparation of new axially chiral carboxylic acids on polysaccharide-based chiral stationary phases under normal phase elution conditions. *Journal of Pharmaceutical and Biomedical Analysis Open, 1*, 100011. doi:https://doi.org/10.1016/j.jpbao.2023.100011

Tietze, L. F., Ma, L., & Jackenkroll, S. (2014). THE PAECILIN PUZZLE – ENANTIOSELECTIVE SYNTHESIS OF THE PROPOSED STRUCTURES OF PAECILIN A AND B *Heterocycles, 88*(2), 1101-1119.

Wang, T., & Chen, Y. W. (1999). Application and comparison of derivatized cellulose and amylose chiral stationary phases for the separation of enantiomers of pharmaceutical compounds by high-performance liquid chromatography. *Journal of Chromatography A, 855*(2), 411-421. doi:https://doi.org/10.1016/S0021-9673(99)00733-5

Wang, T., Chen, Y. W., & Vailaya, A. (2000). Enantiomeric separation of some pharmaceutical intermediates and reversal of elution orders by high-performance liquid chromatography using cellulose and amylose tris(3,5-dimethylphenylcarbamate) derivatives as stationary phases. *Journal of Chromatography A, 902*(2), 345-355. doi:https://doi.org/10.1016/S0021-9673(00)00862-1

Wang, T., & Wenslow, R. M. (2003). Effects of alcohol mobile-phase modifiers on the structure and chiral selectivity of amylose tris(3,5-dimethylphenylcarbamate) chiral stationary phase. *Journal of Chromatography A, 1015*(1), 99-110. doi:https://doi.org/10.1016/S0021-9673(03)01262-7

Yamamoto, C., Yashima, E., & Okamoto, Y. (2002). Structural Analysis of Amylose Tris(3,5-dimethylphenylcarbamate) by NMR Relevant to Its Chiral Recognition Mechanism in HPLC. *Journal of the American Chemical Society, 124*(42), 12583-12589. doi:10.1021/ja020828g

Ye, Y. K., Bai, S., Vyas, S., & Wirth, M. J. (2007). NMR and Computational Studies of Chiral Discrimination by Amylose Tris(3,5-dimethylphenylcarbamate). *The Journal of Physical Chemistry B, 111*(5), 1189-1198. doi:10.1021/jp0637173

3.5 1-deoxy-d-xylulose 5-phosphate reductoisomerase (DXR) as target for anti *Toxoplasma gondii* agents: crystal structure, biochemical characterization and *in vitro* biological evaluation of fosmidomycin and reverse analogues as potent inhibitors

Authors

Flaminia Mazzone, Astrid Hoeppner, Jens Reiners, Mona A. Abdullaziz, Julia Gottstein, Martina Wesemann, Thomas Kurz, Sander H.J. Smits & Klaus Pfeffer.

Published in

Manuscript to be submitted

Impact factor

-

DOI

-

Own contributions to this work

Overall: 70%

Conducted all of the following experiments:

- Construction of the expression plasmid
- Protein expression and purification
- Quality, purity and protein integrity assessment (SDS page, WB)
- Enzyme kinetic characterisation and optimisation
- Enzyme inhibition assays
- *Toxoplasma gondii* proliferation assays
- Cytotoxicity assays (MTT assays) in human fibroblasts Hs27

Other major contributions

Design of experiments, methodology, conduction of experiments, data analysis, manuscript preparation.

1-deoxy-d-xylulose 5-phosphate reductoisomerase (DXR) as target for anti *Toxoplasma gondii* agents: crystal structure, biochemical characterization and *in vitro* biological evaluation of fosmidomycin and reverse analogues as potent inhibitors

Flaminia Mazzone[1]*, Astrid Hoeppner[2], Jens Reiners[2], Mona A. Abdullaziz[3], Julia Gottstein[4], Martina Wesemann[4], Thomas Kurz[3]†, Sander H. J. Smits[2,4]† and Klaus Pfeffer[1]†*

[1]Institute of Medical Microbiology and Hospital Hygiene, Heinrich Heine University, Düsseldorf, Germany

[2]Center for Structural Studies, Heinrich Heine University, Düsseldorf, Germany

[3]Institute of Pharmaceutical and Medicinal Chemistry, Heinrich Heine University, Düsseldorf, Germany

[4]Institute of Biochemistry, Heinrich Heine University, Düsseldorf, Germany

†These authors share last authorship

*Authors for correspondence:

Flaminia Mazzone
flaminia.mazzone@uni-duesseldorf.de,

Sander H.J. Smits
sander.smits@hhu.de,

Klaus Pfeffer
klaus.pfeffer@hhu.de.

Abstract

Toxoplasma gondii is a widely distributed apicomplexan parasite responsible of toxoplasmosis, a critical heath issue for immunocompromised individuals and for congenitally infected foetuses. The current treatment options are limited in number and associated with severe side effects. Thus, novel anti-toxoplasma agents need to the identified and developed. 1-deoxy-D-xylulose 5-phosphate reductoisomerase (DXR) is the rate-limiting enzyme in the non-mevalonate pathway for the biosynthesis of isoprenoids in the parasite, and has been deeply investigated for its key role in the pathway in various species, and in particularly, for the development of novel antimicrobial agents. In the present study, we present the first crystal structure of *T. gondii* DXR in a tertiary complex with the inhibitor fosmidomycin and the cofactor NADPH in dimeric conformation at 2.5 Å resolution. The structure reveals crucial inhibitor´s binding interactions. In addition, we biologically characterize α-phenyl-ß-thia and -oxa reverse fosmidomycin analogues and show that they are strong inhibitors of *Tg*DXR *in vitro* which also inhibit *T. gondi in vivo*, thereby establishing themselves as potent anti-toxoplasma agents. These findings could support the future design and development of more potent anti-toxoplasma compounds.

Keywords

Toxoplasma gondii, DXR, Crystal structure, Enzymatic assay, Growth inhibition, SAXS, fosmidomycin, DXR inhibitors, parasite, antiinfective

1 Introduction

Toxoplasma gondii (*T. gondii*), the causative agent of toxoplasmosis, is an obligate coccidian parasite member of the phylum Apicomplexa (Levine, 2018). As all apicomplexans, *T. gondii* possesses a complex and heteroxenous life cycle alternating between sexual stages that occur exclusively in the intestinal epithelium of their definitive hosts (the family *Felidae*), and asexual stages that can take place virtually in any warm-blooded animal, including humans (Lourido, 2019). Therefore, the pathogenesis of *T. gondii* is profoundly influenced by the growth rate of its asexual stages (White & Suvorova, 2018). It has reported that, in the United States, around 11% of the population aged 6 years and older have been infected with *T. gondii* (Prevention). In humans, the

primary route of infection is foodborne, caused by the consumption of raw or undercooked meat that contain tissue cysts (bradyzoites) or by ingestion of contaminated vegetables or water containing spores (sporulated oocysts) (Krueger, Hilborn, Converse, & Wade, 2014; Pleyer, Gross, Schlüter, Wilking, & Seeber, 2019). In healthy and immunocompetent individuals, toxoplasmosis typically remains asymptomatic or manifests with flu-like symptoms, since the infection is efficiently controlled by a fully functional immune system (Johnson, 1992; Montoya & Liesenfeld, 2004). In the other hand, the disease poses a significant concern in immunocompromised individuals, for the reactivation of latent infection with severe clinical manifestations, such as chorioretinitis, encephalitis, pneumonitis and sepsis-like symptoms (Basavaraju, 2016). Moreover, pregnant women are at relevant risk, as they can transmit the infection congenitally to the foetus, which could have devastating consequences and even be fatal for the unborn child (Deganich, Boudreaux, & Benmerzouga, 2022).

Currently, the gold-standard treatment for toxoplasmosis remains the antifolate combination of pyrimethamine and sulfadiazine (PYR-SLZ) (Dunay, Gajurel, Dhakal, Liesenfeld, & Montoya, 2018). Despite the advancements in target-based drug development in the post-genomic era, human toxoplasmosis lacks sufficient treatment options (Hemphill & Müller, 2023). Furthermore, all the current available regimens suffer from several limitations and negative aspects that compromise patient compliance and overall effectiveness. These limitations include: a lack of specificity, that cause severe and potentially fatal side effects; and the inability to effectively target bradyzoites, the dormant cyst-form of the parasite, responsible for the latency of the infection (Alday & Doggett, 2017). Therefore, novel, safer and more efficient therapeutic options are urgently needed.

Since its discovery, the apicoplast, a non-photosynthetic plastid organelle in the apicomplexan parasites has emerged has an attractive target for anti-infective drugs due to its absence in mammalian cells (Hajj et al., 2021; McFadden, 2011). This plastid is responsible for essential metabolic pathways for the parasite such as fatty acid, haem, iron sulphur cluster, and isoprenoids synthesis among others (Lim & McFadden, 2010). The 2-*C*-methyl-D-erythritol 4-phosphate (MEP) pathway, also called non-mevalonate pathway (NMP), for the biosynthesis of isopentenyl pyrophosphate (IPP) and dimethylallyl diphosphate (DMAPP), crucial metabolites for biosynthesis of isoprenoids and essential for the organism, has gathered high interest as a potential drug target (**Figure 1**). Its enzymes are highly conserved in plastid-bearing organisms and most gram-

negative bacteria, and there are no mammalian orthologues, as humans and animals use the mevalonate pathway for the biosynthesis of isoprenoids (Allamand, Piechowiak, Lièvremont, Rohmer, & Grosdemange-Billiard, 2023; Ball et al., 2021; Wang & Dowd, 2018; Xu et al., 2013).

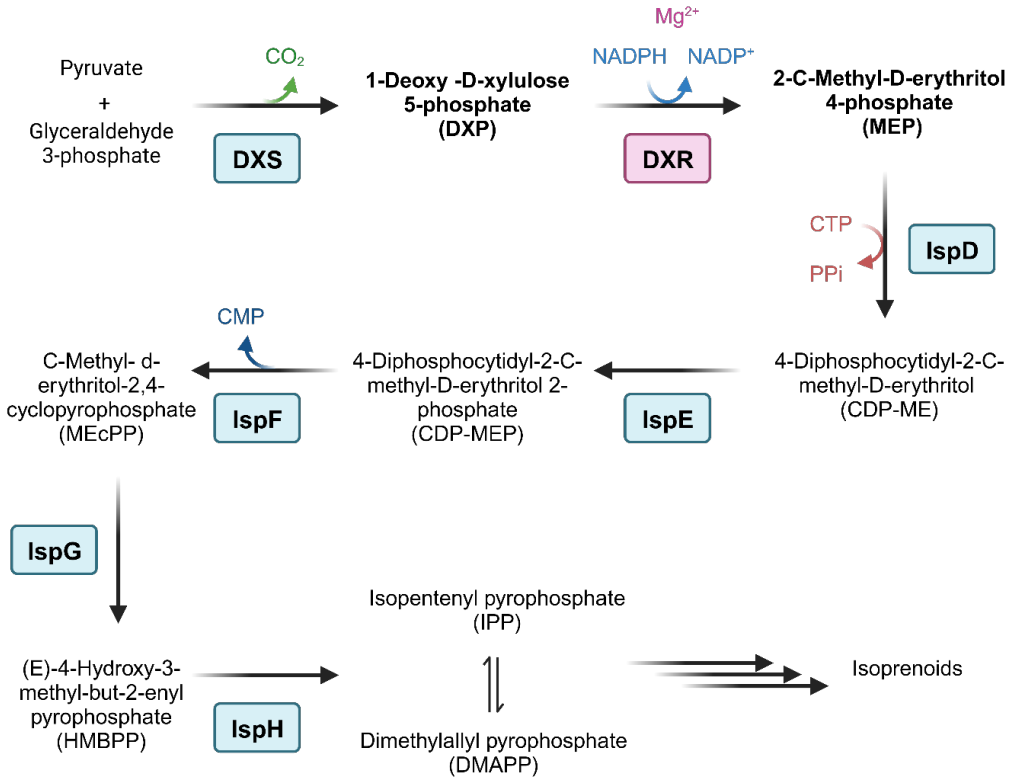

Figure 1: The MEP pathway for the biosynthesis of isoprenoids

Modified from Frank *et al.*(Frank & Groll, 2017). Created with BioRender.com.

The 1-deoxy-d-xylulose 5-phosphate reductoisomerase (DXR, IspC, EC 1.1.1.267), the second and rate-limiting enzyme in the MEP pathway, catalyses the isomerization and the reduction of 1-deoxy-D-Xylulose 5-phosphate (DXP) into MEP via dependency of a divalent metal cation and NADPH-dependent reduction (**Figure 2, A**). DXR enzymes have been extensively investigated and characterized for their key role in the pathway, and in particularly, for the development of novel antibacterial and antimalarial agents (Proteau, 2004; Singh, Chevé, Avery, & McCurdy, 2007). Moreover, several structural studies of this enzyme from a wide range of sources have been reported with high and medium resolution, such as the crystal structure of DXR from *E. coli* (Mac Sweeney et al., 2005), *M. tuberculosis* (Andaloussi et al., 2011), *P. falciparum* (Sooriyaarachchi et al., 2016), but not from *T. gondii*.

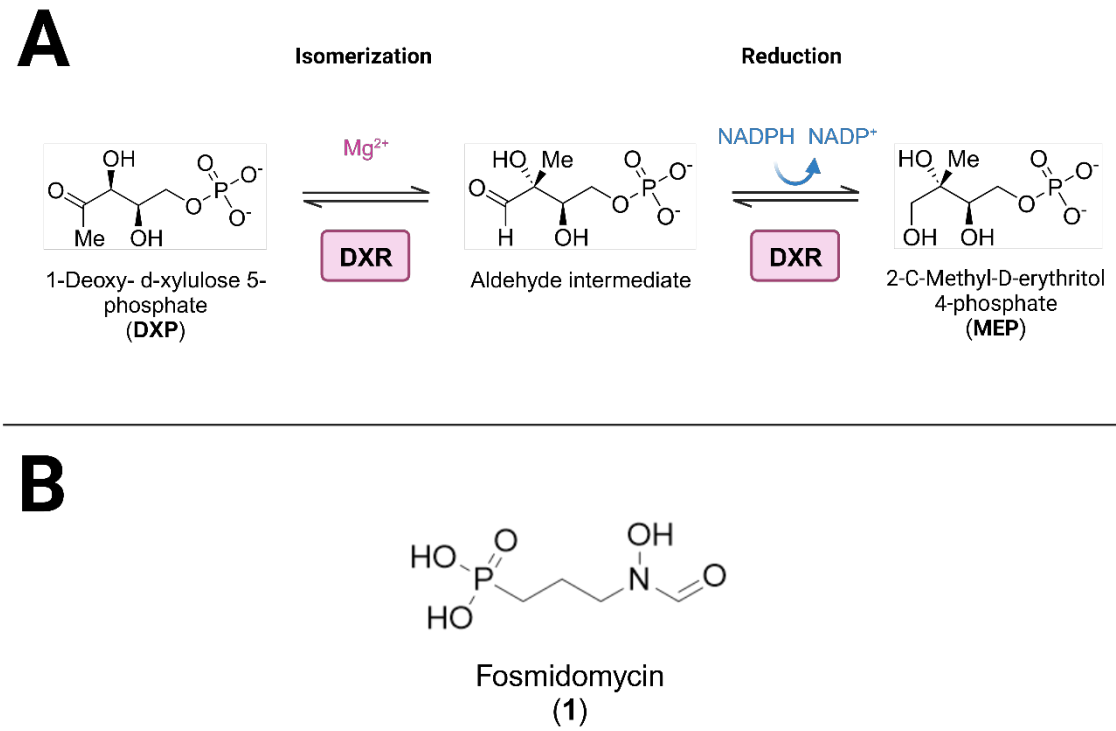

Figure 2: Reaction catalysed by 1-Deoxy-D-xylulose 5-phosphate reductoisomerase (DXR) and the inhibitor fosmidomycin

(**A**): The DXR enzyme catalyses the conversion of the substrate 1-deoxy-D-xylulose 5-phosphate (DXP) into the product 2-C-methyl-D-erythritol-4-phosphate (MEP). The catalysis occurs with dependency of a metallic dication (Mg^{2+}) and NADPH as cofactors, via a two-step reaction: first, the retro-aldol/aldol isomerization of DXP with the formation of the aldehyde intermediate (Munos, Pu, Mansoorabadi, Kim, & Liu, 2009); then, a NADPH- depend reduction of the intermediate to MEP (Murkin, Manning, & Kholodar, 2014). Modified from Kuzuyama *et al.*(T. Kuzuyama, Takahashi, Takagi, & Seto, 2000). (**B**): Chemical structure of the DXR inhibitor fosmidomycin. Created with BioRender.com.

Fosmidomycin (**1**) (**Figure 2, B**), a natural product originally isolated from the bacteria *Streptomyces lavendulae* (Okuhara et al., 1980) was identified as a potent and specific inhibitor of the DXR enzymes from *E.coli* (Tomohisa Kuzuyama, Shimizu, Takahashi, & Seto, 1998) and *P. falciparum* (Jomaa et al., 1999). Unfortunately, this molecule faces several limitations as a clinical therapeutic related to its pharmacokinetics: short plasma half-life and rapid plasma clearance (Na-Bangchang, Ruengweerayut, Karbwang, Chauemung, & Hutchinson, 2007); poor bioavailability due to the highly ionized nature of the phosphonate group of fosmidomycin at physiological pH (Kuemmerle et al., 1985). Its polarity affects also the permeability in several cell membranes, except *E. coli* (Sakamoto, Furukawa, Ogihara, & Yamasaki, 2003) and *P. falciparium* (Baumeister et al., 2011) that actively transport the compound. However, it is not effective in *M.*

tuberculosis (Brown & Parish, 2008) and *T. gondii* (Nair et al., 2011) due to the lack of uptake systems.

Given the significance of this class of the compounds and with the aim to find more potent inhibitors of *Tg*DXR with a better profile than fosmidomycin, in the present study we successfully cloned, expressed, purified and biochemically characterized the recombinant *Tg*DXR. We report an X-ray structure of *Tg*DXR in a tertiary complex with the cofactor NADPH and the inhibitor fosmidomycin, further defined by small-angle X-ray scattering (SAXS) analysis. Moreover, we assessed the *in vitro* activity of previously described ß-thia and ß-oxa isosters of reversed hydroxamic acid analogues of fosmidomycin (Brücher et al., 2012; Kunfermann et al., 2013; Lienau et al., 2019) against the activity of the recombinant *Tg*DXR enzyme and *T. gondii* proliferation. These findings could support the future design and development of novel anti-toxoplasma agents.

2 Results

2.1 Biochemical characterisation

2.1.1 *Tg*DXR enzyme properties

We set out to functionally and structurally characterize the His_{10}-*Tg*DXR, which contain the catalytic domain. To achieve this, we constructed a plasmid, which contains the catalytic centre consisting of the NADPH binding site as well as the substrate-binding site of the *Tg*DXR protein (amino acid 182 to 632) contains the catalytic centre consisting of the NADPH binding site as well as the substrate-binding site (**Figure S1**). After expression, the *Tg*DXR was purified to homogeneity as observed by a single symmetric peak on the size exclusion chromatography profile and SDS-PAGE analysis (**Figure 3**). The purified *Tg*DXR was then evaluated for its enzymatic activity through a spectrophotometric assay measuring the oxidation of NADPH over time under various conditions. The optimum of its catalytic capacity was reached with 100 µM of 1-deoxy-D-xylulose 5-phosphate (DXP), 100 µM of NADPH, 4 mM of $MgCl_2$ and a pH of 7.5 at concertation of 100 nM of *Tg*DXR (**Figure 3**). The kinetics parameters of *Tg*DXR were also evaluated: the Km value for DXP was determined to be 30.58 ± 6.33 µM, which is comparable with the *Tg*DXR K_m value obtained previously (Cai et al., 2013) and the reported DXR K_m values from other species, such as *Pf*DXR (67 µM) (L Goble et al., 2013) and *Mt*DXR (47 µM) (Dhiman et al., 2005); the Km for NADPH was determinated

as 51.30 ± 11.84 µM (**Figure 3**).The V_{max} was shown to be 0.83 mmol/min/mg, comparable to *Pf*DXR (1.04 mmol/min/mg) (L Goble et al., 2013).

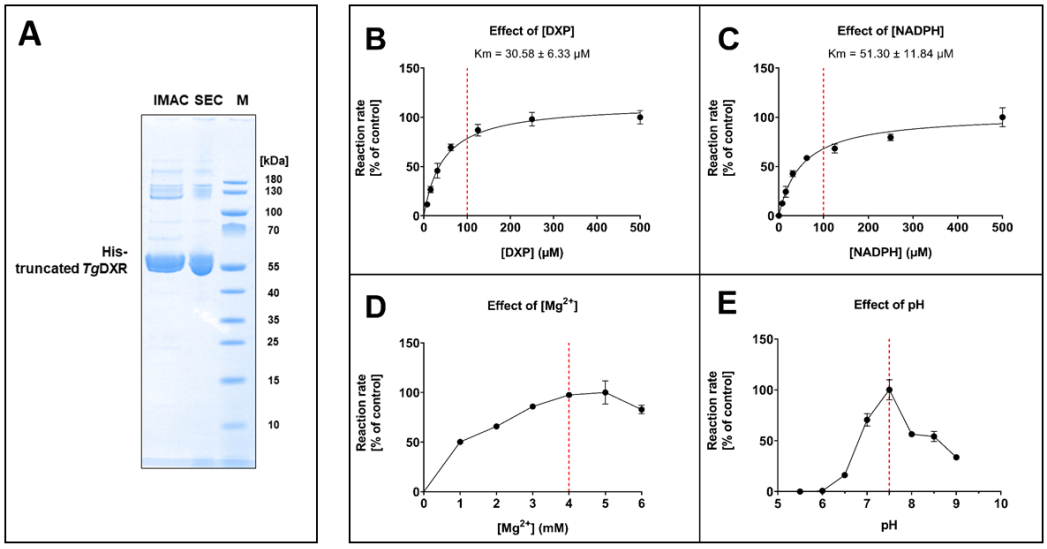

Figure 3: Purification of the His$_{10}$-truncated *Tg*DXR and its optimisation and kinetic characterisation (**A**): SDS-PAGE of samples taken during the purification of truncated His$_{10}$-truncated *Tg*DXR after immobilized metal ion affinity chromatography (IMAC) and size exclusion chromatography (SEC). Marker (M): PageRuler™ Prestained Protein Ladder, Thermo Scientific™, Thermo Fisher Scientific, Waltham, MA, USA, #26616, molecular weights in kDa are indicated. Running Buffer: 20X NuPAGE™ MOPS SDS Running buffer, Thermo Fisher Scientific, Waltham, MA, USA, #NP000102; (**B**): Effects of [DXP] on *Tg*DXR catalysed reaction. Km values of DXP and NADPH are shown; (**C**): Effects of [NADPH] on the *Tg*DXR catalysed reaction; (**D**): Effects of [Mg^{2+}] on the *Tg*DXR catalysed reaction; (**E**): Effects of pH on the *Tg*DXR catalysed reaction. See Materials and Methods section for the experimental conditions. Optimal and selected concentrations or values are indicated (red line). Data shown are from the means of four independent experiments, each performed in duplicate (n = 8) ± S.D.

2.2 Structural characterisation of the *Tg*DXR catalytic domain

*Tg*DXR was crystallised in the presence of the known inhibitor fosmidomycin using the sitting drop method. The 3µl drops consisted of 1.5 µl protein (7.5 mg/ml in 20 mM TRIS pH 7.5, 150 mM NaCl, 2% glycerol supplemented with 1mM fosmidomycin) mixed with crystallisation buffer 1.5 µl 200 mM Na citrate tribasic, 27% PEG smear low, 150 mM HEPES pH 7.8.

Crystals appeared within a few days and grew to their final dimensions within two weeks. Before the crystals were flash-cooled in liquid nitrogen, they were transferred to a drop

of the reservoir solution complemented with mineral oil. A high-resolution dataset was collected and phased using the model of the DXR protein from *E.coli* (PDB entry: 1K5H) (Reuter et al., 2002) revealing a dimer in the asymmetric unit**.**

2.2.1 The overall structure

The structure of *Tg*DXR was solved and refined to 2.5 Å resolution (data-collection and refinement statistics are summarised in **Table S2**). The asymmetric unit contains one homodimer. The r.m.s. difference between Cα atom positions within in the two subunits when they are superimposed is 0.3 Å using all 347 Cα atoms. Residues 25–472 could be modelled for both molecules from the electron-density map except the loop ranging from amino acid 182–221 and were therefore not modelled in either of the two subunits. We describe the overall structure for monomer A.

*Tg*DXR is composed of three domains: an N-terminal NADPH-binding domain, a connective domain and a C-terminal α-helical domain (**Figure 4, A**). These are arranged in a V shape, where the N-terminal and C-terminal domains form the two arms and the central domain lies at the vertex.

The N-terminal domain (residues 25–171) consists of a Rossmann fold, with a ß-sheet containing seven parallel ß -strands (ß1– ß7, including a kink at residue 56 in ß2), which is flanked by a total of six α-helices (α1–α6).

The N-terminal domain is connected via a long loop (residues 172-227) to the catalytic domain. Of this loop, the largest part is not visible in the electron density and appears to be flexible although NADPH and the inhibitor fosmidomycin are present. The catalytic domain (residues 228-385) includes a four-stranded ß -sheet ordered ß9 - ß8 - ß10 - ß11, where ß10 is positioned antiparallel to the other strands. This sheet adheres to the other two domains by virtue of a layer of helices. ß8 extents into a flexible loop consisting of a broken helix α7 which then returns into the four-stranded ß-sheet via α helix α8.

The C-terminal domain residues (386-472) features a four-helix bundle. The dimer interface is created by interactions between the catalytic and connecting regions of each subunit. A twisted eight-stranded ß-sheet is formed using the four ß-strands of each catalytic domain, with the respective ß11 strands positioned antiparallel at its central point (**Figure 4, B**). Further antiparallel interactions between the ß12 strands of each subunit are found on the concave surface of this larger sheet; interactions at the C-terminal end

of the ß12 strand links them to the sheet, thus forming an imperfect ten-stranded ß-barrel as the core of the dimer interface.

In the electron density, NADPH can unambiguously be identified and modelled. NADPH is bound to the Rossmann fold by interactions typically observed, while the pyrophosphate moiety interacts with the consensus sequence GGGNGA, establishing further interactions with the co-substrate NADPH which is bound at the identical position as found in other DXR proteins (Henriksson et al., 2007; Mac Sweeney et al., 2005; Umeda et al., 2011; Yajima et al., 2007). The binding of the adenine and pentose phosphate moieties of NADPH is identical to that observed in the structure of the *E. coli* DXR, in contrast, the nicotinamide ring of NADPH is ordered in this fosmidomycin complex (**Figure 4, C**).

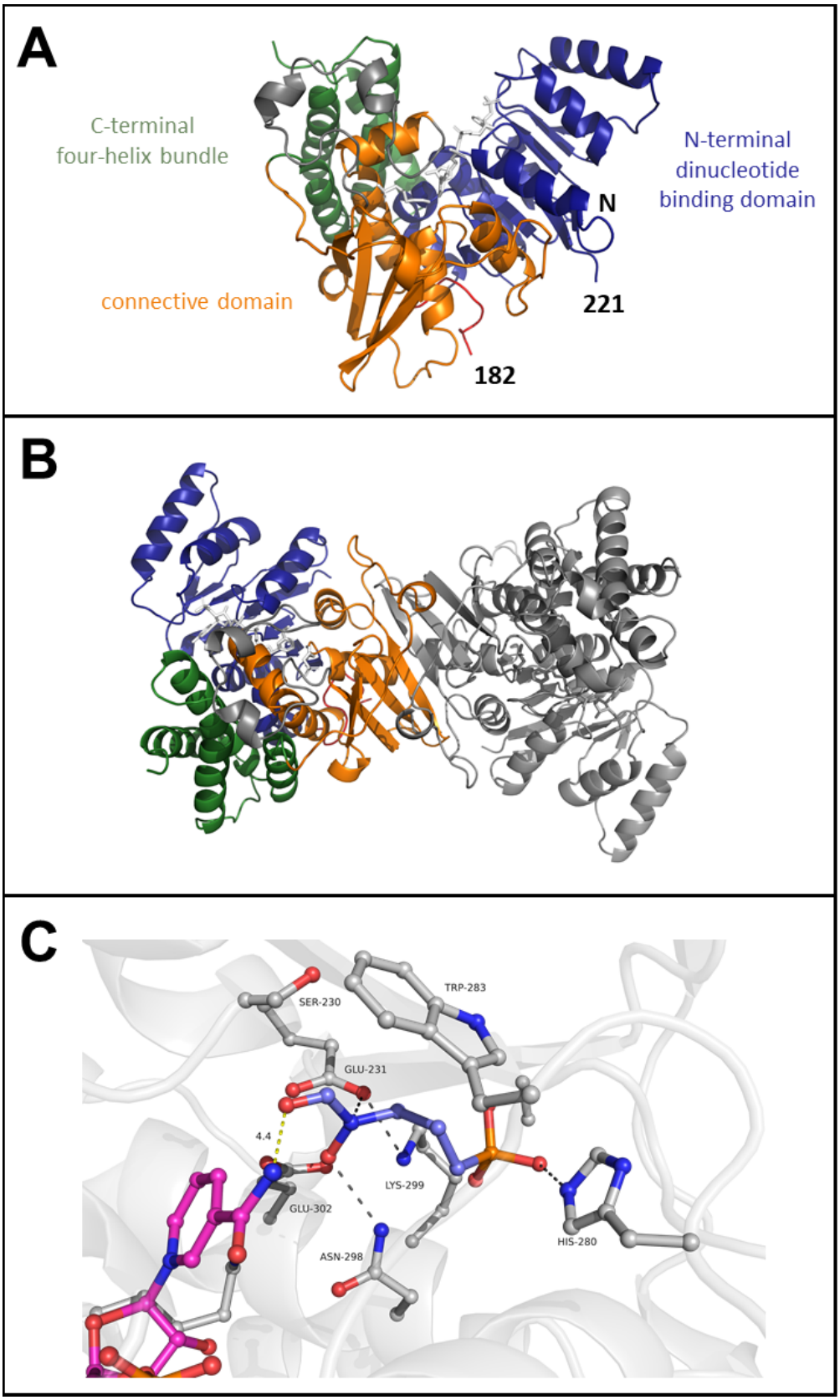

Figure 4: Structure of *Tg*DXR A

Overall structure of *Tg*DXR as observed in the crystal structure. Shown is chain A which is similar to chain B, as calculated by comparing the RMSD of both monomers after superimposing which is 0.3 Å overall. Three different domains are observed and colour coded being the N-terminal nucleotide binding domain

(blue) the connective domain (orange) and the C-terminal four helix bundle (green). **B:** The dimer of *Tg*DXR is highlighted as observed in the asymmetric unit of the crystal. The dimer interface is mediated by the connective domain highlighted in orange in chain A. **C:** The binding site of fosmidomycin is shown with in ball and stick representation. Fosmidomycin (blue) is bound via interaction with the sidechains of Glu231, His280, and Asn298. All distances are indicated with black line with a maximum distance of 3.6Å. The distance of fosmidomycin to NADPH (purple) is 4.4 Å, which is too large to allow activity.

2.2.2 Fosmidomycin binding site

Within the solvent-shielded cavity that is formed upon closure of the "lid" residues 281-285 the inhibitor backbone lies parallel to the β-indole of Trp283 at a distance of approximately 4 Å. The hydroxamic acid moiety of the inhibitor binds to the side-chain of Glu231. The sidechain of Glu231 itself is stabilized and positioned via interaction with Lys299 (**Figure 4, C**). Fosmidomycin further interacts with the sidechains of Asn298 and His280. The sidechain of Glu302 also points towards the fosmidomycin, however the distance is roughly 4 Å indicating a very weak interaction or maybe this interaction is water mediated which however cannot be conclusively modelled at this resolution.

2.2.3 Small angle X-ray scattering of *Tg*DXR

The *Tg*DXR protein was successfully crystallised and forms a dimeric conformation in solution. However, parts of the protein were not visible in the electron density, likely due to the flexibility, e.g. parts from the N-terminus and more importantly the flexible loop region from the *Tg*DXR protein. These loop regions are special in this *Tg*DXR variant and are not present in homolog structures. We used small-angle X-ray scattering to determine the structure of the *Tg*DXR protein in solution. In the SEC-SAXS elution profile (**Figure 5**, **A**; and **Figure S2**, **A**), *Tg*DXR elutes in one homogenous peak. Evaluation of the data revealed a dimer in solution with the same shape and orientation as determined by X-ray crystallography, with an R_g value of 3.33 nm and a D_{max} value of 10.44 nm (**Table S3**). With the Ensemble Optimization Method (EOM), we modelled the missing amino acids from the loop region and the N-terminus to each protomer, which completed the structure. The corresponding scattering data with the EOM fit (χ^2: 1.207) is shown in **Figure 5**, **B** and the most representative EOM model in **Figure 5, C**. The remodelled loops (37 amino acids each), covers the area between both protomers of *Tg*DXR. Its flexibility, evidenced by the absence of electron density in the crystal

structure, led us to analyse the loop's position with EOM, resulting in a 60% occupancy in this conformation.

The loop is located at the back side of the *Tg*DXR protein (**Figure 5, D**) and therefore does not play an immediate role in catalysis. Likely this highly flexible loop serves a more stabilizing function.

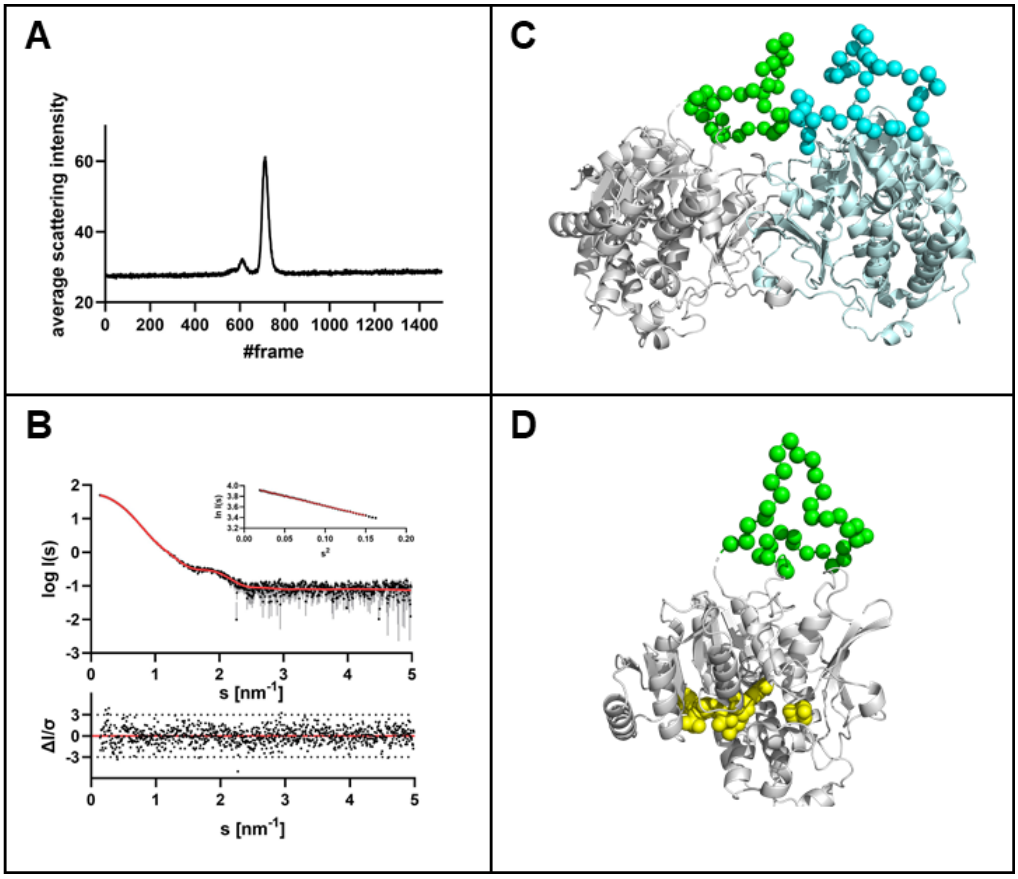

Figure 5: Small-angle X-ray scattering data from DXR and the most representative (62%) EOM model

A: Chromixs SEC SAXS elution profile. Each frame corresponds to two sec. **B:** Scattering data of *Tg*DXR. Experimental data are shown in black dots, with grey error bars. The EOM ensemble model fit is shown as red line and below is the residual plot of the data. The Guinier plot of *Tg*DXR is added in the right corner. **C:** The rigid body protomers of *Tg*DXR from the crystal are shown in grey and cyan cartoon representation. The determined flexible loop is shown as green and blue spheres. (The other EOM models can be found in the supplementary part). **D**: The SAXS completed model of *Tg*DXR is shown as monomer with the flexible loop shown in green spheres. The NADPH and fosmidomycin binding site is highlighted in yellow. It is clear that the flexible loop is remote of the active site and likely serves a more stabilizing role in the dimer of *Tg*DXR.

2.3 *In vitro* biological evaluation

2.3.1 Reverse fosmidomycin thia analogues strongly inhibits the activity of *Tg*DXR

Based on previous studies, demonstrating the effectiveness of reversed hydroxamic acid analogues of fosmidomycin (**1**) as DXR inhibitors, with either a sulphur or an oxygen atom located at the ß-methylene group of the main chain of the ligand (Brücher et al., 2012; Kunfermann et al., 2013; Lienau et al., 2019), we tested 5 reverse thia (**Figure 6, 2 – 6**) and 4 reverse oxa analogues (**Figure 6, 7 – 10)** for their enzymatic activity against the purified recombinant truncated His_{10}-*Tg*DXR and determined their inhibitory concentrations (IC_{50}) and inhibitory constant (Ki) values.

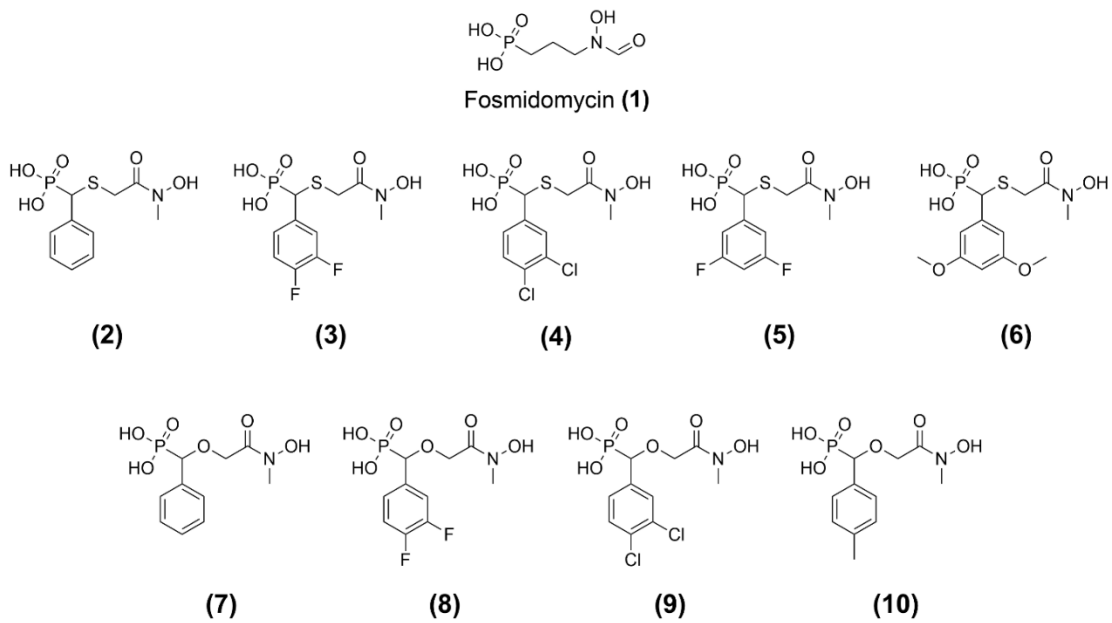

Figure 6: Chemical structures of DXR inhibitors investigated in this study

Interestingly, all the investigated compounds possessed *Tg*DXR inhibitory activity. In particular, the reverse thia isosters revealed a marked increase on the activity than the cognate reverse oxa compounds (**Figure 7**, **Table 1** and **Figure S5)**. Moreover, the substitution at positions 3 and 4 of the phenyl moiety conferred the highest inhibitory activity. The 3,4-difluorophenyl- (**3**) and 3,4-diclorophenyl- (**4**) substituted thia analogues resulted in the most active compounds with a comparable IC_{50} and Ki values lower than the thia analogue **2**, containing an unsubstituted phenyl moiety, the 3,5-difluorophenyl-

(**5**) and 3,5-dimethoxyphenyl- (**6**) substituted derivatives, and additionally, more active than **1** (**Figure 7**, **Table 1** and **Figure S5**).

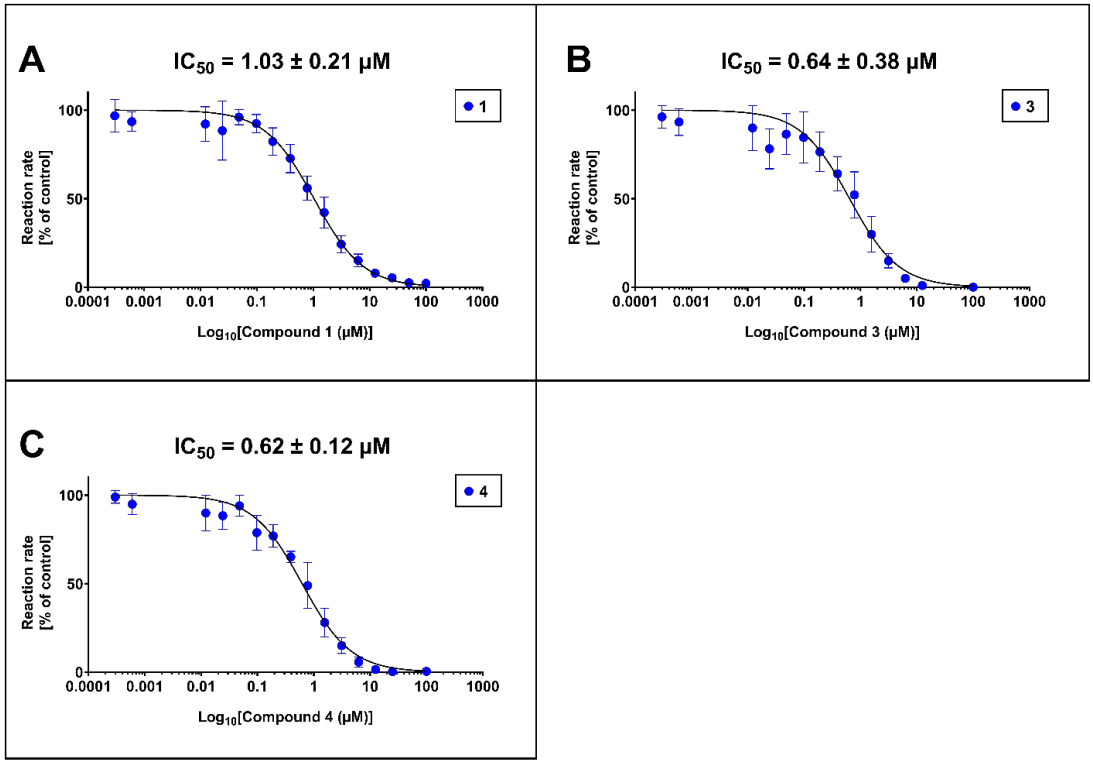

Figure 7: *In vitro* inhibition of *Tg*DXR by most potent DXR inhibitors

The enzymatic inhibitory activity of **1** (**A**), **3** (**B**) and **4** (**C**) were determined by enzymatic assays *in vitro*. Assays were performed in 96 well plates at 30 °C, containing 100 nM of purified *Tg*DXR protein in dimeric state, 100 µM of NADPH and 4 mM of $MgCl_2$ as cofactors, 100 µM of DXP as substrate in 50mM HEPES buffer (pH 7.5) containing 50 µg/mL of bovine serum albumin (BSA). The investigated compounds were tested in a concentration range of 3.05 nM to 100 µM. Data shown are from the means of three independent experiments each performed in duplicate (n = 6) ± S.D. IC_{50} values of each compound are shown.

Table 1 | *In vitro* activity (IC_{50} and K_i values) of DXR inhibitors against *Tg*DXR enzyme

Compound	IC_{50} ± S.D. (µM)	K_i (µM)
1	1.03 ± 0.21	0.31
2	1.23 ± 0.12	0.37
3	0.64 ± 0.38	0.19
4	0.62 ± 0.12	0.19
5	2.45 ± 0.54	0.74
6	3.90 ± 1.06	1.18
7	5.82 ± 1.52	2.69
8	52.14 ± 0.34	11.00
9	2.44 ± 0.43	0.74
10	7.68 ± 0.87	2.51

Values shown in the table represent the means of three independent experiments each done in duplicate (n = 6) ± S.D.

2.3.2 Reverse fosmidomycin analogues inhibit the growth of *T. gondii in vitro*

To determine if reverse thia and reverse oxa analogues of **1** (**Figure 5**) could inhibit *T. gondii* proliferation *in vitro*, we conducted an evaluation to assess their anti-parasitic activity and their IC_{50} values against the proliferation of *T. gondii* type II ME49 strain with an ^{3}[H]-uracil incorporation assay *in vitro*. Interestingly, contrary to **1** that showed no activity as also previously reported (Baumeister et al., 2011; Brown & Parish, 2008; Brücher et al., 2012; Cai et al., 2013; Kunfermann et al., 2013; Lienau et al., 2019; Nair et al., 2011)**,** the investigated compounds **3**, **4**, **5**, **6**, **7** demonstrated activity against *T. gondii* growth (**Figure 8, Table 2, Figure S6**). Moreover, as was first shown in the enzymatic assays, a marked increase in activity for the thia isosters compared to the oxa isoster was observed. Notably, the thia analogue **4** demonstrated the highest inhibitory activity (IC_{50} = 5.46 µM) (**Figure 8** , **Table 2** and **Figure S6**). This compound differ from the other thia compounds for a 3,4-dichlorophenyl on main chain of the ligand.

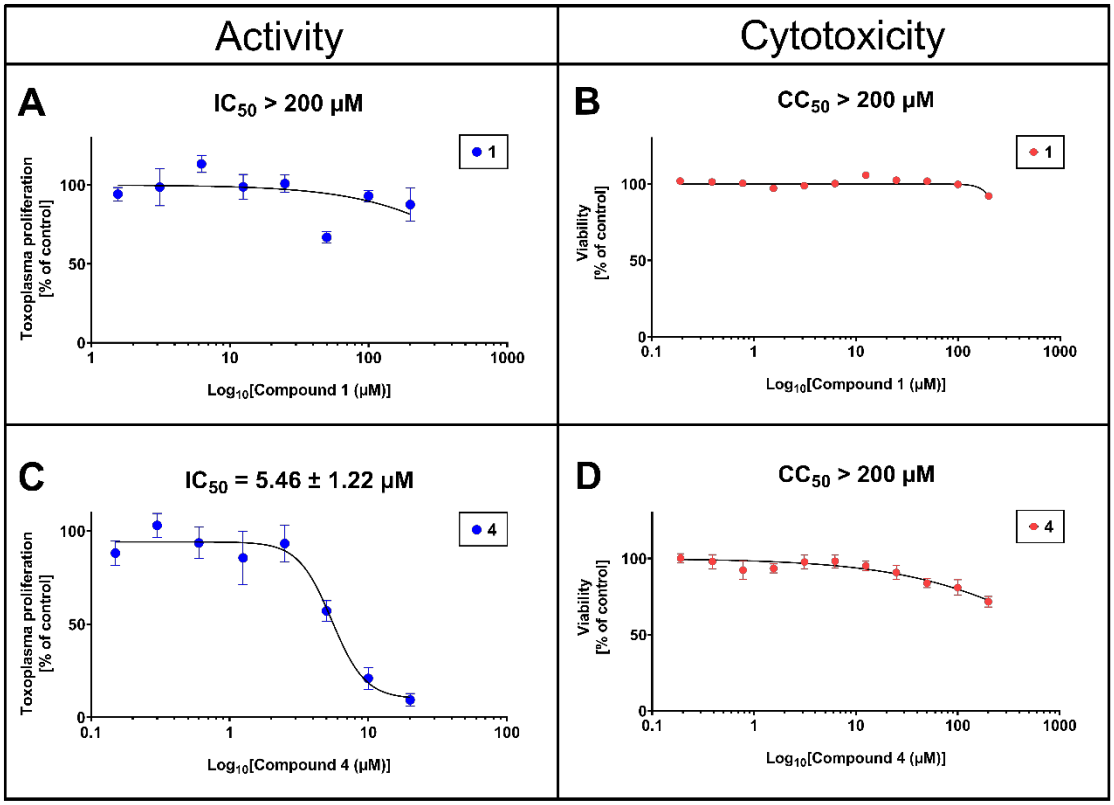

Figure 8: Anti-toxoplasma activity and cytotoxicity on human fibroblasts Hs27 of fosmidomycin and the 3,4-dichlorophenyl-thia analogue

The antiprotozoal activity of **4** (**A**) was determined by the *T. gondii* inhibition assay via the amount of [^{3}H]-uracil incorporation into the RNA of the parasite *in vitro*. Cytotoxicity of **4** (**B**) was measured by MTT assays on human fibroblasts Hs27. Data shown are the means of three independent experiments each performed in duplicate (n = 6) ± SEM. IC_{50} ± S.D. and CC_{50} values of compound **4** are shown.

Table 2 | *In vitro* activity against *T. gondii* ME49 tachyzoites and their cytotoxicity on human fibroblasts Hs27 of DXR inhibitors

Compound	IC_{50} ± S.D. (µM)	CC_{50} (µM)
1	> 200	> 200
2	> 100	> 200
3	14.39 ± 1.94	> 200
4	5.46 ± 1.22	> 200
5	55.99 ± 6.11	> 200
6	12.51 ± 5.56	> 200
7	48.20 ± 8.56	> 200
8	> 100	> 200
9	> 100	> 200
10	> 100	> 200

Values shown in the table represent the means of three independent experiments each done in duplicate (n = 6) ± S.D.

2.3.3 Reverse fosmidomycin analogues are not cytotoxic on human host cells

In order to assess the host cell cytotoxicity of the investigated compounds, MTT assays with Hs27 cells and the compounds were performed. Similar to **1**, all the reverse thia and oxa analogues did not show any detectable host cytotoxicity at the concentration range of 0.19 – 200 µM (**Figure 7, Table 2** and **Figure S6**). Therefore these compounds appear to have a good therapeutic index.

3 Discussion

Toxoplasmosis is a widespread disease and current treatment regimens are related with adverse effects and additionally, are not able to eradicate the latent phase of the infection. Thus, the identification of novel drug targets is crucial for the development of novel, potent and safer anti-toxoplasma compounds for improving the health of patients at risk of toxoplasmosis (Angel et al., 2020). The MEP pathway has been well established as a

promising drug target for novel antimicrobial agents, due to its crucial role on the viability of the microorganism and, additionally, its absence in the human host, that allows the development of novel drugs that selectively inhibit this biochemical pathway and reducing the risk of harmful side effects (Rodriguez-Concepcion, 2004).

DXR inhibitors are a class of antimicrobial agents studied intensively in *P. falciparum*, *E. coli* and *M. tuberculosis*. From previous SAR studies, it has been shown that the retro-inversion of the hydroxamate moiety of **1** and its N-methylation strongly improve the hydrophobic interaction of Trp212 of *Ec*DXR (Woo, Fernandes, & Proteau, 2006) and that the addition of the α-phenyl substitution of the N-methylated reverse fosmidomycin analogues strongly inhibits the growth of the apicomplexan parasite *P. falciparum* (Behrendt et al., 2010; Behrendt et al., 2011). Moreover, the investigation of the biosteric α-phenyl-ß-oxa and ß-thia-substituted analogues resulted in increased activity of the thia analogues against *Ec*DXR and *Mt*DXR than the cognate carba analogues, due the interaction of the sulphur atom with the conserved Met298 within the flexible loop of the enzymes (Behrendt et al., 2011; Knak et al., 2022; Kunfermann et al., 2013).

DXR inhibitors against *T. gondii* have been already investigated by Cai *et al.*, precisely α-phenyl and α-pyridine substituted fosmidomycin analogues, pyridine containing phosphonate compounds, non-hydroxamate phosphonate inhibitors containing a pyridine and 1-hydroxy-5-phenylpyridin-2-one moiety without a phosphonate group. All the compounds were active against *Tg*DXR, but none of them inhibited the parasite growth, probably due to the permeability barrier posed by parasite plasma membrane of *T. gondii* that is lacking the fosmidomycin transporter GlpT (Nair et al., 2011).

In the present study, we present the first crystal structure of *Tg*DXR in tertiary complex with NADPH and the inhibitor **1**. No magnesium ion was observed in this structure despite the fact that it is essential for activity and was included in the crystallization experiments, which also was the case for the *E.coli* DXR protein (Mac Sweeney et al., 2005). The overall structure of *Tg*DXR is resembling its counterparts in various species (Henriksson et al., 2007; Mac Sweeney et al., 2005; Reuter et al., 2002; Umeda et al., 2011). The binding site for fosmidomycin consists of the same amino acids as seen for the *Ec*DXR, indicating that the domain of *Tg*DXR is similar to the *Ec*DXR domain (**Figure 4, C**). The distance of the hydroxymate region of fosmidomycin to the NADPH is 4.4 Å, which is too large for conversion (indicated by the yellow line in **Figure 4, C**). With the substrate DXP, the distance to NADPH is reduced, as an additional bond length is strategically positioned to facilitate the occurrence of the reaction. Since the structure

is of medium resolution, we could not identify water molecules with certainty, likely however they play a role in catalysis as shown before (Mac Sweeney et al., 2005). Moreover the parts of the protein that were not visible in the electron density were determinated through SAXS, unveiling their peculiarity. With SAXS however only the position of the C-alpha atoms can be determined, and atomic detail of the side chains is lacking which would allow a more detailed description.

In addition, we performed a biological investigation on *Tg*DXR, repurposing already investigated reverse α-phenyl-ß-oxa and ß-thia-substituted analogues of (**1**) which were previously described as potent inhibitors of *P. falciparum*, *E. coli* and *M. tuberculosis* DXR enzymes (Brücher et al., 2012; Kunfermann et al., 2013; Lienau et al., 2019) against the activity of *T*gDXR and for inhibition of *T. gondii* proliferation. We show that all the investigated compounds possess *Tg*DXR inhibitor activity, with the thia analogues presenting a more pronounced activity than the reverse oxa analogues. Moreover, we noticed that the 3,4 halogen substitution of the phenyl moiety of the reverse thia analogues confers the highest potency against the enzyme activity of *T*gDXR. In the cell-based assays, we demonstrated that reverse analogues **3** - **7** inhibit *T. gondii* proliferation in contrast to (**1**). Once more, we observed a trend within the thia analogues, showing higher potency compared to the cognate oxa analogues. Furthermore, in this context, the reverse 3,4-dichlorophenyl substituted compound **4** emerged as the most potent one in inhibiting *T. gondii* proliferation, with an IC_{50} of 5.46 µM, presumably due the improved lipophilicity of the 3,4-dichlorophenyl substitution that enhance cellular uptake (Haemers et al., 2006).

4 Conclusions

In summary, in the present study we report for the first time the X-ray structure of *Tg*DXR co-crystallized with fosmidomycin and the cofactor NADPH and its biochemical characterization, as well as the identification of reverse α-phenyl-ß-thia- and oxa-isosters of fosmidomycin as novel anti-*T. gondii* agents with *Tg*DXR inhibitory activity. The x-ray structure of *Tg*DXR and all the information it provide could support the future design, target-based optimization and development of novel DXR inhibitors against *T. gondii*. Further studies are needed for the identification of enhanced derivatives and to explore the efficacy and the mode of action *in vivo*.

5 Material and Methods

5.1 Biochemical characterisation

5.1.1 Sequence alignment

The amino acid sequence of the investigated protein *Tg*DXR (NCBI Reference Sequence: XP_018635719.1) was compared with a multiple sequence alignment using Clustal Omega sequence analysis tool (https://www.ebi.ac.uk/Tools/msa/clustalo/) (Madeira et al., 2022) with its default settings with DXR enzymes from other species that have been extensively studied: *P. falciparum* DXR (*Pf*DXR, NCBI Reference Sequence: AAD03739.1), *M. tuberculosis* DXR (*Mt*DXR, NCBI Reference Sequence: OHO19719.1) and *E. coli* DXR (*Ec*DXR, NCBI Reference Sequence: WP_302347400.1) and visualized and the percentage of identity analysed with Jalview software version 2.11.2.7 (Waterhouse, Procter, Martin, Clamp, & Barton, 2009) (**Figure S1**).

5.1.2 *Tg*DXR

The gene of 1-deoxy-D-xylulose 5-phosphate reductoisomerase of *T. gondii* (*Tg*DXR) ME49 strain was identified using ToxoDB database (http://ToxoDB.org). The gene of *Tg*DXR (NCBI: NC_031478.1), optimized for expression in *Escherichia coli* (*E. coli*), was obtained from GenScript (Piscataway Township, NJ, USA) as a synthetic gene subcloned into the pET-16b plasmid, using NdeI/BamHI restriction sites. The resulting expressed protein carries an N-terminal decahistidine tag (His_{10}). However, the purification of the recombinant His_{10}-tagged *Tg*DXR proved to be challenging. To overcome these issues and generate a soluble recombinant protein, another expression plasmid was designed. We deleted 181 amino acids (2 – 182) of the *Tg*DXR sequence representing the bipartite apicoplast targeting peptide (Cai et al., 2013) in order to generate a soluble truncated His_{10}-tagged *Tg*DXR contain the sequence of the catalytic domain (**Figure S1**).

5.1.3 Cloning of truncated His_{10}-*Tg*DXR and construction of the expression plasmid

The generation of the truncated His_{10}-*Tg*DXR commenced with the deletion of 181 amino acids via Site-Directed-Mutagenesis method (Carter, 1986). For this purpose, the coding sequence of the truncated *Tg*DXR was amplified from the pET-16b plasmid construct with a polymerase chain reaction (PCR) (Manual, 2017) using the primers TgDXR-del181AA_For and TgDXR-del181AA_REV (**Table S1**). Then, the coding sequence was purified through an 1% agarose gel purification (Lee, Costumbrado, Hsu, & Kim, 2012) and ligate with a KLD- Enzyme Mix (KLD Enzyme Mix, New England BioLabs, Frankfurt am Main, Germany, #M0554S) and the plasmids transformed into an *E.coli* DH5α (DH5α Competent Cells, Thermo Fisher Scientific, Waltham, MA, USA, #EC0112), streaked onto Luria-Bertani (LB) agar-plates containing ampicillin (100µg/mL) (Ampicillin, Thermo Fisher Chemicals, Thermo Fisher Scientific, Waltham, MA, USA, #J60977.14). To confirm the successful cloning, positive clones were identified through PCR. Additionally, DNA sequencing was performed using T7 forward and reverse primers for further verifications. The plasmid was extracted with a plasmid miniprep kit (Monarch® Plasmid Miniprep Kit, New England BioLabs, Frankfurt am Main, Germany, #T1010L).

5.1.4 Expression of truncated His_{10}-*Tg*DXR

The expression plasmid *Tg*DXR was transformed into the chemically competent *E. coli* BL21 (DE3) cells (BL21 (DE3) Singles™ Competent Cells – Novagen, Merck KGaA, Darmstadt, Germany, #70235). Then *E. coli* transformants were streaked onto Lauria-Bertani (LB) agar-plates containing ampicillin (100µg/mL) (Ampicillin, Thermo Fisher Chemicals, Thermo Fisher Scientific, Waltham, MA, USA, #J60977.14) and incubated overnight at 37°C.

To express the His-tagged protein, 100 mL overnight pre-cultures were prepared using fresh colonies from LB agar plates or 50% glycerol cryo stock stored at -80°C. The day after, 1 liter (L) of freshly prepared and autoclaved LB media (10g Triptone, 5g yeast extract and 5 NaCl) was supplemented with 100 µg/mL of ampicillin and inoculated with the pre-cultures to an optical density at 600 nm (OD_{600}) of 0.1. The main culture was then incubated with shaking at 37°C and 180 rpm. At an OD_{600} of 0.6, protein expression was induced with the supplementation in the culture of isopropyl-β-D-thiogalactopyranosid

(IPTG, Merck KGaA, Darmstadt, Germany, #I6758) to a final concentration of 1 mM. The main culture was further incubated for additional 2 hours with shaking at 37°C and 180 rpm. Afterwards, cells were harvested via centrifugation at 5,000 g, for 15 min at 4°C (rotor SLC-6000, Sorvall, Thermo Fischer, Waltham, MA, USA), the supernatant discarded, the pellet used subsequently or snap frozen in liquid nitrogen and short-term stored at -20°C.

5.1.5 Purification of truncated His_{10}-*Tg*DXR

Truncated His_{10}-*Tg*DXR purification involved two main steps: immobilized metal ion affinity chromatography (Ni-IMAC) and size exclusion chromatography (SEC).
Cells were thawed at 4°C and suspended with ice-cold lysis buffer A (50 mM NaH_2PO_4, 300 mM NaCl, 20 mM imidazole, pH 8) supplemented with protease inhibitor cocktail (cOmplete Protease Inhibitor Cocktail, Roche, Basel, Switzerland). Subsequently, cell lysis was performed through the application of shear force using a cell disruptor/homogenizer (M-110P Microfluidizer, Microfluidics Inc., Westwood, MA, USA). This method was employed to effectively broke down the cells and release their content. To eliminate cell membranes and other insoluble detritus, ultracentrifugation of the lysate was performed at 45000 rpm, for 45 min at 4°C (Beckman Optima XE, Beckman Coulter Inc., Brea, CA, USA). Then, the collected supernatant was purified via Ni-IMAC at 4 °C on a Ni^{2+} pre-treated HiTrap IMAC FF 5mL column (Cytiva life science, Marlborough, MA, USA, #17092104) using a protein purification system (Äkta purifier 10, GE Healthcare, Chicago, IL, USA). The protein was loaded on the column with a flow rate of 1 mL/min. After binding, the resin was washed with buffer B (50 mM NaH_2PO_4, 150 mM NaCl, 20 mM imidazole, pH 8) with the aim of remove the nonspecifically bound proteins. Afterwards, the protein then eluted with gradually increasing concentration of imidazole with buffer C (50 mM NaH_2PO_4, 150 mM NaCl, 300 mM imidazole, pH 8). As determined by absorption at λ 280 nm, the fractions containing proteins were then pooled, concentrated and subjected to a SEC to further improve its purity. SEC was performed on Äkta purifier 10 equipped with a pre-equilibrated Superdex 200 Increase 10/300 GL column (Cytiva life science, Marlborough, MA, USA, #28990944) at a flow rate of 0.5 ml/min with buffer D (20 mM Tris/HCl, 150 mM NaCl, 2% Glycerol pH 7.5). Dimeric protein was collected, concentrated, aliquoted and snap frozen for their storage at −80°C.

5.1.6 Determination of Protein concentration

The concentration of the protein was assessed by measuring its absorbance with a microvolume UV-Vis spectrophotometer (NanoDrop ™ One, Thermo Fisher Scientific, MA, USA) using protein-specific parameters, including the molecular weight (51,808 Da) and the extinction coefficient of the protein (34,420 M^{-1} cm^{-1}) obtained with the web-software tool Expasy ProtParam (Gasteiger et al., 2005).

5.1.7 Sodium Dodecyl Sulfate Polyacrylamide Gel Electrophoresis (SDS-PAGE)

After IMAC and SEC, in order to detect the fraction contain the desired protein and assess its purity and integrity, Sodium Dodecyl Sulfate – PolyAcrylamid Gel Electrophoresis (SDS-PAGE) was performed (**Figure 4**) following the method described by Laemmli (1970)(Laemmli, 1970). In brief, 10 µg of protein samples were mixed with a 5x protein loading buffer (Pierce™ Lane Marker Reducing Sample Buffer, Thermo Fisher Scientific, Waltham, MA, USA, #39000). Then, the mixture was boiled at 98°C for 5 min, thawed at room temperature and loaded onto a polyacrylamide gel (NuPAGE™ 4-12% Bis-Tris Gel, Invitrogen™, Thermo Fisher Scientific, Waltham, MA, USA, #NP0335BOX), including a prestained ladder (PageRuler™ Prestained Protein Ladder, Thermo Scientific™, Thermo Fisher Scientific, Waltham, MA, USA, # 26616). The polyacrylamide gel was placed into a gel chamber (XCELL SureLock Mini-Well, Invitrogen™, Thermo Fisher Scientific, Waltham, MA, USA, #EI0002), containing a SDS running buffer (20x NuPAGE™ MOPS SDS Running buffer, Thermo Fisher Scientific, Waltham, MA, USA, #NP000102). After the electrophoresis separation at 120V for 1 hour, the polyacrylamide gel was incubated with a Coomassie dye solution (PageBlue™ Protein Staining Solution, Thermo Fisher Scientific, Waltham, MA, USA, #24620). Gel imaging and visual documentation was employed with a gel imaging systems (Gel Doc XR^+ Gel Documentation System, Bio-Rad Laboratories GmbH, Hercules, CA, USA).

5.1.8 *T. gondii* DXR enzyme kinetic characterization and optimisation

In order to biochemically characterize the catalytic ability of the truncated *Tg*DXR for the conversion of DXP into MEP in the presence of the cofactors Mg^{2+} and NADPH, and to determine the optimum conditions for maximum enzyme activity, the enzymatic assays were monitored at 340 nm (maximal absorbance of NADPH) in different conditions.

The enzymatic activity was evaluated in fixed conditions, using 50mM HEPES buffer containing 50 µg/mL of bovine serum albumin (BSA) containing 100 nM of purified *Tg*DXR protein in dimeric state. In each experimental evaluation, only one parameter was varied: either the substrate (DXP) concentration (ranging from 7.8 µM to 500 µM), or the cofactor NADPH (ranging from 7.8 µM to 500 µM), or Mg^{2+}´concentration (ranging from 1 mM to 6 mM) or the pH (ranging from 5.5 to 9) (**Figure 4**)

For the determination of the kinetic parameters, various concentration of the substrate DXP or NADPH were employed for the determination of the apparent K_m (substrate concentration that yield a half-maximal velocity) and V_{max} (maximum velocity) for the enzyme. These parameters where calculated by a non-linear regression with the software GraphPad PRISM™ (Version 9.5.1; San Diego, CA) plotting the initial velocity of the reactions and using the Michaelis-Menten model (**Figure 4**).

5.2 Structural characterisation of the DXR catalytic domain

5.2.1 Crystallization and structure determination of *Tg*DXR

*Tg*DXR was crystallized by sitting-drop vapor-diffusion at 12 °C at a concentration of 20 mM TRIS pH 7.5, 150 mM NaCl, 2% glycerol mit 1 mM Fosmidomycin. Crystals formed after a couple of days, were harvested cryo-protected with 20% ethylene glycol, washed in mineral oil and flash frozen in liquid nitrogen. Diffraction data were collected at 100 K at beamline ID23-1 (ESRF, Grenoble, France) using a 0.9793 Å wavelength. Data reduction was performed using XDS (Kabsch, 2010) and aimless (Evans & Murshudov, 2013) from the CCP4 suite (Winn et al., 2011). The structure was solved via molecular replacement with Phaser (McCoy et al., 2007). The initial model was refined alternating cycles of manual model building in COOT (Emsley & Cowtan, 2004; Emsley, Lohkamp, Scott, & Cowtan, 2010) and automatic refinement using Phenix (Liebschner et al., 2019) version 1.19.2_4158. Data collection and refinement statistics are reported in **Table S2**.

5.2.2 Small-angle-X-ray-scattering from DXR

We collected the SEC-SAXS data on beamline BM29 at the ESRF Grenoble (Pernot et al., 2013; Pernot et al., 2010). The BM29 beamline was equipped with a PILATUS 2M detector (Dectris) at a fixed distance of 2.827 m.

The SEC-SAXS measurement was performed at 10°C with a DXR protein concentration of 8.00 mg/ml. The SEC-SAXS run was performed on a Superdex 200 increase 10/300 column (300 µl inject, Buffer: 20 mM Tris/HCl, 150 mM NaCl, 40 mM $MgCl_2$, 2% glycerol, pH 7.5) with a flowrate of 0.5 ml/min. We collected 1500 frames with an exposer time of 2 sec/frame and scaled the data to absolute intensity against water.

All used programs for data processing were part of the ATSAS Software package (Version 3.0.5) (Manalastas-Cantos et al., 2021). Primary data reduction was performed with the programs CHROMIXS (Panjkovich & Svergun, 2017) and PRIMUS (Konarev, Volkov, Sokolova, Koch, & Svergun, 2003). With the Guinier approximation (Guinier, 1939), we determine the forward scattering *I(0)* and the radius of gyration (R_g). The program GNOM (Svergun, 1992) was used to estimate the maximum particle dimension (D_{max}) with the pair-distribution function *p(r)*. We used the partially solved crystal structure as template in an Ensemble Optimization Method (EOM) (Bernado, Mylonas, Petoukhov, Blackledge, & Svergun, 2007; Tria, Mertens, Kachala, & Svergun, 2015) and added the missing amino acids from the loop region and the N-terminus to each protomer.

5.2.3 Visualization and analysis of molecular structures

For figure preparation of the crystal structures of *Tg*DXR enzyme we utilized PyMOL software suite (www.pymol.org) (DeLano, 2002).

5.3 *In vitro* biological evaluation

5.3.1 Compounds

Fosmidomycin (**1**) (Fosmidomycin sodium salt, Invitrogen, Thermos Fisher Scientific, Waltham, MA, USA, #FR-31564) was dissolved in Dulbecco´s Phosphate Buffered Saline (DPBS (1x), Gibco-Thermo Fisher Scientific, Waltham, MA, USA, #14190144). DXR inhibitors (((2-(hydroxy(methyl)amino)-2-oxoethyl)thio)(phenyl)methyl)phosphonic acid (**2**); ((3,4-difluorophenyl)((2-

(hydroxy(methyl)amino)-2-oxoethyl)thio)methyl)phosphonic acid (**3**), ((3,4-dichlorophenyl)((2-(hydroxy(methyl)amino)-2-oxoethyl)thio)methyl)phosphonic acid (**4**), ((3,5-difluorophenyl)((2-(hydroxy(methyl)amino)-2-oxoethyl)thio)methyl)phosphonic acid (**5**), ((3,5-dimethoxyphenyl)((2-(hydroxy(methyl)amino)-2-oxoethyl)thio)methyl)phosphonic acid (**6**), ((2-(hydroxy(methyl)amino)-2-oxoethoxy)(phenyl)methyl)phosphonic acid (**7**), ((3,4-difluorophenyl)(2-(hydroxy(methyl)amino)-2-oxoethoxy)methyl)phosphonic acid (**8**), ((3,4-dichlorophenyl)(2-(hydroxy(methyl)amino)-2-oxoethoxy)methyl)phosphonic acid (**9**), ((2-(hydroxy(methyl)amino)-2-oxoethoxy)(p-tolyl)methyl)phosphonic acid (**10**) employed in this study (**Figure 5**) were prepared using procedures from previously published methods (Brücher et al., 2012; Kunfermann et al., 2013; Lienau et al., 2019) and dissolved in DMSO (Dimethyl sulfoxide, ≥99%, Thermo Scientific Chemicals, Waltham, MA, USA, #A12380.36). Staurosporine (Merck, Darmstadt, Germany, #S4400) was dissolved in DMSO. All the compounds were prepared as 10 mM stock solutions and stored at -20 °C. Before use, these solutions were thawed and diluted in culture medium to produce the appropriate concentrations (ranging from 0.0003 to 200 µM).

5.3.2 *T.gondii* DXR enzyme inhibition assays

The enzymatic assays were conducted at 30 °C in 96 well plates using a total reaction volume of 150 µL containing 100 nM of purified *Tg*DXR protein in dimeric state, 100 µM of NADPH and 4 mM of $MgCl_2$ as cofactors, 100 µM of DXP as substrate in 50mM HEPES buffer (pH 7.5) containing 50 µg/mL of bovine serum albumin (BSA). For the screening, DXR inhibitors were tested for their inhibitory activity and their IC_{50} measurements at concentrations ranging from 100 µM to 3.05 nM, in dilution steps 1:2.
To optimize and ensure the interaction of NADPH and its enzyme binding pocket, the assay solution was incubated for 10 min at 37°C. Then, the reaction was commenced with the addiction of 100 µM of DXP to the complete assay mixture. The reaction was monitored by measuring the absorption at 340 nm every minute for 1 hour using a microplate reader (Tecan® 200 Pro, Tecan group, Männedorf, Switzerland). The initial velocity of the reactions were calculated, the values were then used in the software GraphPad PRISM™ (Version 9.5.1; San Diego, CA) for the determinations of the IC_{50} value. The inhibitor constant values (Ki) of all inhibitors were determinated using the

Michaelis-Menten formula $K_i = IC_{50}/(1+[S]/K_m)$, [S] is the concentration of DXP (100 µM) and K_m was calculated as 30.58 µM.

5.3.3 *Toxoplasma gondii* and host cells in vitro culture

T. gondii tachyzoites of the ME49 strain (ATCC/LGC Standards GmbH, Wesel, Germany, #50611), were cultured and maintained by repeat passage in monolayers of human foreskin fibroblasts Hs27 (ATCC/LGC Standards GmbH, Wesel, Germany, #CRL-1634) as host cells. Cultures were grown in Iscove's Modified Dulbecco's medium (IMDM; Gibco-Thermo Fisher Scientific, Waltham, MA, USA, #12440053) supplemented with 10% heat-inactivated fetal bovine serum (FBS Standard; South America origin, fetal bovine serum, 2µm sterile filtered, PAN-Biotech, Aidenbach, Germany, #P30-3306) and 50 mM 2-mercaptoethanol (Gibco-Thermo Fisher Scientific, Waltham, MA, USA, #21985023) at 37°C and 5% CO_2 as previously described (Klischan et al., 2023; Mazzone et al., 2022; Merkt et al., 2021).

5.3.4 *Toxoplasma gondii* in vitro growth assay

With the aim to assess the inhibitory *in vitro* effect on parasite growth, *T. gondii* growth assays were performed as described previously (Klischan et al., 2023; Mazzone et al., 2022; Merkt et al., 2021). Compounds, previously diluted in culture media in appropriate stock solutions, were added to confluent monolayers of Hs27 cells in 96-flat well plates at various concentrations. Then, freshly harvested tachyzoites were added to the cultures at a multiplicity of infection (MOI) of 1:1 (parasite/host cell ratio). As controls, untreated and uninfected Hs27 cells, 24 hours pre-stimulated and *T. gondii* infected cells with human interferon γ (IFN γ) (300 U/ml) (Merck, Darmstadt, Germany, #I17001) and *T. gondii* infected cells only were employed. After 48h incubation, proliferating toxoplasmas were labeled with 0.3 µCi/well of tritiated uracil (^{3}H-U; 5 mCi, Hartmann Analytic, Braunschweig, Germany, #ART1782) (Pfefferkorn & PFEFFERKORN, 1977). After 28 – 30 hours of incubation, plates were frozen at -20°C overnight. Cells were then thawed and harvested (Basic96 Harvester; Zinsser Analytic, Skatron Instruments, Northridge, CA, USA), purified with glass fiber filters (Printed Filtermat A 102 mm × 258 mm; PerkinElmer, Waltham, MA, USA) and dried at 130 °C for 15 – 20 minutes. Dried filters were then wrapped into transparent plastic covers, dunked with 10 mL scintillation cocktail (Betaplate Scint; PerkinElmer, Waltham, MA, USA, #1205-440),

sealed and then loaded into metal cassettes and the incorporation of ^{3}H-uracil into the RNA of proliferating toxoplasmas was measured using a ß-counter, a liquid scintillation counter that measure the Cherenkov radiation (Betaplate Liquid Scintillation Counter 1205; LKB-WALLAK, Melbourne, Australia). All data sets were normalized to 100% of the positive control. The dose-response curves of the compounds were fitted by means of the statistics software GraphPad PRISM^{TM} (Version 9.5.1; San Diego, CA). The minimal concentrations of compounds required for 50% inhibition of the parasite (IC_{50} values) were determined by non-linear regression analysis.

5.3.5 Cytotoxicity assays

The method based on the reduction of the tetrazolium dye MTT [3- (4,5-dimethylthiazole-2-yl)-2,5-diphenyltetrazolium bromide] to its purple insoluble formazan by mitochondrial NAD(P)H-dependent cellular oxidoreductase enzymes in living cells, previously described by Mosmann (Mosmann, 1983) was employed to assess the cytotoxic effects of the examined DXR inhibitors on the host cells, as previously described (Klischan et al., 2023; Mazzone et al., 2022; Merkt et al., 2021). Briefly, Hs27 cells were cultured in 96-well plates at a concentration of $5x10^{4}$/well in Iscove's modified Dulbecco's medium (IMDM, Gibco–Thermo Fisher Scientific, Waltham, MA, USA, #12440053) with a volume of 100 µL per well and incubated at 37°C overnight. Then, eleven two-fold serially diluted concentrations of the investigated compounds ranging from 200 to 0.09 µM were prepared and added to each well. Hs27 cells were then incubated for 24 hours in humidified atmosphere of 5 % CO2 in air. Controls included, wells containing medium alone without cells (blank), untreated Hs27 cell, DMSO (negative control) and staurosporine (0.031, 0.062, 0.125, 0.25, 0.5, 1 µM) (Merck, Darmstadt, Germany, #S4400) as apoptosis inducer (Belmokhtar, Hillion, & Ségal-Bendirdjian, 2001) were employed. After incubation time, the culture media was replaced with 100 µL of DMEM medium without phenol (Gibco-Thermo Fisher Scientific, Waltham, MA, USA, #21041025) plus 10 % heat-inactivated fetal bovine serum (FBS Standard, South America origin, fetal bovine serum, 2µm sterile filtered, PAN-Biotech, Aidenbach, Germany, #P30-3306), and 50 mM 2-mercaptoethanol (Gibco-Thermo Fisher Scientific Waltham, MA, USA, #21985023). Thereafter, the MTT reagent was added to each well and analysis conducted following the manufacture instructions (CyQuant MTT Cell Viability Assay Kit, Thermo Fisher Scientific, Waltham, MA, USA, #V-13154). The absorbance was

measured at 570 nm on an ELISA microplate reader (TECAN Sunrise, Männedorf, Switzerland) and the percentage of viability was calculated when compared to untreated control. The data set was subsequently adjusted by applying blank correction. Cell viability values expressed as percentage of the negative control value were calculated as follows:

$$\%\ \text{Cell viability} = \frac{\text{mean absorbance of treated wells} - \text{blank}}{\text{mean absorbance of negative control} - \text{blank}}\ x\ 100$$

The cytotoxicity of each compound was expressed as half maximal cytotoxic concentration (CC_{50} values) against Hs27 cells. These values were calculated by a non-linear regression using GraphPad PRISM^{TM} statistics software package (Version 9.5.1; San Diego, CA) plotting the percentage viability against the log of compound concentrations.

6 Author contribution

F.M. performed all experiments and wrote the first draft of the manuscript; J.R. J.G., A.H., M.W., T.K., S.H.J.S., K.P. designed and supervised the experiments, assisted in drafting and critical reading; M.A.A. provided the investigated molecules; F.M., S.H.J.S. wrote the manuscript. K.P. corrected and proofed the manuscript. All authors discussed and contributed to the article and approved the submitted version.

7 Funding

This work was supported by the Deutsche Forschungsgemeinschaft (DFG, German Research Foundation)–project number 270650915/GRK 2158 (to TK, SHJS, and KP). The Center for Structural Studies (CSS) is funded by the DFG (Grant number 417919780 NST 208/740-1 FUGG and INST 208/761-1 FUGG to S.S.).

8 Acknowledgements

We gratefully acknowledge the DFG (GRK2158), the Heinrich Heine University (HHU) for their generous support. We thank Karin Buchholz, Daniel Degrandi and Ursula Sorg for scientific consultation. Furthermore, we thank Christian Mammen for experimental assistance and Eymen Hachani for MALS-SEC measurement and analysis. We acknowledge the European Synchrotron Radiation Facility for provision of synchrotron radiation facilities and we would like to thank Petra Pernot for assistance in using

beamline BM29. We also thank the beamline staff of the beamline ID23-1 at the ESRF for help during remote collection of the data. Initial crystals were also tested at the EMBL beamline at the DESY synchrotron in Hamburg, Germany which we would also like to acknowledge.

9 Conflict of interest

The authors declare that they have no conflicts of interest with the content of this article.

10 Data availability Statements

All supporting data are included within the main article and its supplementary files. We uploaded the SAXS data to the Small Angle Scattering Biological Data Bank (SASBDB) (Kikhney, Borges, Molodenskiy, Jeffries, & Svergun, 2020), with the accession codes SASDS47.

11 References

Alday, P. H., & Doggett, J. S. (2017). Drugs in development for toxoplasmosis: advances, challenges, and current status. *Drug design, development and therapy, 11*, 273-293. doi:10.2147/dddt.S60973

Allamand, A., Piechowiak, T., Lièvremont, D., Rohmer, M., & Grosdemange-Billiard, C. (2023). The Multifaceted MEP Pathway: Towards New Therapeutic Perspectives. *Molecules, 28*(3), 1403.

Andaloussi, M., Henriksson, L. M., Więckowska, A., Lindh, M., Björkelid, C., Larsson, A. M., . . . Karlén, A. (2011). Design, Synthesis, and X-ray Crystallographic Studies of α-Aryl Substituted Fosmidomycin Analogues as Inhibitors of Mycobacterium tuberculosis 1-Deoxy-d-xylulose 5-Phosphate Reductoisomerase. *Journal of Medicinal Chemistry, 54*(14), 4964-4976. doi:10.1021/jm2000085

Angel, S. O., Vanagas, L., Ruiz, D. M., Cristaldi, C., Saldarriaga Cartagena, A. M., & Sullivan Jr, W. J. (2020). Emerging therapeutic targets against Toxoplasma gondii: update on DNA repair response inhibitors and genotoxic drugs. *Frontiers in Cellular and Infection Microbiology, 10*, 289.

Ball, H. S., Girma, M. B., Zainab, M., Soojhawon, I., Couch, R. D., & Noble, S. M. (2021). Characterization and inhibition of 1-Deoxy-d-Xylulose 5-phosphate reductoisomerase: a promising drug target in Acinetobacter baumannii and Klebsiella pneumoniae. *ACS Infectious Diseases, 7*(11), 2987-2998.

Basavaraju, A. (2016). Toxoplasmosis in HIV infection: An overview. *Trop Parasitol, 6*(2), 129-135. doi:10.4103/2229-5070.190817

Baumeister, S., Wiesner, J., Reichenberg, A., Hintz, M., Bietz, S., Harb, O. S., . . . Seeber, F. (2011). Fosmidomycin uptake into Plasmodium and Babesia-infected erythrocytes is facilitated by parasite-induced new permeability pathways. *PloS one, 6*(5), e19334. doi:10.1371/journal.pone.0019334

Behrendt, C. T., Kunfermann, A., Illarionova, V., Matheeussen, A., Gräwert, T., Groll, M., . . . Fischer, M. (2010). Synthesis and antiplasmodial activity of highly active reverse analogues of the antimalarial drug candidate fosmidomycin. *ChemMedChem, 5*(10), 1673-1676.

Behrendt, C. T., Kunfermann, A., Illarionova, V., Matheeussen, A., Pein, M. K., Gräwert, T., . . . Illarionov, B. (2011). Reverse fosmidomycin derivatives against the antimalarial drug target IspC (Dxr). *Journal of Medicinal Chemistry, 54*(19), 6796-6802.

Belmokhtar, C. A., Hillion, J., & Ségal-Bendirdjian, E. (2001). Staurosporine induces apoptosis through both caspase-dependent and caspase-independent mechanisms. *Oncogene, 20*(26), 3354-3362.

Bernado, P., Mylonas, E., Petoukhov, M. V., Blackledge, M., & Svergun, D. I. (2007). Structural characterization of flexible proteins using small-angle X-ray scattering. *J Am Chem Soc, 129*(17), 5656-5664. doi:10.1021/ja069124n

Brown, A. C., & Parish, T. (2008). Dxr is essential in Mycobacterium tuberculosis and fosmidomycin resistance is due to a lack of uptake. *BMC microbiology, 8*, 1-9.

Brücher, K., Illarionov, B., Held, J., Tschan, S., Kunfermann, A., Pein, M. K., . . . Kurz, T. (2012). α-Substituted β-Oxa Isosteres of Fosmidomycin: Synthesis and Biological Evaluation. *Journal of Medicinal Chemistry, 55*(14), 6566-6575. doi:10.1021/jm300652f

Cai, G., Deng, L., Xue, J., Moreno, S. N., Striepen, B., & Song, Y. (2013). Expression, characterization and inhibition of Toxoplasma gondii 1-deoxy-D-xylulose-5-phosphate reductoisomerase. *Bioorganic & Medicinal Chemistry Letters, 23*(7), 2158-2161.

Carter, P. (1986). Site-directed mutagenesis. *Biochemical Journal, 237*(1), 1.

Deganich, M., Boudreaux, C., & Benmerzouga, I. (2022). Toxoplasmosis infection during pregnancy. *Tropical Medicine and Infectious Disease, 8*(1), 3.

DeLano, W. L. (2002). The PyMOL molecular graphics system. *http://www. pymol. org/*.

Dhiman, R. K., Schaeffer, M. L., Bailey, A. M., Testa, C. A., Scherman, H., & Crick, D. C. (2005). 1-Deoxy-D-xylulose 5-phosphate reductoisomerase (IspC) from Mycobacterium tuberculosis: towards understanding mycobacterial resistance to fosmidomycin. *Journal of bacteriology, 187*(24), 8395-8402.

Dunay, I. R., Gajurel, K., Dhakal, R., Liesenfeld, O., & Montoya, J. G. (2018). Treatment of toxoplasmosis: historical perspective, animal models, and current clinical practice. *Clinical Microbiology Reviews, 31*(4), 10.1128/cmr. 00057-00017.

Emsley, P., & Cowtan, K. (2004). Coot: model-building tools for molecular graphics. *Acta Crystallogr D Biol Crystallogr, 60*(Pt 12 Pt 1), 2126-2132. doi:10.1107/s0907444904019158

Emsley, P., Lohkamp, B., Scott, W. G., & Cowtan, K. (2010). Features and development of Coot. *Acta Crystallogr D Biol Crystallogr, 66*(Pt 4), 486-501. doi:10.1107/s0907444910007493

Evans, P. R., & Murshudov, G. N. (2013). How good are my data and what is the resolution? *Acta Crystallogr D Biol Crystallogr, 69*(Pt 7), 1204-1214. doi:10.1107/s0907444913000061

Frank, A., & Groll, M. (2017). The Methylerythritol Phosphate Pathway to Isoprenoids. *Chemical reviews, 117*(8), 5675-5703. doi:10.1021/acs.chemrev.6b00537

Gasteiger, E., Hoogland, C., Gattiker, A., Duvaud, S. e., Wilkins, M. R., Appel, R. D., & Bairoch, A. (2005). *Protein identification and analysis tools on the ExPASy server*: Springer.

Guinier, A. (1939). Diffraction of X-rays of very small angles-application of ultramicroscopic phenomenon. *Ann. Phys., 12*, 161.

Haemers, T., Wiesner, J., Poecke, S. V., Goeman, J., Henschker, D., Beck, E., . . . Calenbergh, S. V. (2006). Synthesis of α-substituted fosmidomycin analogues as highly potent Plasmodium falciparum growth inhibitors. *Bioorganic & Medicinal Chemistry Letters, 16*(7), 1888-1891. doi:https://doi.org/10.1016/j.bmcl.2005.12.082

Hajj, R. E., Tawk, L., Itani, S., Hamie, M., Ezzeddine, J., El Sabban, M., & El Hajj, H. (2021). Toxoplasmosis: Current and emerging parasite druggable targets. *Microorganisms, 9*(12), 2531.

Hemphill, A., & Müller, J. (2023). Toxoplasma gondii infection: Novel emerging therapeutic targets. *Expert opinion on therapeutic targets*(just-accepted).

Henriksson, L. M., Unge, T., Carlsson, J., Aqvist, J., Mowbray, S. L., & Jones, T. A. (2007). Structures of Mycobacterium tuberculosis 1-deoxy-D-xylulose-5-phosphate reductoisomerase provide new insights into catalysis. *J Biol Chem, 282*(27), 19905-19916. doi:10.1074/jbc.M701935200

Johnson, L. L. (1992). SCID mouse models of acute and relapsing chronic Toxoplasma gondii infections. *Infection and immunity, 60*(9), 3719-3724.

Jomaa, H., Wiesner, J., Sanderbrand, S., Altincicek, B., Weidemeyer, C., Hintz, M., . . . Lichtenthaler, H. K. (1999). Inhibitors of the nonmevalonate pathway of isoprenoid biosynthesis as antimalarial drugs. *Science, 285*(5433), 1573-1576.

Kabsch, W. (2010). XDS. *Acta Crystallogr D Biol Crystallogr, 66*(Pt 2), 125-132. doi:10.1107/s0907444909047337

Kikhney, A. G., Borges, C. R., Molodenskiy, D. S., Jeffries, C. M., & Svergun, D. I. (2020). SASBDB: Towards an automatically curated and validated repository for biological scattering data. *Protein Science, 29*(1), 66-75. doi:https://doi.org/10.1002/pro.3731

Klischan, M. K. T., Mazzone, F., Berning, L., Greb, J., Schlamkow, M., Haase, M., . . . Pietruszka, J. (2023). Modular Approach for the Synthesis and Bioactivity Profiling of 8,8′-Biflavones. *ACS omega*. doi:10.1021/acsomega.3c06503

Knak, T., Abdullaziz, M. A., Höfmann, S., Alves Avelar, L. A., Klein, S., Martin, M., . . . Kurz, T. (2022). Over 40 Years of Fosmidomycin Drug Research: A Comprehensive Review and Future Opportunities. *Pharmaceuticals, 15*(12), 1553.

Konarev, P. V., Volkov, V. V., Sokolova, A. V., Koch, M. H. J., & Svergun, D. I. (2003). PRIMUS: a Windows PC-based system for small-angle scattering data analysis. *Journal of Applied Crystallography, 36*, 1277-1282. doi:10.1107/S0021889803012779

Krueger, W. S., Hilborn, E. D., Converse, R. R., & Wade, T. J. (2014). Drinking water source and human Toxoplasma gondii infection in the United States: a cross-sectional analysis of NHANES data. *BMC Public Health, 14*(1), 1-10.

Kuemmerle, H., Murakawa, T., Sakamoto, H., Sato, N., Konishi, T., & De Santis, F. (1985). Fosmidomycin, a new phosphonic acid antibiotic. Part II: 1. Human pharmacokinetics. 2. Preliminary early phase IIa clinical studies. *International journal of clinical pharmacology, therapy, and toxicology, 23*(10), 521-528.

Kunfermann, A., Lienau, C., Illarionov, B., Held, J., Gräwert, T., Behrendt, C. T., . . . Riederer, U. (2013). IspC as target for antiinfective drug discovery: synthesis, enantiomeric separation, and structural biology of fosmidomycin thia isosters. *Journal of Medicinal Chemistry, 56*(20), 8151-8162.

Kuzuyama, T., Shimizu, T., Takahashi, S., & Seto, H. (1998). Fosmidomycin, a specific inhibitor of 1-deoxy-D-xylulose 5-phosphate reductoisomerase in the nonmevalonate pathway for terpenoid biosynthesis. *Tetrahedron Letters, 39*(43), 7913-7916.

Kuzuyama, T., Takahashi, S., Takagi, M., & Seto, H. (2000). Characterization of 1-deoxy-D-xylulose 5-phosphate reductoisomerase, an enzyme involved in isopentenyl diphosphate biosynthesis, and identification of its catalytic amino acid residues. *J Biol Chem, 275*(26), 19928-19932. doi:10.1074/jbc.M001820200

L Goble, J., Johnson, H., De Ridder, J., L Stephens, L., Louw, A., L Blatch, G., & Boshoff, A. (2013). The druggable antimalarial target PfDXR: overproduction strategies and kinetic characterization. *Protein and Peptide Letters, 20*(2), 115-124.

Laemmli, U. K. (1970). Cleavage of structural proteins during the assembly of the head of bacteriophage T4. *Nature, 227*(5259), 680-685.

Lee, P. Y., Costumbrado, J., Hsu, C. Y., & Kim, Y. H. (2012). Agarose gel electrophoresis for the separation of DNA fragments. *J Vis Exp*(62). doi:10.3791/3923

Levine, N. D. (2018). *The Protozoan Phylum Apicomplexa: Volume 2* (Vol. 2): CRC press.

Liebschner, D., Afonine, P. V., Baker, M. L., Bunkóczi, G., Chen, V. B., Croll, T. I., . . . Adams, P. D. (2019). Macromolecular structure determination using X-rays, neutrons and electrons: recent developments in Phenix. *Acta Crystallogr D Struct Biol, 75*(Pt 10), 861-877. doi:10.1107/s2059798319011471

Lienau, C., Gräwert, T., Avelar, L. A. A., Illarionov, B., Held, J., Knaab, T. C., . . . Geissler, S. (2019). Novel reverse thia-analogs of fosmidomycin: Synthesis and antiplasmodial activity. *European Journal of Medicinal Chemistry, 181*, 111555.

Lim, L., & McFadden, G. I. (2010). The evolution, metabolism and functions of the apicoplast. *Philosophical Transactions of the Royal Society B: Biological Sciences, 365*(1541), 749-763.

Lourido, S. (2019). Toxoplasma gondii. *Trends in Parasitology, 35*(11), 944-945.

Mac Sweeney, A., Lange, R., Fernandes, R. P., Schulz, H., Dale, G. E., Douangamath, A., . . . Oefner, C. (2005). The crystal structure of E.coli 1-deoxy-D-xylulose-5-phosphate reductoisomerase in a ternary complex with the antimalarial compound

fosmidomycin and NADPH reveals a tight-binding closed enzyme conformation. *J Mol Biol, 345*(1), 115-127. doi:10.1016/j.jmb.2004.10.030

Madeira, F., Pearce, M., Tivey, A. R., Basutkar, P., Lee, J., Edbali, O., . . . Lopez, R. (2022). Search and sequence analysis tools services from EMBL-EBI in 2022. *Nucleic acids research, 50*(W1), W276-W279.

Manalastas-Cantos, K., Konarev, P. V., Hajizadeh, N. R., Kikhney, A. G., Petoukhov, M. V., Molodenskiy, D. S., . . . Franke, D. (2021). ATSAS 3.0: expanded functionality and new tools for small-angle scattering data analysis. *Journal of Applied Crystallography, 54*(1). doi:doi:10.1107/S1600576720013412

Manual, I. (2017). Phusion® High-Fidelity PCR Kit.

Mazzone, F., Simons, V. E., van Geelen, L., Frank, M., Mándi, A., Kurtán, T., . . . Kalscheuer, R. (2022). In Vitro Biological Activity of Natural Products from the Endophytic Fungus Paraboeremia selaginellae against Toxoplasma gondii. *Antibiotics, 11*(9), 1176.

McCoy, A. J., Grosse-Kunstleve, R. W., Adams, P. D., Winn, M. D., Storoni, L. C., & Read, R. J. (2007). Phaser crystallographic software. *J Appl Crystallogr, 40*(Pt 4), 658-674. doi:10.1107/s0021889807021206

McFadden, G. I. (2011). The apicoplast. *Protoplasma, 248*(4), 641-650.

Merkt, F. K., Mazzone, F., Sazzadeh, S. S., Bonda, L., Hinz, L. K., Gruber, I., . . . Müller, T. J. (2021). Fluorescent Indolo [3, 2-a] phenazines against Toxoplasma gondii: Concise Synthesis by Gold-Catalyzed Cycloisomerization with 1, 2-Silyl Migration and ipso-Iodination Suzuki Sequence. *Chemistry–A European Journal, 27*(38), 9774-9781.

Montoya, J. G., & Liesenfeld, O. (2004). Toxoplasmosis. *The Lancet, 363*(9425), 1965-1976. doi:10.1016/S0140-6736(04)16412-X

Mosmann, T. (1983). Rapid colorimetric assay for cellular growth and survival: application to proliferation and cytotoxicity assays. *J Immunol Methods, 65*(1-2), 55-63. doi:10.1016/0022-1759(83)90303-4

Munos, J. W., Pu, X., Mansoorabadi, S. O., Kim, H. J., & Liu, H.-w. (2009). A secondary kinetic isotope effect study of the 1-deoxy-D-xylulose-5-phosphate reductoisomerase-catalyzed reaction: Evidence for a retroaldol-aldol rearrangement. *Journal of the American Chemical Society, 131*(6), 2048-2049.

Murkin, A. S., Manning, K. A., & Kholodar, S. A. (2014). Mechanism and inhibition of 1-deoxy-d-xylulose-5-phosphate reductoisomerase. *Bioorganic Chemistry, 57*, 171-185. doi:https://doi.org/10.1016/j.bioorg.2014.06.001

Na-Bangchang, K., Ruengweerayut, R., Karbwang, J., Chauemung, A., & Hutchinson, D. (2007). Pharmacokinetics and pharmacodynamics of fosmidomycin monotherapy and combination therapy with clindamycin in the treatment of multidrug resistant falciparum malaria. *Malaria journal, 6*(1), 1-10.

Nair, S. C., Brooks, C. F., Goodman, C. D., Strurm, A., McFadden, G. I., Sundriyal, S., . . . Striepen, B. (2011). Apicoplast isoprenoid precursor synthesis and the molecular basis of fosmidomycin resistance in Toxoplasma gondii. *Journal of Experimental Medicine, 208*(7), 1547-1559.

Okuhara, M., KURODA, Y., GOTO, T., OKAMOTO, M., TERANO, H., KOHSAKA, M., . . . IMANAKA, H. (1980). Studies on new phosphonic acid antibiotics III. isolation and characterization of FR-31564. *J Antibiot (Tokyo), 33*(1), 24-28.

Panjkovich, A., & Svergun, D. I. (2017). CHROMIXS: automatic and interactive analysis of chromatography-coupled small angle X-ray scattering data. *Bioinformatics*. doi:10.1093/bioinformatics/btx846

Pernot, P., Round, A., Barrett, R., De Maria Antolinos, A., Gobbo, A., Gordon, E., . . . McSweeney, S. (2013). Upgraded ESRF BM29 beamline for SAXS on macromolecules in solution. *J Synchrotron Radiat, 20*(Pt 4), 660-664. doi:10.1107/S0909049513010431

Pernot, P., Theveneau, P., Giraud, T., Fernandes, R. N., Nurizzo, D., Spruce, D., . . . Cipriani, F. (2010). New beamline dedicated to solution scattering from biological macromolecules at the ESRF. *Journal of Physics: Conference Series, 247*(1), 012009. Retrieved from http://stacks.iop.org/1742-6596/247/i=1/a=012009

Pfefferkorn, E., & PFEFFERKORN, L. C. (1977). Specific labeling of intracellular Toxoplasma gondii with uracil. *J Protozool, 24*(3), 449-453.

Pleyer, U., Gross, U., Schlüter, D., Wilking, H., & Seeber, F. (2019). Toxoplasmosis in Germany: Epidemiology, diagnosis, risk factors, and treatment. *Deutsches Ärzteblatt International, 116*(25), 435.

Prevention, C.-C. f. D. C. a. (September 4, 2018). Parasites - Toxoplasmosis (Toxoplasma infection) - Epidemiology & Risk Factors. Retrieved from https://www.cdc.gov/parasites/toxoplasmosis/epi.html

Proteau, P. J. (2004). 1-Deoxy-d-xylulose 5-phosphate reductoisomerase: an overview. *Bioorganic Chemistry, 32*(6), 483-493. doi:https://doi.org/10.1016/j.bioorg.2004.08.004

Reuter, K., Sanderbrand, S., Jomaa, H., Wiesner, J., Steinbrecher, I., Beck, E., . . . Stubbs, M. T. (2002). Crystal structure of 1-deoxy-D-xylulose-5-phosphate reductoisomerase, a crucial enzyme in the non-mevalonate pathway of isoprenoid biosynthesis. *J Biol Chem, 277*(7), 5378-5384. doi:10.1074/jbc.M109500200

Rodriguez-Concepcion, M. (2004). The MEP pathway: a new target for the development of herbicides, antibiotics and antimalarial drugs. *Current pharmaceutical design, 10*(19), 2391-2400.

Sakamoto, Y., Furukawa, S., Ogihara, H., & Yamasaki, M. (2003). Fosmidomycin resistance in adenylate cyclase deficient (cya) mutants of Escherichia coli. *Bioscience, biotechnology, and biochemistry, 67*(9), 2030-2033.

Singh, N., Chevé, G., Avery, M. A., & McCurdy, C. R. (2007). Targeting the methyl erythritol phosphate (MEP) pathway for novel antimalarial, antibacterial and herbicidal drug discovery: inhibition of 1-deoxy-D-xylulose-5-phosphate reductoisomerase (DXR) enzyme. *Current pharmaceutical design, 13*(11), 1161-1177.

Sooriyaarachchi, S., Chofor, R., Risseeuw, M. D., Bergfors, T., Pouyez, J., Dowd, C. S., . . . Van Calenbergh, S. (2016). Targeting an Aromatic Hotspot in Plasmodium falciparum 1-Deoxy-d-xylulose-5-phosphate Reductoisomerase with β-Arylpropyl Analogues of Fosmidomycin. *ChemMedChem, 11*(18), 2024-2036.

Svergun, D. I. (1992). Determination of the Regularization Parameter in Indirect-Transform Methods Using Perceptual Criteria. *Journal of Applied Crystallography, 25*, 495-503. doi:Doi 10.1107/S0021889892001663

Tria, G., Mertens, H. D., Kachala, M., & Svergun, D. I. (2015). Advanced ensemble modelling of flexible macromolecules using X-ray solution scattering. *IUCrJ, 2*(Pt 2), 207-217. doi:10.1107/S205225251500202X

Umeda, T., Tanaka, N., Kusakabe, Y., Nakanishi, M., Kitade, Y., & Nakamura, K. T. (2011). Molecular basis of fosmidomycin's action on the human malaria parasite Plasmodium falciparum. *Scientific Reports, 1*(1), 9. doi:10.1038/srep00009

Wang, X., & Dowd, C. S. (2018). The Methylerythritol Phosphate Pathway: Promising Drug Targets in the Fight against Tuberculosis. *ACS Infect Dis, 4*(3), 278-290. doi:10.1021/acsinfecdis.7b00176

Waterhouse, A. M., Procter, J. B., Martin, D. M. A., Clamp, M., & Barton, G. J. (2009). Jalview Version 2—a multiple sequence alignment editor and analysis workbench. *Bioinformatics, 25*(9), 1189-1191. doi:10.1093/bioinformatics/btp033

White, M. W., & Suvorova, E. S. (2018). Apicomplexa cell cycles: something old, borrowed, lost, and new. *Trends in Parasitology, 34*(9), 759-771.

Winn, M. D., Ballard, C. C., Cowtan, K. D., Dodson, E. J., Emsley, P., Evans, P. R., . . . Wilson, K. S. (2011). Overview of the CCP4 suite and current developments. *Acta Crystallogr D Biol Crystallogr, 67*(Pt 4), 235-242. doi:10.1107/s0907444910045749

Woo, Y. H., Fernandes, R. P., & Proteau, P. J. (2006). Evaluation of fosmidomycin analogs as inhibitors of the Synechocystis sp. PCC6803 1-deoxy-D-xylulose 5-phosphate reductoisomerase. *Bioorg Med Chem, 14*(7), 2375-2385. doi:10.1016/j.bmc.2005.11.012

Xu, M., Zhu, J., Diao, Y., Zhou, H., Ren, X., Sun, D., . . . Zhu, L. (2013). Novel selective and potent inhibitors of malaria parasite dihydroorotate dehydrogenase: discovery and optimization of dihydrothiophenone derivatives. *Journal of Medicinal Chemistry, 56*(20), 7911-7924.

Yajima, S., Hara, K., Iino, D., Sasaki, Y., Kuzuyama, T., Ohsawa, K., & Seto, H. (2007). Structure of 1-deoxy-D-xylulose 5-phosphate reductoisomerase in a quaternary

complex with a magnesium ion, NADPH and the antimalarial drug fosmidomycin. *Acta Crystallogr Sect F Struct Biol Cryst Commun, 63*(Pt 6), 466-470. doi:10.1107/s1744309107024475

Supplementary Informations

1-deoxy-d-xylulose 5-phosphate reductoisomerase (DXR) as target for anti *Toxoplasma gondii* agents: crystal structure, biochemical characterization and *in vitro* biological evaluation of fosmidomycin and reverse analogues as potent inhibitors

Flaminia Mazzone[1]*, Astrid Hoeppner[2], Jens Reiners[2], Mona A. Abdullaziz[3], Julia Gottstein[4], Martina Wesemann[4], Thomas Kurz[3]†, Sander H. J. Smits[2,4]†*, Klaus Pfeffer[1]†*

[1]Institute of Medical Microbiology and Hospital Hygiene, Heinrich Heine University, Düsseldorf, Germany

[2]Center for Structural Studies, Heinrich Heine University, Düsseldorf, Germany

[3]Institute of Pharmaceutical and Medicinal Chemistry, Heinrich Heine University, Düsseldorf, Germany

[4]Institute of Biochemistry, Heinrich Heine University, Düsseldorf, Germany

†These authors share last authorship

*Authors for correspondence:

Sander H.J. Smits
sander.smits@hhu.de,
Klaus Pfeffer
klaus.pfeffer@hhu.de
Flaminia Mazzone
flaminia.mazzone@uni-duesseldorf.de,

1 Multiple sequence alignment

Previous studies on *P. falciparum, E. coli*, and *M. tuberculosis* showed that the DXR enzyme is the biological target of the reverse thia and oxa analogues employed in this study [1-3]. The DXR enzyme of these species have been extensively studied [1, 4-6], but very less is known for *T. gondii* DXR [7]. *Tg*DXR shares an high degree of sequence similarity with DXRs from other species [7], resulting in an highly conserved catalytic domain among all species in comparison (**Figure S1**). *Tg*DXR sequence is composed of 632 residues. The initial 186 amino acids from the N-terminal region (1 – 186) represent the bipartite apicoplast targeting peptide, since this extension in only present in the apicomplexan parasites *T. gondii* and *P. falciparum* [7, 8]. The NADPH binding domain includes amino acids 187 – 342 and the metal/substrate binding domain (405 – 632) resulted highly conserved among all the species. Special feature of the *Tg*DXR is the linker region ranging from amino acids (343 – 404). Apart of this region, the amino acids involved in direct contact with the NADH ligand and substrate are strictly conserved (**Figure S1**).

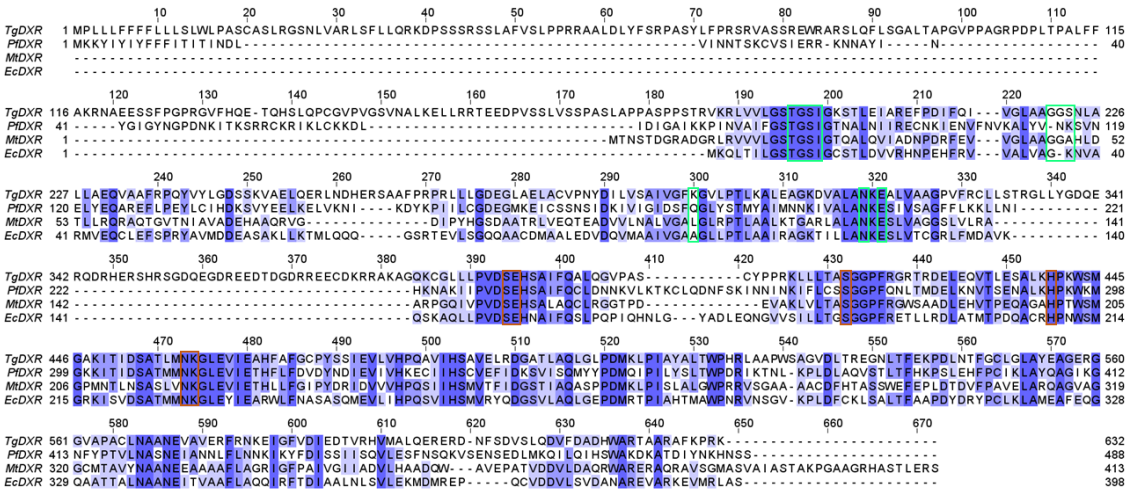

Supplementary Figure S1. Multiple sequence alignment of the amino acids sequence of the putative *T. gondii* DXR

*Tg*DXR, *T. gondii* (NCBI Reference Sequence: XP_018635719.1); *Pf*DXR, *P. falciparum* (NCBI Reference Sequence: AAD03739.1); *Mt*DXR, *M. tuberculosis* (NCBI Reference Sequence: OHO19719.1) and *Ec*DXR, *E. coli* (NCBI Reference Sequence:

WP_302347400.1). Identical amino acids are shaded in dark blue, similar amino acids in lighter shades. *Tg*DXR residues are highlighted according to their function: residues interacting with the NADPH cofactor are highlighted in green, those binding the inhibitor **1** are highlighted in orange. Alignment coloured using Jalview 2.11.2.7.

2 Enzyme production

Supplementary Table S1. List of the primers used in this work and their parameters

Primer name	Sequence	CG %	Tm
TgDXR-del181AA_For	TCCACGCGTGTGAAGAGACTTGTGG	56	75.1
TgDXR-del181AA_Rev	CATATGACGACCTTCGATATGGCCGCTG	53.5	76.6
T7 promoter primer (5')	TAATACGACTCACTATAGGG	40	53.2
T7 terminator primer (3')	GCTAGTTATTGCTCAGCGG	47	54.5

3 Crystal structure parameters and refinement

Supplementary Table S2. Data collection and refinement statistics.

	***Tg*DXR**
Wavelength	0.91677
Resolution range	54.97 - 2.56 (2.651 - 2.56)
Space group	P 65
Unit cell	159.524 159.524 75.873 90 90 120
Total reflections	67947 (6688)
Unique reflections	35325 (3503)
Multiplicity	1.9 (1.9)
Completeness (%)	99.04 (99.54)
Mean I/sigma(I)	11.53 (1.17)
Wilson B-factor	65.83
R-merge	0.03397 (0.4448)
R-meas	0.04804 (0.629)
R-pim	0.03397 (0.4448)
CC1/2	0.999 (0.76)
CC*	1 (0.929)
Reflections used in refinement	35299 (3500)
Reflections used for R-free	1999 (197)
R-work	0.1941 (0.3214)
R-free	0.2260 (0.3795)
CC(work)	0.966 (0.837)
CC(free)	0.960 (0.804)
Number of non-hydrogen atoms	6416
macromolecules	6283
ligands	124

solvent	9
Protein residues	821
RMS(bonds)	0.022
RMS(angles)	2.03
Ramachandran favored (%)	96.43
Ramachandran allowed (%)	2.95
Ramachandran outliers (%)	0.62
Rotamer outliers (%)	0.31
Clashscore	18.58
Average B-factor	81.21
macromolecules	81.05
ligands	90.29
solvent	66.19

Statistics for the highest-resolution shell are shown in parentheses.

4 DXR SEC-SAXS data

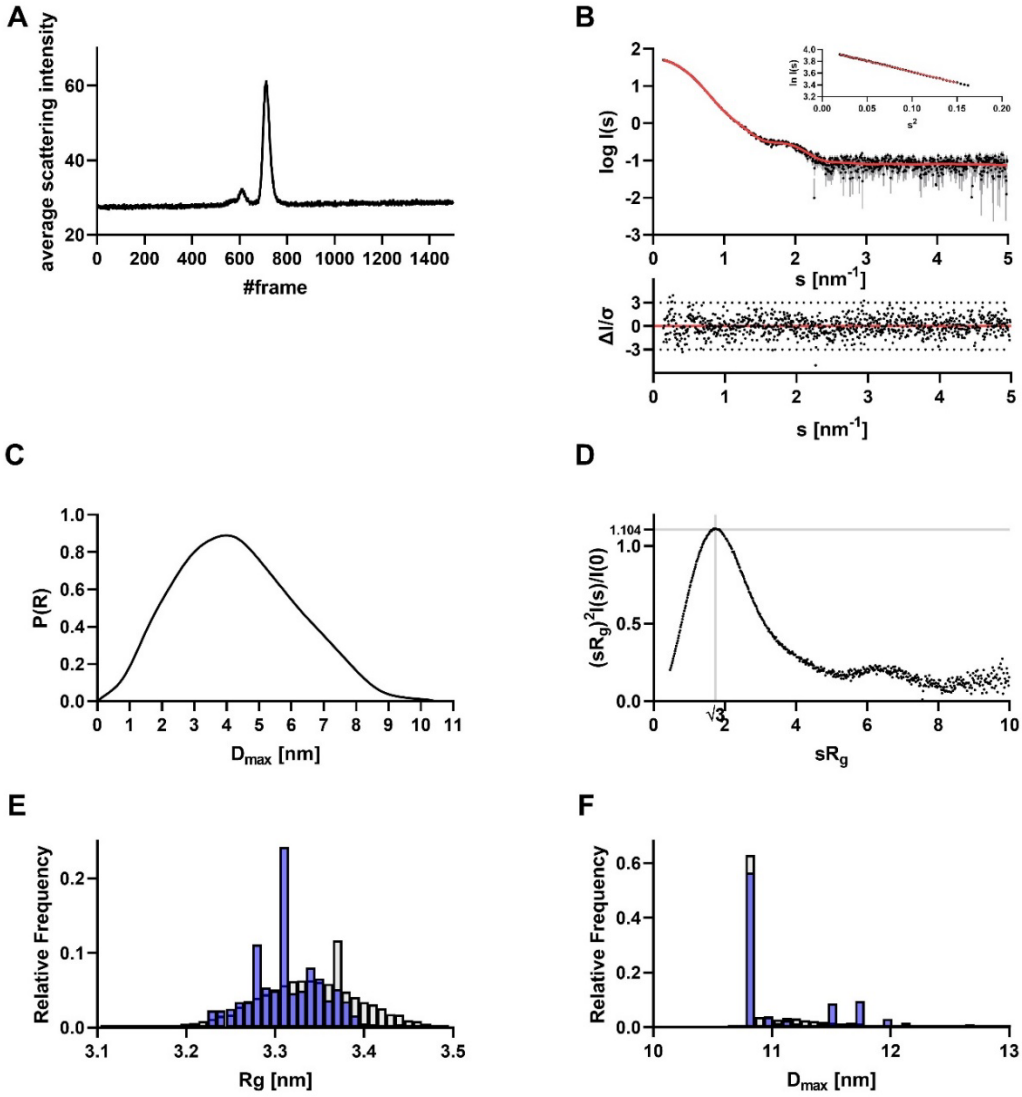

Supplementary Figure S2. Small-angle X-ray scattering data from DXR apo. A: CHROMIXS SEC SAXS elution profile. Each frame corresponds to 2 sec exposer time. **B:** Scattering data of DXR. Experimental data are shown in black dots, with grey error bars. The EOM ensemble model fit is shown as red line and below is the residual plot of the data. The Guinier plot of DXR is added in the right corner. **C:** *p(r)* function of DXR apo offers a D_{max} values of 10.44 nm. **D:** Dimensionless Kratky plot of DXR apo showed a compact practical. **E & F:** R_g and D_{max} distribution of DXR apo. Ensemble pool is shown in grey, selected EOM models are shown in blue.

4.1 EOM: Ensemble Optimization Method

Protein sequence (monomer) used for EOM.

Black parts are solved in the crystal and were extracted and used as rigid body. Missing amino acids are shown in green. These were added and orientated from EOM until the models describes the scattering data.

MGHHHHHHHHHHSSGHIEGRHMSTRVKRLVVLGSTGSIGKSTLEIAREFPDIFQI
VGLAAGGSNLALLAQVAAFRPQYVYLGDSSKVAELQERLNDHERSAAFPRPRL
LLGDEGLAELACVPNYDILVSAIVGFKGVLPTLKALEAGKDVALANKEALVAA
GPVFRCLLSTRGLLYGDQERQDRHERSHRSGDQEGDREEDTDGDRREECDKRR
AKAGQKCGLLLPVDSEHSAIFQALQGVPASCYPPRKLLLTASGGPFRGRTRDEL
EQVTLESALKHPKWSMGAKITIDSATLMNKGLEVIEAHFAFGCPYSSIEVLVHP
QAVIHSAVELRDGATLAQLGLPDMKLPIAYALTWPHRLAAPWSAGVDLTREG
NLTFEKPDLNTFGCLGLAYEAGERGGVAPACLNAANEVAVERFRNKEIGFVDIE
DTVRHVMALQERERDNFSDVSLQDVFDADHWARTAARAFKPR

Supplementary Table S3. Overall SAXS Data

Data collection parameters	
SAXS Device	BM29, ESRF Grenoble [9, 10]
Detector	PILATUS 2 M
Detector distance (m)	2.827
Beam size	200 µm x 200 µm
Wavelength (nm)	0.099
Sample environment	Quartz glass capillary, 1 mm ø
Absolute scaling method	Comparison with scattering from pure H_2O
Normalization	To transmitted intensity by beam-stop counter
Scattering intensity scale	Absolute scale, cm^{-1}
s range (nm^{-1}), ($s = 4\pi\sin(\theta)/\lambda$)	0.025–5.5
Sample	**1-Deoxy-D-xylulose-5-phosphate reductoisomerase (DXR)**
Organism	*Toxoplasma gondii (ME49)*
UniProt ID	*V5B5Y5*
Mode of measurement	SEC-SAXS
SEC-Column	Superdex 200 increase 10/300
Flowrate (ml/min)	0.5
Injection volume (µl)	300
Temperature (°C)	10
Exposure time (# frames)	2 s (1500 frames)
# frames used for averaging	35
Protein buffer	20 mM Tris/HCl, 150 mM NaCl, 40 mM MgCl2, 2% glycerol, pH 7.5
Protein concentration (mg/ml)	8.00
Structural parameters	
Guinier Analysis (PRIMUS)	
$I(0) \pm \sigma$ (cm^{-1})	54.11 ± 0.033
$R_g \pm \sigma$ (nm)	3.33 ± 0.0032
s-range (nm^{-1})	0.140 – 0.387
min < sRg < max limit	0.47 – 1.29
Data point range	1 - 49
Linear fit assessment (R^2)	0.9996
PDDF/P(r) Analysis (GNOM 5)	

$I(0) \pm \sigma$ (cm^{-1})	53.99 ± 0.032
$R_g \pm \sigma$ (nm)	3.31 ± 0.0025
D_{max} (nm)	10.44
Porod volume (nm^3)	176.01
s-range (nm^{-1})	0.140 – 5.029
$\chi 2$ / CorMap P-value	1.207 / 0.108
Molecular mass (kDa)	
From $I(0)$	not determined
From Qp [11]	105.53
From MoW2 [12]	108.24
From Vc [13]	101.69
Bayesian Inference [14]	104.90
From sequence	51.81 (monomer), 103.62 (dimer)
Modelling	
EOM (Ensemble Optimization Method)	
Constant subtraction	0.007
s-range for fit ($s_{min} - s_{max}$; nm^{-1})	0.140 – 4.988
No. of representative structures	3
χ^2, CorMap *P*-value	1.259 / 0.108
SASBDB accession codes	SASDS47
Software	
ATSAS Software Version [15]	3.0.5
Primary data reduction	CHROMIXS [16]/ PRIMUS [17]
Data processing	GNOM [18]
Ensemble modelling	EOM [19, 20]
Model visualization	PyMOL [21]

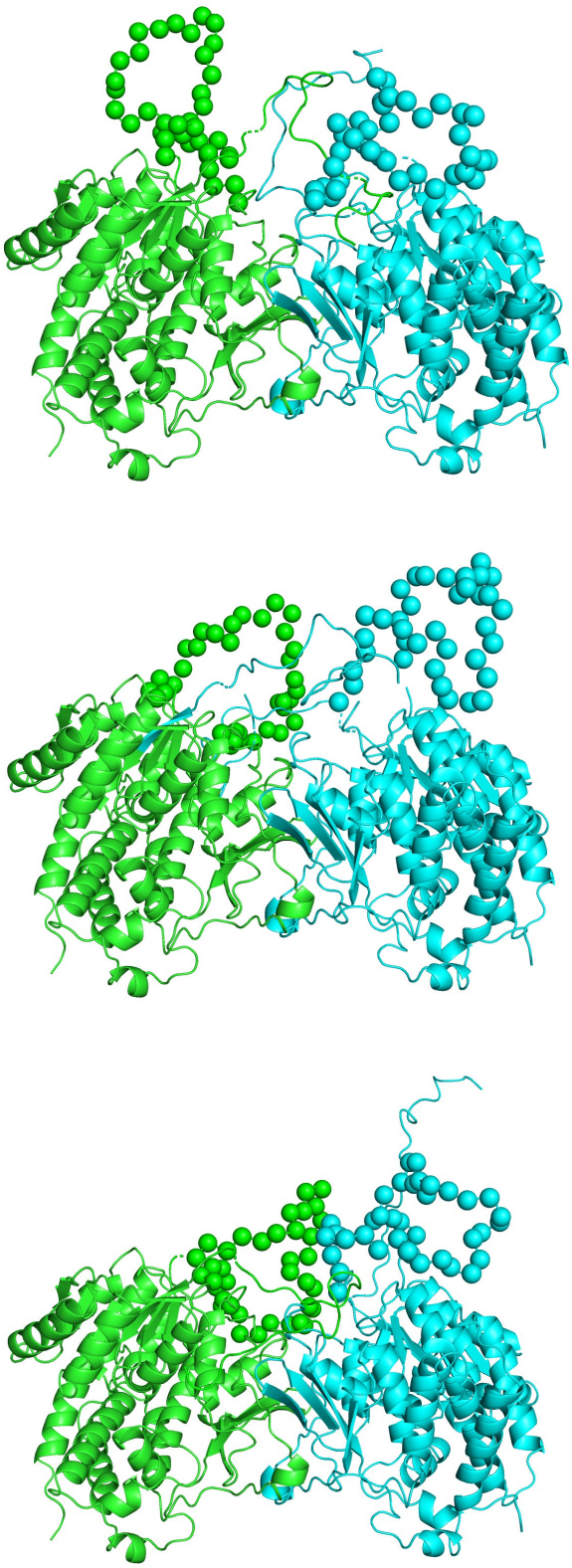

Supplementary Figure S4. Overlay view from the three EOM calculated models.

The rigid body protomers of DXR from the crystal are shown in green and cyan cartoon representation. The loop region of each protomer is shown in spheres representation. The

upper model corresponds to a volume fraction of 12 %, the middle on to a volume fraction of 25 % and the lower one to a volume fraction of 62 %.

5 Biological Data

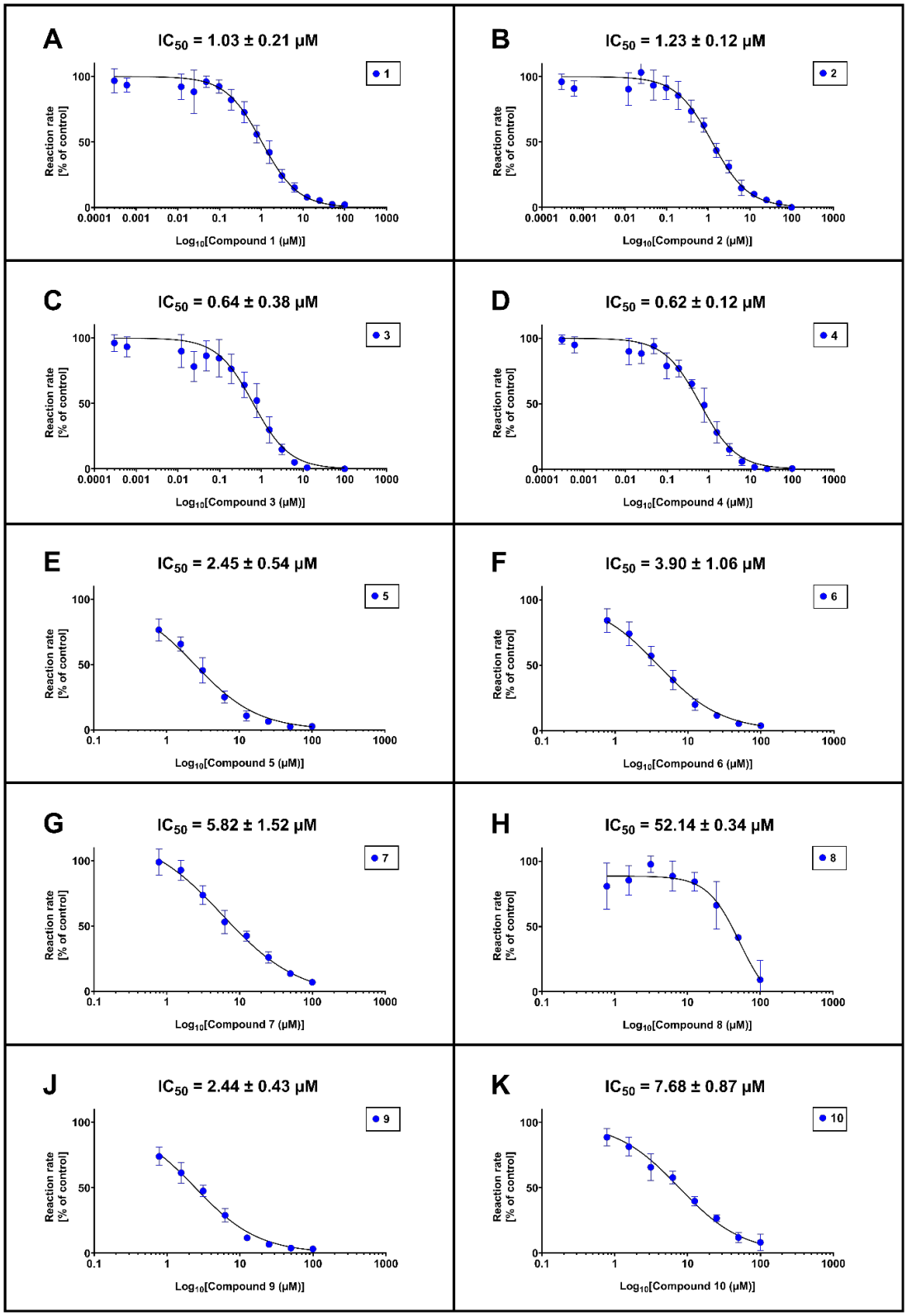

Supplementary Figure S5. *In vitro* enzymatic inhibition of *Tg*DXR of investigated compounds.

The enzymatic inhibitory activity of **1** (**A**), **2** (**B**), **3** (**C**), **4** (**D**), **5** (**E**), **6** (**F**), **7** (**G**), **8** (**H**), **9** (**J**) and **10** (**K**) were determined by enzymatic assays *in vitro*. Experiments were conducted in 96 well plates at 30 °C containing 100 nM of purified *Tg*DXR protein in dimeric state, 100 µM of NADPH and 4 mM of $MgCl_2$ as cofactors, 100 µM of DXP as substrate in50mM Hepes buffer (pH 7.5) containing 50 µg/mL of bovine serum albumin (BSA). The investigated compounds were tested in serial dilution 1:2. Data shown are from the means of three independent experiments each performed in duplicate (n = 6) ± S.D. IC_{50} of each compound are shown.

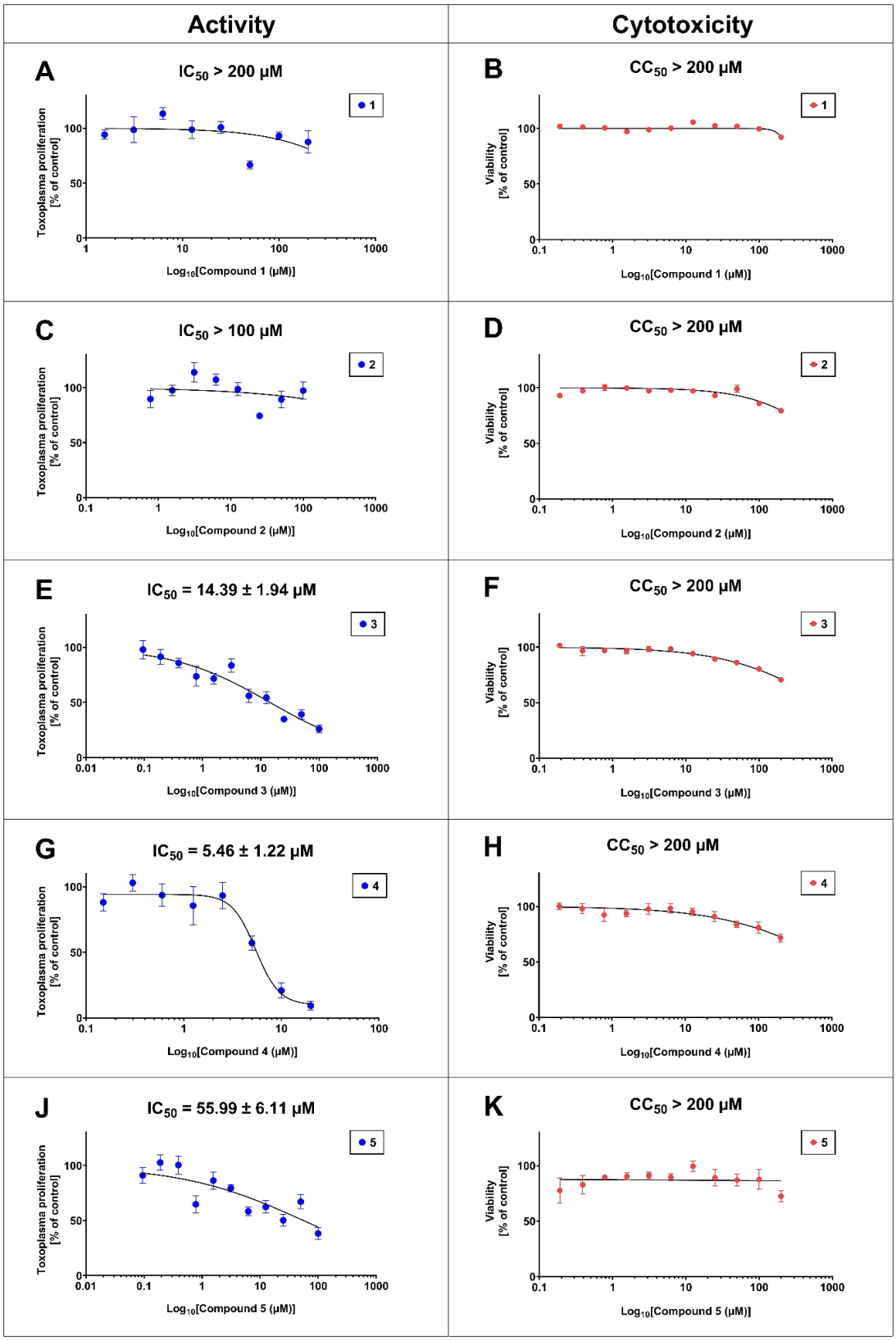
Activity
Cytotoxicity
A
IC50 > 200 µM
Toxoplasma proliferation [% of control]
Log10[Compound 1 (µM)]
B
CC50 > 200 µM
Viability [% of control]
Log10[Compound 1 (µM)]
C
IC50 > 100 µM
Toxoplasma proliferation [% of control]
Log10[Compound 2 (µM)]
D
CC50 > 200 µM
Viability [% of control]
Log10[Compound 2 (µM)]
E
IC50 = 14.39 ± 1.94 µM
Toxoplasma proliferation [% of control]
Log10[Compound 3 (µM)]
F
CC50 > 200 µM
Viability [% of control]
Log10[Compound 3 (µM)]
G
IC50 = 5.46 ± 1.22 µM
Toxoplasma proliferation [% of control]
Log10[Compound 4 (µM)]
H
CC50 > 200 µM
Viability [% of control]
Log10[Compound 4 (µM)]
J
IC50 = 55.99 ± 6.11 µM
Toxoplasma proliferation [% of control]
Log10[Compound 5 (µM)]
K
CC50 > 200 µM
Viability [% of control]
Log10[Compound 5 (µM)]

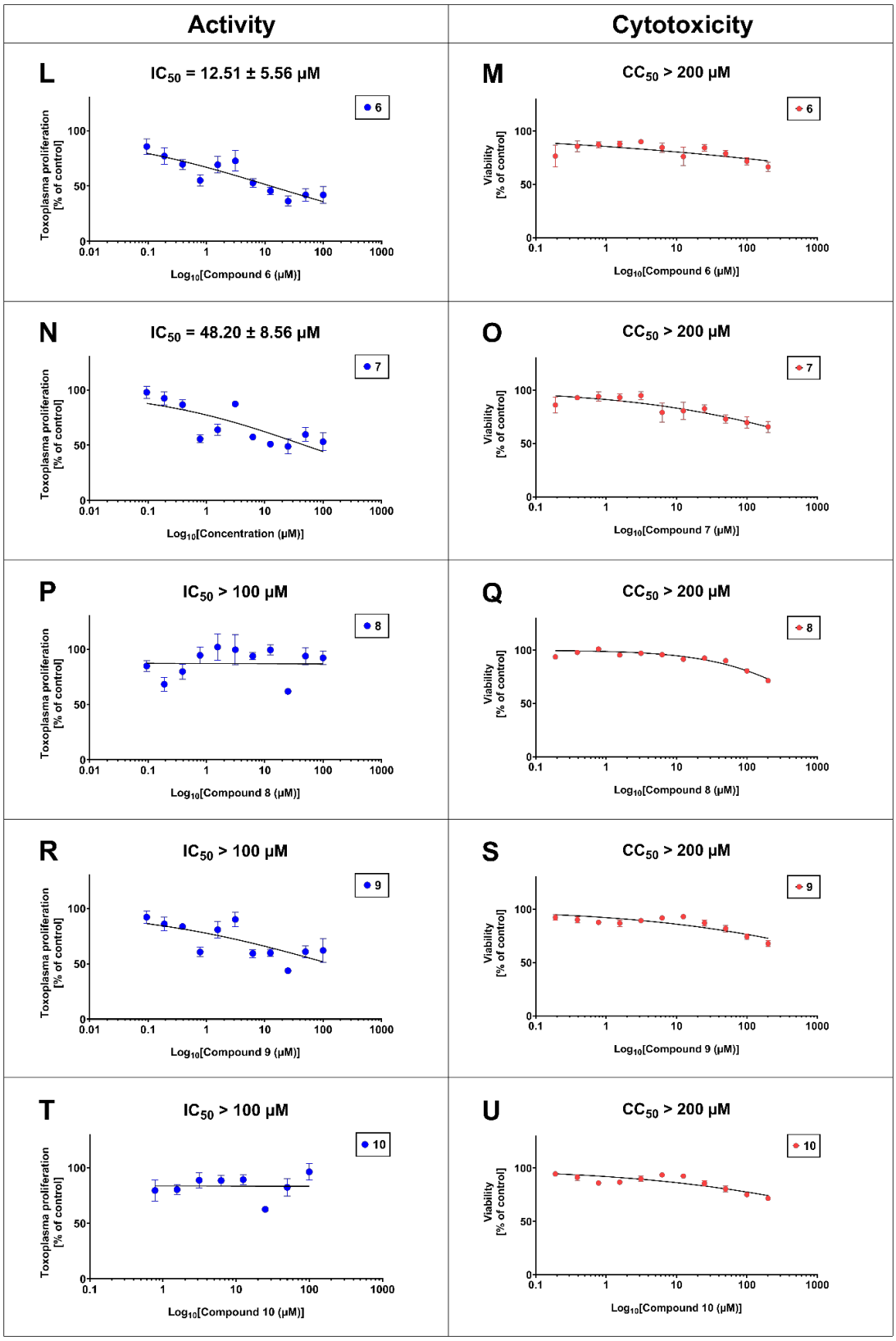

Supplementary Figure S6. Anti-toxoplasma activity and cytotoxicity on human fibroblasts Hs27 of the investigated compounds. The inhibitory activities of **1** (**A**), **2** (**C**), **3** (**E**), **4** (**G**), **5** (**J**), **6** (**L**) **7** (**N**) **8** (**P**) **9** (**R**) **10** (**T**) were determined by the *T. gondii*

in vitro inhibition assay via the [^{3}H]-uracil incorporation into the RNA of the parasite. Cytotoxicity of **1** (**B**), **2** (**D**), **3** (**F**), **4** (**H**), **5** (**K**), **6** (**M**) **7** (**O**) **8** (**Q**) **9** (**S**) **10** (**U**) were measured by MTT assays on human fibroblasts Hs27. Data shown are from the means of three independent experiments each performed in duplicate (n = 6) ± SEM. IC_{50} ± S.D. and CC_{50} values of each compound are shown.

6 References

1. Kunfermann, A., et al., *IspC as target for antiinfective drug discovery: synthesis, enantiomeric separation, and structural biology of fosmidomycin thia isosters.* Journal of medicinal chemistry, 2013. **56**(20): p. 8151-8162.

2. Lienau, C., et al., *Novel reverse thia-analogs of fosmidomycin: Synthesis and antiplasmodial activity.* European Journal of Medicinal Chemistry, 2019. **181**: p. 111555.

3. Brücher, K., et al., *α-Substituted β-Oxa Isosteres of Fosmidomycin: Synthesis and Biological Evaluation.* Journal of Medicinal Chemistry, 2012. **55**(14): p. 6566-6575.

4. Mac Sweeney, A., et al., *The crystal structure of E.coli 1-deoxy-D-xylulose-5-phosphate reductoisomerase in a ternary complex with the antimalarial compound fosmidomycin and NADPH reveals a tight-binding closed enzyme conformation.* J Mol Biol, 2005. **345**(1): p. 115-27.

5. Andaloussi, M., et al., *Design, Synthesis, and X-ray Crystallographic Studies of α-Aryl Substituted Fosmidomycin Analogues as Inhibitors of Mycobacterium tuberculosis 1-Deoxy-d-xylulose 5-Phosphate Reductoisomerase.* Journal of Medicinal Chemistry, 2011. **54**(14): p. 4964-4976.

6. Sooriyaarachchi, S., et al., *Targeting an Aromatic Hotspot in Plasmodium falciparum 1-Deoxy-d-xylulose-5-phosphate Reductoisomerase with β-Arylpropyl Analogues of Fosmidomycin.* ChemMedChem, 2016. **11**(18): p. 2024-2036.

7. Cai, G., et al., *Expression, characterization and inhibition of Toxoplasma gondii 1-deoxy-D-xylulose-5-phosphate reductoisomerase.* Bioorganic & medicinal chemistry letters, 2013. **23**(7): p. 2158-2161.

8. Jomaa, H., et al., *Inhibitors of the nonmevalonate pathway of isoprenoid biosynthesis as antimalarial drugs.* Science, 1999. **285**(5433): p. 1573-1576.

9. Pernot, P., et al., *New beamline dedicated to solution scattering from biological macromolecules at the ESRF.* Journal of Physics: Conference Series, 2010. **247**(1): p. 012009.

10. Pernot, P., et al., *Upgraded ESRF BM29 beamline for SAXS on macromolecules in solution.* J Synchrotron Radiat, 2013. **20**(Pt 4): p. 660-4.

11. Porod, G., *Die Röntgenkleinwinkelstreuung Von Dichtgepackten Kolloiden Systemen - 1 Teil.* Kolloid-Zeitschrift and Zeitschrift Fur Polymere, 1951. **124**(2): p. 83-114.

12. Fischer, H., et al., *Determination of the molecular weight of proteins in solution from a single small-angle X-ray scattering measurement on a relative scale.* Journal of Applied Crystallography, 2010. **43**: p. 101-109.

13. Rambo, R.P. and J.A. Tainer, *Accurate assessment of mass, models and resolution by small-angle scattering.* Nature, 2013. **496**(7446): p. 477-81.

14. Hajizadeh, N.R., et al., *Consensus Bayesian assessment of protein molecular mass from solution X-ray scattering data.* Sci Rep, 2018. **8**(1): p. 7204.

15. Manalastas-Cantos, K., et al., *ATSAS 3.0: expanded functionality and new tools for small-angle scattering data analysis.* Journal of Applied Crystallography, 2021. **54**(1).

16. Panjkovich, A. and D.I. Svergun, *CHROMIXS: automatic and interactive analysis of chromatography-coupled small angle X-ray scattering data.* Bioinformatics, 2017.

17. Konarev, P.V., et al., *PRIMUS: a Windows PC-based system for small-angle scattering data analysis.* Journal of Applied Crystallography, 2003. **36**: p. 1277-1282.

18. Svergun, D.I., *Determination of the Regularization Parameter in Indirect-Transform Methods Using Perceptual Criteria.* Journal of Applied Crystallography, 1992. **25**: p. 495-503.

19. Tria, G., et al., *Advanced ensemble modelling of flexible macromolecules using X-ray solution scattering.* IUCrJ, 2015. **2**(Pt 2): p. 207-17.

20. Bernado, P., et al., *Structural characterization of flexible proteins using small-angle X-ray scattering.* J Am Chem Soc, 2007. **129**(17): p. 5656-64.

21. PyMOL, *The PyMOL Molecular Graphics System, Version 2.5 Schrödinger, LLC.* 2022.

3.5.1 Inhibitors of 1-deoxy-D-xylulose 5-phosphate reductoisomerase: Unpublished data

Manuscript in preparation. Submission expected: 2024

Pivaloyloxymethyl (POM) esters of fosmidomycin derivatives as prodrugs

In the investigation in chapter 3.5, a significant disparity between the IC_{50} values of the reverse thia and oxa analogues of FSM for the inhibition of the parasite proliferation and their activity on inhibiting the enzymatic activity of the *Tg*DXR enzyme was observed, exhibiting only a reduced efficacy in the biological level. This divergence could be attributed to the anionic nature of the phosphonic moiety that could limit the drug uptake and its membrane permeability (Knak et al., 2022).

A strategy to address the permeability challenges, arising from the high negative charge of the phosphonate moieties at physiological pH, is to shield this moiety using a variety of protective groups producing prodrugs (Greene & Wuts, 1999). Prior to reach their target, these inactive molecules undergo to enzymatic cleavage of the protecting groups, leading to the release of the active molecules, which can subsequently interact with their targets (Rautio et al., 2008). This strategy could enhance the permeability through the biological obstacles and, additionally, enhancing the bioavailability *in vivo* (Heidel & Dowd, 2019). Pivaloyloxymethyl (POM) esters are widely used as prodrugs of phosphonate containing compounds (Hecker & Erion, 2008). Moreover, several studies of POM-esters of FSM analogues report the enhancement of permeability and consequent potency for *M. tuberculosis* (Jackson et al., 2014) and *P. falciparum* growth inhibition (K. Brücher et al., 2015; X. Wang et al., 2018; Xu Wang et al., 2023).

Thus, four novel derivatives of FSM and their respective POM esters were successfully synthesised (**Figure 11**) and evaluated their inhibitory activities on the *Tg*DXR enzyme and their anti-toxoplasma capacity.

Free phosphonate / parental	POM ester / prodrug
MAMK 89 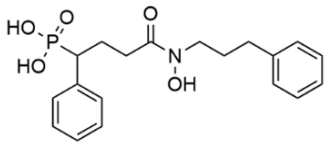	**MAMK 136** 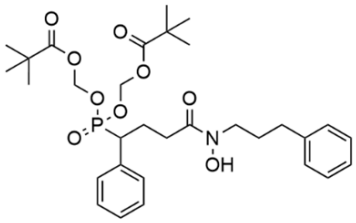
MAMK 150 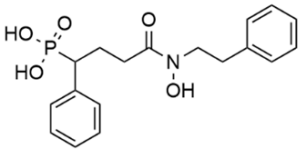	**MAMK 151** 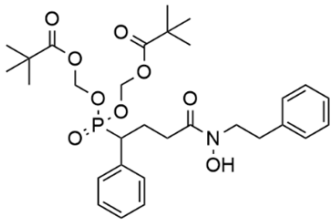
MAMK 145 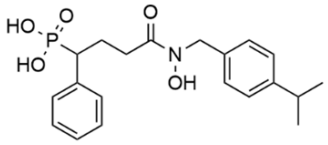	**MAMK 149** 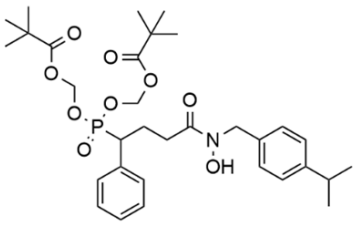
CBK 52 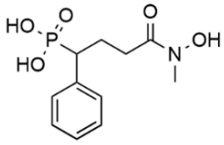	**MAMK 169** 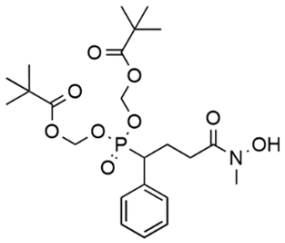

Figure 11: The novel free-phosphonate compound and their POM esters

Chemical structures of the novel fosmidomycin derivatives **MAMK 89**, **MAMK 150**, **MAMK 145** and **CBK 52** and their POM esters **MAMK 136**, **MAMK 151**, **MAMK 149**, **and MAMK 169** are shown. Molecules were synthesised by Mona A. Abdullaziz.

Enzymatic inhibition assays

The four free-phosphonate compounds and their POM ester counterparts were tested for their anti-toxoplasma capacity. Experiments were performed as described in the Material and Method section in chapter 3.5. All the free-phosphonate compounds exerted high potency on inhibiting the *Tg*DXR enzyme, with IC_{50} ranging from 3.24 – 12.26 μM, with the compounds MAMK 89 and CBK 52 exerting the highest activities (**Table 2** and **Figure 12**).

The POM esters, showed only weak or no inhibition activity, perhaps because they are too bulky to interact with the active site of *Tg*DXR (K. Brücher et al., 2015)

Parental (free phosphonate)			POM esters (prodrugs)		
Compound	**IC_{50} (µM)**	**K_i (µM)**	**Compound**	**IC_{50} (µM)**	**K_i (µM)**
MAMK 89	3.24 ± 1.19	1.35	**MAMK 136**	35.96 ± 7.72	15.01
MAMK 150	4.17 ± 1.00	1.74	**MAMK 151**	41.60 ± 5.71	17.36
MAMK 145	12.26 ± 0.66	5.11	**MAMK 149**	> 100	> 100
CBK 52	3.83 ± 1.01	1.60	**MAMK 169**	> 100	> 100
Fosmidomycin	1.03 ± 0.21	0.43			

Table 2: *In vitro* enzymatic inhibitory activity (IC_{50} and K_i values) of the investigated compounds against *Tg*DXR

Values shown in the table represent the means of three independent experiments each done in duplicate (n = 6) ± S.D.

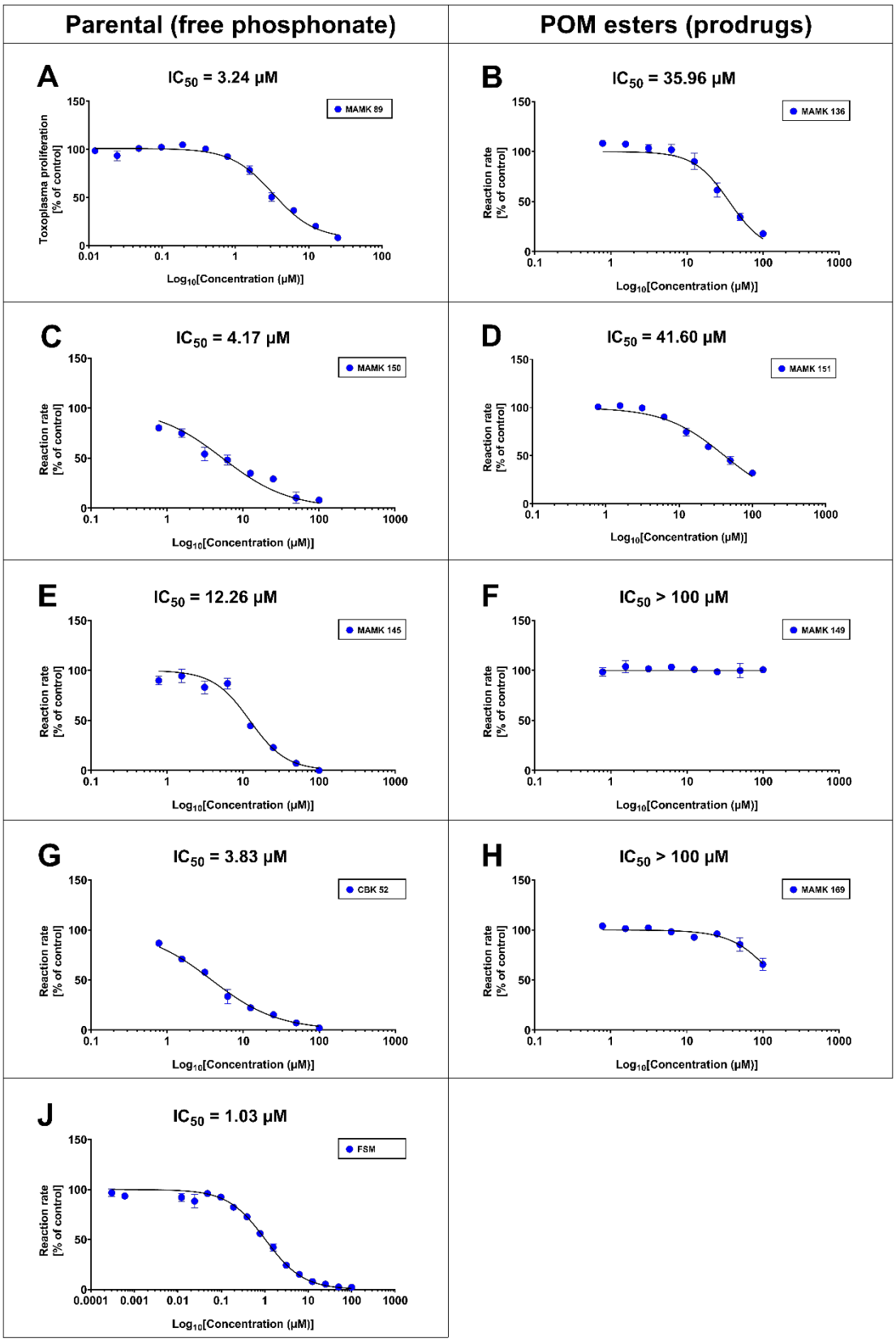

Figure 12: *In vitro* enzymatic inhibition of *Tg*DXR of the investigated compounds

The enzymatic inhibitory activities of **MAMK 89** (**A**), **MAMK 136** (**B**), **MAMK 150** (**C**), **MAMK 151** (**D**), **MAMK 145** (**E**), **MAMK 149** (**F**), **CBK 52** (**G**), **MAMK 169** (**H**), **Fosmidomycin** (**FSM**) (**J**) were determined by enzymatic assays *in vitro* conducted in 96 well plates at 30 °C containing 100 nM of purified *Tg*DXR protein

in dimeric state, 100 µM of NADPH and 4 mM of $MgCl_2$ as cofactors, 100 µM of DXP as substrate in 50mM HEPES buffer (pH 7.5) containing 50 µg/mL of bovine serum albumin (BSA). The investigated compounds were tested in different concentration ranges. Data shown are from the means of three independent experiments each performed in duplicate (n = 6) ± SEM. IC_{50} of each compound are shown.

Anti-*T. gondii* proliferation assay

After the evaluation at the enzymatic level, I commenced the investigation on testing the free phosphonate and the POM esters for their ability to inhibit *T. gondii* proliferation using the [^{3}H]-uracil incorporation assay on *T. gondii* ME49 detailed in the Material and Methods section of chapter 3.5. As shown in **Figure 13** and **Table 3** the free-phosphonate compounds **MAMK 89**, **MAMK 150**, **MAMK 145** and **CBK 52** showed low activity within a concentration of 50 µM.

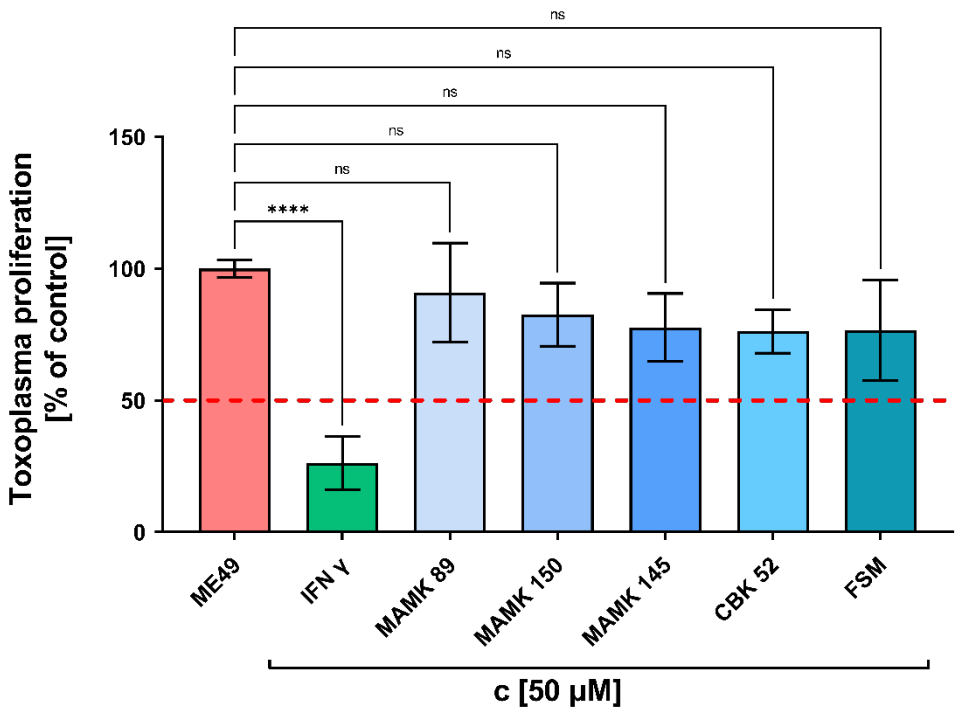

Figure 13: Anti-toxoplasma activity of the investigated free-phosphonate compounds

The inhibitory activities of **MAMK 89**, **MAMK 150**, **MAMK 145**, **CBK 52** and **Fosmidomycin** (**FSM**) were determined via the [^{3}H]-uracil incorporation assay on *T. gondii* treated *in vitro* with fixed concentration of the investigated compounds (50 µM). **ME49** represent the proliferation of not-inhibited *T. gondii* (100% control). Interferon γ (**IFN γ**) is used as positive control. Not-infected host cells, were used as control (0% control). Data shown are from the means of three independent experiments each performed in duplicate (n = 6) ± SEM. Statistical analysis was performed by the one-way analysis of variance (ANOVA) and Tukey multiple comparison test. ****P < 0.0001 vs 100% control group (ME49). Ns, not significant.

The scenario was distinct with the POM esters. **MAMK 136**, **MAMK 151**, **MAMK 149** and **MAMK 169** showed anti-toxoplasma activity *in vitro*, with IC_{50} values ranging from 5.27 – 8.16 µM (**Figure 14** and **Table 3**).

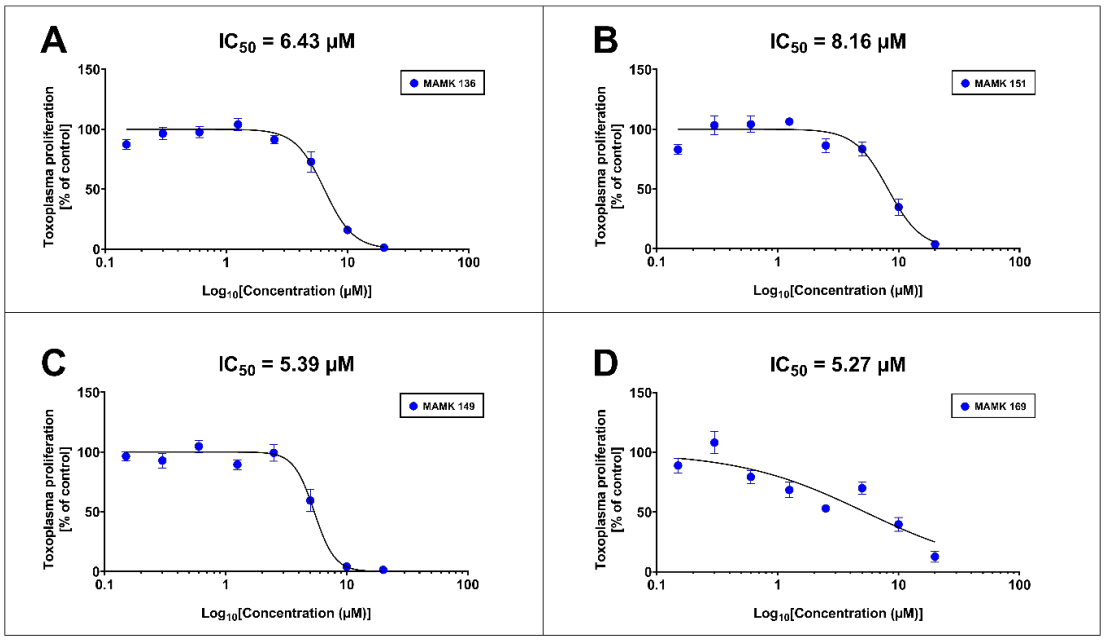

Figure 14: Anti-toxoplasma activity of the investigated POM ester compounds

The inhibitory activities of **MAMK 136** (**A**), **MAMK 151** (**B**), **MAMK 149** (**C**), **MAMK 169** (**D**), were determined by the *T. gondii in vitro* inhibition assay via the [^{3}H]-uracil incorporation into the RNA of the parasite. Data shown are from the means of three independent experiments each performed in duplicate (n = 6) ± SEM. IC_{50} values of each compound are shown.

Parental (free phosphonate)			POM esters (prodrugs)		
Compound	**IC_{50} (µM)**	**CC_{50} (µM)**	**Compound**	**IC_{50} (µM)**	**CC_{50} (µM)**
MAMK 89	> 50	> 100	**MAMK 136**	6.43 ± 0.8	> 100
MAMK 150	> 50	> 100	**MAMK 151**	8.16 ± 1.68	> 100
MAMK 145	> 50	> 100	**MAMK 149**	5.39 ± 0.47	80.56 ± 10.54
CBK 52	> 50	> 100	**MAMK 169**	5.27 ± 1.52	> 100
Fosmidomycin	> 50	> 100			

Table 3: In vitro activity against *T. gondii* ME49 tachyzoites and their cytotoxicity on human fibroblasts Hs27 of DXR inhibitors.

Values shown in the table represent the means of three independent experiments each done in duplicate (n = 6) ± S.D.

Cytotoxicity assays

I further investigated the cytotoxic effects of *T. gondii* host cells for all compounds, in order to address the selectivity of their anti-toxoplasma activity. The experiments were performed as described in the Material and Methods section in chapter 3.5. All the examined compounds showed low or no cytotoxic effect on human fibroblasts Hs27, indicating the selectivity of their activity (**Figure 15**).

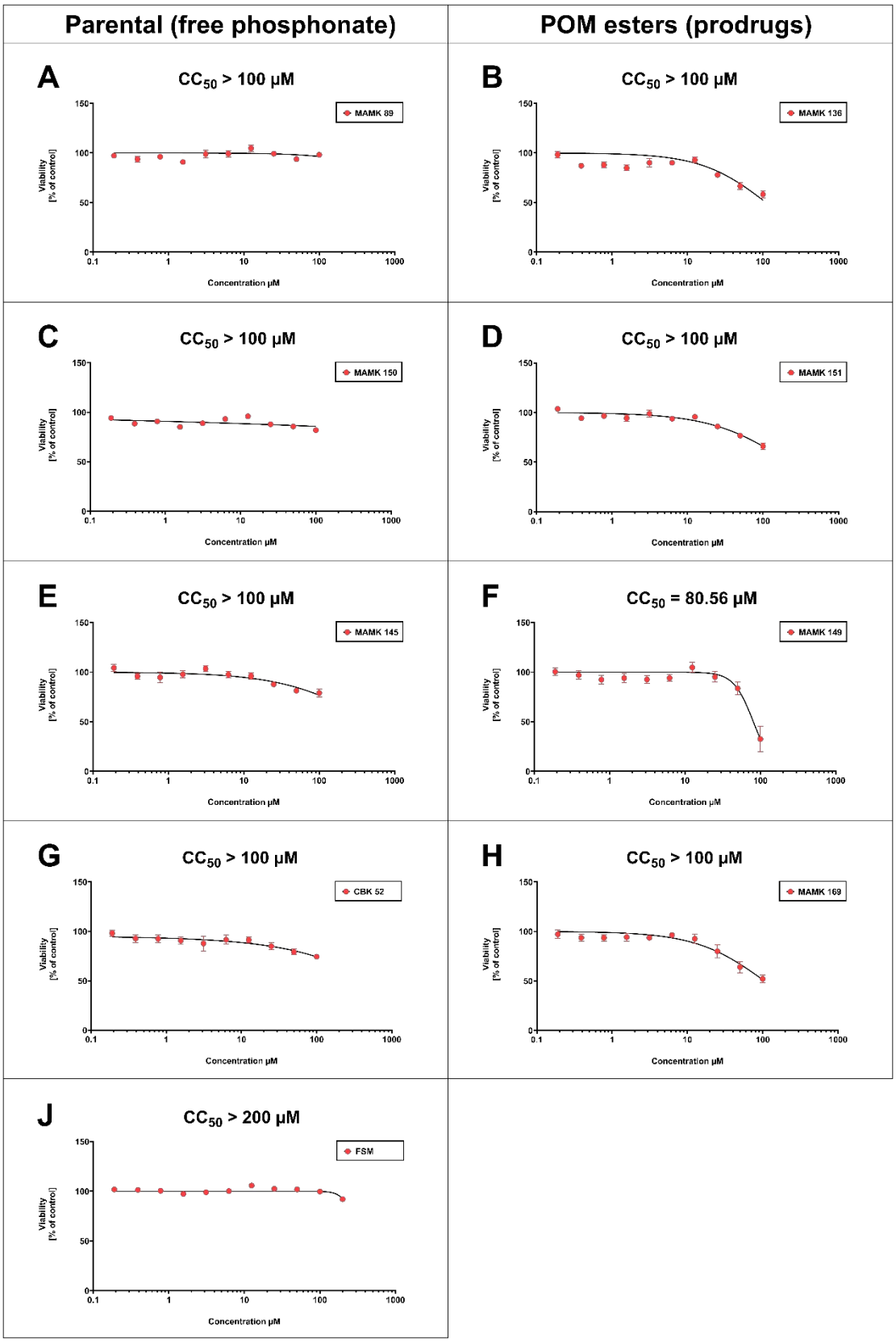

Figure 15: Effect of the investigated phosphonate and POM ester compounds on the viability of human fibroblasts Hs27

Cytotoxic effect of **MAMK 89** (**A**); **MAMK 136** (**B**); **MAMK 150** (**C**); **MAMK 151** (**D**); **MAMK 145** (**E**); **MAMK 149** (**F**); **CBK 52** (**G**); **MAMK 169** (**H**); **Fosmidomycin** (**I**); against human cell lines Hs27 as

determined by MTT assay. 100% growth control DMSO, 0% growth control staurosporine. Values shown in the figures represent the means of three independent experiments each done in duplicate (n = 6) ± SEM.

4 Additional Unpublished Work

4.1 In vitro evaluation of a Histone Deacetilase Inhibitor (HDACi) library against *Toxoplasma gondii*

Compound	IC_{50} (μM)	CC_{50} (μM)
LAK 39	0.20	> 200
LAK 41	0.02	> 200
YAK 31	0.04	> 200
LAK 17	> 50	-
BBK 69	1.12	> 200
MPK 409	0.03	> 200
LAK 67	0.11	> 200
LAK 86	> 50	-
LAK 88	> 50	-
LAK 88	> 50	-
LAK 107	> 50	-
LAK 110	> 50	-
LAK 121	> 50	-
FFK 29	> 50	-
MPK 187	> 50	-
MPK 472	0.59	> 200
MPK 541	0.19	174.33
MPK 576	> 50	-
YAK 545	> 50	-
MPK 508	0.99	> 200
MPK 807	> 50	-
KSK 75	> 50	-
YAK 448	5.61	> 200
YAK577	> 50	-
YAK 576	0.9	125.66
LAK- ZnfD	> 50	-
LAK119	> 50	-
LAK 31	> 50	-
LMK 179	2.46	-

LMK 174	1.32	> 200
HP7 Hy	0.93	> 200
KSK 23	0.42	> 200
KSK 17	0.54	> 200
KSK 25	0.5	> 200
KSK 29	0.36	> 200
KSK 81	0.72	> 200
KSK 83	0.83	> 200
KSK 119	1.48	> 200
LAK 21	0.21	> 200
LAK 37	0.58	> 200
LAK 65	0.21	> 200
YAK 40	0.036	> 200
YAK 61	0.047	> 200
YAK 63	0.45	> 200
YAK 70	0.42	> 200
MPK 406	1.86	> 180
MPK 415	0.44	> 200
BLK 195	0.66	> 200
MPK 377	> 3.89	-
YSKK 74	0.53	105.99
YSKK 43	0.84	> 200
YAK 466	0.84	> 200
YAK 477	0.061	166
YAK 483	0.92	71
MPK 803	< 0.115	> 200
KSK 43	< 0.105	> 200
LAK 29	0.37	> 200
YAK 77	2.9	-
YAK 320	< 0.19	> 200
FFK 22	1.27	> 200
FFK 23	0.63	> 200
VWK 408	0.44	> 200
FFK 70	0.19	> 200
FFK 85	0.31	> 200
LAK 40	0.81	> 200

SAHA	0.026	> 200
Panobinostat	0.001	92.33
Nexturastat A	0.22	> 200
Pyrimethamine	0.06	> 100

Table 4: Anti-toxoplasma activity and cytotoxicity against human fibroblasts Hs27 of HDACi against *T. gondii*

Molecules synthesised by members of the research group of Prof. Dr. Thomas Kurz.

5 Discussion

The treatment for human toxoplasmosis faces various limitations. Therapy is mostly relying on the use of antifolates, based on the inhibition of the folate metabolic pathway of the parasite at specific steps. The most effective chemotherapeutic of this class in PYR, a DHFR inhibitor widely used for the treatment and prophylaxis of toxoplasmosis. As the administration of PYR alone results usually ineffective, it is often combined with sulphonamides (especially SDZ), that inhibit the DHPS enzyme in the same pathway for a synergistic effect that increases drug efficacy. Moreover, PYR is an unspecific inhibitor, unable to distinguish between parasite and host enzymes, resulting in off-target toxicity and severe adverse effects. In addition, the raise of drug resistances and the absence of a vaccine for the medical prevention emphasize the urgent need for novel therapeutic alternatives (Dunay et al., 2018; Montazeri et al., 2018; Y. Zhang et al., 2022).

With the aim to identify new drug candidates that might address the critical need for novel chemotherapeutics for the treatment of toxoplasmosis, a screening of different mini-libraries of NPs, NPs analogues and NPs-inspired molecules was performed to assess their inhibitory activity on inhibiting the proliferation of *T. gondii* tachyozoites of the ME49 strain, a type II strain which is the predominant type associated with human infection (F. G. Araujo & Slifer, 2003). Molecular, cellular, structural biology, and biochemical approaches were employed for the elucidation, evaluation and characterization of their mechanism of action.

Natural products from the endophytic fungus *Paraboeremia selaginellae*

Endophytes are endosymbiont microorganisms, often fungi or bacteria, that colonize plants for all or part of their life cycle establishing an interaction with their host, without causing a disease (Gouda, Das, Sen, Shin, & Patra, 2016). Likewise, endophytes can have an essential defence role against pathogens for their hosts, i.e. releasing secondary metabolites. These are biologically active substances that could provide protection directly, through their intrinsic antibiotic activity, or indirectly, triggering the mechanisms of defences of the host or promoting its growth (Alvin, Miller, & Neilan, 2014). Thus, endophytes in general, and especially fungal endophytes, have gathered a high interest for drug discovery due to their enormous potential as source of structurally diverse NPs that could serve a potential leads (Aly, Debbab, & Proksch, 2011). With the raise of antimicrobial resistance (AMR) and the emergency for novel antibiotics, nowadays fungal endophytes are still playing a crucial role in natural product drug discovery (Gakuubi, Munusamy, Liang, & Ng, 2021; Tiwari & Bae, 2022).

Hence, with the aim to identify NPs with anti-toxoplasma activity, the endophytic fungus *Paraboeremia selaginellae* (*P. selaginellae*) from the ornamental plant *Philodendron monster* was investigated for its potential as a source of anti-toxoplasma agents (chapter 3.1) (Mazzone et al., 2022). After the isolation and purification of eight NPs from solid rice cultures, six of them could be identified which showed an anti-toxoplasma activity (**Figure 16**), with low or no cytotoxicity in different human cell lines and no activity in gram-positive, gram-negative representatives and *Mycobacterium tuberculosis* (*M. tuberculosis*).

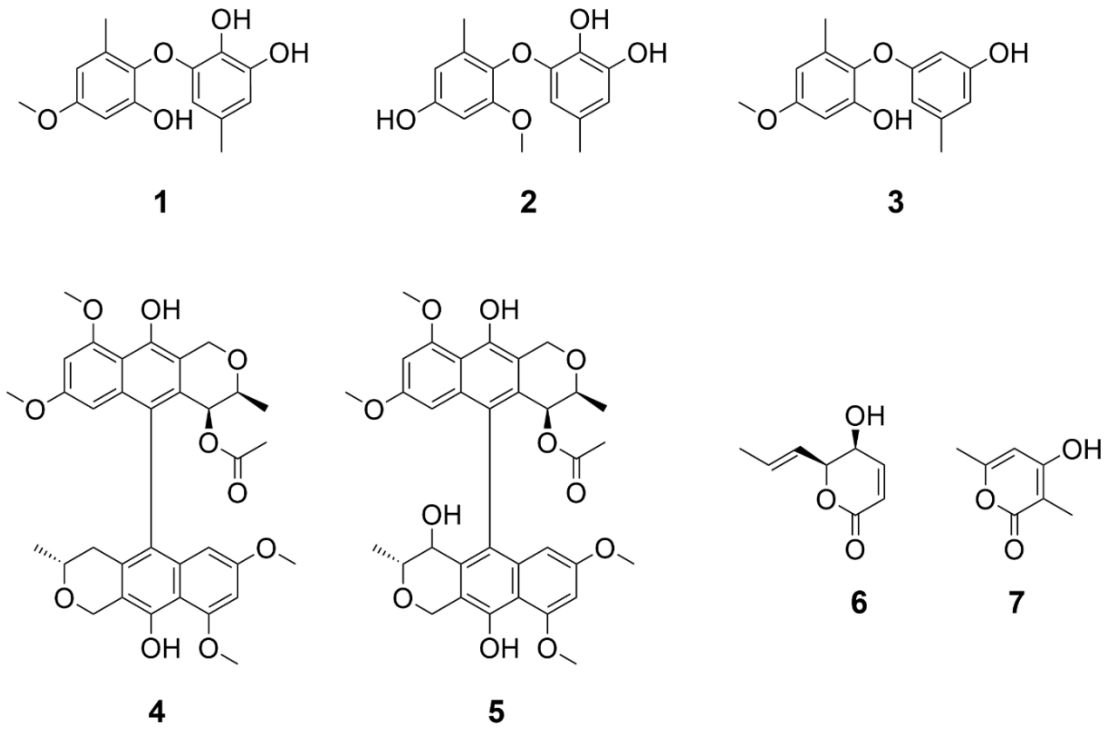

Figure 16: Natural products isolated from the endophytic fungus *P. selaginella* with anti-toxoplasma activity

Diphenyl ethers NK-A 17e233 (**1**), 1,2-benzenediol, 3-(4-hydroxy-2-methoxy-6-methylphenoxy)-5-methyl-(ACI) (**2**) and cyperin (**3**); bioxantracenes ES-242-1 (**4**) ES-242-3 (**5**); and lactones 5*S*,6*S*-phomalactone (**6**) and methyltriaceticlactone (**7**). Molecules isolated by Viktor E Simons.

The experimental results of diphenyl ethers, bioxanthracenes and lactones highlighted the specificity and selectivity of their inhibition of *T. gondii* proliferation and, additionally, that they may have a wide therapeutic window that could minimize the risk of adverse effects *in vivo*. Since no one of the tested compounds reached an IC_{50} value in the nanomolar range as the current treatment in clinical use PYR, these results could be a starting point for employing a semi-synthetic approach for the identification of more potent derivatives. This approach would be suitable especially for the diphenyl ethers (**Figure 16**), due the absence of stereocenters in their structure and their low molecular weight. These molecules have the

same scaffold as triclosan, an NP with a broad-spectrum antibacterial and antifungal property which is widely used in consumer products (Fang et al., 2010), Triclosan was shown to act as an inhibitor of the microbial enoyl reductase (FabI) in a microbial lipid biosynthetic pathway (McMurry, Oethinger, & Levy, 1998). Considering the structural similarities, the diphenyl ethers **1**, **2** and **3** might have a common target with triclosan.

More structural complex molecules are bioxantracenes, where interestingly the IC_{50} of **4** and **5** were comparable with the previously reported IC_{50} values for the inhibition of *Plasmodium falciparum* (*P. falciparum*), suggesting maybe that they may share the same mode of action and the same target in apicomplexans. Phomalactone (**6**) is a widely spread secondary metabolite that has been isolated in several genus encompassing *Phoma* (Hussain et al., 2014), *Nigrospora* (J. C. Kim, Choi, Park, Kim, & Cho, 2001), *Xilaria* (Jiménez-Romero, Ortega-Barría, Arnold, & Cubilla-Rios, 2008), *Aspergillus* (Komai et al., 2003), *Verticillium* (Khambay, Bourne, Cameron, Kerry, & Zaki, 2000). A wide spectrum of bioactivities have been reported (Khambay et al., 2000; Komai et al., 2003; Krasnoff & Gupta, 1994) including a weak antimalarial activity (Jiménez-Romero et al., 2008). In the present study, it is reported for the first time the isolation of **6** from the genus *Selaginellae* and its more effective anti-toxoplasma capacity *in vitro* (IC_{50} 5.13 μM) than its reported activity on the apicomplexan *P. falciparum* (IC_{50} 84.32 μM) (Jiménez-Romero et al., 2008). This finding emphasizes that the strategy of repurposing previously identified substances with anti-apicomplexan activity remains a powerful tool for the anti-toxoplasma drug discovery. Indeed, the modes of action of bioxantracenes, biphenyl ethers and lactones on *T. gondii* remain still unknown and in-depth investigations in this issue are needed. The discovery of their targets could be beneficial for the drug optimisation process and additionally for potential target-oriented syntheses strategies.

Indolo[3,2-*a*]phenazines

Indolo[3,2-*a*]phenazines are poorly investigated penta-heterocycles wherein a carbazole moiety is fused with a phenazine moiety (**Figure 17**) (K. S. Kumar et al., 2017; Pramanik & Ghatak, 2022; Rinderspacher, 2013; Shoker, Ghattass, Fettinger, Kurth, & Haddadin, 2012; Yang et al., 2022). Very few synthetic strategies have been proposed for this class of compounds, such as carbonyl cyclocondensation approaches (Shoker et al., 2012; Teuber & Staiger, 1954) or the acid-catalysed cycloisomerization of indole-substituted 3-ethynylquinoxalines (K. S. Kumar et al., 2017). The only proposed pharmacological assessment for indolophenazines is their potential as anti-cancer agents as inhibitor of the

NAD(P)H quinoneoxido reductase (NQO1) *in silico* (Nolan, Timson, Stratford, & Bryce, 2006) and their cytotoxic proprieties against the two cancer cell lines TZM-BL (human cervical carcinoma cells) and A549 (human lung carcinoma cells) *in vitro* (K. S. Kumar et al., 2017). In this study (chapter 3.2), a gold-catalysed 1,2-silyl migratory cycloisomerization of 3-(TMS)ethynyl quinoxalines and subsequent one-pot *ipso*-iodination Suzuki coupling for the synthesis of 6-aryl-indolo[3,2-*a*]phenazines was proposed which resulted in moderate to good yields. The combined presence of a donor (carbazole) and an acceptor (phenazine) moiety serves as luminophore, conferring intriguing photophysical proprieties to these molecules, where their emission colour and the yield of their fluorescent quantum can differ depending on their substituents. Donor-acceptor moieties are commonly found within scaffolds of NPs, such as in berberine (Rajapakse et al., 2023). The latter is a penta-heterocyclic NP, belonging to the protoberberine group of benzylisoquinoline alkaloids, featuring electron-donating methylenedioxy and methoxy groups and an electron-accepting isoquinolium moiety (Rajapakse et al., 2023), such exhibiting structural similarities to indolophenazines (**Figure 17**).

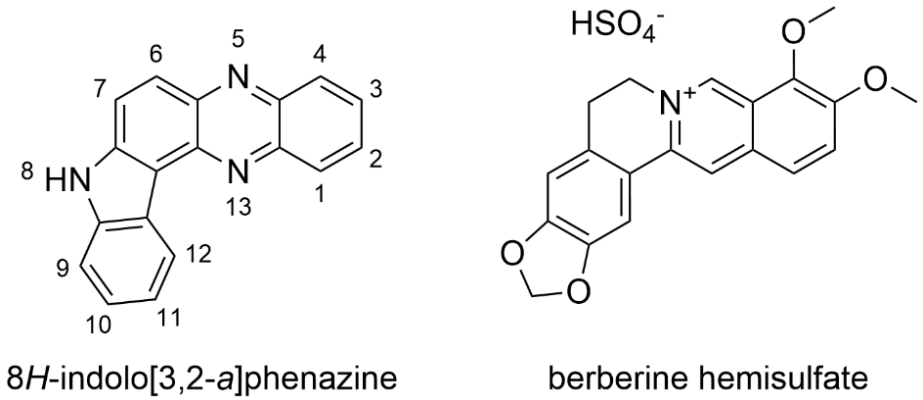

Figure 17: The penta-heterocyclic structures of 8*H*-indolo[3,2-*a*]phenazine and berberine hemisulfate in comparison.

Several pharmacological activities have been reported for berberine, such as anti-microbial, anti-cancer, anti-inflammatory, anti-depressant, analgesic, anti-protozoal (A. Kumar et al., 2015), including anti-toxoplasma (Krivogorsky, Pernat, Douglas, Czerniecki, & Grundt, 2012) activities. In light of these prior findings, the investigation of the anti-toxoplasma activity of seven selected synthetic indolo[3,2-*a*]phenazines was performed (Merkt et al., 2021). The results showed that all investigated molecules strongly inhibited *T. gondii* proliferation *in vitro*, with the phenyl (IC_{50} 0.73 μM) and p-tolyl (IC_{50} 0.67 μM) substituted derivatives (**Figure 18**) showing IC_{50} values lower than berberine (IC_{50} 0.94 μM).

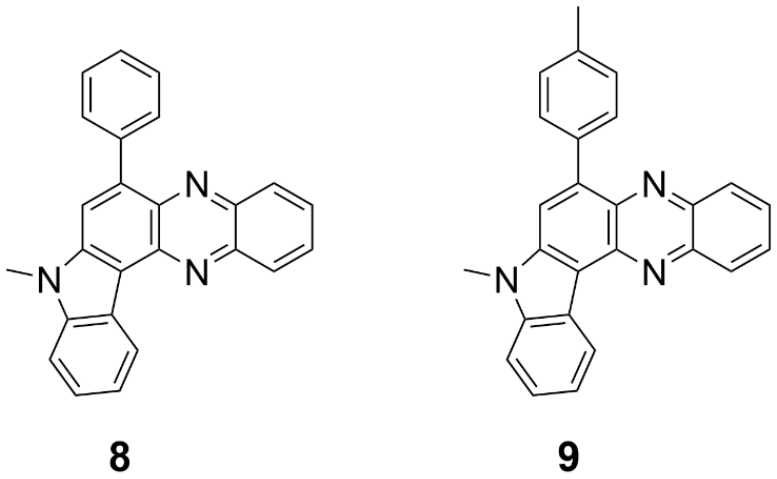

Figure 18: Most active indolo[3,2-*a*]phenazines of the first cohort against *T. gondii*
8-methyl-6-phenyl-8*H*-indolo[3,2-*a*]phenazine (**8**) and 8-methyl-6-(p-tolyl)-8*H*-indolo[3,2-*a*]phenazine (**9**). Molecules were synthesised by Franziska K. Merkt.

These findings established indolo[3,2-*a*]phenazines as novel anti-toxoplasma agents, and additionally, compounds with phenyl and p-tolyl moieties bound to the phenazine core-structure as promising leads for future drug optimisation studies. Regrettably, all the investigated compounds demonstrated cytotoxic effects on human fibroblasts Hs27 starting from 5 μM. Moreover, some compounds presented limited solubility in water, emphasizing the need of analogues with a broader therapeutic window and improved pharmakinetics. Thus, was commenced a systematic process with the objective to identify novel leads characterized by a superior profile, featuring lower cytotoxicity in human host cells, enhanced solubility in water, improved potency and with good synthetic yields. In total, fifteen novel derivatives were synthesised, with a diverse pool of substituents with electron withdrawing or electro donating abilities in position 6 and with or without halogen substitution in position 11 (chapter 3.2.1). Thus, the novel derivatives were screened for their activity against *T. gondii* proliferation and their cytotoxic effects on the human host fibroblasts Hs27. Compound LHP 091 (**10**), featuring the electron-rich thiophen-2-yl moiety in position 6 (**Figure 19**), exhibited the most promising profile with IC_{50} of 1.36 μM against *T. gondii* accompanied by no cytotoxic effects toward the host cells at a concentration up to 100 μM.

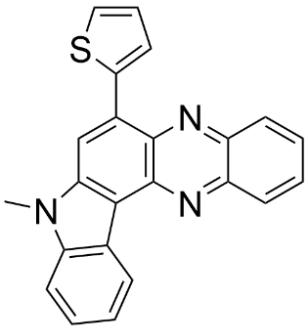

10

Figure 19: Chemical structure of the indolo[3,2-*a*]phenazine lead compound LHP 091
8-methyl-6-(thiophen-2-yl)-8*H*-indolo[3,2-*a*]phenazine (**10**). The molecule was synthesised by Larissa K.E Hinz.

The improved solubility in water and the efficient yield in the synthesis process, established **10** as our new lead compound. Given that *in vitro* parameters may not accurately reflects the more complex scenario *in vivo*, it is an imperative to investigate in the future the activity, safety and pharmacokinetic / pharmacodynamic profile of the lead compound **10** *in vivo*, in a *T. gondii* infection mouse model. Moreover, the mechanism of inhibition of indolo[3,2-*a*]phenazines on *T. gondii* proliferation remains elusive. Natural and synthetic phenazines have demonstrated to possess intriguing wide range of biological activities (Yan et al., 2021), including antiplasmodial activity (Makgatho et al., 2000). As mechanism of actions, a dual inhibition of topoisomerase I and II and radical scavenging activity has been proposed, which could enable these molecules to act on a wide range of microorganisms and cancer cells (Serafim, Bernardino, Freitas, & Torres, 2023). Thus, it would therefore be interesting to explore these possible modes of action in *T. gondii*. Additionally, given the interesting photophysical properties of indolo[3,2-*a*]phenazines, which allow them to emit luminescence, the exploitation of this propriety as a tool for molecule localization at the cellular level and monitoring protein interactions could be an interesting strategy for the target identification. In addition, another promising strategy to exploit the photophysical properties of indolo[3,2-*a*]phenazines involves a photo cross-linking approach combined with FPLC/HPLC MS (fast protein liquid chromatography/high-performance liquid chromatography with mass spectrometry) (Kozoriz et al., 2023), which could allow the identification of their biological target in the parasite. Finally, comparison between the mechanism of action of berberine and indolo[3,2-*a*]phenazines would be intriguing. Therefore, a viable strategy to isolate and selectively identify the target proteins of both molecules would be the derivatisation of berberine and indolo[3,2-a]phenazines by affixing

a biotin tag and subsequent affinity purification with streptavidin pull-down, where the purified proteins can be identified by MS (Tabana, Babu, Fahlman, Siraki, & Barakat, 2023). Another alternative that could allow the identification of receptor size or confirmation of target binding candidates would be the far Western blot, a rapid method to detect receptor-ligand interactions (Peng, Ramatchandirin, Pearah, & He, 2023).

Biflavones

Flavones are a class of flavonoids that is widely distributed as secondary metabolites in plants, playing a central role in the adaptation of plants to their environment by exercising several functions, including plant signalling and defence (Andersen & Markham, 2005). These molecules are based on a 2-phenylchromen-4-one (2-phenyl-1-benzopyran-4-one) backbone. Due to their variety of biological activities, the scaffold of flavones has been deeply investigated in medicinal chemistry for structure-activity relationships studies. These studies generated the synthesis and the development of semi-synthetic or total synthetic derivatives, showing a wide range of applications such as anti-inflammatory, anti-oxidant, anti-cancer and antimicrobial activities (M. Singh, Kaur, & Silakari, 2014). Flavone dimers, termed biflavones, have shown interesting bioactivities with potential for drug discovery (Chen et al., 2019; Menezes & Diederich, 2019), particularly the antiprotozoal and anticancer activity of non-C2-symmetric biflavones (H. P. Kim, Park, Son, Chang, & Kang, 2008; Y. M. Lin et al., 1999; Yu et al., 2017). The 8,8'-biflavones are a less studied type of symmetrical biflavones. NP cupressuflavone (CUF), a dimer of two monomeric units of apigenin (Murti, Raman, & Seshadri, 1967), has been little studied for its antioxidant and antimicrobial activity (Al-Sayed & Abdel-Daim, 2014; Al-Sayed, Gad, El-Shazly, Abdel-Daim, & Nasser Singab, 2018). Since different bioactivities have been reported for the monomeric unit apigenin (Imran et al., 2020; Salehi et al., 2019), and in some cases, dimers have been shown to exhibit higher potency than their monomeric counterpart (Frank et al., 2015; W. Zhang et al., 2008), in chapter 3.3 the investigation focused on the synthesis and biological evaluation of monomeric flavones and dimers. Specifically, the aim of the study was to propose a modular and scalable approach for the synthesis of a diversity-oriented library of 8,8'-biflavones, followed by the biological evaluation of their anti-toxoplasmic activity, their cytotoxic effects on human fibroblasts (Hs27) and malignant (HeLa) cell lines, and their antioxidant capacity, including the comparison of the bioactivities of monomeric and dimeric molecules (Klischan et al., 2023). The synthesis of a mini-library of 14 flavones and 13 of the corresponding biflavones was performed in excellent yields, without the need for chromatographic isolation.

Overall, biological investigations showed the potential of this library as anti-toxoplasma, anti-cancer and anti-oxidant agents, with the 8,8'-biflavones having a significantly increased potency compared to their monomeric counterparts. 4-NMe_2-substituted biflavone (**11**) (**Figure 20**) showed to be the most potent in the mini-library for both its anti-toxoplasma activity and anti-cancer capacity with comparable IC_{50} values, making it a lead compound for future investigations.

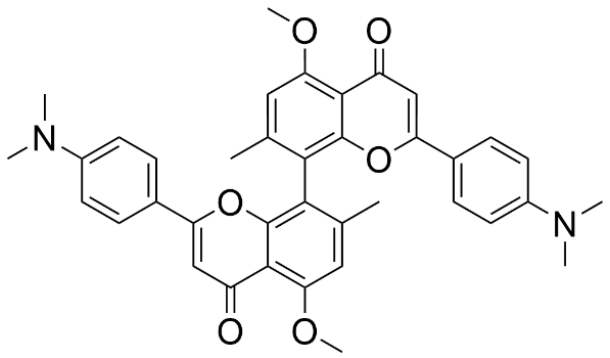

11

Figure 20. Chemical structure of the 8,8'-biflavone lead compound
2,2'-bis(4-(dimethylamino)phenyl)-5,5'-dimethoxy-7,7'-dimethyl-4*H*,4'*H*-[8,8'-bichromene]-4,4'-dione (**11**).
The molecule was synthesised by Moritz K.T Klischan.

Additionally, compound **11** showed no cytotoxic effects of the host-human fibroblasts Hs27 cells, demonstrating high selectivity and a potentially wide therapeutic window, that are excellent proprieties for the future investigation in *in vivo* in mouse models. The mechanism of action remains still unknown, and due the wide range of bioactivities of flavones, it may be possible that it executes interactions with multiple targets in the microorganism, leading to a strong potency. Fishing strategies, based on proteome-based affinity chromatography followed by high-resolution mass spectrometry analysis, could be interesting approaches for the simultaneously identification of multiple targets. In summary, our investigation highlights that nature is still a major source of scaffolds with diverse bioactivities, and continues to inspire medicinal chemistry for the optimisation of potential novel leads for drug development.

Bichalcones

Chalcones are naturally occurring secondary metabolites belonging to the family of flavonoids widely distributed throughout the plant kingdom (Rozmer & Perjési, 2016). They

have a 1,3-diaryl-2-propen-1-ones skeleton, existing as open-chain precursors for the biosynthesis of flavonoids and isoflavonoids, including flavones (N. Jiang, Doseff, & Grotewold, 2016; Rudrapal et al., 2021). For decades, chalcones have attracted the attention of medicinal chemistry research, especially in the fields of synthesis and drug discovery, due to the simplicity of their scaffolding and their wide range of bioactivity, earning them the appellation of "privileged scaffold in medicinal chemistry" (Zhuang et al., 2017). Amongst these bioactivities, chalcones were shown to possess potential anti-parasitic effects (Díaz-Carrillo et al., 2018; González et al., 2020; Montes-Avila, Díaz-Camacho, Sicairos-Félix, Delgado-Vargas, & Rivero, 2009; Sinha et al., 2019), including activity against *T. gondii* (AL-Hilli, Ghazzay, Hasan, Al-Kelaby, & Zarka, 2021; Ghazzay, Hasan, DeliKhudhair, & Abbas, 2023; L. Jiang et al., 2022; Si et al., 2018). Bichalcones, are a less investigated sub-class of chalcones, that were shown to possess anti-protozoal activity (Mihigo, Mammo, Bezabih, Andrae-Marobela, & Abegaz, 2010), particularly as antimalarial agents (Domínguez et al., 2013; Ram, Saxena, Srivastava, & Chandra, 2000; Sharma et al., 2018). Bichalcones consist of two monomeric subunits connected by distinct linkers. In particular, A-A'-bichalcones have only been scarcely explored in terms of synthesis and for their bioactivity profile. The synthetic approaches that have been proposed are lacking scalability (Li, Nehira, Hagiwara, & Harada, 1997; G.-Q. Lin & Zhong, 1997), a crucial value in natural product synthesis approaches (Kuttruff, Eastgate, & Baran, 2014). Moreover, some studies reported increased potency of bichalcones compared to their respective monomer counterparts (Pereira, Silva, Ribeiro, Silva, & Fernandes, 2023). As monomeric chalcones and A-A'-bichalcones represent essential synthetic intermediates in the construction of the flavones and 8-8´biflavones described in this thesis (see chapter 3.4), further investigation was based on the *in vitro* assessment of these previously synthesised intermediates within the mini-library. This involved *in vitro* screening for their anti-toxoplasma activity and their cytotoxic profile in the human host fibroblasts Hs27, as part of a comparative analysis of the dimeric A-A'-bichalcones with their monomeric counterparts. As result, the dimeric A-A'-bichalcones exhibited a notable increase in potency compared to their monomeric counterparts. Especially, the bichalcone **12**, with a benzene moiety as the B-ring and a methyl group (Me) at R (**Figure 21**), exhibited the highest potency and selectivity, being the only NP in the series with an IC_{50} in the nanomolar range. Notably, the bichalcone **13** with a methoxy group at R (**Figure 21**) showed a substantial decrease in potency, highlighting the importance of the smaller methyl group for the anti-toxoplasma activity.

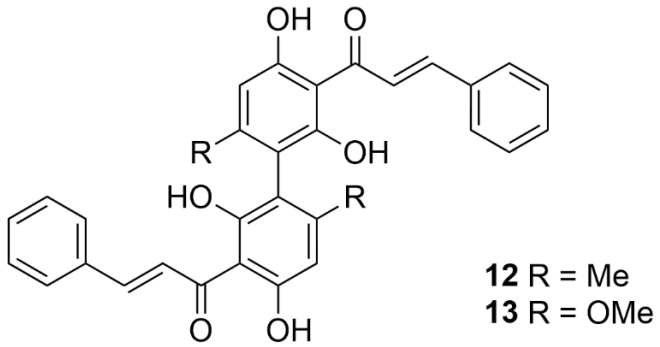

Figure 21. Chemical structures of bichalcones 12 and 13

(2*E*,2´*E*)-1,1´-(2,2´,4,4´-tetrahydroxy-6,6´-dimethyl-[1,1´-biphenyl]-3,3´-diyl)bis(3-phenylprop-2en-1-one) (**12**) and (2*E*,2´*E*)-1,1´-(2,2´,4,4´-tetrahydroxy-6,6´-dimethoxy-[1,1´-biphenyl]-3,3´-diyl)bis(3-phenylprop-2en-1-one) (**13**). Molecules were synthesised by Moritz K.T Klischan.

Since initially racemic mixtures were screened, the focus was redirected on the synthesis of both enantiomers of compound **12** followed by their biological evaluation, with the aim of identifying potential variations in potency and selectivity between them related to their absolute configuration. The enantiomers were also compared with the racemic mixture. After synthesizing enantiomers S_a and R_a of **12** (**Figure 22**), yielding 83% and 76%, respectively, the anti-toxoplasma evaluation revealed a two-fold increase in the activity of enantiomer ***R*$_a$-12** (IC_{50} 0.10 μM) compared to ***S*$_a$-12** (IC_{50} 0.31 μM).

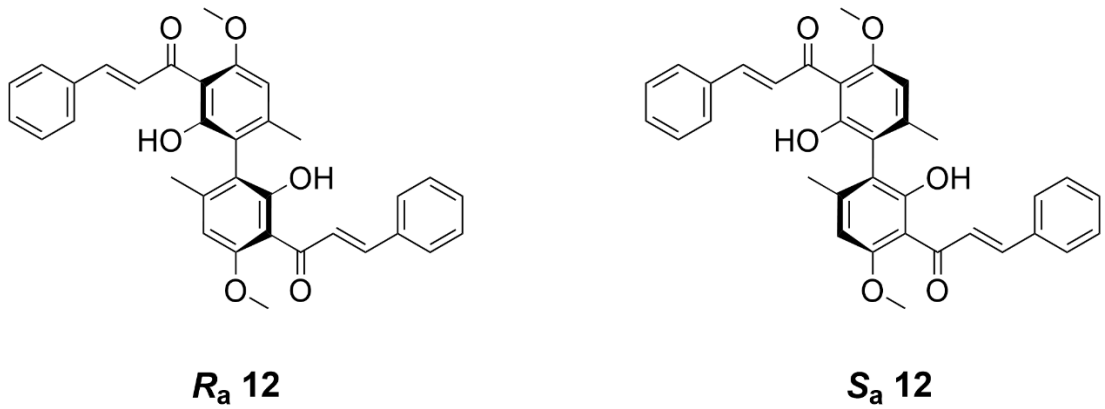

Figure 22: Chemical structures of enantiomers *R*$_a$-12 and *S*$_a$-12

Molecules were synthesised by Moritz K.T Klischan and Julian Greb.

With an IC_{50} value of ***R*$_a$-12** comparable to that of the racemic mixture, it indicates that ***R*$_a$-12** is the eutomer. Furthermore, the comparison with the IC_{50} of the standard treatment PYR IC_{50} 0.22 μM) underscores the potential of ***R*$_a$-12** as a novel anti-toxoplasma agent. As future prospects, it is crucial to identify the target of the biflavone ***R*$_a$-12** and to elucidate the mechanism of action of A-A'-bichalcones, an elusive sub-class of flavonoids that has not

been thoroughly explored for its biological potential and for their target in apicomplexa. Moreover, exploring the binding interactions with crystallography or docking analysis of stereoisomers ***R*$_a$-12** and ***S*$_a$-12** with their target and understanding the reasons behind the higher potency of ***R*$_a$-12** would be intriguing. Since the racemic mixture showed to be slightly more active than the pure enantiomer ***R*$_a$-12**, both enantiomers may exhibit a synergistic effect, involving agonistic binding to the same receptor, or interactions with other biological targets leading to a cooperative effect. Furthermore, the effect of pharmacokinetics could be crucial. However, these aspects warrant further investigation which is beyond this thesis. In this regard, it could be speculated that a potential target of bichalcone **12** for future deeper investigation could be the *T. gondii* silent information regulator 2 (SIR2), an NAD-dependent histone deacetylase (HDAC) belonging to the protein family of sirtuins (Imai, Armstrong, Kaeberlein, & Guarente, 2000). SIR2 was found to be a transcriptional regulator of mating-type loci, telomeres and ribosomal DNA in mammalian cells (Guarente, 2011; Haigis & Sinclair, 2010). While performing a structure-based virtual screening for the identification of novel modulators or inhibitors of sirtuins, Karaman *et al.* identified that rhuschalcone IV and a rhuschalcone I analogue inhibited human sirtuins SIRT-1 and SIRT-2 (Karaman et al., 2018). Given the structural similarities between rhuschalcone and the bichalcone **12** from our library (**Figure 23**), combined with the high degree of similarity between the humans and the parasite sirtuin proteins, it could be speculated that *T. gondii* SIR2 could be a potential target for bichalcone **12**.

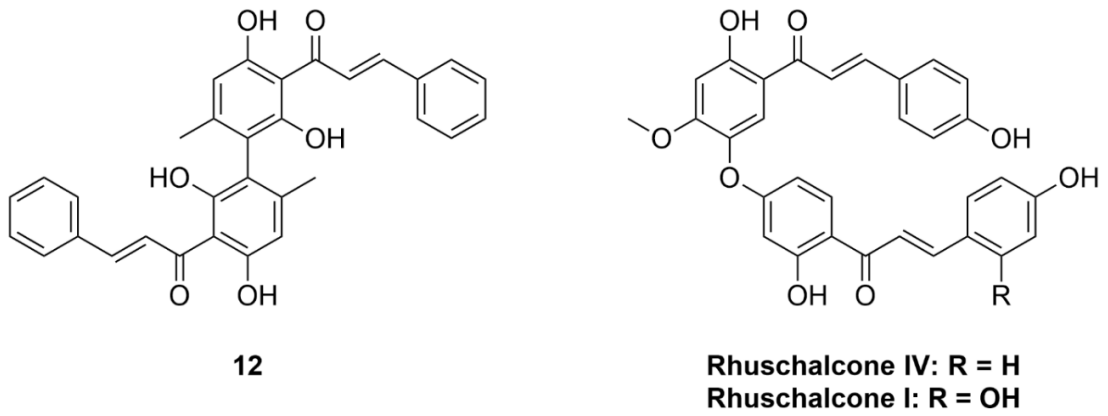

Figure 23: Chemical structures of bichalcone 12 and rhuschalcones IV and I

Comparison of chemical structures of the lead bichalcone **12** from our library and rhuschalcone IV and I investigated by (Karaman et al., 2018)

Unfortunately, the docking analysis did not resulted into a stable protein-ligand complex which might explain the inhibitory properties of the enantiomers ***S*$_a$** and ***R*$_a$** of **12** on *T. gondii*

SIR2. Thus, further investigations *in vitro* are necessary to validate this speculation. The expression of a recombinant *T. gondii* SIR2 and the subsequent *in vitro* investigation through an enzymatic assay wherein the enantiomers ***R*$_a$-12** and ***S*$_a$-12** are tested against *T. gondii* SIR2, and crystallography analysis of the *T. gondii* SIR2 in complex with the enantiomers, could be crucial to explore and to verify this hypothesis.

Reverse hydroxamate-based inhibitors of 1-deoxy-D-xylulose 5-phosphate reductoisomerase

The 2-C-methyl-D-erythritol-4-phosphate (MEP) pathway for the biosynthesis of isoprenoids has gathered high interest as a novel target for antimalarial, antibacterial and herbicidal effects (N. Singh, Chevé, Avery, & McCurdy, 2007). The MEP pathway is absent in humans and animals, which use the mevalonate (MVA) pathway for the biosynthesis of isoprenoids. The MEP pathway is exclusively present in eubacteria, plants and eukaryotic parasites such as Apicomplexans, including *T. gondii*. In this microorganism, the MEP pathway is located within the apicoplast (Rodriguez-Concepcion, 2004), a subcellular organelle responsible for essential metabolic pathways for the parasite (Kloehn et al., 2021a). The 1-deoxy-D-xylulose 5-phosphate reductoisomerase (DXR) enzyme, the second in the cascade of the MEP pathway, catalyzes the isomerization and the NADPH-reduction processes, transforming the substrate 1-deoxy-D-xylulose 5-phosphate (DXP) into MEP. As the rate-limiting enzyme of the pathway, it is referred to as a key enzyme (N. Singh et al., 2007). Hence, extensive research has been conducted on the DXR enzyme, and several crystal structures of the protein from various microorganisms have been reported (Henriksson et al., 2007; Reuter et al., 2002; Ricagno et al., 2004; Umeda et al., 2011). Unfortunately, the *T. gondii* DXR crystal structure remains still elusive. Fosmidomycin (FSM) (**Figure 24**), a natural product from the genus *Streptomyces*, composed of a phosphonic acid group linked to N-formylated moiety by a propyl linker, has been found to be a potent inhibitor of the DXR enzyme, gathering an high interest in drug development, especially as antimalarial (Knak et al., 2022).

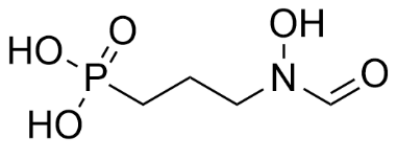

14

Figure 24: Chemical structure of the natural product fosmidomycin (FSM)

Due to its low bioavailability and its short plasma half-life, medicinal chemistry is directed on the synthesis of more stable and potent derivatives (Knak et al., 2022). Reverse hydroxamate-based inhibitors of DXR have shown their potential as potent antimalarial, antibacterial and antitubercular agents (Karin Brücher et al., 2012; Kunfermann et al., 2013; Lienau et al., 2019). Thus, the aim of this investigation (see chapter 3.5) was the expression and the purification of a recombinant truncated *T. gondii* DXR (*Tg*DXR) and the biochemical characterization as well as the determination of the structure of *Tg*DXR and its configuration through crystallographic and small-angle X-ray scattering (SAXS) analysis. As no DXR inhibitors have been described with anti-toxoplasma activity, the aim was to assess the *in vitro* inhibitory activity of previously investigated ß-thia and ß-oxa isosters of reversed hydroxamic acid analogues of FSM (Karin Brücher et al., 2012; Kunfermann et al., 2013; Lienau et al., 2019) (**Figure 25**), against the activity of *T*gDXR, and biologically, against the proliferation of *T. gondii*.

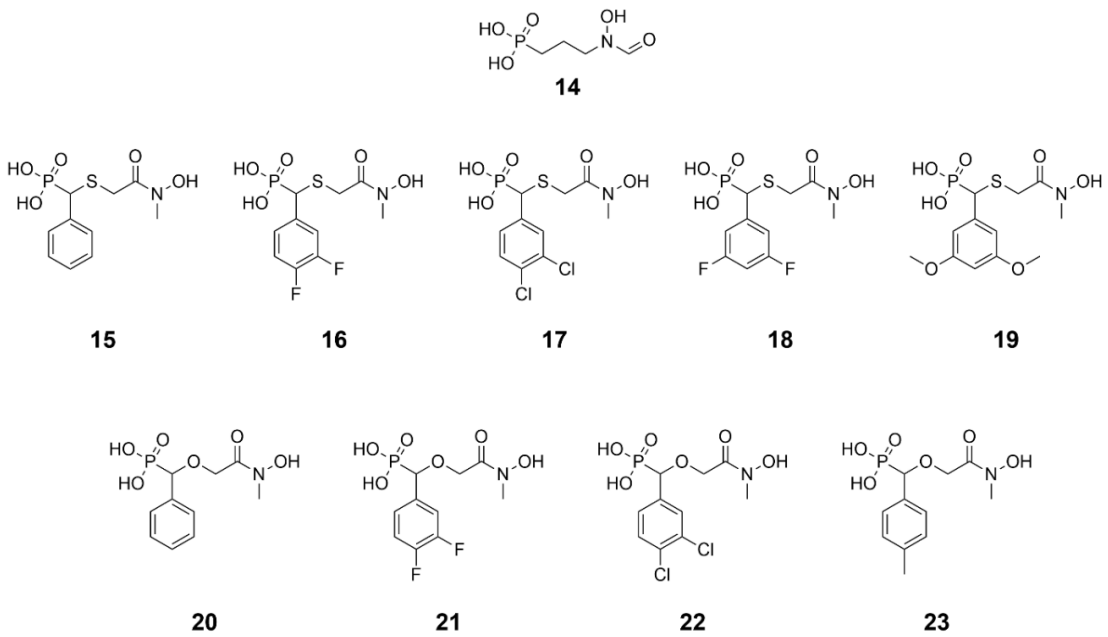

Figure 25: Chemical structures of fosmidomycin and the investigated reverse ß-thia and ß-oxa analogues of fosmidomycin

Compounds were previously investigated by (Karin Brücher et al., 2012; Kunfermann et al., 2013; Lienau et al., 2019).

Here, the first crystal structure of the *Tg*DXR enzyme was presented in complex with FSM and the co-factor NADPH. Overall, the structure of the NADPH-FSM complexed enzyme was similar to the ones described before from *M. tuberculosis*, *E. coli* and *P. falciparum*

(Henriksson et al., 2007; Umeda et al., 2011; Yajima et al., 2007). NADPH bound in a similar way as in the other DXR proteins. The binding pattern of the adenine and pentose phosphate moieties of NADPH is consistent with the ones observed in the DXR enzyme of *Escherichia coli* (*E. coli*) (Mac Sweeney et al., 2005). In contrast, the nicotinamide ring of NADPH exhibits orderliness in the FSM complex (**Figure 26**).

.

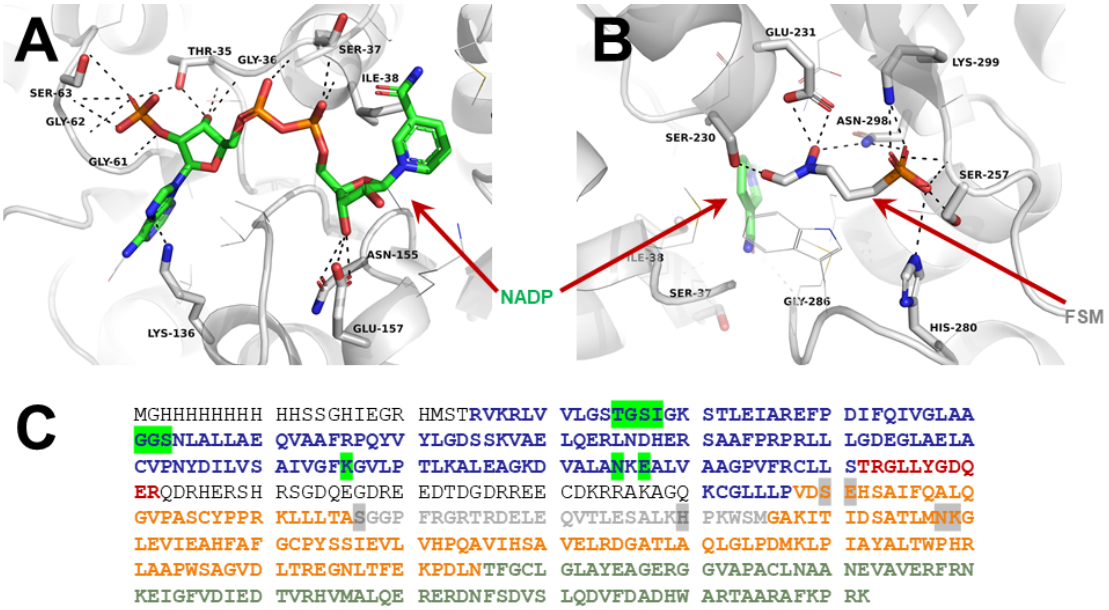

Figure 26: Detailed view of the active site of *Tg*DXR

(**A**) Binding interactions of *Tg*DXR amino acids residues and NADP (green); (**B**) Binding interactions of *Tg*DXR amino acid residues and FSM (grey). NADP and FSM are indicated with red arrows; (**C**) The amino acid sequence of the truncated His_{10}-*Tg*DXR and its domains: N-terminal dinucleotide domain (blue), additional loop (red), connective domain (orange), flexible loop (light grey) and C-terminal four-helix bundle (dark green). Binding interactions of NADP (green) and FMS (grey) in the amino acids sequence are highlighted. Figure created by Prof. Dr. Sander H.J. Smits.

Regarding the inhibition mode of FSM it can be noted that the hydroxamic acid moiety of FSM binds to the side-chain of Glu231 and to the backbone nitrogen of Ser25 (**Figure 26**). Unfortunately, no magnesium ion was observed in the crystal. In addition, due their flexibility, the long linker (from amino acids 182 -632) and the N-terminal domain with the histidine tag were not visible in the electron density map derived from the diffraction data of the crystal structure analysis. Therefore a SAXS analysis was performed. Here the structure including the missing parts could be completed, and additionally, the SAXS analysis revealed that in solution *Tg*DXR is in a dimeric state. Of note, a tendency could be found for ß-thia FSM analogues to exert an increased potency than the cognate ß-oxa FSM analogues which

could be observed on both the enzymatic and the biologic level. This tendency was also observed against the *E. coli* DXR and *M. tuberculosis* DXR in previous investigations (Kunfermann et al., 2013). Their crystal structures revealed that the interaction of the sulphur atom with the conserved Met298 of the flexible loop of the DXR enzymes play a crucial role on improving potency (Behrendt et al., 2011; Kunfermann et al., 2013). In particular, in this study, compound **17** (**Figure 25**), a reverse ß-thia-analogue with 3,4 halogen substitutions at the phenyl moiety, showed the highest potency against the enzymatic activity and against *T. gondii* proliferation. The enhanced lipophilicity and electronegative properties resulting from the 3,4-dichlorophenyl substitution may play a pivotal role in augmenting cellular uptake (T. Haemers et al., 2006). It was observed that the IC_{50} for the inhibition of *T. gondii* parasite proliferation is much higher compared to the inhibition at the enzymatic level. This is perhaps due to the permeability barrier posed by the lipophilic membranes, impeding a compound originating from the extracellular space of the host cell from reaching the DXR enzyme in the *T. gondii* apicoplast (J. Kloehn, C. E. M. Lacour, & D. Soldati-Favre, 2021b) where halogenated molecules might easier translocate (Timothy Haemers et al., 2006). Thus, novel potent and more lipophilic DXR inhibitors, capable to over cross the several hydrophobic membranes and reach the target at the apicoplast are needed for the future. Overall, these findings demonstrate that the *Tg*DXR enzyme is a druggable target for the future investigation into anti-toxoplasma agents. The crystal structure of *Tg*DXR holds promise for aiding in future docking analyses, facilitating the modelling of more potent inhibitors. Henceforth, crystallographic analyses on complexes of *Tg*DXR with reverse ß-thia-analogues of FSM would be of significant interest. Those analyses would provide close insights on the binding interactions with the target, allowing for a comparison with FSM, and additionally, a comparative assessment into their interaction with other protein homologues.

To address the permeability issues related to the phosphonic acid moiety, which could limit the cellular uptake and decrease its potency for inhibition of parasite proliferation, a second screening of novel five phosphonate compounds and their corresponding POM-esters was commenced. The aim was to identify POM-prodrugs with improved lipophilicity that are able to cross the biological membrane barriers better than their respective free-phosphonate compounds, thus undergoing bioactivation and subsequently reaching the *Tg*DXR enzyme, leading to an enhanced anti-toxoplasma activity *in vitro* (chapter 3.5.1). Our findings showed that all the examined free-phosphonate compounds present a DXR inhibitor activity at the enzymatic level, and low or no activity on the inhibition of the proliferation of the

intracellular parasite. On the other hand, all the investigated POM-esters showed anti-toxoplasma activity and low or no activity on the enzymatic level, clearly suggesting a prodrug activity (Walther, Rautio, & Zelikin, 2017). Further investigations are needed for the validation of the prodrug activities especially *in vivo*. Metabolomics through ion chromatography-mass spectrometry (IC-MS) on the MEP pathway of POM-esters treated *T. gondii*, associated with stability tests of the free-phosphonate compounds and POM-esters, could provide enhanced insights and understanding of the activity of POM-esters for the future *in vivo* investigation in a mouse model.

6 Concluding Remarks

Overall, the outcomes of this thesis comprise a variety of molecules from different natural and synthetic sources, ranging from isolated NPs, derivatives of NPs to fully synthetic molecules that draw inspiration from natural scaffolds (**Figure 27**). These findings confirmed the pivotal role of Nature in the drug discovery for novel anti-toxoplasma leads. The chemical diversity and unique structures of NPs are often associated with a diverse array of bioactivities that may remain undiscovered. Thus, drug repurposing of already known NPs, is still a viable, cost-effective and rapid strategy for the only scarcely explored field of anti-toxoplasma drug discovery. The recent advances in artificial intelligence (AI), HTS and the availability of modern large databases, such as sequence data, coupled with the almost inexhaustible reservoir of natural products, could synergistically enhance the repurposing approach. Additionally, the comprehensive understanding of novel therapeutic targets, through crystallography and other biochemical methods, can support the structure-based optimization of already known NPs, leading to the synthesis and development of more potent and stable derivatives. In conclusion, the findings gained through this thesis will hopefully support the future preclinical research for the discovery of anti-toxoplasma drugs. Lead structures developed and tested within this work can now be tested in *in vivo T. gondii* infection animal models.

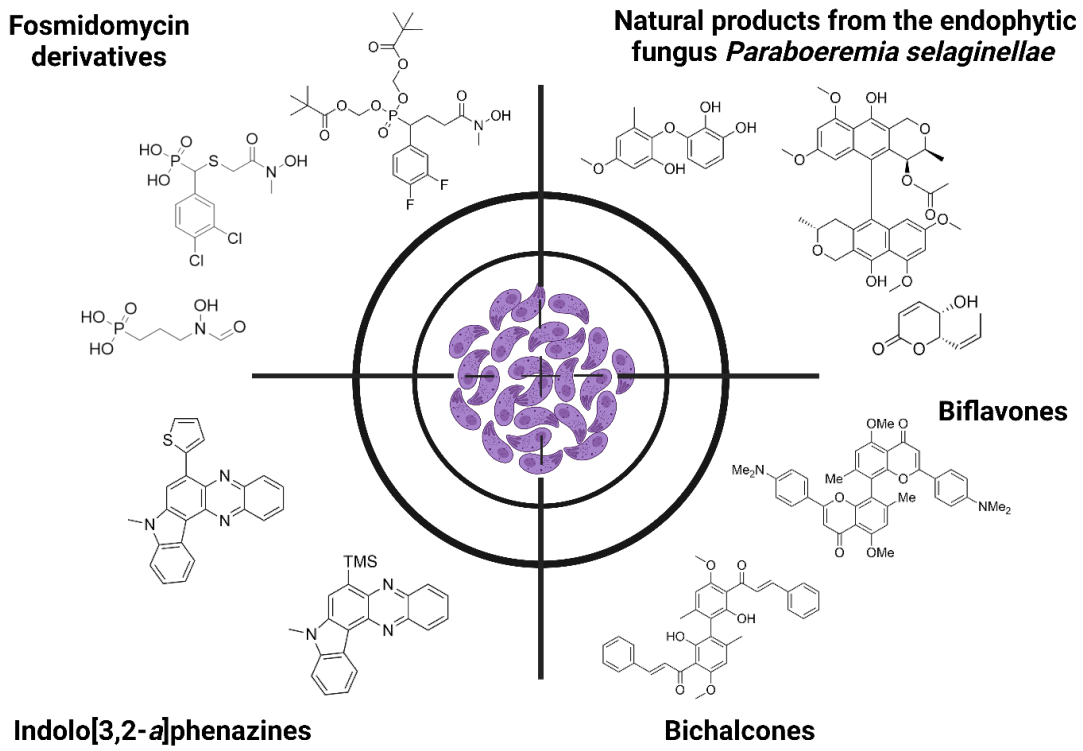

Figure 27: *T. gondii* under the scope: summary of the compound classes investigated

Chemical structures representativs of fosmidomycin derivatives, natural products from the endophytic fungus *P. selaginellae*, biflavones, bichalcones and indolo[3,2-*a*]phenazines investigated in this dissertation for anti-toxoplasma activities are shown.
Created with BioRender.com.

Literature

Adeyemi, O. S., Sugi, T., Han, Y., & Kato, K. (2018). Screening of chemical compound libraries identified new anti-Toxoplasma gondii agents. *Parasitol Res, 117*(2), 355-363. doi:10.1007/s00436-017-5698-1

Adl, S. M., Leander, B. S., Simpson, A. G., Archibald, J. M., Anderson, O. R., Bass, D., . . . Karpov, S. (2007). Diversity, nomenclature, and taxonomy of protists. *Systematic biology, 56*(4), 684-689.

Akira, S. (2000). The role of IL-18 in innate immunity. *Current opinion in immunology, 12*(1), 59-63.

AL-Hilli, E. S. A., Ghazzay, M. H., Hasan, S. A., Al-Kelaby, K. K. A., & Zarka, M. A. (2021). THERAPEUTIC EFFECT OF CHALCONE ON TOXOPLASMA GONDII ISOLATED FROM RECURRENT PREGNANCY LOSS CASES IN AL-NAJAF CITY" INVITRO STUDY". *Journal of Natural Remedies, 22*(1 (2)), 32-40.

Al-Malki, E. S. (2021). Toxoplasmosis: stages of the protozoan life cycle and risk assessment in humans and animals for an enhanced awareness and an improved socio-economic status. *Saudi Journal of Biological Sciences, 28*(1), 962-969.

Al-Sayed, E., & Abdel-Daim, M. M. (2014). Protective role of Cupressuflavone from Cupressus macrocarpa against carbon tetrachloride-induced hepato-and nephrotoxicity in mice. *Planta medica, 80*(18), 1665-1671.

Al-Sayed, E., Gad, H. A., El-Shazly, M., Abdel-Daim, M. M., & Nasser Singab, A. (2018). Anti-inflammatory and analgesic activities of cupressuflavone from Cupressus macrocarpa: Impact on pro-inflammatory mediators. *Drug Development Research, 79*(1), 22-28. doi:https://doi.org/10.1002/ddr.21417

Alday, P. H., & Doggett, J. S. (2017). Drugs in development for toxoplasmosis: advances, challenges, and current status. *Drug design, development and therapy, 11*(null), 273-293. doi:10.2147/DDDT.S60973

Ali, M. I., Abd El Wahab, W. M., Hamdy, D. A., & Hassan, A. (2019). Toxoplasma gondii in cancer patients receiving chemotherapy: seroprevalence and interferon gamma level. *J Parasit Dis, 43*(3), 464-471. doi:10.1007/s12639-019-01111-9

Alvin, A., Miller, K. I., & Neilan, B. A. (2014). Exploring the potential of endophytes from medicinal plants as sources of antimycobacterial compounds. *Microbiological Research, 169*(7), 483-495. doi:https://doi.org/10.1016/j.micres.2013.12.009

Aly, A. H., Debbab, A., & Proksch, P. (2011). Fifty years of drug discovery from fungi. *Fungal Diversity, 50*(1), 3-19. doi:10.1007/s13225-011-0116-y

Amouei, A., Sarvi, S., Sharif, M., Aghayan, S. A., Javidnia, J., Mizani, A., . . . Daryani, A. (2020). A systematic review of Toxoplasma gondii genotypes and feline:

Geographical distribution trends. *Transboundary and Emerging Diseases, 67*(1), 46-64. doi:https://doi.org/10.1111/tbed.13340

Andersen, O. M., & Markham, K. R. (2005). *Flavonoids: chemistry, biochemistry and applications*: CRC press.

Antczak, M., Dzitko, K., & Długońska, H. (2016). Human toxoplasmosis–Searching for novel chemotherapeutics. *Biomedicine & Pharmacotherapy, 82*, 677-684. doi:https://doi.org/10.1016/j.biopha.2016.05.041

Araujo, F., Shepard, R., & Remington, J. (1991). In vivo activity of the macrolide antibiotics azithromycin, roxithromycin and spiramycin against Toxoplasma gondii. *European Journal of Clinical Microbiology and Infectious Diseases, 10*, 519-524.

Araujo, F. G., Huskinson, J., & Remington, J. S. (1991). Remarkable in vitro and in vivo activities of the hydroxynaphthoquinone 566C80 against tachyzoites and tissue cysts of Toxoplasma gondii. *Antimicrob Agents Chemother, 35*(2), 293-299. doi:10.1128/aac.35.2.293

Araujo, F. G., & Slifer, T. (2003). Different strains of Toxoplasma gondii induce different cytokine responses in CBA/Ca mice. *Infect Immun, 71*(7), 4171-4174. doi:10.1128/iai.71.7.4171-4174.2003

Atanasov, A. G., Waltenberger, B., Pferschy-Wenzig, E.-M., Linder, T., Wawrosch, C., Uhrin, P., . . . Heiss, E. H. (2015). Discovery and resupply of pharmacologically active plant-derived natural products: A review. *Biotechnology Advances, 33*(8), 1582-1614.

Atanasov, A. G., Waltenberger, B., Pferschy-Wenzig, E.-M., Linder, T., Wawrosch, C., Uhrin, P., . . . Stuppner, H. (2015). Discovery and resupply of pharmacologically active plant-derived natural products: A review. *Biotechnology Advances, 33*(8), 1582-1614. doi:https://doi.org/10.1016/j.biotechadv.2015.08.001

Atanasov, A. G., Zotchev, S. B., Dirsch, V. M., Orhan, I. E., Banach, M., Rollinger, J. M., . . . the International Natural Product Sciences, T. (2021). Natural products in drug discovery: advances and opportunities. *Nature Reviews Drug Discovery, 20*(3), 200-216. doi:10.1038/s41573-020-00114-z

Becker, B., & Cooper, M. A. (2013). Aminoglycoside Antibiotics in the 21st Century. *ACS Chemical Biology, 8*(1), 105-115. doi:10.1021/cb3005116

Beckers, C. J., Roos, D. S., Donald, R. G., Luft, B. J., Schwab, J. C., Cao, Y., & Joiner, K. A. (1995). Inhibition of cytoplasmic and organellar protein synthesis in Toxoplasma gondii. Implications for the target of macrolide antibiotics. *J Clin Invest, 95*(1), 367-376. doi:10.1172/jci117665

Behrendt, C. T., Kunfermann, A., Illarionova, V., Matheeussen, A., Pein, M. K., Gräwert, T., . . . Illarionov, B. (2011). Reverse fosmidomycin derivatives against the antimalarial drug target IspC (Dxr). *Journal of Medicinal Chemistry, 54*(19), 6796-6802.

Ben-Harari, R. R., Goodwin, E., & Casoy, J. (2017). Adverse Event Profile of Pyrimethamine-Based Therapy in Toxoplasmosis: A Systematic Review. *Drugs in R&D, 17*(4), 523-544. doi:10.1007/s40268-017-0206-8

Benoit-Vical, F., Santillana-Hayat, M., Kone-Bamba, D., Mallie, M., & Derouin, F. (2000). Anti-Toxoplasma activity of vegetal extracts used in West African traditional medicine. *Parasite, 7*(1), 3-7. Retrieved from https://doi.org/10.1051/parasite/2000071003

Blackman, M. J., & Bannister, L. H. (2001). Apical organelles of Apicomplexa: biology and isolation by subcellular fractionation. *Molecular and biochemical parasitology, 117*(1), 11-25.

Blader, I. J., Coleman, B. I., Chen, C. T., & Gubbels, M. J. (2015). Lytic Cycle of Toxoplasma gondii: 15 Years Later. *Annu Rev Microbiol, 69*, 463-485. doi:10.1146/annurev-micro-091014-104100

Blake, D. P., & Tomley, F. M. (2014). Securing poultry production from the ever-present Eimeria challenge. *Trends in Parasitology, 30*(1), 12-19.

Bollani, L., Auriti, C., Achille, C., Garofoli, F., De Rose, D. U., Meroni, V., . . . Tzialla, C. (2022). Congenital toxoplasmosis: the state of the art. *Frontiers in Pediatrics, 10*, 894573.

Boothroyd, J. C. (2009). Toxoplasma gondii: 25 years and 25 major advances for the field. *International journal for parasitology, 39*(8), 935-946. doi:https://doi.org/10.1016/j.ijpara.2009.02.003

Bouwknegt, M., Devleesschauwer, B., Graham, H., Robertson, L. J., & van der Giessen, J. W. (2018). Prioritisation of food-borne parasites in Europe, 2016. *Euro Surveill, 23*(9). doi:10.2807/1560-7917.Es.2018.23.9.17-00161

Brücher, K., Gräwert, T., Konzuch, S., Held, J., Lienau, C., Behrendt, C., . . . Kurz, T. (2015). Prodrugs of reverse fosmidomycin analogues. *J Med Chem, 58*(4), 2025-2035. doi:10.1021/jm5019719

Brücher, K., Illarionov, B., Held, J., Tschan, S., Kunfermann, A., Pein, M. K., . . . Kurz, T. (2012). α-Substituted β-Oxa Isosteres of Fosmidomycin: Synthesis and Biological Evaluation. *Journal of Medicinal Chemistry, 55*(14), 6566-6575. doi:10.1021/jm300652f

CDC. (2018). Parasites -Toxoplasmosis (Toxoplasma infection). Toxoplasmosis Epidemiology & Risk Factors. Retrieved from https://www.cdc.gov/parasites/toxoplasmosis/epi.html

Chan, P. F., Holmes, D. J., & Payne, D. J. (2004). Finding the gems using genomic discovery: antibacterial drug discovery strategies – the successes and the challenges. *Drug Discovery Today: Therapeutic Strategies, 1*(4), 519-527. doi:https://doi.org/10.1016/j.ddstr.2004.11.003

Chang, H. R., & Pechère, J. C. (1988). In vitro effects of four macrolides (roxithromycin, spiramycin, azithromycin [CP-62,993], and A-56268) on Toxoplasma gondii. *Antimicrob Agents Chemother, 32*(4), 524-529. doi:10.1128/aac.32.4.524

Chen, T.-R., Wei, L.-H., Guan, X.-Q., Huang, C., Liu, Z.-Y., Wang, F.-J., . . . Guo, W.-Z. (2019). Biflavones from Ginkgo biloba as inhibitors of human thrombin. *Bioorganic Chemistry, 92*, 103199. doi:https://doi.org/10.1016/j.bioorg.2019.103199

Chessa, G., Chisu, V., Porcu, R., & Masala, G. (2014). Molecular characterization of Toxoplasma gondii Type II in sheep abortion in Sardinia, Italy. *Parasite, 21*, 6. doi:10.1051/parasite/2014007

Chopra, I., & Roberts, M. (2001). Tetracycline antibiotics: mode of action, applications, molecular biology, and epidemiology of bacterial resistance. *Microbiology and molecular biology reviews, 65*(2), 232-260.

Conly, J. M., & Johnston, B. L. (2005). Where are all the new antibiotics? The new antibiotic paradox. *Canadian Journal of Infectious Diseases and Medical Microbiology, 16*, 892058. doi:10.1155/2005/892058

Conrado, R., Gomes, T. C., Roque, G. S. C., & De Souza, A. O. (2022). Overview of Bioactive Fungal Secondary Metabolites: Cytotoxic and Antimicrobial Compounds. *Antibiotics, 11*(11), 1604. Retrieved from https://www.mdpi.com/2079-6382/11/11/1604

Cowell, A. N., & Winzeler, E. A. (2019). The genomic architecture of antimalarial drug resistance. *Brief Funct Genomics, 18*(5), 314-328. doi:10.1093/bfgp/elz008

Cragg, G. M., Newman, D. J., & Snader, K. M. (1997). Natural Products in Drug Discovery and Development. *J Nat Prod, 60*(1), 52-60. doi:10.1021/np9604893

D'Angelo, J. G., Bordon, C., Posner, G. H., Yolken, R., & Jones-Brando, L. (2009). Artemisinin derivatives inhibit Toxoplasma gondii in vitro at multiple steps in the lytic cycle. *Journal of antimicrobial chemotherapy, 63*(1), 146-150.

da Rosa, R., Schenkel, E. P., & Campos Bernardes, L. S. (2020). Semisynthetic and newly designed derivatives based on natural chemical scaffolds: moving beyond natural products to fight Trypanosoma cruzi. *Phytochemistry Reviews, 19*(1), 105-122. doi:10.1007/s11101-020-09659-8

Davies, J. (2006). Where have All the Antibiotics Gone? *Can J Infect Dis Med Microbiol, 17*(5), 287-290. doi:10.1155/2006/707296

Demain, A. L., & Elander, R. P. (1999). The β-lactam antibiotics: past, present, and future. *Antonie Van Leeuwenhoek, 75*, 5-19.

Deng, H., Cummins, R., Schares, G., Trevisan, C., Enemark, H., Waap, H., . . . Opsteegh, M. (2021). Mathematical modelling of Toxoplasma gondii transmission: A systematic review. *Food and waterborne parasitology, 22*, e00102. doi:https://doi.org/10.1016/j.fawpar.2020.e00102

Deshmukh, S. K., Dufossé, L., Chhipa, H., Saxena, S., Mahajan, G. B., & Gupta, M. K. (2022). Fungal Endophytes: A Potential Source of Antibacterial Compounds. *Journal of Fungi, 8*(2), 164. Retrieved from https://www.mdpi.com/2309-608X/8/2/164

Díaz-Carrillo, J. T., Díaz-Camacho, S. P., Delgado-Vargas, F., Rivero, I. A., López-Angulo, G., Sarmiento-Sánchez, J. I., & Montes-Avila, J. (2018). Synthesis of leading chalcones with high antiparasitic, against Hymenolepis nana, and antioxidant activities. *Brazilian Journal of Pharmaceutical Sciences, 54*.

Domínguez, J. N., Gamboa de Dominguez, N., Rodrigues, J., Acosta, M. E., Caraballo, N., & León, C. (2013). Synthesis and antimalarial activity of urenyl Bis-chalcone in vitro and in vivo. *Journal of Enzyme Inhibition and Medicinal Chemistry, 28*(6), 1267-1273.

Donald, L., Pipite, A., Subramani, R., Owen, J., Keyzers, R. A., & Taufa, T. (2022). Streptomyces: Still the Biggest Producer of New Natural Secondary Metabolites, a Current Perspective. *Microbiology Research, 13*(3), 418-465. Retrieved from https://www.mdpi.com/2036-7481/13/3/31

Dubey, J. (1998). Advances in the life cycle of Toxoplasma gondii. *International journal for parasitology, 28*(7), 1019-1024.

Dubey, J. (2002). A review of toxoplasmosis in wild birds. *Veterinary Parasitology, 106*(2), 121-153.

Dubey, J., Murata, F., Cerqueira-Cézar, C., Kwok, O., & Villena, I. (2021). Congenital toxoplasmosis in humans: an update of worldwide rate of congenital infections. *Parasitology, 148*(12), 1406-1416.

Dubey, J. P. (1996). Infectivity and pathogenicity of Toxoplasma gondii oocysts for cats. *J Parasitol, 82*(6), 957-961.

Dubey, J. P. (2008). The history of Toxoplasma gondii—the first 100 years. *Journal of Eukaryotic Microbiology, 55*(6), 467-475.

Dubey, J. P., Lindsay, D. S., & Speer, C. A. (1998). Structures of Toxoplasma gondii tachyzoites, bradyzoites, and sporozoites and biology and development of tissue cysts. *Clin Microbiol Rev, 11*(2), 267-299. doi:10.1128/cmr.11.2.267

Dubey, J. P., Miller, N. L., & Frenkel, J. K. (1970). Toxoplasma gondii life cycle in cats. *J Am Vet Med Assoc, 157*(11), 1767-1770.

Duggar, B. M. (1948). Aureomycin-a New Antibiotic. *Annals of the New York Academy of Sciences, 51*(Art. 2), 177-342.

Dunay, I. R., Gajurel, K., Dhakal, R., Liesenfeld, O., & Montoya, J. G. (2018). Treatment of Toxoplasmosis: Historical Perspective, Animal Models, and Current Clinical Practice. *Clinical Microbiology Reviews, 31*(4), 10.1128/cmr.00057-00017. doi:doi:10.1128/cmr.00057-17

Eyles, D. E., & Coleman, N. (1952). Tests of 2,4-diaminopyrimidines on toxoplasmosis. *Public Health Rep (1896), 67*(3), 249-252.

Fang, J.-L., Stingley, R. L., Beland, F. A., Harrouk, W., Lumpkins, D. L., & Howard, P. (2010). Occurrence, Efficacy, Metabolism, and Toxicity of Triclosan. *Journal of Environmental Science and Health, Part C, 28*(3), 147-171. doi:10.1080/10590501.2010.504978

Farmhealthonline.com. Toxoplasmosis edited Life Cycle from elifesciences.org. Retrieved from https://www.farmhealthonline.com/disease-management/sheep-diseases/toxoplasmosis/

Fast, N. M., Xue, L., Bingham, S., & Keeling, P. J. (2002). Re-examining alveolate evolution using multiple protein molecular phylogenies. *Journal of Eukaryotic Microbiology, 49*(1), 30-37.

Fernandes, E. S., da Silva Figueiredo, I. F., Monteiro, C. R. A. V., & Monteiro-Neto, V. (2023). Antimicrobial and Anti-Infective Activity of Natural Products—Gaining Knowledge from Novel Studies. *Antibiotics, 12*(6), 1051. Retrieved from https://www.mdpi.com/2079-6382/12/6/1051

Feustel, S. M., Meissner, M., & Liesenfeld, O. (2012). Toxoplasma gondii and the blood-brain barrier. *Virulence, 3*(2), 182-192. doi:10.4161/viru.19004

Frank, M., Niemann, H., Böhler, P., Stork, B., Wesselborg, S., Lin, W., & Proksch, P. (2015). Phomoxanthone A--From Mangrove Forests to Anticancer Therapy. *Curr Med Chem, 22*(30), 3523-3532. doi:10.2174/0929867322666150716115300

Frenkel, J. K., & Jacobs, L. (1958). Ocular toxoplasmosis; pathogenesis, diagnosis and treatment. *AMA Arch Ophthalmol, 59*(2), 260-279.

Fry, L. M., Schneider, D. A., Frevert, C. W., Nelson, D. D., Morrison, W. I., & Knowles, D. P. (2016). East coast fever caused by Theileria parva is characterized by macrophage activation associated with vasculitis and respiratory failure. *PloS one, 11*(5), e0156004.

Gakuubi, M. M., Munusamy, M., Liang, Z.-X., & Ng, S. B. (2021). Fungal Endophytes: A Promising Frontier for Discovery of Novel Bioactive Compounds. *Journal of Fungi, 7*(10), 786. Retrieved from https://www.mdpi.com/2309-608X/7/10/786

Garin, J. P., & Eyles, D. E. (1958). [Spiramycin therapy of experimental toxoplasmosis in mice]. *Presse Med (1893), 66*(42), 957-958.

Genilloud, O. (2017). Actinomycetes: still a source of novel antibiotics. *Natural Product Reports, 34*(10), 1203-1232. doi:10.1039/C7NP00026J

Ghazzay, M. H., Hasan, S. A., DeliKhudhair, O., & Abbas, K. K. (2023). Synthesis, Characterization, and Anti-parasitic Activity Evaluation of the Synthesized Chalcone against Toxoplasma Gondii Isolated from Cases of Abortion in Al-Najaf City.

Goldstein, E. J., Montoya, J. G., & Remington, J. S. (2008). Management of Toxoplasma gondii infection during pregnancy. *Clinical Infectious Diseases, 47*(4), 554-566.

González, L. A., Upegui, Y. A., Rivas, L., Echeverri, F., Escobar, G., Robledo, S. M., & Quiñones, W. (2020). Effect of substituents in the A and B rings of chalcones on antiparasite activity. *Archiv der Pharmazie, 353*(12), 2000157.

Gouda, S., Das, G., Sen, S. K., Shin, H. S., & Patra, J. K. (2016). Endophytes: A Treasure House of Bioactive Compounds of Medicinal Importance. *Front Microbiol, 7*, 1538. doi:10.3389/fmicb.2016.01538

Greene, T. W., & Wuts, P. G. (1999). Protective groups in organic synthesis. *(No Title), 2*.

Griffith, M. B., Pearce, C. S., & Heaslip, A. T. (2022). Dense granule biogenesis, secretion, and function in Toxoplasma gondii. *J Eukaryot Microbiol, 69*(6), e12904. doi:10.1111/jeu.12904

Grossman, P. L., & Remington, J. S. (1979). The effect of trimethoprim and sulfamethoxazole on Toxoplasma gondii in vitro and in vivo. *Am J Trop Med Hyg, 28*(3), 445-455. doi:10.4269/ajtmh.1979.28.445

Guarente, L. (2011). Sirtuins, aging, and medicine. *New England Journal of Medicine, 364*(23), 2235-2244.

Haemers, T., Wiesner, J., Poecke, S. V., Goeman, J., Henschker, D., Beck, E., . . . Calenbergh, S. V. (2006). Synthesis of α-substituted fosmidomycin analogues as highly potent Plasmodium falciparum growth inhibitors. *Bioorganic & Medicinal Chemistry Letters, 16*(7), 1888-1891. doi:https://doi.org/10.1016/j.bmcl.2005.12.082

Haemers, T., Wiesner, J., Van Poecke, S., Goeman, J., Henschker, D., Beck, E., . . . Van Calenbergh, S. (2006). Synthesis of alpha-substituted fosmidomycin analogues as highly potent Plasmodium falciparum growth inhibitors. *Bioorg Med Chem Lett, 16*(7), 1888-1891. doi:10.1016/j.bmcl.2005.12.082

Haigis, M. C., & Sinclair, D. A. (2010). Mammalian sirtuins: biological insights and disease relevance. *Annual Review of Pathology: Mechanisms of Disease, 5*, 253-295.

Hartley, W., & Marshall, S. (1957). Toxoplasmosis as a cause of ovine perinatal mortality. *New Zealand Veterinary Journal, 5*(4), 119-124.

Harvey, A. L., Edrada-Ebel, R., & Quinn, R. J. (2015). The re-emergence of natural products for drug discovery in the genomics era. *Nat Rev Drug Discov, 14*(2), 111-129. doi:10.1038/nrd4510

Hecker, S. J., & Erion, M. D. (2008). Prodrugs of phosphates and phosphonates. *J Med Chem, 51*(8), 2328-2345. doi:10.1021/jm701260b

Heidel, K. M., & Dowd, C. S. (2019). Phosphonate prodrugs: an overview and recent advances. *Future Med Chem, 11*(13), 1625-1643. doi:10.4155/fmc-2018-0591

Henriksson, L. M., Unge, T., Carlsson, J., Aqvist, J., Mowbray, S. L., & Jones, T. A. (2007). Structures of Mycobacterium tuberculosis 1-deoxy-D-xylulose-5-phosphate reductoisomerase provide new insights into catalysis. *J Biol Chem, 282*(27), 19905-19916. doi:10.1074/jbc.M701935200

Henry, R. J. (1943). THE MODE OF ACTION OF SULFONAMIDES. *Bacteriol Rev, 7*(4), 175-262. doi:10.1128/br.7.4.175-262.1943

Hernandez, A., Thota, P., Pellegrino, D., Pasupuleti, V., Benites-Zapata, V., Deshpande, A., . . . Vidal, J. (2017). A systematic review and meta-analysis of the relative efficacy and safety of treatment regimens for HIV-associated cerebral toxoplasmosis: is trimethoprim-sulfamethoxazole a real option? *HIV Medicine, 18*(2), 115-124. doi:https://doi.org/10.1111/hiv.12402

Hill, D., & Dubey, J. P. (2002). Toxoplasma gondii: transmission, diagnosis and prevention. *Clinical microbiology and infection, 8*(10), 634-640.

Hitchings, G. H., Falco, E. A., Vanderwerff, H., Russell, P. B., & Elion, G. B. (1952). Antagonists of nucleic acid derivatives. VII. 2, 4-Diaminopyrimidines. *J Biol Chem, 199*(1), 43-56.

Hoffman, S. L., Subramanian, G. M., Collins, F. H., & Venter, J. C. (2002). Plasmodium, human and Anopheles genomics and malaria. *Nature, 415*(6872), 702-709.

Holfels, E., McAuley, J., Mack, D., Milhous, W. K., & McLeod, R. (1994). In vitro effects of artemisinin ether, cycloguanil hydrochloride (alone and in combination with sulfadiazine), quinine sulfate, mefloquine, primaquine phosphate, trifluoperazine hydrochloride, and verapamil on Toxoplasma gondii. *Antimicrobial Agents and Chemotherapy, 38*(6), 1392-1396.

Holland, G. N. (2004). Ocular toxoplasmosis: a global reassessment: part II: disease manifestations and management. *American journal of ophthalmology, 137*(1), 1-17.

Holmes, K. K., Kaplan, J. E., & Masur, H. (2002). Guidelines for preventing opportunistic infections among HIV-infected persons--2002: recommendations of the US Public Health Service and the Infectious Diseases Society of America.

Howe, D. K., Honoré, S., Derouin, F., & Sibley, L. D. (1997). Determination of genotypes of Toxoplasma gondii strains isolated from patients with toxoplasmosis. *J Clin Microbiol, 35*(6), 1411-1414. doi:10.1128/jcm.35.6.1411-1414.1997

Howe, D. K., & Sibley, L. D. (1995). Toxoplasma gondii comprises three clonal lineages: correlation of parasite genotype with human disease. *J Infect Dis, 172*(6), 1561-1566. doi:10.1093/infdis/172.6.1561

Howe, D. K., & Sibley, L. D. (1995). Toxoplasma gondii Comprises Three Clonal Lineages: Correlation of Parasite Genotype with Human Disease. *The Journal of Infectious Diseases, 172*(6), 1561-1566. doi:10.1093/infdis/172.6.1561

Hussain, H., Kock, I., Al-Harrasi, A., Al-Rawahi, A., Abbas, G., Green, I. R., . . . Krohn, K. (2014). Antimicrobial chemical constituents from endophytic fungus Phoma

sp. *Asian Pacific Journal of Tropical Medicine, 7*(9), 699-702. doi:https://doi.org/10.1016/S1995-7645(14)60119-X

Hutchings, M. I., Truman, A. W., & Wilkinson, B. (2019). Antibiotics: past, present and future. *Current Opinion in Microbiology, 51*, 72-80. doi:https://doi.org/10.1016/j.mib.2019.10.008

Igarashi, M. (2019). New natural products to meet the antibiotic crisis: a personal journey. *J Antibiot (Tokyo), 72*(12), 890-898. doi:10.1038/s41429-019-0224-6

Imai, S.-i., Armstrong, C. M., Kaeberlein, M., & Guarente, L. (2000). Transcriptional silencing and longevity protein Sir2 is an NAD-dependent histone deacetylase. *Nature, 403*(6771), 795-800.

Imran, M., Aslam Gondal, T., Atif, M., Shahbaz, M., Batool Qaisarani, T., Hanif Mughal, M., . . . Sharifi-Rad, J. (2020). Apigenin as an anticancer agent. *Phytotherapy Research, 34*(8), 1812-1828.

Innes, E. (2010). A brief history and overview of Toxoplasma gondii. *Zoonoses and public health, 57*(1), 1-7.

Innes, E. A., Hamilton, C., Garcia, J. L., Chryssafidis, A., & Smith, D. (2019). A one health approach to vaccines against Toxoplasma gondii. *Food and waterborne parasitology, 15*, e00053. doi:https://doi.org/10.1016/j.fawpar.2019.e00053

Jackson, E. R., San Jose, G., Brothers, R. C., Edelstein, E. K., Sheldon, Z., Haymond, A., . . . Dowd, C. S. (2014). The effect of chain length and unsaturation on Mtb Dxr inhibition and antitubercular killing activity of FR900098 analogs. *Bioorg Med Chem Lett, 24*(2), 649-653. doi:10.1016/j.bmcl.2013.11.067

Jacobs, L., Remington, J. S., & Melton, M. L. (1960). The resistance of the encysted form of Toxoplasma gondii. *J Parasitol, 46*(1), 11-21.

Jakubiec-Krzesniak, K., Rajnisz-Mateusiak, A., Guspiel, A., Ziemska, J., & Solecka, J. (2018). Secondary Metabolites of Actinomycetes and their Antibacterial, Antifungal and Antiviral Properties. *Pol J Microbiol, 67*(3), 259-272. doi:10.21307/pjm-2018-048

Janku, J. (1923). Pathogenesa a patologicka anatomie tak nazvaneho vrozenehonalezem parasitu v sitnici. *Cas Lek Ces, 62*, 1021-1027.

Jiang, L., Liu, B., Hou, S., Su, T., Fan, Q., Alyafeai, E., . . . Li, J. (2022). Discovery and evaluation of chalcone derivatives as novel potential anti-Toxoplasma gondii agents. *European Journal of Medicinal Chemistry, 234*, 114244.

Jiang, N., Doseff, A. I., & Grotewold, E. (2016). Flavones: From Biosynthesis to Health Benefits. *Plants (Basel), 5*(2). doi:10.3390/plants5020027

Jiménez-Romero, C., Ortega-Barría, E., Arnold, A. E., & Cubilla-Rios, L. (2008). Activity against Plasmodium falciparum of lactones isolated from the endophytic fungus Xylaria sp. *Pharmaceutical Biology, 46*(10-11), 700-703.

Jones, J. L., Muccioli, C., Belfort, R., Jr., Holland, G. N., Roberts, J. M., & Silveira, C. (2006). Recently acquired Toxoplasma gondii infection, Brazil. *Emerg Infect Dis, 12*(4), 582-587. doi:10.3201/eid1204.051081

Jones, J. L., Parise, M. E., & Fiore, A. E. (2014). Neglected parasitic infections in the United States: toxoplasmosis. *Am J Trop Med Hyg, 90*(5), 794-799. doi:10.4269/ajtmh.13-0722

Karaman, B., Alhalabi, Z., Swyter, S., Mihigo, S. O., Andrae-Marobela, K., Jung, M., . . . Ntie-Kang, F. (2018). Identification of bichalcones as sirtuin inhibitors by virtual screening and in vitro testing. *Molecules, 23*(2), 416.

Katris, N. J., van Dooren, G. G., McMillan, P. J., Hanssen, E., Tilley, L., & Waller, R. F. (2014). The apical complex provides a regulated gateway for secretion of invasion factors in Toxoplasma. *PLoS Pathog, 10*(4), e1004074. doi:10.1371/journal.ppat.1004074

Khambay, B. P. S., Bourne, J. M., Cameron, S., Kerry, B. R., & Zaki, M. J. (2000). A nematicidal metabolite from Verticillium chlamydosporium. *Pest Management Science: formerly Pesticide Science, 56*(12), 1098-1099.

Khan Assir, M. Z., Ahmad, H. I., Akram, J., Yusuf, N. W., & Kamran, U. (2014). An outbreak of pyrimethamine toxicity in patients with ischaemic heart disease in Pakistan. *Basic & clinical pharmacology & toxicology, 115*(3), 291-296.

Khan, S. M., & Witola, W. H. (2023). Past, current, and potential treatments for cryptosporidiosis in humans and farm animals: A comprehensive review. *Frontiers in Cellular and Infection Microbiology, 13*, 1115522.

Khurana, S., & Batra, N. (2016). Toxoplasmosis in organ transplant recipients: Evaluation, implication, and prevention. *Trop Parasitol, 6*(2), 123-128. doi:10.4103/2229-5070.190814

Khurana, S., & Batra, N. (2016). Toxoplasmosis in organ transplant recipients: Evaluation, implication, and prevention. *Tropical Parasitology, 6*(2), 123.

Kim, H. P., Park, H., Son, K. H., Chang, H. W., & Kang, S. S. (2008). Biochemical pharmacology of biflavonoids: implications for anti-inflammatory action. *Arch Pharm Res, 31*(3), 265-273. doi:10.1007/s12272-001-1151-3

Kim, J. C., Choi, G. J., Park, J. H., Kim, H. T., & Cho, K. Y. (2001). Activity against plant pathogenic fungi of phomalactone isolated from Nigrospora sphaerica. *Pest Manag Sci, 57*(6), 554-559. doi:10.1002/ps.318

Klischan, M. K. T., Mazzone, F., Berning, L., Greb, J., Schlamkow, M., Haase, M., . . . Pietruszka, J. (2023). Modular Approach for the Synthesis and Bioactivity Profiling of 8,8′-Biflavones. *ACS omega*. doi:10.1021/acsomega.3c06503

Kloehn, J., Lacour, C. E., & Soldati-Favre, D. (2021a). The metabolic pathways and transporters of the plastid organelle in Apicomplexa. *Current Opinion in Microbiology, 63*, 250-258.

Kloehn, J., Lacour, C. E. M., & Soldati-Favre, D. (2021b). The metabolic pathways and transporters of the plastid organelle in Apicomplexa. *Current Opinion in Microbiology, 63*, 250-258. doi:https://doi.org/10.1016/j.mib.2021.07.016

Knak, T., Abdullaziz, M. A., Höfmann, S., Alves Avelar, L. A., Klein, S., Martin, M., . . . Kurz, T. (2022). Over 40 Years of Fosmidomycin Drug Research: A Comprehensive Review and Future Opportunities. *Pharmaceuticals, 15*(12), 1553.

Komai, S.-i., Hosoe, T., Nozawa, K., Okada, K., de Campos Takaki, G. M., Fukushima, K., . . . Kawai, K.-i. (2003). Antifungal activity of pyranone and furanone derivatives, isolated from Aspergillus sp. IFM51759, against Aspergillus fumigatus. *MYCOTOXINS-TOKYO-, 53*(1), 11-18.

Konstantinovic, N., Guegan, H., Stäjner, T., Belaz, S., & Robert-Gangneux, F. (2019). Treatment of toxoplasmosis: Current options and future perspectives. *Food and waterborne parasitology, 15*, e00036. doi:https://doi.org/10.1016/j.fawpar.2019.e00036

Kortagere, S. (2012). Screening for small molecule inhibitors of Toxoplasma gondii. *Expert Opinion on Drug Discovery, 7*(12), 1193-1206. doi:10.1517/17460441.2012.729036

Kovacs, J. A., & AIDS, T. N.-C. C. I. (1992). Efficacy of atovaquone in treatment of toxoplasmosis in patients with AIDS. *The Lancet, 340*(8820), 637-638.

Kozoriz, K., Shkel, O., Hong, K. T., Kim, D. H., Kim, Y. K., & Lee, J.-S. (2023). Multifunctional Photo-Cross-Linking Probes: From Target Protein Searching to Imaging Applications. *Accounts of Chemical Research, 56*(1), 25-36. doi:10.1021/acs.accounts.2c00505

Krasnoff, S. B., & Gupta, S. (1994). Identification of the antibiotic phomalactone from the entomopathogenic fungus Hirsutella thompsonii var. synnematosa. *Journal of Chemical Ecology, 20*, 293-302.

Krivogorsky, B., Pernat, J. A., Douglas, K. A., Czerniecki, N. J., & Grundt, P. (2012). Structure–activity studies of some berberine analogs as inhibitors of Toxoplasma gondii. *Bioorganic & Medicinal Chemistry Letters, 22*(8), 2980-2982. doi:https://doi.org/10.1016/j.bmcl.2012.02.038

Kumar, A., Ekavali, Chopra, K., Mukherjee, M., Pottabathini, R., & Dhull, D. K. (2015). Current knowledge and pharmacological profile of berberine: An update. *European Journal of Pharmacology, 761*, 288-297. doi:https://doi.org/10.1016/j.ejphar.2015.05.068

Kumar, K. S., Bhaskar, B., Ramulu, M. S., Kumar, N. P., Ashfaq, M. A., & Pal, M. (2017). Metal catalyst free cyclization of 3-alkynyl substituted 2-(indol-3-yl)quinoxalines in TFA alone: a new synthesis of indolophenazines. *Organic & Biomolecular Chemistry, 15*(1), 82-87. doi:10.1039/C6OB02340A

Kunfermann, A., Lienau, C., Illarionov, B., Held, J., Gräwert, T., Behrendt, C. T., . . . Riederer, U. (2013). IspC as target for antiinfective drug discovery: synthesis,

enantiomeric separation, and structural biology of fosmidomycin thia isosters. *Journal of Medicinal Chemistry, 56*(20), 8151-8162.

Kuttruff, C. A., Eastgate, M. D., & Baran, P. S. (2014). Natural product synthesis in the age of scalability. *Nat Prod Rep, 31*(4), 419-432. doi:10.1039/c3np70090a

Lachance, H., Wetzel, S., Kumar, K., & Waldmann, H. (2012). Charting, navigating, and populating natural product chemical space for drug discovery. *Journal of Medicinal Chemistry, 55*(13), 5989-6001.

Lélu, M., Villena, I., Dardé, M. L., Aubert, D., Geers, R., Dupuis, E., . . . Gilot-Fromont, E. (2012). Quantitative estimation of the viability of Toxoplasma gondii oocysts in soil. *Appl Environ Microbiol, 78*(15), 5127-5132. doi:10.1128/aem.00246-12

Li, H.-Y., Nehira, T., Hagiwara, M., & Harada, N. (1997). Total Synthesis and Absolute Stereochemistry of the Natural Atropisomer of the Biflavone 4‘,4‘‘‘,7,7‘‘-Tetra-O-methylcupressuflavone. *The Journal of Organic Chemistry, 62*(21), 7222-7227. doi:10.1021/jo970670w

Lienau, C., Gräwert, T., Alves Avelar, L. A., Illarionov, B., Held, J., Knaab, T. C., . . . Kurz, T. (2019). Novel reverse thia-analogs of fosmidomycin: Synthesis and antiplasmodial activity. *Eur J Med Chem, 181*, 111555. doi:10.1016/j.ejmech.2019.07.058

Lim, L., & McFadden, G. I. (2010). The evolution, metabolism and functions of the apicoplast. *Philosophical Transactions of the Royal Society B: Biological Sciences, 365*(1541), 749-763.

Lin, G.-Q., & Zhong, M. (1997). The first enantioselective synthesis of optically pure (R)-and (S)-5, 5 ″-dihydroxy-4′, 4‴, 7, 7 ″-tetramethoxy-8, 8 ″-biflavone and the reconfirmation of their absolute configuration. *Tetrahedron Letters, 38*(6), 1087-1090.

Lin, Y. M., Flavin, M. T., Schure, R., Chen, F. C., Sidwell, R., Barnard, D. L., . . . Kern, E. R. (1999). Antiviral activities of biflavonoids. *Planta Med, 65*(2), 120-125. doi:10.1055/s-1999-13971

Luft, B. J., & Chua, A. (2000). Central Nervous System Toxoplasmosis in HIV Pathogenesis, Diagnosis, and Therapy. *Curr Infect Dis Rep, 2*(4), 358-362. doi:10.1007/s11908-000-0016-x

Luft, B. J., & Remington, J. S. (1992). Toxoplasmic Encephalitis in AIDS. *Clinical Infectious Diseases, 15*(2), 211-222. doi:10.1093/clinids/15.2.211

Lyons, R. E., McLeod, R., & Roberts, C. W. (2002). Toxoplasma gondii tachyzoite–bradyzoite interconversion. *Trends in Parasitology, 18*(5), 198-201.

Mac Sweeney, A., Lange, R., Fernandes, R. P., Schulz, H., Dale, G. E., Douangamath, A., . . . Oefner, C. (2005). The crystal structure of E.coli 1-deoxy-D-xylulose-5-phosphate reductoisomerase in a ternary complex with the antimalarial compound fosmidomycin and NADPH reveals a tight-binding closed enzyme conformation. *J Mol Biol, 345*(1), 115-127. doi:10.1016/j.jmb.2004.10.030

Machala, L., Kodym, P., Malý, M., Geleneky, M., Beran, O., & Jilich, D. (2015). [Toxoplasmosis in immunocompromised patients]. *Epidemiologie, mikrobiologie, imunologie : casopis Spolecnosti pro epidemiologii a mikrobiologii Ceske lekarske spolecnosti J.E. Purkyne, 64*(2), 59-65. Retrieved from http://europepmc.org/abstract/MED/26099608

Majhi, S., & Das, D. (2021). Chemical derivatization of natural products: Semisynthesis and pharmacological aspects- A decade update. *Tetrahedron, 78*, 131801. doi:https://doi.org/10.1016/j.tet.2020.131801

Makgatho, M. E., Anderson, R., O'Sullivan, J. F., Egan, T. J., Freese, J. A., Cornelius, N., & van Rensburg, C. E. J. (2000). Tetramethylpiperidine-substituted phenazines as novel anti-plasmodial agents. *Drug Development Research, 50*(2), 195-202. doi:https://doi.org/10.1002/1098-2299(200006)50:2<195::AID-DDR10>3.0.CO;2-T

Maldonado, Y. A., & Read, J. S. (2017). Diagnosis, Treatment, and Prevention of Congenital Toxoplasmosis in the United States. *Pediatrics, 139*(2). doi:10.1542/peds.2016-3860

Martorelli Di Genova, B., Wilson, S. K., Dubey, J. P., & Knoll, L. J. (2019). Intestinal delta-6-desaturase activity determines host range for Toxoplasma sexual reproduction. *PLoS Biol, 17*(8), e3000364. doi:10.1371/journal.pbio.3000364

Mazzone, F., Simons, V. E., van Geelen, L., Frank, M., Mándi, A., Kurtán, T., . . . Kalscheuer, R. (2022). In Vitro Biological Activity of Natural Products from the Endophytic Fungus Paraboeremia selaginellae against Toxoplasma gondii. *Antibiotics, 11*(9), 1176.

McCabe, R. E., & Oster, S. (1989). Current recommendations and future prospects in the treatment of toxoplasmosis. *Drugs, 38*, 973-987.

McFadden, G. I., Reith, M. E., Munholland, J., & Lang-Unnasch, N. (1996). Plastid in human parasites. *Nature, 381*(6582), 482-482.

McLeod, R., Boyer, K., Karrison, T., Kasza, K., Swisher, C., Roizen, N., . . . Noble, A. G. (2006). Outcome of treatment for congenital toxoplasmosis, 1981–2004: the national collaborative Chicago-based, congenital toxoplasmosis study. *Clinical Infectious Diseases, 42*(10), 1383-1394.

McLeod, R., Van Tubbergen, C., Montoya, J., & Petersen, E. (2014). Chapter 4-Human Toxoplasma Infection. *Toxoplasma gondii: The Model Apicomplexan-Perspectives and Methods*, 99-159.

McMurry, L. M., Oethinger, M., & Levy, S. B. (1998). Triclosan targets lipid synthesis. *Nature, 394*(6693), 531-532. doi:10.1038/28970

Menezes, J. C. J. M. D. S., & Diederich, M. F. (2019). Natural dimers of coumarin, chalcones, and resveratrol and the link between structure and pharmacology. *European Journal of Medicinal Chemistry, 182*, 111637. doi:https://doi.org/10.1016/j.ejmech.2019.111637

Mercier, C., Adjogble, K. D. Z., Däubener, W., & Delauw, M.-F.-C. (2005). Dense granules: Are they key organelles to help understand the parasitophorous vacuole of all apicomplexa parasites? *International journal for parasitology, 35*(8), 829-849. doi:https://doi.org/10.1016/j.ijpara.2005.03.011

Merkt, F. K., Mazzone, F., Sazzadeh, S. S., Bonda, L., Hinz, L. K., Gruber, I., . . . Müller, T. J. (2021). Fluorescent Indolo [3, 2-a] phenazines against Toxoplasma gondii: Concise Synthesis by Gold-Catalyzed Cycloisomerization with 1, 2-Silyl Migration and ipso-Iodination Suzuki Sequence. *Chemistry–A European Journal, 27*(38), 9774-9781.

Mihigo, S. O., Mammo, W., Bezabih, M., Andrae-Marobela, K., & Abegaz, B. M. (2010). Total synthesis, antiprotozoal and cytotoxicity activities of rhuschalcone VI and analogs. *Bioorg Med Chem, 18*(7), 2464-2473. doi:10.1016/j.bmc.2010.02.055

Miller, E. L. (2002). The penicillins: A review and update11This article reviews modes of action, indications, adverse effects and spectrums of activity for the various classes of penicillin used in primary care. *Journal of Midwifery & Women's Health, 47*(6), 426-434. doi:https://doi.org/10.1016/S1526-9523(02)00330-6

Molinari, G. (2009). Natural products in drug discovery: present status and perspectives. *Pharmaceutical Biotechnology*, 13-27.

Mondragon, R., Howe, D. K., Dubey, J. P., & Sibley, L. D. (1998). Genotypic analysis of Toxoplasma gondii isolates from pigs. *J Parasitol, 84*(3), 639-641.

Montazeri, M., Mehrzadi, S., Sharif, M., Sarvi, S., Tanzifi, A., Aghayan, S. A., & Daryani, A. (2018). Drug Resistance in Toxoplasma gondii. *Front Microbiol, 9*, 2587. doi:10.3389/fmicb.2018.02587

Montes-Avila, J., Díaz-Camacho, S. P., Sicairos-Félix, J., Delgado-Vargas, F., & Rivero, I. (2009). Solution-phase parallel synthesis of substituted chalcones and their antiparasitary activity against Giardia lamblia. *Bioorg Med Chem, 17*(18), 6780-6785.

Montoya, J. G., Boothroyd, J. C., & Kovacs, J. A. (2015). 280 - Toxoplasma gondii. In J. E. Bennett, R. Dolin, & M. J. Blaser (Eds.), *Mandell, Douglas, and Bennett's Principles and Practice of Infectious Diseases (Eighth Edition)* (pp. 3122-3153.e3127). Philadelphia: W.B. Saunders.

Montoya, J. G., & Liesenfeld, O. (2004). Toxoplasmosis. *Lancet, 363*(9425), 1965-1976. doi:10.1016/s0140-6736(04)16412-x

Murti, V., Raman, P., & Seshadri, T. (1967). Cupressuflavone, a new biflavonyl pigment. *Tetrahedron, 23*(1), 397-404.

Mzabi, A., Aubert, D., & Villena, I. (2017). Mechanisms of Drug Resistance in Toxoplasma gondii. In D. L. Mayers, J. D. Sobel, M. Ouellette, K. S. Kaye, & D. Marchaim (Eds.), *Antimicrobial Drug Resistance: Mechanisms of Drug Resistance, Volume 1* (pp. 677-684). Cham: Springer International Publishing.

Nicolle, C. (1908). Sur une infection a corps de Leishman (on organismes voisons) du gondi. *CR Acad Sci, 147*, 736.

Nicolle, C., & Manceaux, L. (1909). Sur un Protozoaire nouveau du Gondi (Toxoplasma n. gen.). Retrieved from https://eurekamag.com/research/023/735/023735829.php

Nolan, K. A., Timson, D. J., Stratford, I. J., & Bryce, R. A. (2006). In silico identification and biochemical characterization of novel inhibitors of NQO1. *Bioorganic & Medicinal Chemistry Letters, 16*(24), 6246-6254. doi:https://doi.org/10.1016/j.bmcl.2006.09.015

Pagano, L., Trapè, G., Putzulu, R., Caramatti, C., Picardi, M., Nosari, A., . . . Del Favero, A. (2004). Toxoplasma gondii infection in patients with hematological malignancies. *Ann Hematol, 83*(9), 592-595. doi:10.1007/s00277-004-0898-z

Papich, M. G. (2016). Atovaquone. In M. G. Papich (Ed.), *Saunders Handbook of Veterinary Drugs (Fourth Edition)* (pp. 58-60). St. Louis: W.B. Saunders.

Park, Y. H., & Nam, H. W. (2013). Clinical features and treatment of ocular toxoplasmosis. *Korean J Parasitol, 51*(4), 393-399. doi:10.3347/kjp.2013.51.4.393

Peng, J., Ramatchandirin, B., Pearah, A., & He, L. (2023). Far-western Blotting Detection of the Binding of Insulin Receptor Substrate to the Insulin Receptor. *Bio Protoc, 13*(4), e4619. doi:10.21769/BioProtoc.4619

Pereira, R., Silva, A. M., Ribeiro, D., Silva, V. L., & Fernandes, E. (2023). Bis-chalcones: A review of synthetic methodologies and anti-inflammatory effects. *European Journal of Medicinal Chemistry, 252*, 115280.

Pramanik, A., & Ghatak, A. (2022). Current Trends on C–C Bond Formation Through Regioselective Hydroarylation of Alkynes and Alkenes Using Metal Free Catalysts. *Tetrahedron, 112*, 132757. doi:https://doi.org/10.1016/j.tet.2022.132757

Prestes-Carneiro, L. E., Rubinsky-Elefant, G., Ferreira, A. W., Araujo, P. R., Troiani, C., Zago, S. C., . . . Vaz, A. (2013). Seroprevalence of toxoplasmosis, toxocariasis and cysticercosis in a rural settlement, São Paulo State, Brazil. *Pathogens and Global Health, 107*(2), 88-95. doi:10.1179/2047773213Y.0000000079

Rajapakse, R. M. G., Horrocks, B. R., Malikaramage, A. U., Gunarathna, H., Egodawele, M., Jayasinghe, J. M. S., . . . Velauthapillai, D. (2023). Berberine isolation from Coscinium fenestratum: optical, electrochemical, and computational studies. *RSC Adv, 13*(25), 17062-17073. doi:10.1039/d3ra01769a

Ram, V. J., Saxena, A. S., Srivastava, S., & Chandra, S. (2000). Oxygenated chalcones and bischalcones as potential antimalarial agents. *Bioorg Med Chem Lett, 10*(19), 2159-2161. doi:10.1016/s0960-894x(00)00409-1

Rautio, J., Kumpulainen, H., Heimbach, T., Oliyai, R., Oh, D., Järvinen, T., & Savolainen, J. (2008). Prodrugs: design and clinical applications. *Nature Reviews Drug Discovery, 7*(3), 255-270. doi:10.1038/nrd2468

Remington, J. S. (1974). Toxoplasmosis in the adult. *Bull N Y Acad Med, 50*(2), 211-227.

Remington, J. S., & Klein, J. O. (2001). *Infectious diseases of the fetus and newborn infant*: London: WB Saunders, 2001.

Remington, J. S., Wilson, C. B., Nizet, V., Klein, J. O., & Maldonado, Y. (2010). *Infectious diseases of the fetus and newborn E-book*: Elsevier Health Sciences.

Reuter, K., Sanderbrand, S., Jomaa, H., Wiesner, J., Steinbrecher, I., Beck, E., . . . Stubbs, M. T. (2002). Crystal structure of 1-deoxy-D-xylulose-5-phosphate reductoisomerase, a crucial enzyme in the non-mevalonate pathway of isoprenoid biosynthesis. *J Biol Chem, 277*(7), 5378-5384. doi:10.1074/jbc.M109500200

Ricagno, S., Grolle, S., Bringer-Meyer, S., Sahm, H., Lindqvist, Y., & Schneider, G. (2004). Crystal structure of 1-deoxy-d-xylulose-5-phosphate reductoisomerase from Zymomonas mobilis at 1.9-A resolution. *Biochim Biophys Acta, 1698*(1), 37-44. doi:10.1016/j.bbapap.2003.10.006

Rinderspacher, A. (2013). Chapter 5.2 - Six-Membered Ring Systems: Diazines and Benzo Derivatives. In G. W. Gribble & J. A. Joule (Eds.), *Progress in Heterocyclic Chemistry* (Vol. 25, pp. 357-390): Elsevier.

Robert-Gangneux, F., & Dardé, M.-L. (2012). Epidemiology of and Diagnostic Strategies for Toxoplasmosis. *Clinical Microbiology Reviews, 25*(2), 264-296. doi:doi:10.1128/cmr.05013-11

Robert-Gangneux, F., Murat, J.-B., Fricker-Hidalgo, H., Brenier-Pinchart, M.-P., Gangneux, J.-P., & Pelloux, H. (2011). The placenta: a main role in congenital toxoplasmosis? *Trends in Parasitology, 27*(12), 530-536.

Rodriguez-Concepcion, M. (2004). The MEP pathway: a new target for the development of herbicides, antibiotics and antimalarial drugs. *Current pharmaceutical design, 10*(19), 2391-2400.

Rozmer, Z., & Perjési, P. (2016). Naturally occurring chalcones and their biological activities. *Phytochemistry Reviews, 15*(1), 87-120. doi:10.1007/s11101-014-9387-8

Rudrapal, M., Khan, J., Dukhyil, A. A. B., Alarousy, R., Attah, E. I., Sharma, T., . . . Bendale, A. R. (2021). Chalcone Scaffolds, Bioprecursors of Flavonoids: Chemistry, Bioactivities, and Pharmacokinetics. *Molecules, 26*(23). doi:10.3390/molecules26237177

Saadatnia, G., & Golkar, M. (2012). A review on human toxoplasmosis. *Scand J Infect Dis, 44*(11), 805-814.

Sabin, A. B., & Feldman, H. A. (1948). Dyes as Microchemical Indicators of a New Immunity Phenomenon Affecting a Protozoon Parasite (Toxoplasma). *Science, 108*(2815), 660-663. doi:10.1126/science.108.2815.660

Sabin, A. B., & Warren, J. (1942). Therapeutic Effectiveness of Certain Sulfonamides on Infection by an Intracellular Protozoon (Toxoplasma). *Proceedings of the Society for Experimental Biology and Medicine, 51*(1), 19-23. doi:10.3181/00379727-51-13809

Salehi, B., Venditti, A., Sharifi-Rad, M., Kręgiel, D., Sharifi-Rad, J., Durazzo, A., . . . Martins, N. (2019). The Therapeutic Potential of Apigenin. *International Journal of Molecular Sciences, 20*(6), 1305. Retrieved from https://www.mdpi.com/1422-0067/20/6/1305

Sam-Yellowe, T. Y. (1996). Rhoptry organelles of the apicomplexa: Their role in host cell invasion and intracellular survival. *Parasitol Today, 12*(8), 308-316. doi:10.1016/0169-4758(96)10030-2

Scallan, E., Hoekstra, R. M., Angulo, F. J., Tauxe, R. V., Widdowson, M.-A., Roy, S. L., . . . Griffin, P. M. (2011). Foodborne illness acquired in the United States—major pathogens. *Emerging infectious diseases, 17*(1), 7.

Schatz, A., Bugle, E., & Waksman, S. A. (1944). Streptomycin, a Substance Exhibiting Antibiotic Activity Against Gram-Positive and Gram-Negative Bacteria.∗†. *Proceedings of the Society for Experimental Biology and Medicine, 55*(1), 66-69. doi:10.3181/00379727-55-14461

Schoch, C. L., Ciufo, S., Domrachev, M., Hotton, C. L., Kannan, S., Khovanskaya, R., . . . Karsch-Mizrachi, I. (2020). NCBI Taxonomy: a comprehensive update on curation, resources and tools. *Database (Oxford), 2020*. doi:10.1093/database/baaa062

Secrieru, A., Costa, I. C. C., O'Neill, P. M., & Cristiano, M. L. S. (2020). Antimalarial Agents as Therapeutic Tools Against Toxoplasmosis-A Short Bridge between Two Distant Illnesses. *Molecules, 25*(7). doi:10.3390/molecules25071574

Selim, M. S. M., Abdelhamid, S. A., & Mohamed, S. S. (2021). Secondary metabolites and biodiversity of actinomycetes. *J Genet Eng Biotechnol, 19*(1), 72. doi:10.1186/s43141-021-00156-9

Serafim, B., Bernardino, A. R., Freitas, F., & Torres, C. A. V. (2023). Recent Developments in the Biological Activities, Bioproduction, and Applications of Pseudomonas spp. Phenazines. *Molecules, 28*(3), 1368. Retrieved from https://www.mdpi.com/1420-3049/28/3/1368

Shammaa, A. M., Powell, T. G., & Benmerzouga, I. (2021). Adverse outcomes associated with the treatment of Toxoplasma infections. *Sci Rep, 11*(1), 1035. doi:10.1038/s41598-020-80569-7

Sharif, M., Sarvi, S., Pagheh, A. S., Asfaram, S., Rahimi, M. T., Mehrzadi, S., . . . Daryani, A. (2016). The efficacy of herbal medicines against Toxoplasma gondii during the last 3 decades: a systematic review. *Canadian Journal of Physiology*

and Pharmacology, 94(12), 1237-1248. doi:10.1139/cjpp-2016-0039 %M 27564395

Sharma, U. K., Mohanakrishnan, D., Sharma, N., Equbal, D., Sahal, D., & Sinha, A. K. (2018). Facile synthesis of vanillin-based novel bischalcones identifies one that induces apoptosis and displays synergy with Artemisinin in killing chloroquine resistant Plasmodium falciparum. *Eur J Med Chem, 155*, 623-638. doi:10.1016/j.ejmech.2018.06.025

Sheffield, H. G., & Melton, M. L. (1968). The fine structure and reproduction of Toxoplasma gondii. *J Parasitol*, 209-226.

Sheffield, H. G., & Melton, M. L. (1975). Effect of pyrimethamine and sulfadiazine on the fine structure and multiplication of Toxoplasma gondii in cell cultures. *J Parasitol, 61*(4), 704-712.

Shiojiri, D., Kinai, E., Teruya, K., Kikuchi, Y., & Oka, S. (2019). Combination of Clindamycin and Azithromycin as Alternative Treatment for Toxoplasma gondii Encephalitis. *Emerg Infect Dis, 25*(4), 841-843. doi:10.3201/eid2504.181689

Shivaprasad, H. N., Sirisha Mulukuri, N. V. L., Chandrasekar, S. B., Baheti, A. M., & Pawar, A. T. (2023). Chapter 59 - Role of natural products in infectious diseases. In D. Bagchi, A. Das, & B. W. Downs (Eds.), *Viral, Parasitic, Bacterial, and Fungal Infections* (pp. 757-770): Academic Press.

Shoker, T. A., Ghattass, K. I., Fettinger, J. C., Kurth, M. J., & Haddadin, M. J. (2012). Unusual Friedlander reactions: a route to novel quinoxaline-based heterocycles. *Org Lett, 14*(14), 3704-3707. doi:10.1021/ol301550e

Si, H., Xu, C., Zhang, J., Zhang, X., Li, B., Zhou, X., & Zhang, J. (2018). Licochalcone A: an effective and low-toxicity compound against Toxoplasma gondii in vitro and in vivo. *International Journal for Parasitology: Drugs and Drug Resistance, 8*(2), 238-245.

Sibley, L. D., & Boothroyd, J. C. (1992). Virulent strains of Toxoplasma gondii comprise a single clonal lineage. *Nature, 359*(6390), 82-85. doi:10.1038/359082a0

Sibley, L. D., Khan, A., Ajioka, J. W., & Rosenthal, B. M. (2009). Genetic diversity of Toxoplasma gondii in animals and humans. *Philosophical Transactions of the Royal Society B: Biological Sciences, 364*(1530), 2749-2761. doi:doi:10.1098/rstb.2009.0087

Singh, M., Kaur, M., & Silakari, O. (2014). Flavones: An important scaffold for medicinal chemistry. *European Journal of Medicinal Chemistry, 84*, 206-239. doi:https://doi.org/10.1016/j.ejmech.2014.07.013

Singh, N., Chevé, G., Avery, M. A., & McCurdy, C. R. (2007). Targeting the methyl erythritol phosphate (MEP) pathway for novel antimalarial, antibacterial and herbicidal drug discovery: inhibition of 1-deoxy-D-xylulose-5-phosphate reductoisomerase (DXR) enzyme. *Current pharmaceutical design, 13*(11), 1161-1177.

Sinha, S., Batovska, D. I., Medhi, B., Radotra, B. D., Bhalla, A., Markova, N., & Sehgal, R. (2019). In vitro anti-malarial efficacy of chalcones: cytotoxicity profile, mechanism of action and their effect on erythrocytes. *Malaria journal, 18*(1), 421. doi:10.1186/s12936-019-3060-z

Smith, R. D., & Coast, J. (2002). Antimicrobial resistance: a global response. *Bulletin of the World Health Organization, 80*, 126-133.

Splendore, A. (1908). Un nuovo protozoa parassita deconigli incontrato nelle lesioni anatomiche d'une malattia che ricorda in molti punti il Kala-azar dell'uoma. Nota preliminare pel. *Rev Soc Sci Sao Paulo, 3*, 109-112.

Stopić, M., Štajner, T., Marković-Denić, L., Nikolić, V., Djilas, I., Srzentić, S. J., . . . Bobić, B. (2022). Epidemiology of Toxoplasmosis in SERBIA: A Cross-Sectional Study on Blood Donors. *Microorganisms, 10*(3), 492. Retrieved from https://www.mdpi.com/2076-2607/10/3/492

Strang, A. G. G. F., Ferrari, R. G., do Rosário, D. K., Nishi, L., Evangelista, F. F., Santana, P. L., . . . Guilherme, A. L. F. (2020). The congenital toxoplasmosis burden in Brazil: Systematic review and meta-analysis. *Acta Tropica, 211*, 105608. doi:https://doi.org/10.1016/j.actatropica.2020.105608

Tabana, Y., Babu, D., Fahlman, R., Siraki, A. G., & Barakat, K. (2023). Target identification of small molecules: an overview of the current applications in drug discovery. *BMC Biotechnol, 23*(1), 44. doi:10.1186/s12896-023-00815-4

Teuber, H. J., & Staiger, G. (1954). Reaktionen mit Nitrosodisulfonat, VI. Mitteil.: Oxyindole und Indolchinone aus Dihydroindolen. *Chemische Berichte, 87*(9), 1251-1255.

Thaker, M. N., Waglechner, N., & Wright, G. D. (2014). Antibiotic resistance-mediated isolation of scaffold-specific natural product producers. *Nat Protoc, 9*(6), 1469-1479. doi:10.1038/nprot.2014.093

Tiwari, P., & Bae, H. (2022). Endophytic Fungi: Key Insights, Emerging Prospects, and Challenges in Natural Product Drug Discovery. *Microorganisms, 10*(2), 360. Retrieved from https://www.mdpi.com/2076-2607/10/2/360

Torrey, E. F., & Yolken, R. H. (2013). Toxoplasma oocysts as a public health problem. *Trends in Parasitology, 29*(8), 380-384.

Trouiller, P., Olliaro, P., Torreele, E., Orbinski, J., Laing, R., & Ford, N. (2002). Drug development for neglected diseases: a deficient market and a public-health policy failure. *Lancet, 359*(9324), 2188-2194. doi:10.1016/s0140-6736(02)09096-7

Umeda, T., Tanaka, N., Kusakabe, Y., Nakanishi, M., Kitade, Y., & Nakamura, K. T. (2011). Molecular basis of fosmidomycin's action on the human malaria parasite Plasmodium falciparum. *Scientific Reports, 1*(1), 9. doi:10.1038/srep00009

Vogel, N., Kirisits, M., Michael, E., Bach, H., Hostetter, M., Boyer, K., . . . Mack, D. (1996). Congenital toxoplasmosis transmitted from an immunologically

competent mother infected before conception. *Clinical Infectious Diseases, 23*(5), 1055-1060.

Votýpka, J., Modrý, D., Oborník, M., Šlapeta, J., & Lukeš, J. (2017). Apicomplexa. In J. M. Archibald, A. G. B. Simpson, C. H. Slamovits, L. Margulis, M. Melkonian, D. J. Chapman, & J. O. Corliss (Eds.), *Handbook of the Protists* (pp. 1-58). Cham: Springer International Publishing.

Walther, R., Rautio, J., & Zelikin, A. N. (2017). Prodrugs in medicinal chemistry and enzyme prodrug therapies. *Advanced Drug Delivery Reviews, 118*, 65-77. doi:https://doi.org/10.1016/j.addr.2017.06.013

Wang, X., Edwards, R. L., Ball, H., Johnson, C., Haymond, A., Girma, M., . . . Dowd, C. S. (2018). MEPicides: α,β-Unsaturated Fosmidomycin Analogues as DXR Inhibitors against Malaria. *J Med Chem, 61*(19), 8847-8858. doi:10.1021/acs.jmedchem.8b01026

Wang, X., Edwards, R. L., Ball, H. S., Heidel, K. M., Brothers, R. C., Johnson, C., . . . Dowd, C. S. (2023). MEPicides: α,β-unsaturated Fosmidomycin N-Acyl Analogs as Efficient Inhibitors of Plasmodium falciparum 1-Deoxy-d-xylulose-5-phosphate reductoisomerase. *ACS Infectious Diseases, 9*(7), 1387-1395. doi:10.1021/acsinfecdis.3c00132

Wolf, A., Cowen, D., & Paige, B. (1939). Human toxoplasmosis: occurrence in infants as an encephalomyelitis verification by transmission to animals. *Science, 89*(2306), 226-227.

Yabsley, M. J., & Shock, B. C. (2013). Natural history of zoonotic Babesia: role of wildlife reservoirs. *International Journal for Parasitology: Parasites and Wildlife, 2*, 18-31.

Yajima, S., Hara, K., Iino, D., Sasaki, Y., Kuzuyama, T., Ohsawa, K., & Seto, H. (2007). Structure of 1-deoxy-D-xylulose 5-phosphate reductoisomerase in a quaternary complex with a magnesium ion, NADPH and the antimalarial drug fosmidomycin. *Acta Crystallogr Sect F Struct Biol Cryst Commun, 63*(Pt 6), 466-470. doi:10.1107/s1744309107024475

Yan, J., Liu, W., Cai, J., Wang, Y., Li, D., Hua, H., & Cao, H. (2021). Advances in phenazines over the past decade: Review of their pharmacological activities, mechanisms of action, biosynthetic pathways and synthetic strategies. *Mar Drugs, 19*(11), 610.

Yang, W., Ning, W., Jungchi, H., Liu, T., Yin, X., Ye, C., . . . Yang, C. (2022). Polycyclic phenazine-derived rigid donors construct thermally activated delayed fluorescence emitters for highly efficient orange OLEDs with extremely low roll-off. *Chemical Engineering Journal, 438*, 135571. doi:https://doi.org/10.1016/j.cej.2022.135571

Yu, S., Yan, H., Zhang, L., Shan, M., Chen, P., Ding, A., & Li, S. F. (2017). A Review on the Phytochemistry, Pharmacology, and Pharmacokinetics of Amentoflavone, a Naturally-Occurring Biflavonoid. *Molecules, 22*(2). doi:10.3390/molecules22020299

Zhang, M., Joyce, B. R., Sullivan, W. J., Jr., & Nussenzweig, V. (2013). Translational control in Plasmodium and toxoplasma parasites. *Eukaryot Cell, 12*(2), 161-167. doi:10.1128/ec.00296-12

Zhang, W., Krohn, K., Flörke, U., Pescitelli, G., Di Bari, L., Antus, S., . . . Schulz, B. (2008). New Mono-and Dimeric Members of the Secalonic Acid Family: Blennolides A–G Isolated from the Fungus Blennoria sp. *Chemistry–A European Journal, 14*(16), 4913-4923.

Zhang, Y., Li, D., Lu, S., & Zheng, B. (2022). Toxoplasmosis vaccines: what we have and where to go? *npj Vaccines, 7*(1), 131. doi:10.1038/s41541-022-00563-0

Zhuang, C., Zhang, W., Sheng, C., Zhang, W., Xing, C., & Miao, Z. (2017). Chalcone: A Privileged Structure in Medicinal Chemistry. *Chemical reviews, 117*(12), 7762-7810. doi:10.1021/acs.chemrev.7b00020

Acknowledgements

I want to express my heartfelt gratitude to everyone who stood by me throughout my Ph.D. journey, offering unwavering support in bringing this dissertation to fruition.

First and foremost, I extend my deepest appreciation to my supervisor Prof. Dr. med. Klaus Pfeffer. His guidance has been the beacon that illuminated the path of this extraordinary three-and-a-half year journey within his laboratories, which have become like a second home to me. I want to express my gratitude to Klaus for entrusting me with this fantastic project and for placing such great trust in me. The research and study of the various topics were enlightening, I enjoyed every single day spent in Klaus' lab. I am particularly thankful for Klaus's role as an exceptional mentor. His wealth of insights and invaluable feedback, shared during our meetings, not only encouraged me to consistently deliver my best but also provided unwavering support during challenging times. Beyond that, Klaus played a crucial role in both my professional and personal growth. I am grateful for the opportunity to work closely with him. Thank you for your great support Klaus, both professional and personal, I will never forget it. You have been and will always be a great inspiration to me.

I express my gratitude to my second supervisor, Prof. Dr. Rainer Kalscheuer. I am thankful for his kindness and willingness to help me. Each meeting with him has been not only pleasant but also motivating. I appreciate every piece of advice and feedback he has provided, contributing significantly to the refinement of my work. Thank you for allowing me to collaborate on the project involving natural products derived from the endophytic fungus *Paraboeremia selaginellae*. It has been truly fruitful, and your contribution has been invaluable.

I would like to express my sincerest gratitude to Prof. Dr. Sander Smits. He was a fantastic guide and supervisor, and meeting him significantly shaped my Ph.D. journey. I am grateful for giving me the opportunity to conduct my "endless lab rotation" in his laboratories in Biochemistry I. It has undoubtedly been the most fun and richest experience of my Ph.D. path. I appreciate Sander transmitting his extraordinary enthusiasm to me. Thanks to Sander, I delved deeper into the realms of biochemistry and protein studies. His substantial contribution to the study of *Tg*DXR is truly remarkable. Thank you very much, Sander. You are amazing!

Furthermore, I extend my gratitude to my research partners for the fruitful collaboration we have cultivated. Special thanks to Dr. Viktor Simons, Dr. Franziska Merkt, Larissa Hinz, Moritz Klischan, Julian Greb, Mona Abdullaziz Mahmood, Dr. Philipp Westhoff, Fabian Fisher, Prof. Dr. Rainer Kalscheuer, Prof. Dr. Sander Smits, Prof Dr. Thomas J.J. Müller, Prof. Dr. Jörg Pietruszka and Prof. Dr. Thomas Kurz. Collaborating with each of you has been truly extraordinary.

I would like to convey my sincere gratitude to the laboratory technicians Karin Buchholz, Nicole Küpper and Julia Mock for their unwavering assistance in the laboratory, especially during challenging moments, and for imparting valuable knowledge about laboratory methods. I extend special thanks to Karin for her crucial role during the initial stages of my PhD. and the management of my orders.

I express my sincere gratitude for the outstanding support of Dr. Daniel Degrandi. Conversing in Italian with you has consistently provided a sense of home. Your advice and support have proven to be truly invaluable.

I extend my gratitude to Dr. Ursula Sorg for the myriad pieces of advice she provided during our Wednesday meetings. Thank you for consistently being kind and willing to assist me.

I also want to thank my colleagues and former colleagues of the Pfeffer team Marcel Helle, Veronica Raba, Dr. Sebastian Scharf, Imke Bradtmöller, Anna Rommerskirschen, Gowshiga Sivalingam, Sophia Kasbrink, Sebastian Hachenberg, Sina Waeteraere, Dr. Jennifer Jaufmann and Dr. Elisabeth Kravetz. Your unwavering assistance has been priceless; there wasn't a day when I couldn't depend on your support. All of you have contributed to my education, skill enhancement, and personal development. I appreciate your motivation, positive words, and the lively atmosphere you brought to the institute.

I would like to thank my “amazing office” 22.21, 00 OG, Raum 55.00 made up of Veronica Raba, Mahamudul Bhuyan, Lars Vogelgsang, Adarsh Nair, Mick Gottemeier, Nick Komischke and Dana Belick for making my working days super colourful. Thank you for the many "scientific discussions" strictly with the door closed. The laughter, the long conversations and your great support helped make my Ph.D. super fun. Thanks to you I will remember everything with a smile.

I extend my gratitude to my former colleagues and friends from the Proksch team Nam Tran-Cong, Haiqian Yu, Kim Thao Le Tran-Cong, and Dina Hassouna El-Kashef. I am truly grateful for your ongoing support, which evolves from professional connections into authentic friendships. Special thanks goes to Nam, who has been more than a colleague – he has been a personal mentor. I want to express my deep thanks for guiding me towards pursuing an academic career and convincing me to embark on the PhD journey. Without your influence, I would not be in the position I am today. Thank you for being a pillar of support and encouragement on this remarkable path.

I want to express my special gratitude to all members of Biochemistry I. Your warm welcome to your laboratories and your support played a crucial role during my laboratory period. Heartfelt thanks go to Dr. Julia Gottstein, Dr. Marten Exterkate and Prof. Dr. Miriam Kutsch, with whom important friendships were created. Really thank you, my dears.

I extend my gratitude to GRK2158 for providing me with the opportunity to pursue a well-structured doctorate, complete with diverse lessons and workshops in the realms of preclinical studies and soft skills. These experiences have significantly enriched my cultural knowledge. I express my thanks to all the members of GRK2158 for the unforgettable symposiums and retreats and the numerous collaborations that have emerged from them.
In particular, I would like to convey my appreciation to Dr. Martina Holz for her exceptional organization of every single event, lesson, and workshop, along with her valuable guidance on navigating the bureaucratic aspects associated with every conferences. It's always a pleasure to engage in conversations with you, and I must say, "sei bellissima!".

Voglio ringraziare i miei amici, tutti. In particolare, i miei punti di riferimento qui a Düsseldorf: Vanessa Cristofaro, Sara Oriente, Giuseppe Andreacchio, Barbara Coglitore, Giulia Morro e Fabio D'Addelfio. Grazie per supportarmi tra un calice di vino e l'altro, per avermi sostenuta durante i miei periodi più difficili, ve ne sarò sempre grata. Ringrazio anche i miei amici in Sicilia, che nonostante il tempo e lo spazio che ci distanzia (2.031km di distanza, per l'esattezza) sono ancora al mio fianco e fanno una gran festa ogni qual volta che sono giù in terra natia. Mi mancate sempre, soprattutto Gaetano Gennuso, Ylenia Sanfilippo, Giovanni Massimino, Dr. Stefano Amantia, Stefania Scalone, Nicoletta Dammone Sessa. Grazie di vero cuore.

Desidero ringraziare di cuore tutta la mia amata famiglia per il calore avvolgente che mi dona ogni volta che ne ho bisogno. In particolare, i miei genitori e mio fratello. In questo momento così significativo, giunta alla conclusione della mia tesi di dottorato, desidero ringraziarvi di cuore per il vostro fondamentale contributo. Voi siete la ragione per cui ho perseverato nei momenti difficili e il vostro amore e il vostro sostegno sono la linfa vitale che ha alimentato il mio intero percorso accademico. Il vostro amore ha reso possibile ogni cosa, ogni mio passo in avanti e ogni piccolo e grande successo raggiunto. Grazie per avermi insegnato i valori che hanno plasmato il mio percorso, e devo a voi il raggiungimento di questo importante traguardo. Con tutto il mio amore, grazie per essere la luce che guida il mio cammino nella vita.

Last, but not least, thank you to my love Pascal. Thank you for your great love, for constantly being by my side and for providing me with support in the most difficult moments. You are the most beautiful aspect of my life. Your love is a source of strength and inspiration, pushing me to achieve goals I never thought possible, like completing the last page of my thesis. I would like to dedicate this doctoral thesis to our love, because it is the catalyst for everything; the love that moves the sun and the other stars, my love for you. Ti amo amore mio.

Statutory Declaration / Eidesstattliche Erklärung

Statutory Declaration

I declare under oath that I have produced my thesis independently and without any undue assistance by third parties under consideration of the "Principles for the Safeguarding of Good Scientific Practice at Heinrich Heine University Düsseldorf".

Eidesstattliche Erklärung

Ich erkläre an Eides statt, dass ich meine Dissertation selbstständig und ohne unzulässige Unterstützung durch Dritte unter Beachtung der "Grundsätze zur Sicherung guter wissenschaftlicher Praxis an der Heinrich-Heine-Universität Düsseldorf" angefertigt habe.

_____

Flaminia Mazzone

Düsseldorf, / /